行政院國家科學委員會補助專題研究計畫 □ 成 果 報 告
■期中進度報告

冷媒流量和熱通量振盪引起之暫態新冷媒和 FC-72 流動沸騰研究(一)

計畫類別：■ 個別型計畫　　□ 整合型計畫
計畫編號：NSC 96－2221－E－009－133－MY3
執行期間：民國 96 年 08 月 01 日 起至民國 97 年 07 月 31 日

計畫主持人：林清發 教授
共同主持人：
計畫參與人員：陳建安 楊政陞

成果報告類型(依經費核定清單規定繳交)：■精簡報告　□完整報告

本成果報告包括以下應繳交之附件：
□赴國外出差或研習心得報告一份
□赴大陸地區出差或研習心得報告一份
□出席國際學術會議心得報告及發表之論文各一份
□國際合作研究計畫國外研究報告書一份

處理方式：除產學合作研究計畫、提升產業技術及人才培育研究計畫、列管計畫及下列情形者外，得立即公開查詢
□涉及專利或其他智慧財產權，□一年□二年後可公開查詢

執行單位：國立交通大學機械工程研究所

中　華　民　國　九十七　年　　五　　月　　日

ABSTRACT

This study intends to explore how a time periodic coolant flow rate affects the transient forced convective boiling heat transfer and associated bubble characteristics of FC-72 over a small heated circular copper plate flush mounted on the bottom of a horizontal rectangular channel with a cross section of 20 mm in width and 5 mm in height. The diameter of the copper plate is 10 mm. More specifically, the effects of the coolant flow rate oscillation in the form of nearly triangular wave on the transient flow boiling will be examined in detail. In the experiment the time-average coolant mass flux $\overline{G}$ is varied from 300 to 400 kg/m^{2}s and the amplitude of the coolant mass flux oscillation is fixed at 0%, 5% and 10% of $\overline{G}$. The period of the coolant mass flux oscillation varies from 10s to 30s. Besides, the liquid subcooling at the inlet of the channel ranges from 0°C to 10°C and the heat flux imposed on the heated plate varies from 0.1 to 10 W/cm^2.

The experimental results show that the time-average data of the FC-72 transient saturated and subcooled flow boiling heat transfer characteristics are not affected to a significant degree by the amplitude and period of the coolant mass flux oscillation. In fact, they resemble these for the stable flow boiling. However, in the transient saturated and subccoled flow boiling of FC-72 significant temporal oscillations in the boiling heat transfer coefficient, bubble departure diameter and frequency, and active nucleation site density appear for the imposed heat flux slightly higher than that for ONB. They oscillate at the same frequency as the mass flux oscillation. Besides, at a higher imposed heat flux and for a larger amplitude of the mass flux oscillation stronger oscillations in $h_{2\phi}$, d_p, f and N_{ac} are noted. But they are only slightly affected by the period of the mass flux oscillation. Furthermore, in the time duration in which the mass flux rises with time both the size of the departing bubbles and active

nucleation site density decrease, but the bubble departure frequency increases. The opposite processes occur for a sink of mass flux with time. We also note that an increases in the inlet liquid subcooling causes stronger oscillations in the boiling heat transfer coefficient.

TABLE OF CONTENTS

LIST OF TABLES

LIST OF FIGURES

Experiment Apparatus

Saturated Flow Boiling

NOMENCLATURE

A	area, m^2
B	element height, m
c_p	specific heat, J/kg℃
D	hydraulic diameter of rectangular-channel, m
G	mass flux, kg/m^2s
g	acceleration due to gravity, m/s^2
H	height, m
h	heat transfer coefficient, $W/m^2 \cdot K$
I	measured current from DC power supply, A
i_{lv}	enthalpy of vaporization, $J/kg \cdot K$
k	thermal conductivity, $W/m \cdot K$
L	length, mm
$\dot{m}$	mass flow rate, kg/s
Ja'	Jacob number based on ΔT_{sub}, $Ja' = \frac{\rho_l \cdot C_{pl} \cdot \Delta T_{sub}}{\rho_v \cdot i_{lv}}$, dimensionless
Nu	Nusselt number, $Nu = \frac{h \cdot L}{k}$, dimensionless
P	system pressure, kPa
Pr	Prandtl number, $Pr = \frac{\mu \cdot C_p}{k}$, dimensionless
N_{ac}	Active nucleation site density, n/m^2
Q	heat transfer rate, W

q	average imposed heat flux, W/cm^2
Re	Reynolds number, $Re = \frac{G \cdot D}{\mu}$, dimensionless
S	element space between two adjacent elements, m
T	temperature,℃
V	coolant FC-72 flow velocity, m/s
V	measured voltage from DC power supply, V
W	width, m

Greek Symbols

ΔT	temperature difference, ℃
μ	dynamic viscosity, $N \cdot s/m^2$
ν	specific volume, m^3/kg
ρ	density, kg/m^3
ε	relative heat loss, dimensionless

Subscripts

ave	average
c,h	from heater surface to cooper surface
cop	copper
cs	cross-section of rectangular-channel
d	diameter

e	effective
f	fin
fin	mean bubble departure frequency
g	gas
h	hydraulic
i	at the inlet of the test section
in	at the inlet of the test section
i,o	at inlet and exit of the test section
l	all-liquid nonboiling heat transfer
lv	liquid phase to vapor phase
m	average value for the two phase mixture or between the inlet and exit
M	mica
n	net power input to the coolant FC-72
n	active nucleation site density
o	at the outlet of the test section
p	preheater
pool	pool boiling
r	coolant FC-72
s	surface
sat	saturated state for coolant FC-72
sp	single-phase convective heat transfer

sub	subcooled state for coolant FC-72
T	teflon
t	total
t-g	thermal-grease
tp	two-phase boiling heat transfer
v	vapor
w	wall
w	water
1ϕ	single-phase
2ϕ	two-phase

CHAPTER 1

INTRODUCTION

1.1 Motive of the Present Study

Energy conservation is a major concern in many countries relying heavily on the imported oil. Thus improving the energy utilization efficiency is relatively important in designing most engineering systems. In the past decade the use of variable frequency compressors in air conditioning and refrigeration systems to meet the changing heat load is found to significantly improve their thermal efficiencies. It is important to note that two-phase flow in these systems is subject to time varying refrigerant flow rate and time varying imposed heat flux. It is also well known that the junction temperature of IC must be kept under 85^{o}C to maintain its normal operation [1]. To solve the heat transfer problem of high power density in advanced CPU chips, methods employing boiling and condensation have been proposed and used recently. Moreover, the power dissipation in IC chips are also time dependent in practical operation. Therefore the coolant flow rate must be varied in time to meet the required time varying cooling load. Consequently, a detailed understanding of the phase-change processes subject to the time varying coolant flow rate and imposed heat flux is essential in thermal design for electronics cooling. Although considerable research has been carried out in the past for the two-phase flow and heat transfer under the condition of fixed flow rate and imposed heat flux, the corresponding research for the transient flow rate and imposed heat flux remains largely unexplored. In the present study an initial attempt is made to unravel how the characteristics of FC-72 flow boiling heat transfer and bubble motion in a channel are affected by the time varying refrigerant flow rate for a fixed imposed heat flux.

Due to thermally and chemically stable, the dielectric fluorocarbon liquid FC-72 is currently considered as a suitable coolant for electronics cooling. Hence FC-72 is chosen as the working fluid in the present experiment. Some thermophysical properties for FC-72 are given in Table 1.1.

1.2 Literature Review

In what follows the literature relevant to the present study is reviewed. Specifically, the literature on the use of boiling of dielectric liquids for cooling of electronic equipments will be examined.

1.2.1 Stable Single-Phase and Convective Boiling Heat Transfer

Boiling heat transfer from a small heated patch in the size of 0.25 × 2.0 mm (width × length) to R-113 and FC-72 was investigated by Samant and Simon [2]. They observed temperature excursions and boiling hysteresis at the onset of nucleate boiling, which were less pronounced at increasing velocity and/or liquid subcooling. They combined the experimental data for R-113 and FC-72 to develop an empirical correlation. Besides, in the nucleate boiling region the slope of the boiling curve increases with the coolant flow velocity. Garimella and Eibeck [3] analyzed the heat transfer characteristics of an array of protruding elements in single-phase forced convection of water for the channel Reynolds number ranging from 150 to 5,150. They noted that the heat transfer coefficient decreased with decreasing Reynolds number and the Nusselt number decreased with increasing ratio of the channel height to element height. Incropera et al. [4] experimentally investigated single-phase convective heat transfer from a single heat source and four-row arrays of 12 discrete heat sources flush-mounted in a horizontal rectangular channel. The working fluids they used were water and FC-77 for the channel Reynolds number ranging from 1,000 to 14,000. They developed a model to predict the relation between the Reynolds

number and Nusselt number for the turbulent flow regime with $5{,}000 < Re_D < 14{,}000$. Unfortunately, their measured data were significantly under-predicted in the laminar flow regime. Slightly later, Incropera et al. [5, 6] examined single-phase liquid convection and flow boiling of water and FC-72 in a horizontal rectangular channel with a 1×10 array flush mounted discrete heat sources. They found in the single-phase forced convection experiment that when the Reynolds number is raised from a very low value to a very high value, the resulting flow regimes included laminar mixed convection, transition from laminar mixed convection to laminar forced convection, laminar forced convection, transition from laminar forced convection to turbulent forced convection, and turbulent forced convection. Besides, they defined the wall temperature overshoot at the boiling inception as the constant heat flux temperature difference between the maximum temperature recorded under the single-phase convection condition and the corresponding theoretical temperature under boiling conditions. According to their experimental results, at increasing velocity the heat flux increases but the temperature overshoot decreases.

Mudawar and Maddox [7] investigated the critical heat flux for FC-72 boiling on a single heat source flush mounted on one wall of a vertical rectangular channel. They noted an increase in the channel pressure drop and a decrease in the critical heat flux at increasing void fraction. In a continuing study Mudawar et al. [8, 9] experimentally examined flow boiling of FC-72 over flush-mounted heat sources. The multi-heat sources in the vertical flow channel were arranged in an 1×9 array for the flow velocity ranging from 13 cm/s to 400 cm/s and for the liquid subcooling from 3 ^{o}C to 36 ^{o}C with the system pressure at 1.36 bar. They observed that increases in the flow velocity and subcooling resulted in a delay in the incipence of nucleate boiling and an increase in the critical heat flux. Besides, they proposed an empirical correlation for the heat transfer coefficient measured in the single-phase region. The chip surface

temperature was noted to increase slightly at decreasing velocity, and the result was opposite to that of Tso et al. [10]. Yun et al. [11] investigated flow boiling heat transfer of carbon dioxide in mini tubes. They noted that the effects of the heat flux on the heat transfer coefficient before critical vapor quality were strong at all mass flux. Besides, when the mass flux is less than 500 kg/m^{2}s, the effects of the mass flux on the heat transfer coefficient before the critical quality are significant.

The single-phase heat transfer correlations proposed in the above studies are listed in Table 1.2

1.2.2 Unstable Convective Boiling Heat Transfer

Two-phase flow instabilities in flow boiling of various liquids in long heated channels have been recognized for several decades [12, 13]. Under certain operating condition significant temporal oscillations in pressure, temperature, mass flux and boiling onset appear. Recently, some detailed characteristics associated with these instabilities were explored through experimental measurement and theoretical modeling. Specifically in flow boiling of refrigerant R-11 in a vertical channel, the pressure drop and thermal oscillations were observed by Kakac et al. [14]. Meanwhile, a two-phase homogeneous model along with the thermodynamic equilibrium assumption was used to predict the conditions leading to the thermal oscillation. Besides, they also predicted the periods and amplitudes of the oscillations, which were in good agreement with their measured data. Slightly later, Kakac and his colleagues [15] further noted the presence of density-wave oscillation superimposed on the pressure-drop oscillations. Moreover, the drift-flux model was employed in their numerical prediction. In a continuing study for R-11 in a horizontal tube of 106 cm long [16], the research group led by Kakac examined the dependence of the oscillation amplitude and period on the system parameters and located the boundaries

of various oscillations on the steady-state pressure drop vs. mass flux characteristic curves. A similar experimental study was carried out by Comakli et al. [17] for a longer tube (L=319.5 cm). They showed that the channel length has an important effect on the two-phase flow dynamic instabilities.

Analysis of the dynamic behavior of a horizontal boiling channel connected with a surge tank for liquid supply also receives some attention. Mawasha and Gross [18] used a constitutive model containing a cubic nonlinearity combined with the homogeneous two-phase flow model to simulate the pressure-drop oscillation. The prediction is in qualitative agreement with the measured data. Later, the effects of the channel wall heat capacity are included in the analysis [19] to allow the wall temperature and heat transfer coefficient to vary with time.

The boiling onset in a upward flow of subcooled water in a vertical tube of 7.8 m long with a liquid surge tank was noted by Wang et al. [20] to cause substantial flow pressure and density-wave oscillations. These boiling onset oscillations were attributed to a sudden increase of pressure drop across the channel and a large change in the water flow rate at the onset of nucleate boiling, which resulted in the feedback of the pressure drop and flow rate by the system and caused the location of the boiling onset to move in and out of the channel. Therefore, large flow oscillations appear in the channel.

Aside from the boiling instabilities in conventional channels, pressure-drop oscillations of n-pentane liquid in a vertical small rectangular channel (D_h=0.889 mm and L=50 & 200 mm) were reported recently by Brutin et al. [21]. Besides, a non-stationary state of two-phase flow was observed. The effects of the inlet flow conditions on the boiling instabilities were found to be relatively significant [22]. A similar study for subcooled flow boiling of deionized water was conducted by Shuai et al. [23] and the pressure-drop oscillations were also noted.

1.2.3 Bubble Characteristics

Experiments conducted by Chang et al. [24] for water focused on the behavior of near-wall bubbles in subcooled flow boiling. The number of near-wall bubbles increases with the increase in the heat flux and in the superheated liquid layer with very small bubbles attach on the heated wall. In addition, the size of coalesced bubbles decreases with the increase in the mass flux of the flow. In a recent experiment Bang et al. [25] examined boiling of R-134a in a vertical rectangular channel focusing on the characteristic structures in the near-wall region. They noted the presence of the vapor remants below the discrete bubbles and coalesced bubbles and the presence of an interleaved liquid layer between the vapor remants and bubbles. Besides, the bubble layer was divided into two types, a near wall-bubble layer dominated by small bubbles and a following bubble layer prevailed by large coalesced bubbles. Kandlikar [26] examined the subcooled flow boiling for water in a rectangular horizontal channel. They concluded that the bubble growth was slow at high subcooling and the departure diameter decreased as the flow rate increased.

By using optical measurement techniques, Maurus et al. [27, 28] examined the bubble distribution and local void fraction in subcooling flow boiling of water at atmospheric pressure. They reported that the bubble size increased with an increase in the heat flux but reduced with an increase in the mass flux. The total bubble life time, the remaining lifetime after the detachment process and the waiting time between two bubble cycles decreased significantly as the mass flux increased. In a recent study Maurus and Sattelmayer [29] further defined the bubbly region by the ratio of the averaged phase boundary velocity to the averaged fluid velocity. On the other hand, an experimental analysis was carried out by Thorncroft et al. [30] to investigate the vapor bubble growth and departure in vertical upflow and downflow boiling of FC-87. They found that the bubble growth rate and bubble departure diameter increased with

the Jacob number (increasing ΔT_{sat}) and decreased at increasing mass flux in both upflow and downflow. Bubble rise characteristics after the bubble departure from a nucleation site in vertical upflow tube boiling were investigated by Okawa et al. [31-33]. They noted that the inertia force had a significant influence on the onset of detachment but the influence was gradually reduced with time. They also observed three different bubble rise paths after the departure from nucleation sites. Specifically, some bubbles slide upward along the vertical wall, some bubbles detach from the wall after sliding, and other bubbles remain close to the wall and reattach to the wall. Forced convection boiling experiments conducted by Situ et al. [34, 35] for water in a vertical annular channel revealed that the bubble departure frequency increased as the heat flux increased. Moreover, the experimental results indicate that bubble lift-off diameter increases at increasing inlet temperature and heat flux. In addition, Yin et al. [36] examined the subcooled flow boiling of R-134a in a horizontal annular duct and noted that both the bubble departure size and frequency reduced at increasing liquid subcooling. They found that only the liquid subcooling showed a large effect on the bubble size.

1.3 Objective of This Study

The above literature review clearly indicates that the two-phase instabilities in the flow boiling of liquids in a long heated channel has received considerable attention. However, the unstable characteristics of flow boiling heat transfer and associated bubble behavior in a channel subject to imposed time varying liquid flow rate and heat flux remain largely unexplored. In this study, an experimental study will be carried out to investigate how the imposed inlet flow rate oscillation affects the transient flow boiling heat transfer of FC-72 and associated bubble characteristics on a heated flat plate flush mounted on the bottom of a horizontal rectangular channel

with a constant imposed heat flux. The use of this flat heater intends to simulate the power dissipating chip in an electronic system. In the experiment both the transient saturated and subcooled flow boiling will be examined. Effects of the period and amplitude of the flow rate oscillation on the boiling characteristics will be inspected in detail for various average mass fluxes of FC-72 and imposed heat fluxes at different degrees of inlet liquid subcooling.

Table 1.1 Thermodynamic properties for FC-72.

Properties	FC-72
Appearance	Clear, colorless
Average Molecular Weight	338
Boiling Point (1 atm)	55.7^{o}C
Pour Point	-90^{o}C
Estimated Critical Temperature	449K
Estimated Critical Pressure	1.83×10^{6} pascals
Vapor Pressure	30.9×10^{3} pascals
Latent Heat of Vaporization (at normal boiling point)	88 J/g
Liquid Density	1680 kg/m^{3}
Kinematic Viscosity	0.38 centistokes
Absolute Viscosity	0.64 centipoise
Liquid Specific Heat	1100 J kg^{-1} C^{-1}
Liquid Thermal Conductivity	0.057 W m^{-1} ^{o}C^{-1}
Coefficient of Expansion	0.00156 ^{o}C^{-1}
Surface Tension	10 dynes/cm
Refractive Index	1.251
Water Solubility	10 ppmw
Solubility in Water	<5 ppmw
Ozone Depletion Potential	0

Table 1.2 Some single-phase convection heat transfer correlations for electronics cooling.

Reference	**Working Fluid**	**Heat Transfer Correlation**	**Conditions**
Samant and Simon [2]	R-113 & FC-72	$Nu_H = 0.47Re_H^{0.58}Pr^{0.5}$	Test patch size: 0.25mm × 2.0mm Bulk velocity: 2.05 ~ 16.86 m/s Pressure at the patch: 118.8 ~ 338.1 kPa
Garimella and Eibeck [3]	Water	$Nu = 1.31Re_a^{0.48}(LS / B)^{0.15}$	Heat sources size: 1.9 cm × 1.9 cm $150 < Re_H < 5150$ Arrays: 5 row × 6 line
Incropera et al. [5]	Water & FC-77	$Nu_L = 0.13Re_D^{0.64}Pr^{0.38}(\mu_o / \mu_h)^{0.25}$	Heat sources size: 12.7mm ×12.7mm Arrays: 4 row × 3 line Inlet temperature: 14 &30 ^oC $5000 < Re_D < 14000$
Gersey and Mudawar [8]	FC-72	$Nu_L = 0.362Re_L^{0.614}Pr^{1/3}$	Heat sources size: 10mm ×10mm Arrays: 9 row × 1 line Flow velocity: 13 ~400 cm/s

CHAPTER 2

EXPERIMENTAL APPARATUS AND PROCEDURES

The experimental system established in the present study to investigate the transient flow boiling heat transfer and associated bubble characteristics of the dielectric coolant FC-72 over a small heated copper flat plate flush mounted on the bottom of a horizontal rectangular channel is depicted schematically in Fig. 2.1. This system includes a degassing unit, a coolant loop, a hot-water loop, and a cold water loop. The test section along with the entrance and exit sections are shown in Fig. 2.2 by three-dimensional plots. The liquid coolant FC-72 is driven by a variable speed gear pump and the inlet temperature of the coolant is regulated by a pre-heater with a hot water circulation in it. The coolant vapor generated during boiling in the test section is then condensed in the condenser cooled by another water thermostat and then returns to the receiver. The details of each component in the testing system are described in the following.

2.1 Degassing Unit

Since any non-condensable gas dissolved in the coolant FC-72 can significantly affect the heat transfer performance and nucleate boiling phenomena, we must degas the coolant before beginning the experiments. After a recharge of the coolant or re-arrangement of the piping system, the coolant must be degassed. The degassing unit is a tank of 8 liters patched with a flexible electric heater on its inside surface to heat the coolant to its boiling point. During the degassing process, the air and any non-condensable gas dissolved in the coolant escape from the liquid FC-72 in the tank and pass through the released valve on the top of the tank. Besides, a pressure

transducer and a thermocouple are equipped in the tank to measure the pressure and temperature of FC-72, respectively.

2.2 Coolant Loop

After degassing the coolant FC-72, we remove the non-condensable gases possibly existing in the coolant-loop by using a vacuum pump and then fill the degassed FC-72 liquid into the coolant-loop. The circulation system for the coolant consists of a variable-speed gear pump, a filter, a volume flow meter, a pre-heater, a test section including the inlet and outlet sections, a condenser, and a receiver. The head of this gear pump is coupled with a magnet-driven disk sealed inside an envelope to avoid any contamination from the shaft. The shaft is driven by an variable–speed AC induction motor which is in turn regulated by an inverter. The temporal oscillation of the coolant flow rate can be implemented by an optional external control of the inverter through a programmable DC current or voltage signal sequence. Besides, the average coolant flow rate can be further adjusted by regulating the bypass valve.

The coolant FC-72 at the outlet of the magnetic micro-pump must be kept subcooled to avoid any vapor flow through the volume flow meter. The pre-heater is used to heat the subcooled coolant FC-72 to a specific subcooled or saturated temperature at the test section inlet by receiving heat from the hot water in the hot-water loop. Finally, the vapor-liquid coolant mixture is generated in the test section when the subcooled or saturated coolant flows over the heated copper plate. The vapor flow leaving the test section is re-liquefied by the condenser in the cold-water loop.

After leaving the condenser, the liquid FC-72 flows back to the receiver at the

bottom of the system. An accumulator is connected to a high-pressure nitrogen tank to dampen the fluctuations of the coolant flow rate and pressure. The filter is used to filter the impurities and non-condensable gas possibly existing in the loop. Varying the temperature and flow rate of the hot-water flowing through the pre-heater allows us to control the pressure of the coolant loop. Two absolute pressure transducers are installed at the inlet and outlet of the test section with a resolution up to ± 2kPa. All the refrigerant and water temperatures are measured by calibrated copper-constantan thermocouples (T-type) with a calibrated accuracy of ± 0.2℃. The test section is thermally insulated with a polyethylene insulation layer so that heat loss from it can be reduced significantly.

2.3 Test Section

The test section mainly consists of a circular copper plate flush mounted on the bottom of the horizontal rectangular channel. The rectangular flow-channel includes a gradually diverging section, the main test section, and a gradually converging section (Fig. 2.3). They are all made of stainless steel plate. The installation of the inlet and exit sections avoids the sudden change in the cross section of the channel. The test section is 20 mm in width, 5 mm in height, and 150 mm in length, and the aspect ratio of the test section is 4.0. The heated plate is placed around the geometric center of the bottom plate of the test section. A ladder-shaped acrylic window is installed on the upper lid of the test section right above the heated plate. The temperature and pressure of the FC-72 flow at the inlet and exit of the test section are measured by the calibrated thermocouples and pressure transducers, as schematically shown in Fig. 2.3.

The copper plate module schematically shown in Figs. 2.4 and 2.5 includes a

hollow cylindrical Teflon block, a cylindrical Teflon bolt, a copper plate, two pieces of mica plates, a Teflon plate, and an electric-heater. The diameter of the copper plate is 10 mm and the plate is heated by passing DC current through the electric-heater. Besides, three thermocouples are fixed at the back surface of the copper plate to estimate the temperature of the upper surface of the copper plate and another two thermocouples are fixed at the top and bottom surface of the electric-heater to measure their surface temperatures. The locations of the thermocouples at the backside of the copper plate and at the electric-heater surface are shown in Fig. 2.5. The mica plates are placed between the heater and copper plate and between the heater and Teflon plate, intending to prevent the leaking of the DC current to the copper plate. The detailed structure of the module is shown in Fig. 2.6. The magnitude of heat loss from each surface of the Cylindrical-hollow Teflon block can be evaluated from the temperature measured at selected locations in the block. Locations of the thermocouples are schematically shown in Fig. 2.7.

2.4 Hot-water Loop

In order to maintain the dielectric coolant FC-72 at the preset temperature at the test section inlet, a hot-water loop is used to preheat the coolant before it arrives at the test section inlet. The hot-water loop for the pre-heater includes a thermostat with a 20-liter hot water container and a 2 kW heater in it, and a 0.5-hp water pump which can drive the hot water at a specified flow rate to the pre-heater. Besides, a bypass valve in the loop can further adjust the water flow rate. The hot water passes through the container while the liquid coolant FC-72 flows through the inner coiled pipe in the pre-heater. The connecting pipe between the pre-heater and test section is thermally insulated with a 5-cm thick polyethylene layer to reduce the heat loss from the pipe.

2.5 Cold-water Loop

The cold-water loop is designed for condensing the liquid-vapor mixture of FC-72 delivered from the test section. The maximum cooling capacity of the thermostat is 2,000 Kcal/hr. The cold water at a specific flow rate is driven by a 0.5-hp pump to the condenser and a bypass loop is provided to adjust the flow rate. By adjusting the temperature and flow rate of the cold water, the bulk temperature of FC-72 in the condenser can be controlled at a preset level.

2.6 DC Power Supply

As described above, the copper plate flush mounted on the bottom of the test section is heated by the electric-heater. A 30V-3A (Topward 3303D) DC power supply delivers the required electric current to the heater. A Yokogawa DC meter is used to measure the DC current through the electric-heater with an accuracy of ±1%. Besides, a Yokogawa data logger is used to measure the DC voltage across the electric-heater with an accuracy of ±1%. Thus the power input to the electric-heater can be calculated.

2.7 Data Acquisition

The data acquisition system employed to acquire and process the data from various transducers is a 30-channel data logger (YOKOGAWA MX-100) along with a personal computer. All the voltage signals from the T-type thermocouples, pressure transducers, and volume flow-meters are converted to the temperature, pressure, and volume flow rate by the internal calibration equations in the computer and are displayed on the screen simultaneously.

2.8 Optical Measurement Technique

The optical measurement technique employed in the present study enables us to capture the bubble characteristics in the boiling flow near the copper plate in the present flow boiling experiments. The photographic apparatus consists of a high speed digital video camera (IDT High-speed CMOS Digital Camera), a micro-lens (Optem Zoom160), a three-dimensional positioning mechanism, and a personal computer. The high-speed motion analyzer can take photographs up to 143,307 frames/s. Here, a recording rate of 5000 frames/s is adopted to obtain the images of the bubble ebullition processes. The positioning mechanism is used to hold the camera at the required accurate position. The data for the bubble characteristics are collected in the regions near the geometric center of the plate surface. After the experimental system reaches a statistically steady state, we start recording the boiling activity. The high speed motion analyzer stores the images which are later downloaded to a personal computer. Then, the mean bubble departure diameter and frequency and active nucleation site density are calculated by viewing more than 500 frames for each case. In order to achieve the highest possible resolution and to eliminate errors in calibration, the camera lens is fixed at a constant focal length, resulting in a fixed viewing area. Typically, a total of over 150 bubble diameter measurements are used to construct the present data. The bubble departure frequency is measured by counting the total number of bubbles that emerge from the targeted heating surface area during a period of a second.

2.9 Experimental Procedures

Before conducting the transient flow boiling experiment, the liquid FC-72 is degassed and then filled into the coolant receiver. Besides, the non-condensable gases in the coolant loop are evacuated. In each test, we first turn on the controller for

setting the required variable rotation rate of the AC motor to regulate the FC-72 flow rate to the preset mean level and the period and amplitude of the oscillation. Then the temperature and flow rate of the hot-water loop are selected so that the FC-72 temperature at the test section inlet can be maintained at a preset level. The imposed heat flux from the electric heater to the coolant in the test section is adjusted by varying the electric current delivered from the DC power supply. In addition, we can calculate the heat transfer rate to the coolant by measuring the DC voltage across the electric-heater and the current delivered to the electric-heater. Temperature and flow rate of the cold water in the cold-water loop can be adjusted to condense and subcool the liquid-vapor mixture of FC-72 from the test section. Next, we regulate the FC-72 pressure at the test section inlet by adjusting the gate valve locating right after the outlet of the test section. All measurements proceed when the experimental system has reached statistically stable state. Finally, the scanning rate for each data channel is 2 Hz and all the data channels are scanned for a period of 180 seconds.

2.10 Experimental Parameters

The ranges of the experimental parameters to be covered in the present study are listed in Table 2.1. Moreover, the thermodynamic and transport properties of the dielectric coolant FC-72 are given in Table 2.2 [37].

Table 2.1 Experimental parameters

Parameter	Range	Unit
Flow velocity (V)	16.7 ~ 30	cm/s
Mean mass flux ($\overline{G}$)	300 ~ 400	kg/m^2*s
Oscillation amplitude ($\zeta = \triangle G/\overline{G}$)	±5% ~ 10%	-
Oscillation period	10 ~ 30	sec
Subcooling temperature (ΔT_{sub})	0 ~ 10	^oC
Imposed heat flux (q")	0.1 ~ 10	W/cm^2
System pressure (P)	99.0	kPa

Table 2.2 Thermodynamic and transport properties of the dielectric coolant FC-72 [37]

Temperature T		Pressure P	Latent heat h_{fg}	Density ρ		Dynamic viscosity μ		Specific heat C_p		Conductivity K		Thermal expansion coefficient β	Surface tension σ	Thermal diffusion coefficient α		Prandtl No. Pr	
°C	K	Mpa	kJ/kg	kg/m³(l)	kg/m³(v)	mPa*s(l)	uPa*s(v)	J/kg*K(l)	J/kg*K(v)	mW/mK(l)	mW/mK(v)	1/K(l)	mN/m(l)	m²/s(l)	m³/s(v)	liquid	vapor
20	293.15	0.024	90.4	1687	3.43	0.69	10.76	1045	844	57.9	10.4	0.00157	10.9	3.29E-08	3.6	12.4	0.87
25	298.15	0.03	88.5	1674	4.28	0.64	10.94	1053	851	57.4	10.8	0.00159	10.47	3.26E-08	3	11.8	0.86
30	303.15	0.038	86.7	1660	5.27	0.6	11.11	1061	858	56.9	11.1	0.0016	10.04	3.23E-08	2.5	11.2	0.86
35	308.15	0.046	84.8	1647	6.44	0.56	11.29	1068	866	56.3	11.5	0.00161	9.62	3.20E-08	2.1	10.6	0.85
40	313.15	0.057	82.9	1634	7.78	0.53	11.47	1076	873	55.8	11.8	0.00162	9.2	3.17E-08	1.7	10.2	0.85
45	318.15	0.069	81.1	1621	9.31	0.5	11.64	1084	880	55.2	12.2	0.00164	8.78	3.14E-08	1.5	9.7	0.84
50	323.15	0.083	79.1	1607	11.06	0.47	11.82	1092	887	54.7	12.5	0.00165	8.36	3.12E-08	1.3	9.3	0.84
54.3	327.45	0.097	77.5	1596	12.75	0.44	11.97	1098	892	54.3	12.8	0.00166	8.01	3.09E-08	1.1	9	0.83
55	**328.15**	**0.099**	**77.2**	**1594**	**13.03**	**0.44**	**12**	**1099**	**893**	**54.2**	**12.9**	**0.00166**	**7.95**	**3.09E-08**	**1.1**	**9**	**0.83**
55.7	328.85	0.1013	76.9	1592	13.33	0.44	12.02	1101	894	54.1	12.9	0.00167	7.9	3.09E-08	1.1	8.9	0.83
60	333.15	0.117	75.2	1581	15.25	0.42	12.17	1107	900	53.6	13.2	0.00168	7.55	3.06E-08	1	8.6	0.83
70	343.15	0.16	71.1	1554	20.49	0.38	12.53	1123	913	52.5	13.9	0.00171	6.75	3.01E-08	0.7	8.1	0.82
80	353.15	0.213	66.7	1528	27	0.34	12.88	1138	926	51.5	14.6	0.00174	5.97	2.96E-08	0.6	7.6	0.82

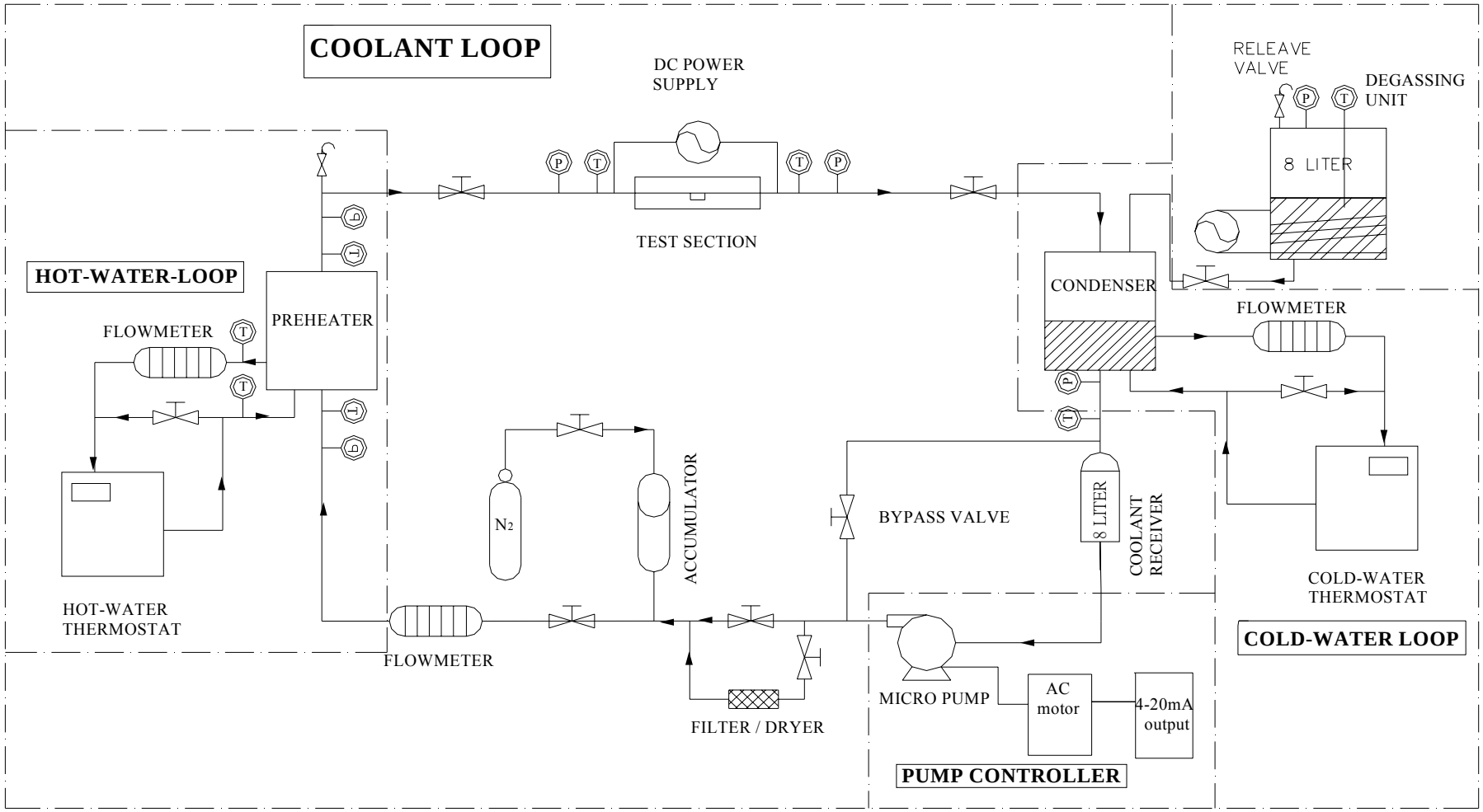

Fig. 2.1 Schematic diagram of experimental apparatus.

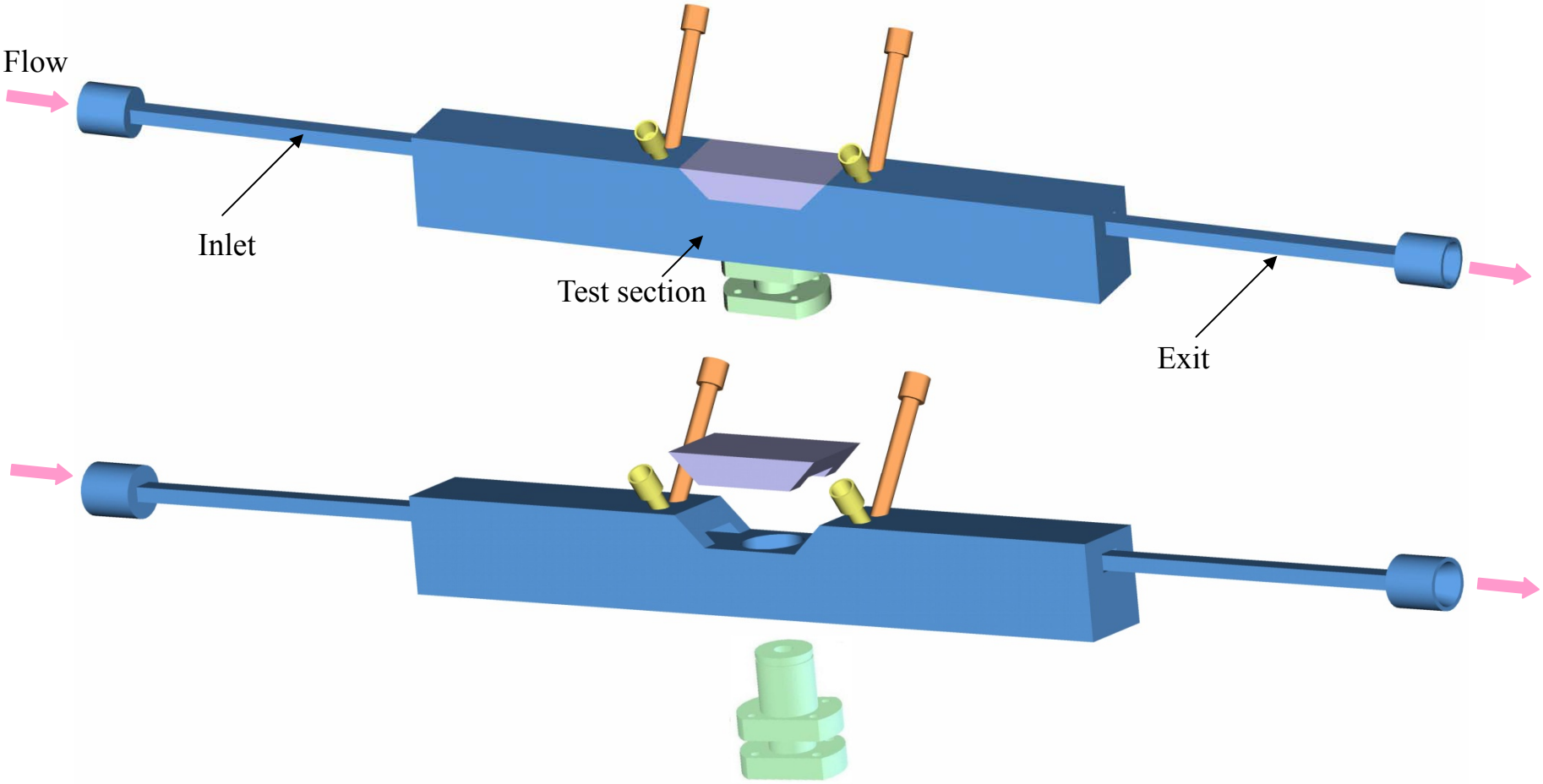

Fig. 2.2 Three-dimensional plots of test section along with inlet and outlet sections.

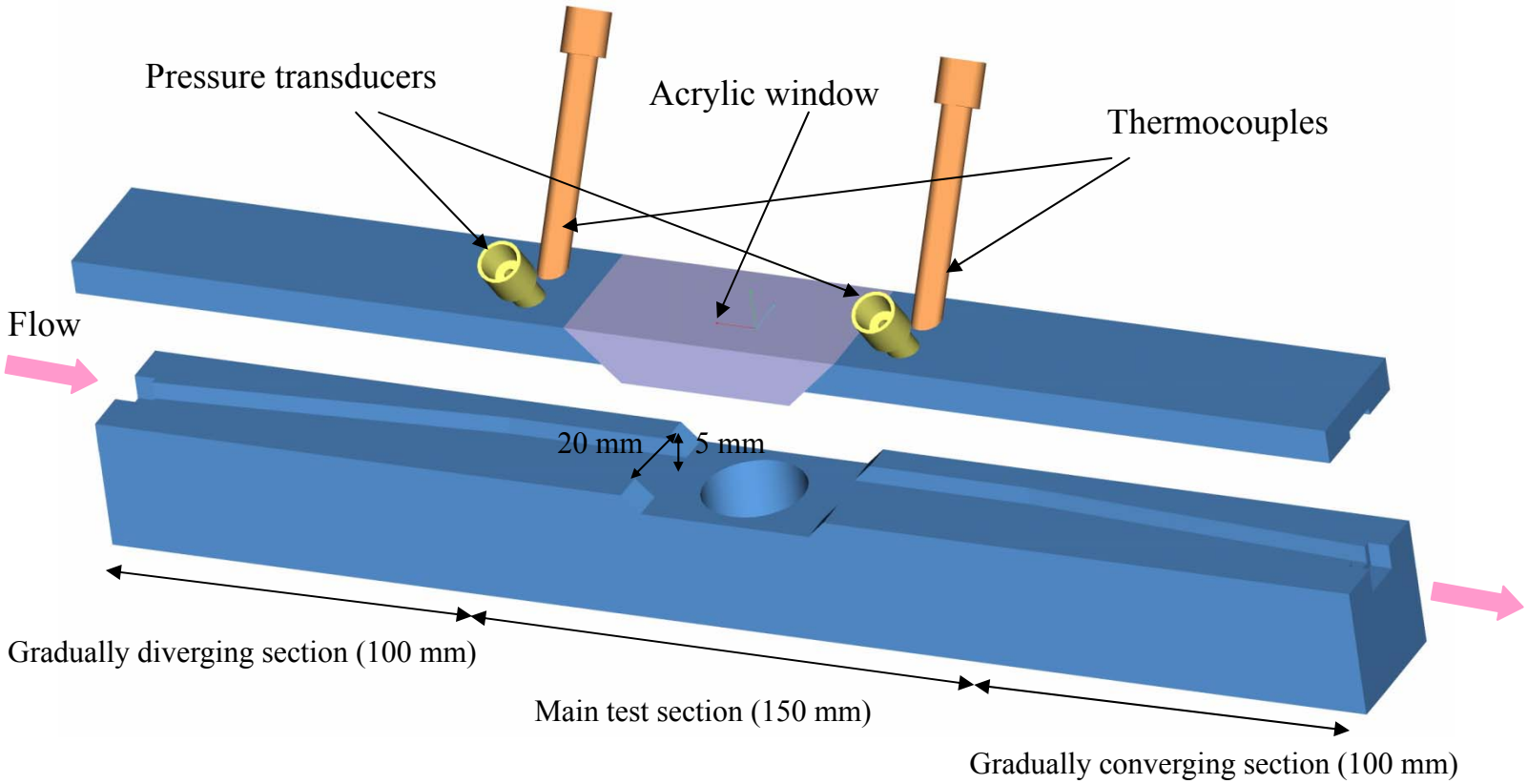

Fig. 2.3 Three-dimensional plots illustrating the test section in the rectangular flow-channel.

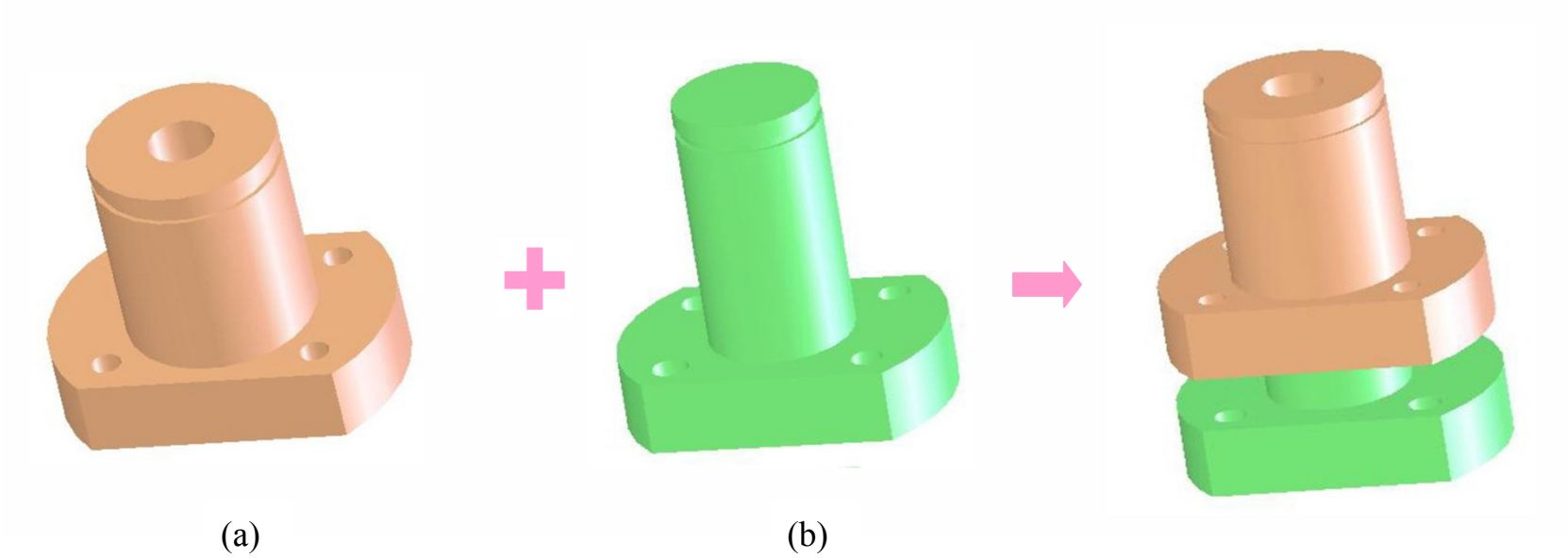

Fig. 2.4 Three-dimensional pictures showing (a) hollow cylindrical Teflon block and (b) cylindrical Teflon bolt.

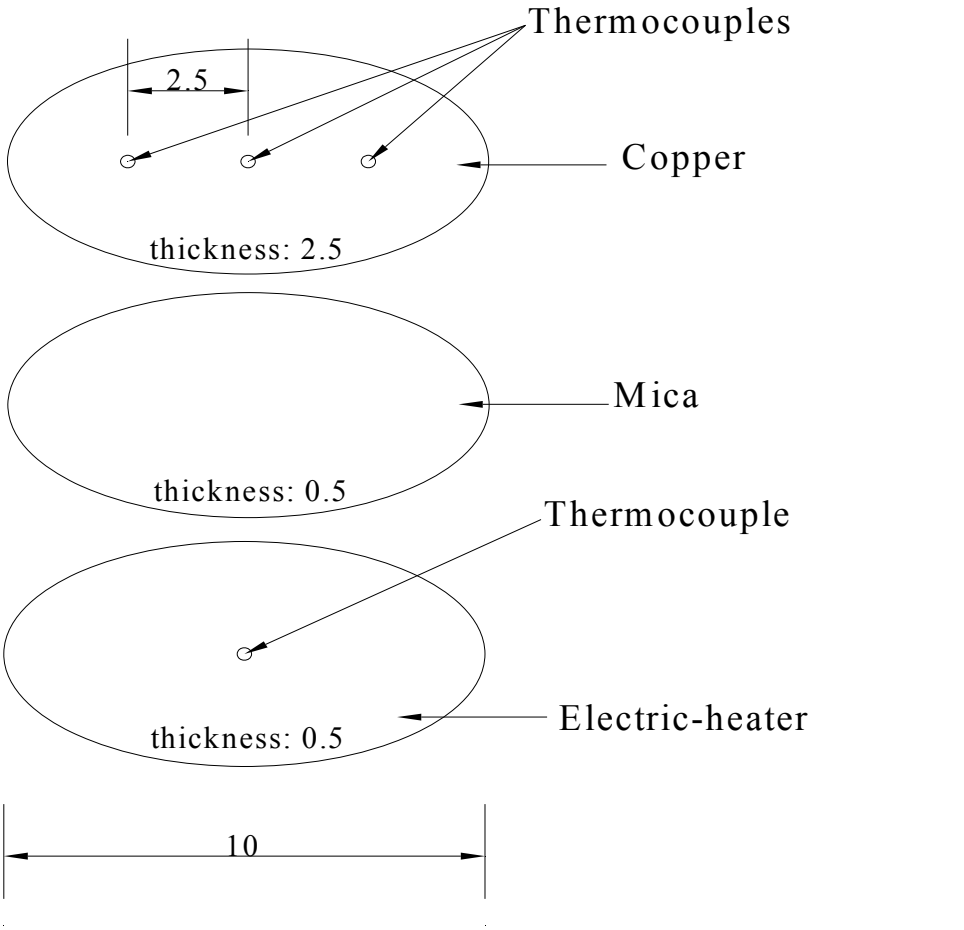

Fig. 2.5 Locations of thermocouples.

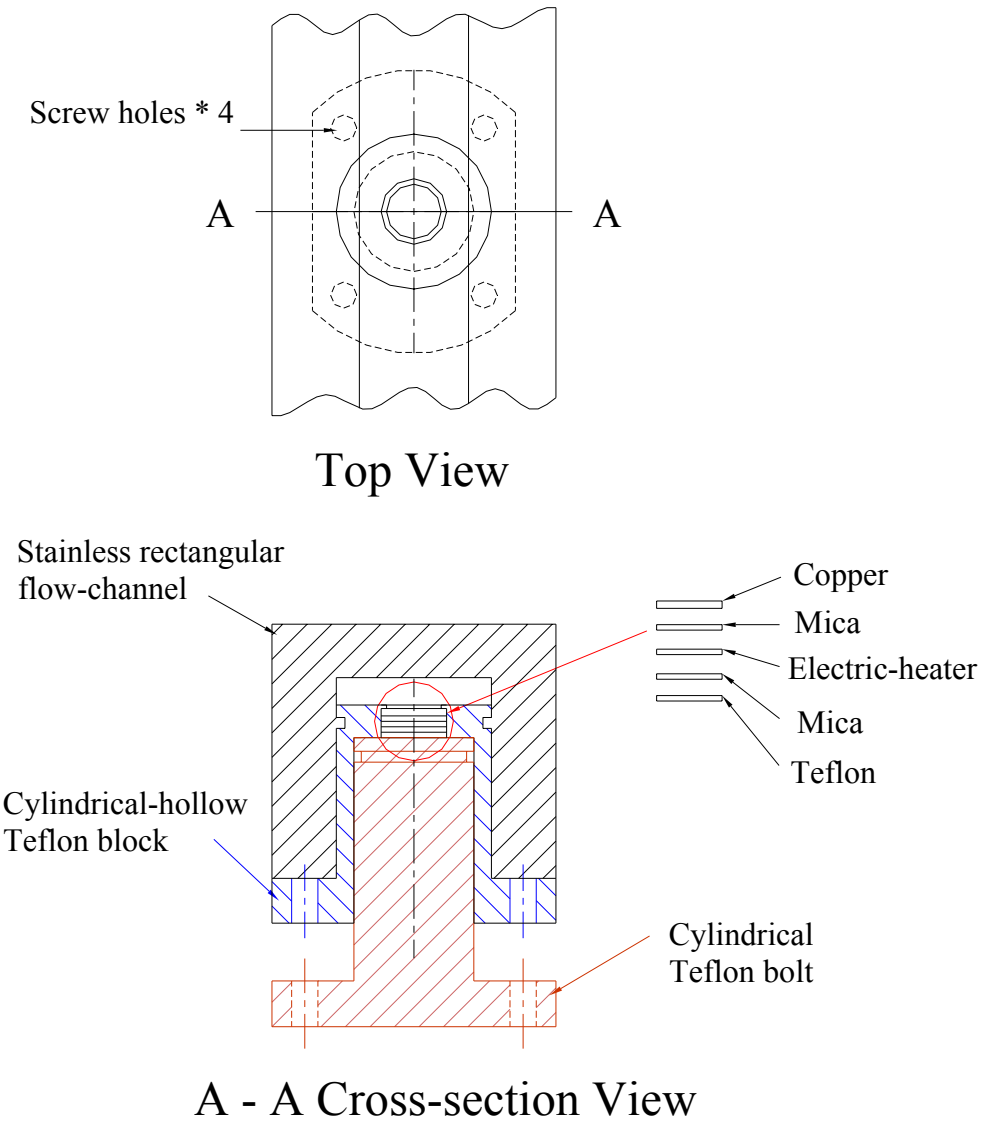

Fig. 2.6 Schematics of the copper plate module.

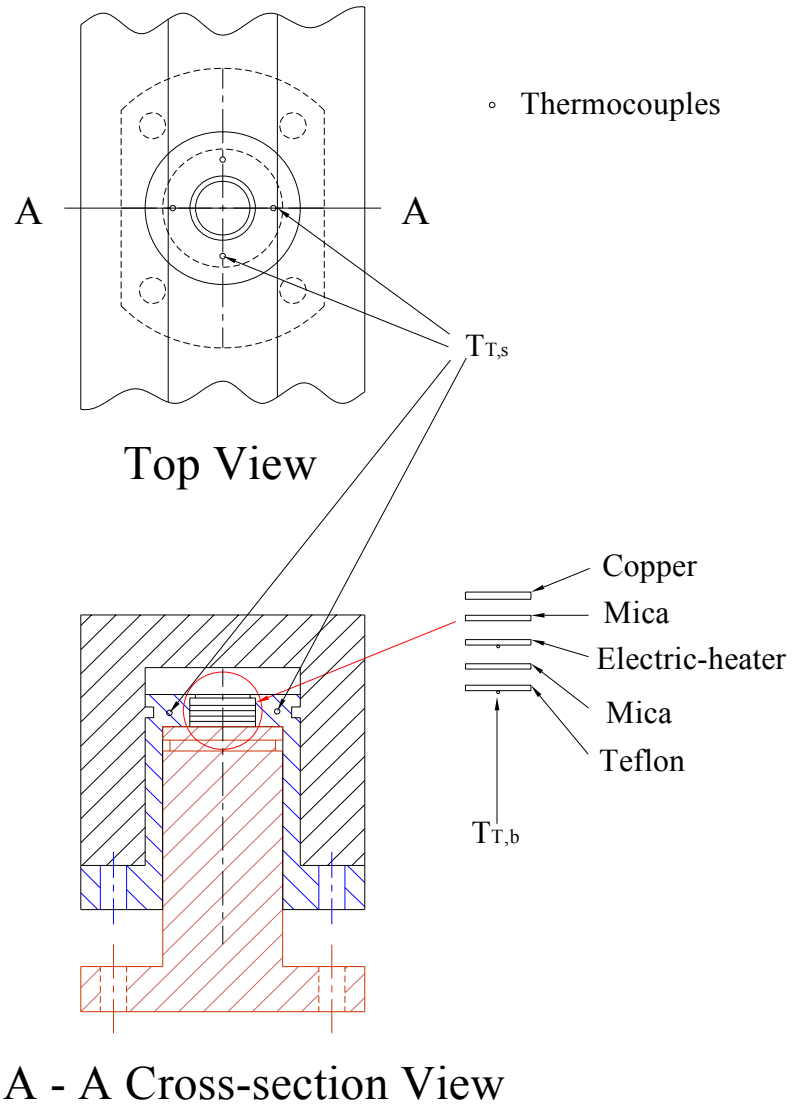

Fig. 2.7 Locations of the thermocouples inside the cylindrical-hollow Teflon block

Chapter 3

DATA REDUCTION

The single-phase liquid convection and two-phase flow boiling heat transfer coefficients of the coolant FC-72 flowing over the small heated plate on the bottom of a horizontal rectangular-channel will be deduced from the measured raw data. The data reduction procedures are described in the following.

3.1 Single-phase Heat Transfer

Before the two-phase experiments, the effective power input Q_e to the coolant flowing over the copper plate is evaluated from the difference between the total power input Q_t to the copper plate and the total heat loss of the test section Q_{loss}. The total power input can be calculated from the measured voltage drop across the electric-heater and the electric current passing through it.

The total power input Q_t and the effective power input Q_e are hence evaluated respectively from the equations:

$$Q_t = V \cdot I \tag{3.1}$$

Where V and I are individually the voltage drop across and current through the electric-heater, and

$$Q_e = Q_t - Q_{loss} \tag{3.2}$$

Here the total heat loss from the copper plate is approximately estimated from the relation

$$Q_{loss} = \frac{2\pi L k_T (T_w - T_{T,s})}{\ln(r_{T,s}/r_w)} + \frac{(T_e - T_{T,b})}{\frac{L_{T,b}}{k_T A_{T,b}} + \frac{L_M}{k_M A_M}} \tag{3.3}$$

Where k_T and k_M are the thermal conductivities of the Teflon and the mica, respectively; $A_{T,b}$ and A_M are respectively the bottom area of the Teflon block and the bottom area of the mica plate; L, $L_{T,b}$ and L_M are individually total thickness of the plates, the thickness of the Teflon plate, and the thickness of the mica; T_w and T_e are respectively the average temperature of the copper plate and the temperature at

the electric-heater, T_T is the temperature of the Teflon block, as schematically shown in Fig. 2.7.

The imposed heat flux at the copper plate surface is defined as

$$q = Q_e / A_{cp} \tag{3.4}$$

where A_{cp} is the surface area of the copper plate. The relative heat loss from the test section is defined as

$$\varepsilon = \frac{Q_{loss}}{Q_t} \times 100\% \tag{3.5}$$

The results from this estimation show that the relative heat losses for all cases investigated here are about 20% at q=10 W/cm^2. The average single-phase liquid convection heat transfer coefficient over the copper plate is defined as

$$h_{1\phi} = \frac{Q_e}{A_{cp} \cdot (T_c - T_{in})} \tag{3.6}$$

where Q_e is the effective power input to the FC-72, T_{in} is the coolant temperature at the inlet of the test section, and T_c is the average temperature of the upper surface of the copper plate.

3.2 Two-phase Flow Boiling Heat Transfer

In the subcooled flow boiling experiment the state of coolant FC-72 at the inlet of the rectangular flow-channel is evaluated from the energy balance for the pre-heater. The total heat transfer rate in the pre-heater is calculated from the temperature drop on the water side as

$$Q_{w,p} = \dot{m}_{w,p} \cdot c_{p,w} \cdot (T_{w,p,i} - T_{w,p,o}) \tag{3.7}$$

where $\dot{m}_{w,p}$ is the mass flow rate of the hot water in the pre-heater, $c_{p,w}$ is the specific heat of water, and $T_{w,p,i}$ and $T_{w,p,o}$ are respectively the temperatures of the water at the pre-heater inlet and outlet. Note that in the pre-heater the coolant FC-72 is still in liquid state. Hence on the coolant side in the pre-heater

$$Q_{w,p} = \dot{m}_r \cdot c_{p,r} \cdot (T_{r,p,o} - T_{r,p,i}) \tag{3.8}$$

where $\dot{m}_r$ is the mass flow rate of the coolant in the pre-heater, $c_{p,r}$ is the specific heat of coolant, and $T_{r,p,o}$ and $T_{r,p,i}$ are the temperatures of the coolant at the pre-heater outlet and inlet, respectively. Combining the above two equations allows us to

calculate $T_{r,p,o}$, which is considered as the temperature of FC-72 at the test section inlet. On the other hand, the average two-phase heat transfer coefficient for the coolant flow over the copper plate is defined as

$$h_{2\phi,sat} = \frac{Q_n}{A_{cp} \cdot (T_c - T_{sat})} \quad \text{for saturated flow boiling,} \tag{3.9}$$

and

$$h_{2\phi,sub} = \frac{Q_n}{A_{cp} \cdot (T_c - T_{r,bulk})} \quad \text{for subcooled flow boiling} \tag{3.10}$$

where T_{sat} is the saturated of the coolant FC-72 and $T_{r,bulk}$ is the bulk liquid temperature which is defined as

$$T_{r,bulk} = \frac{T_{r,i} + T_{r,o}}{2} \tag{3.11}$$

3.3 Uncertainty Analysis

Uncertainties of the single-phase liquid convection and flow boiling heat transfer coefficients and other parameters are estimated by the procedures proposed by Kline and McClintock [38]. The detailed results from this uncertainty analysis are summarized in Table 3.1.

Table 3.1 Summary of the uncertainty analysis

Parameter	**Uncertainty**
Rectangular channel geometry	
Length, width and thickness (%)	±0.5%
Area (%)	±1.0%
Parameter measurement	
Temperature, T (℃)	±0.2
Temperature difference, ΔT (℃)	±0.3
System pressure, P (kPa)	±2
Average mass flux of coolant, $\overline{G}$ (%)	±3
Amplitude of mass flux oscillation (%)	±4.8
Period of mass flux oscillation (sec)	±0.25
Single-phase heat transfer in rectangular channel	
Imposed heat flux, q (%)	±4.2
Heat transfer coefficient, $h_{1\phi}$ (%)	±12.3
Two-phase heat transfer in Rectangular channel	
Imposed heat flux, q (%)	±4.2
Heat transfer coefficient, $h_{2\phi}$ (%)	±12.3

CHAPTER 4

TRANSIENT SATURATED FLOW BOILING OF FC-72 OVER A SMALL HEATED COPPER PLATE

The results obtained in the first part of the study are presented in this chapter to illustrate how the FC-72 mass flux oscillation affects the transient saturated flow boiling heat transfer of FC-72 over a small heated circular copper flat plate flush mounted on the bottom of a horizontal rectangular channel. The present experiments are carried out for the mean FC-72 mass flux fixed at 300 and 400 kg/m^2s for the imposed heat flux varying from 0.1 W/cm^2 to 10 W/cm^2. Besides, the amplitude of the coolant mass flux oscillation is set at 0%, 5% and 10% of the mean coolant mass flux. Moreover, the period of the mass flux oscillation is fixed at 10, 20 and 30 seconds. The coolant in the test section is at slightly subatmospheric pressure of 99 kPa with T_{sat} = 55^{o}C for FC-72. In the following, the effects of the mean level, oscillation amplitude and period of the coolant mass flux, and the imposed heat flux on the transient FC-72 saturated flow boiling heat transfer performance are examined in detail. Note that for the limiting case of 0% mass flux oscillation for a given coolant mass flux we have saturated boiling of FC-72 at a coolant mass flux rate in the test section, which is designated as stable flow boiling. The heat transfer performance is presented mainly in terms of the transient variations of the average surface temperature of the copper plate and the boiling heat transfer coefficient.

4.1 Single-phase Liquid Convective Heat Transfer

Before beginning the two-phase flow boiling experiments, steady single-phase convective heat transfer experiments are conducted for liquid FC-72 flow in the

rectangular channel. The measured average heat transfer coefficients for single-phase convection from the heated copper surface to the coolant are compared with the correlation proposed by Gersey and Mudawar [8]. The correlation of Gersey and Mudawar [8] is

$$\overline{Nu}_L = 0.362 \cdot Re_L^{0.614} \cdot Pr^{1/3} \tag{4.1}$$

where

$$Re_L = \frac{G \cdot L}{\mu_l} \tag{4.2}$$

$$\bar{h}_{1\phi} = \frac{k_l}{L} \cdot \overline{Nu}_L \tag{4.3}$$

for the flow velocity ranging from 13 cm/s to 400 cm/s. Their correlation is based on the experimental data procured from the same liquid and same flow configuration as the present data and the comparison is shown in Fig. 4.1 for the dimensional and dimensionless heat transfer coefficients. The results indicate that our data are in good agreements with their correlation.

It should be mentioned that all of the working fluid properties used in reducing the data for Fig. 4.1 from Equations 4.1 - 4.3 are calculated at the coolant inlet temperature. The copper plate diameter is chosen as the characteristic length in defining the Reynolds number Re_L and average Nusselt number $\overline{Nu}_L$ because of its significant effect on the heat transfer performance [8].

4.2 Stable and Time-average Saturated Flow Boiling Curves and Heat Transfer Coefficient

To illustrate the effects of the mass flux oscillation on the boiling characteristics, data for the FC-72 saturated flow boiling for a constant coolant mass flux are first compared with the time-average data for a transient oscillatory coolant mass flux. The

results from this comparison are shown in Figures 4.2 and 4.3 by presenting the boiling curves for various mean mass fluxes and amplitudes and periods of the mass flux oscillation. Note that for each boiling curve at a given G the mean temperature of the copper plate increases gradually with the imposed heat flux at a low q from the saturated temperature of the coolant to a certain value just slightly higher than T_{sat} and no bubble nucleation is observed. The heat transfer in this region is completely due to the single-phase forced convection. With the continuing increase in the surface heat flux, bubbles begin to appear on the surface and the boiling curve is characterized by a sharp increase in the surface heat flux for a small rise in the temperature of copper surface. We have onset of nucleate boiling (ONB) in the flow. The reason causing the sharp increase in the slope of the boiling curve is due to a significant increase in the surface heat transfer by the boiling processes when ONB occurs. For the cases with oscillating coolant mass fluxes the ONB locations marked in these plots are the time-average values. Note that beyond ONB the coolant mass flux has slight effects on the boiling curves, suggesting that the surface heat transfer is mainly dominated by the fully developed nucleate boiling. Besides, at a higher G the required heat flux for ONB is higher and this implies that more energy is needed for the vapor to nucleate from the wall since the residence time of the coolant on the heated surface is shorter. It can be concluded from the results in Figures 4.2 and 4.3 that the time-average boiling curves are not affected by the amplitude and period of the coolant mass flux oscillation to a significant degree.

We move further to explore how the stable and transient time-average saturated flow boiling heat transfer coefficients $h_{2\phi,sat}$ are affected by the FC-72 coolant mass flux oscillation. The results for the variations of the time-average $h_{2\phi,sat}$ with the surface heat flux presented in Figures 4.4 and 4.5 reveal that the coolant mass flux

oscillation amplitude and period show negligible influences on the time-average flow boiling heat transfer coefficients. However, for a given coolant mass flux the boiling heat transfer coefficient increases substantially with the imposed heat flux. For example, at T_{sat} =55°C and $\bar{G}$ =400 kg/m^{2}s, the saturated boiling heat transfer coefficient for q =9.7 W/cm^2 is about 102% higher than that for q =3.2 W/cm^2 (Figure 4.4(a)).

4.3 Transient Flow Boiling Heat Transfer Characteristics

The transient boiling heat transfer characteristics for FC-72 flow over the heated copper plate resulting from the temporal coolant mass flux oscillation are illustrated by presenting the time variations of the space-average heated surface temperature T_w and heat transfer coefficient $h_{2\phi}$ for various imposed heat fluxes and mass fluxes. For comparison purpose the results for T_w for the limiting cases of constant coolant mass fluxes are shown in Figure 4.6. These data indicate that the fluctuations of the average heated surface temperature with time for various q and G are relatively small. The boiling can be regarded as at a statistically stable state.

Now when the coolant mass flux oscillates periodically in time in a form of nearly a triangular wave, significant temporal oscillations in the space average heated surface temperature occur for the imposed heat flux slightly higher than that for the time average ONB, as evident from the data shown in Figures 4.7 – 4.18 for the oscillation amplitude being 5% and 10% of the mean mass flux. Note that the temporal oscillation of the heated surface temperature is also periodic in time and is at the same frequency as the mass flux. Besides, the T_w oscillation gets stronger for higher imposed heat flux and higher amplitude of the mass flux oscillation. However, the period of the mass flux oscillation only slightly affects the T_w oscillation. It is of

interest to note that at a higher amplitude of the mass flux oscillation with $\triangle G$ being 10% of $\overline{G}$, even in the single-phase forced convection the space average heated surface temperature also oscillates noticeably with time at a relatively low imposed heat flux with $q < \overline{q}_{ONB}$ (Figures 4.13 – 4.18). Here $\overline{q}_{ONB}$ is the time-average heat flux for ONB for the cases with the oscillating mass flux. But for the imposed heat flux around $\overline{q}_{ONB}$ the T_w oscillation is small for most cases except for $\overline{G}$ =300 kg/m^{2}s with an intermediate period of the G oscillation at 20 seconds (Figure 4.15). A close inspection of the data given in Figures 4.7 – 4.18 further reveals that the T_w oscillation slightly lags the mass flux oscillation. Moreover for q substantially above $\overline{q}_{ONB}$ and in the period of time at which the instantaneous mass flux is higher than the average level, the space average heated surface temperature is higher than the corresponding time-average level, suggesting that the flow boiling heat transfer over the heated surface is poorer at a higher instantaneous G. But in the single-phase region the opposite is the case (Figures 4.13 - 4.15 and 4.17 – 4.18). The trend for the single-phase flow is apparently due to the better convection heat transfer for a higher mass flux. This somewhat unusual trend for the boiling flow requires more investigation into the bubble characteristics which will be examined later.

The corresponding time variations of the space-average flow boiling heat transfer coefficient affected by the coolant mass flux oscillation are shown in Figures 4.19 – 4.30. The results manifest that the flow boiling heat transfer coefficients also oscillate periodically in time and at the same frequency as the G oscillation. At a higher imposed heat flux and for the larger amplitude in the mass flux oscillation, the boiling heat transfer coefficients oscillate stronger. Besides in the period of time at which the mass flux is higher than the mean level, the space average boiling heat transfer coefficient is below the corresponding time-average level. Moreover, the oscillation in

$h_{2\phi}$ also lags slightly behind the mass flux oscillation.

In this transient oscillatory boiling flow the time variation of the coolant pressure at the inlet of the test section is also of interest in thermal-fluid design. These data are shown in Figures 4.31 – 4.42 for various cases. The results indicate that the inlet coolant pressure oscillates nearly in phase with the mass flux oscillation. Note that the inlet coolant pressure oscillation becomes somewhat irregular for the larger amplitude of the mass flux oscillation and a higher average mass flux (Figures 4.36, 4.38, 4.40 and 4.42). Finally, the quantitative data evaluated from the above results are summarized in Table 4.1 for the relative oscillation amplitudes of the space average heated surface temperature and boiling heat transfer coefficient $A_{T_w}/\Delta\bar{T}_{sat}$ and $A_{h2\varphi}/\bar{h}_{2\varphi}$ at various imposed heat fluxes and the amplitude and period of the coolant mass flux oscillation.

4.4 Transient Bubble Characteristics in Saturated Flow Boiling

To elucidate the transient saturated flow boiling heat transfer characteristics, the data for the bubble characteristics of FC-72 obtained from the present flow visualization are examined in the following. The top views of the boiling flow in a small region around the geometric center of the heated surface for various coolant mass fluxes and imposed heat fluxes are shown in Figs. 4.43 - 4.67 for the transient saturated flow boiling. At first, the bubble characteristics for the limiting cases of constant mass fluxes are illustrated by the photos in Figure 4.43. It is noted in the flow visualization and the results in Figure 4.43 that the vapor bubbles begin to appear as the heated surface temperature exceeds the boiling incipient superheat. In the beginning, tiny bubbles are observed in the active nucleation sites. The bubbles grow and then detach from the heated surface with certain mean bubble departure diameters.

As the imposed heat flux increases, more bubbles are generated on more active nucleation sites and more bubbles detach from the heated surface. Besides, the detached bubbles tend to merge into larger bubbles. Note that the large bubbles become distorted and elongated as they slide on the heating surface. Moreover, at a higher mass flux the bubbles are smaller and the bubble coalescence is less significant.

Next, the bubble characteristics in the transient flow boiling are illustrated by presenting the photos of the boiling flow at eight selected time instants in a typical periodic cycle in Figures 4.44 – 4.67. In these figures the symbol " $t=t_o$ " signifies the time instant at which the instantaneous mass flux is at the mean level and starts to increase with time. The results indicate that for a given imposed heat flux and fixed mean level, amplitude and period of the mass flux oscillation the bubbles get smaller and become more dispersed in the period the instantaneous mass flux increases. The opposite processes take place when the instantaneous mass flux decreases with time. These changes of the bubble characteristics with the instantaneous mass flux become more significant for an increase in the amplitude of the mass flux oscillation (Figures 4.44 and 4.56 and Figures 4.46 and 4.58). It is of interest to note that the mean level of the mass flux oscillation exhibits significant influences on the bubble characteristics in the transient flow boiling, as evident from comparing the results in Figures 4.44 and 4.46. Besides, the bubble characteristics are only affected slightly by the period of the mass flux oscillation for the small mass flux oscillation amplitude of 5%. But for the large amplitude of the mass flux oscillation of 10% the bubbles are larger for the cases with longer period of the mass flux oscillation (Figures 4.56 and 4.60).

To quantify the bubble characteristics, the measured data for the time variations of the space-average bubble departure diameter and frequency and active nucleation

site density in a typical periodic cycle are given in Figs. 4.68 – 4.94 for various mean coolant mass fluxes, amplitudes and periods of the coolant mass flux oscillations, and imposed heat fluxes.

The results in Fig. 4.68(a) indicate that the mean size of the bubbles departing from the copper plate is somewhat smaller for the mass flux raised from 300 to 400 kg/m^2s in the stable flow boiling. It reflects the fact that the coolant at a higher mass flux and hence at a higher speed tends to sweep the bubbles more quickly away from the heating surface. Now as the coolant mass flux oscillates, the bubble departure diameter varies significantly with time (Figures 4.68(b) - (c)). More specifically, the size of the departing bubbles decreases in the first and fourth quarters of the periodic cycle in which the instantaneous mass flux increases with time. While in the second and third quarters of the cycle an opposite process is noted since the instantaneous mass flux decreases with time. Besides, at a higher imposed heat flux the departing bubbles are larger. Similar trend is noted in Figures 4.69 – 4.71. Comparing the results in Figure 4.68 with Figure 4.69 and Figure 4.70 with Figure 4.71 indicates that at the larger amplitude of the mass flux oscillation the effects of the imposed heat flux on the bubble departure diameter are somewhat smaller. The results in Figures 4.72 – 4.75 indicate that the bubble departure diameters are only affected slightly by the period of the mass flux oscillation.

Next, the data for the variations of the space-average bubble departure frequency with time for various cases are shown in Figures 4.77 – 4.80. In the stable flow boiling the increase in the bubble departure frequency with the imposed heat flux and coolant mass flux is clearly seen. The increase of f with G is ascribed again to the higher drag on the bubbles still attaching to the heated surface by the liquid coolant moving at a higher speed for a higher G. This, in turn, causes an earlier departure of the bubbles from the surface, resulting in a higher departure frequency. For an

oscillation mass flux the bubbles depart from the heated surface at an increasing rate in the first and fourth quarters of the periodic cycle in which the coolant mass flux rises with time. Apparently, in the second and third quarters of the cycle in which G decreases the bubble departing rate reduces. It should be pointed out that the time variations of the bubble departure frequency are somewhat milder when compared with the bubble departure diameter. Figures 4.81 – 4.84 indicate that the bubble departure frequencies are only affected slightly by the period of the mass flux oscillation. The results shown in Figure 4.85 manifest that the mean level of the mass flux oscillation noticeably affects the bubble departure frequency.

Finally, the space-average active nucleation site density on the heated surface affected by the coolant mass flux oscillation is illustrated in Figures 4.86 – 4.89. The results in Figure 4.86(a) indicate that in stable flow boiling the active nucleation site density increases substantially with the imposed heat flux. But the increase is rather mild for the mass flux raised from 300 to 400 kg/m^{2}s. Note that in transient flow boiling the active nucleation site density decreases with time in the first and fourth quarters of the periodic cycle in which G increases. The reverse process appears in the second and third quarters of the cycle in which the coolant flow slows down. At the higher amplitude of the mass flux oscillation and at higher imposed heat flux the temporal variations of N_{ac} is stronger (Figures 4.88 and 4.89). The effects of the period of the mass flux oscillation on the time variations of N_{ac} are rather weak (Figures 4.90 – 4.93). The amplitude of the N_{ac} oscillation is slighter higher for a larger amplitude of the mass flux oscillation (Figure 4.94).

4.5 Correlation Equations

According to the present experimental data, empirical correlations for the space-average bubble departure diameters in FC-72 stable and transient saturated flow boiling on the heated circular copper flat plate flush mounted on the bottom of the

rectangular channel estimated from the present flow visualization are proposed as

$$\frac{d_p}{\sqrt{\sigma/g\cdot\Delta\rho}} = \frac{0.2\cdot(\rho_l/\rho_v)^{0.48}\cdot\overline{Bo}^{0.21}}{\overline{Re_D}^{0.08}} \quad \text{for stable flow boiling} \tag{4.4}$$

where $\overline{Re_D}$ and $\overline{Bo}$ are the mean Reynolds and Boiling numbers respectively. They are defined as

$$\overline{Re_D} = \frac{\bar{G}\cdot D}{\mu_l} \tag{4.5}$$

$$\overline{Bo} = \frac{q''}{\bar{G}\cdot i_{lv}} \tag{4.6}$$

and

$$\frac{d_p}{\sqrt{\sigma/g\cdot\Delta\rho}} = \frac{0.2\cdot(\rho_l/\rho_v)^{0.48}\cdot Bo^{0.22}}{Re_D^{0.08}} \quad \text{for transient flow boiling} \tag{4.7}$$

where Re_D and Bo are respectively the instantaneous Reynolds and Boiling numbers. They are defined as

$$Re_D = \frac{G\cdot D}{\mu_l} \tag{4.8}$$

$$Bo = \frac{q''}{G\cdot i_{lv}} \tag{4.9}$$

where $G(=\bar{G}+\Delta G)$ is the instantaneous coolant mass flux, $\bar{G}$ is the average coolant mass flux, ΔG is the amplitude of the mass flux oscillation, ρ_l is the liquid density, and D is the copper plate diameter. Figures 4.95 and 4.96 show that the present experimental data fall within ± 20 % of the correlations given in Equations (4.4) and (4.7). In addition, empirical equations are provided to correlate the data for the space-average bubble departure frequency as

$$\frac{f\cdot d_p}{\mu_l/\rho_l\cdot D_h} = 0.5\overline{Re_D}^{1.3}\cdot Pr^{0.7}\cdot\overline{Bo}^{0.66} \quad \text{for stable flow boiling} \tag{4.10}$$

and

$$\frac{f\cdot d_p}{\mu_l/\rho_l\cdot D_h} = 0.5Re_D^{1.3}\cdot Pr^{0.7}\cdot Bo^{0.7} \quad \text{for transient flow boiling} \tag{4.11}$$

Figures 4.97 and 4.98 reveal that the present experimental data for $f\cdot d_p$ can be correlated with the deviation less than ± 20 % and ± 25 % by the above two equations. Moreover, empirical correlations for the space-average active nucleation site density in the FC-72 saturated flow boiling deduced from the present flow visualization are proposed as

$$N_{ac} \cdot d_p^{\,2} = -0.065+(85 \cdot \overline{Bo}^{0.83} \cdot \overline{Re_D}^{-0.15}) \quad \text{for stable flow boiling} \tag{4.12}$$

and

$$N_{ac} \cdot d_p^{\,2} = -0.03+(45 \cdot Bo^{0.85} \cdot Re_D^{-0.13}) \quad \text{for transient flow boiling} \tag{4.13}$$

The comparison in Figs. 4.99 and 4.100 shows that more than 85 % of the present experimental data fall within ± 30 % and ± 40 % of the correlation given in Equations (4.12) and (4.13). Finally, the total heat flux input to the stable boiling flow q_t is considered to be roughly composed of two parts: one resulting from the bubble nucleation q_b and another due to the single phase forced convection q_c. Thus

$$q_t = q_b + q_c \tag{4.14}$$

Here q_b and q_c can be individually calculated from the quantitative data for the bubble characteristics examined in section 5.3 and single phase liquid forced convection as

$$q_b = \rho_v \cdot V_v \cdot f \cdot N_{ac} \cdot i_{lv} \tag{4.15}$$

where ρ_v is the vapor density, V_v is the vapor volume of the mean departing bubble defined as $\frac{4\pi}{3}(\frac{d_p}{2})^3$, f is the space-average bubble departure frequency, N_{ac} is the space-average active nucleation site density, i_{lv} is the enthalpy of vaporization, and

$$q_c = E \cdot \bar{h}_{1\phi} \cdot \Delta T_{sat} \tag{4.16}$$

where E is an enhancement factor added to account for the agitating motion of the bubbles which can enhance the single phase liquid convection heat transfer. From the experimental data, E can be empirically correlated as

$$E = 4.5 \cdot N_{conf}^{\,0.5} \cdot \overline{Fr_l}^{0.15} \cdot (1+280 \cdot \overline{Bo})^{1.8} \quad \text{for stable flow boiling} \tag{4.17}$$

Here $\overline{Fr_l}$ is the Froude number and N_{conf} is the Confinement number. They are respectively defined as

$$N_{conf} = \frac{(\sigma/g \cdot \Delta\rho)^{0.5}}{D_h} \tag{4.18}$$

and

$$\overline{Fr_l} = \frac{\bar{G}^2}{\rho_l^2 \cdot g \cdot D_h} \tag{4.19}$$

where g is the acceleration due to gravity, D_h is the hydraulic diameter of the test section, and ΔT_{sat} (= T_w - T_{sat}) is the wall superheat. The results shown in Figure 4.101 indicate that the present data can be correlated with the deviation less than ± 25% by the empirical correlation given in Equations (4.14) - (4.19).

Table 4.1 Relative amplitudes of heated surface temperature and heat transfer coefficient oscillations in transient oscillatory saturated flow boiling for various imposed heat fluxes and the amplitudes and periods of the coolant mass flux oscillation.

$\Delta G/\bar{G}$	t_p (sec)	$\bar{G}$ =300 kg/m^{2}s			$\bar{G}$ =400 kg/m^{2}s		
		q(W/cm^2)	$A_{T_w}/\Delta\bar{T}_{sat}$	$A_{h_{2\varphi}}/\bar{h}_{2\varphi}$	q(W/cm^2)	$A_{T_w}/\Delta\bar{T}_{sat}$	$A_{h_{2\varphi}}/\bar{h}_{2\varphi}$
±5%	10	5.05	0.0097	0.0098	5.05	0.0099	0.0099
		6.23	0.0078	0.0078	6.24	0.0105	0.0105
		8.25	0.0095	0.0094	8.26	0.0096	0.0095
		9.74	0.0089	0.0088	9.74	0.0101	0.0100
	20	4.99	0.0098	0.0110	5.04	0.0179	0.0180
		6.18	0.0104	0.0128	6.18	0.0219	0.0221
		8.24	0.0083	0.0094	8.23	0.0153	0.0153
		9.75	0.0088	0.0087	9.76	0.0156	0.0156
	30	4.95	0.0084	0.0084	5.01	0.0182	0.0183
		6.15	0.0116	0.0116	6.16	0.0184	0.0184
		8.21	0.0094	0.0094	8.20	0.0141	0.0141
		9.70	0.0077	0.0077	9.72	0.0143	0.0144
±10%	10	5.04	0.0082	0.0082	5.03	0.0136	0.0136
		6.15	0.0153	0.0153	6.19	0.0178	0.0177
		8.17	0.0149	0.0149	8.20	0.0185	0.0185
		9.68	0.0151	0.0151	9.70	0.0185	0.0185
	20	4.95	0.0135	0.0135	4.99	0.0285	0.0285
		6.17	0.0177	0.0177	6.19	0.0280	0.0280
		8.21	0.0173	0.0173	8.22	0.0267	0.0267
		9.71	0.0185	0.0185	9.76	0.0230	0.0231
	30	4.94	0.0187	0.0188	5.02	0.0227	0.0227
		6.11	0.0189	0.0188	6.16	0.0226	0.0228
		8.18	0.0184	0.0184	8.20	0.0254	0.0256
		9.69	0.0184	0.0184	9.73	0.0252	0.0253

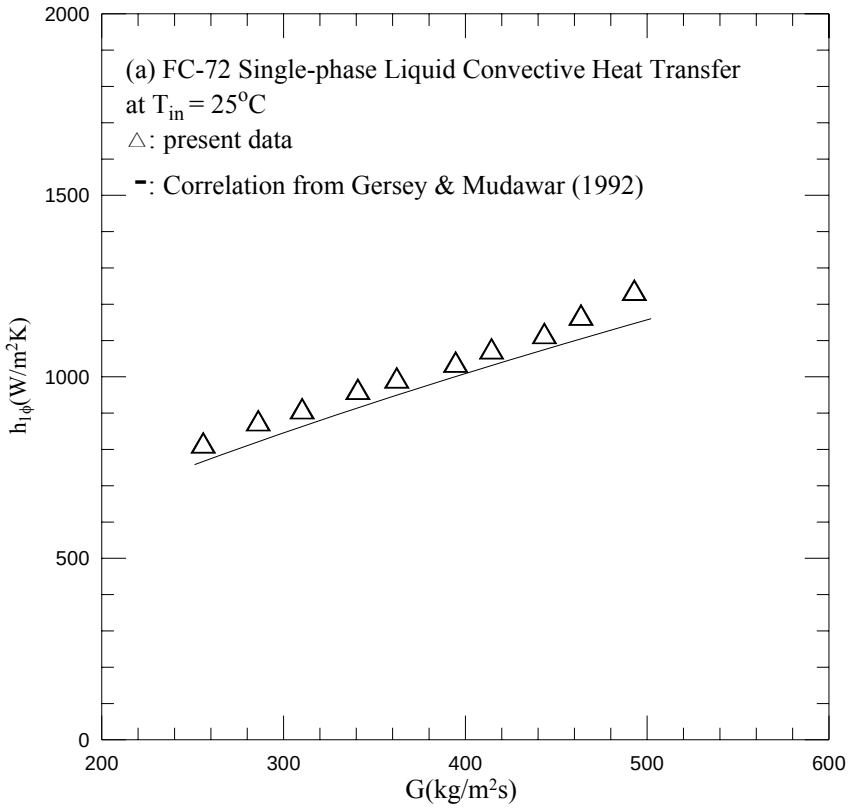

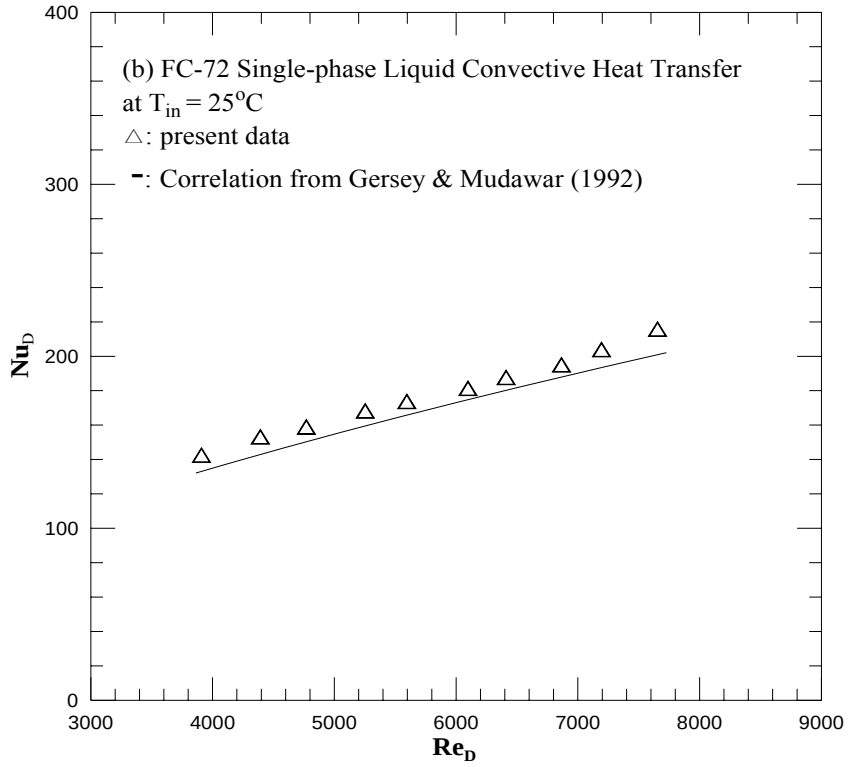

Fig. 4.1 Comparison of the present steady single-phase liquid convection heat transfer data with the correlation of Gersey and Mudawar (1992) for (a) $h_{1\phi}$ vs. G an (b) Nu_L vs. Re_L.

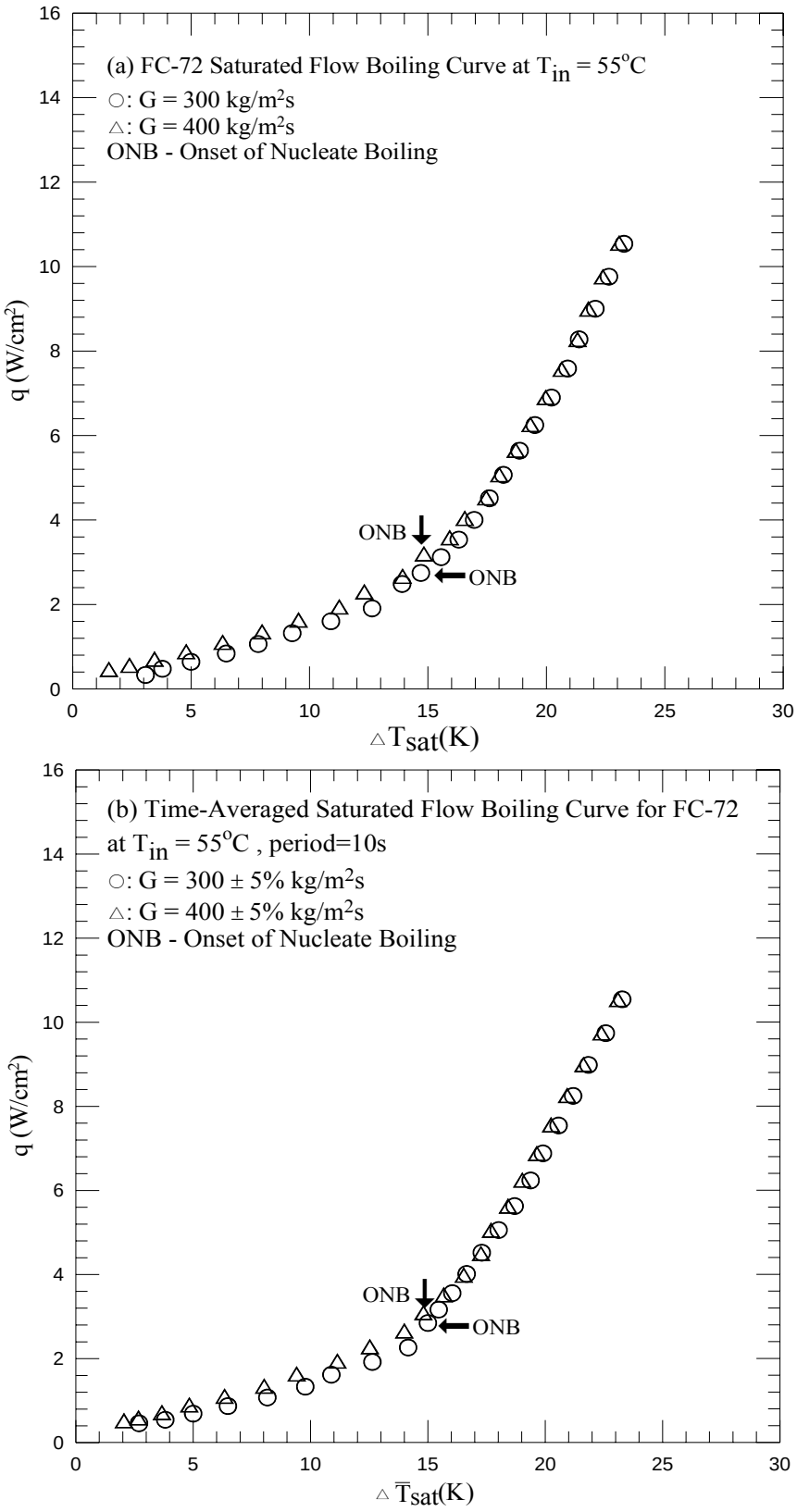

Fig. 4.2 Time-average flow boiling curves for various coolant mass fluxes for stable saturated flow boiling (a) and transient saturated flow boiling for t_p=10 sec (b), 20 sec (c) and 30 sec (d).

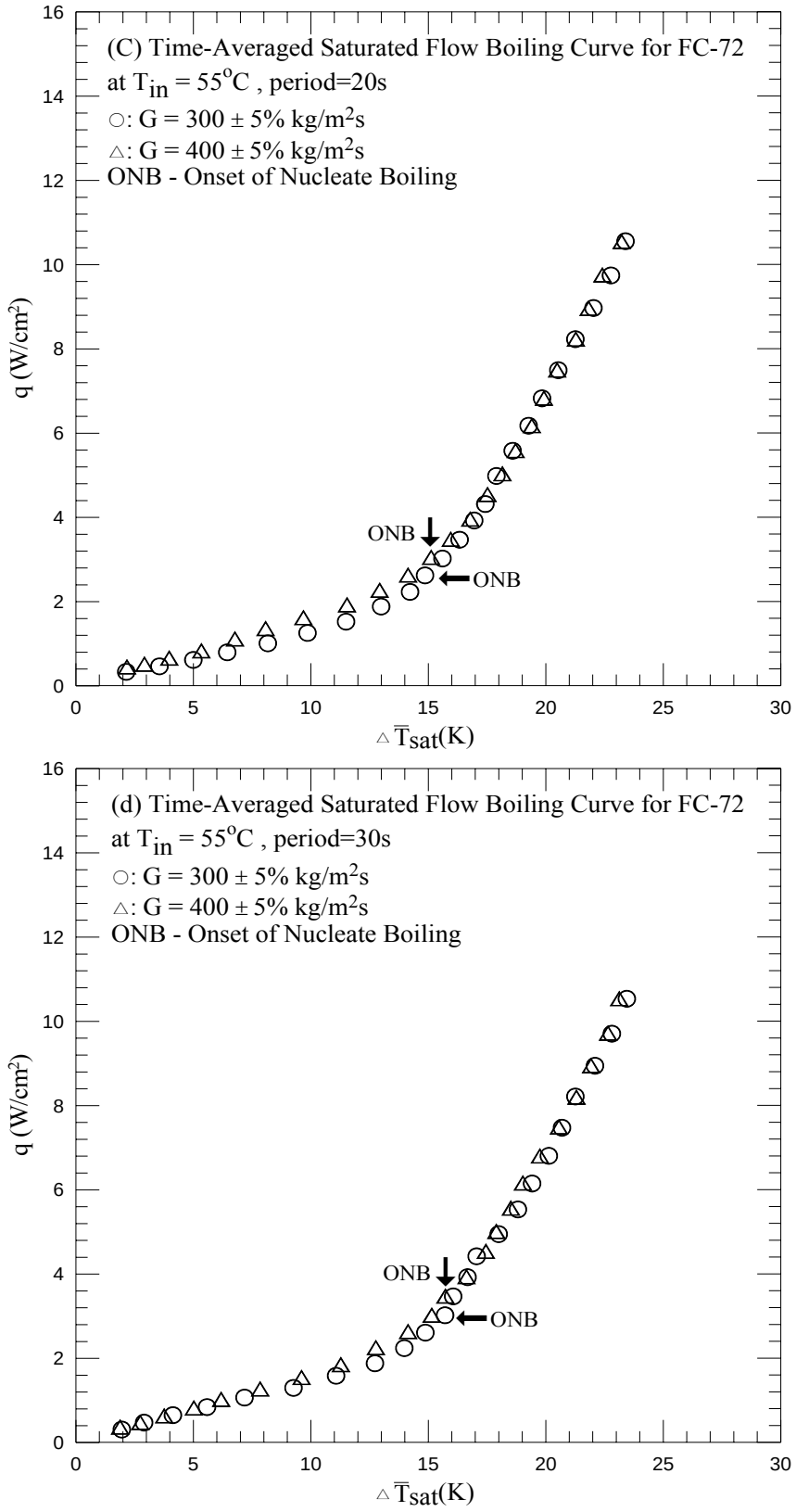

Fig. 4.2 Continued.

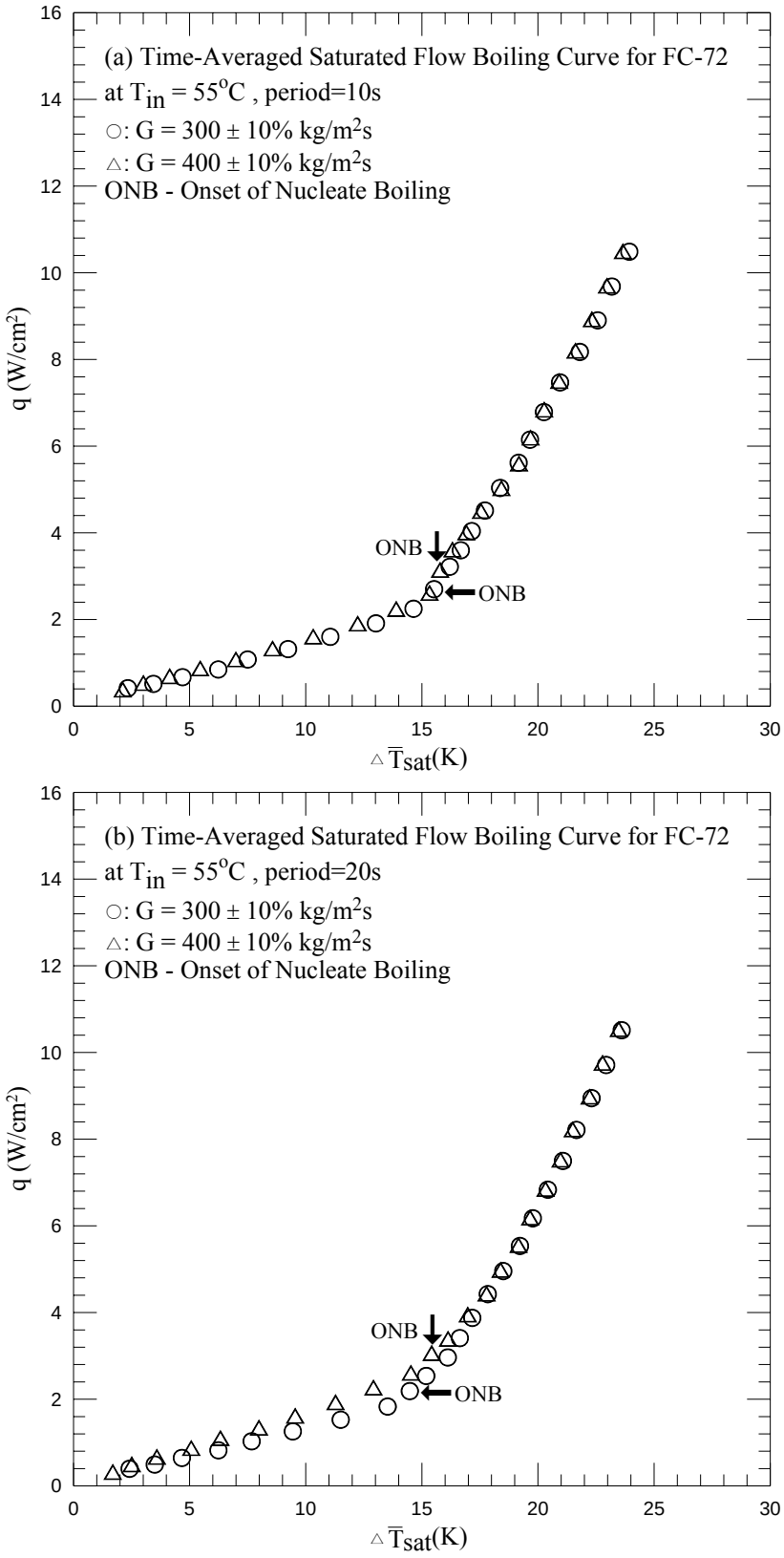

Fig. 4.3 Time-average flow boiling curves for various coolant mass fluxes for transient saturated flow boiling at t_p=10 sec (a), 20 sec (b) and 30 sec (c).

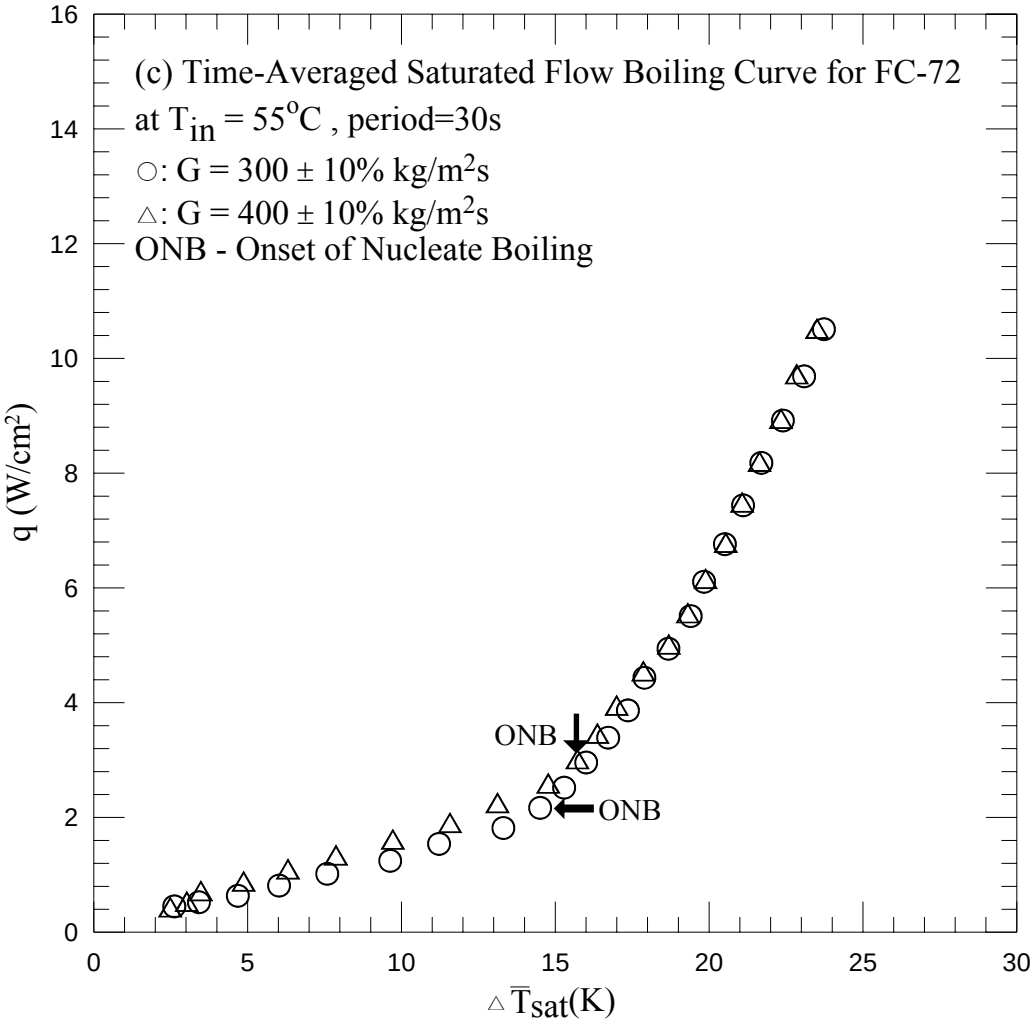

Fig. 4.3 Continued.

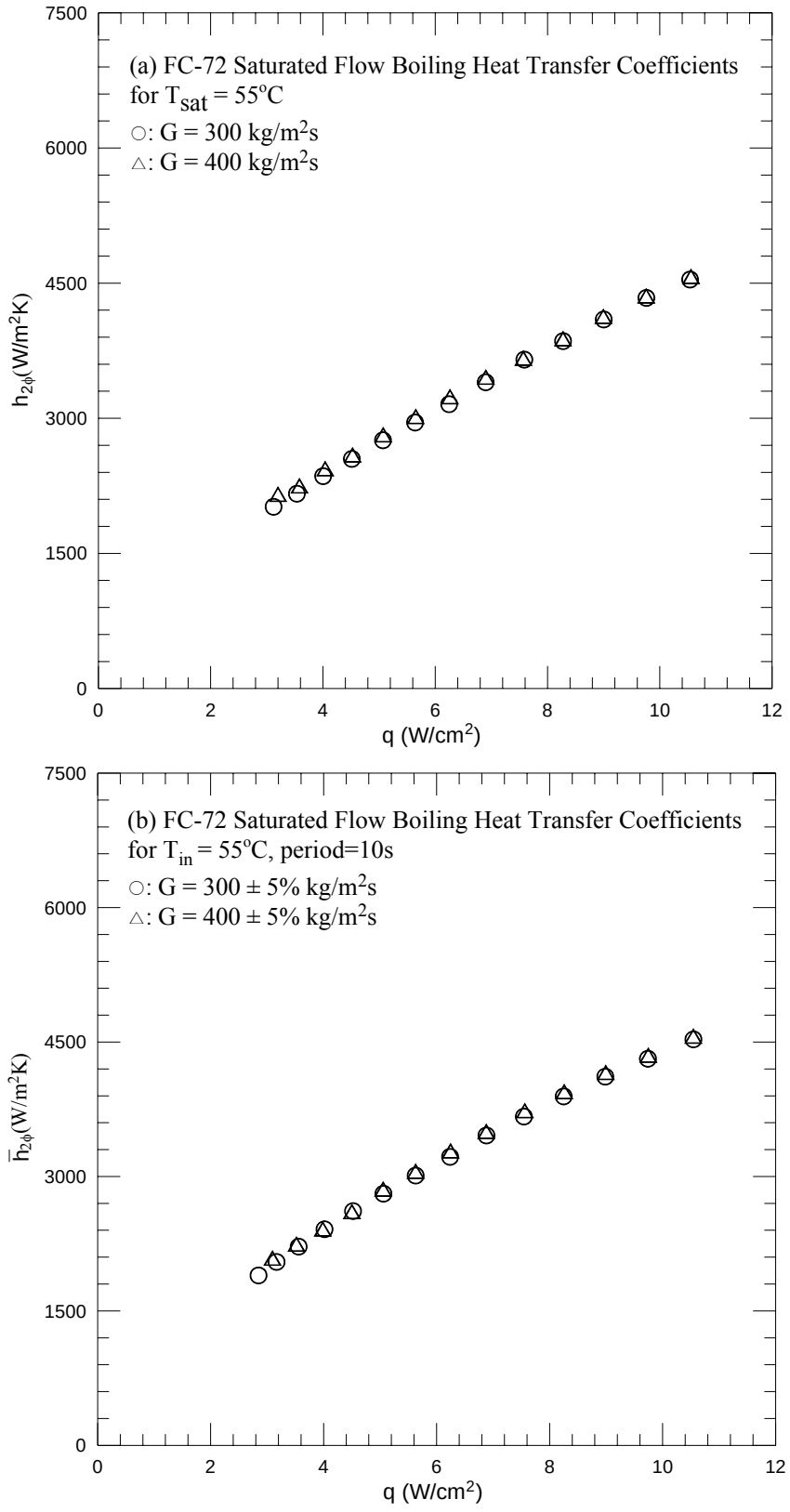

Fig. 4.4 Time-average flow boiling heat transfer coefficients for various coolant mass fluxes for stable saturated flow boiling (a) and transient saturated flow boiling at t_p=10 sec (b), 20 sec (c) and 30 sec (d).

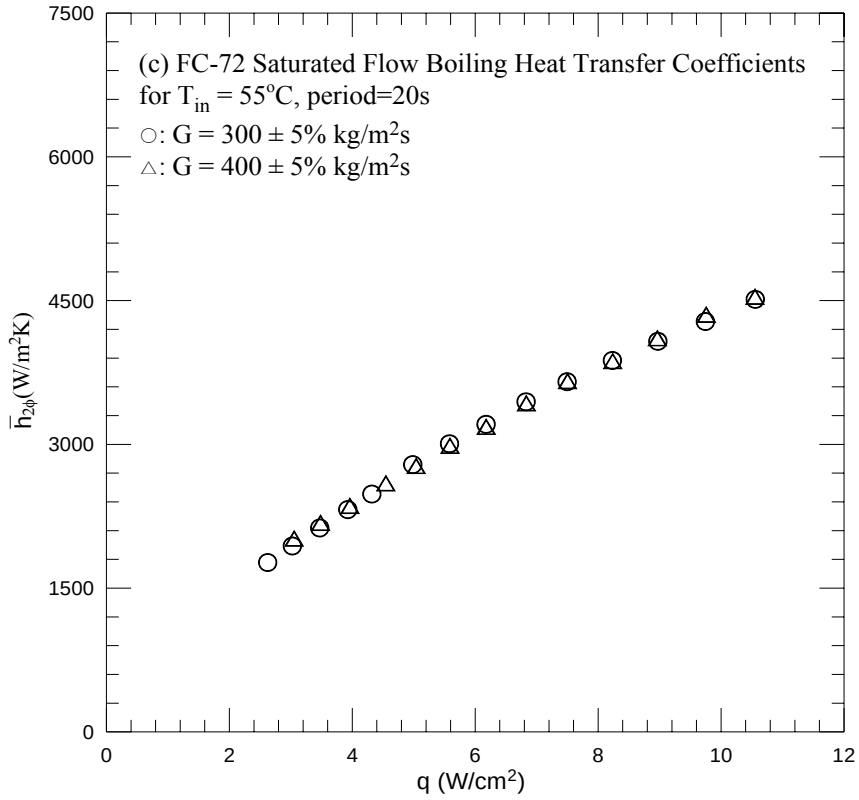

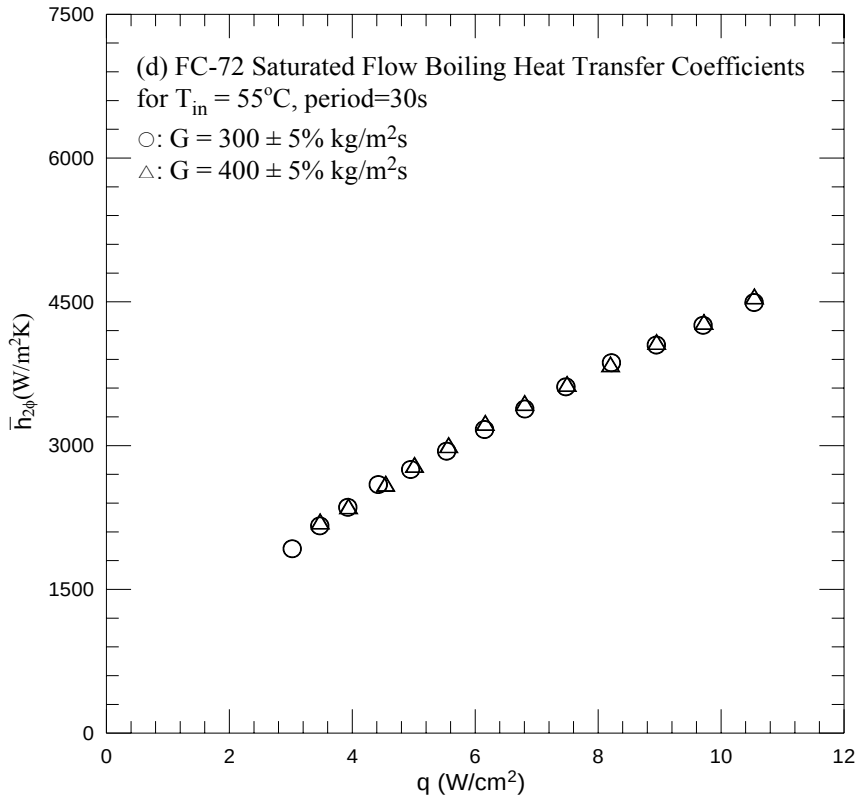

Fig. 4.4 Continued.

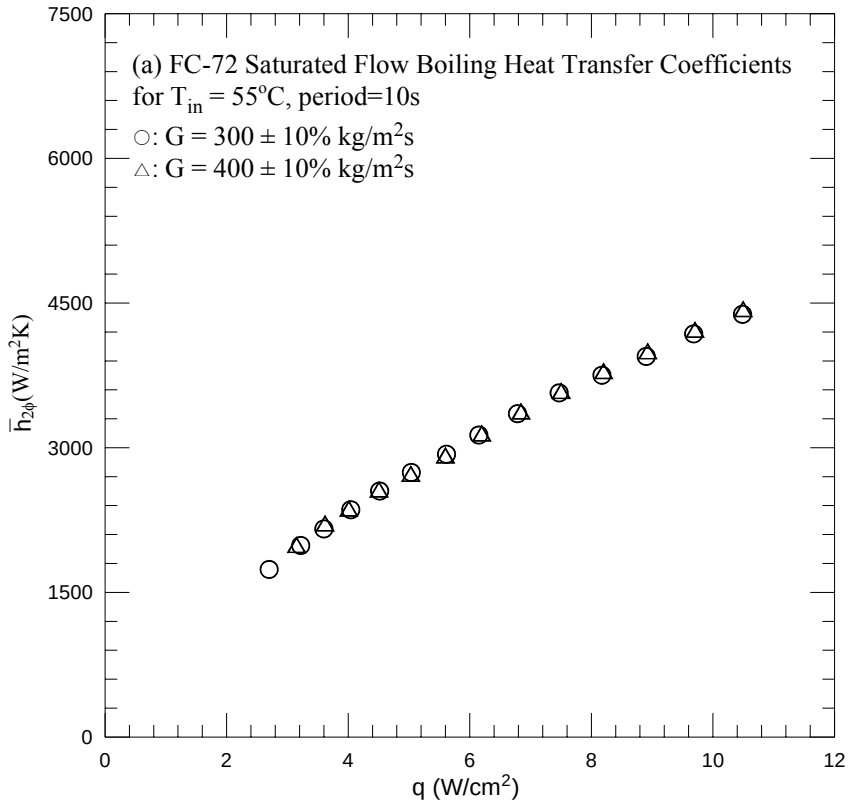

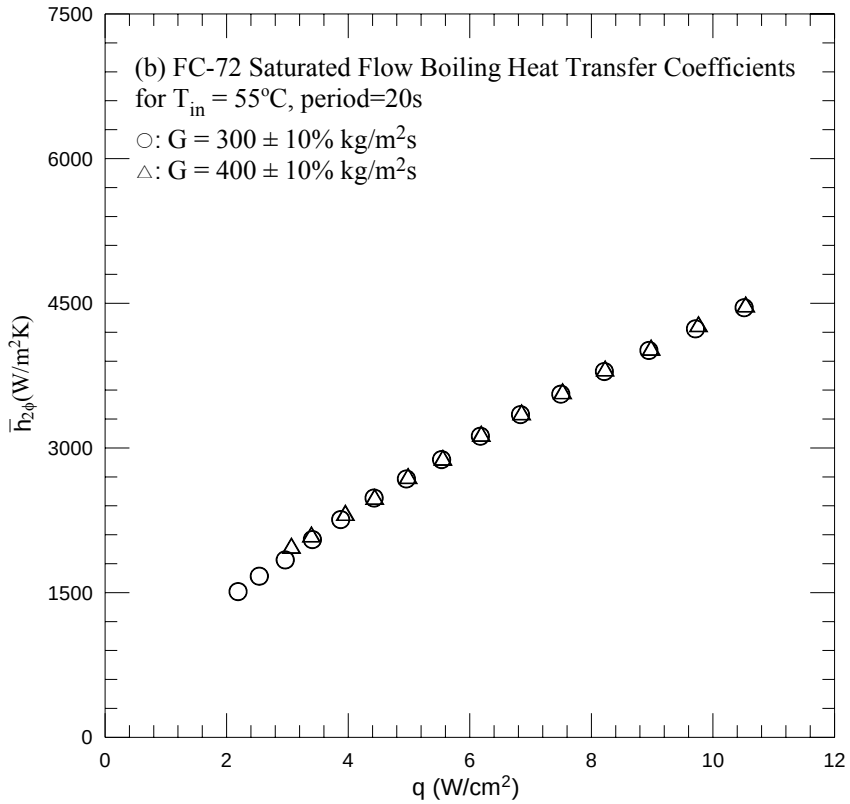

Fig. 4.5 Time-average flow boiling heat transfer coefficients for various coolant mass fluxes for transient saturated flow boiling at t_p=10 sec (a), 20 sec (b) and 30 sec (c).

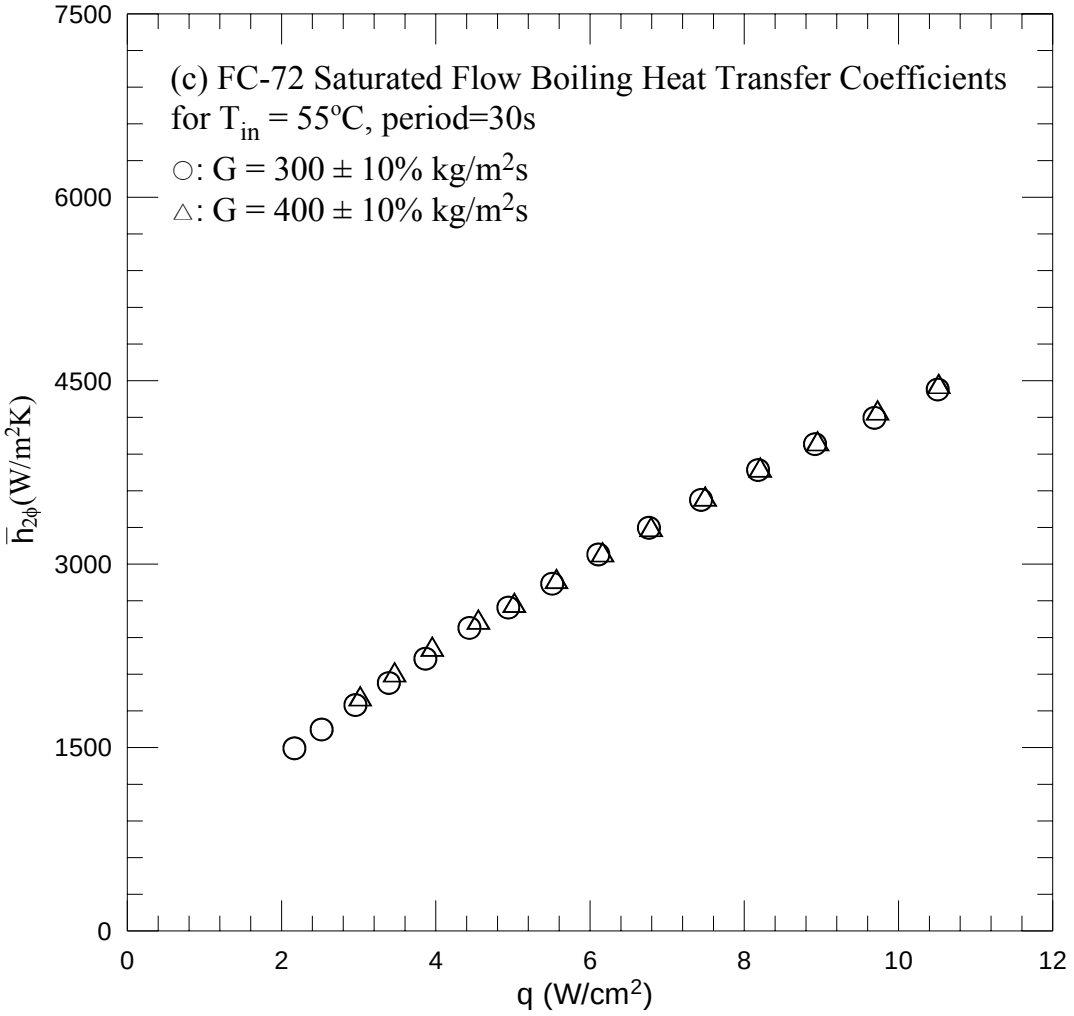

Fig. 4.5 Continued.

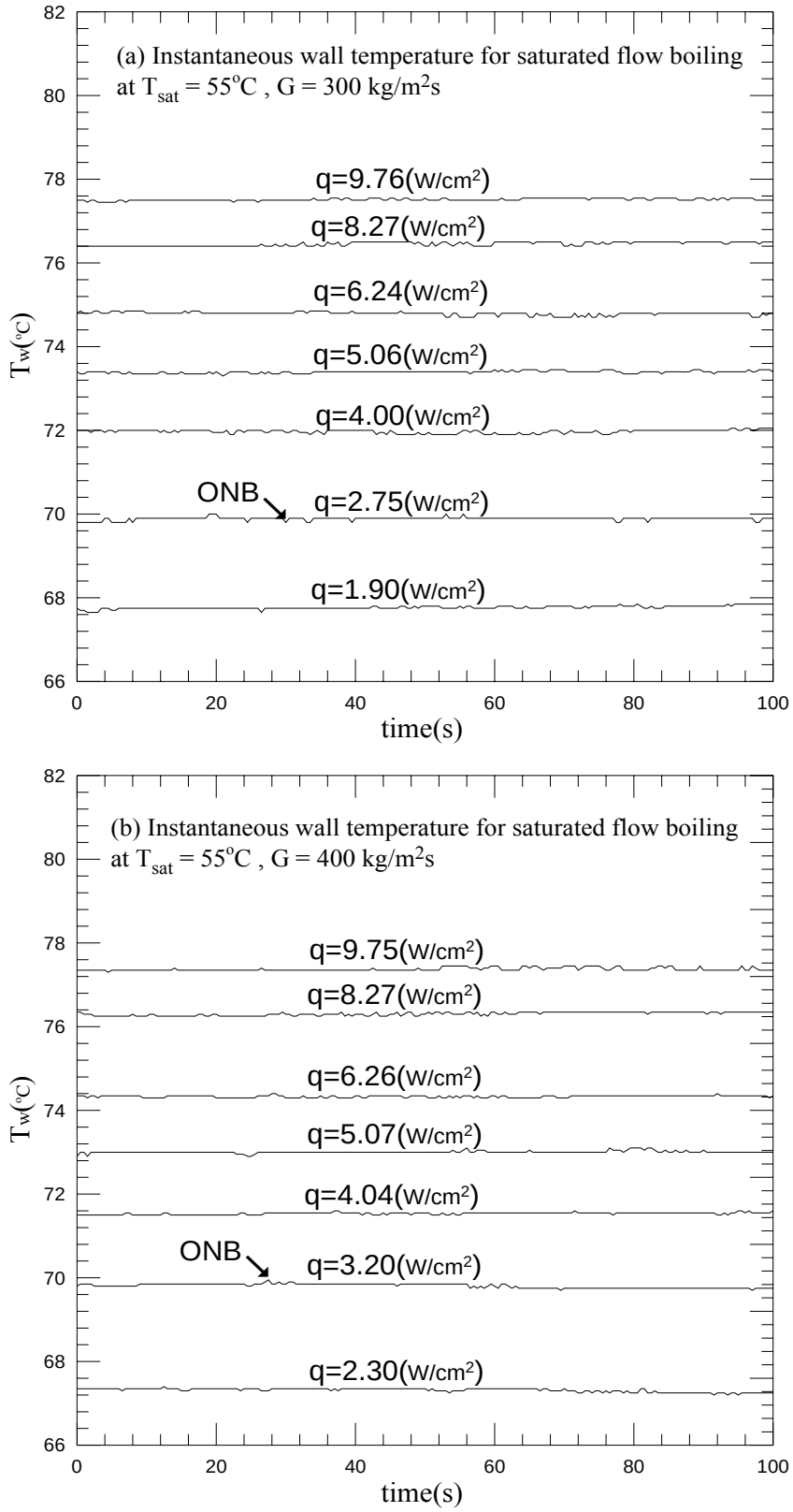

Fig. 4.6 Time variations of the copper plate temperature in stable saturated flow boiling for various imposed heat fluxes at (a) G=300 kg/m^{2}s and (b) G=400 kg/m^{2}s.

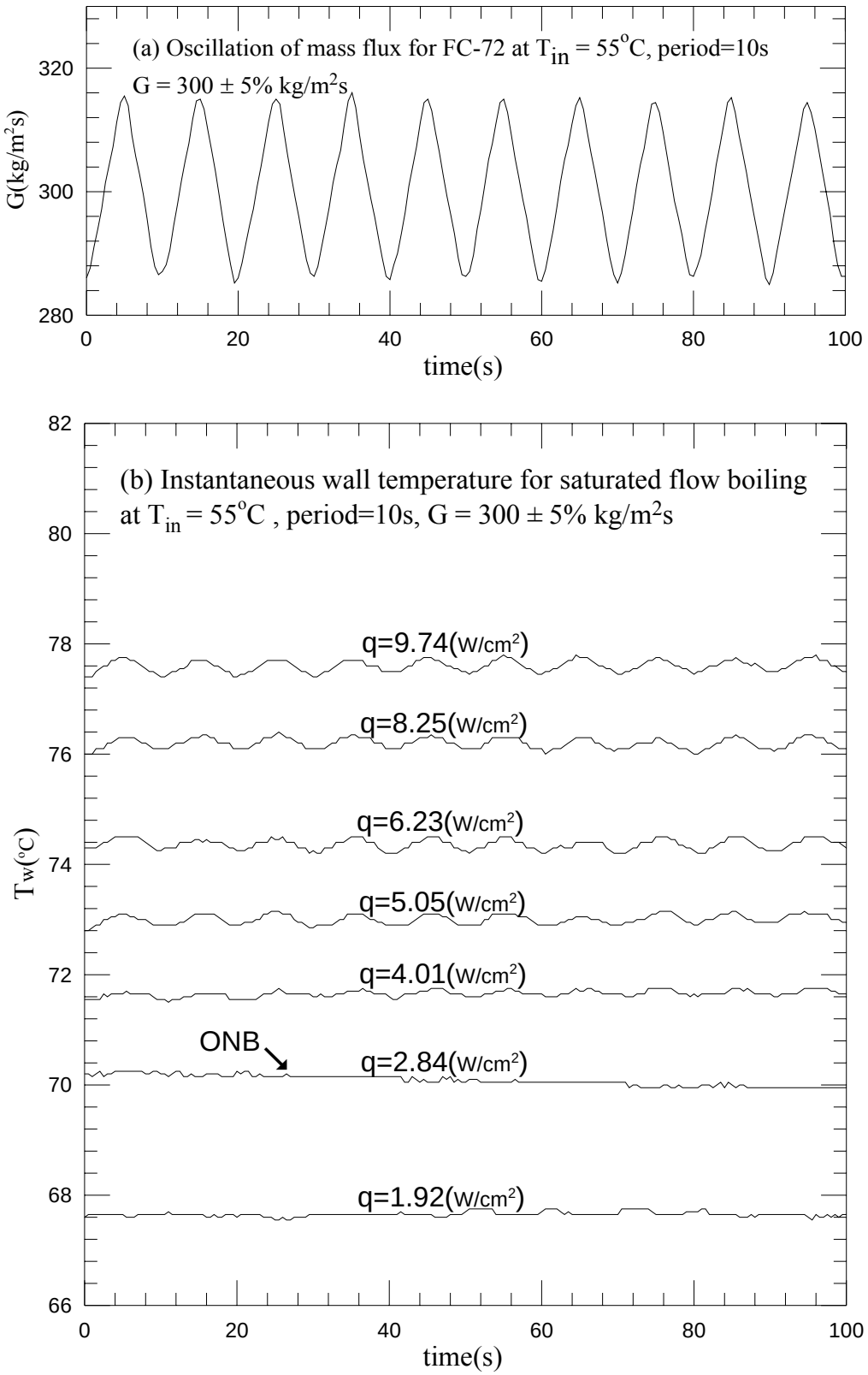

Fig. 4.7 Time variations of (a) imposed coolant mass flux and (b) copper plate temperature in transient oscillatory saturated flow boiling for various imposed heat fluxes for G=300±5% kg/m^{2}s with t_p=10 sec.($\overline{q}_{ONB}$ =2.84 w/cm^2 at G =300 kg/m^{2}S)

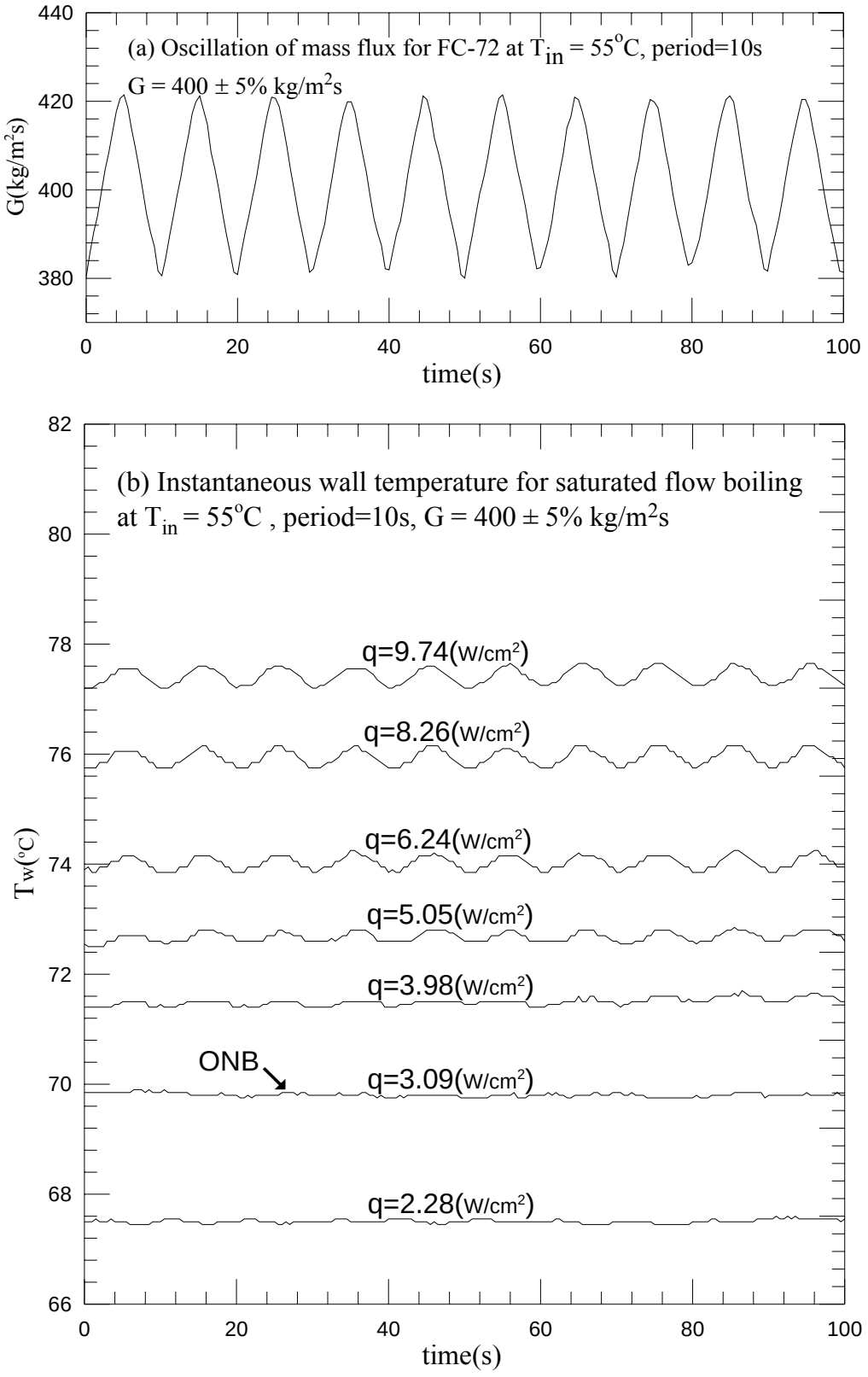

Fig. 4.8 Time variations of (a) imposed coolant mass flux and (b) copper plate temperature in transient oscillatory saturated flow boiling for various imposed heat fluxes for G=400±5% kg/m^{2}s with t_p =10 sec.($\overline{q}_{ONB}$ =3.09 w/cm^2 at G =400 kg/m^{2}S)

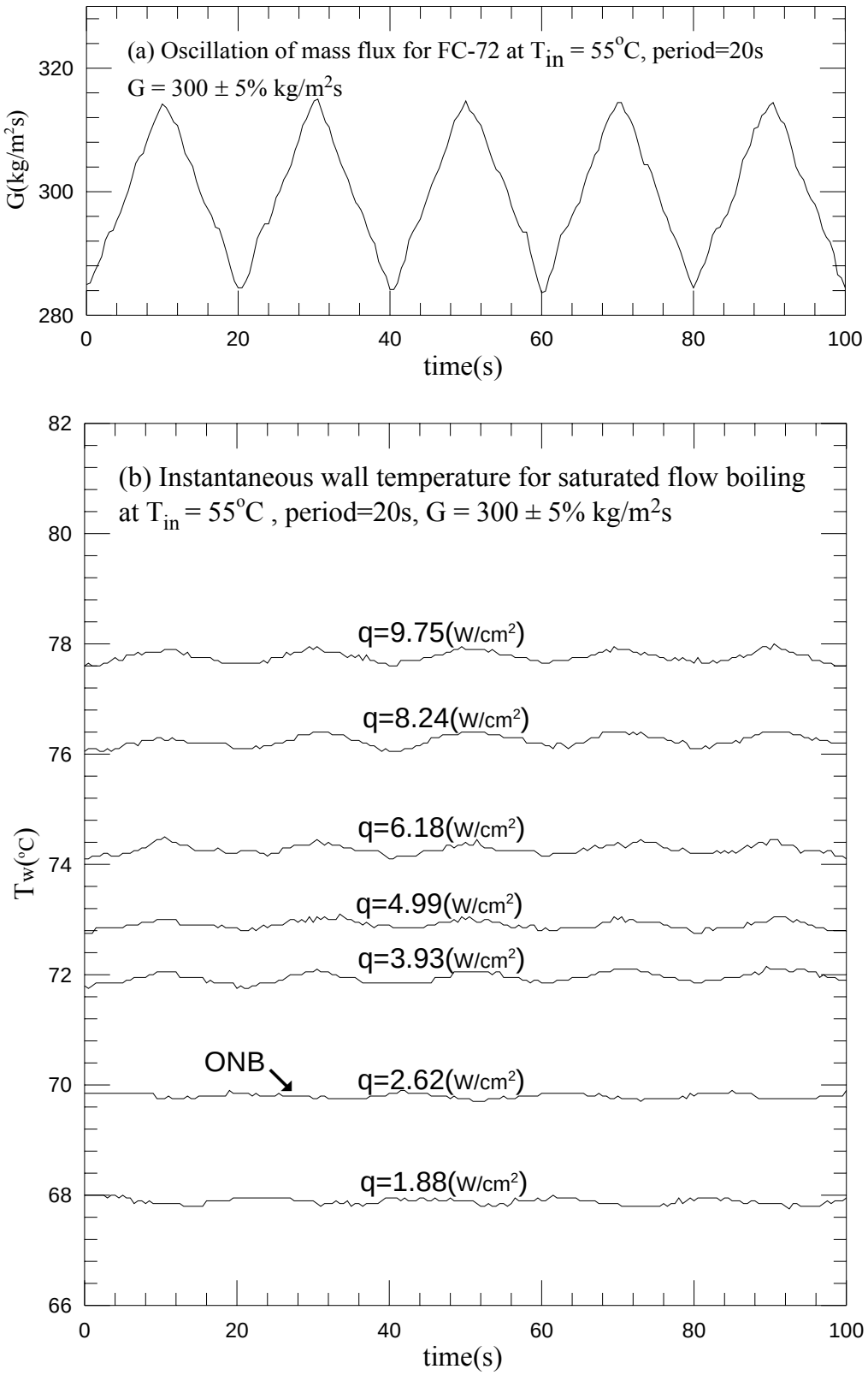

Fig. 4.9 Time variations of (a) imposed coolant mass flux and (b) copper plate temperature in transient oscillatory saturated flow boiling for various imposed heat fluxes for G=300±5% kg/m^{2}s with t_p =20 sec.($\bar{q}_{ONB}$ =2.62 w/cm^2 at G =300 kg/m^{2}s)

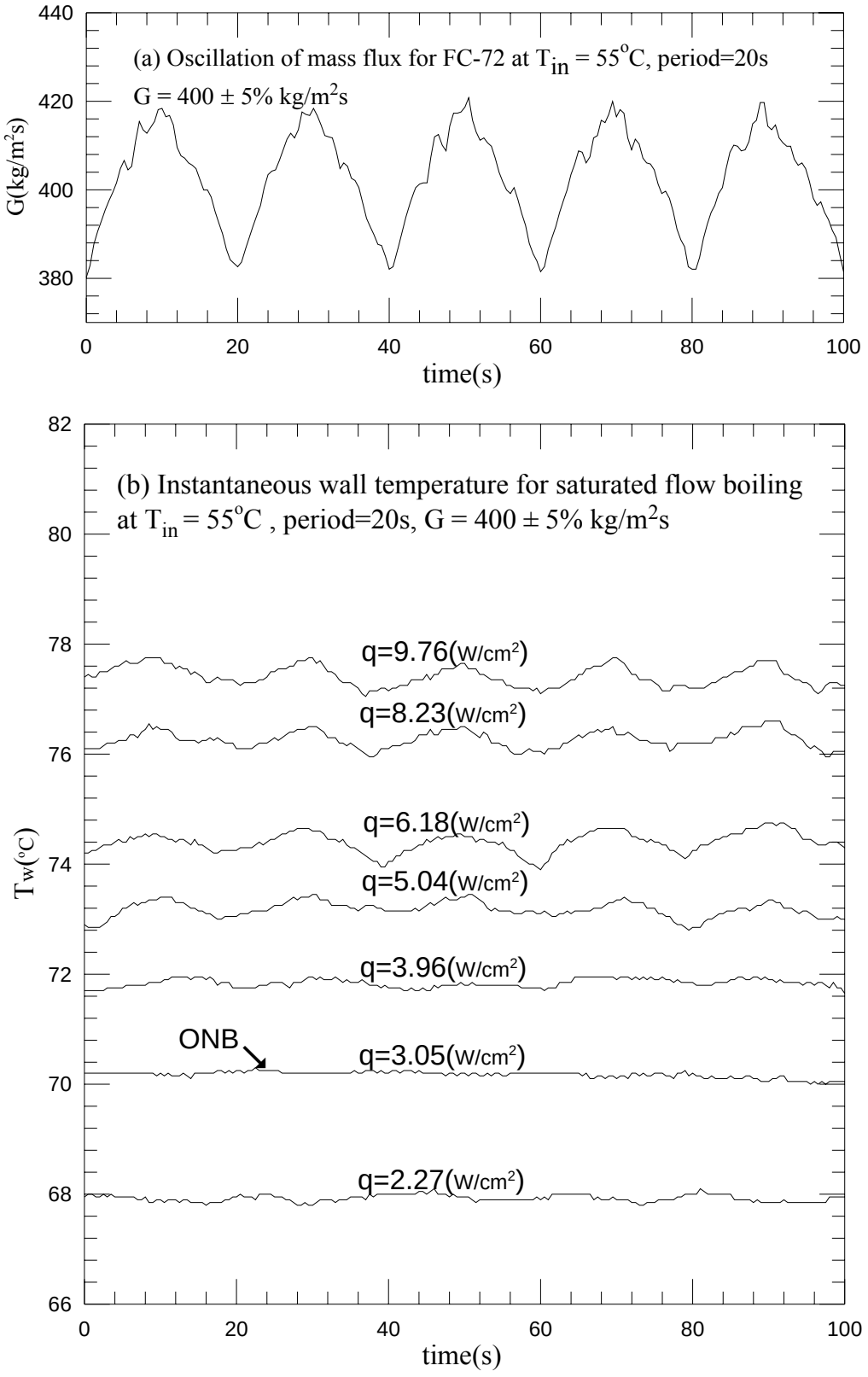

Fig. 4.10 Time variations of (a) imposed coolant mass flux and (b) copper plate temperature in transient oscillatory saturated flow boiling for various imposed heat fluxes for G=400±5% kg/m^{2}s with t_p =20 sec.($\overline{q}_{ONB}$ =3.05 w/cm^2 at G =400 kg/m^{2}S)

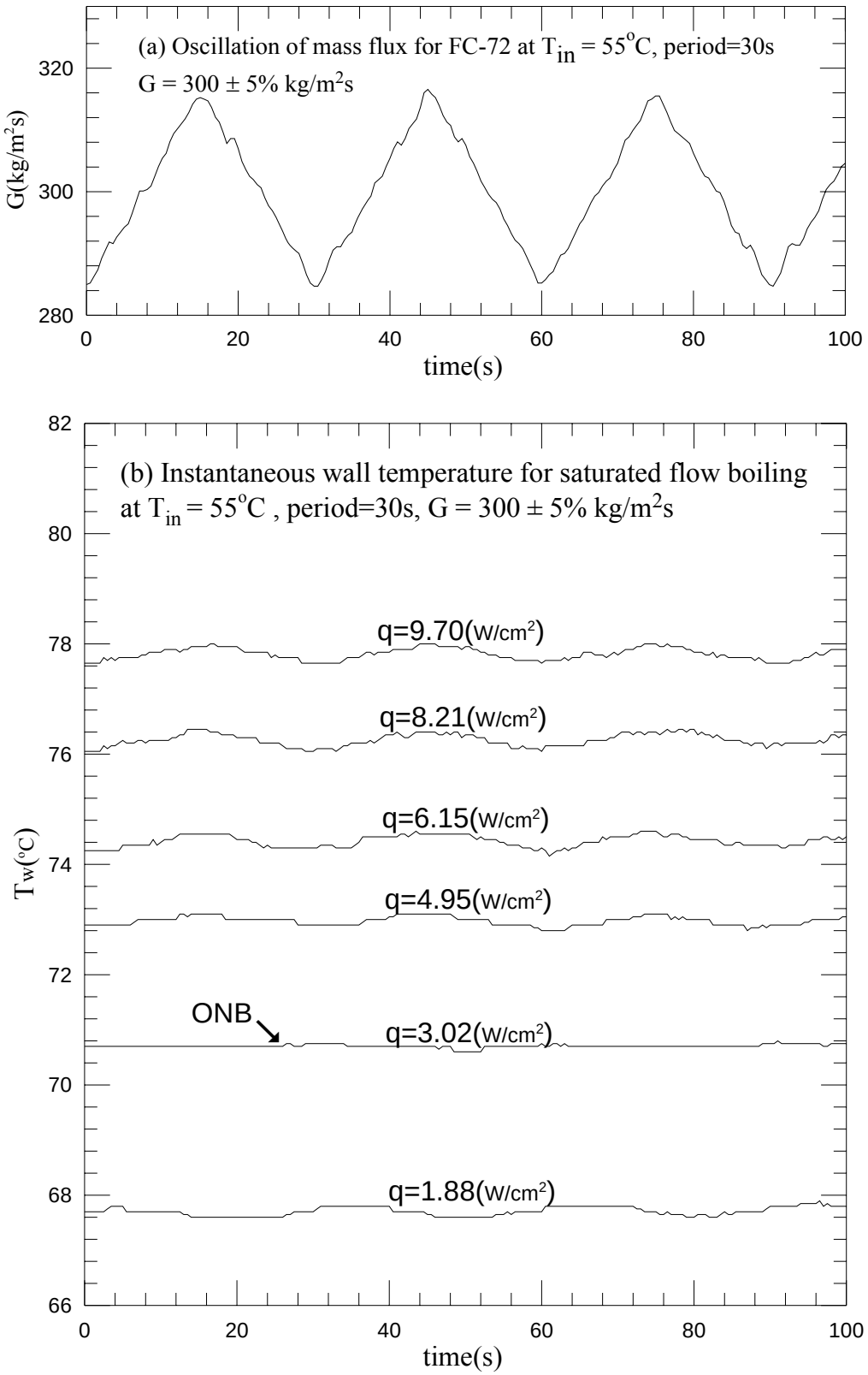

Fig. 4.11 Time variations of (a) imposed coolant mass flux and (b) copper plate temperature in transient oscillatory saturated flow boiling for various imposed heat fluxes for G=300±5% kg/m^{2}s with t_p =30 sec.($\overline{q}_{ONB}$ =3.02 w/cm^2 at G =300 kg/m^{2}S)

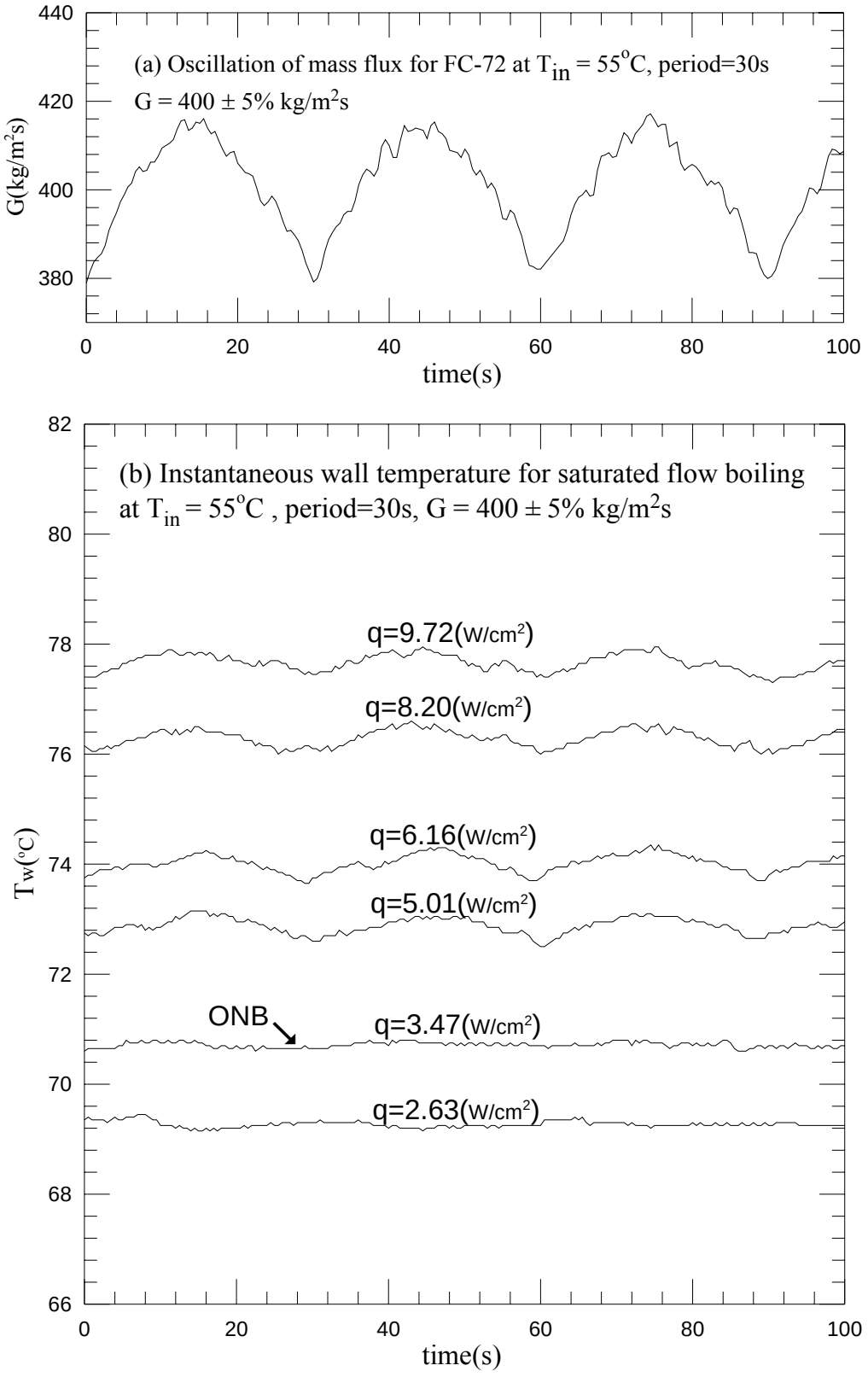

Fig. 4.12 Time variations of (a) imposed coolant mass flux and (b) copper plate temperature in transient oscillatory saturated flow boiling for various imposed heat fluxes for G=400±5% kg/m^{2}s with t_p =30 sec.($\overline{q}_{ONB}$ =3.47 w/cm^2 at G =400 kg/m^{2}S)

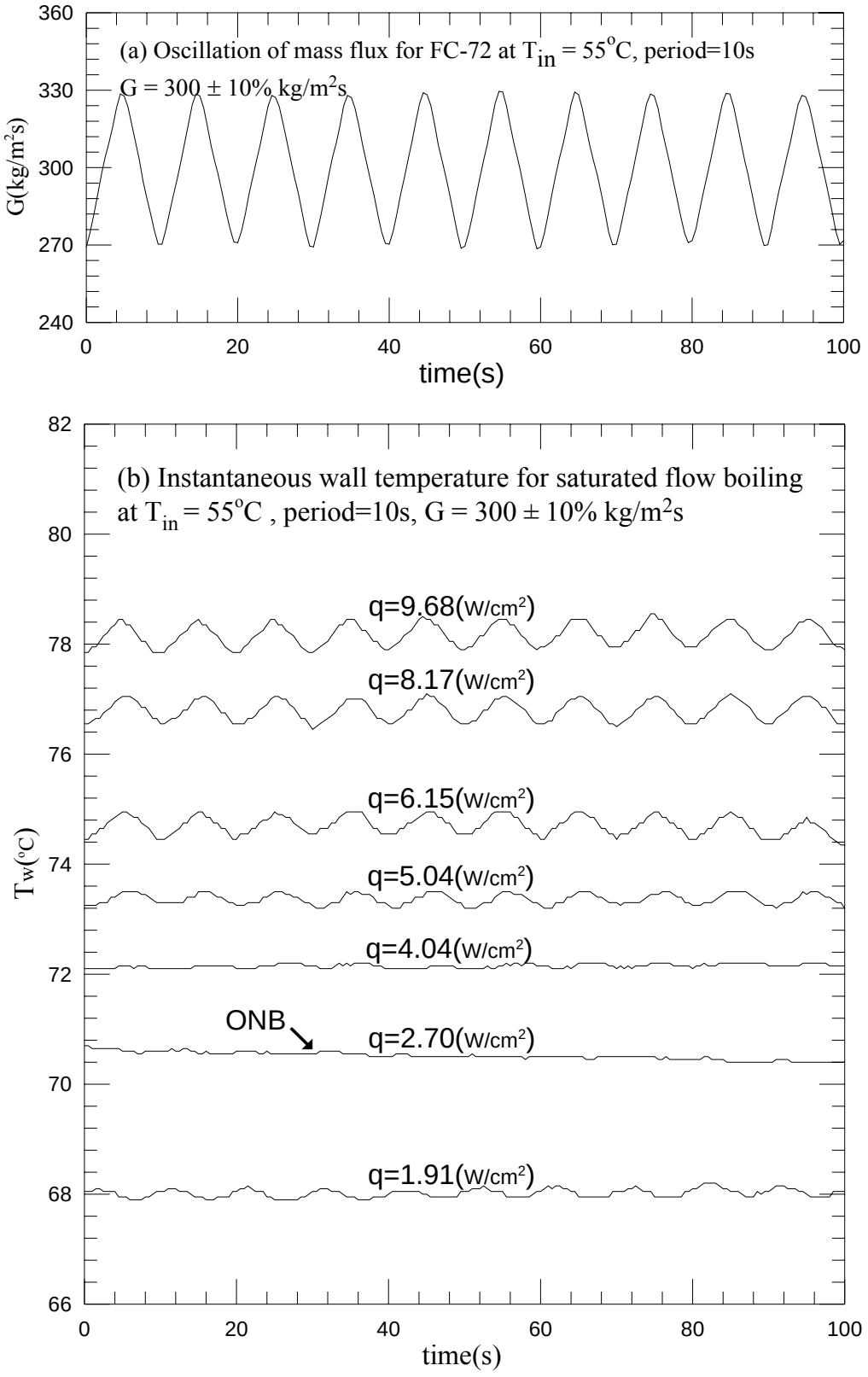

Fig. 4.13 Time variations of (a) imposed coolant mass flux and (b) copper plate temperature in transient oscillatory saturated flow boiling for various imposed heat fluxes for G=300±10% kg/m^{2}s with t_p =10 sec.($\bar{q}_{ONB}$ =2.70 w/cm^2 at G =300 kg/m^{2}S)

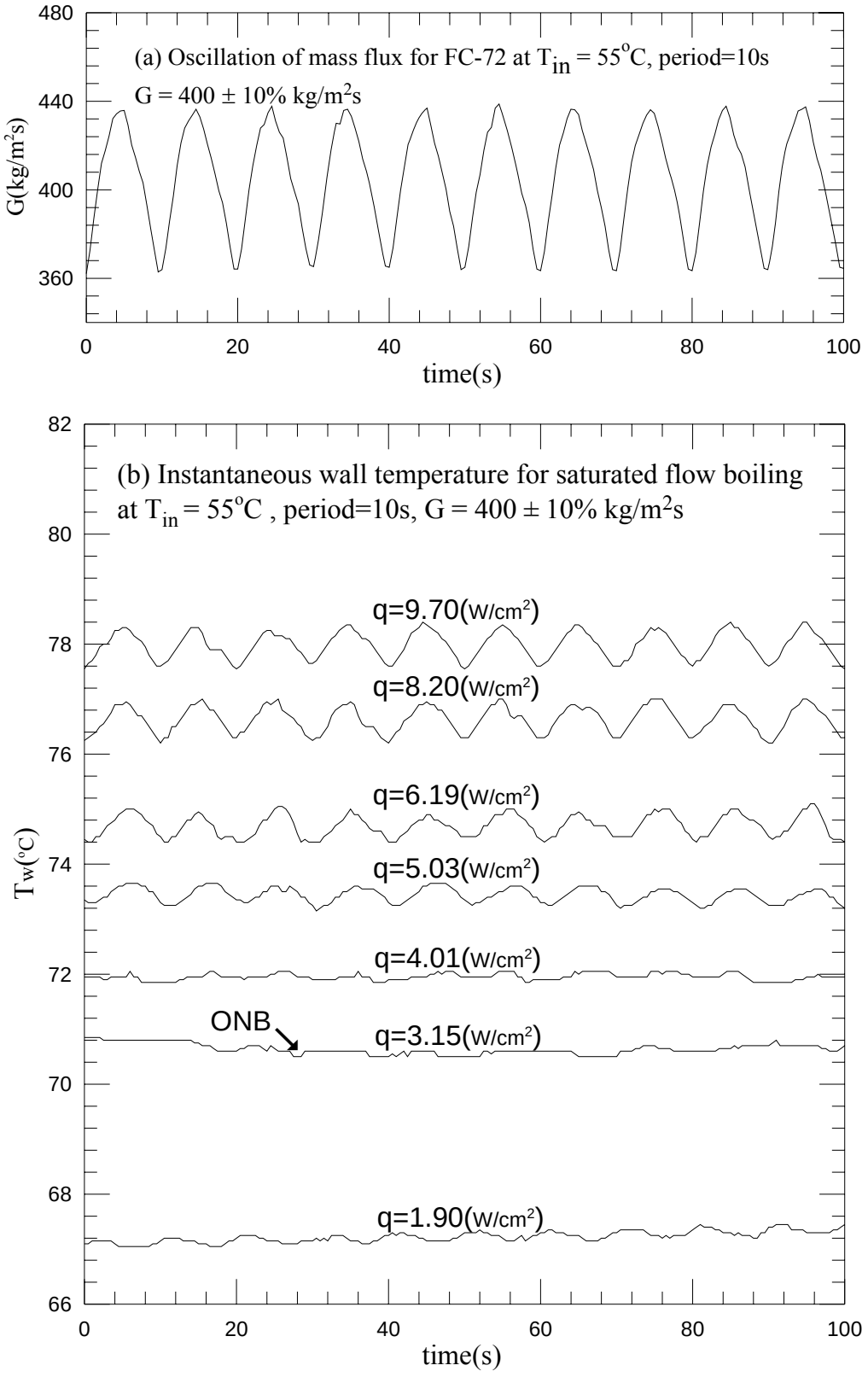

Fig. 4.14 Time variations of (a) imposed coolant mass flux and (b) copper plate temperature in transient oscillatory saturated flow boiling for various imposed heat fluxes for G=400±10% kg/m^{2}s with t_p=10 sec.($\bar{q}_{ONB}$ =3.15 w/cm^2 at G =400 kg/m^{2}s)

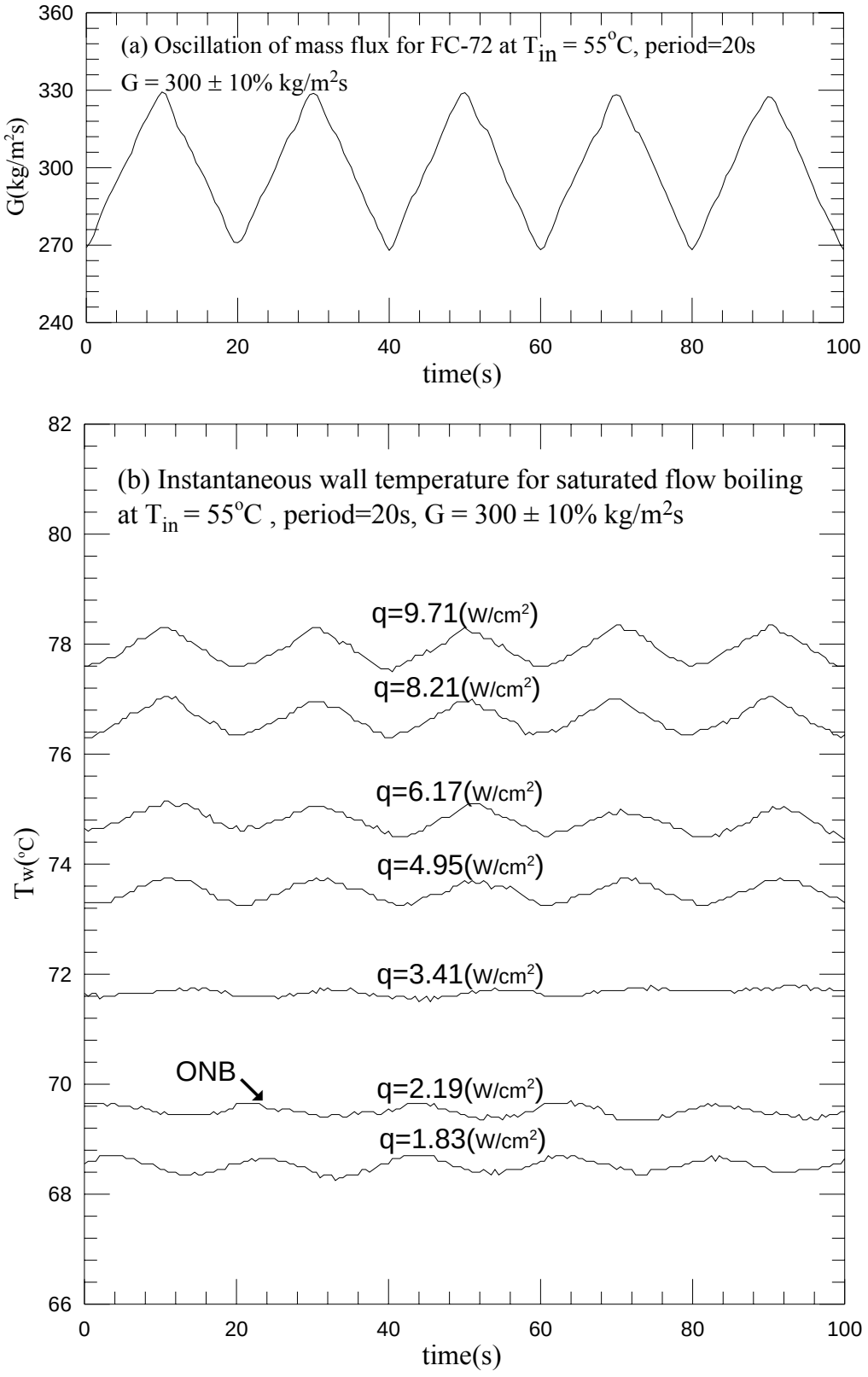

Fig. 4.15 Time variations of (a) imposed coolant mass flux and (b) copper plate temperature in transient oscillatory saturated flow boiling for various imposed heat fluxes for G=300±10% kg/m^{2}s with t_p =20 sec.($\bar{q}_{ONB}$ =2.19 w/cm^2 at G =300 kg/m^{2}S)

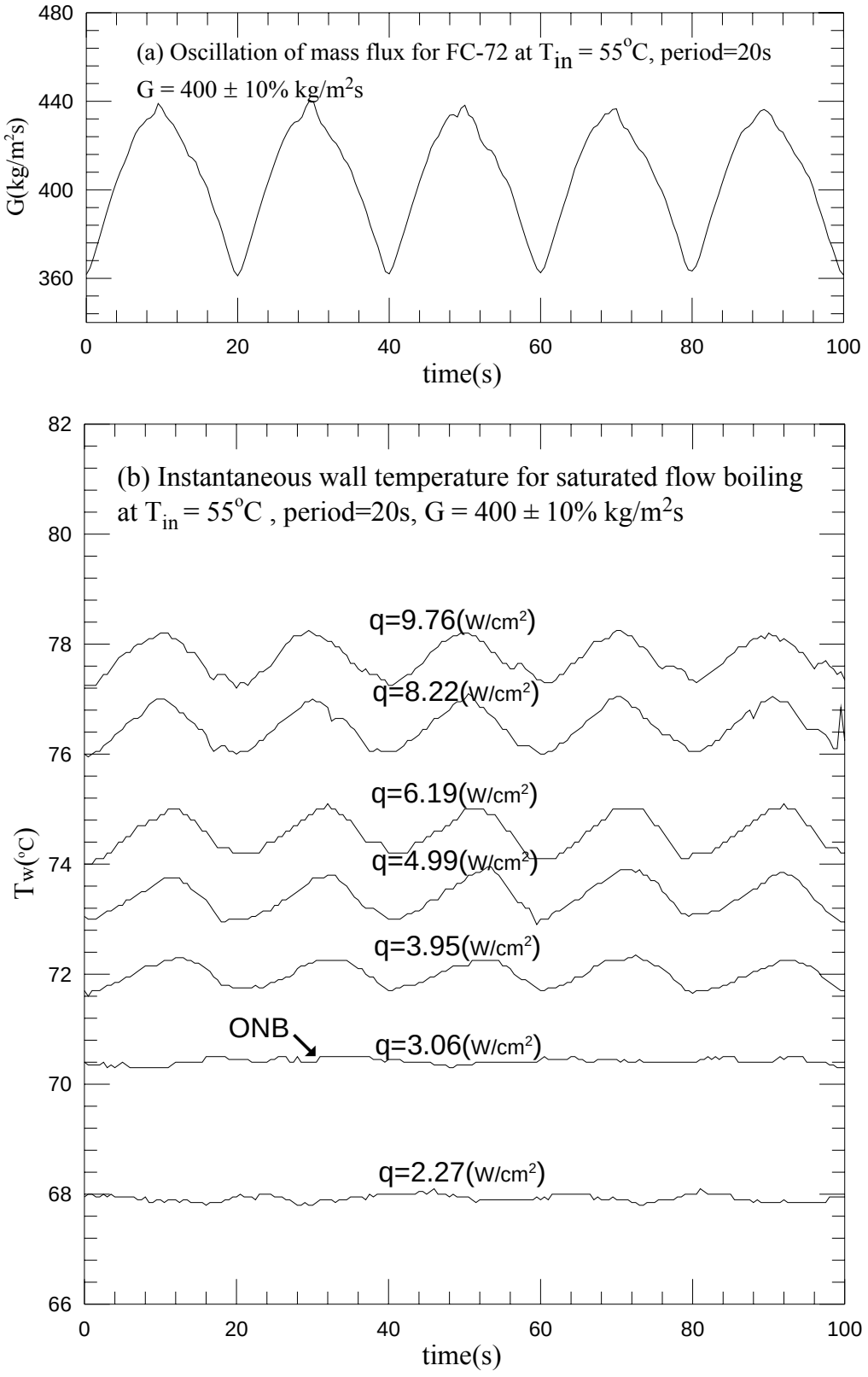

Fig. 4.16 Time variations of (a) imposed coolant mass flux and (b) copper plate temperature in transient oscillatory saturated flow boiling for various imposed heat fluxes for G=400±10% kg/m^{2}s with t_p =20 sec.($\bar{q}_{ONB}$ =3.06 w/cm^2 at G =400 kg/m^{2}S)

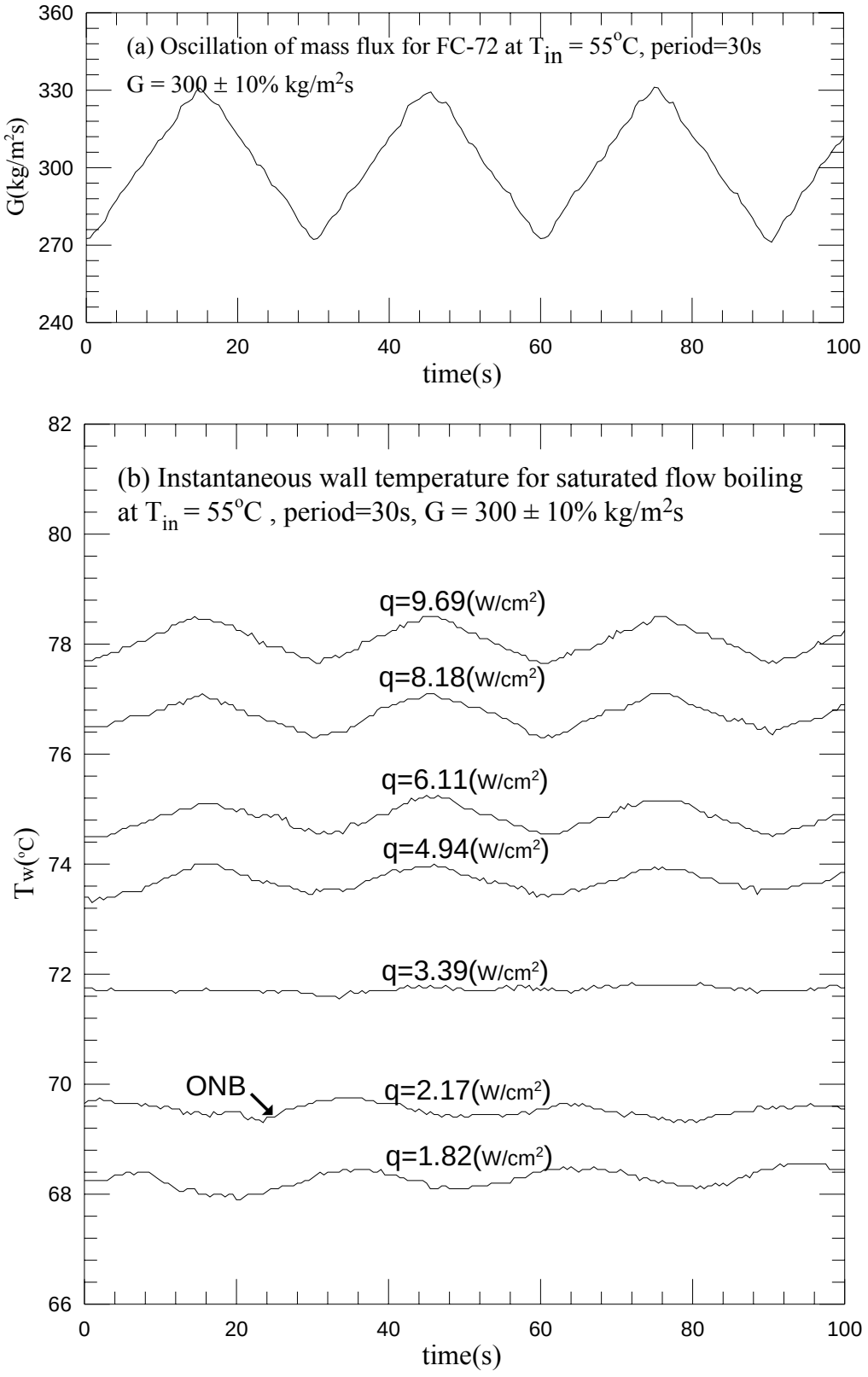

Fig. 4.17 Time variations of (a) imposed coolant mass flux and (b) copper plate temperature in transient oscillatory saturated flow boiling for various imposed heat fluxes for G=300±10% kg/m^{2}s with t_p =30 sec.($\bar{q}_{ONB}$ =2.17 w/cm^2 at G =300 kg/m^{2}S)

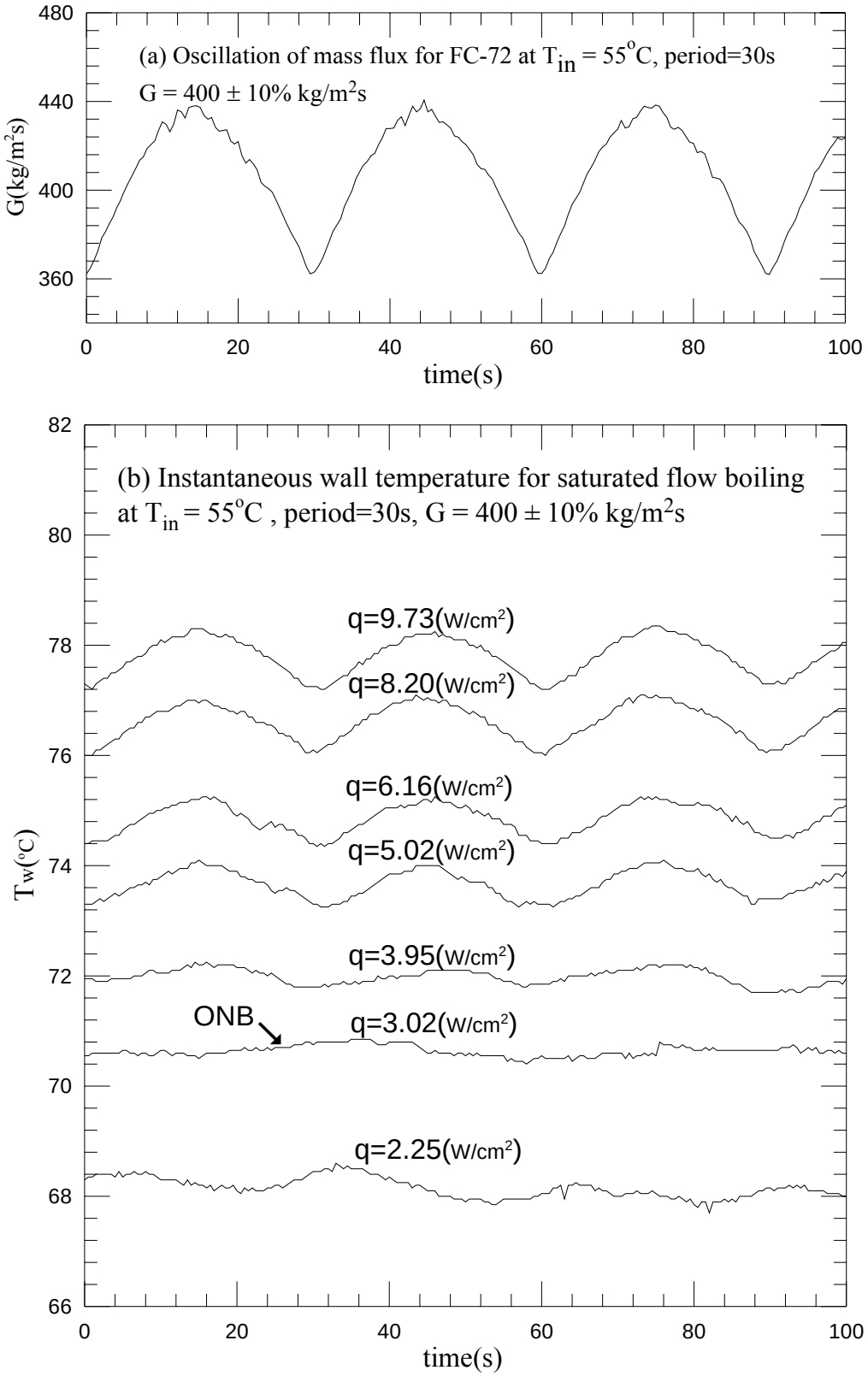

Fig. 4.18 Time variations of (a) imposed coolant mass flux and (b) copper plate temperature in transient oscillatory saturated flow boiling for various imposed heat fluxes for G=400±10% kg/m^{2}s with t_p =30 sec.($\bar{q}_{ONB}$ =3.02 w/cm^2 at G =400 kg/m^{2}S)

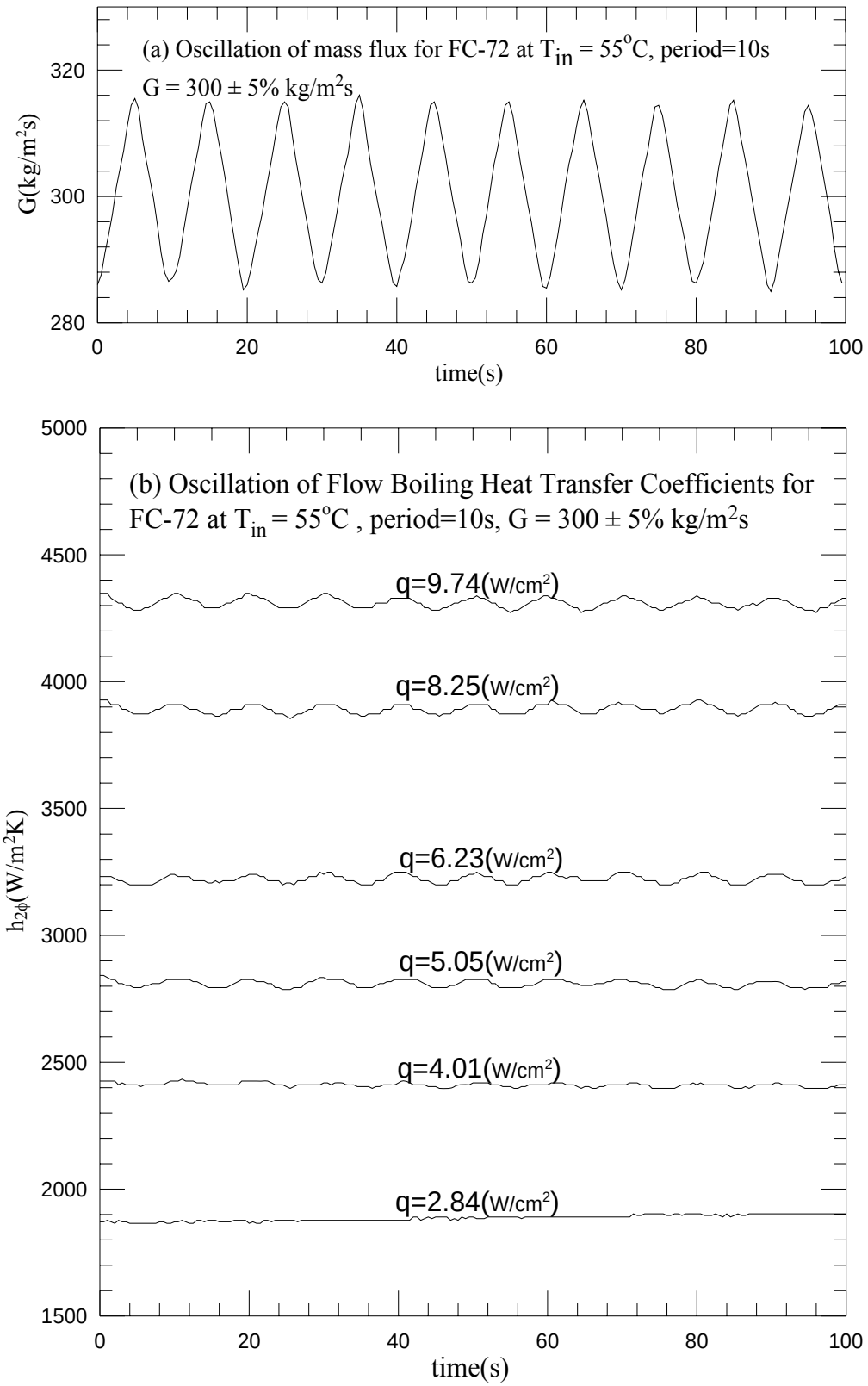

Fig. 4.19 Time variations of (a) imposed coolant mass flux and (b) flow boiling heat transfer coefficients in transient oscillatory saturated flow boiling for various imposed heat fluxes for G=300± 5% kg/m^{2}s with t_p =10 sec.

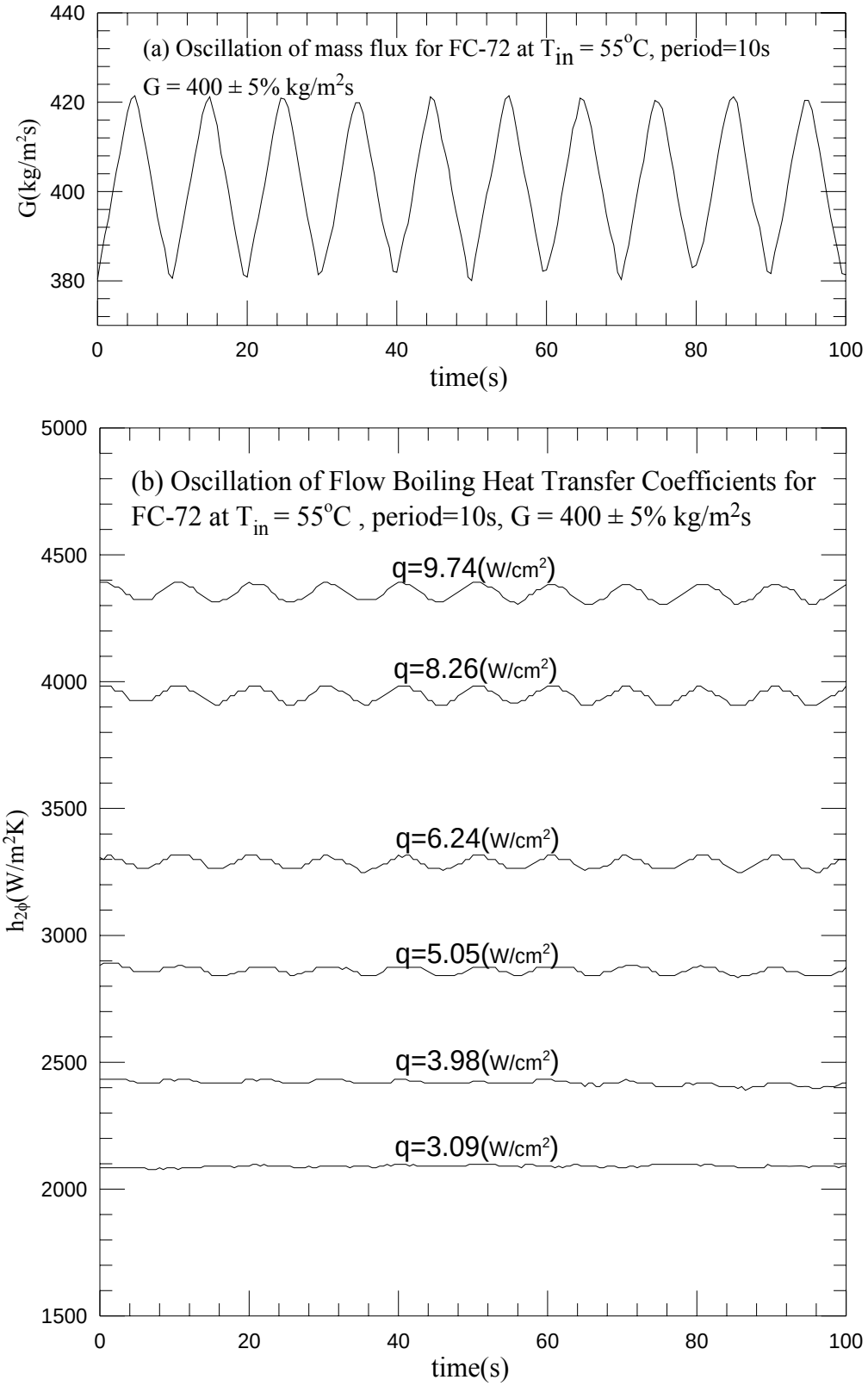

Fig. 4.20 Time variations of (a) imposed coolant mass flux and (b) flow boiling heat transfer coefficients in transient oscillatory saturated flow boiling for various imposed heat fluxes for G=400± 5% kg/m^{2}s with t_p =10 sec.

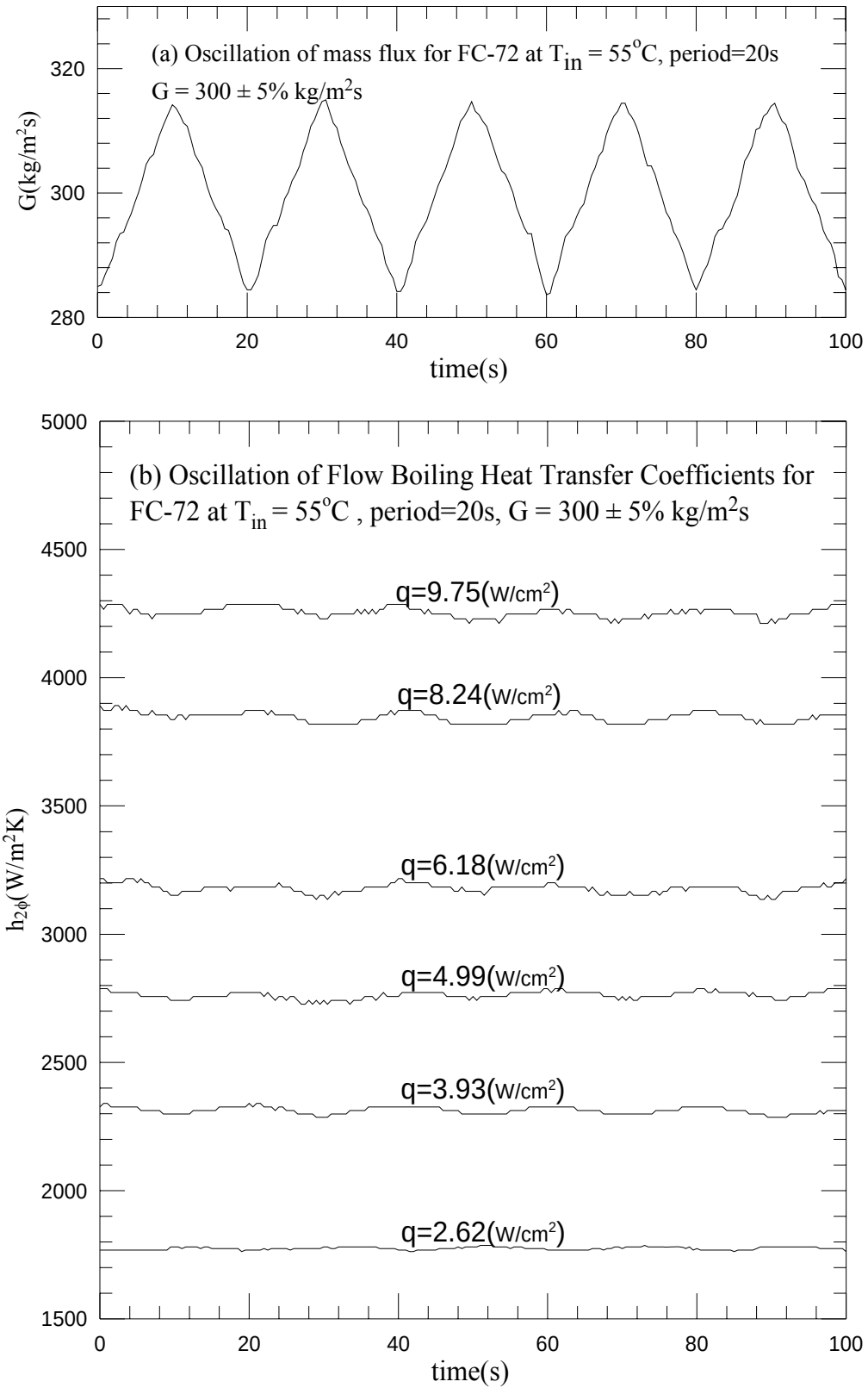

Fig. 4.21 Time variations of (a) imposed coolant mass flux and (b) flow boiling heat transfer coefficients in transient oscillatory saturated flow boiling for various imposed heat fluxes for G=300± 5% kg/m^{2}s with t_p =20 sec.

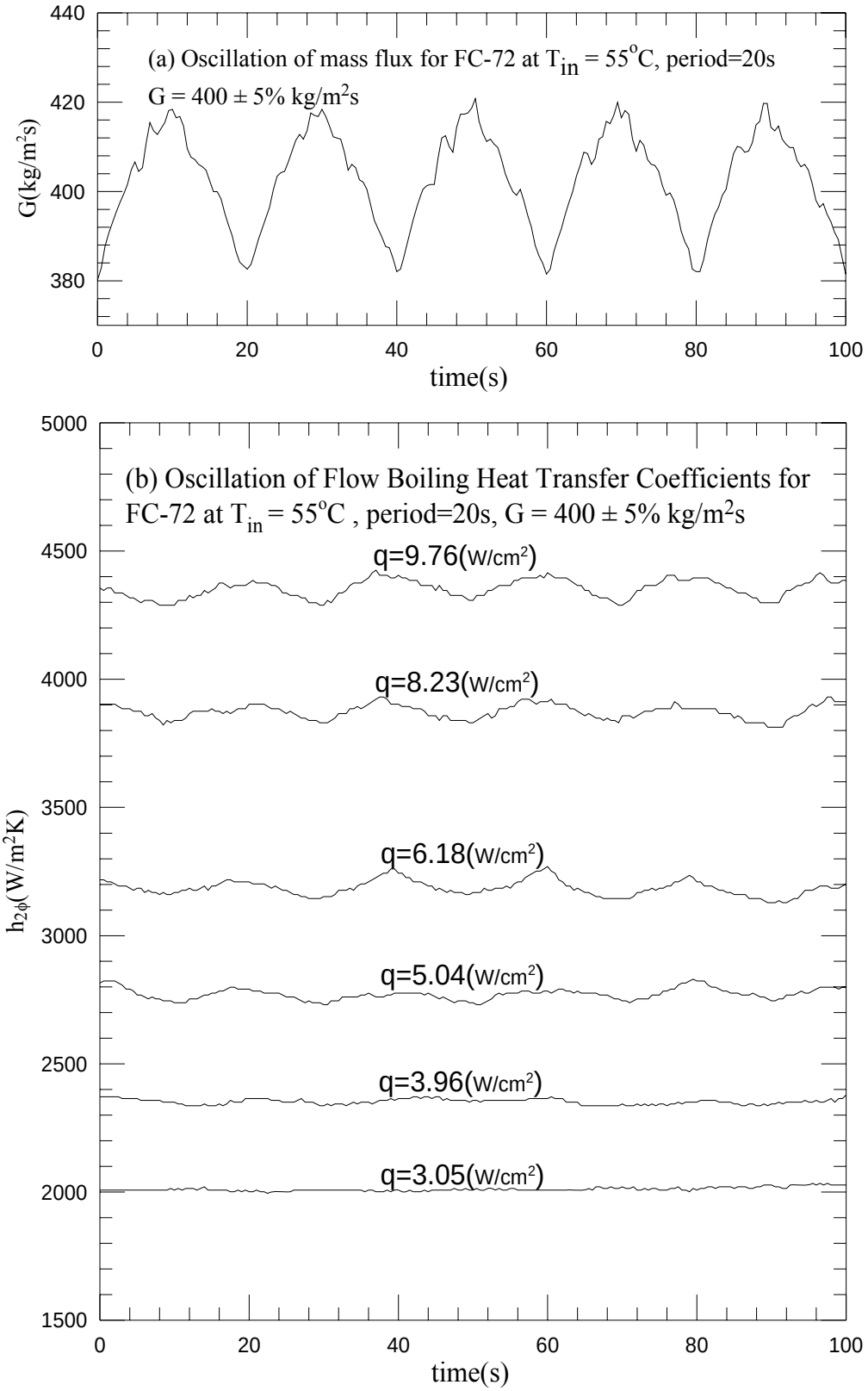

Fig. 4.22 Time variations of (a) imposed coolant mass flux and (b) flow boiling heat transfer coefficients in transient oscillatory saturated flow boiling for various imposed heat fluxes for G=400± 5% kg/m^{2}s with t_p =20 sec.

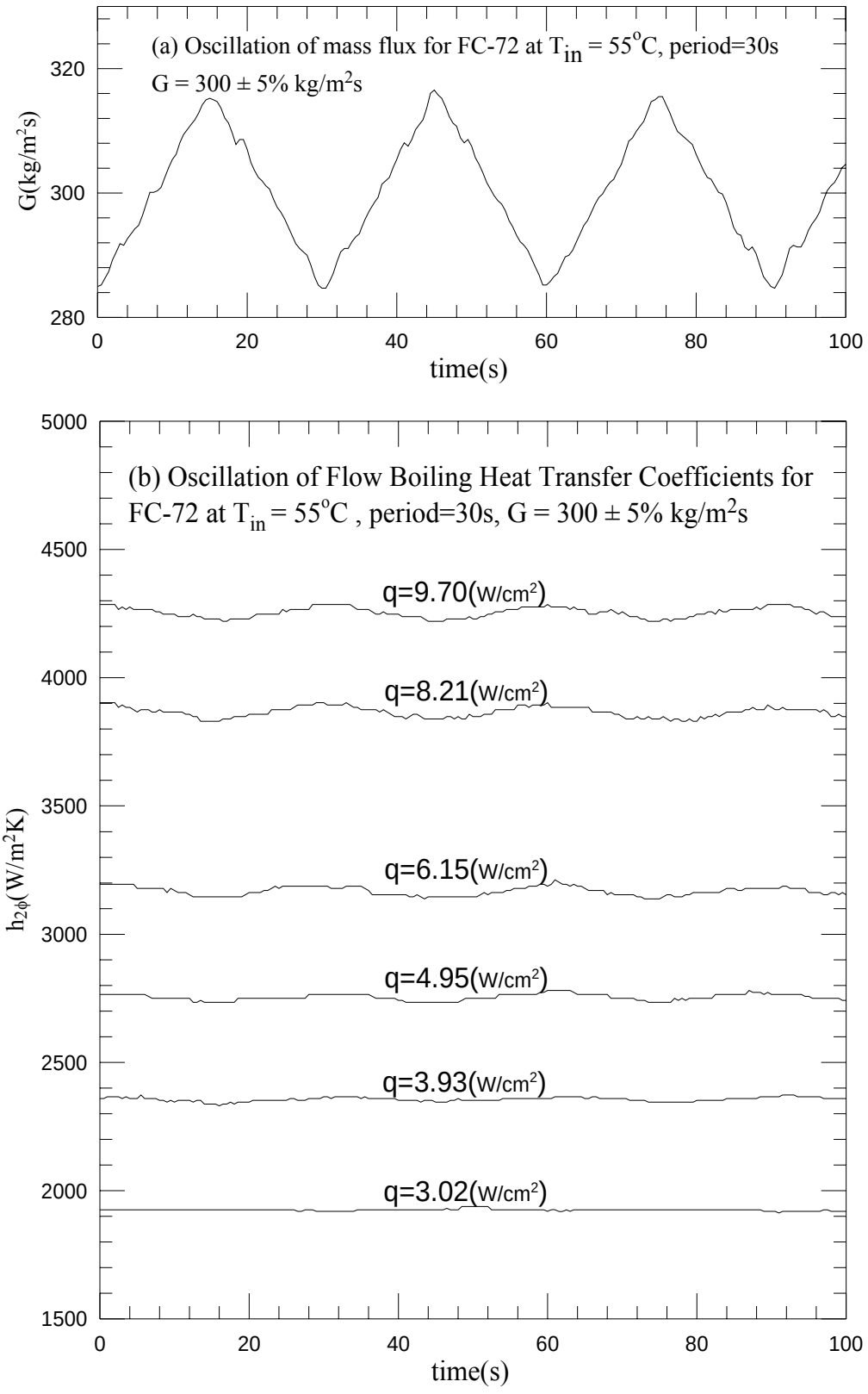

Fig. 4.23 Time variations of (a) imposed coolant mass flux and (b) flow boiling heat transfer coefficients in transient oscillatory saturated flow boiling for various imposed heat fluxes for G=300± 5% kg/m^{2}s with t_p =30 sec.

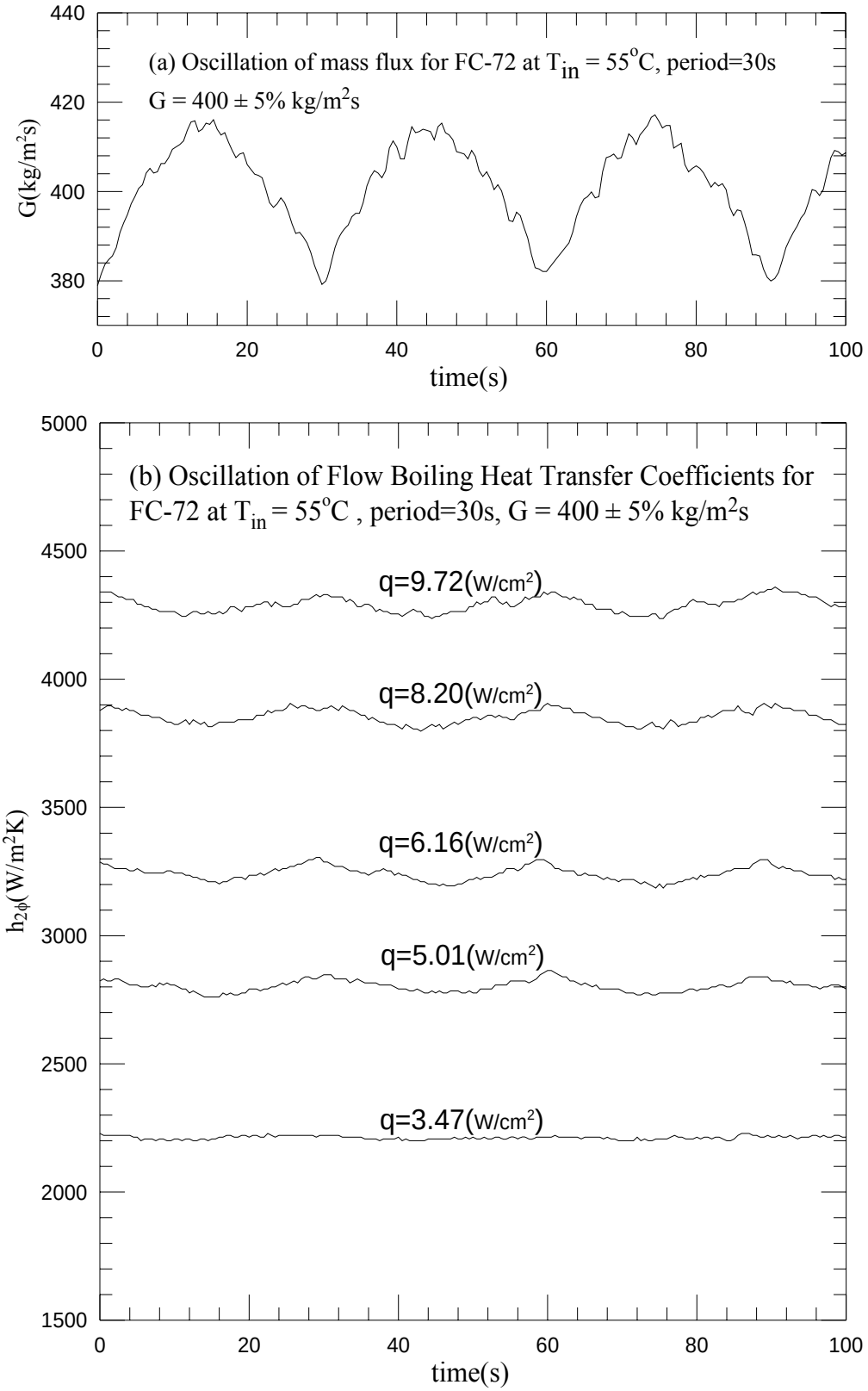

Fig. 4.24 Time variations of (a) imposed coolant mass flux and (b) flow boiling heat transfer coefficients in transient oscillatory saturated flow boiling for various imposed heat fluxes for G=400± 5% kg/m^{2}s with t_p =30 sec.

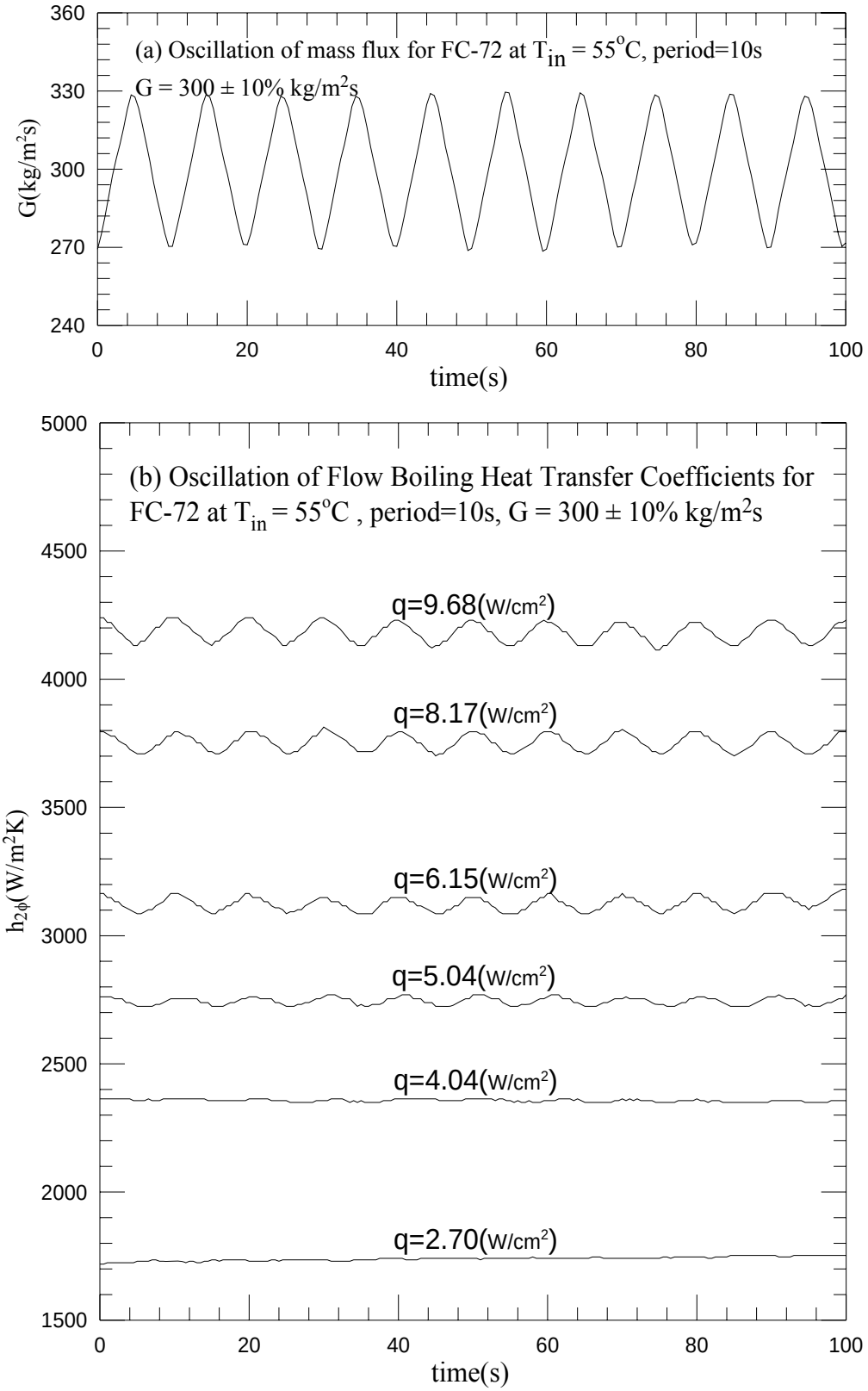

Fig. 4.25 Time variations of (a) imposed coolant mass flux and (b) flow boiling heat transfer coefficients in transient oscillatory saturated flow boiling for various imposed heat fluxes for G=300± 10% kg/m^{2}s with t_p =10 sec.

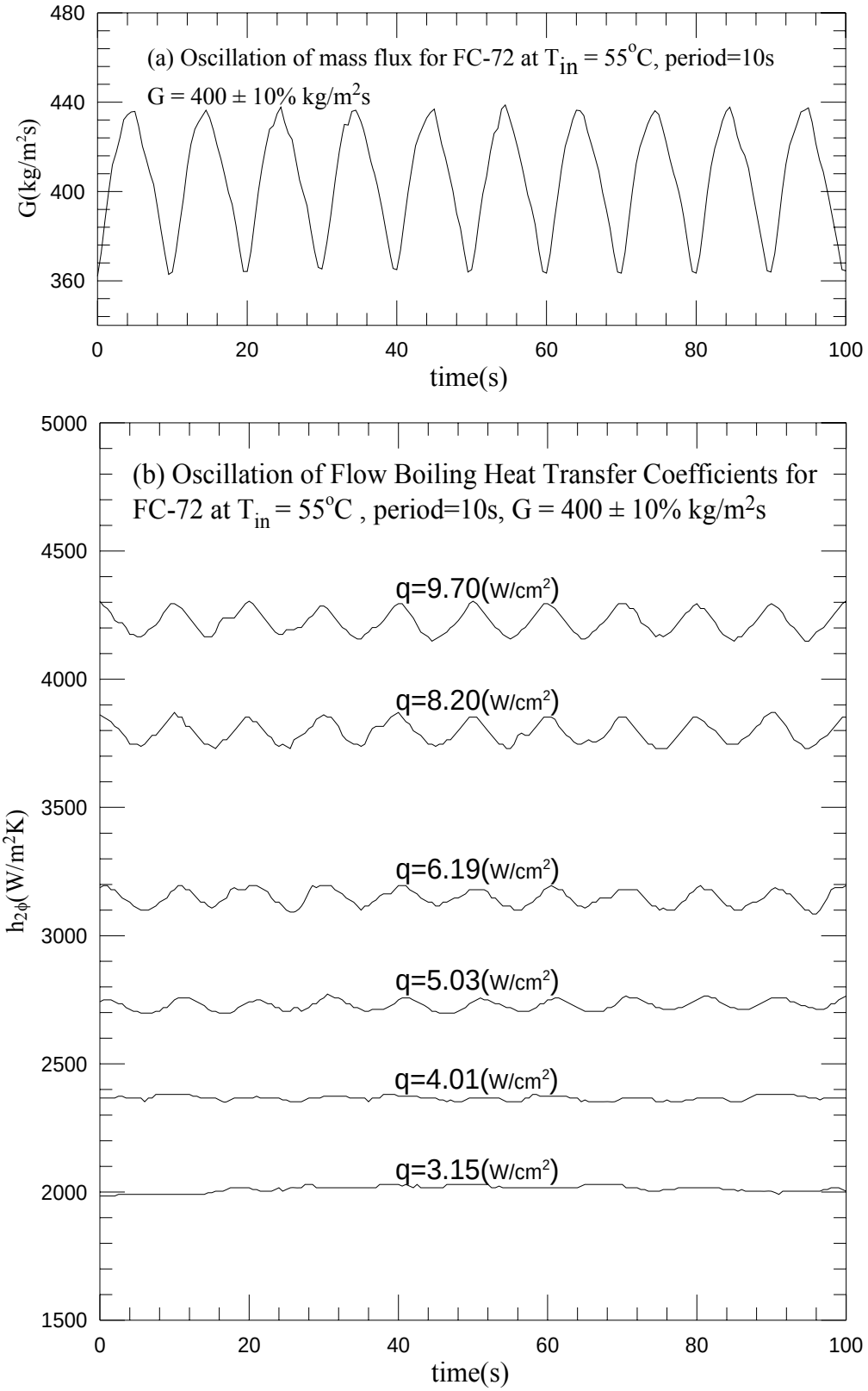

Fig. 4.26 Time variations of (a) imposed coolant mass flux and (b) flow boiling heat transfer coefficients in transient oscillatory saturated flow boiling for various imposed heat fluxes for G=400± 10% kg/m^{2}s with t_p =10 sec.

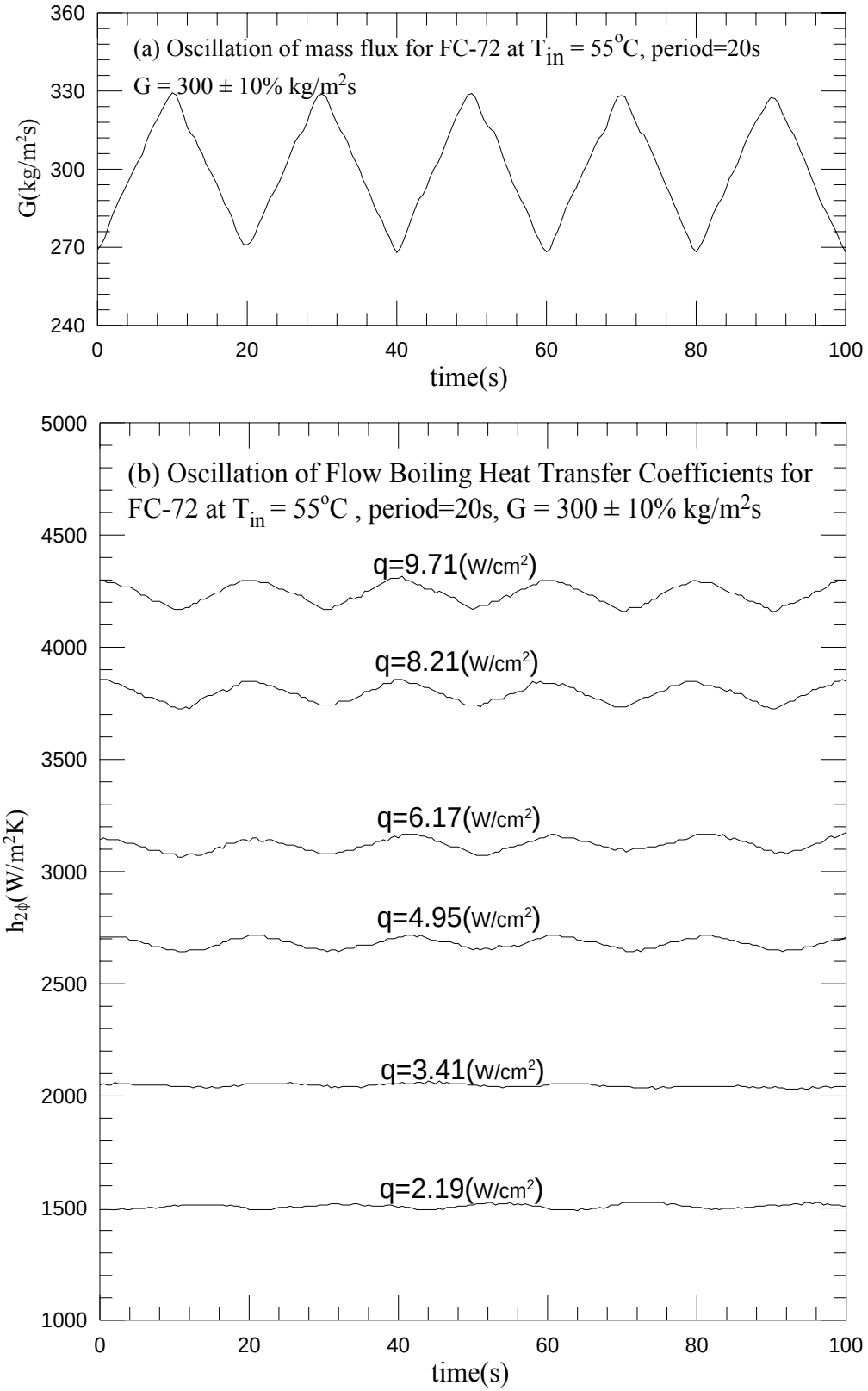

Fig. 4.27 Time variations of (a) imposed coolant mass flux and (b) flow boiling heat transfer coefficients in transient oscillatory saturated flow boiling for various imposed heat fluxes for G=300± 10% kg/m^{2}s with t_p =20 sec.

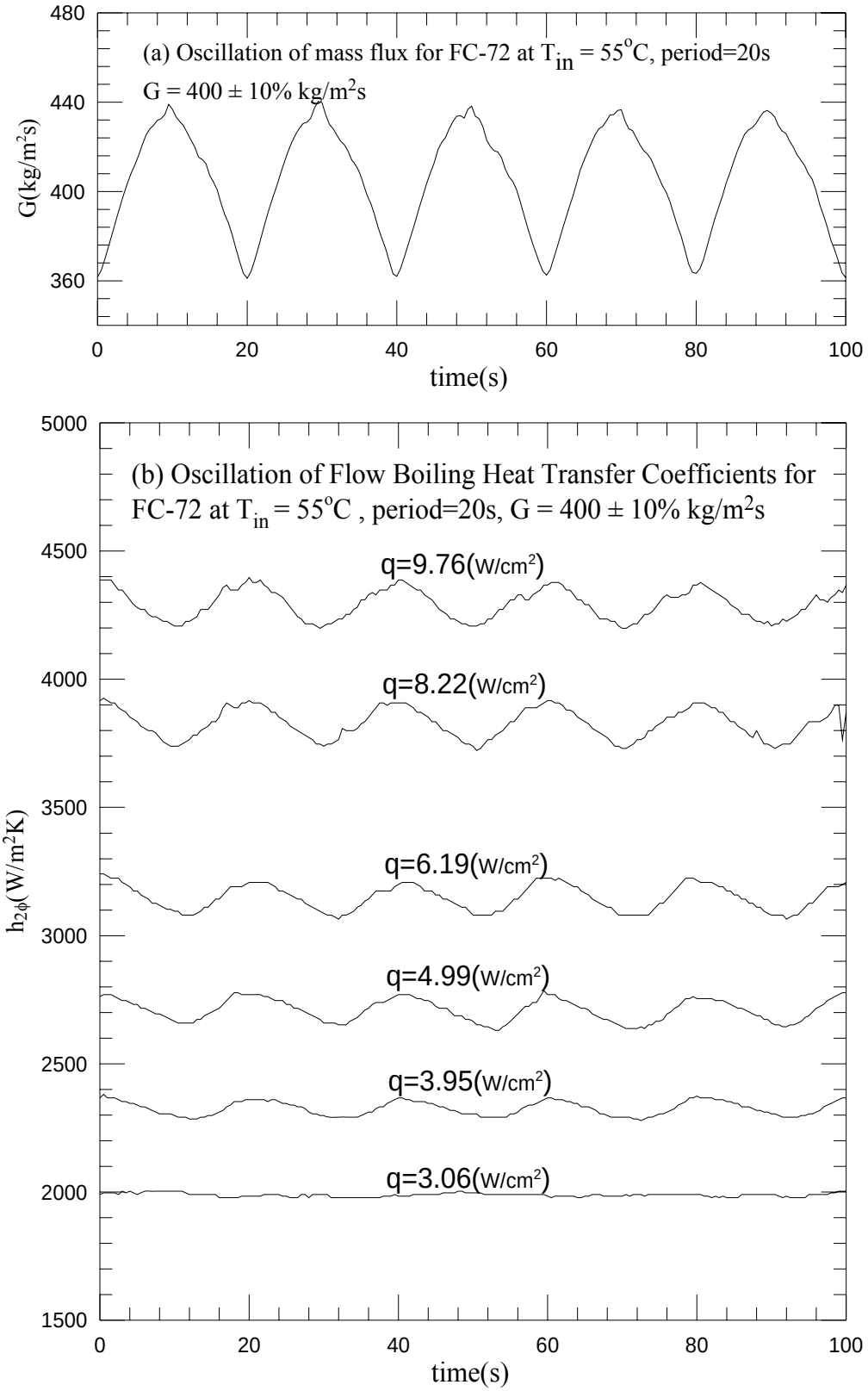

Fig. 4.28 Time variations of (a) imposed coolant mass flux and (b) flow boiling heat transfer coefficients in transient oscillatory saturated flow boiling for various imposed heat fluxes for G=400± 10% kg/m^{2}s with t_p =20 sec.

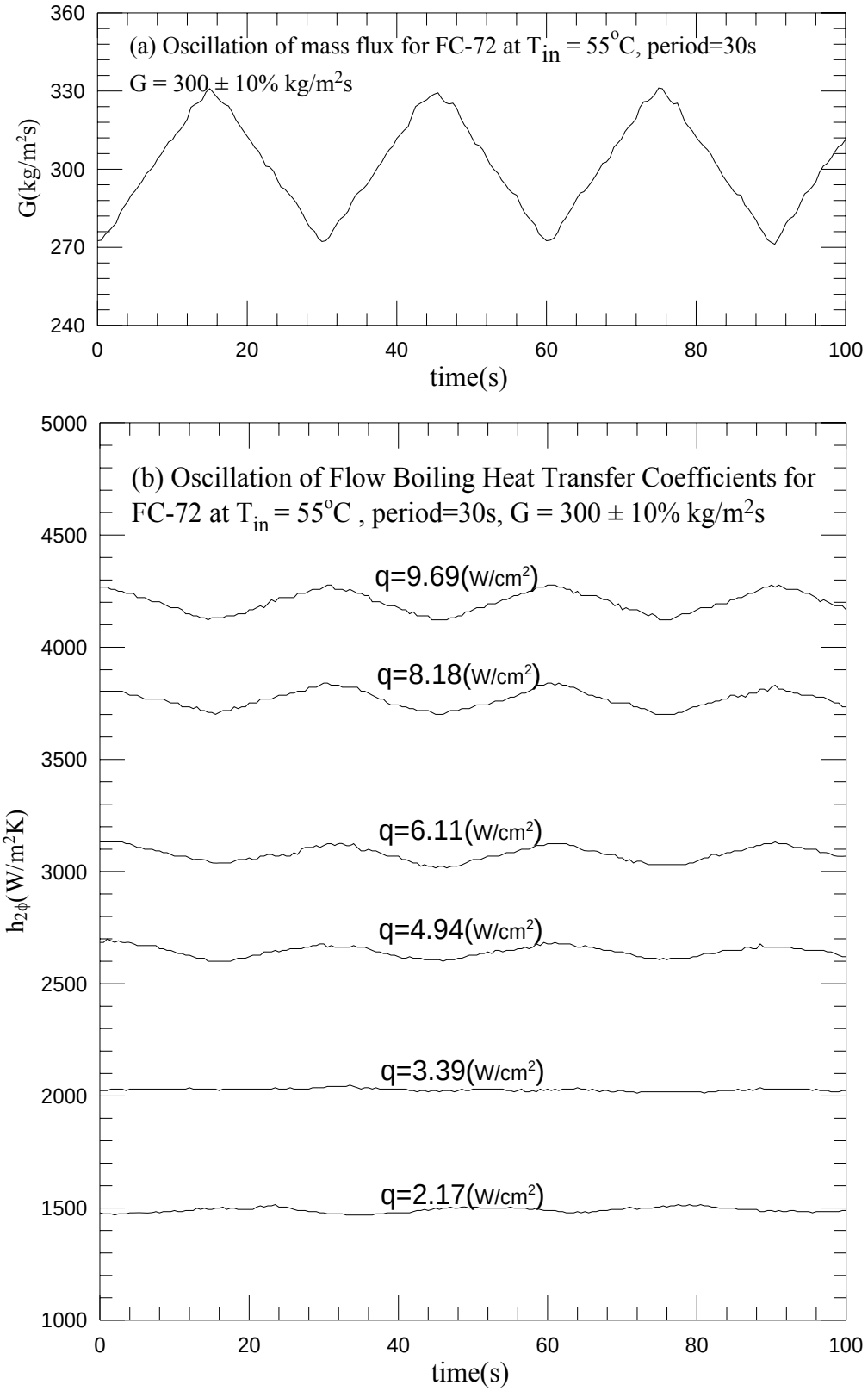

Fig. 4.29 Time variations of (a) imposed coolant mass flux and (b) flow boiling heat transfer coefficients in transient oscillatory saturated flow boiling for various imposed heat fluxes for G=300± 10% kg/m^{2}s with t_p =30 sec.

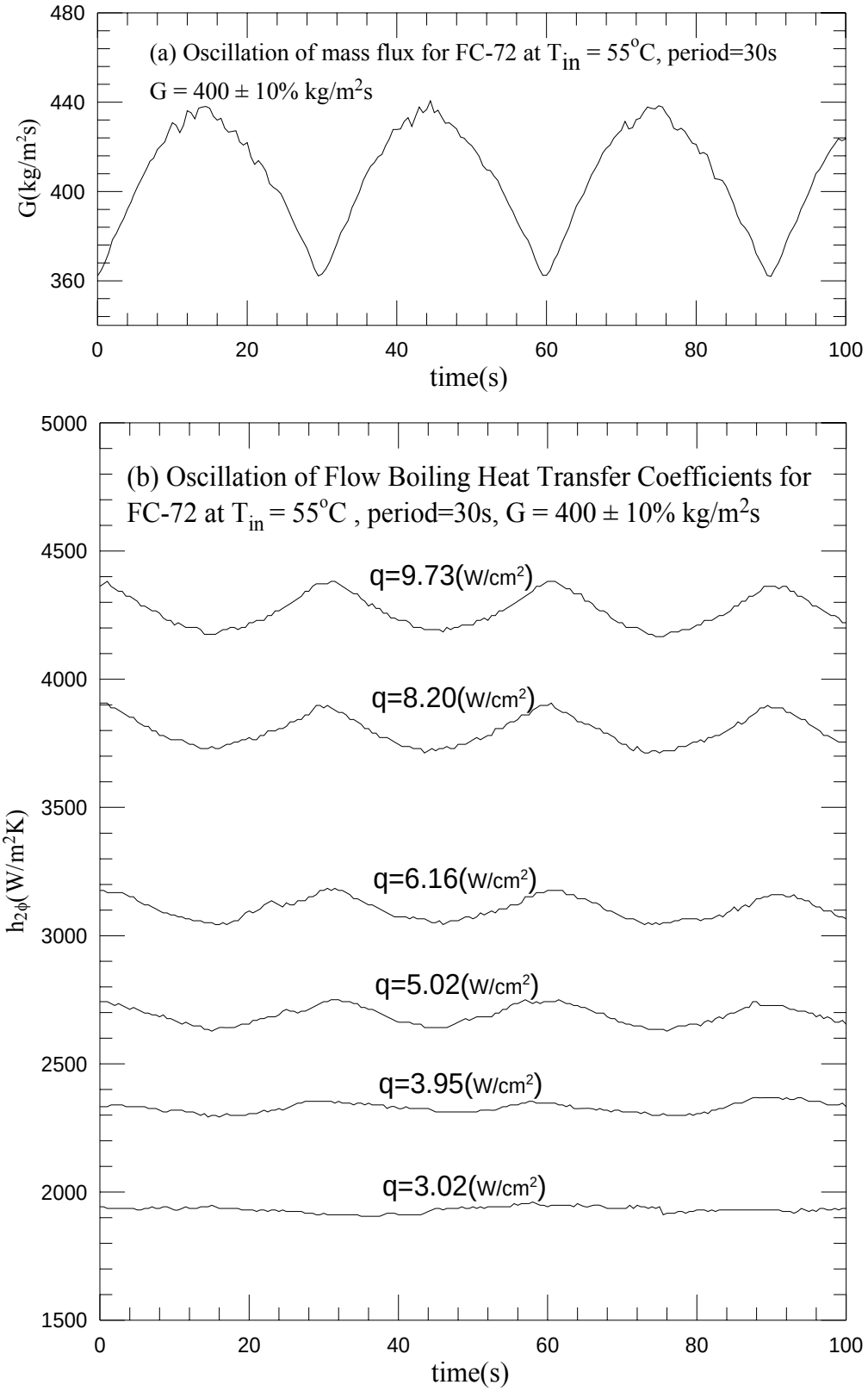

Fig. 4.30 Time variations of (a) imposed coolant mass flux and (b) flow boiling heat transfer coefficients in transient oscillatory saturated flow boiling for various imposed heat fluxes for G=400± 10% kg/m^{2}s with t_p =30 sec.

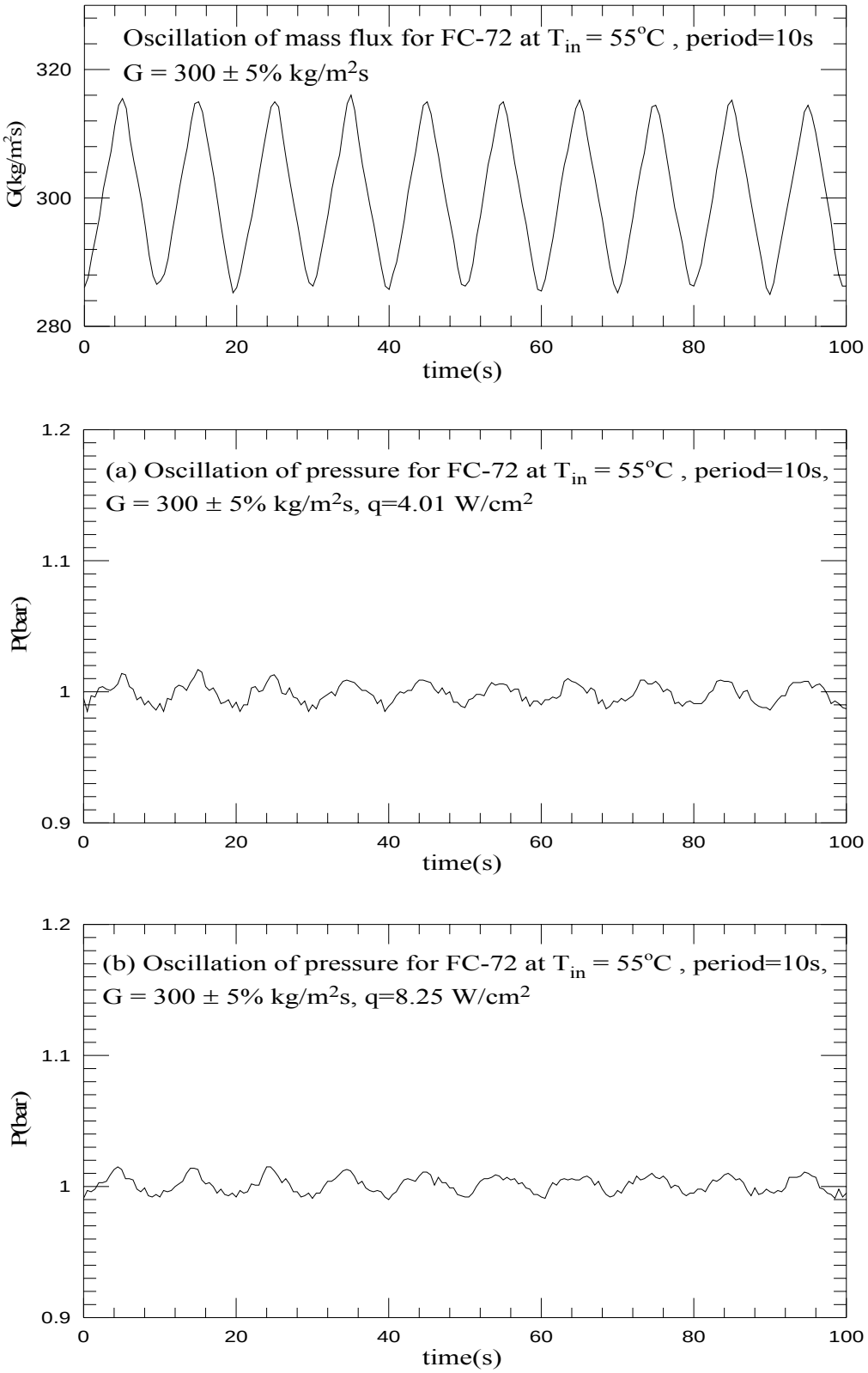

Fig.4.31 Time variations of coolant mass flux and inlet pressure in transient oscillatory saturated flow boiling for various imposed heat fluxes at (a) q=4.01 W/cm^2 and (b) q=8.25 W/cm^2 for G=300±5% kg/m^{2}S with t_p=10 sec.

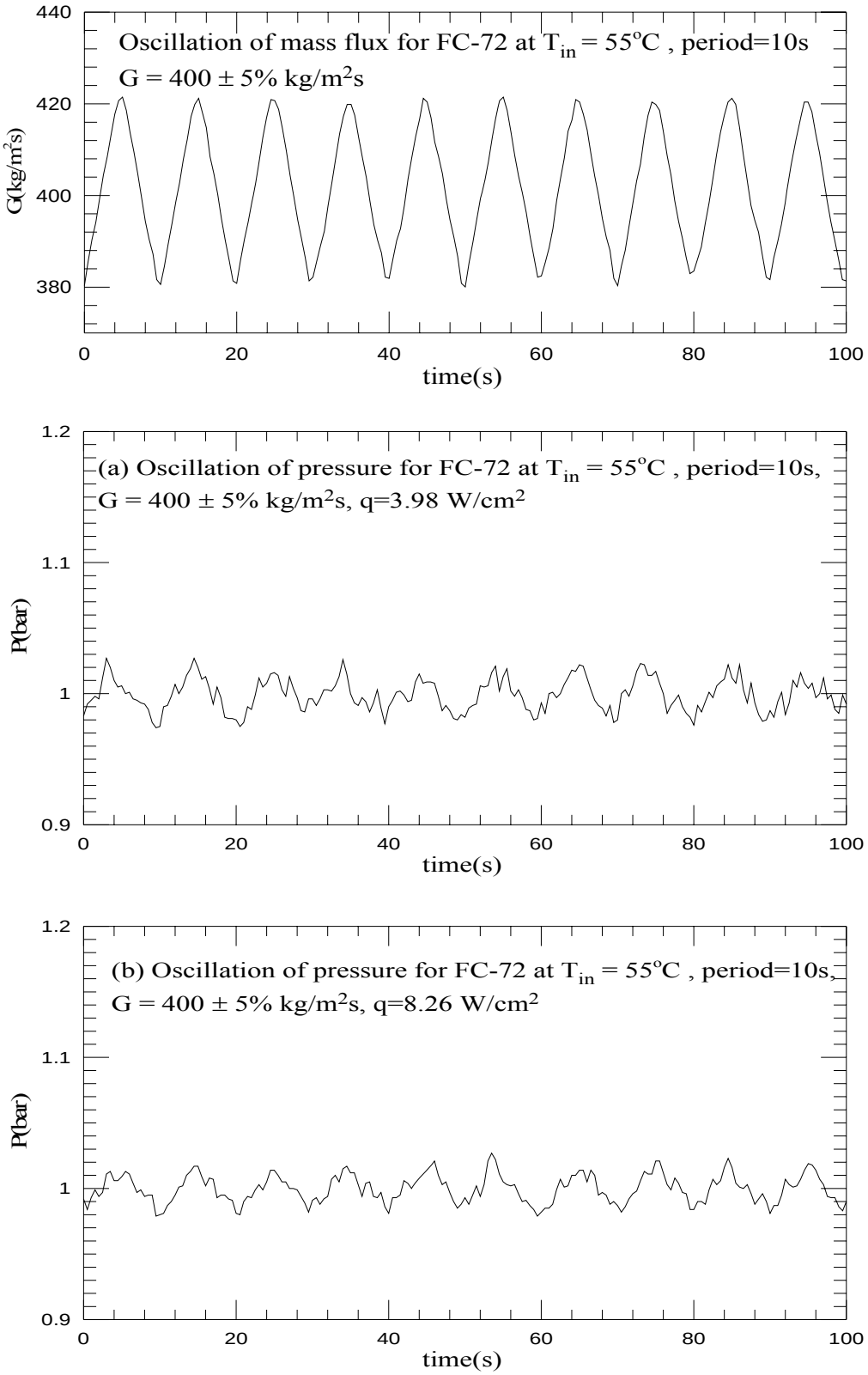

Fig.4.32 Time variations of coolant mass flux and inlet pressure in transient oscillatory saturated flow boiling for various imposed heat fluxes at (a) q=3.98 W/cm^2 and (b) q=8.26 W/cm^2 for G=400±5% kg/m^{2}S with t_p =10 sec.

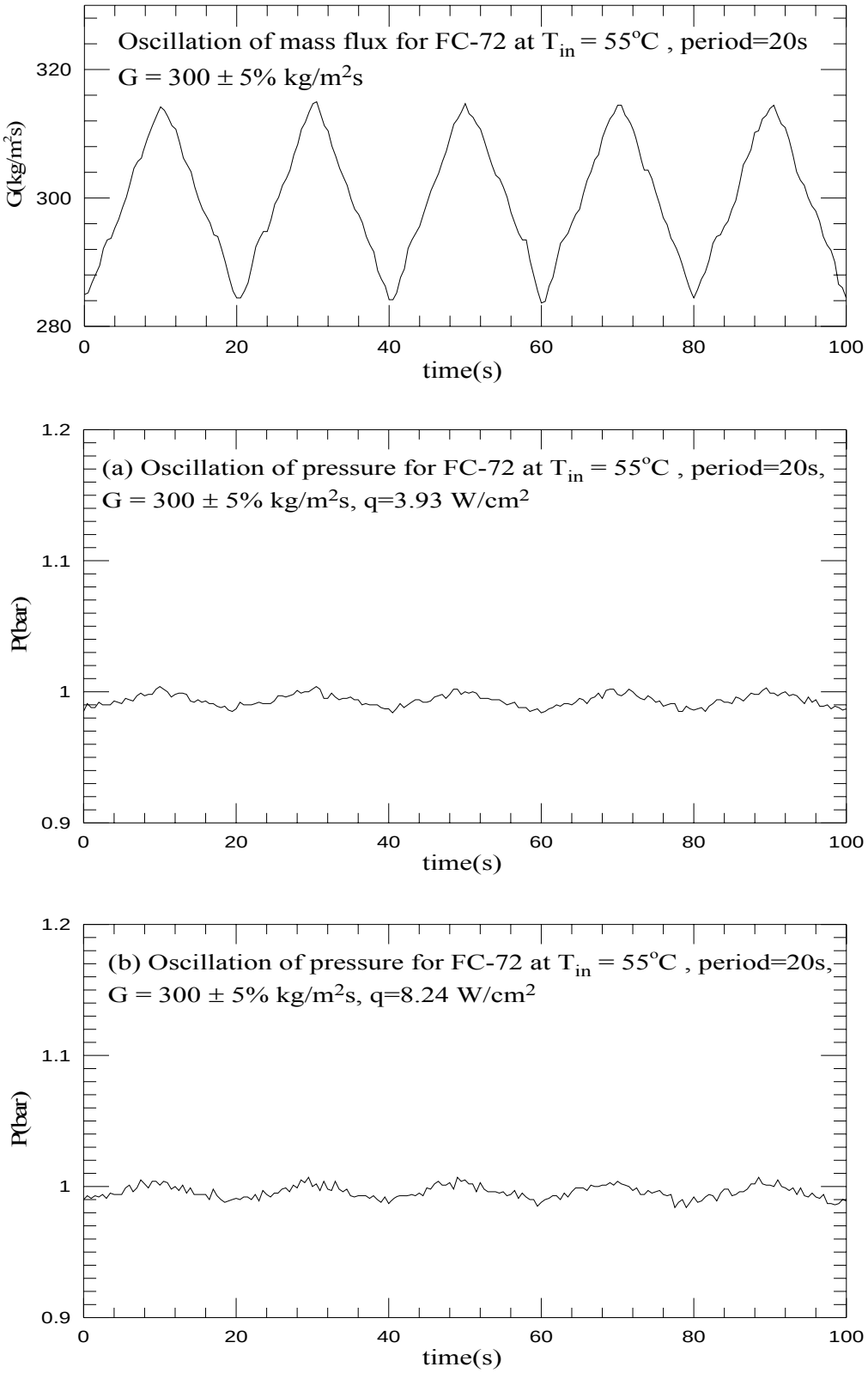

Fig.4.33 Time variations of coolant mass flux and inlet pressure in transient oscillatory saturated flow boiling for various imposed heat fluxes at (a) q=3.93 W/cm^2 and (b) q=8.24 W/cm^2 for G=300±5% kg/m^{2}S with t_p =20 sec.

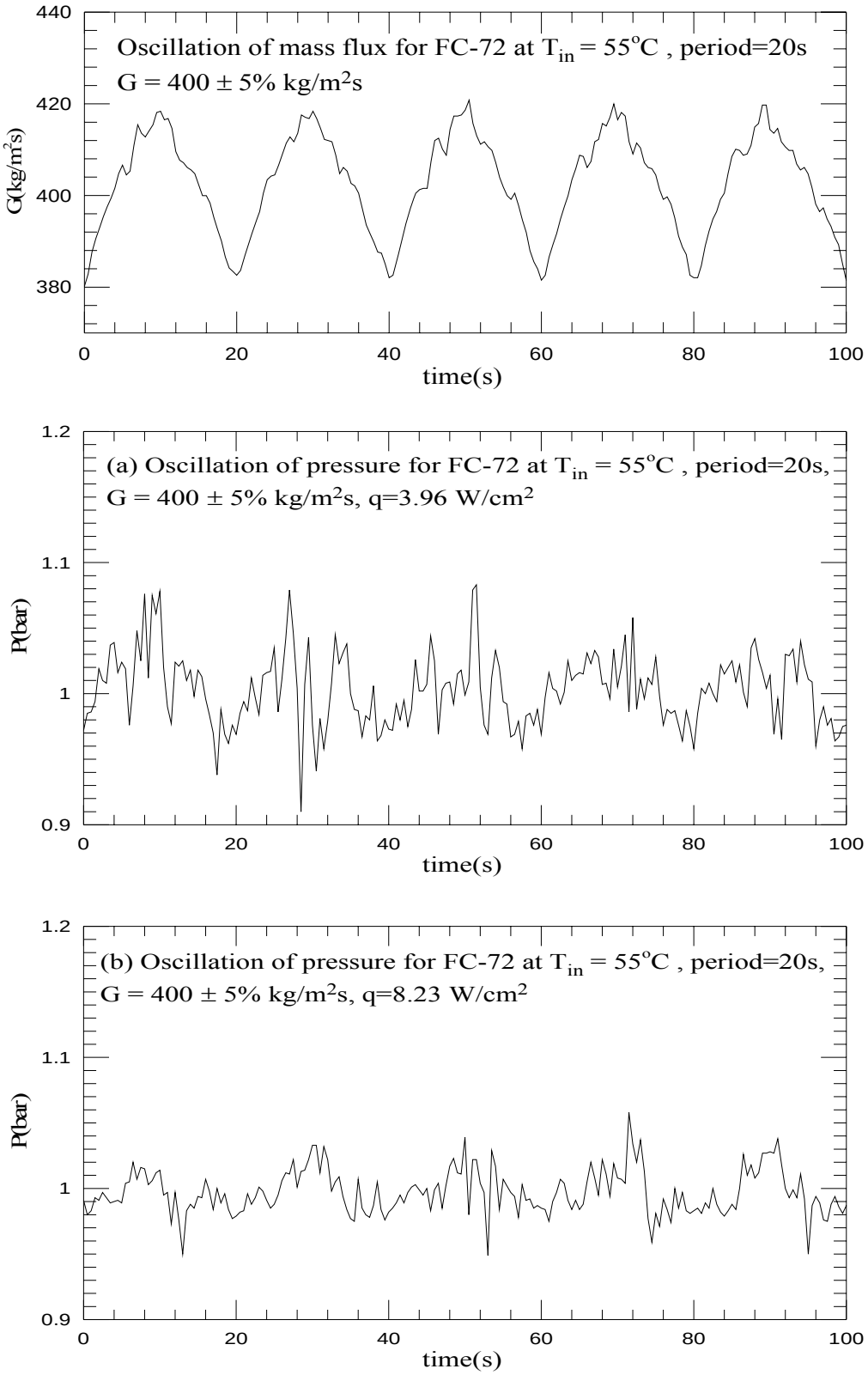

Fig.4.34 Time variations of coolant mass flux and inlet pressure in transient oscillatory saturated flow boiling for various imposed heat fluxes at (a) q=3.96 W/cm^2 and (b) q=8.23 W/cm^2 for G=400±5% kg/m^{2}S with t_p =20 sec.

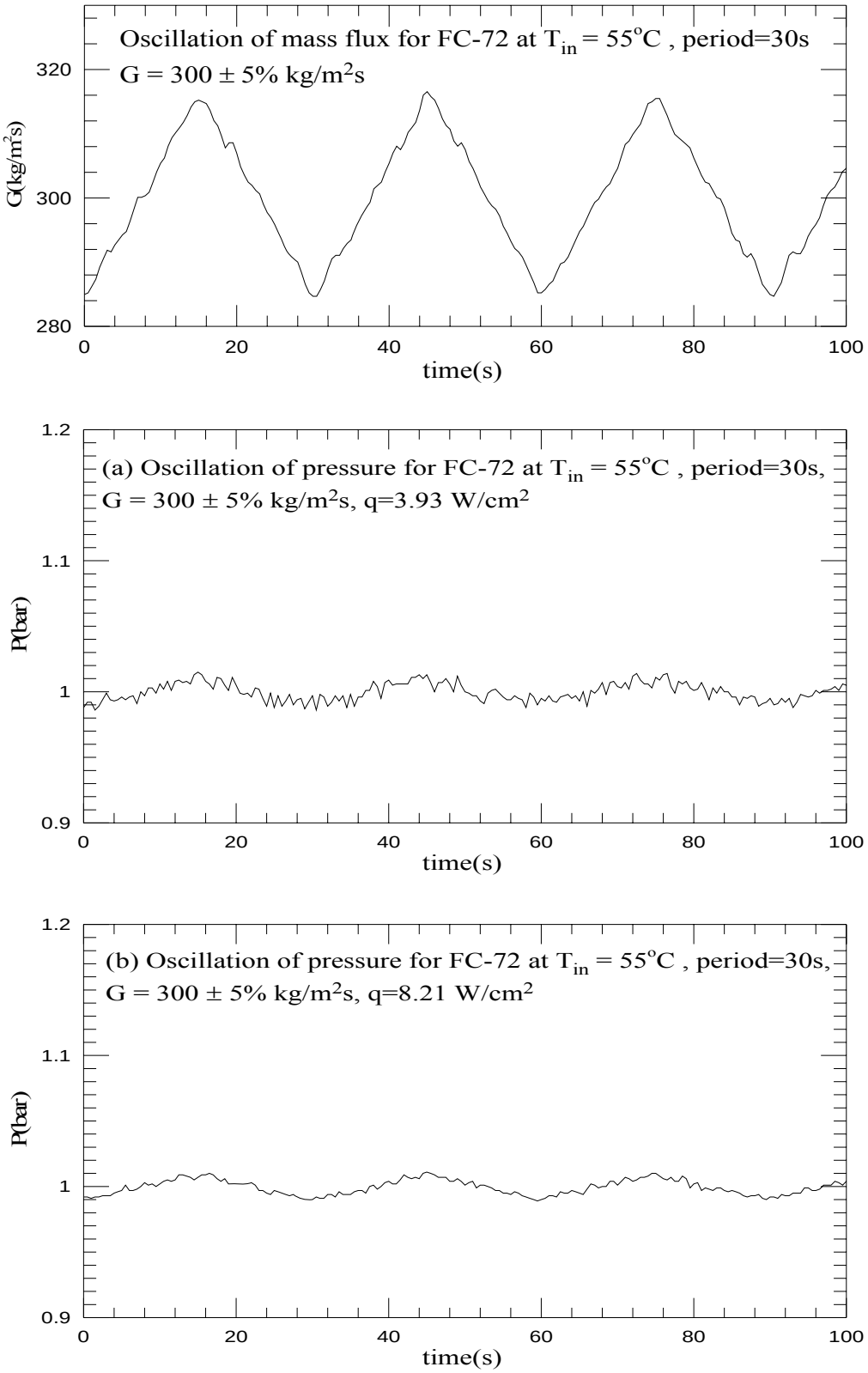

Fig.4.35 Time variations of coolant mass flux and inlet pressure in transient oscillatory saturated flow boiling for various imposed heat fluxes at (a) q=3.93 W/cm^2 and (b) q=8.21 W/cm^2 for G=300±5% kg/m^{2}S with t_p =30 sec.

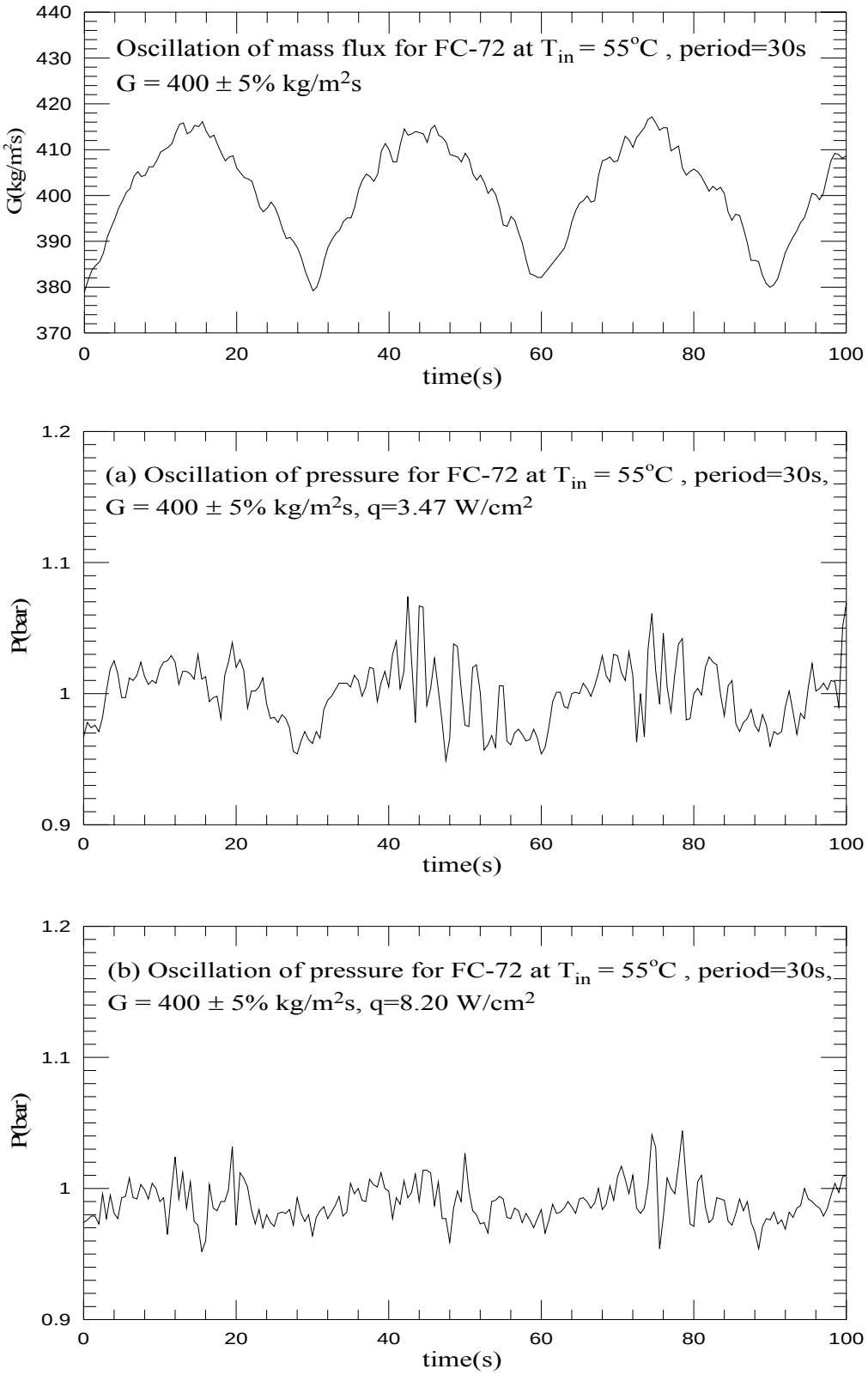

Fig.4.36 Time variations of coolant mass flux and inlet pressure in transient oscillatory saturated flow boiling for various imposed heat fluxes at (a) q=3.47 W/cm^2 and (b) q=8.20 W/cm^2 for G=400±5% kg/m^{2}S with t_p =30 sec.

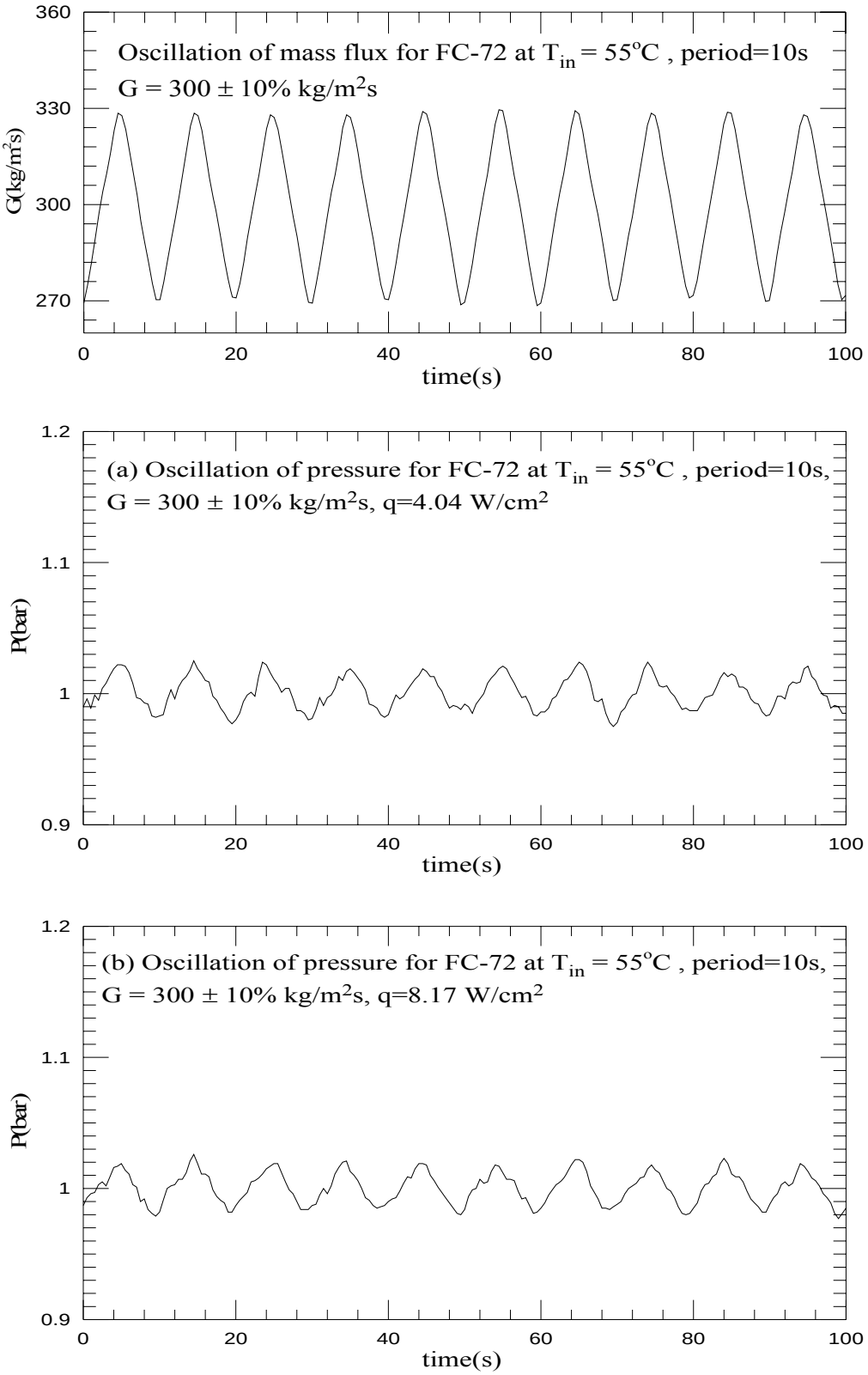

Fig.4.37 Time variations of coolant mass flux and inlet pressure in transient oscillatory saturated flow boiling for various imposed heat fluxes at (a) q=4.04 W/cm^2 and (b) q=8.17 W/cm^2 for G=300±10% kg/m^{2}S with t_p=10 sec.

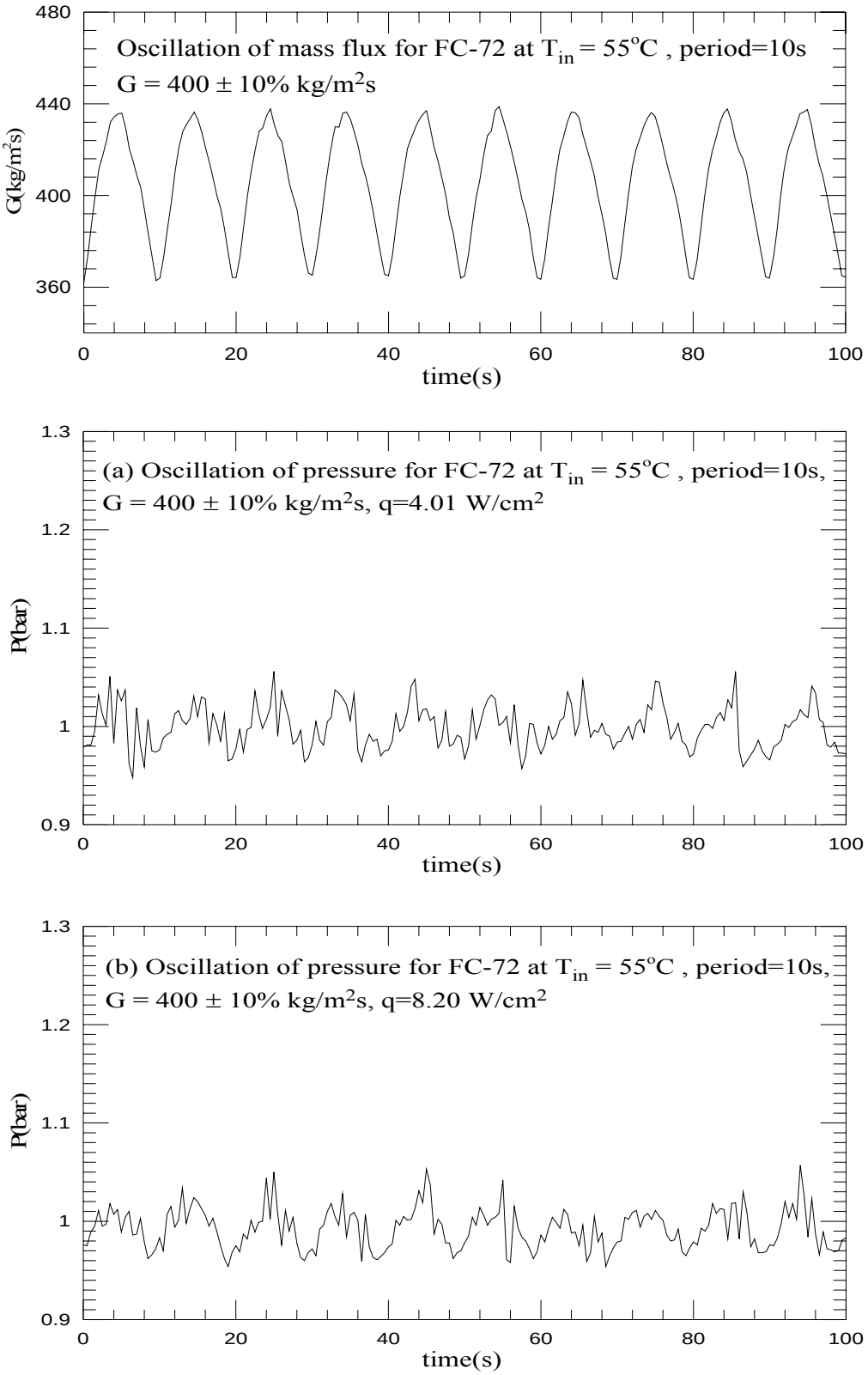

Fig.4.38 Time variations of coolant mass flux and inlet pressure in transient oscillatory saturated flow boiling for various imposed heat fluxes at (a) q=4.01 W/cm^2 and (b) q=8.20 W/cm^2 for G=400±10% kg/m^{2}S with t_p=10 sec.

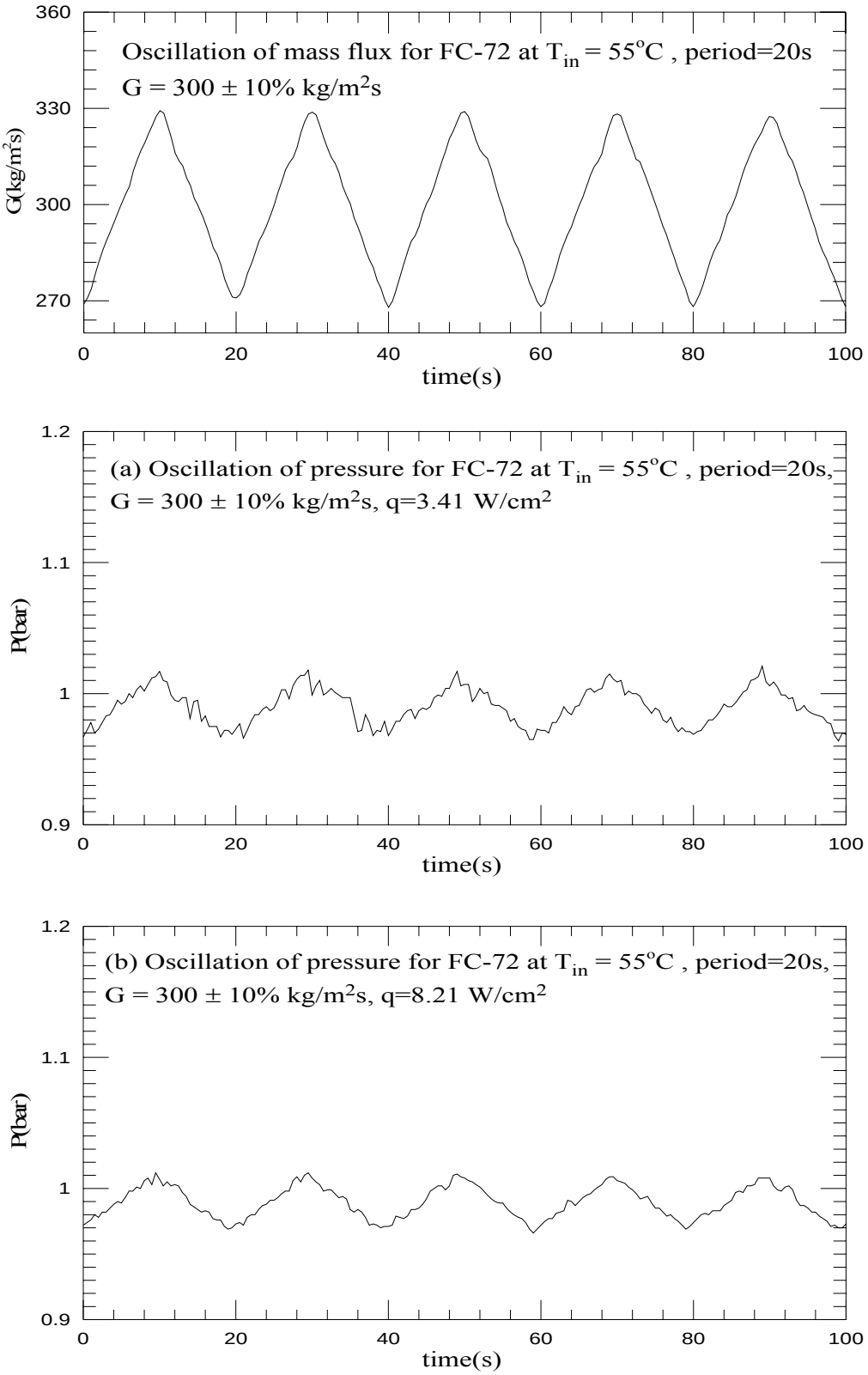

Fig.4.39 Time variations of coolant mass flux and inlet pressure in transient oscillatory saturated flow boiling for various imposed heat fluxes at (a) q=3.41 W/cm^2 and (b) q=8.21 W/cm^2 for G=300±10% kg/m^{2}S with t_p=20 sec.

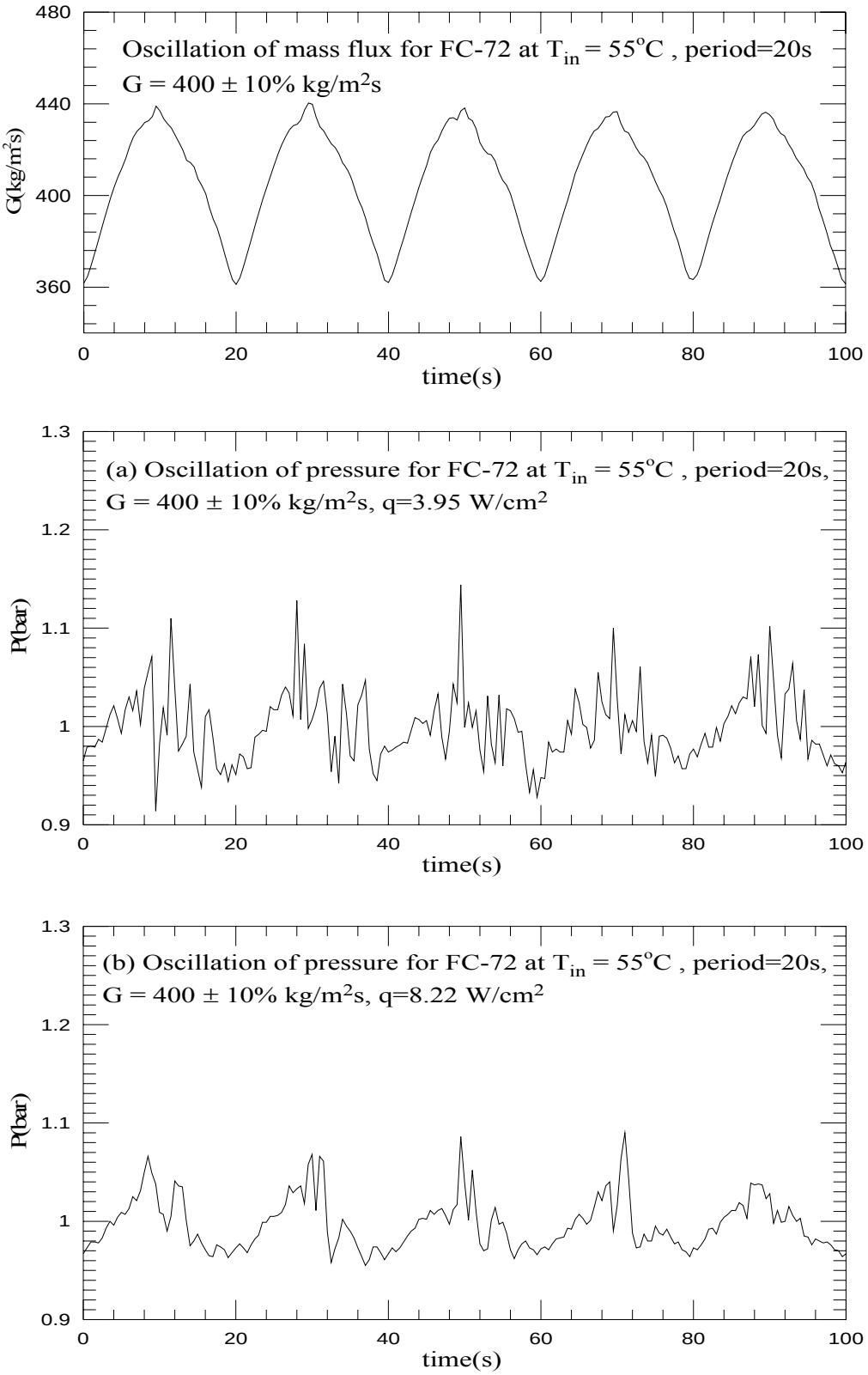

Fig.4.40 Time variations of coolant mass flux and inlet pressure in transient oscillatory saturated flow boiling for various imposed heat fluxes at (a) q=3.95 W/cm^2 and (b) q=8.22 W/cm^2 for G=400±10% kg/m^{2}S with t_p=20 sec.

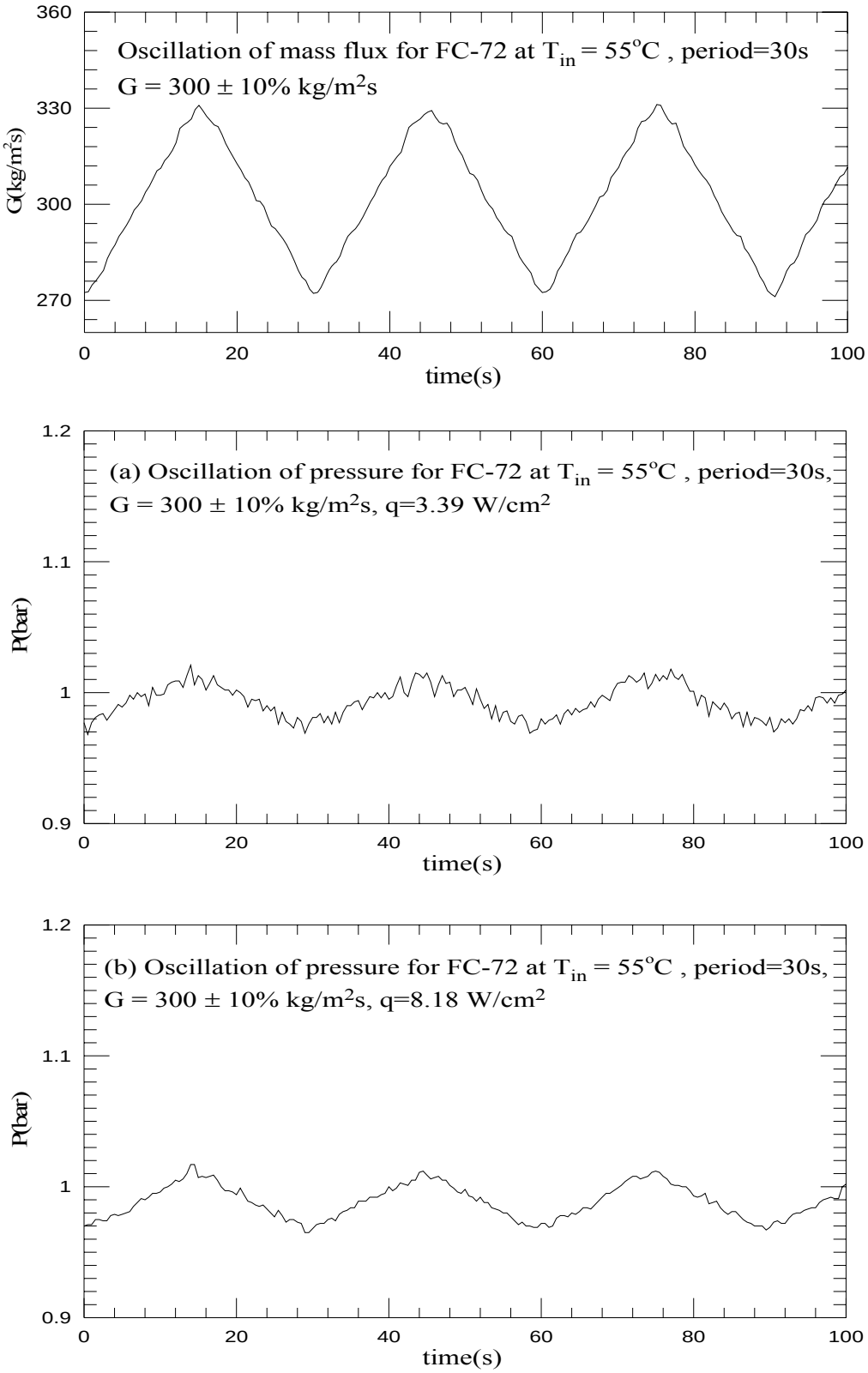

Fig.4.41 Time variations of coolant mass flux and inlet pressure in transient oscillatory saturated flow boiling for various imposed heat fluxes at (a) q=3.39 W/cm^2 and (b) q=8.18 W/cm^2 for G=300±10% kg/m^{2}S with t_p=30 sec.

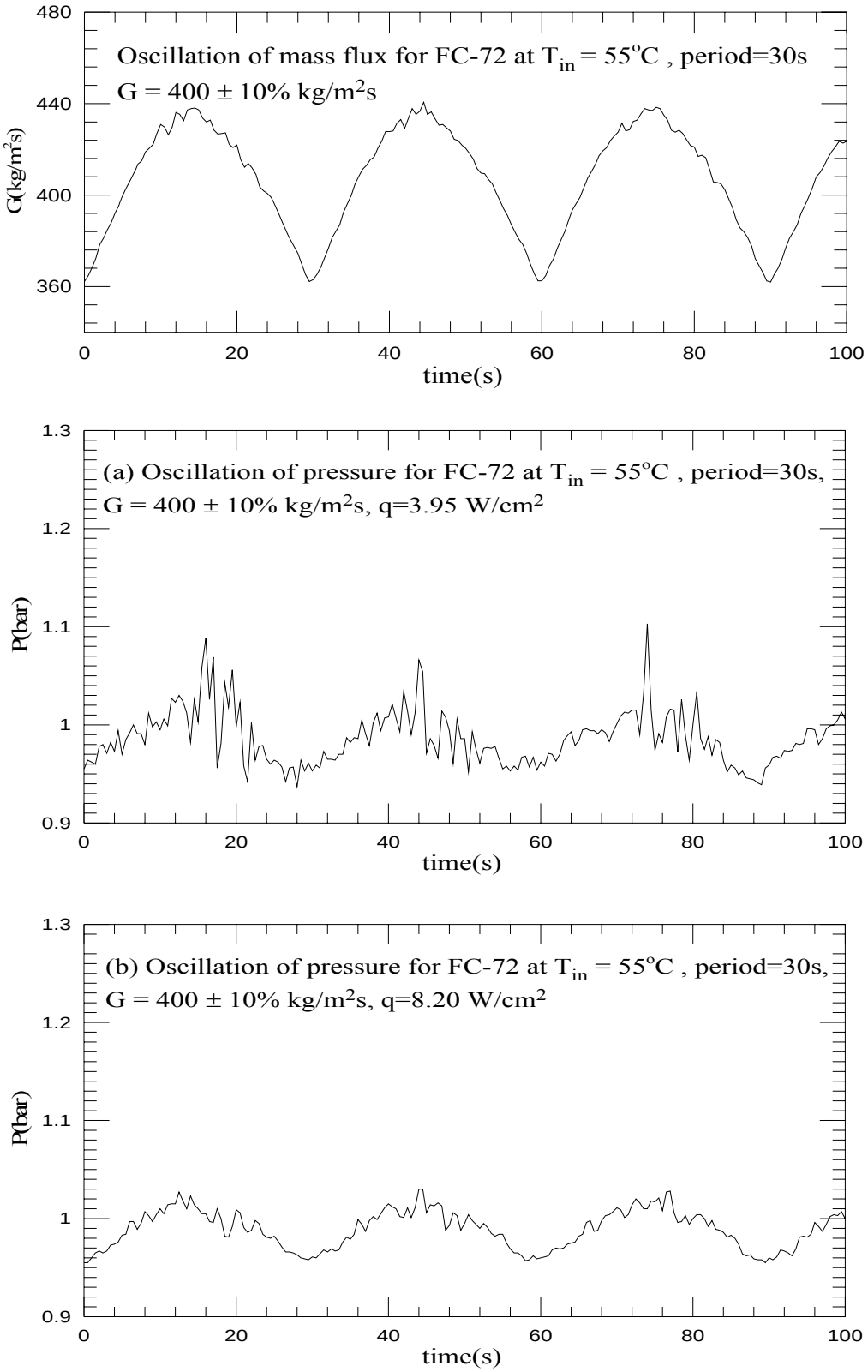

Fig.4.42 Time variations of coolant mass flux and inlet pressure in transient oscillatory saturated flow boiling for various imposed heat fluxes at (a) q=3.95 W/cm^2 and (b) q=8.20 W/cm^2 for G=400±10% kg/m^{2}S with t_p=30 sec.

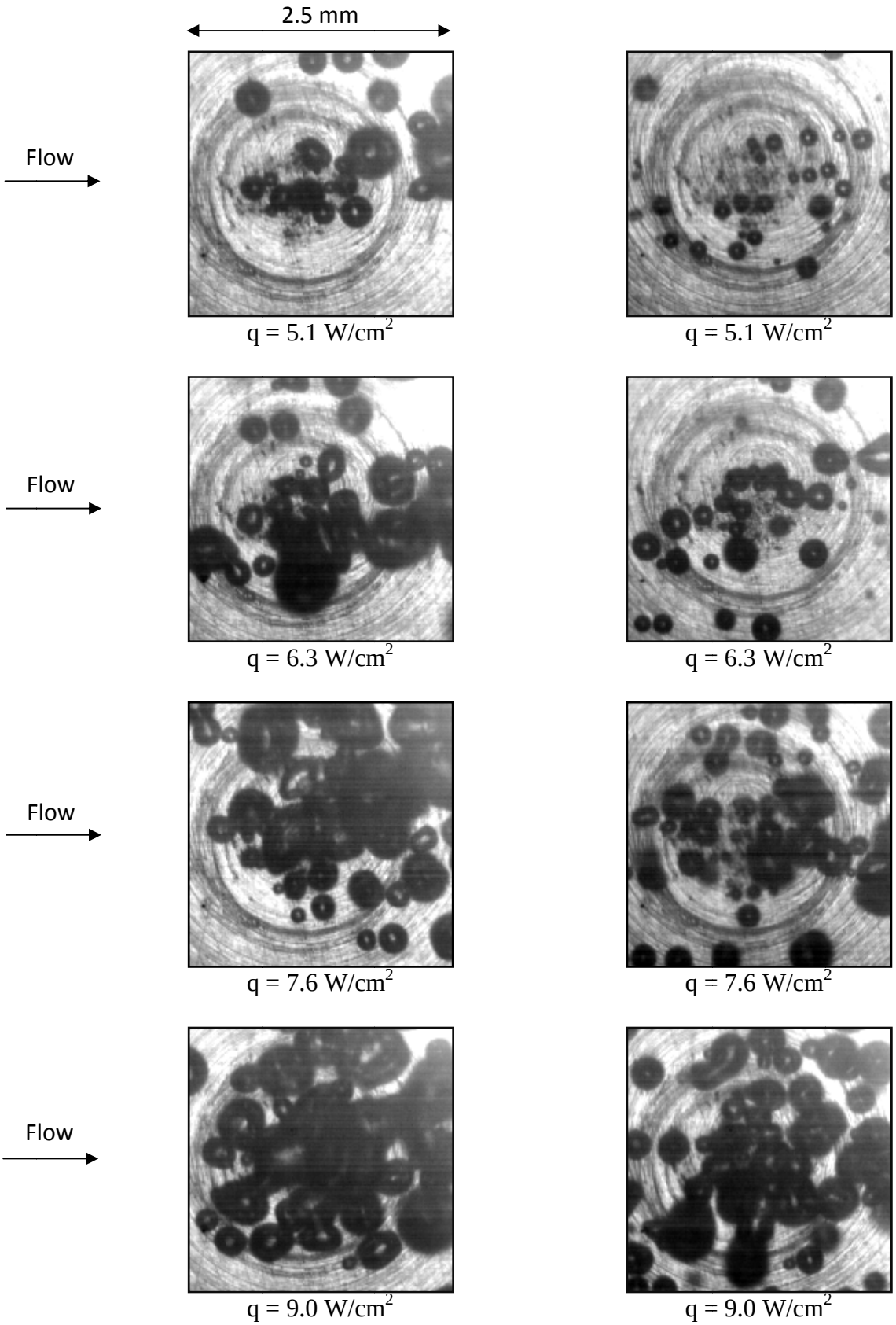

(a) G = 300 kg/m^{2}s (b) G = 400 kg/m^{2}s

Fig.4.43 Photos of stable saturated boiling flow at certain time instants for various imposed heat fluxes for (a) G =300 kg/m^{2}s and (b) G =400 kg/m^{2}s.

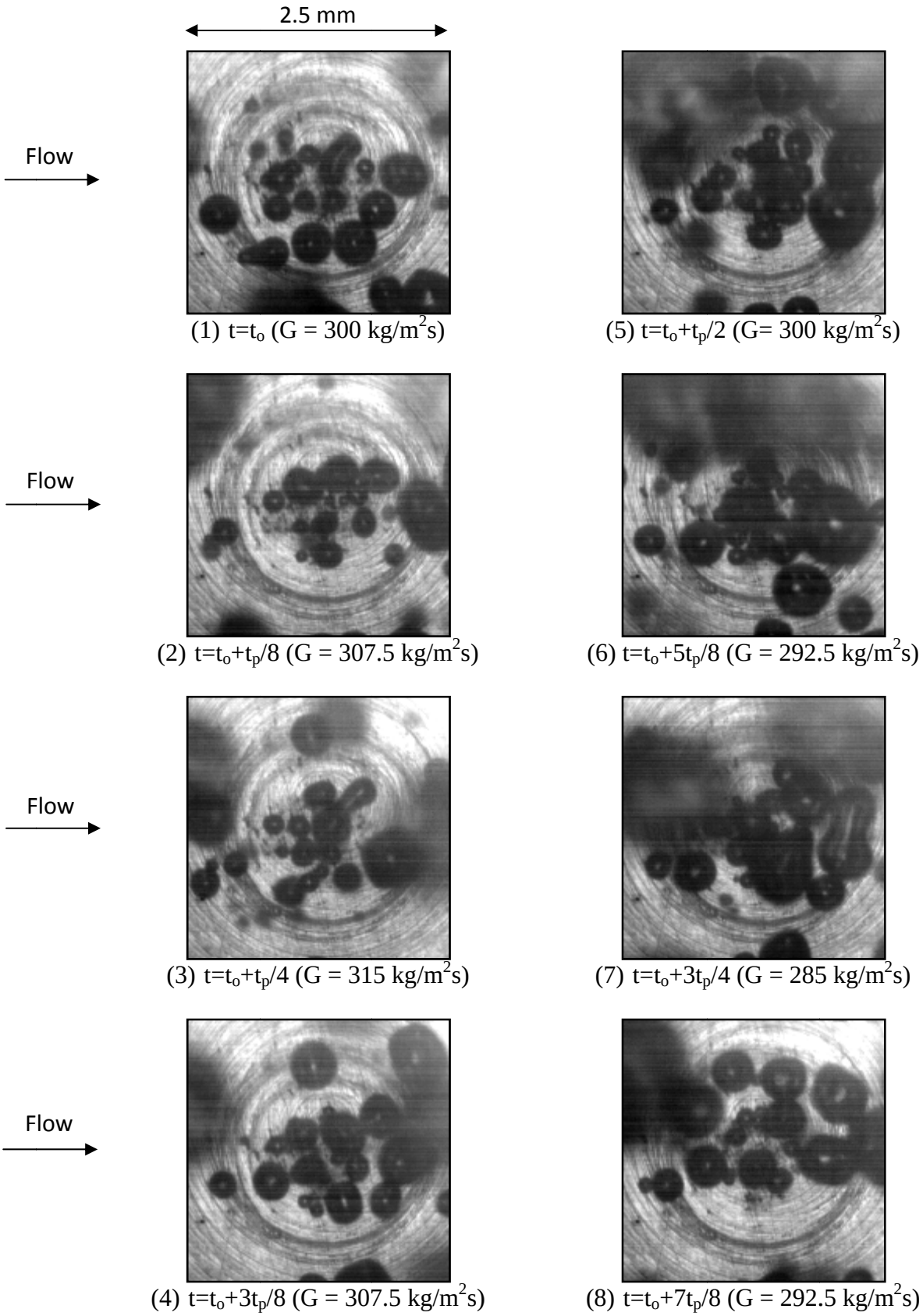

Fig.4.44 Photos of transient oscillatory saturated flow boiling flow at certain time instants for various imposed mass fluxes for q=6.2 W/cm^2 at G=300±5% kg/m^{2}s with oscillation t_p=10s.

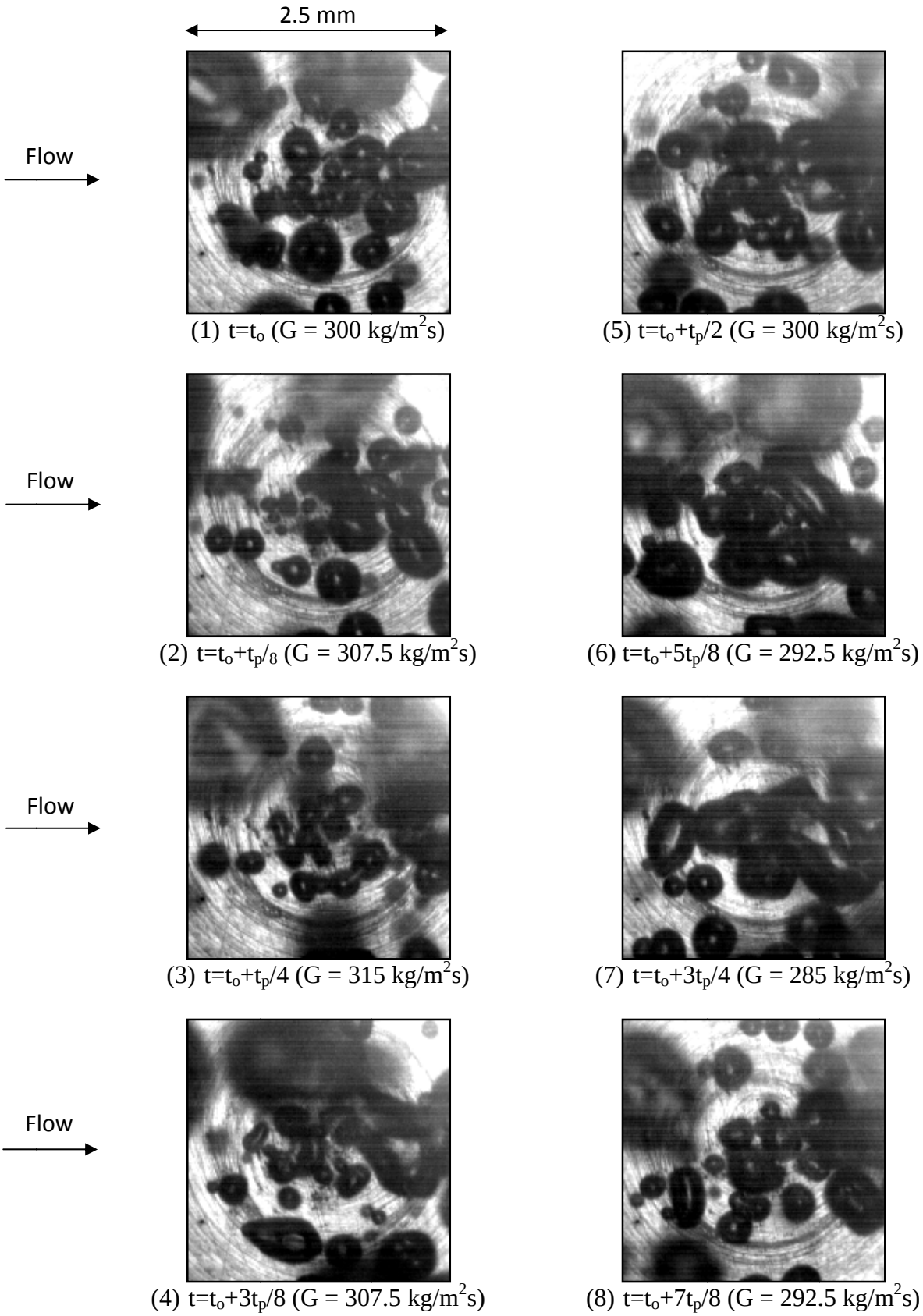

Fig.4.45 Photos of transient oscillatory saturated flow boiling flow at certain time instants for various imposed mass fluxes for q=7.5 W/cm^2 at G=300±5% kg/m^{2}s with oscillation t$_p$=10s.

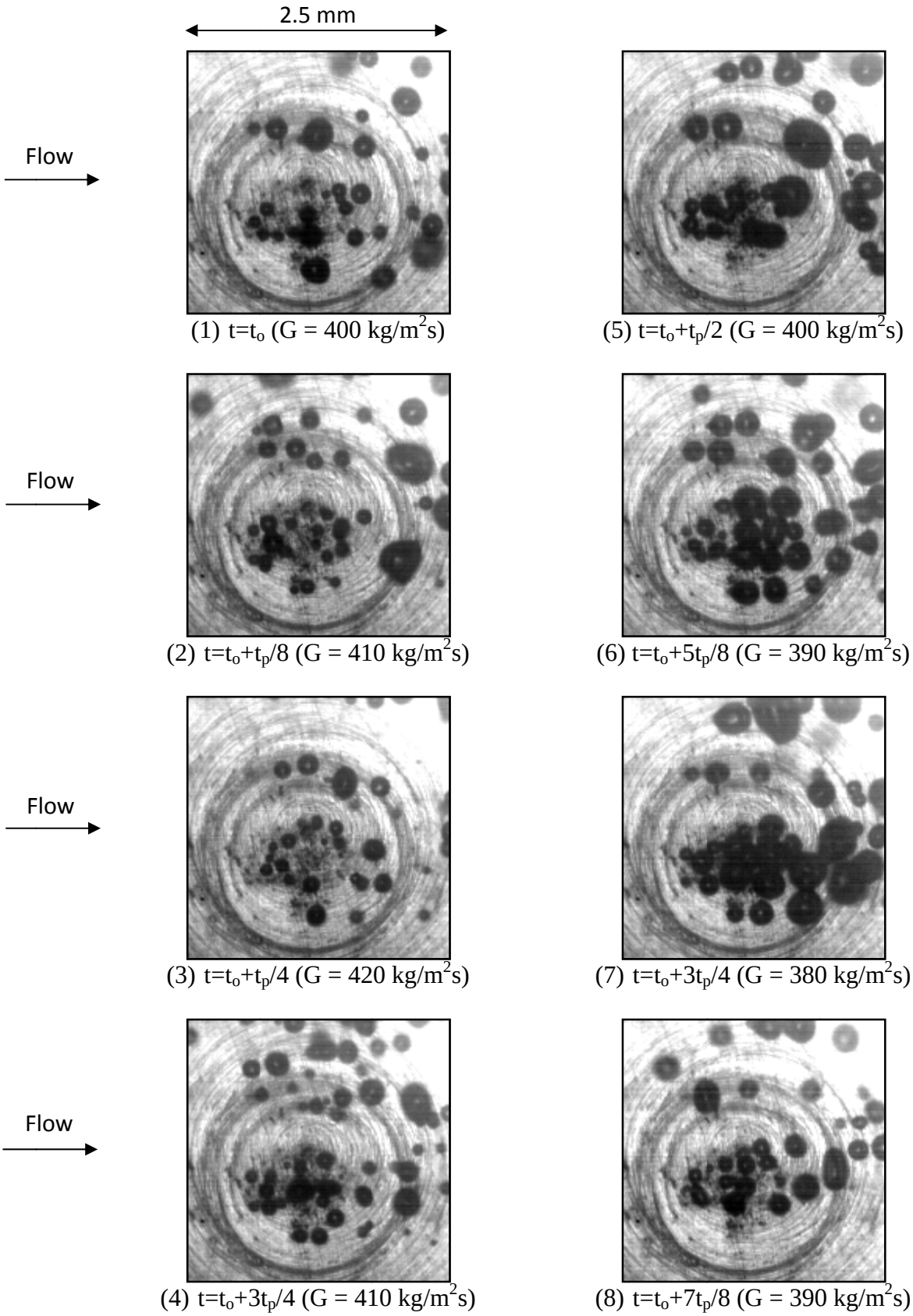

Fig.4.46 Photos of transient oscillatory saturated flow boiling flow at certain time instants for various imposed mass fluxes for q=6.2 W/cm^2 at G=400±5% kg/m^{2}s with oscillation t_p=10s.

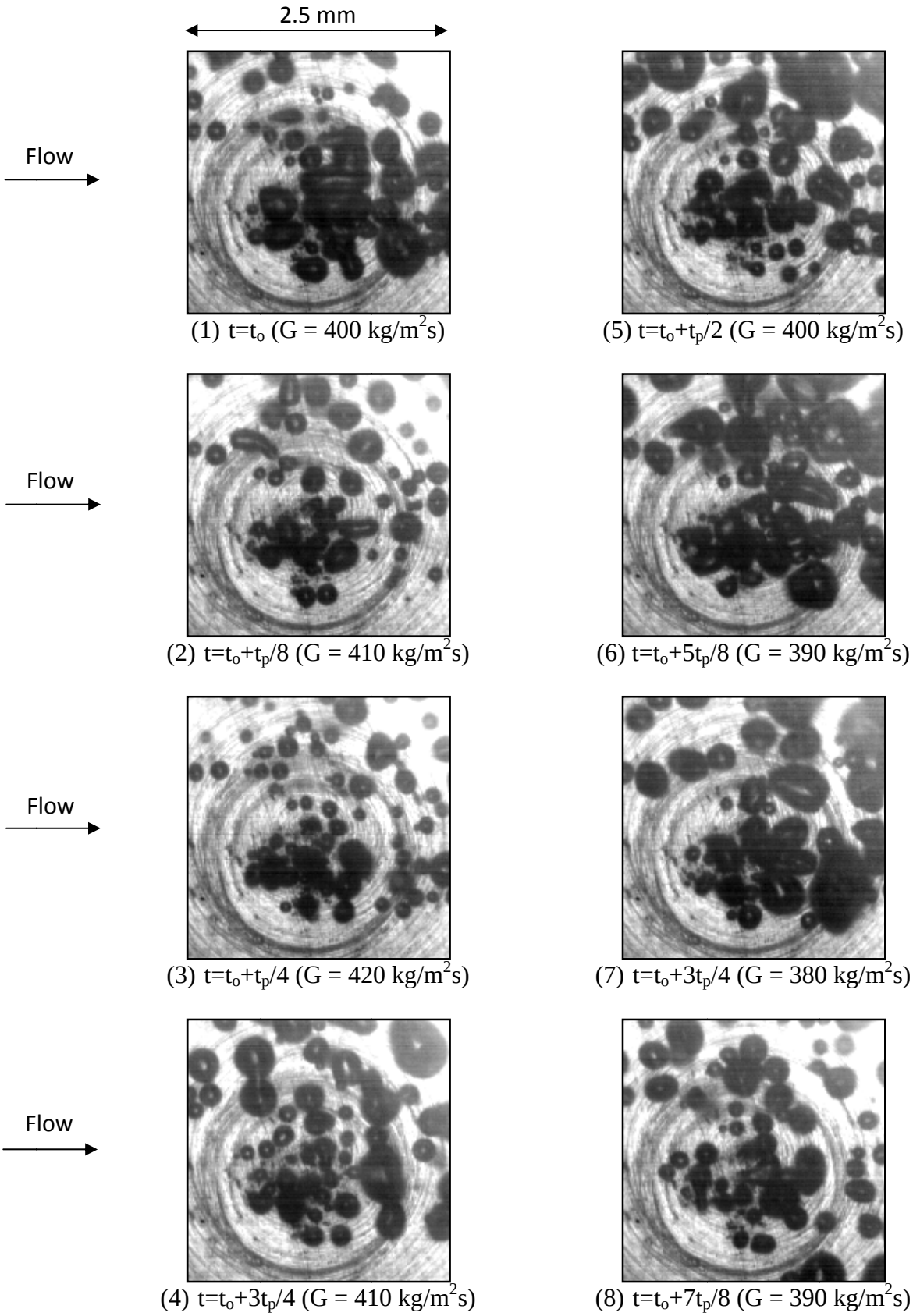

Fig.4.47 Photos of transient oscillatory saturated flow boiling flow at certain time instants for various imposed mass fluxes for q=9.0 W/cm^2 at G=400±5% kg/m^{2}s with oscillation t$_p$=10s.

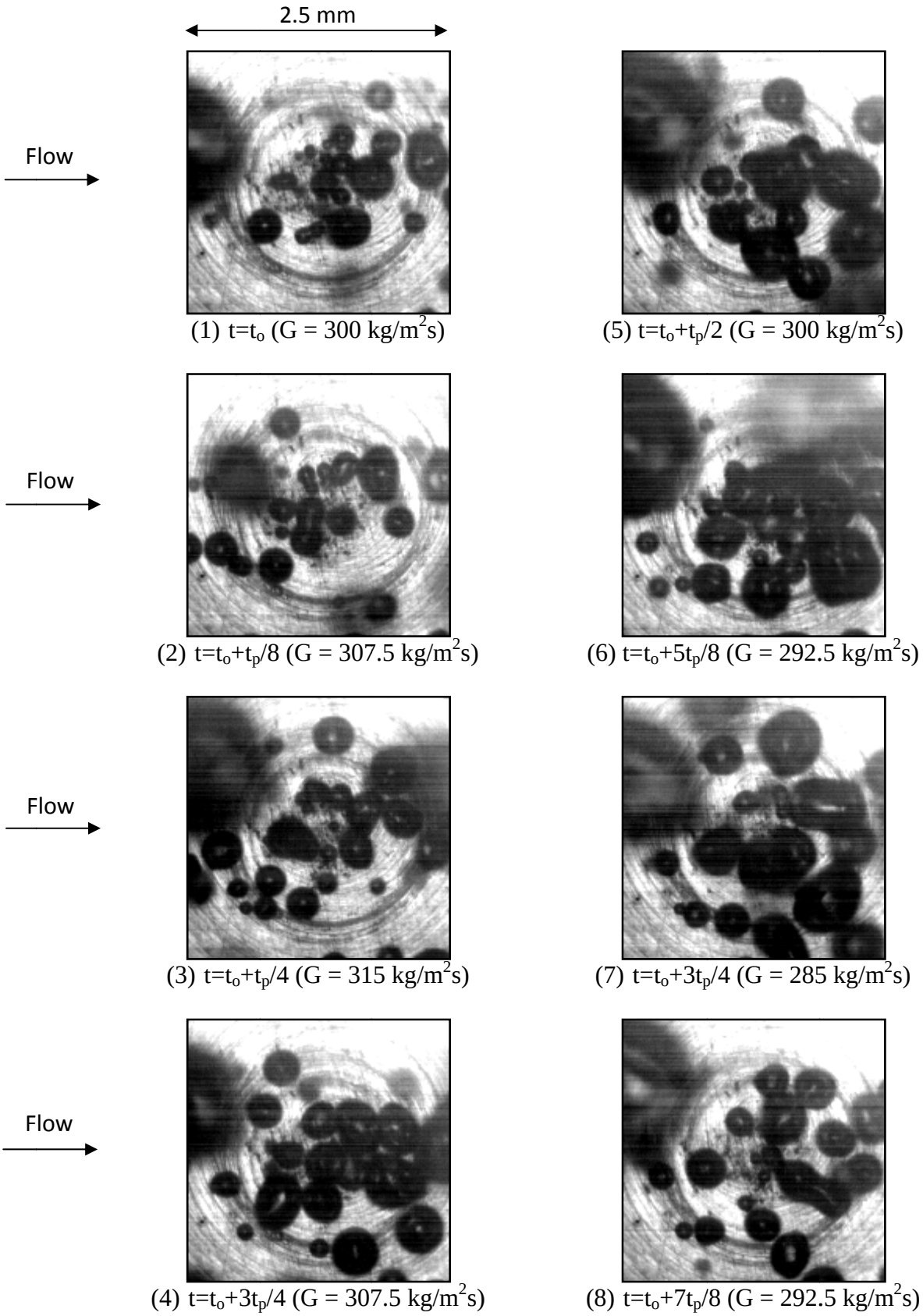

Fig.4.48 Photos of transient oscillatory saturated flow boiling flow at certain time instants for various imposed mass fluxes for q=6.2 W/cm^2 at G=300±5% kg/m^{2}s with oscillation t_p=20s.

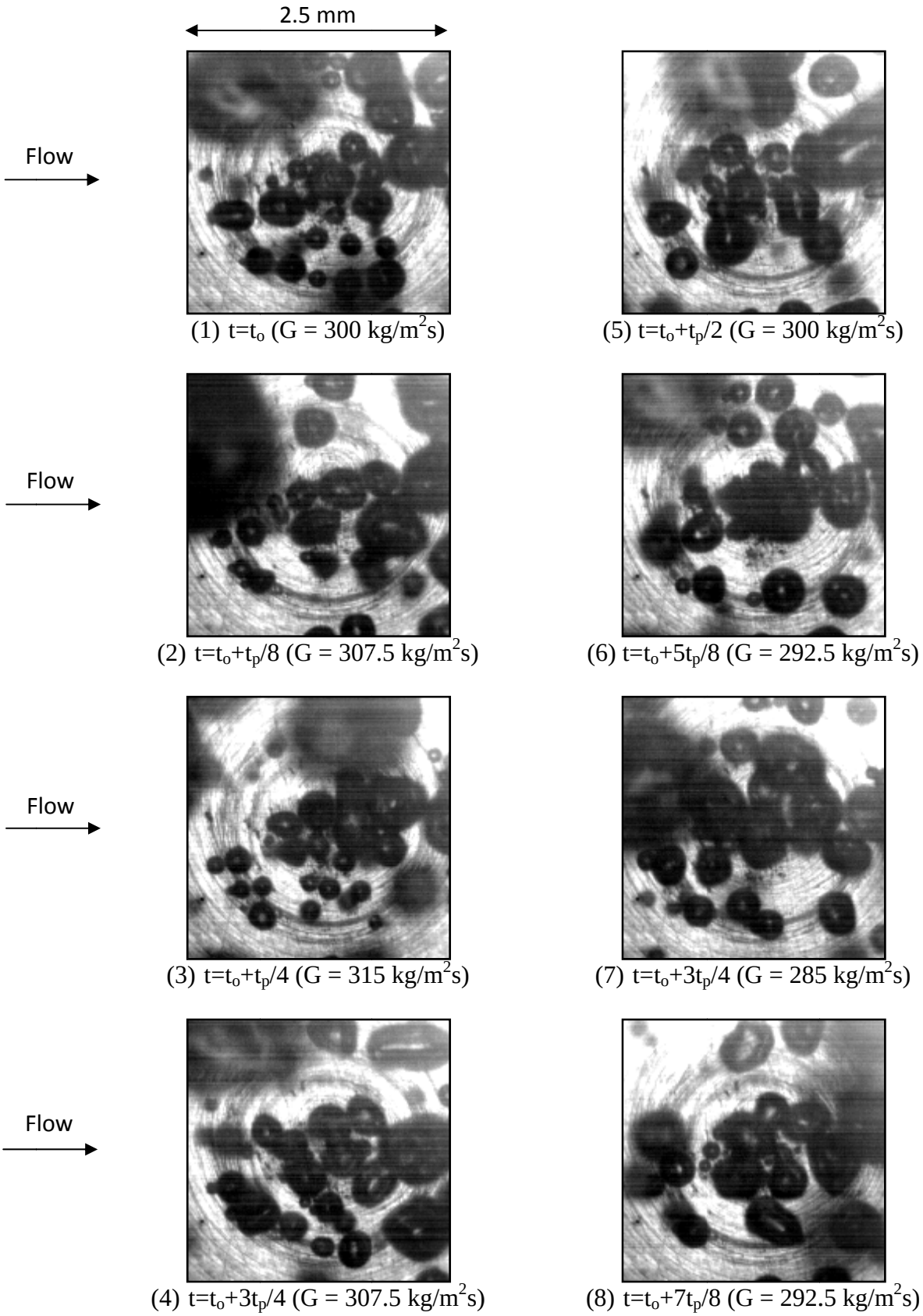

Fig.4.49 Photos of transient oscillatory saturated flow boiling flow at certain time instants for various imposed mass fluxes for q=7.5 W/cm^2 at G=300±5% kg/m^{2}s with oscillation t_p=20s.

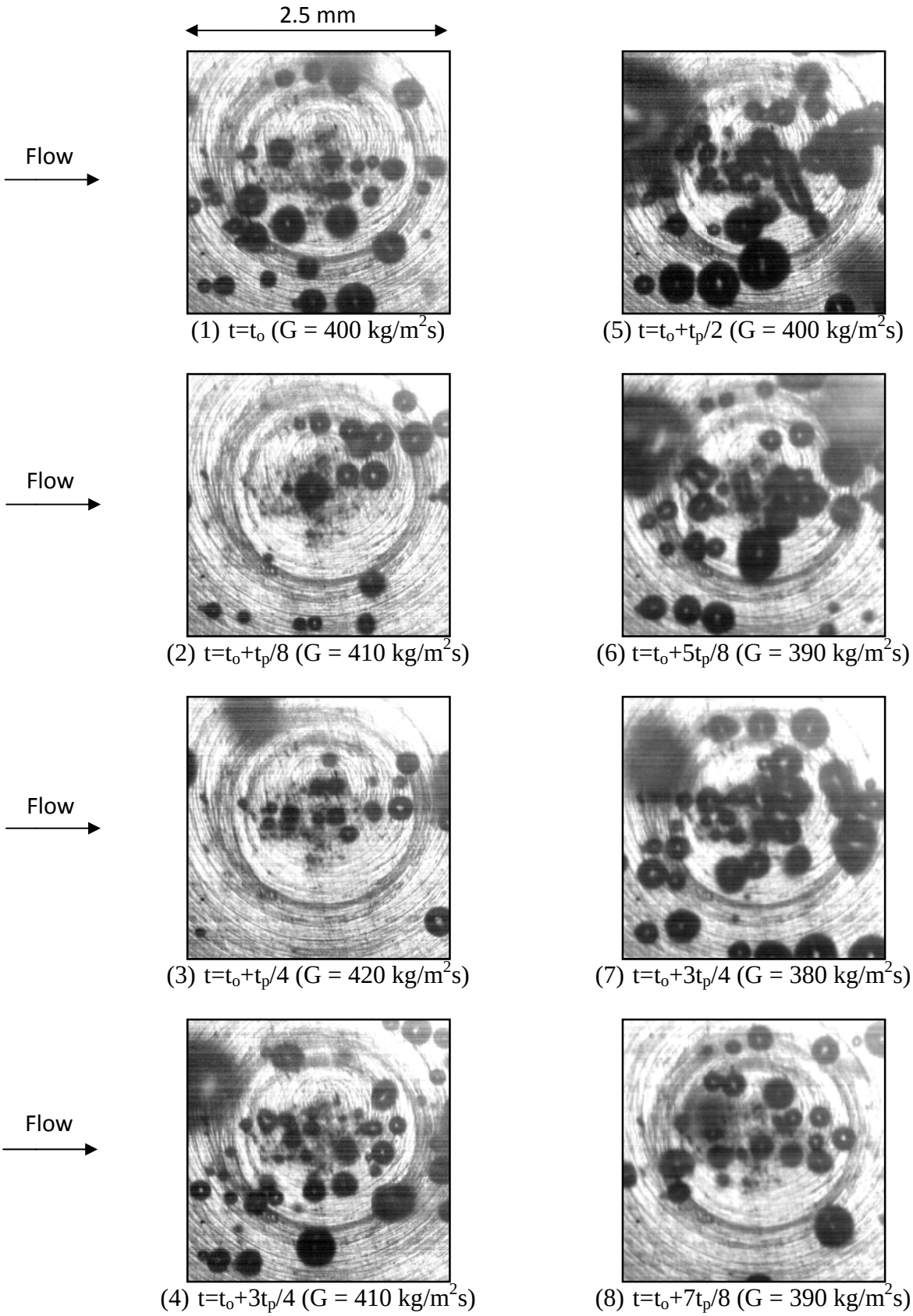

(1) $t=t_o$ (G = 400 kg/m^{2}s) (5) $t=t_o+t_p/2$ (G = 400 kg/m^{2}s)

(2) $t=t_o+t_p/8$ (G = 410 kg/m^{2}s) (6) $t=t_o+5t_p/8$ (G = 390 kg/m^{2}s)

(3) $t=t_o+t_p/4$ (G = 420 kg/m^{2}s) (7) $t=t_o+3t_p/4$ (G = 380 kg/m^{2}s)

(4) $t=t_o+3t_p/4$ (G = 410 kg/m^{2}s) (8) $t=t_o+7t_p/8$ (G = 390 kg/m^{2}s)

Fig.4.50 Photos of transient oscillatory saturated flow boiling flow at certain time instants for various imposed mass fluxes for q=6.2 W/cm^2 at G=400±5% kg/m^{2}s with oscillation t_p=20s.

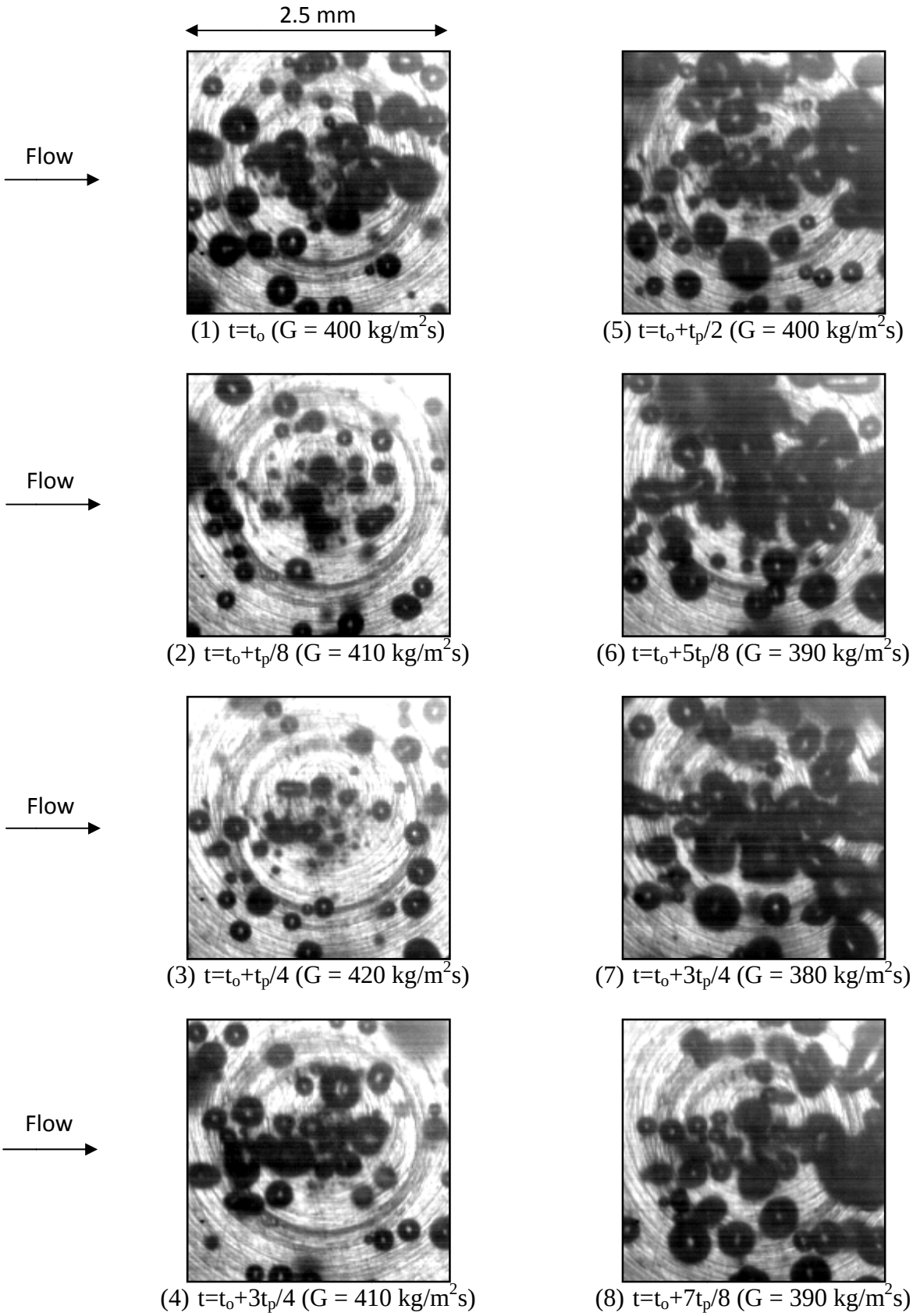

Fig.4.51 Photos of transient oscillatory saturated flow boiling flow at certain time instants for various imposed mass fluxes for q=9.0 W/cm^2 at G=400±5% kg/m^{2}s with oscillation t$_p$=20s.

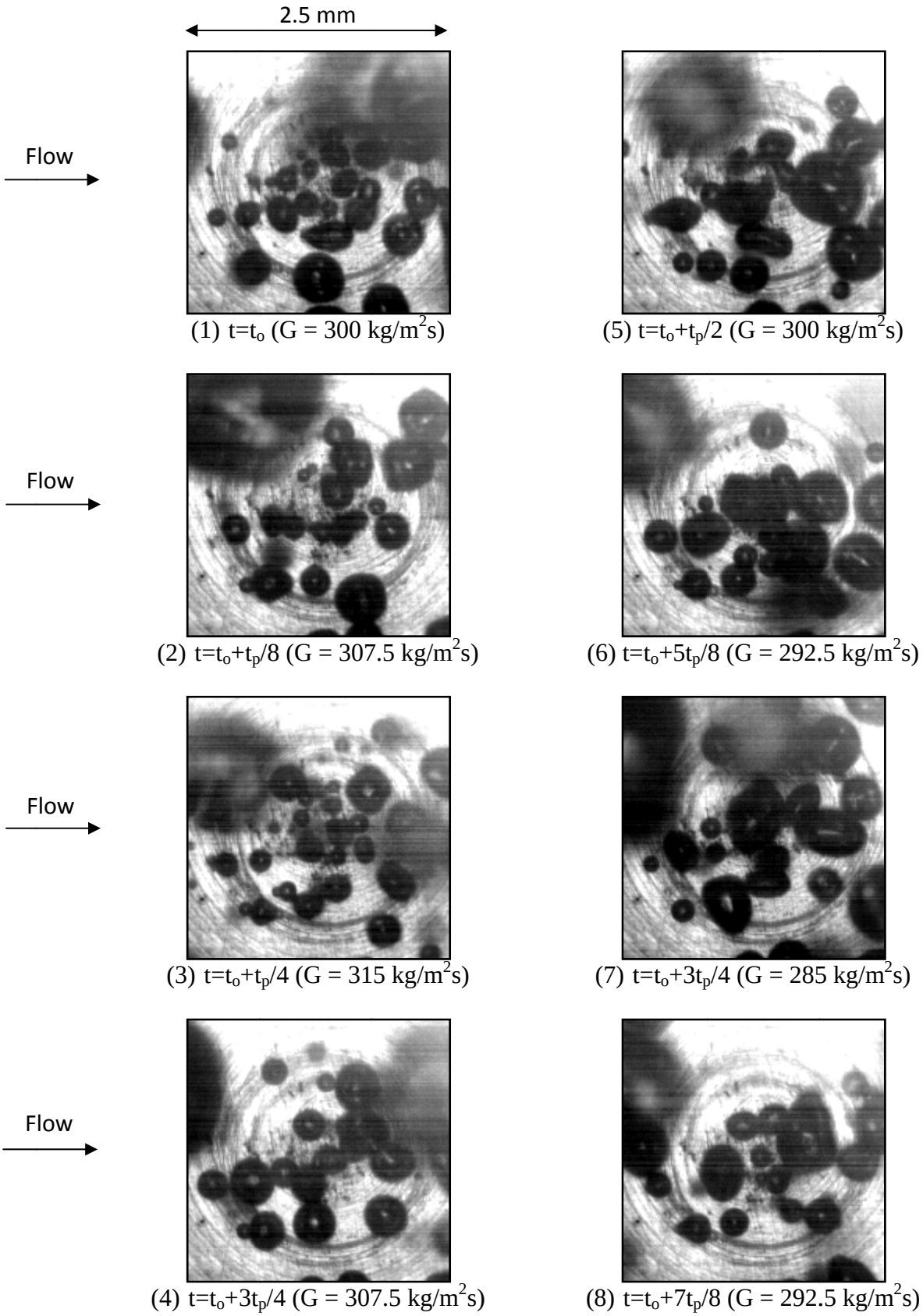

Fig.4.52 Photos of transient oscillatory saturated flow boiling flow at certain time instants for various imposed mass fluxes for q=6.2 W/cm^2 at G=300±5% kg/m^{2}s with oscillation t$_p$=30s.

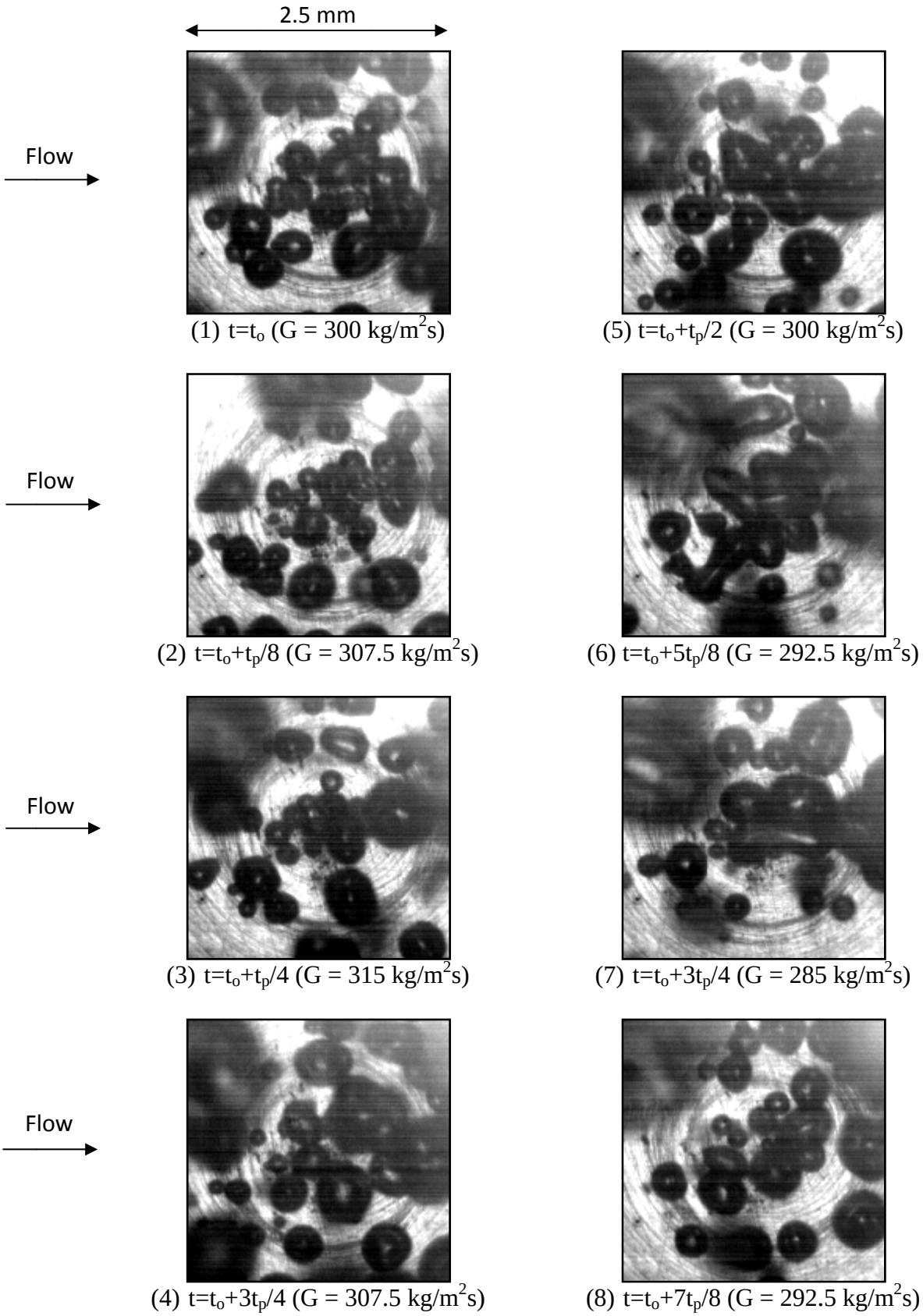

Fig.4.53 Photos of transient oscillatory saturated flow boiling flow at certain time instants for various imposed mass fluxes for q=7.5 W/cm^2 at G=300±5% kg/m^{2}s with oscillation t$_p$=30s.

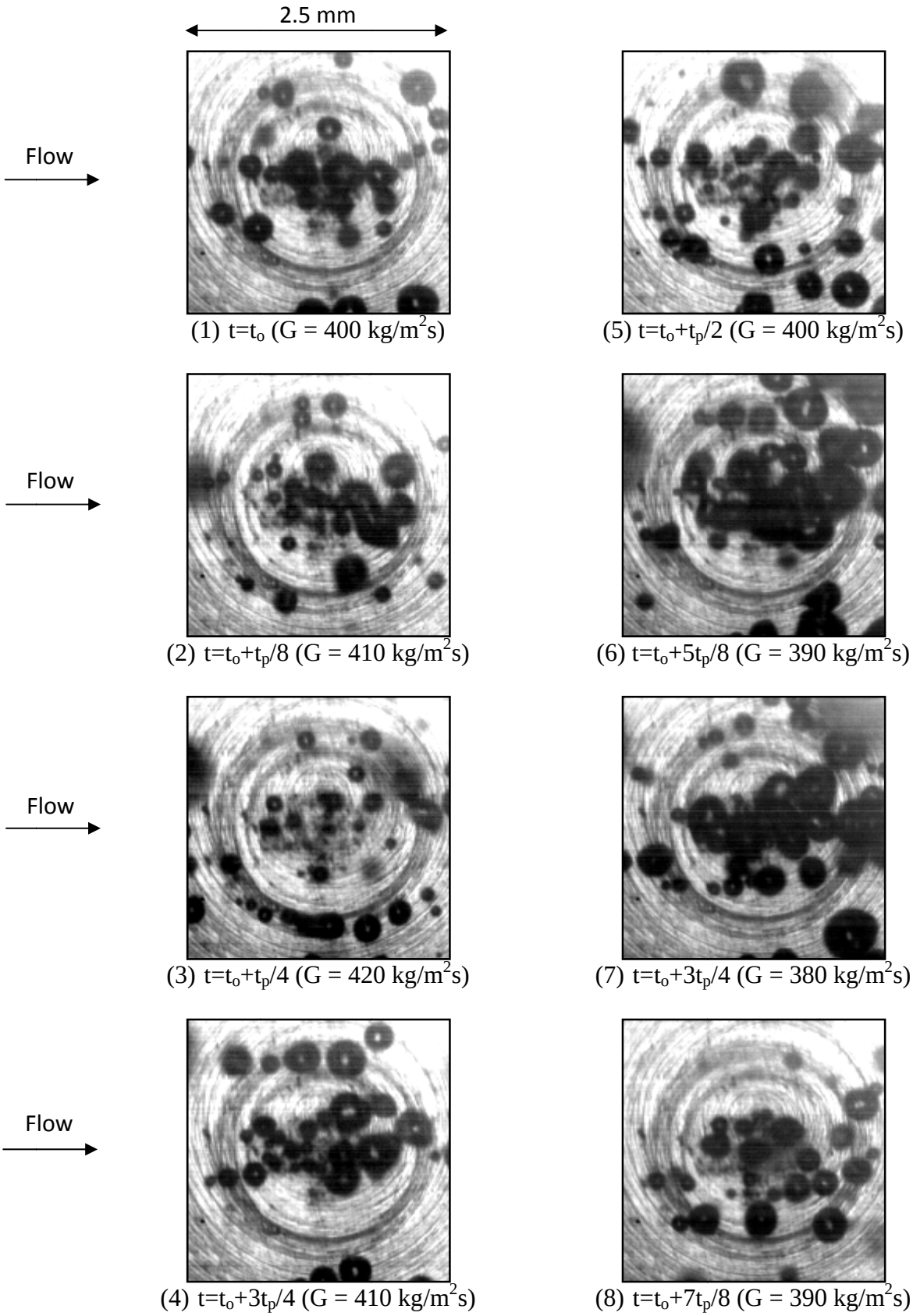

Fig.4.54 Photos of transient oscillatory saturated flow boiling flow at certain time instants for various imposed mass fluxes for q=6.2 W/cm^2 at G=400±5% kg/m^{2}s with oscillation t$_p$=30s.

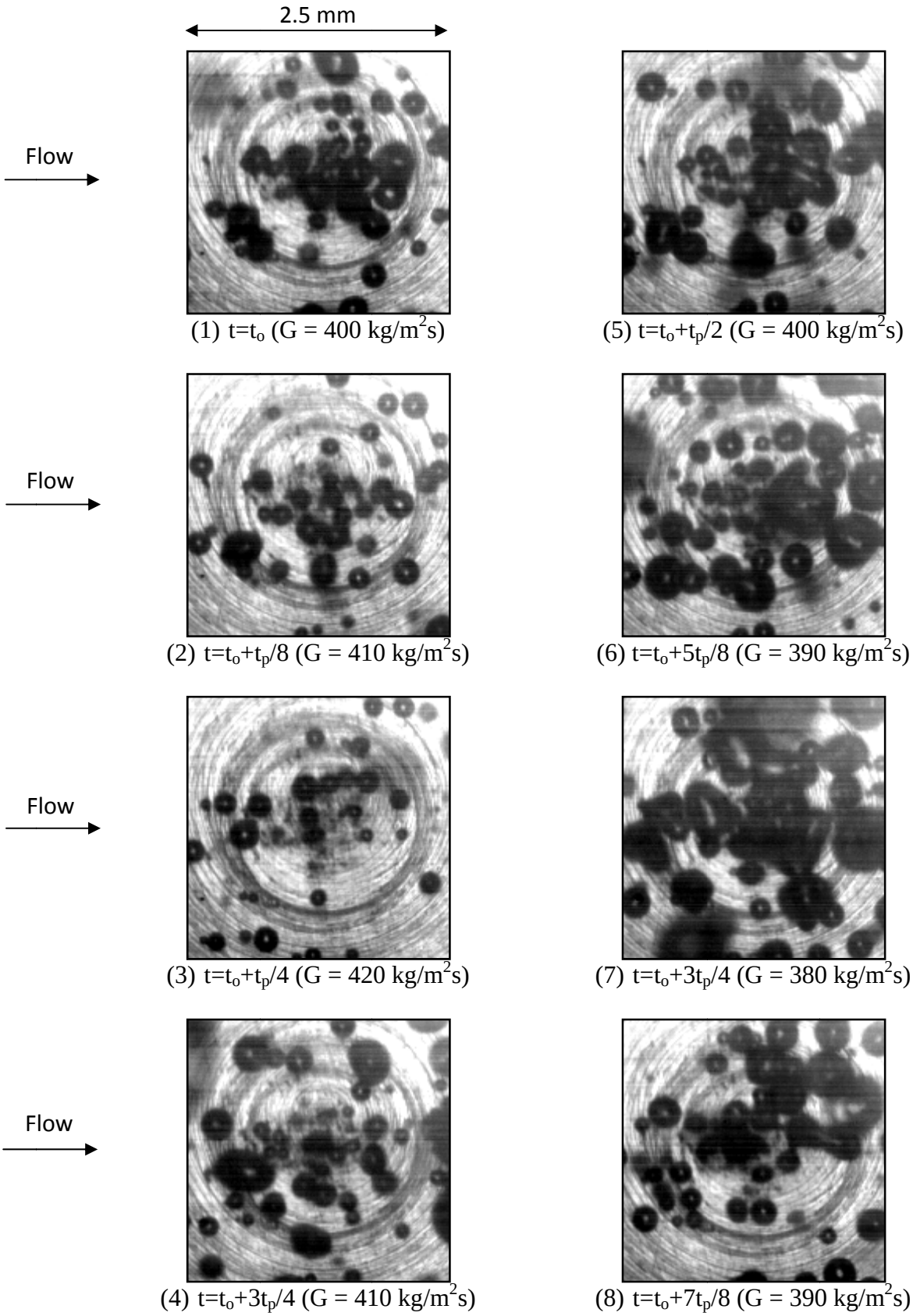

Fig.4.55 Photos of transient oscillatory saturated flow boiling flow at certain time instants for various imposed mass fluxes for q=9.0 W/cm^2 at G=400±5% kg/m^{2}s with oscillation t$_p$=30s.

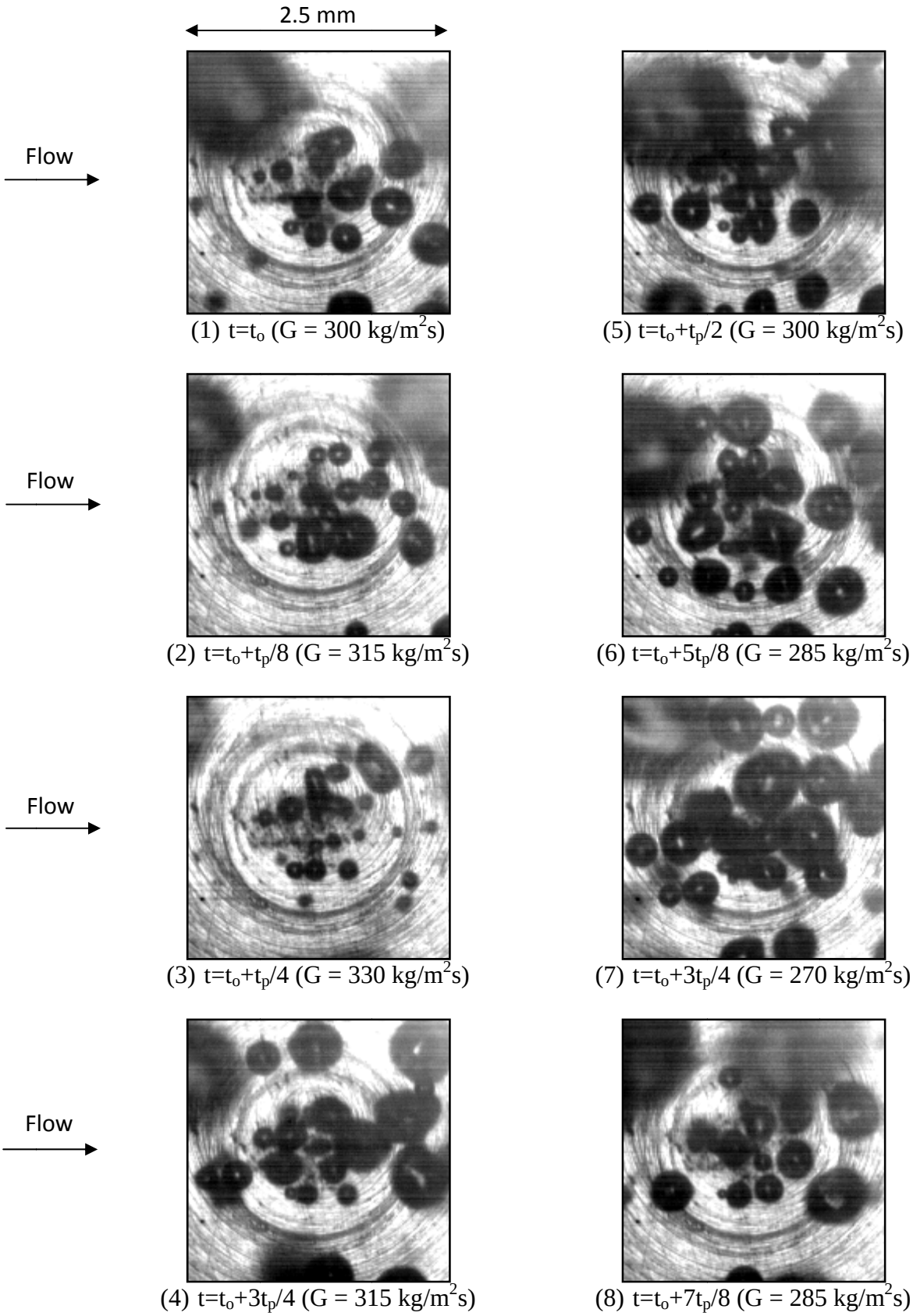

Fig.4.56 Photos of transient oscillatory saturated flow boiling flow at certain time instants for various imposed mass fluxes for q=6.2 W/cm^2 at G=300±10% kg/m^{2}s with oscillation t$_p$=10s.

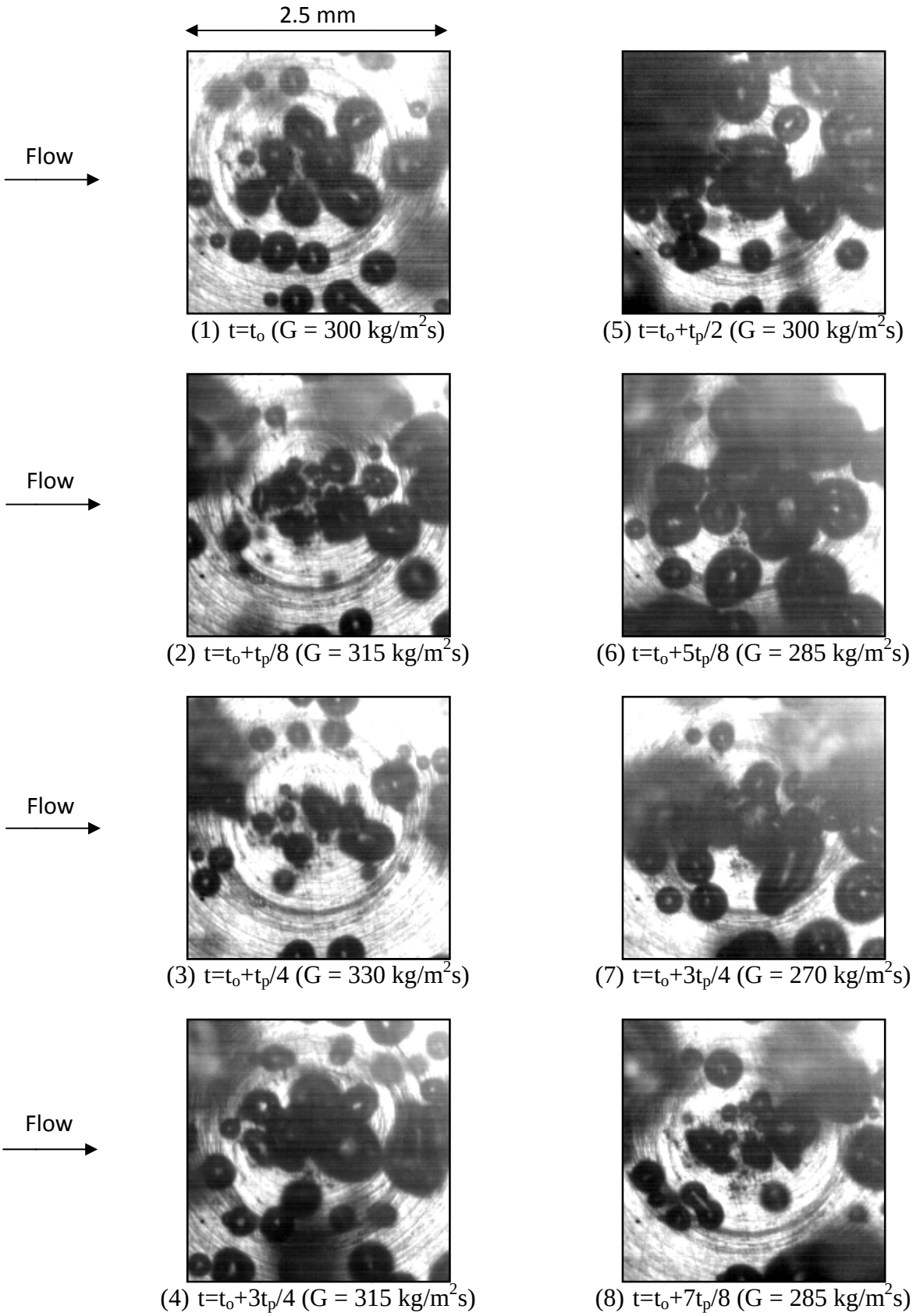

(1) $t=t_o$ (G = 300 kg/m^{2}s) (5) $t=t_o+t_p/2$ (G = 300 kg/m^{2}s)

(2) $t=t_o+t_p/8$ (G = 315 kg/m^{2}s) (6) $t=t_o+5t_p/8$ (G = 285 kg/m^{2}s)

(3) $t=t_o+t_p/4$ (G = 330 kg/m^{2}s) (7) $t=t_o+3t_p/4$ (G = 270 kg/m^{2}s)

(4) $t=t_o+3t_p/4$ (G = 315 kg/m^{2}s) (8) $t=t_o+7t_p/8$ (G = 285 kg/m^{2}s)

Fig.4.57 Photos of transient oscillatory saturated flow boiling flow at certain time instants for various imposed mass fluxes for q=7.5 W/cm^2 at G=300±10% kg/m^{2}s with oscillation t_p=10s.

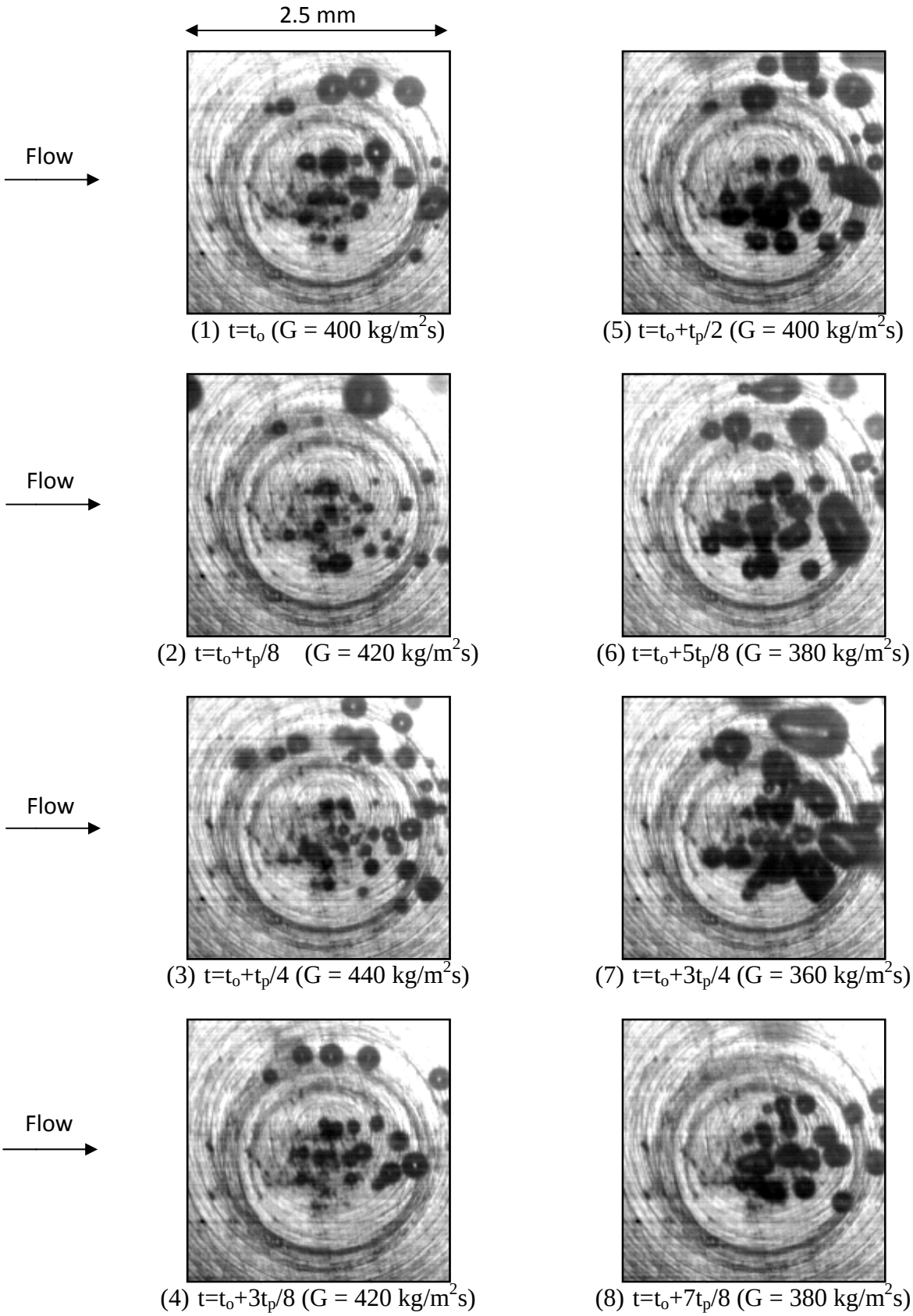

Fig.4.58 Photos of transient oscillatory saturated flow boiling flow at certain time instants for various imposed mass fluxes for q=6.2 W/cm^2 at G=400±10% kg/m^{2}s with oscillation t$_p$=10s.

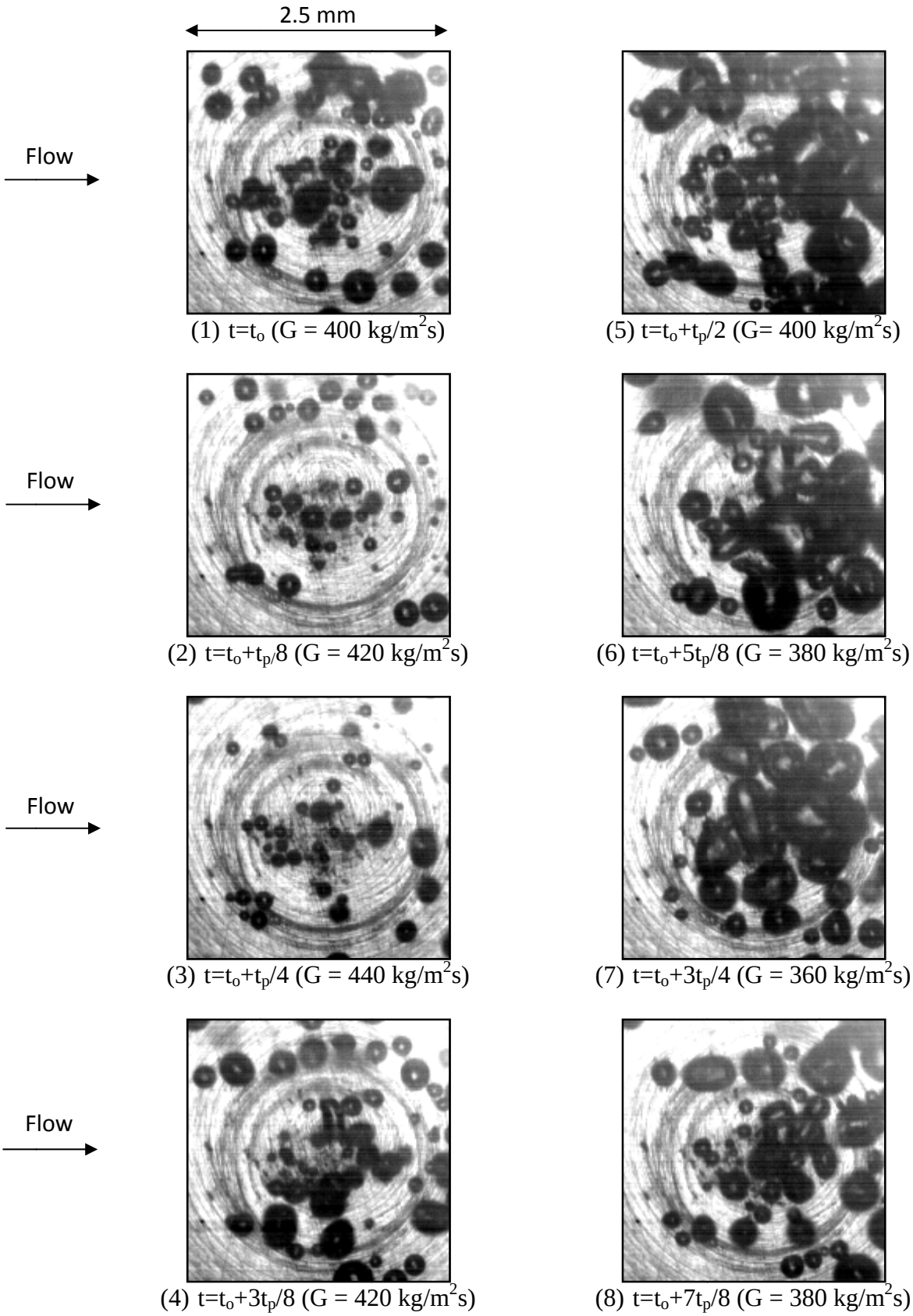

Fig.4.59 Photos of transient oscillatory saturated flow boiling flow at certain time instants for various imposed mass fluxes for q=8.9 W/cm^2 at G=400±10% kg/m^{2}s with oscillation t$_p$=10s.

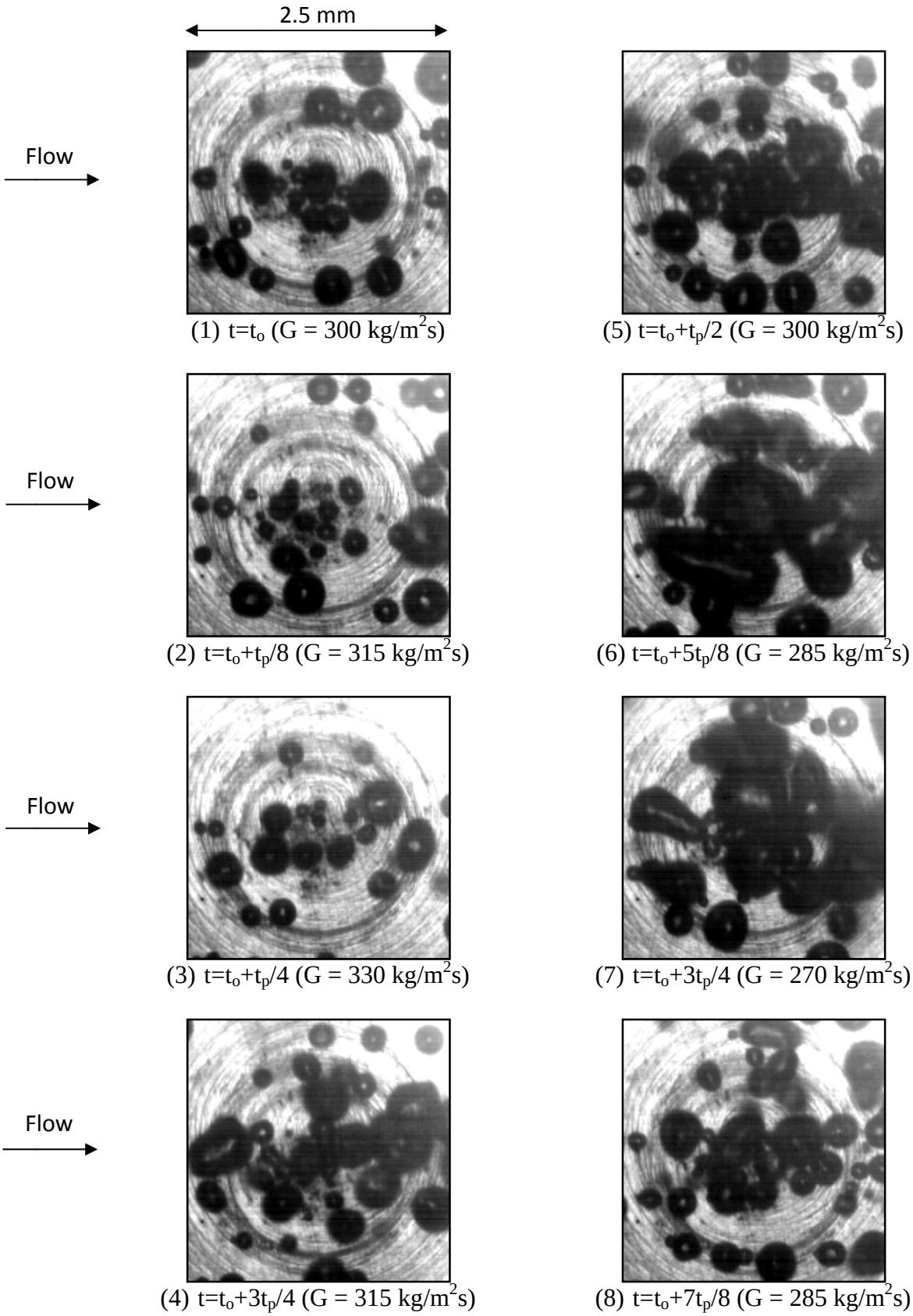

Fig.4.60 Photos of transient oscillatory saturated flow boiling flow at certain time instants for various imposed mass fluxes for q=6.2 W/cm^2 at G=300±10% kg/m^{2}s with oscillation t$_p$=20s.

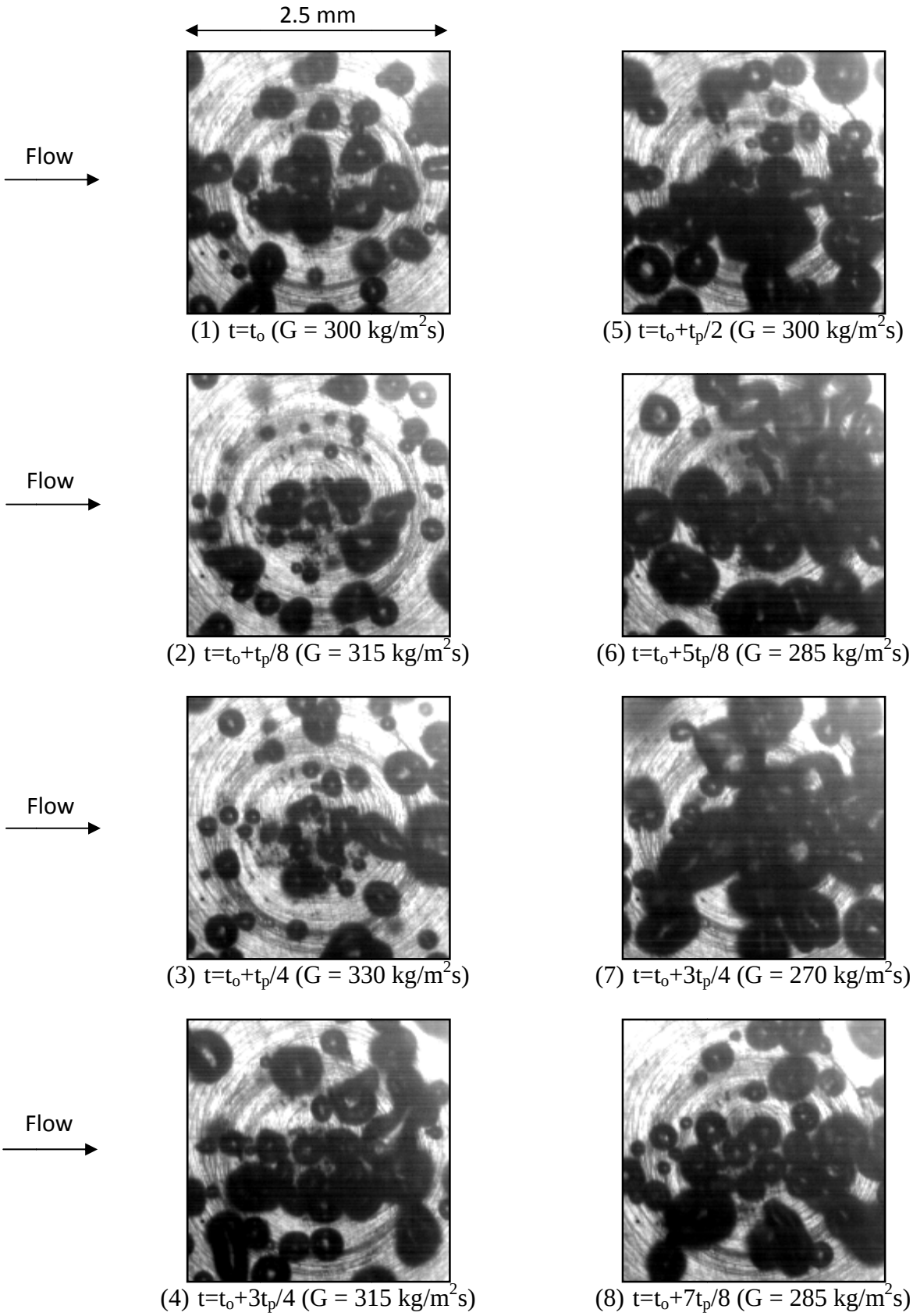

Fig.4.61 Photos of transient oscillatory saturated flow boiling flow at certain time instants for various imposed mass fluxes for q=7.5 W/cm^2 at G=300±10% kg/m^{2}s with oscillation t_p=20s.

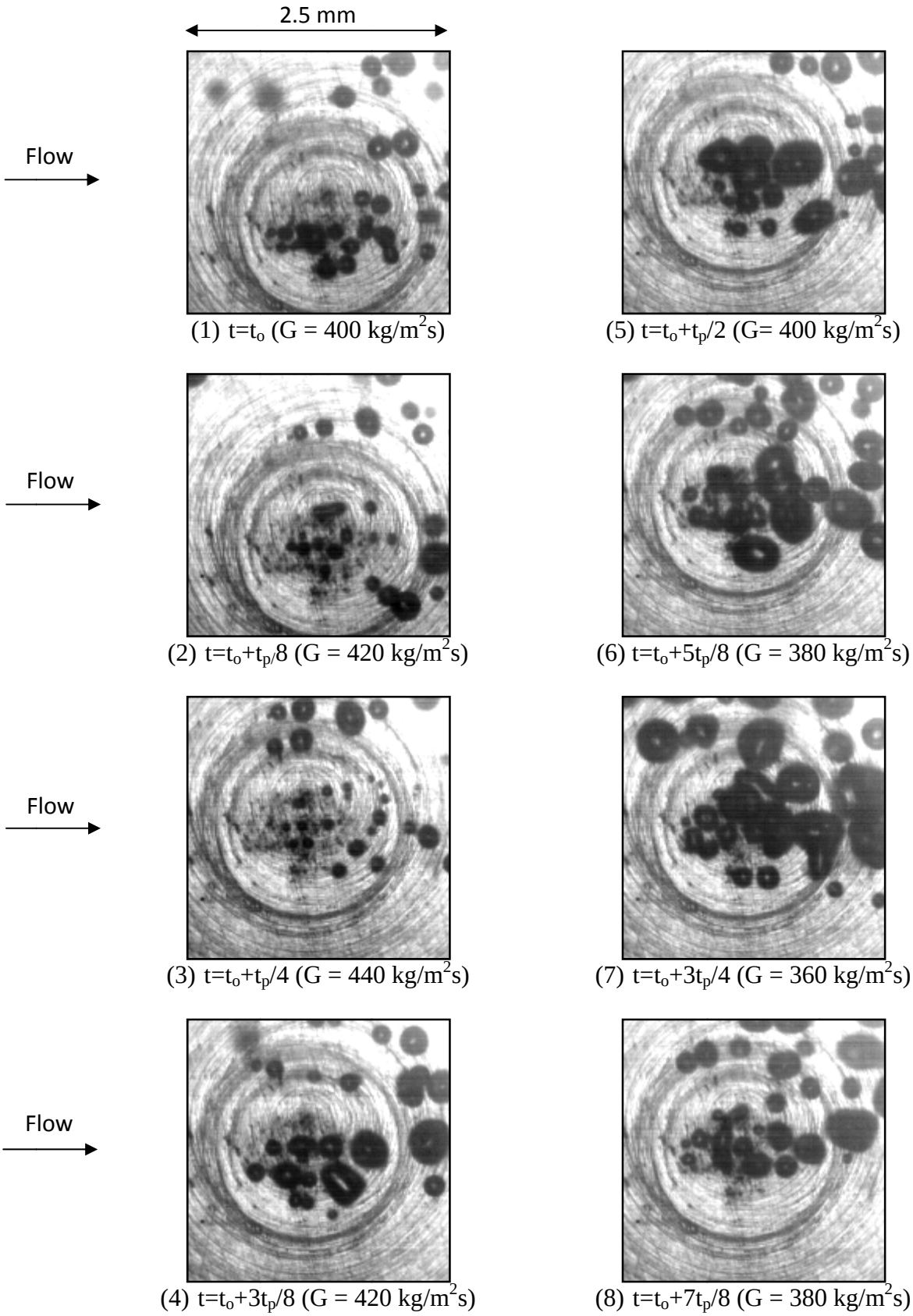

Fig.4.62 Photos of transient oscillatory saturated flow boiling flow at certain time instants for various imposed mass fluxes for q=6.2 W/cm^2 at G=400±10% kg/m^{2}s with oscillation t$_p$=20s.

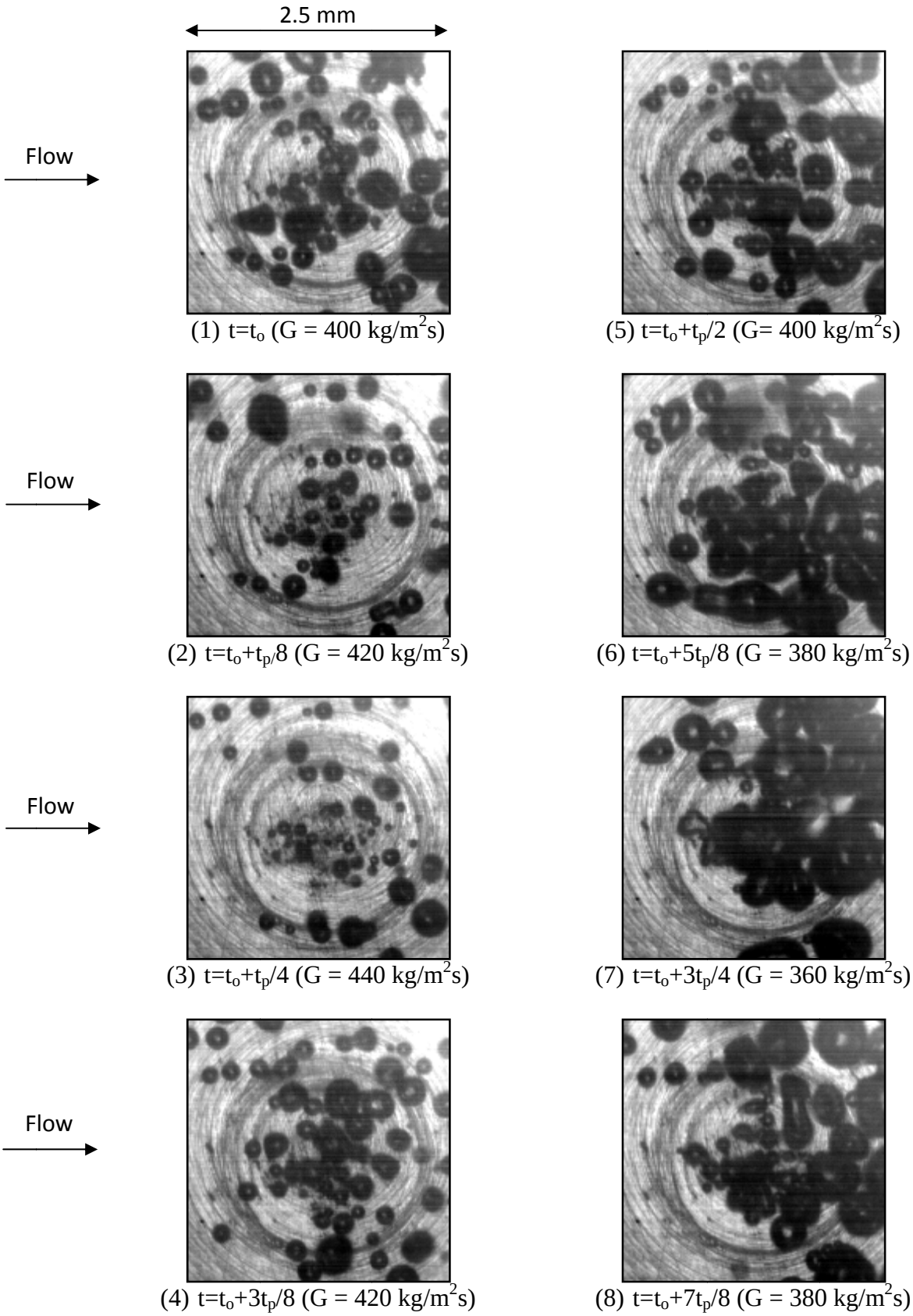

Fig.4.63 Photos of transient oscillatory saturated flow boiling flow at certain time instants for various imposed mass fluxes for q=9.0 W/cm^2 at G=400±10% kg/m^{2}s with oscillation t$_p$=20s.

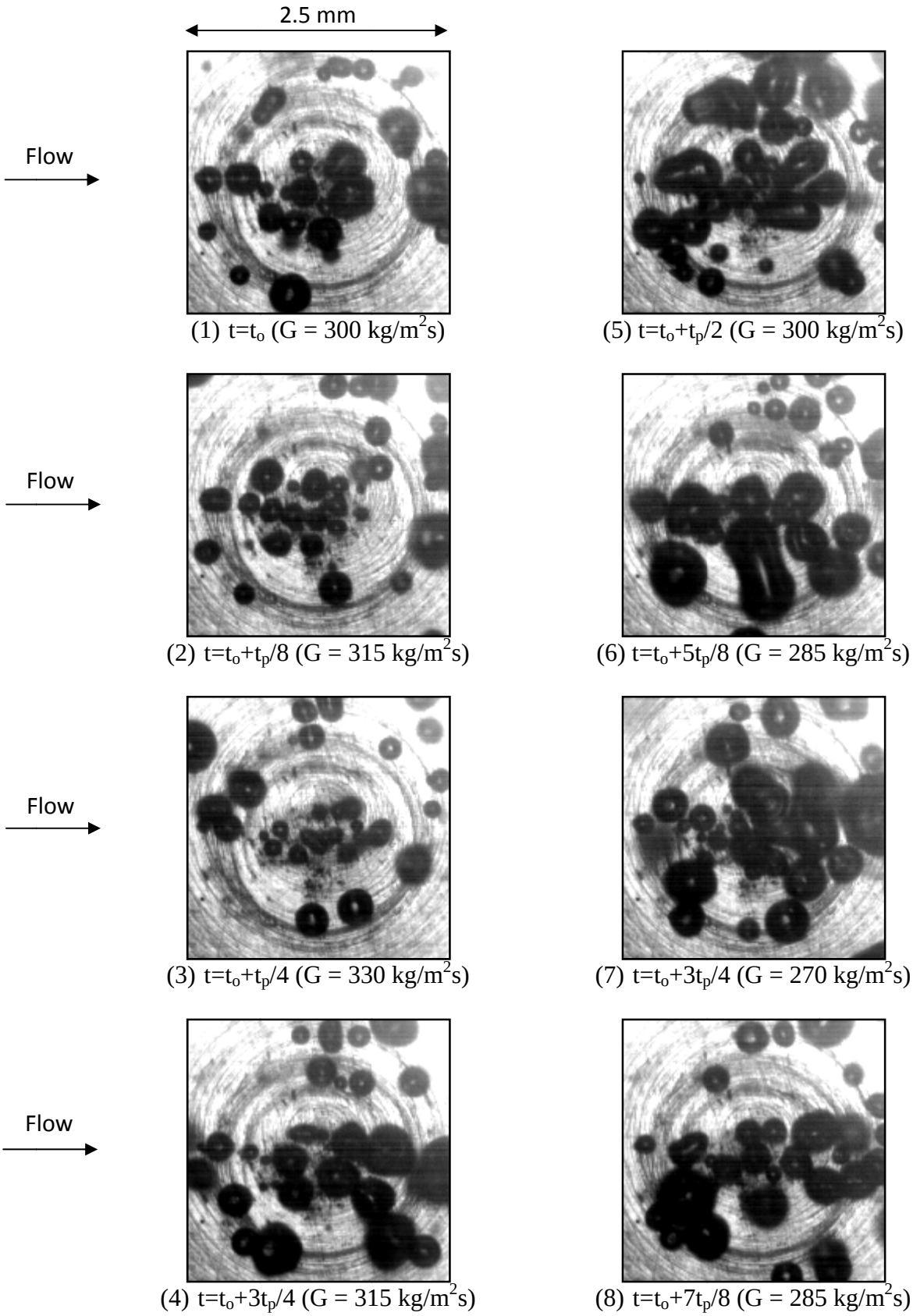

Fig.4.64 Photos of transient oscillatory saturated flow boiling flow at certain time instants for various imposed mass fluxes for q=6.1 W/cm^2 at G=300±10% kg/m^{2}s with oscillation t$_p$=30s.

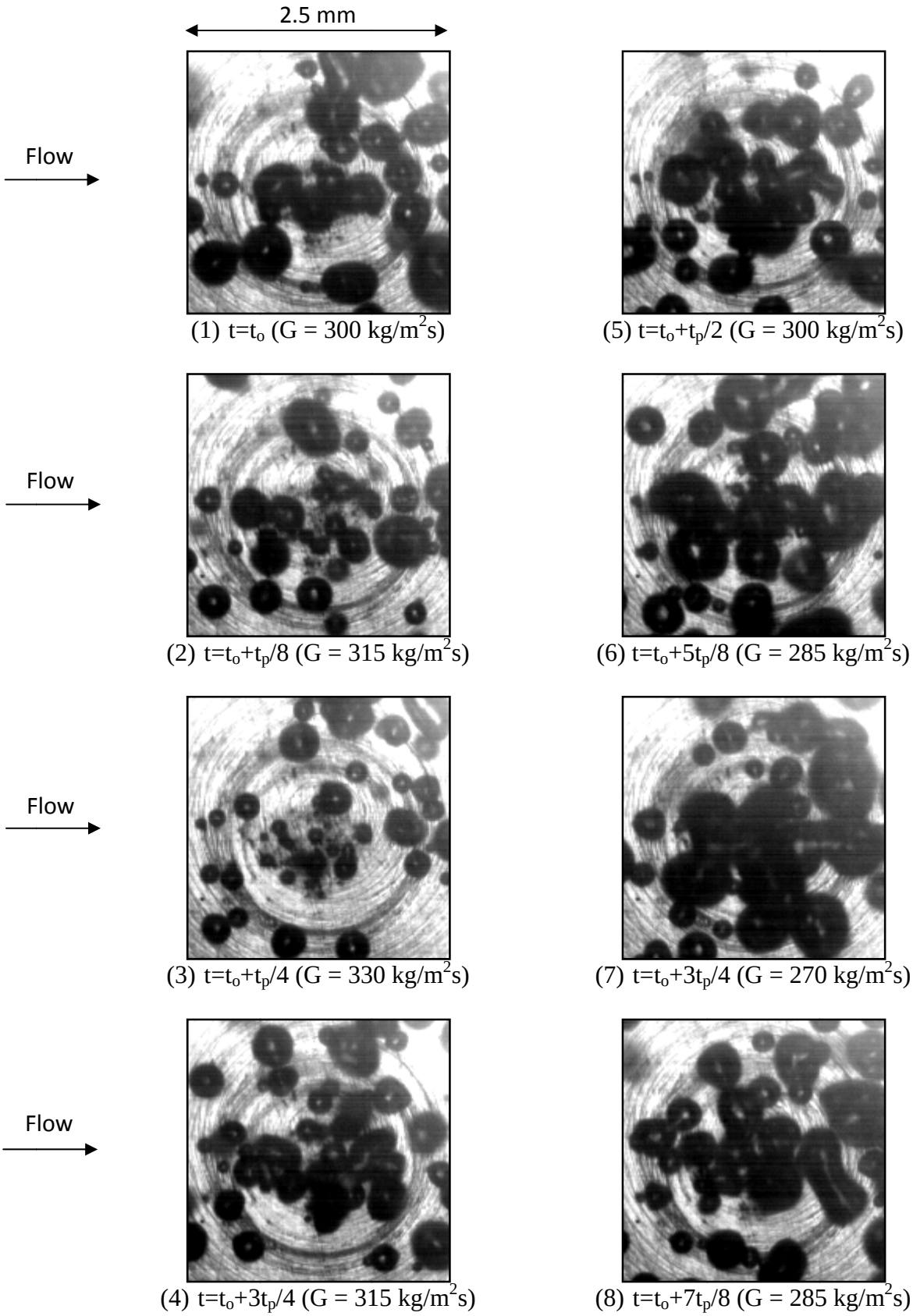

Fig.4.65 Photos of transient oscillatory saturated flow boiling flow at certain time instants for various imposed mass fluxes for q=7.5 W/cm^2 at G=300±10% kg/m^{2}s with oscillation t_p=30s.

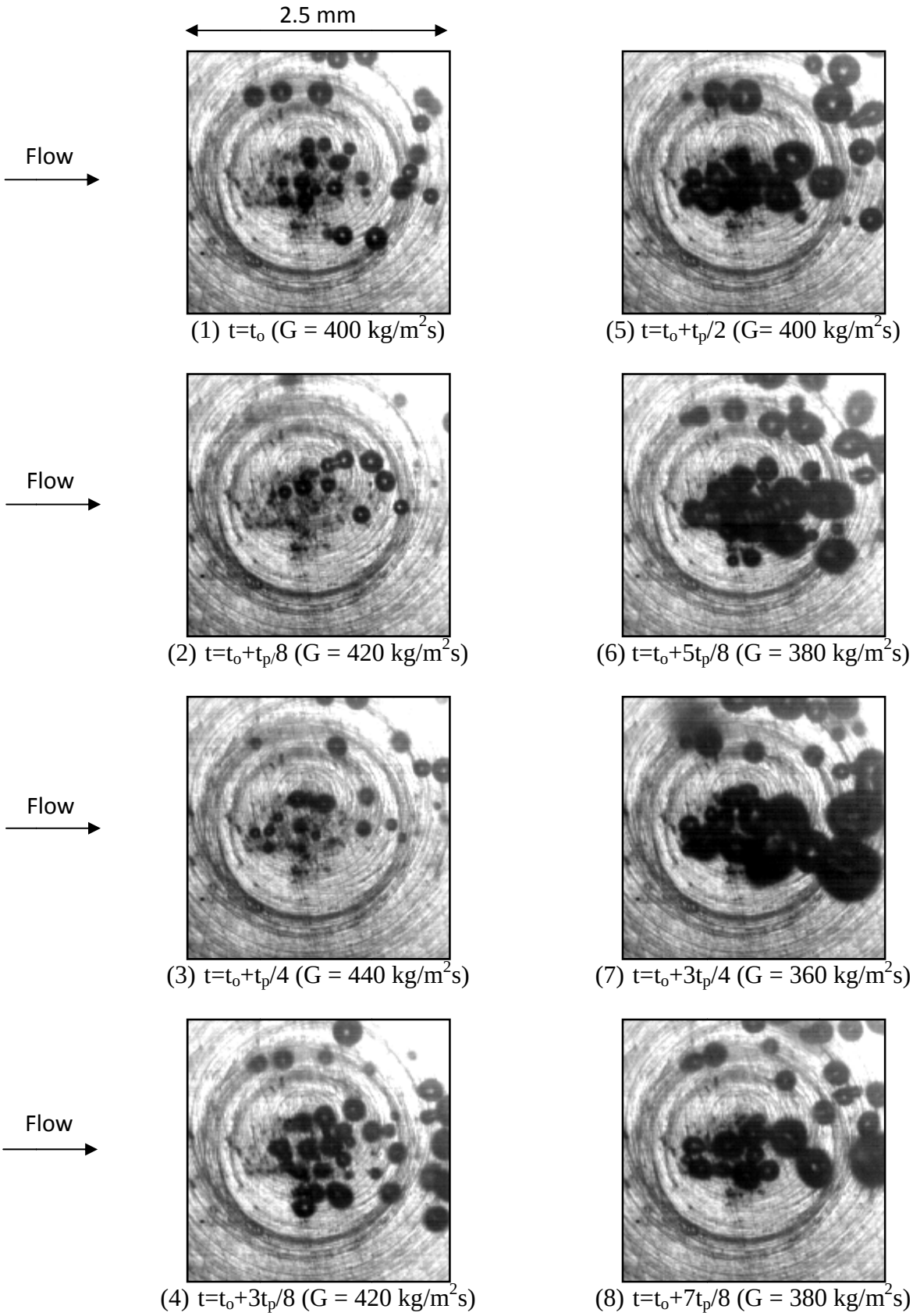

Fig.4.66 Photos of transient oscillatory saturated flow boiling flow at certain time instants for various imposed mass fluxes for q=6.2 W/cm^2 at G=400±10% kg/m^{2}s with oscillation t$_p$=30s.

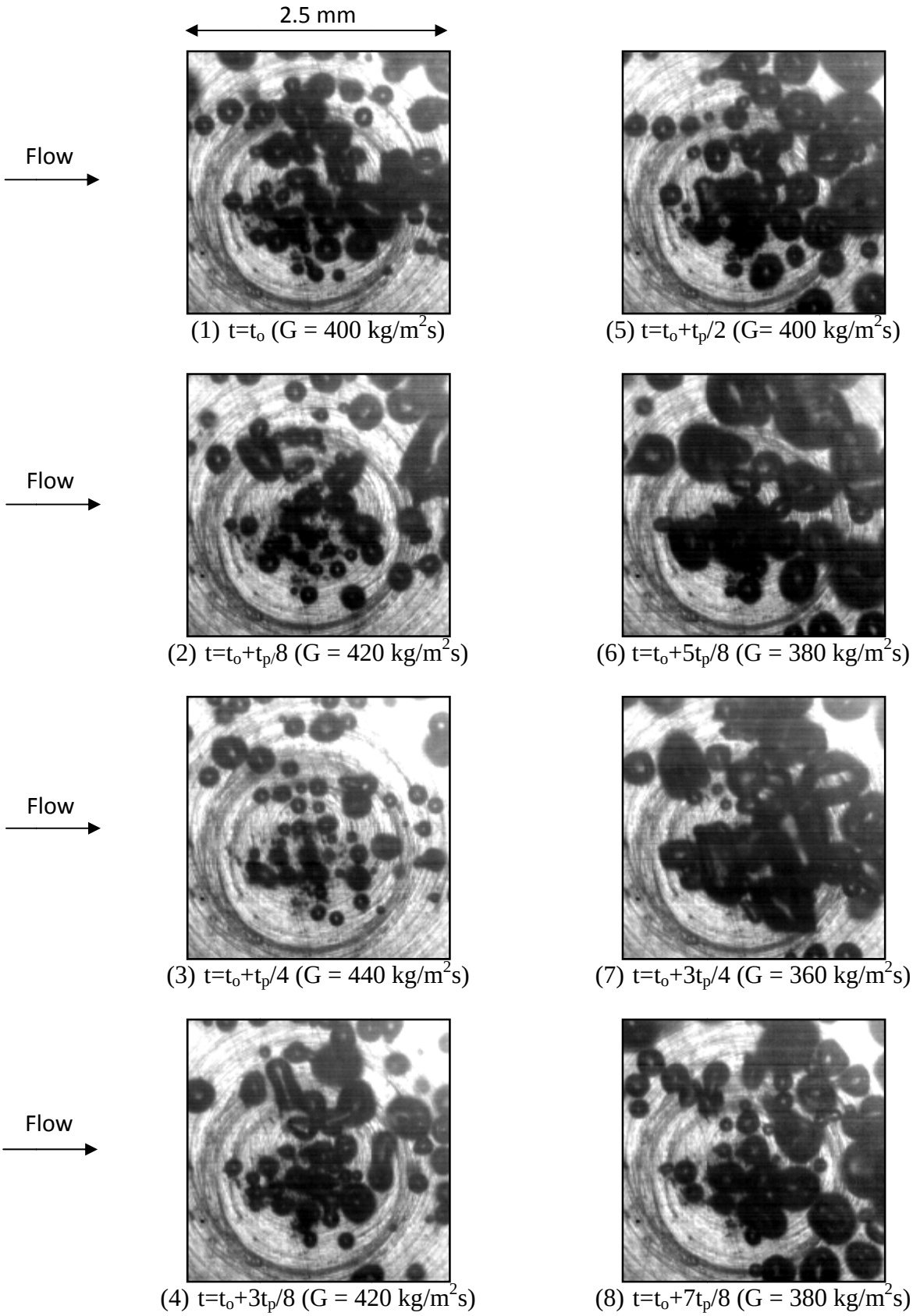

Fig.4.67 Photos of transient oscillatory saturated flow boiling flow at certain time instants for various imposed mass fluxes for q=9.0 W/cm^2 at G=400±10% kg/m^{2}s with oscillation t$_p$=30s.

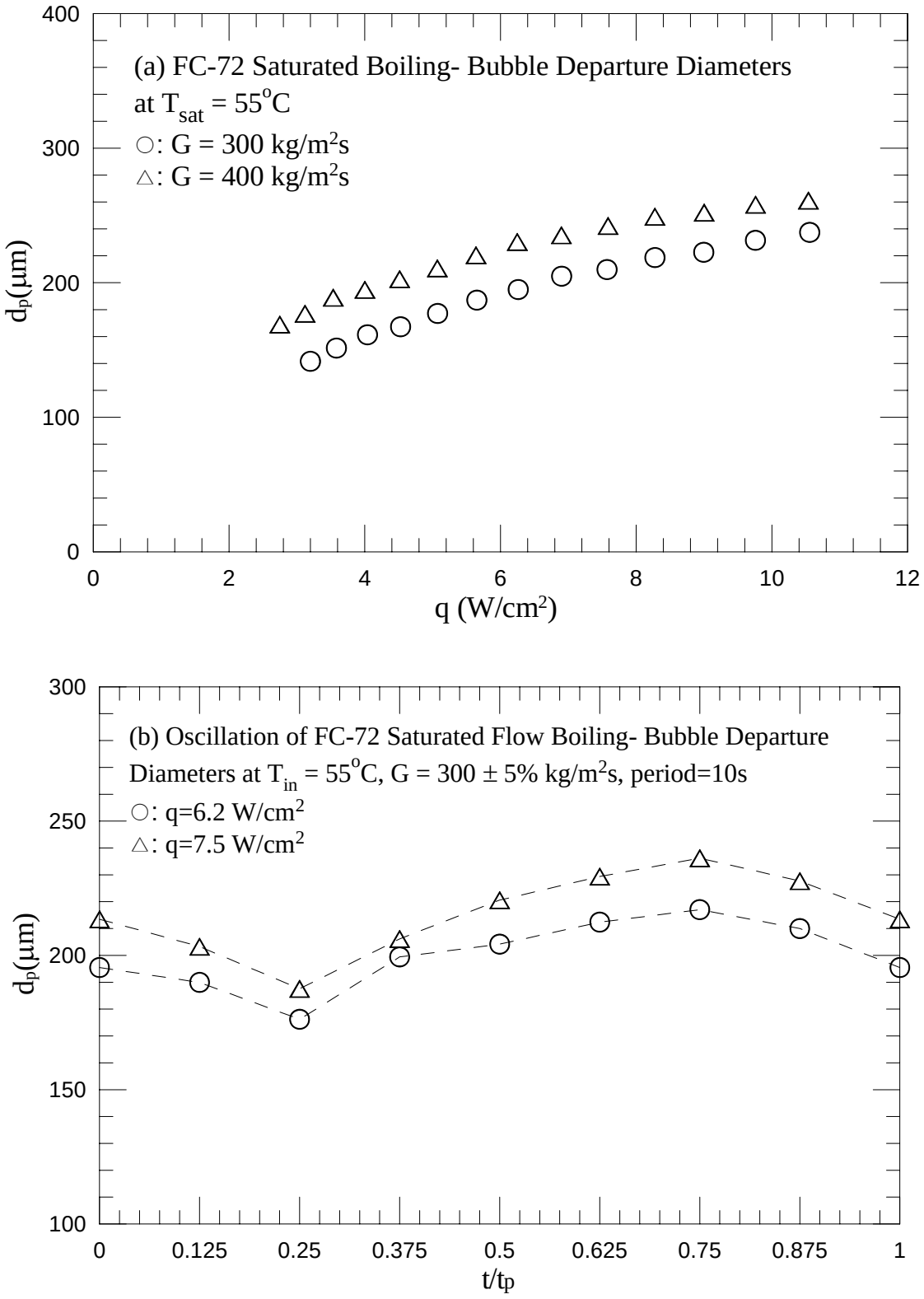

Fig. 4.68 Mean bubble departure diameters for various coolant mass fluxes for stable saturated flow boiling (a) and various imposed heat fluxes for transient saturated flow boiling for G=300±5% kg/m^{2}s with t_p=10 sec (b), 20sec (c) and 30 sec (d).

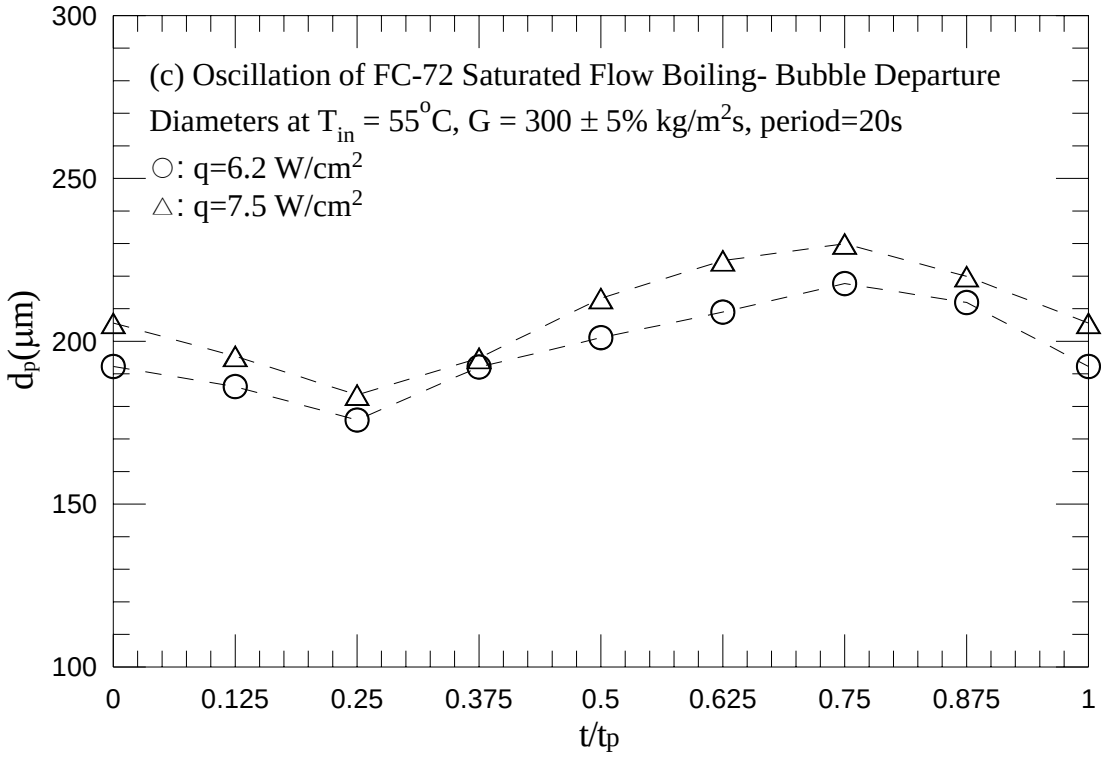

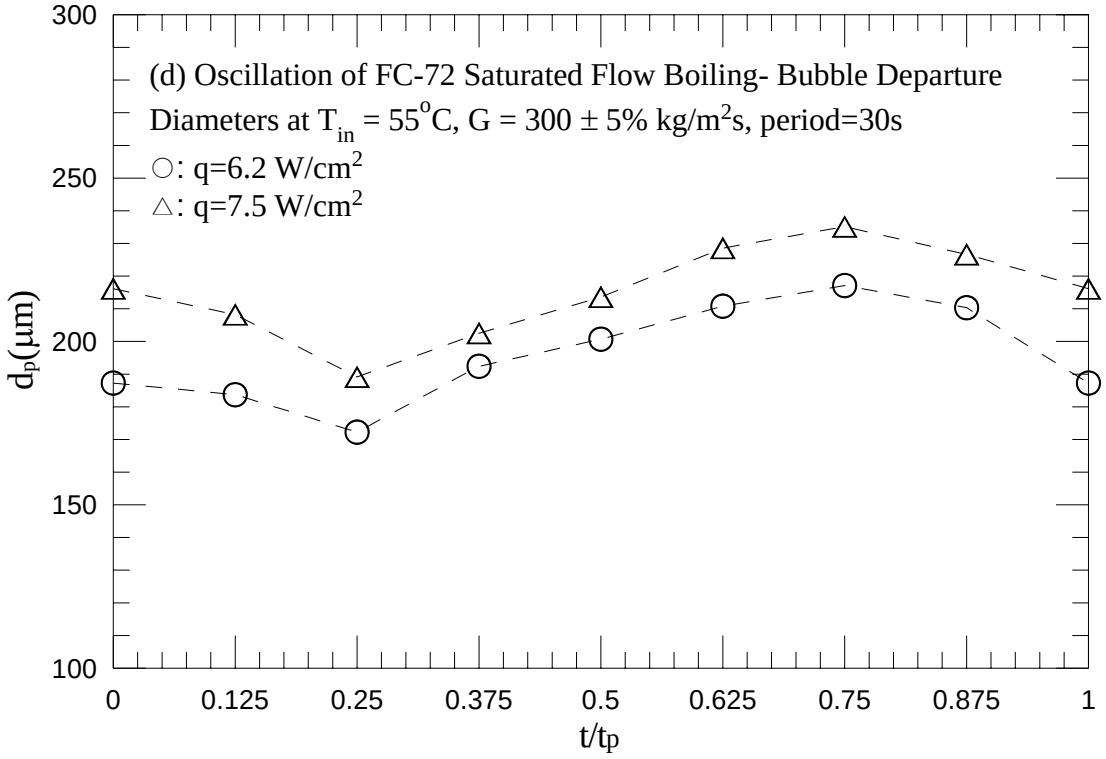

Fig. 4.68 Continued.

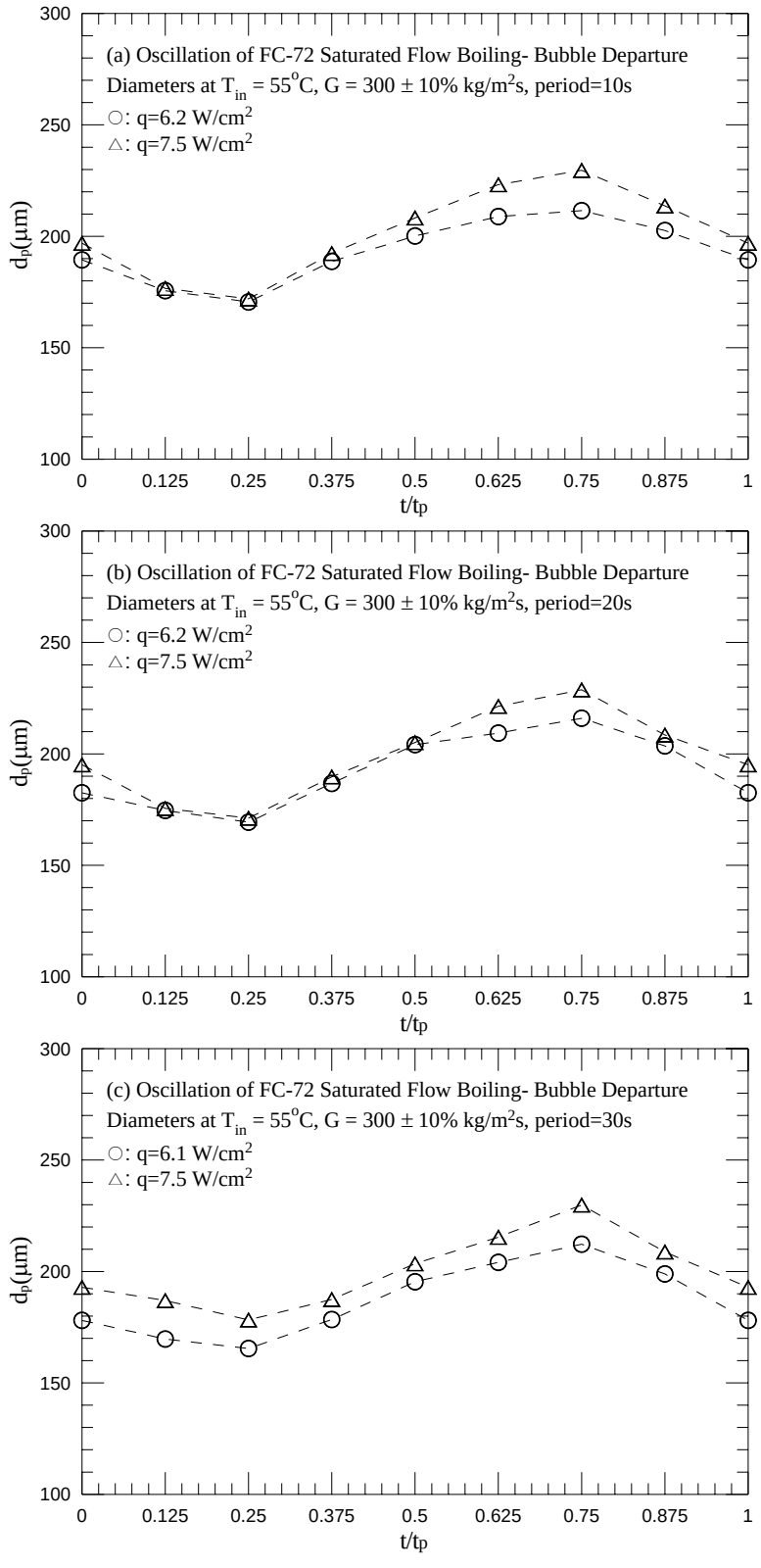

Fig. 4.69 Mean bubble departure diameters for various imposed heat fluxes for transient saturated flow boiling for G=300±10% kg/m^{2}s with t_p=10 sec (a), 20sec (b) and 30 sec (c).

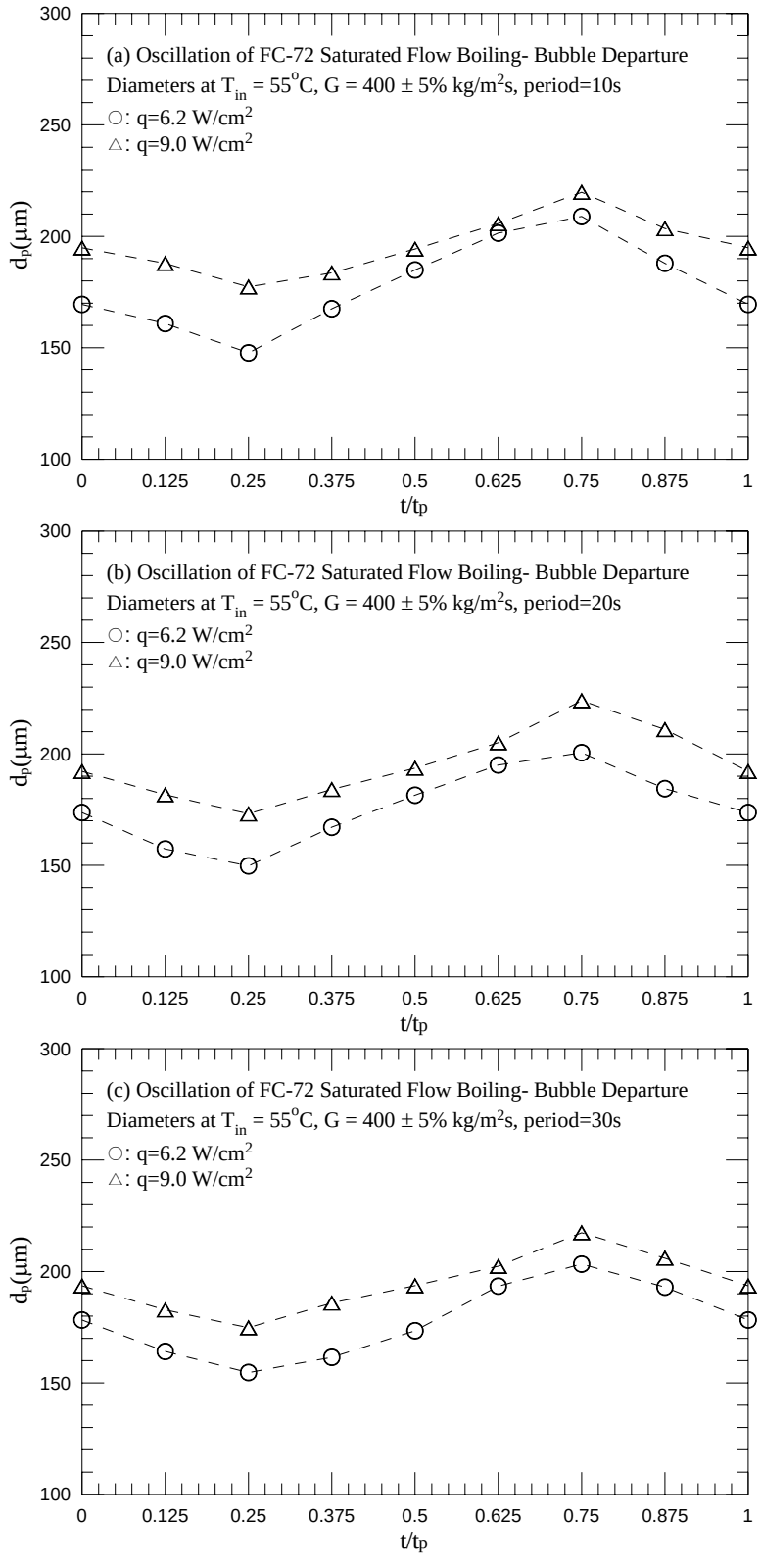

Fig. 4.70 Mean bubble departure diameters for various imposed heat fluxes for transient saturated flow boiling for G=400±5% kg/m^{2}s with t_p=10 sec (a), 20sec (b) and 30 sec (c).

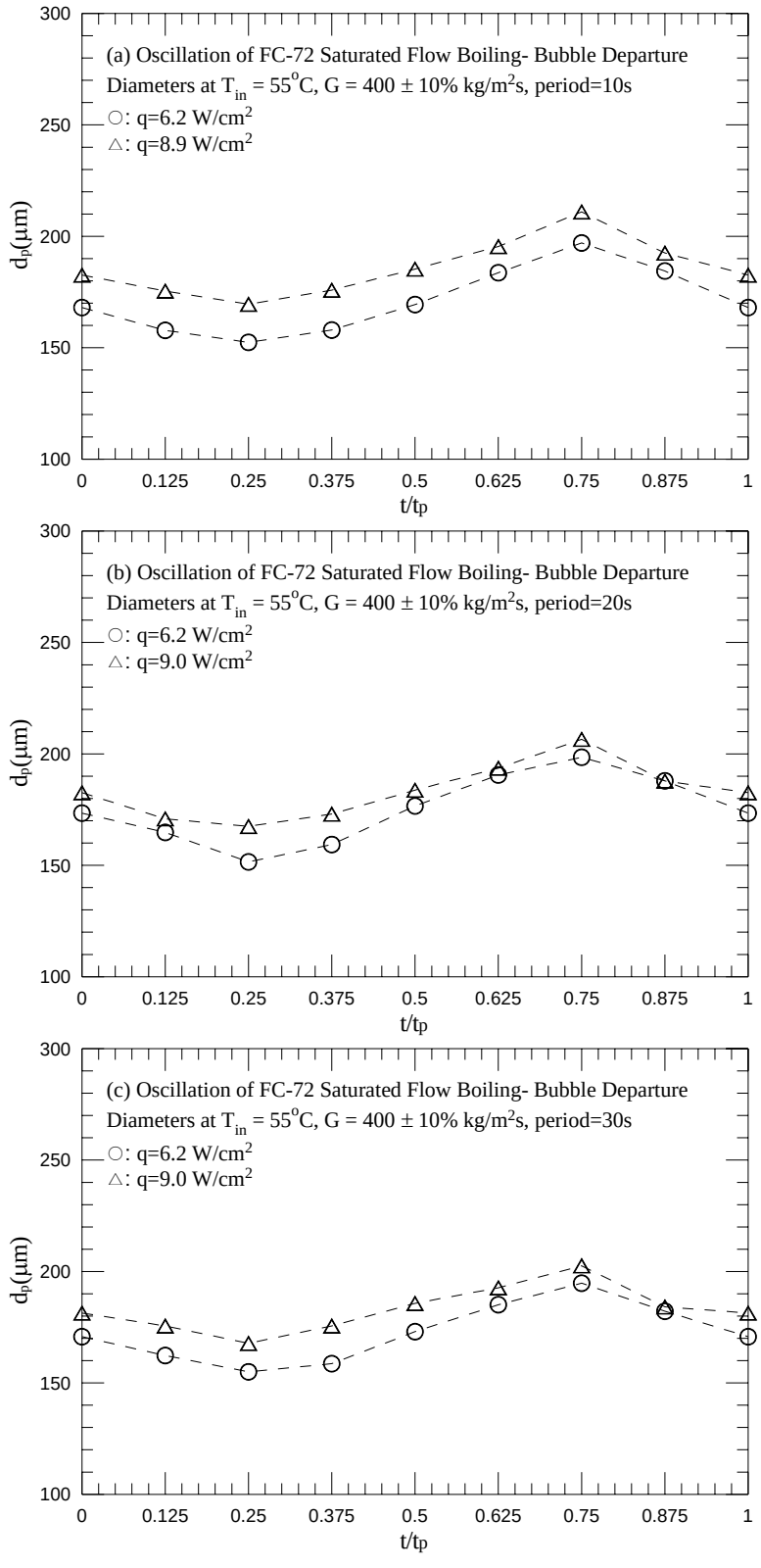

Fig. 4.71 Mean bubble departure diameters for various imposed heat fluxes for transient saturated flow boiling for G=400±10% kg/m^{2}s with t_p=10 sec (a), 20sec (b) and 30 sec (c).

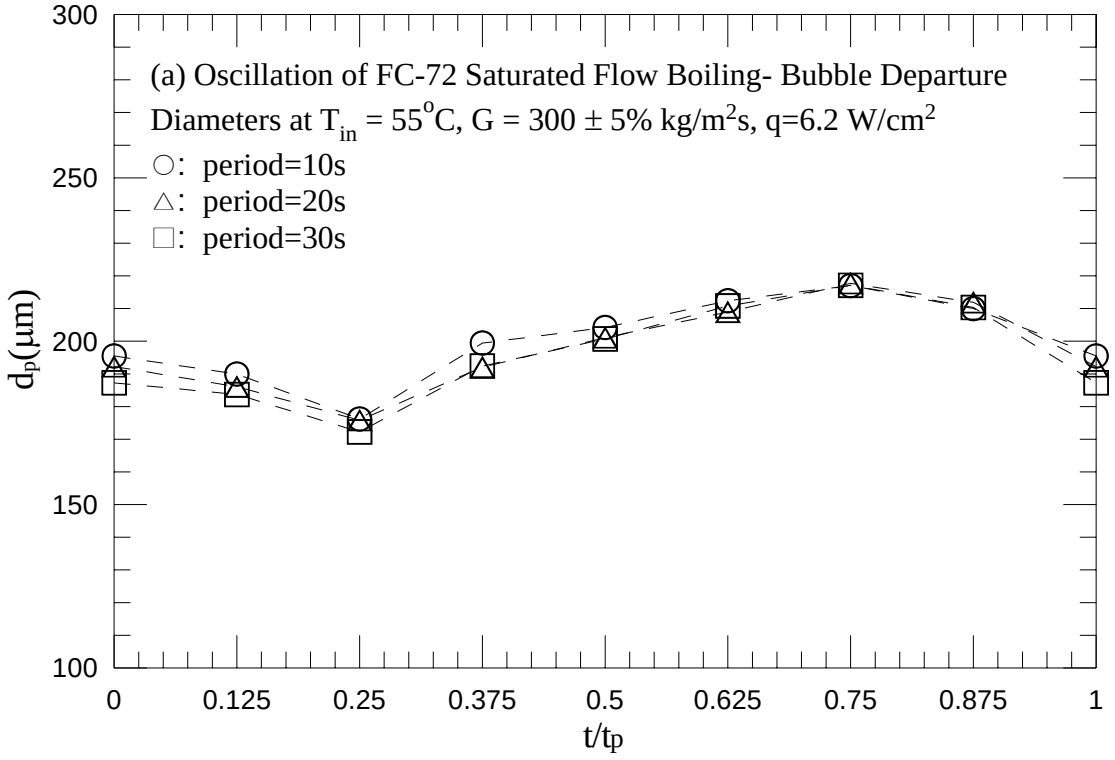

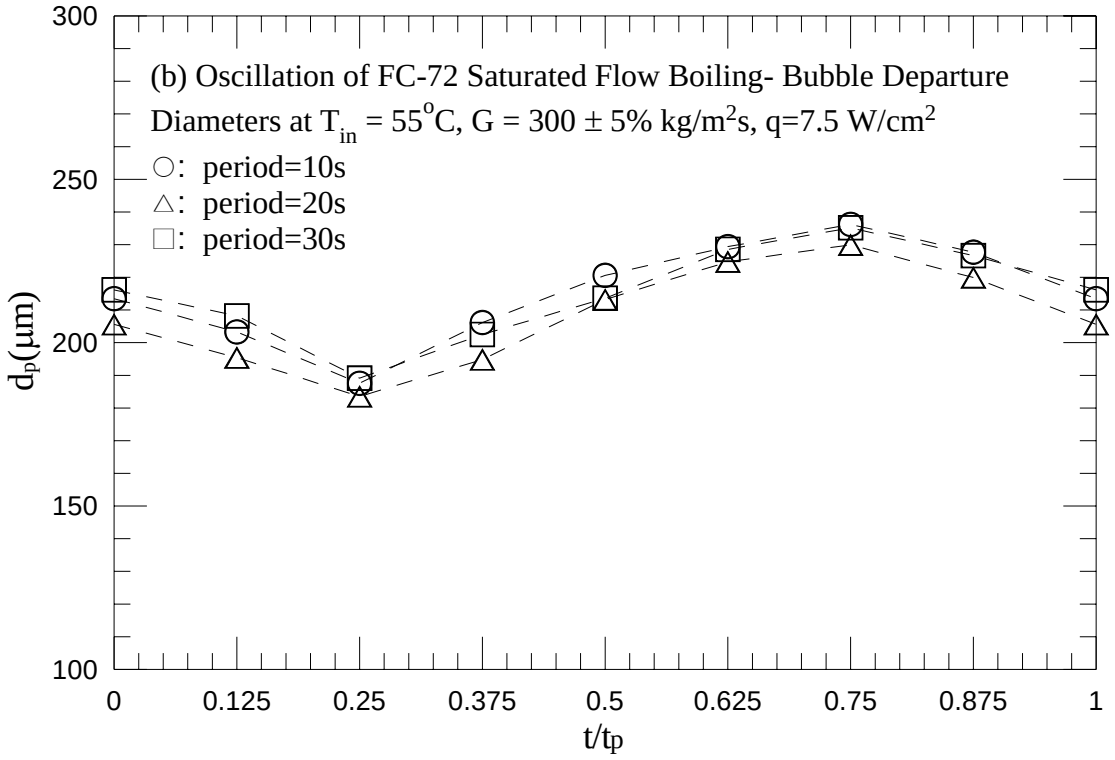

Fig. 4.72 Mean bubble departure diameters for various periods of the mass flux oscillation for transient saturated flow boiling for G=300±5% kg/m^{2}s with (a) q=6.2 W/cm^2 and (b) q=7.5 W/cm^2.

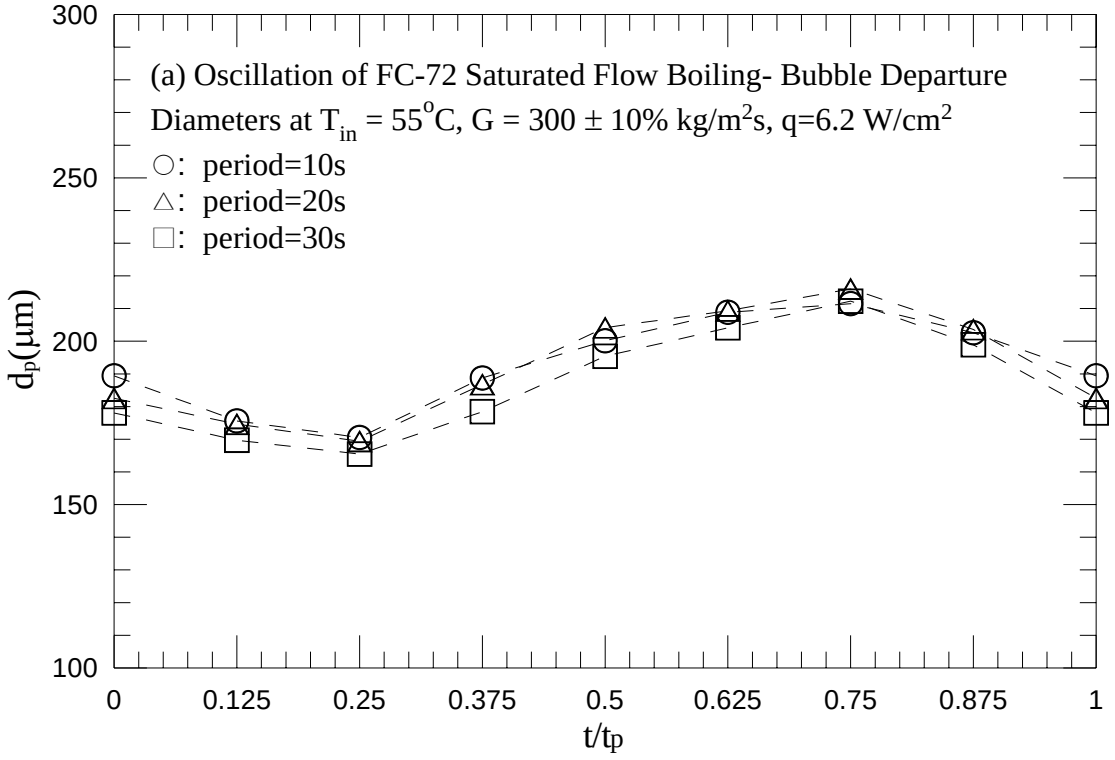

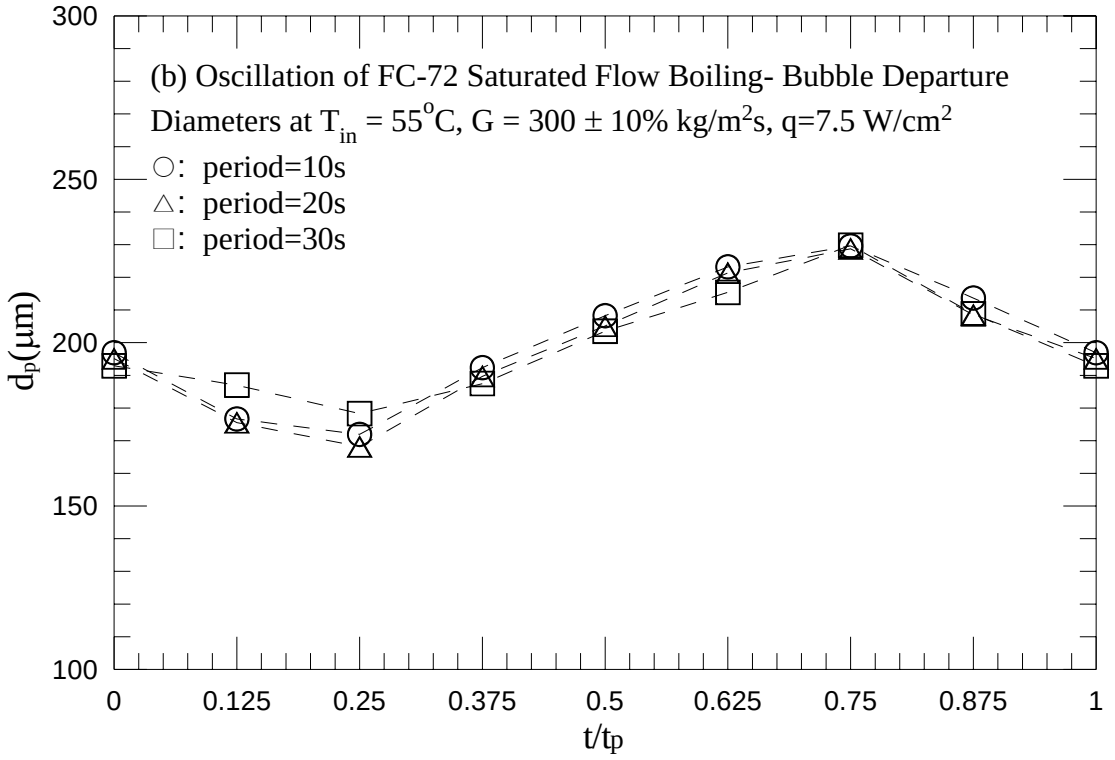

Fig. 4.73 Mean bubble departure diameters for various periods of the mass flux oscillation for transient saturated flow boiling for G=300±10% kg/m^{2}s with (a) q=6.2 W/cm^2 and (b) q=7.5 W/cm^2.

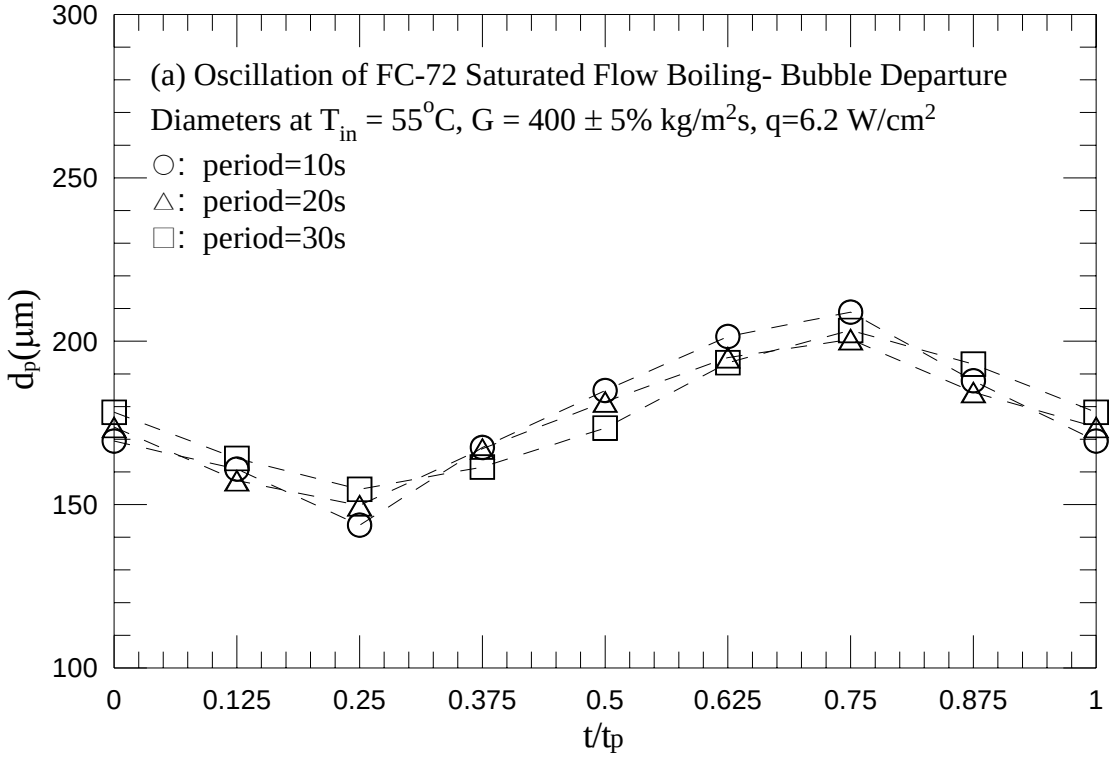

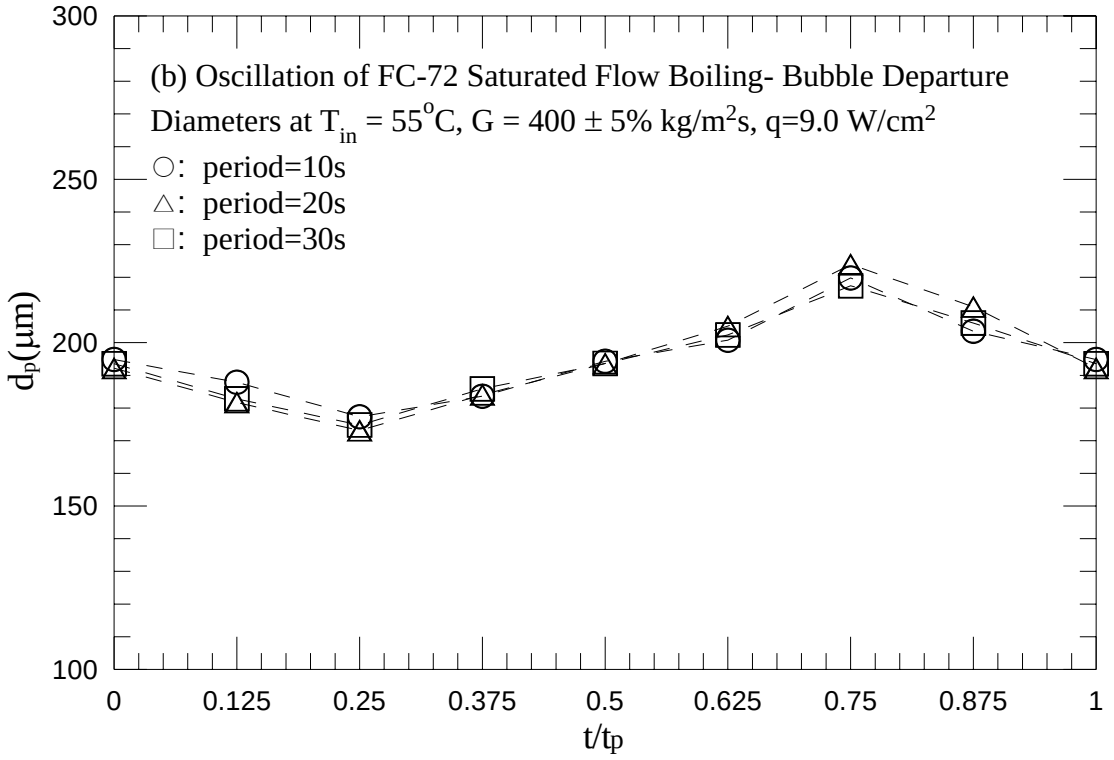

Fig. 4.74 Mean bubble departure diameters for various periods of the mass flux oscillation for transient saturated flow boiling for G=400±5% kg/m^{2}s with (a) q=6.2 W/cm^2 and (b) q=9.0 W/cm^2.

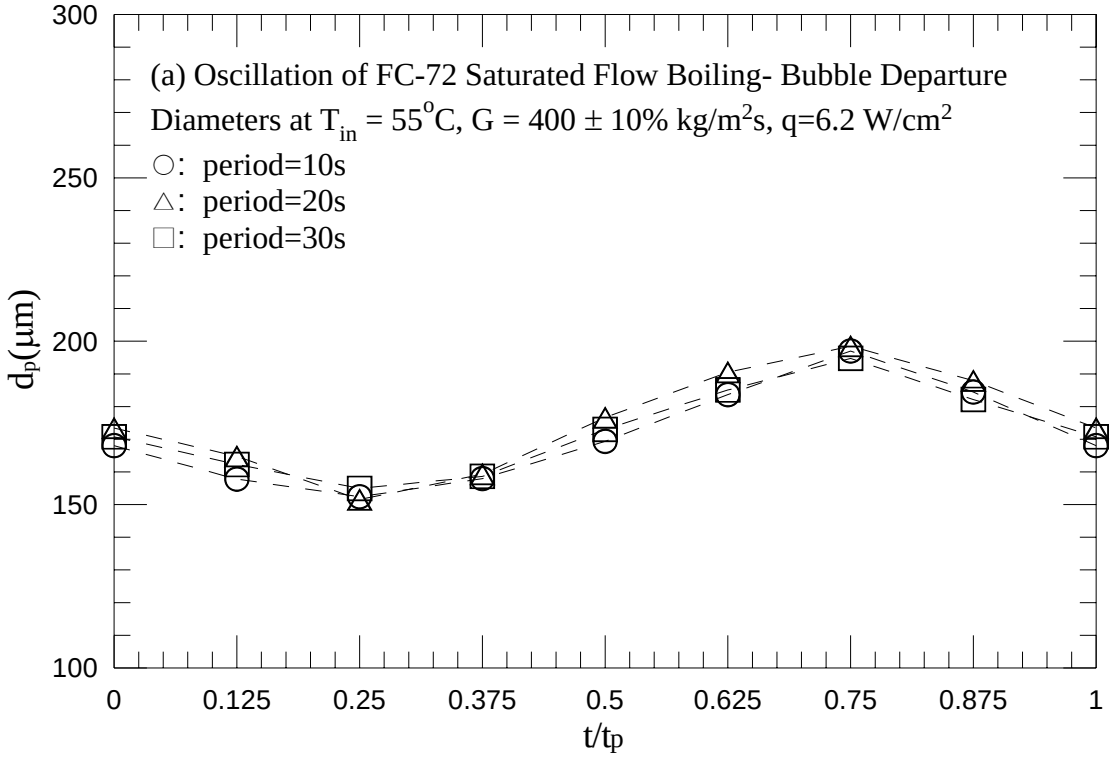

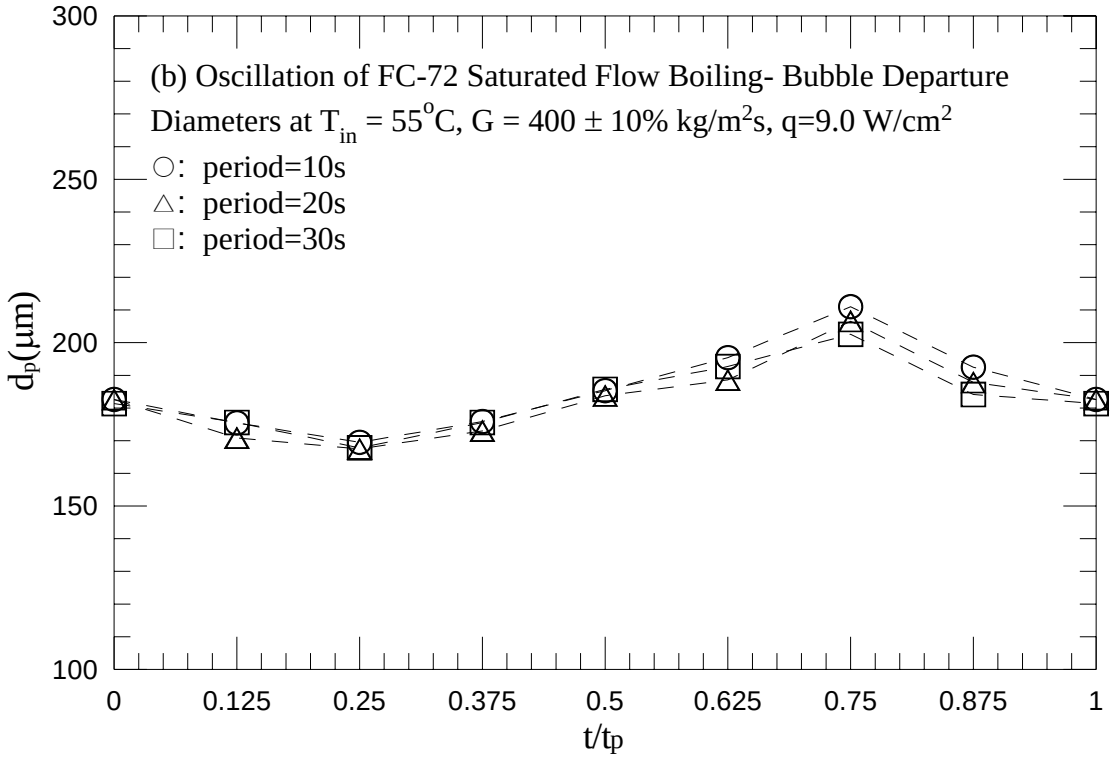

Fig. 4.75 Mean bubble departure diameters for various periods of the mass flux oscillation for transient saturated flow boiling for G=400±10% kg/m^{2}s with (a) q=6.2 W/cm^2 and (b) q=9.0 W/cm^2.

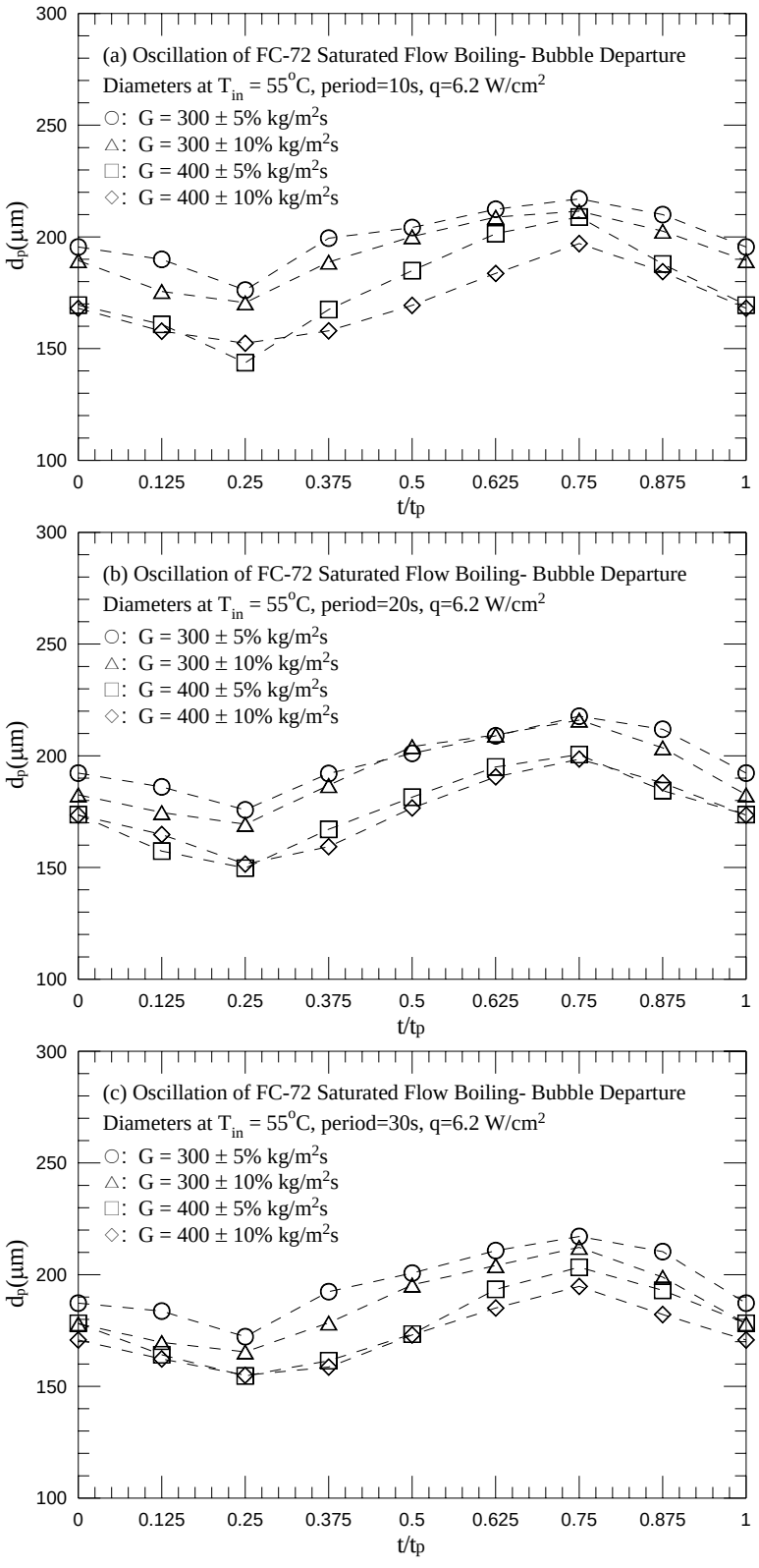

Fig. 4.76 Mean bubble departure diameters for various amplitudes of the mass fluxes oscillation for transient saturated flow boiling for q=6.2 W/cm^2 with period=10 sec (a), 20 sec (b), and 30 sec (c).

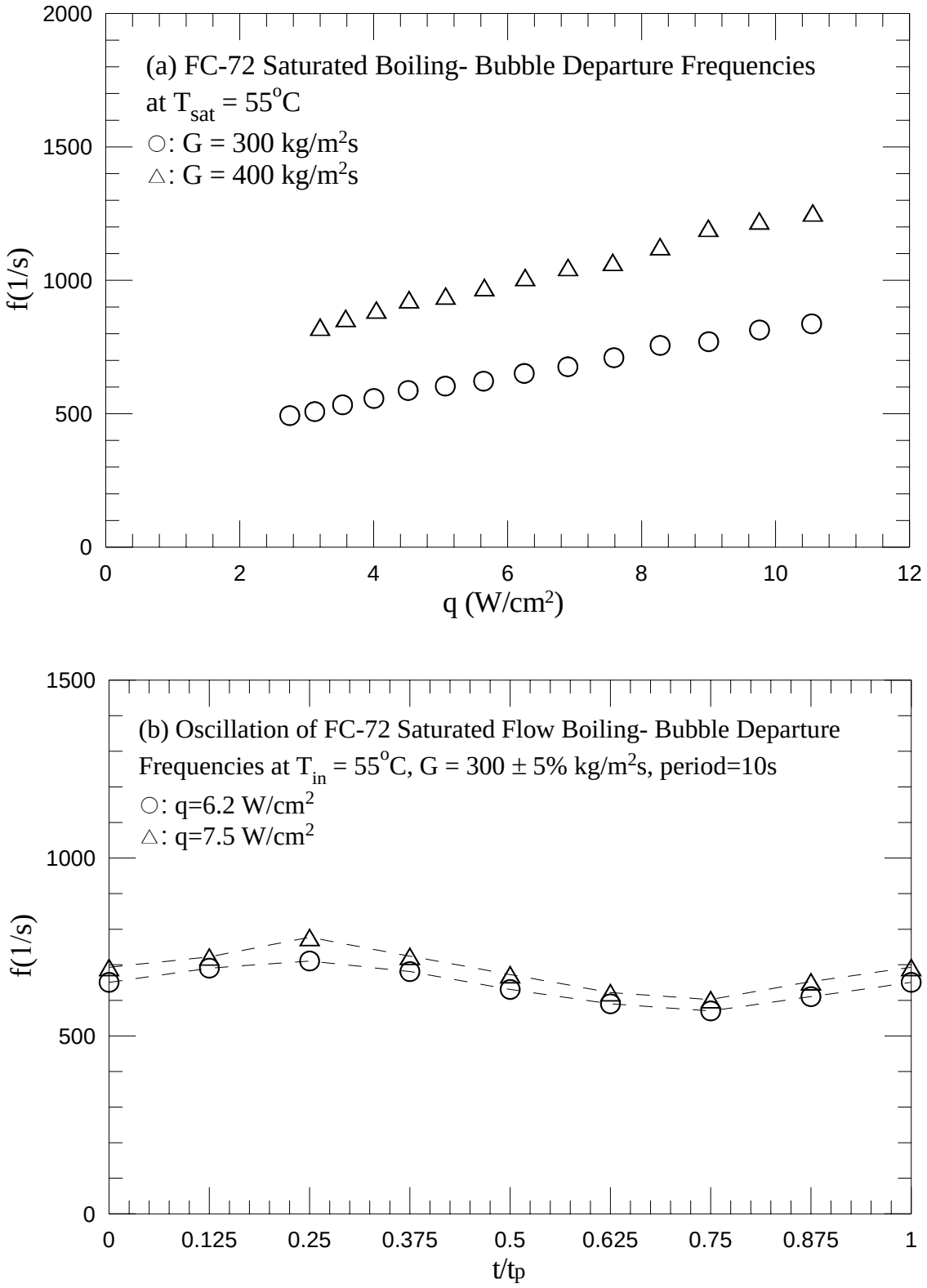

Fig. 4.77 Mean bubble departure frequencies for various coolant mass fluxes for stable saturated flow boiling (a) and various imposed heat fluxes for transient saturated flow boiling for G=300±5% kg/m^{2}s with t_p=10 sec (b), 20sec (c) and 30 sec (d).

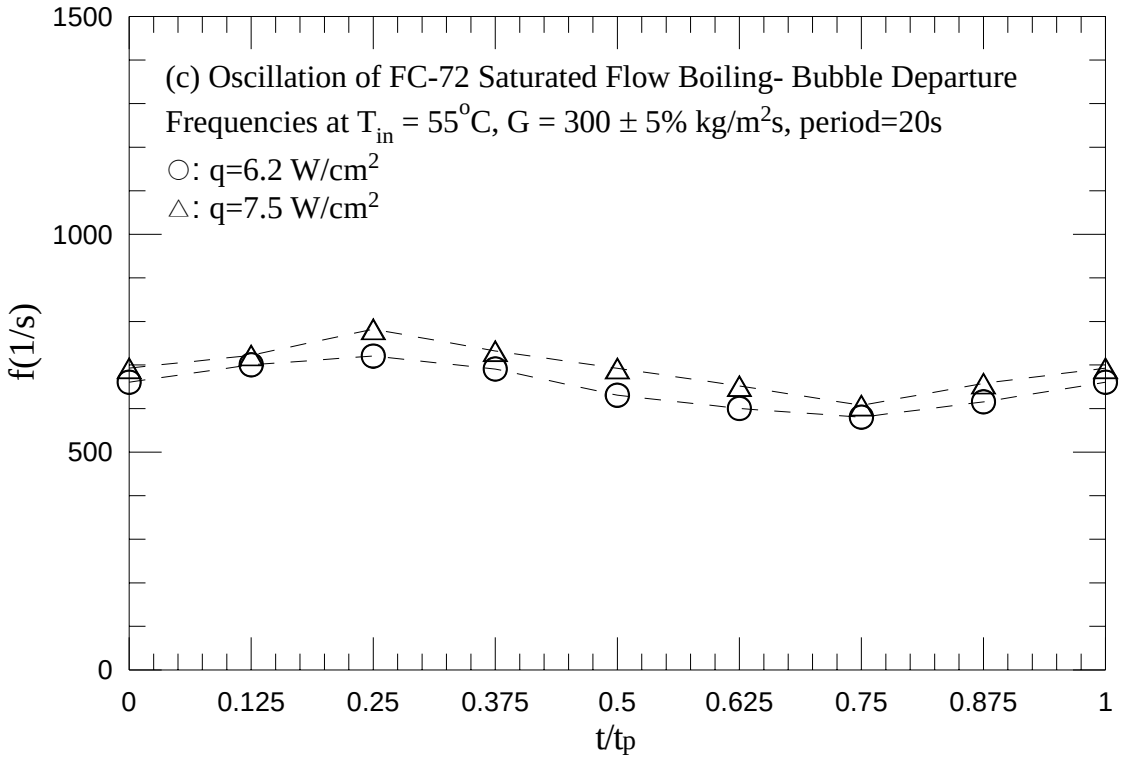

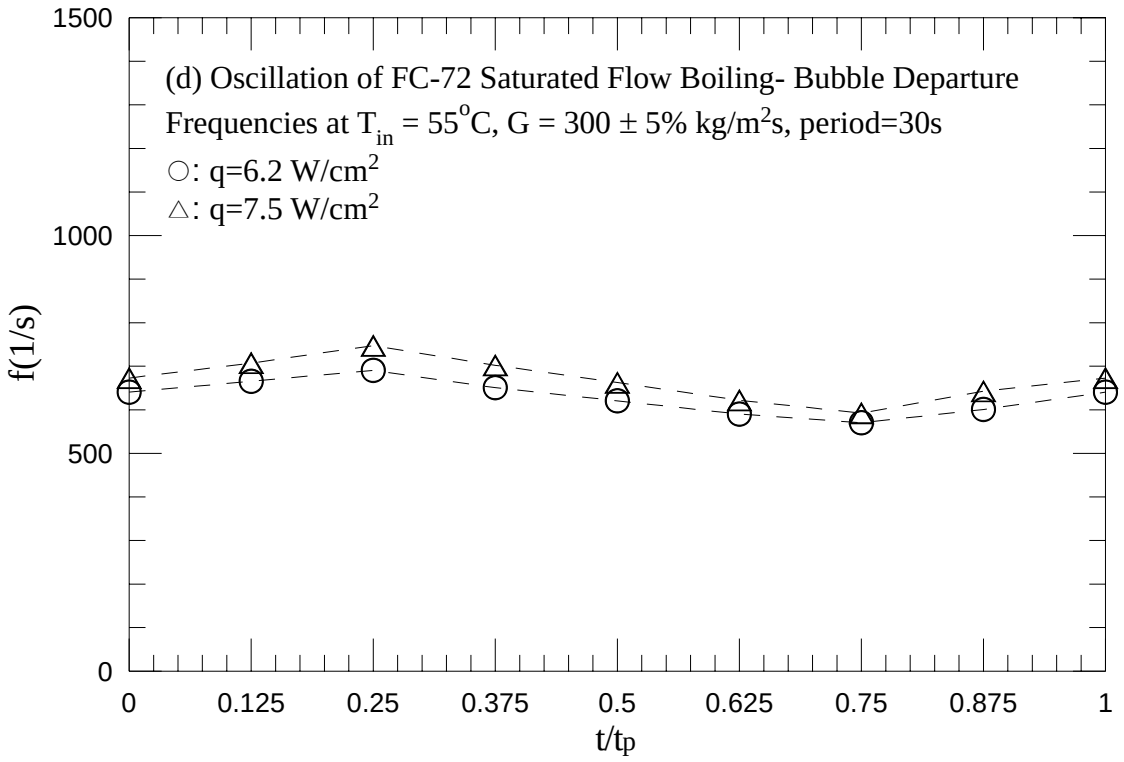

Fig. 4.77 Continued.

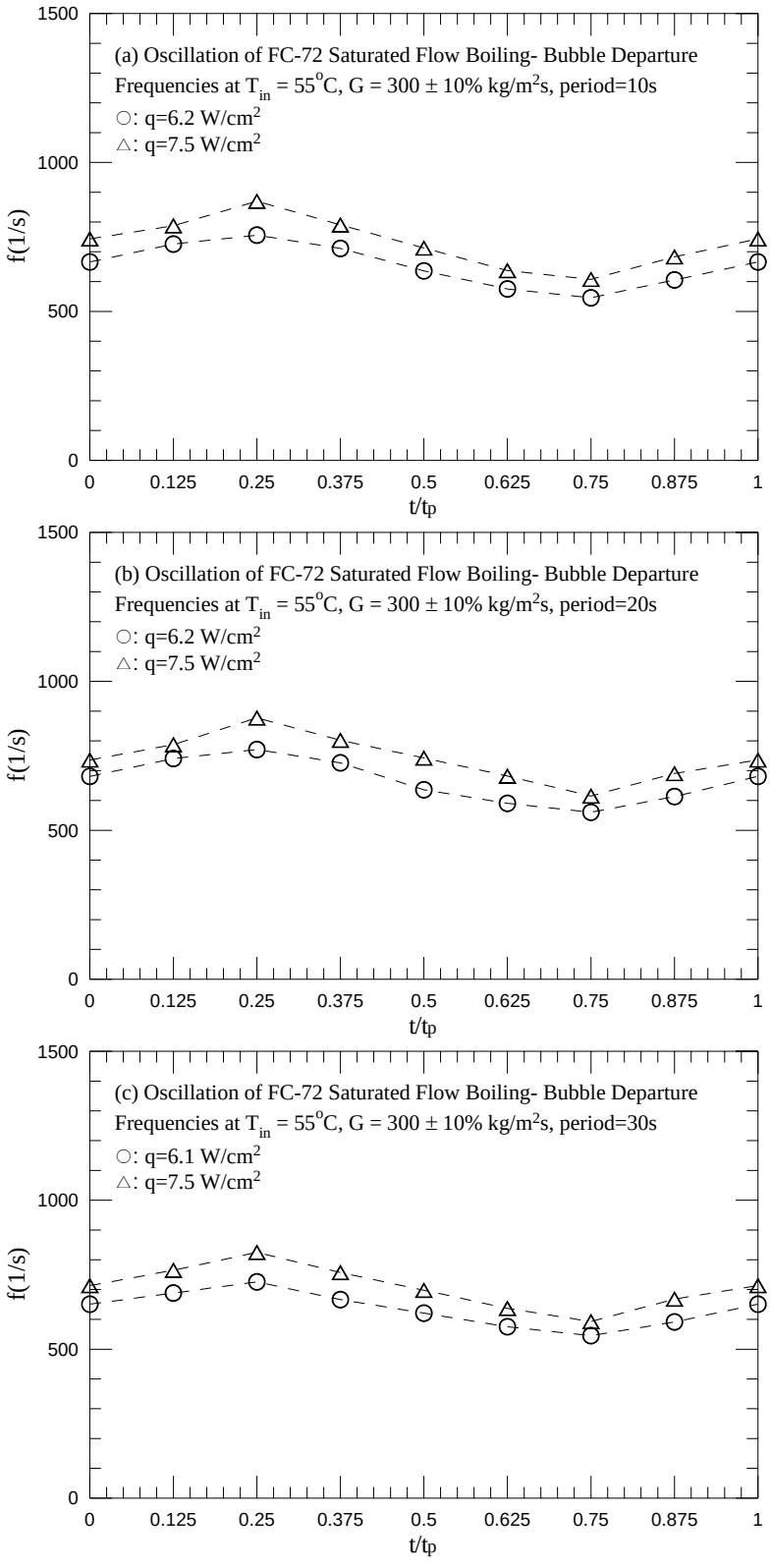

Fig. 4.78 Mean bubble departure frequencies for various imposed heat fluxes for transient saturated flow boiling for G=300±10% kg/m^{2}s with t_p=10 sec (a), 20sec (b) and 30 sec (c).

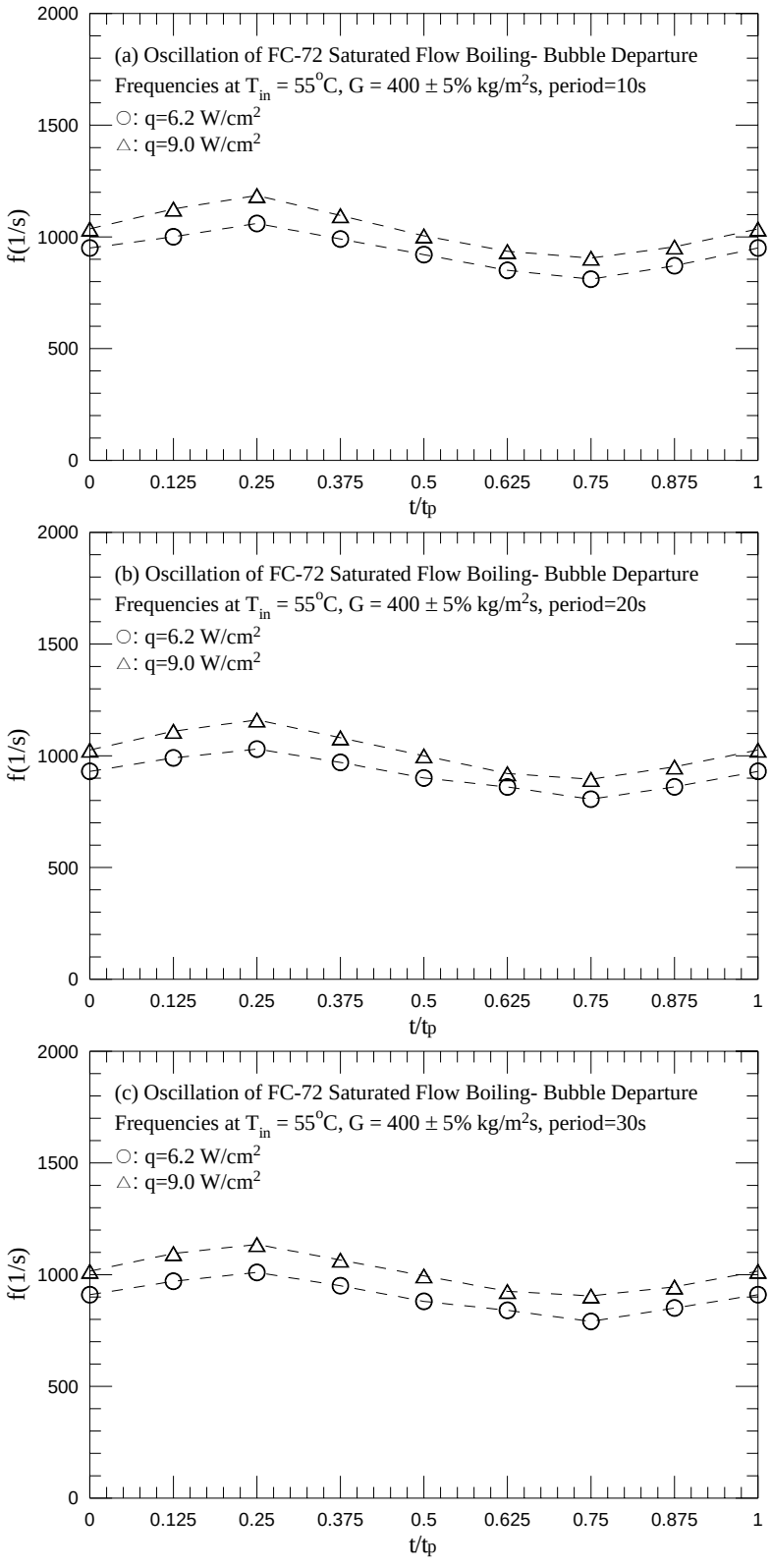

Fig. 4.79 Mean bubble departure frequencies for various imposed heat fluxes for transient saturated flow boiling for G=400±5% kg/m^{2}s with t_p=10 sec (a), 20sec (b) and 30 sec (c).

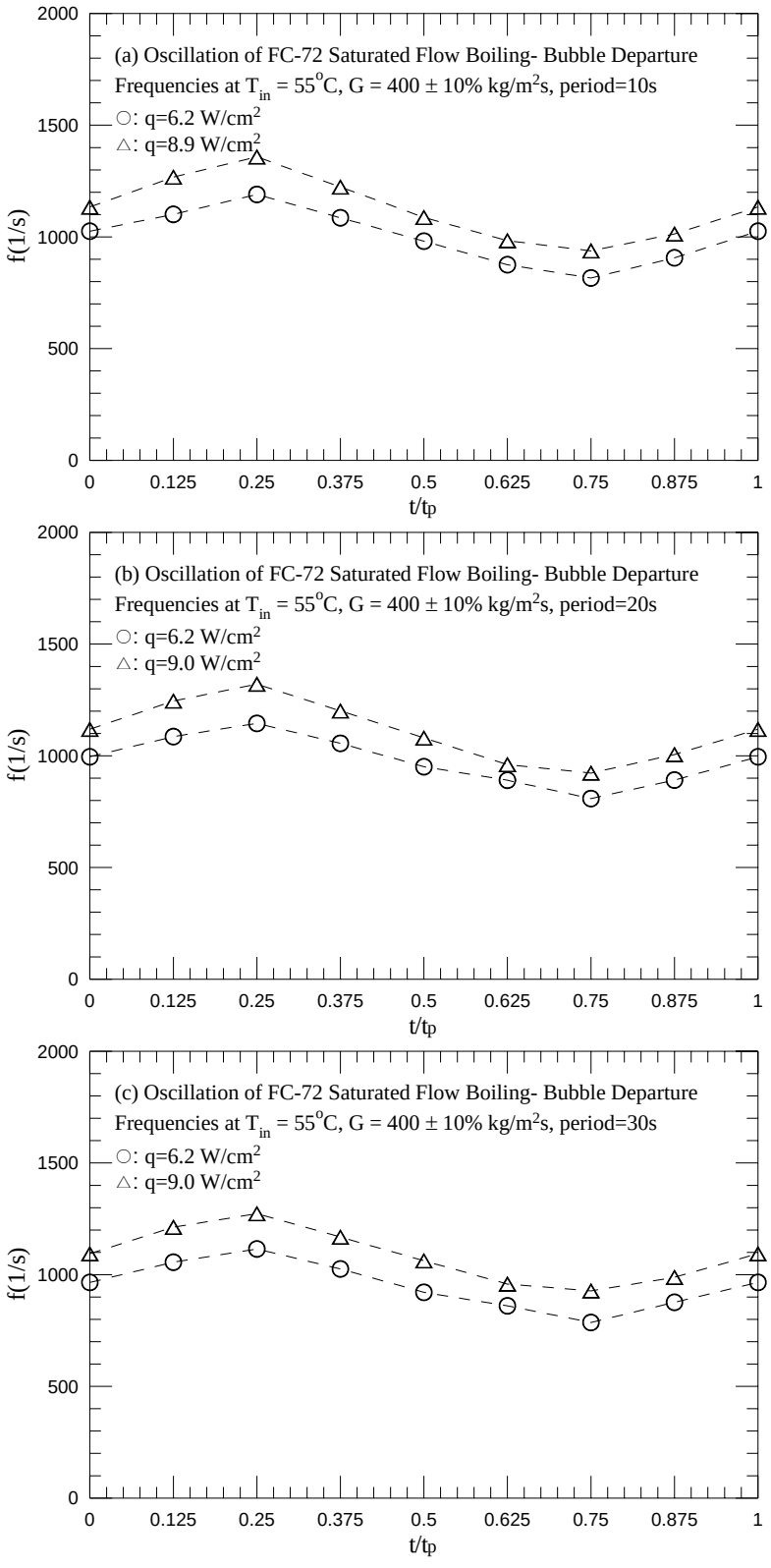

Fig. 4.80 Mean bubble departure frequencies for various imposed heat fluxes for transient saturated flow boiling for G=400±10% kg/m^{2}s with t_p=10 sec (a), 20sec (b) and 30 sec (c).

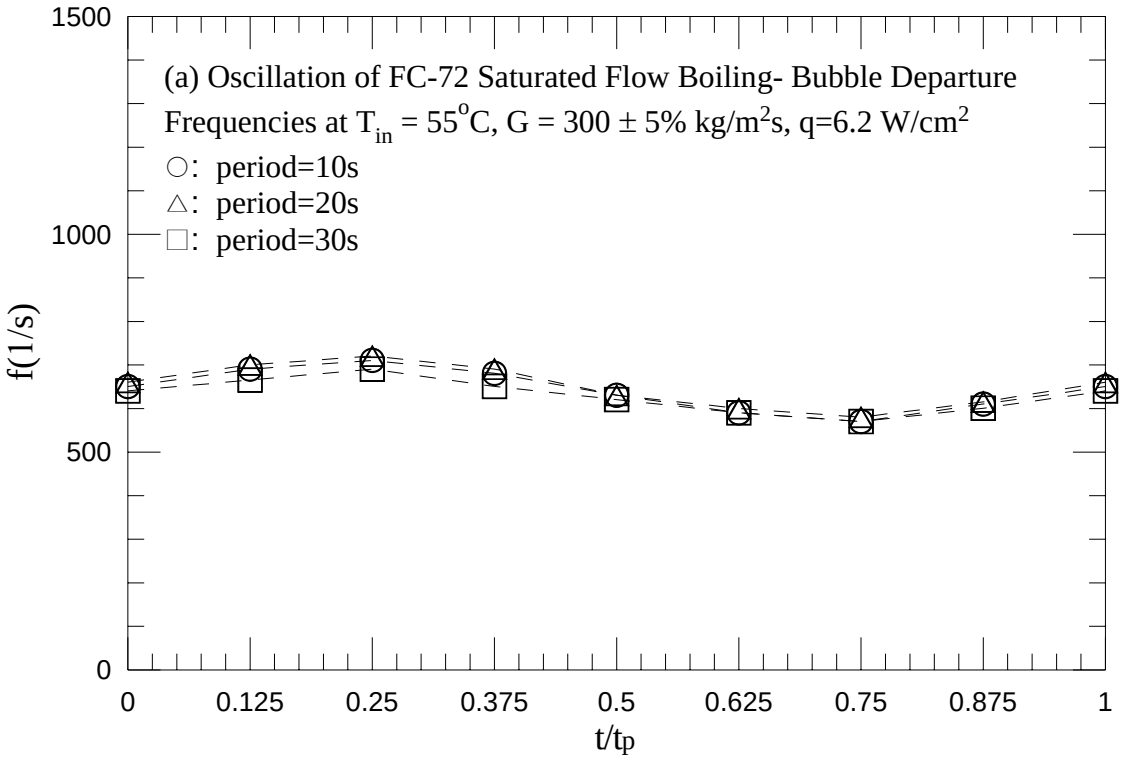

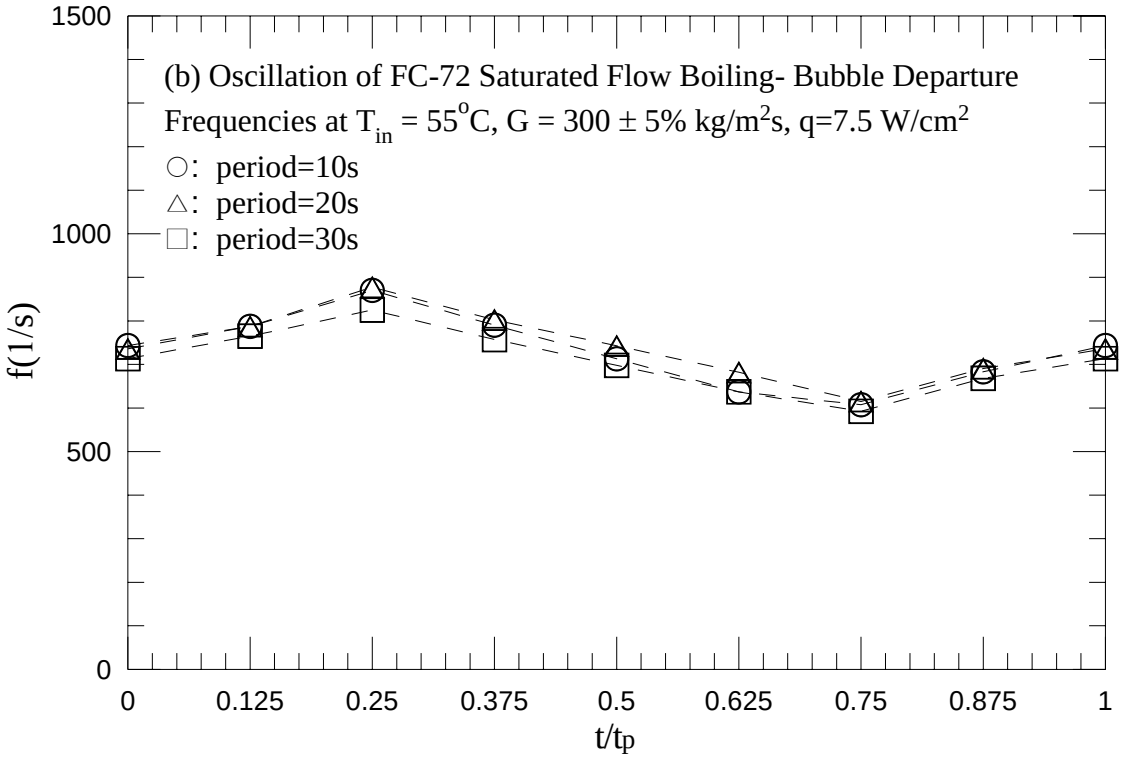

Fig. 4.81 Mean bubble departure frequencies for various periods of mass flux oscillation for transient saturated flow boiling for G=300±5% kg/m^{2}s with (a) q=6.2 W/cm^2 and (b) q=7.5 W/cm^2.

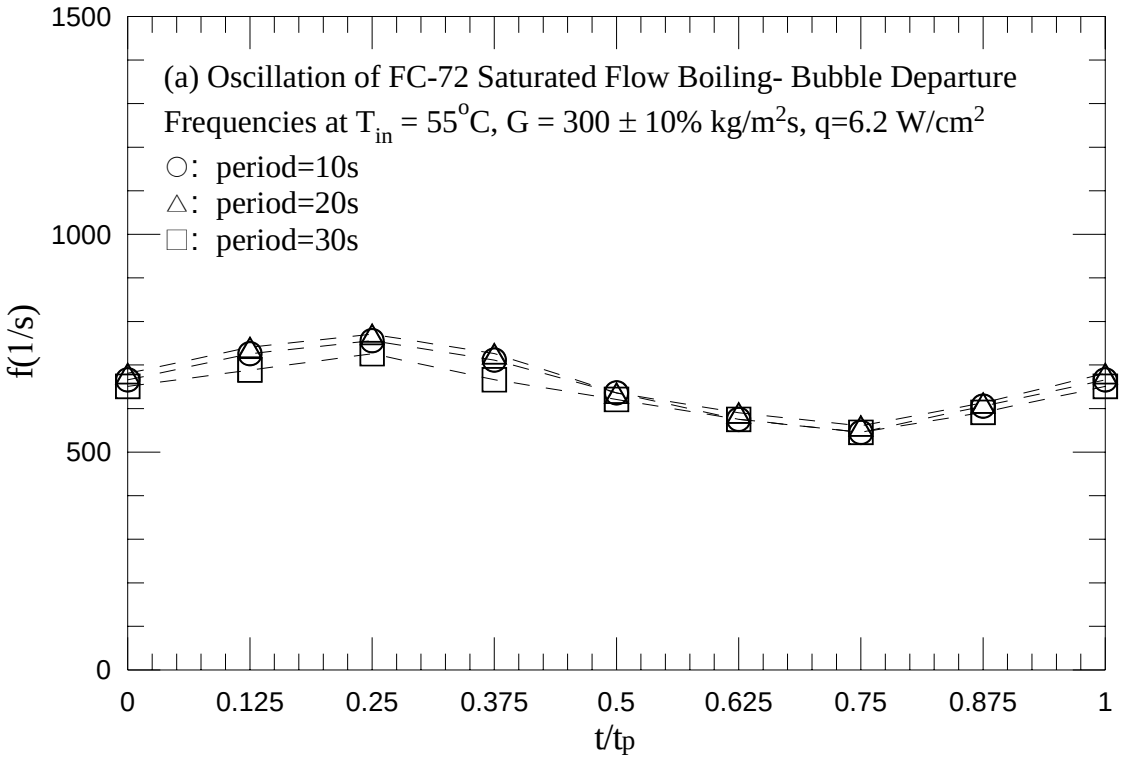

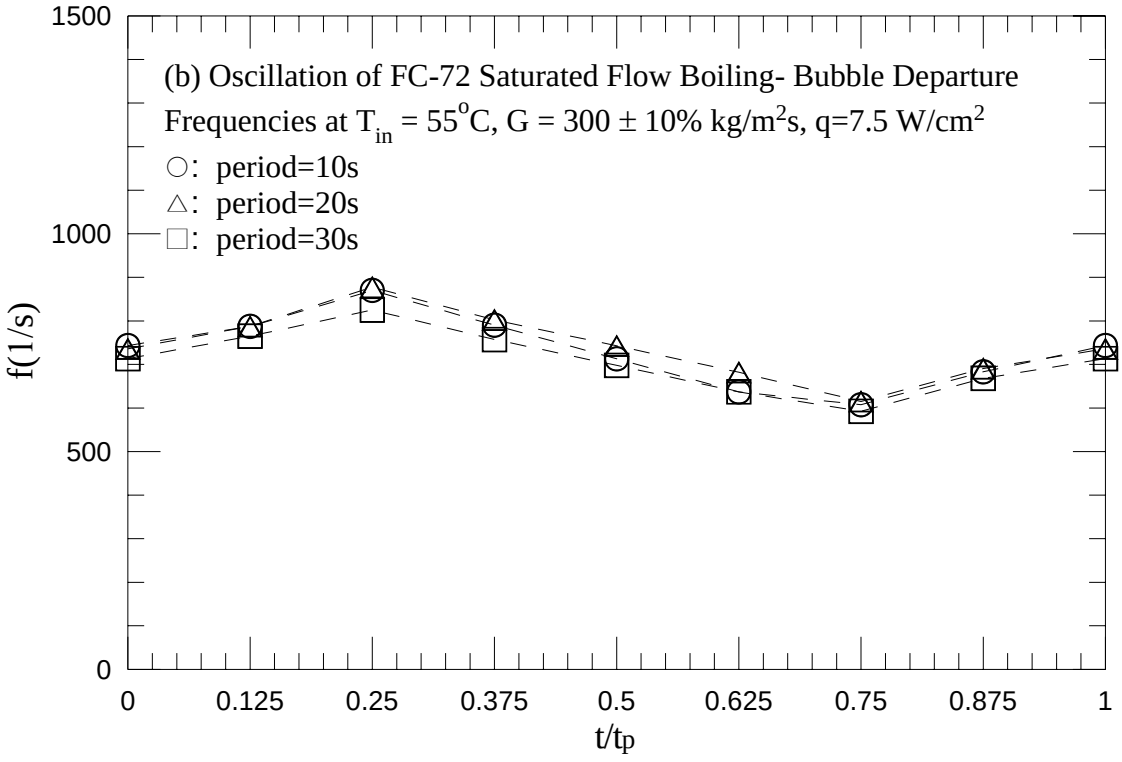

Fig. 4.82 Mean bubble departure frequencies for various periods of mass flux oscillation for transient saturated flow boiling for G=300±10% kg/m^{2}s with (a) q=6.2 W/cm^2 and (b) q=7.5 W/cm^2.

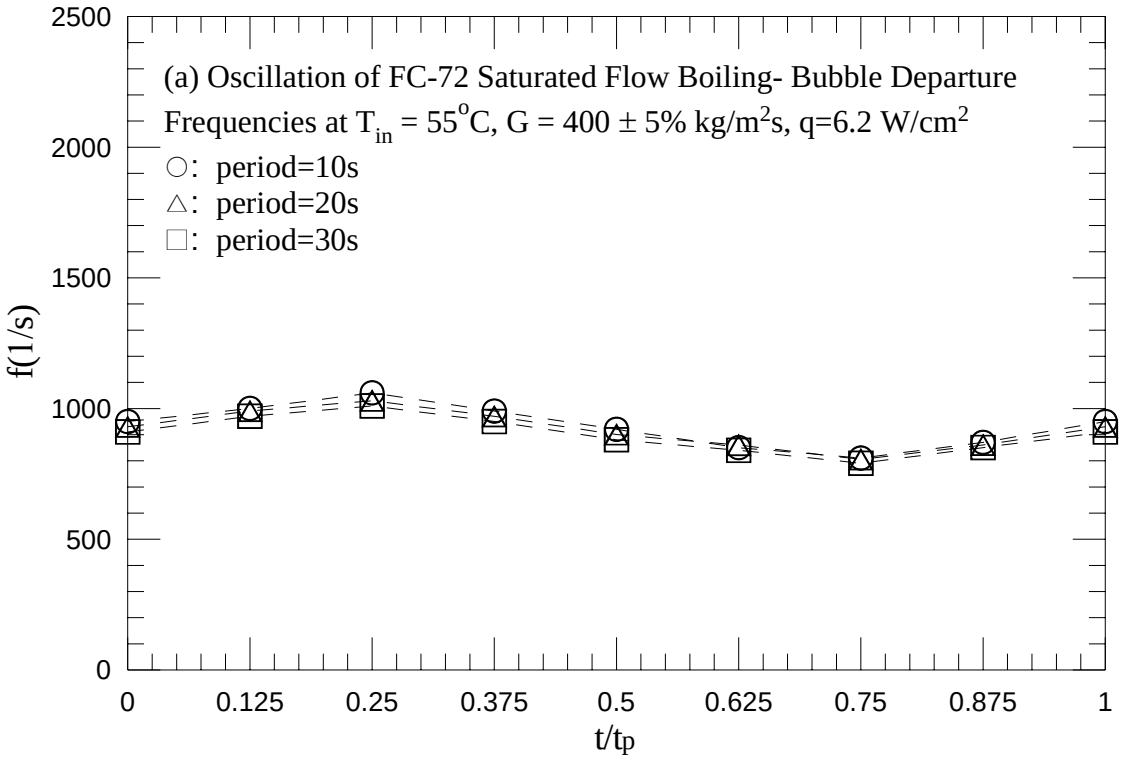

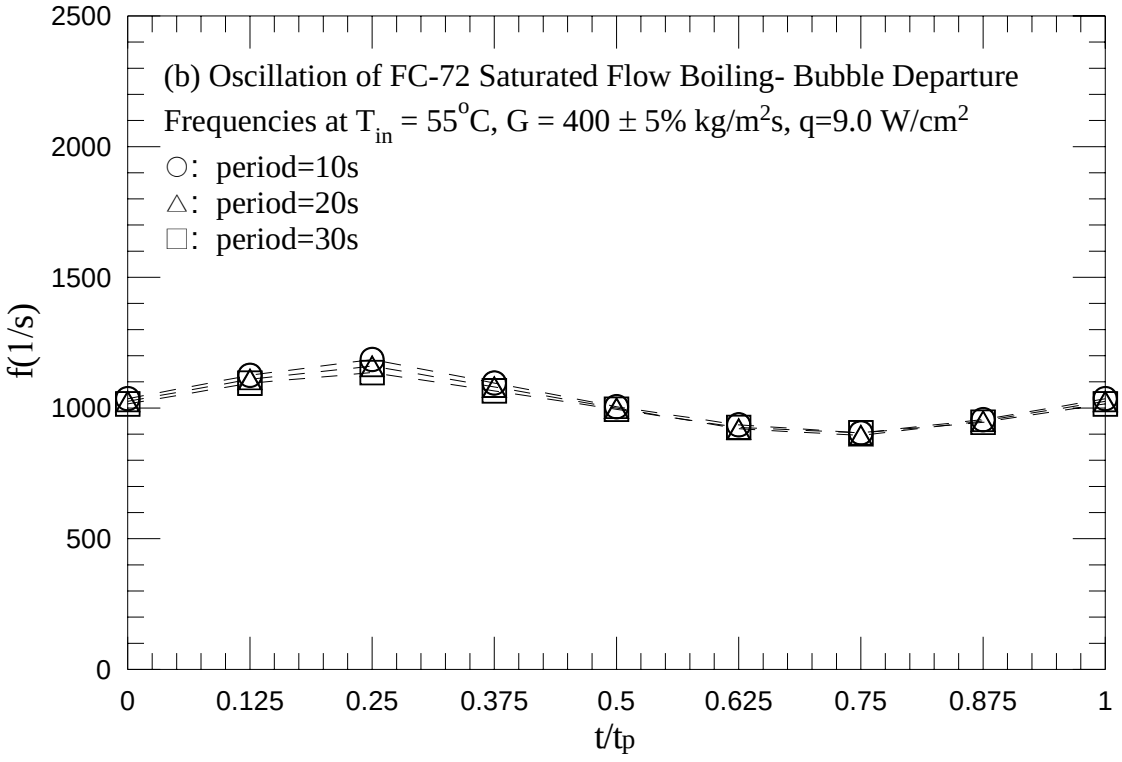

Fig. 4.83 Mean bubble departure frequencies for various periods of mass flux oscillation for transient saturated flow boiling for G=400±5% kg/m^{2}s with (a) q=6.2 W/cm^2 and (b) q=9.0 W/cm^2.

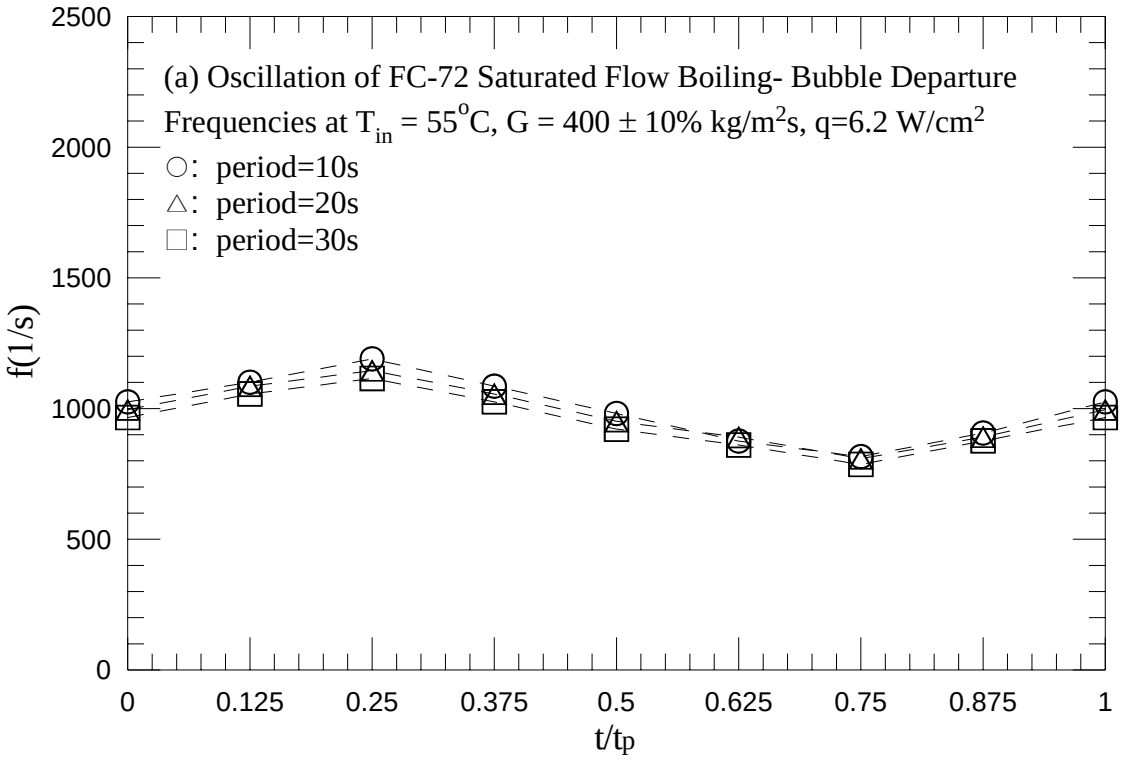

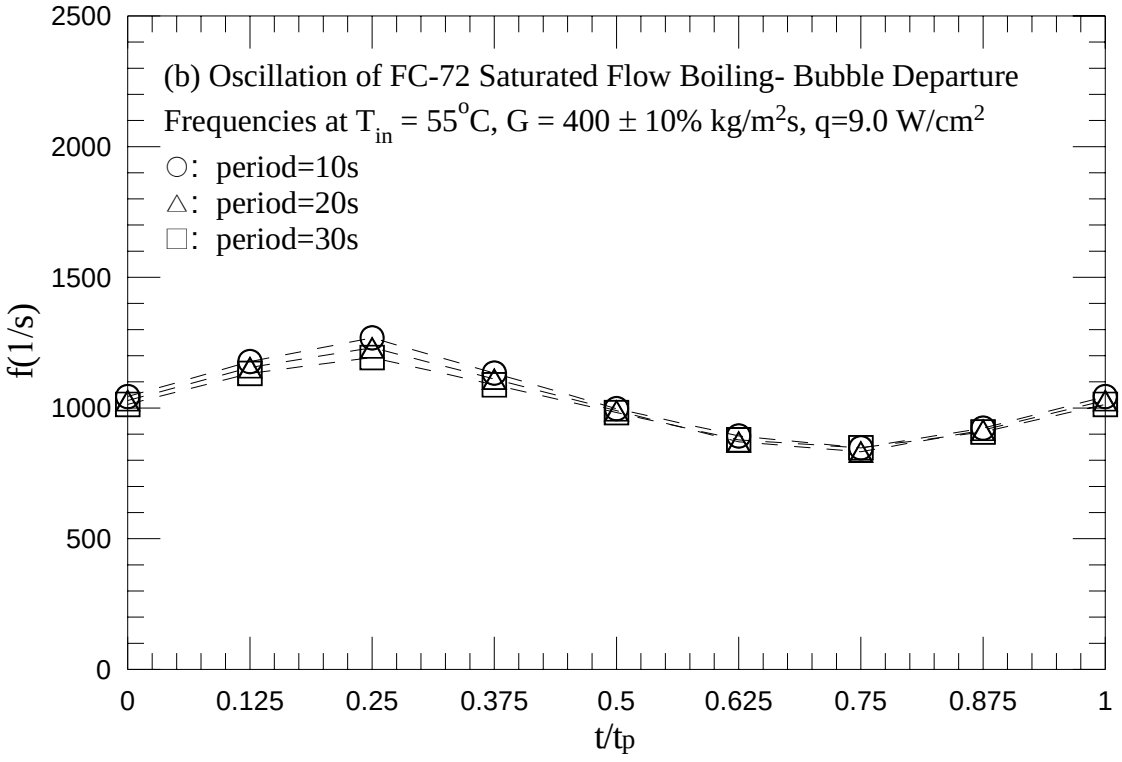

Fig. 4.84 Mean bubble departure frequencies for various periods of mass flux oscillation for transient saturated flow boiling for G=400±10% kg/m^{2}s with (a) q=6.2 W/cm^2 and (b) q=9.0 W/cm^2.

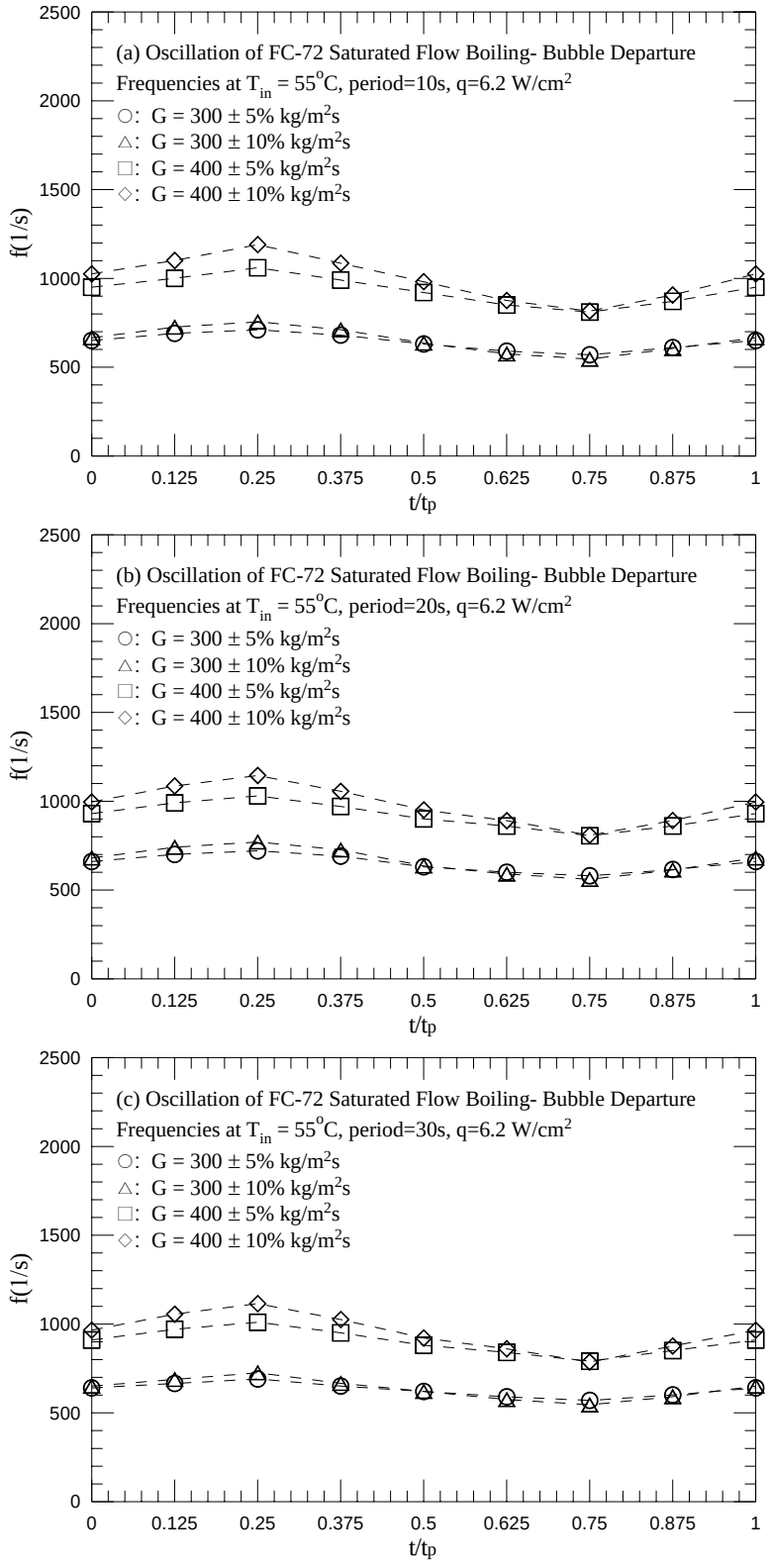

Fig. 4.85 Mean bubble departure frequencies for various amplitudes of the mass fluxes oscillation for transient saturated flow boiling for q=6.2 W/cm^2 with period=10 sec (a), 20 sec (b), and 30 sec (c).

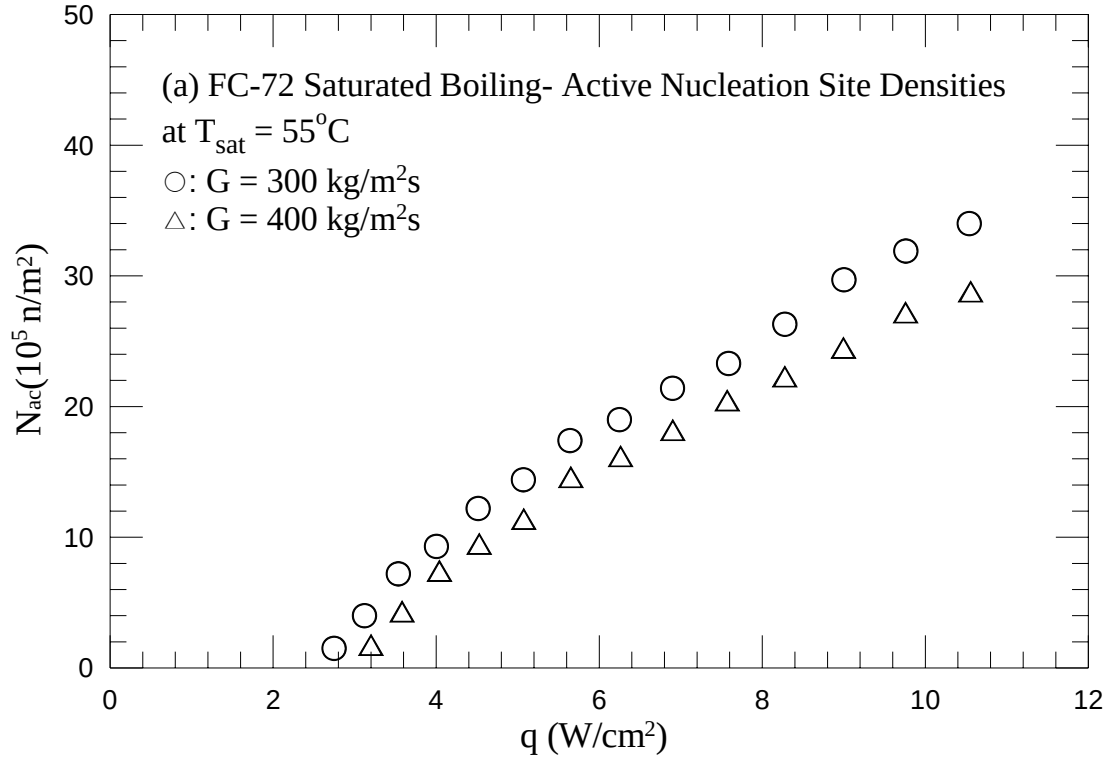

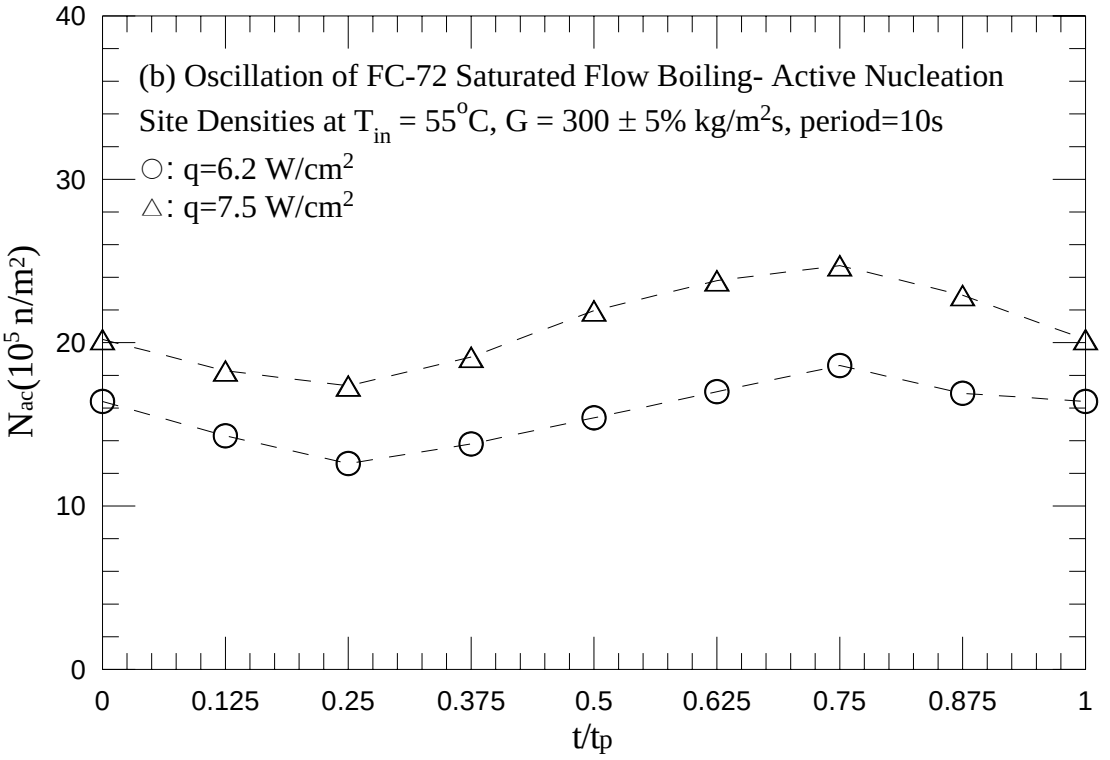

Fig. 4.86 Mean active nucleation site densities for various coolant mass fluxes for stable saturated flow boiling (a) and various imposed heat fluxes for transient saturated flow boiling for G=300±5% kg/m^{2}s with t_p=10 sec (b), 20sec (c) and 30 sec (d).

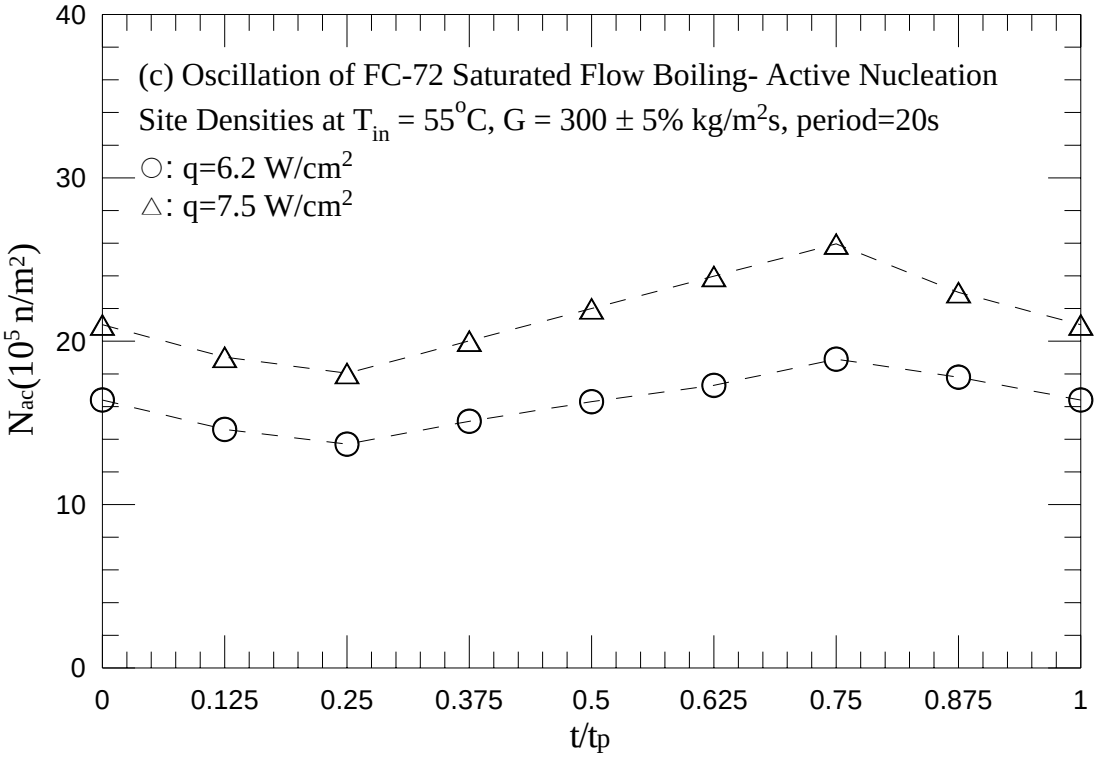

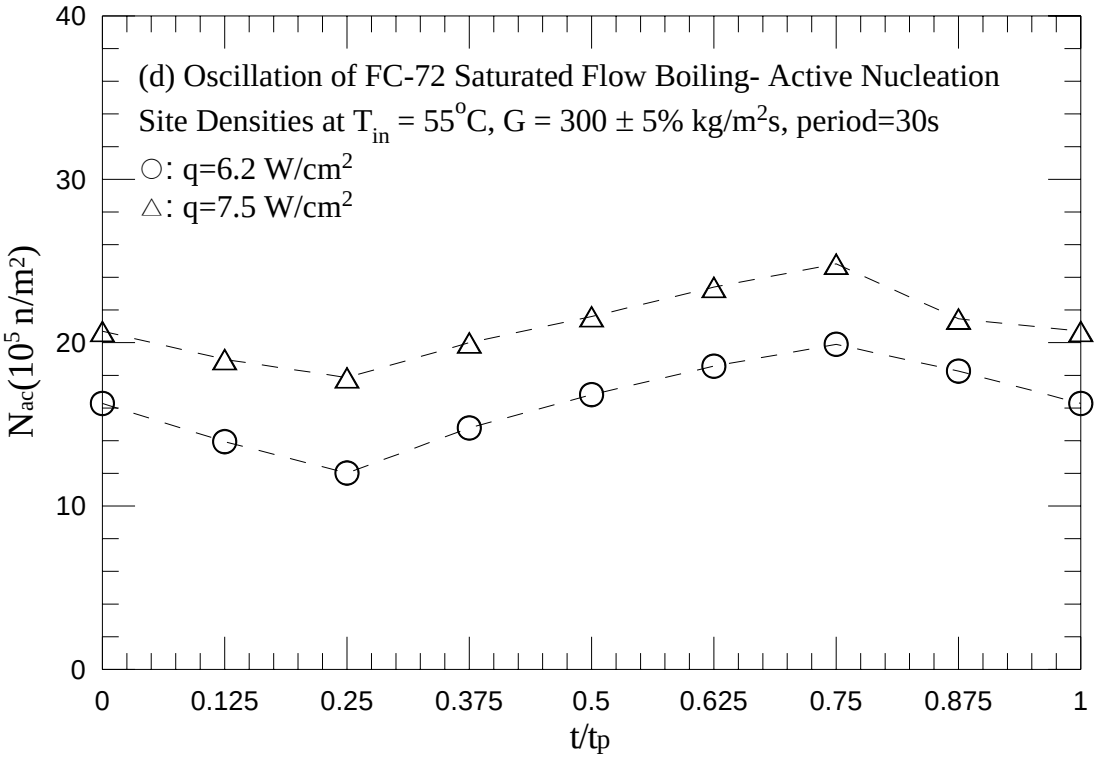

Fig. 4.86 Continued.

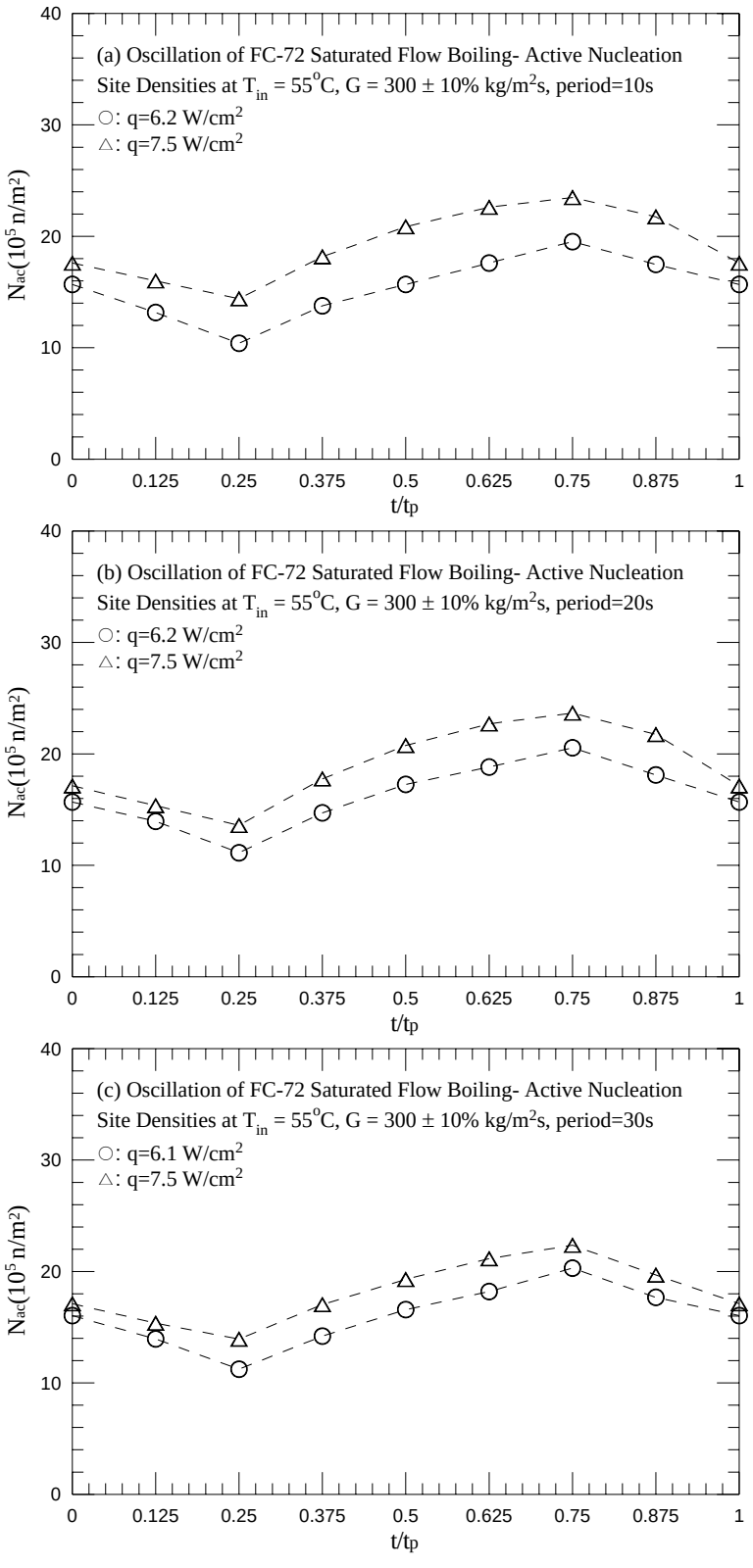

Fig. 4.87 Mean active nucleation site densities for various imposed heat fluxes for transient saturated flow boiling for G=300±10% kg/m^{2}s with t_p=10 sec (a), 20sec (b) and 30 sec (c).

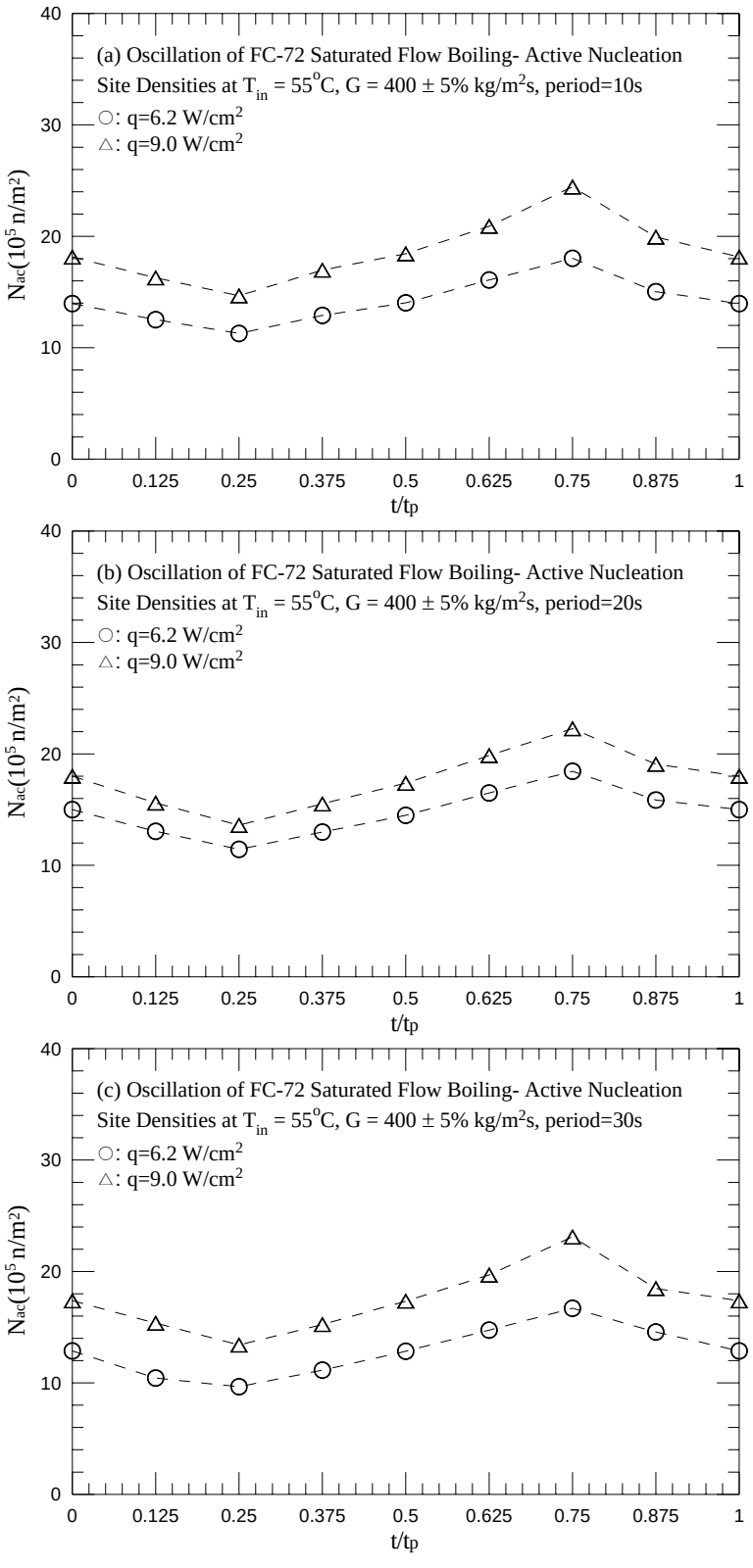

Fig. 4.88 Mean active nucleation site densities for various imposed heat fluxes for transient saturated flow boiling for G=400±5% kg/m^{2}s with t_p=10 sec (a), 20sec (b) and 30 sec (c).

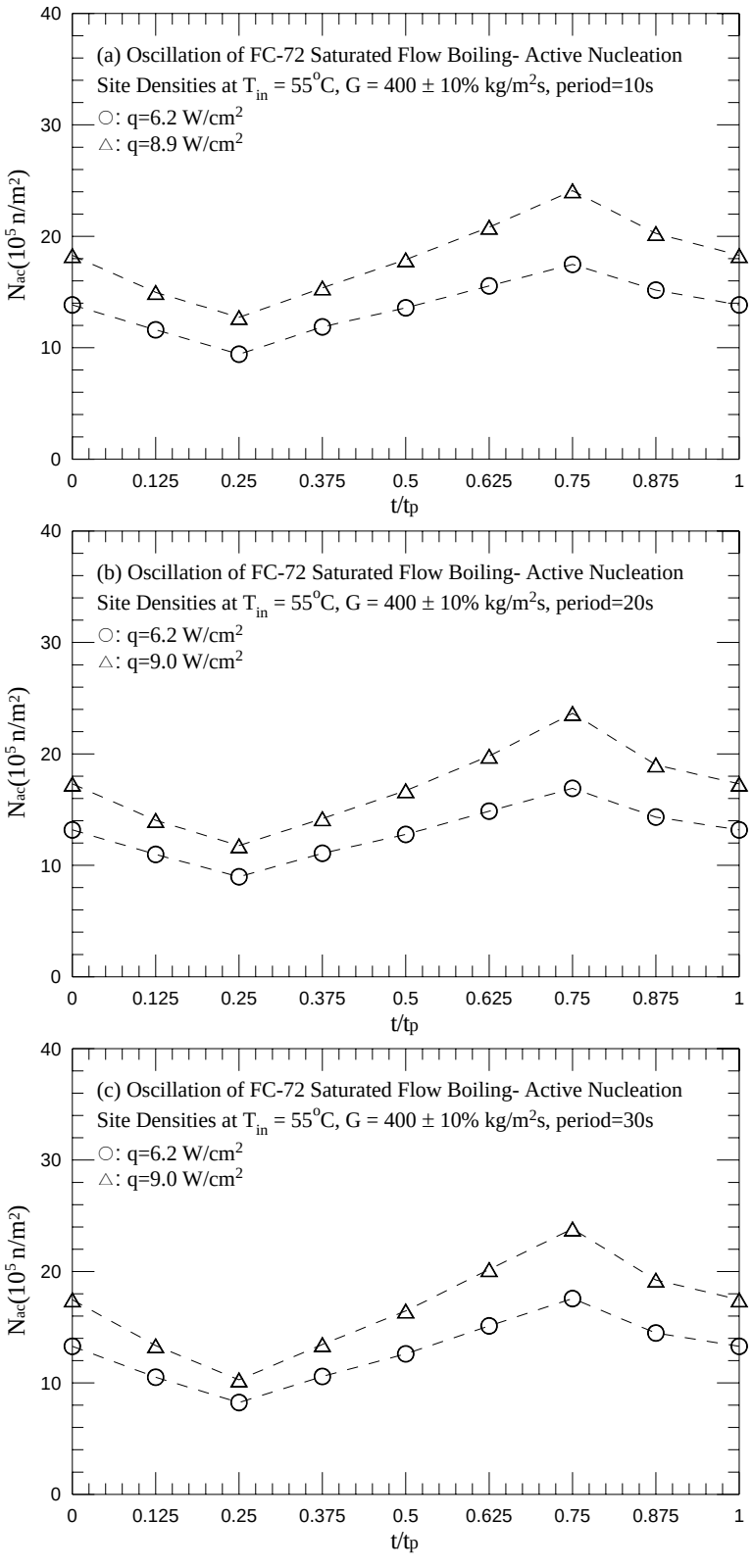

Fig. 4.89 Mean active nucleation site densities for various imposed heat fluxes for transient saturated flow boiling for G=400±10% kg/m^{2}s with t_p=10 sec (a), 20sec (b) and 30 sec (c).

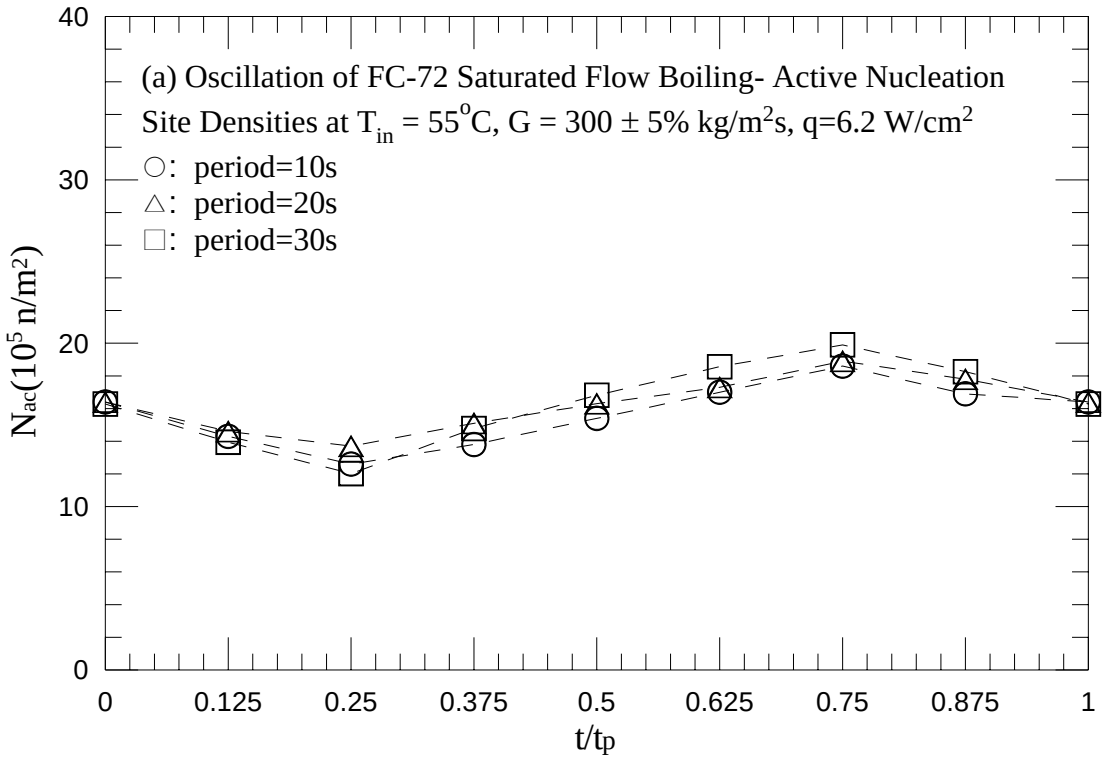

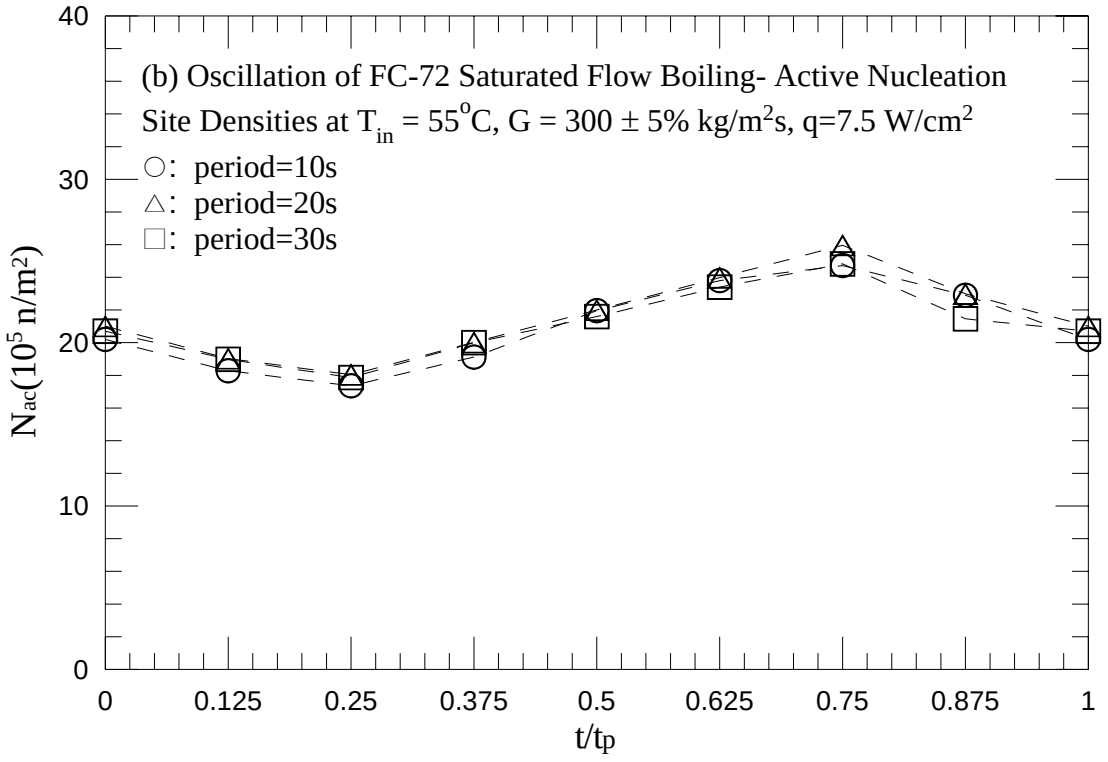

Fig. 4.90 Mean active nucleation site densities for various periods of mass flux oscillation for transient saturated flow boiling for G=300±5% kg/m^{2}s with (a) q=6.2 W/cm^2 and (b) q=7.5 W/cm^2.

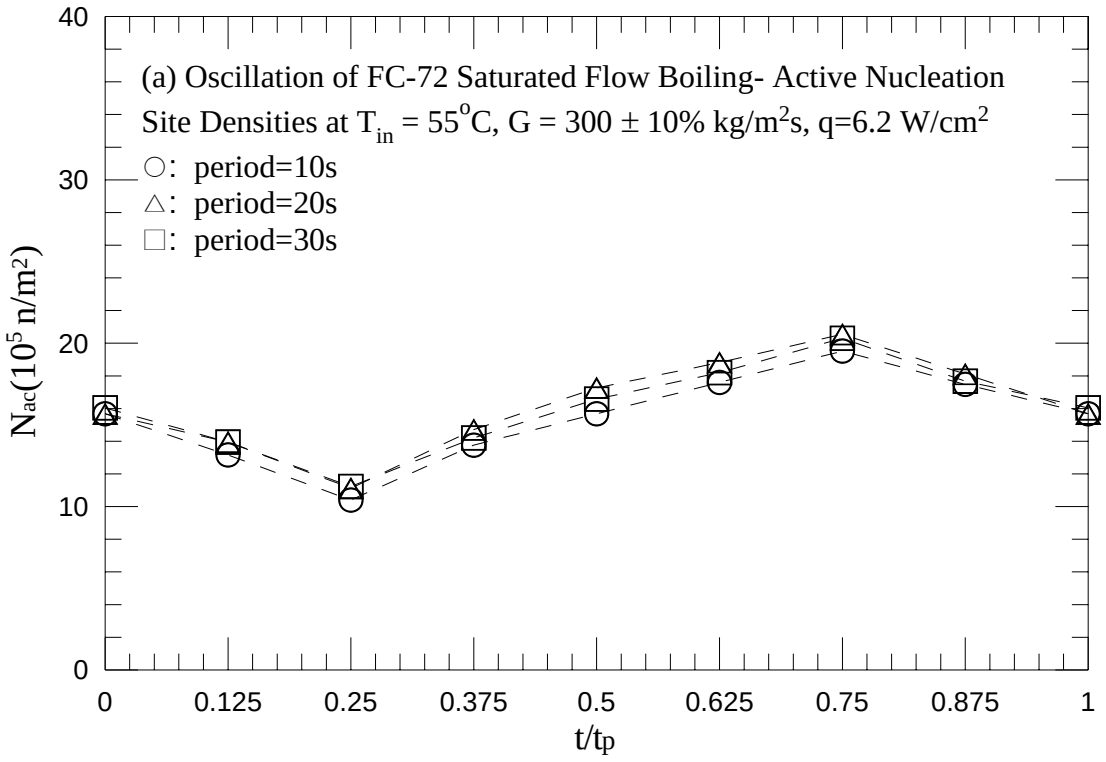

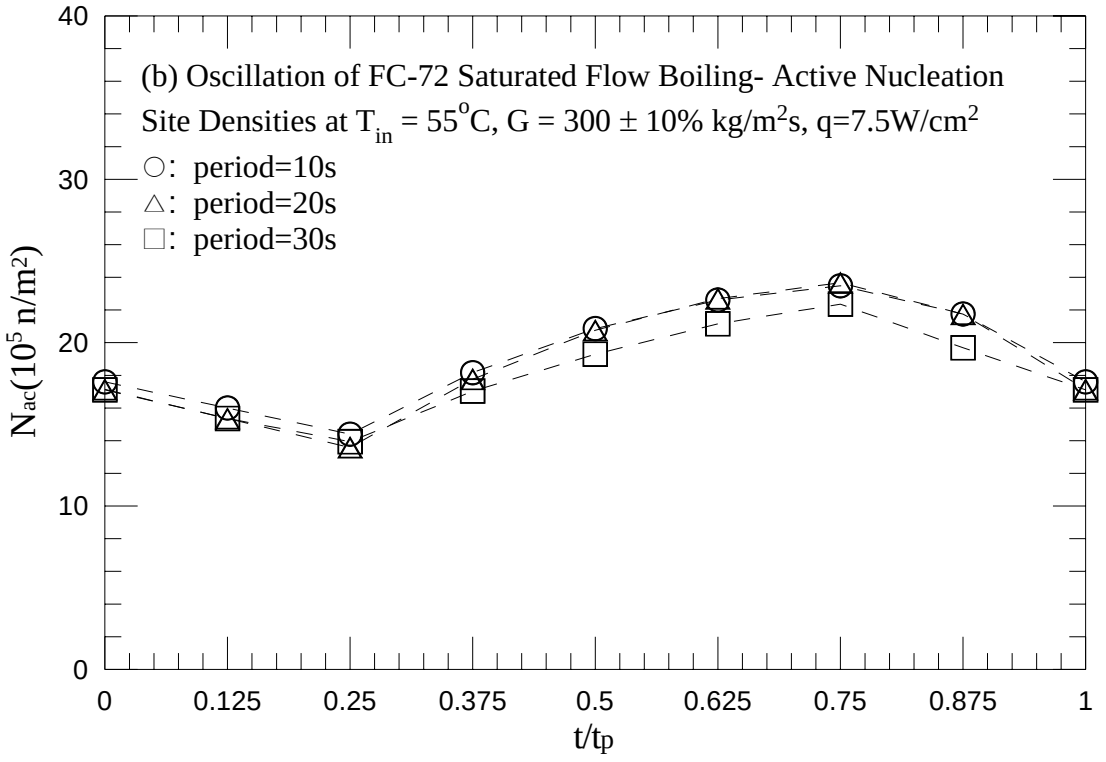

Fig. 4.91 Mean active nucleation site densities for various periods of mass flux oscillation for transient saturated flow boiling for G=300±10% kg/m^{2}s with (a) q=6.2 W/cm^2 and (b) q=7.5 W/cm^2.

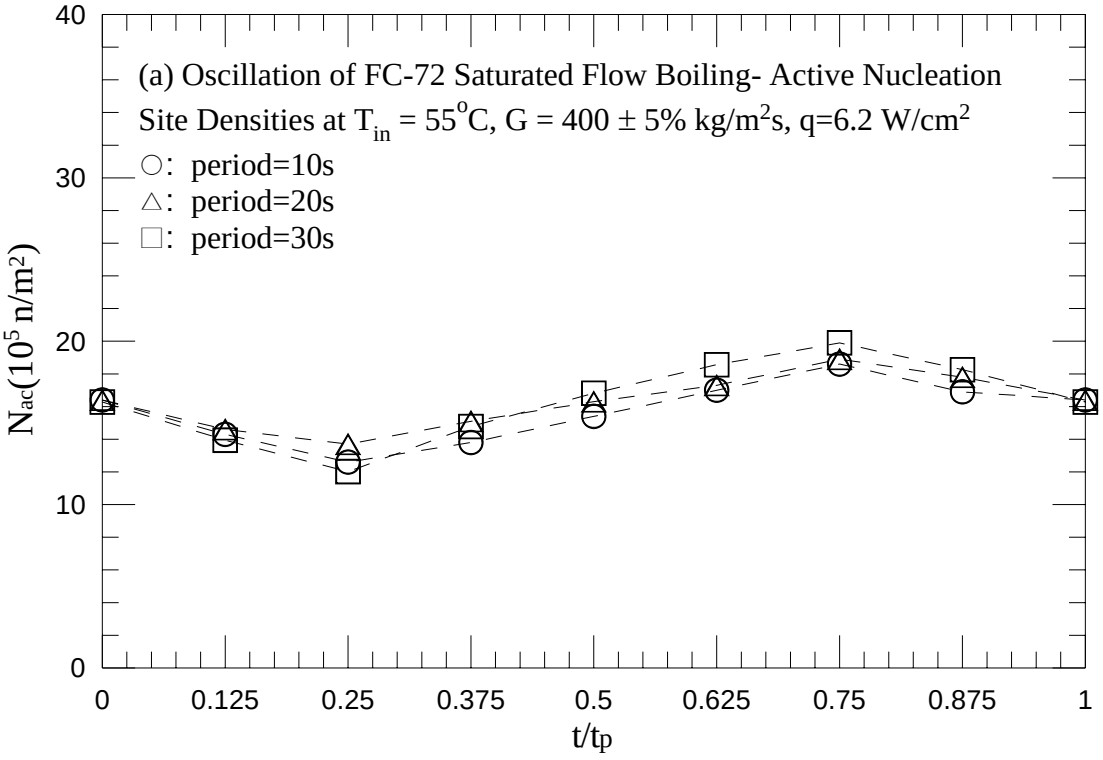

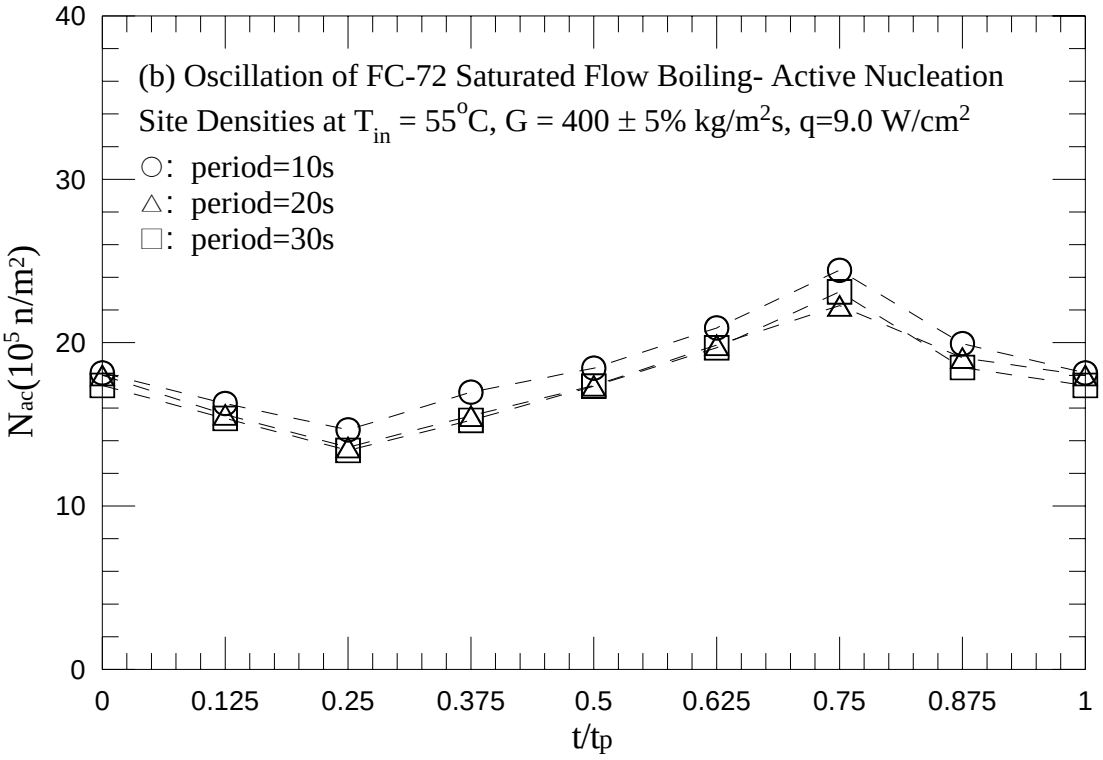

Fig. 4.92 Mean active nucleation site densities for various periods of mass flux oscillation for transient saturated flow boiling for G=400±5% kg/m^{2}s with (a) q=6.2 W/cm^2 and (b) q=9.0 W/cm^2.

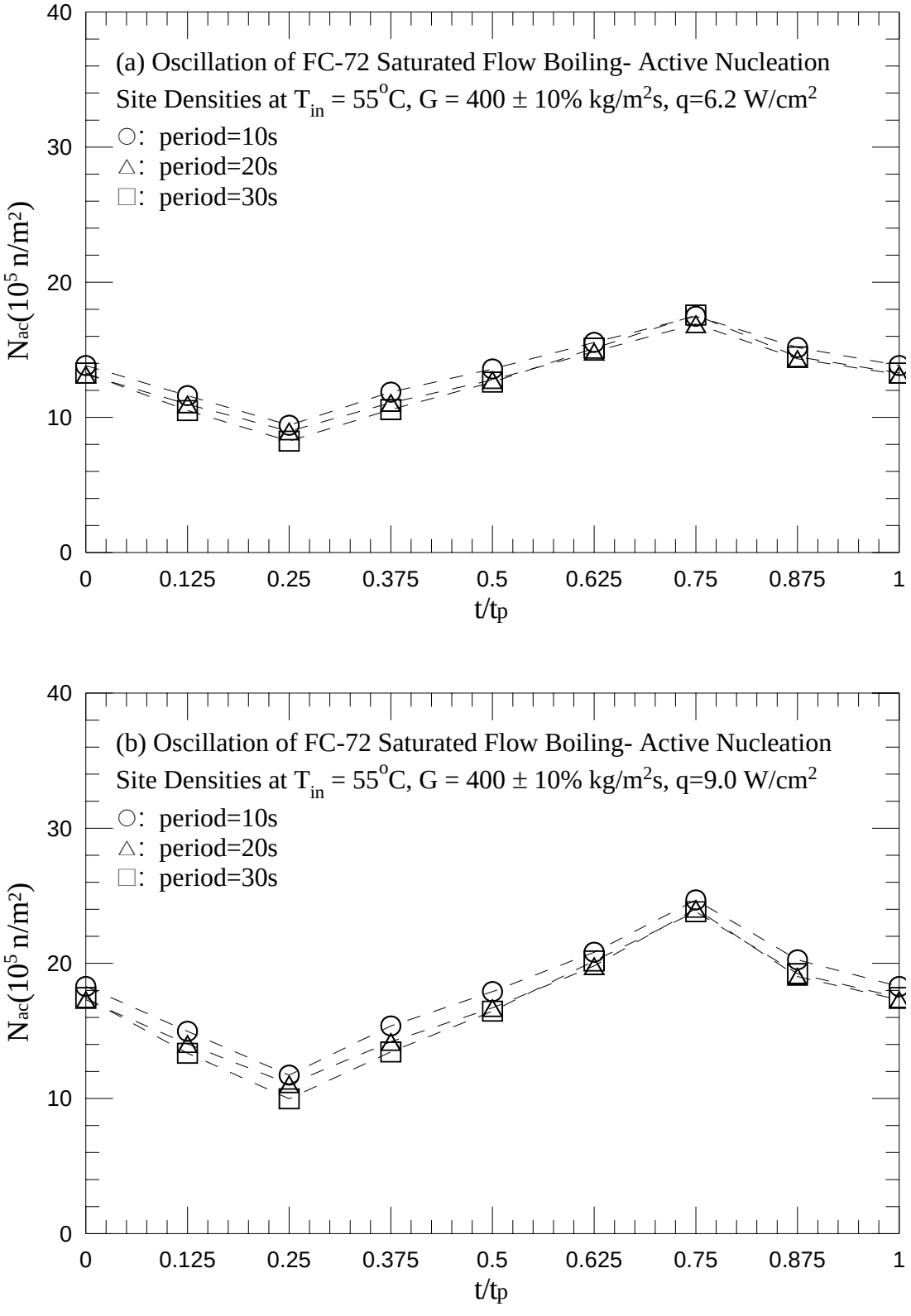

Fig. 4.93 Mean active nucleation site densities for various periods of mass flux oscillation for transient saturated flow boiling for G=400±10% kg/m^{2}s with (a) q=6.2 W/cm^2 and (b) q=9.0 W/cm^2.

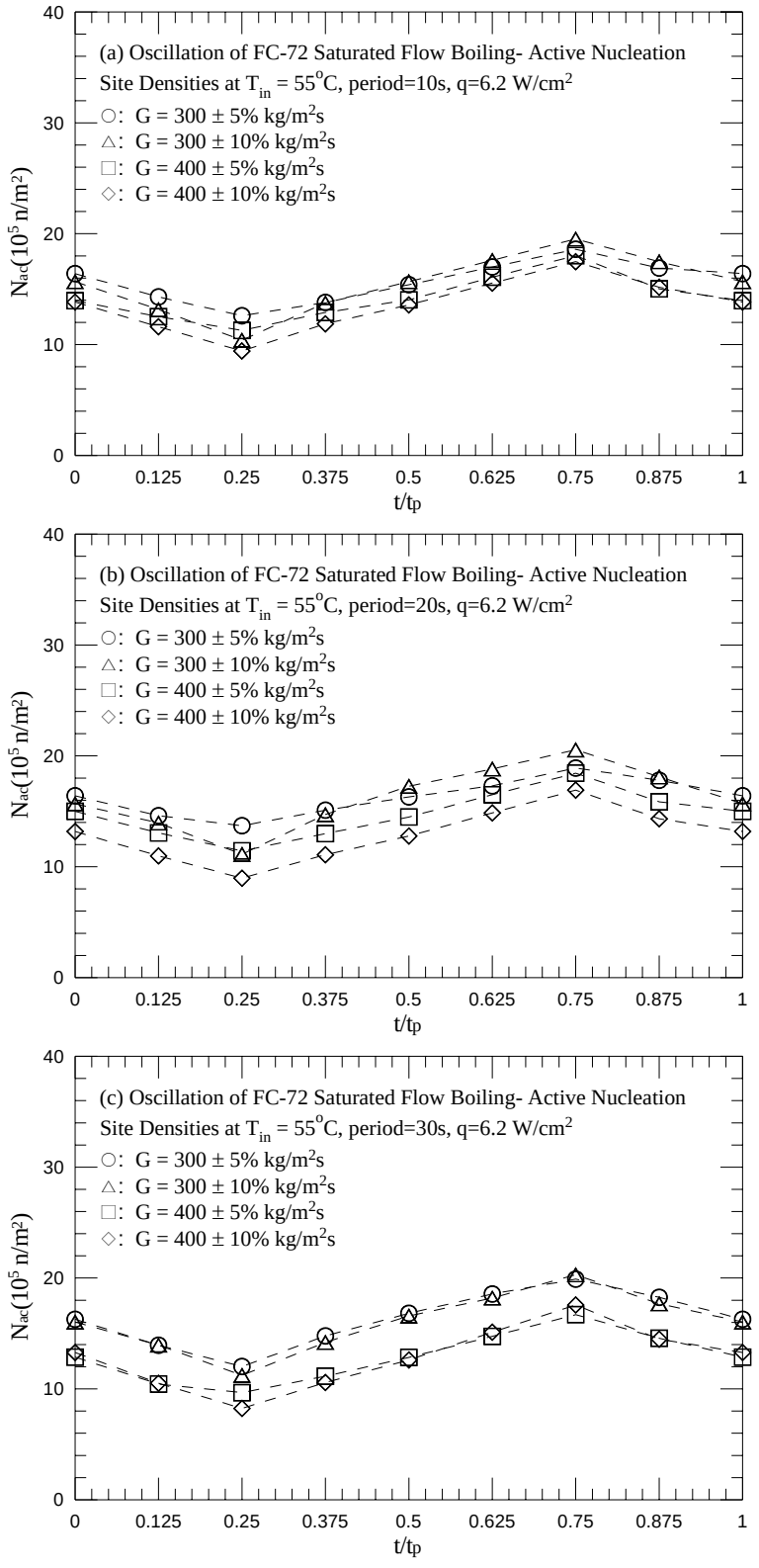

Fig. 4.94 Mean active nucleation site densities for various amplitudes of the mass fluxes oscillation for transient saturated flow boiling for q=6.2 W/cm^2 with period=10 sec (a), 20 sec (b), and 30 sec (c).

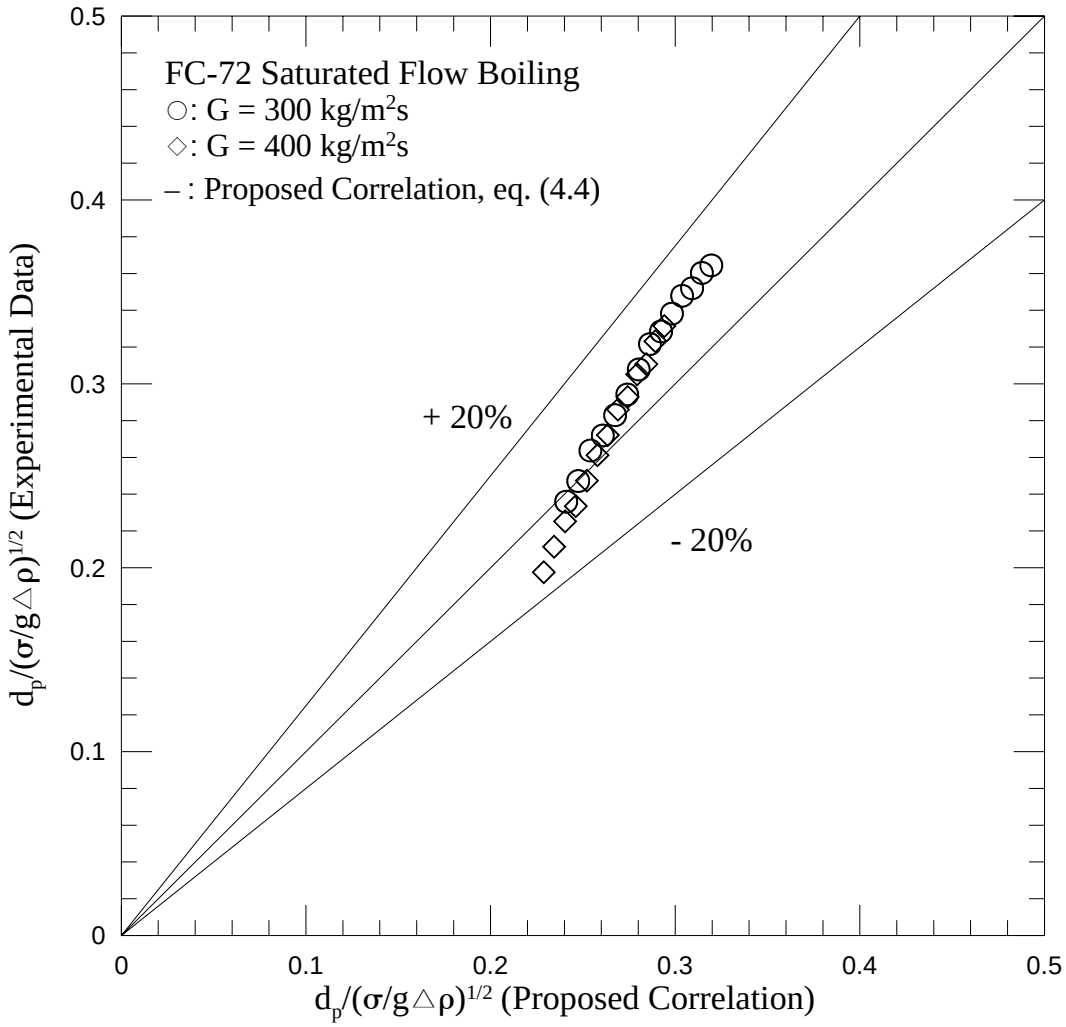

Fig. 4.95 Comparison of the measured data for mean bubble departure diameter for stable saturated flow boiling of FC-72 with the proposed correlation.

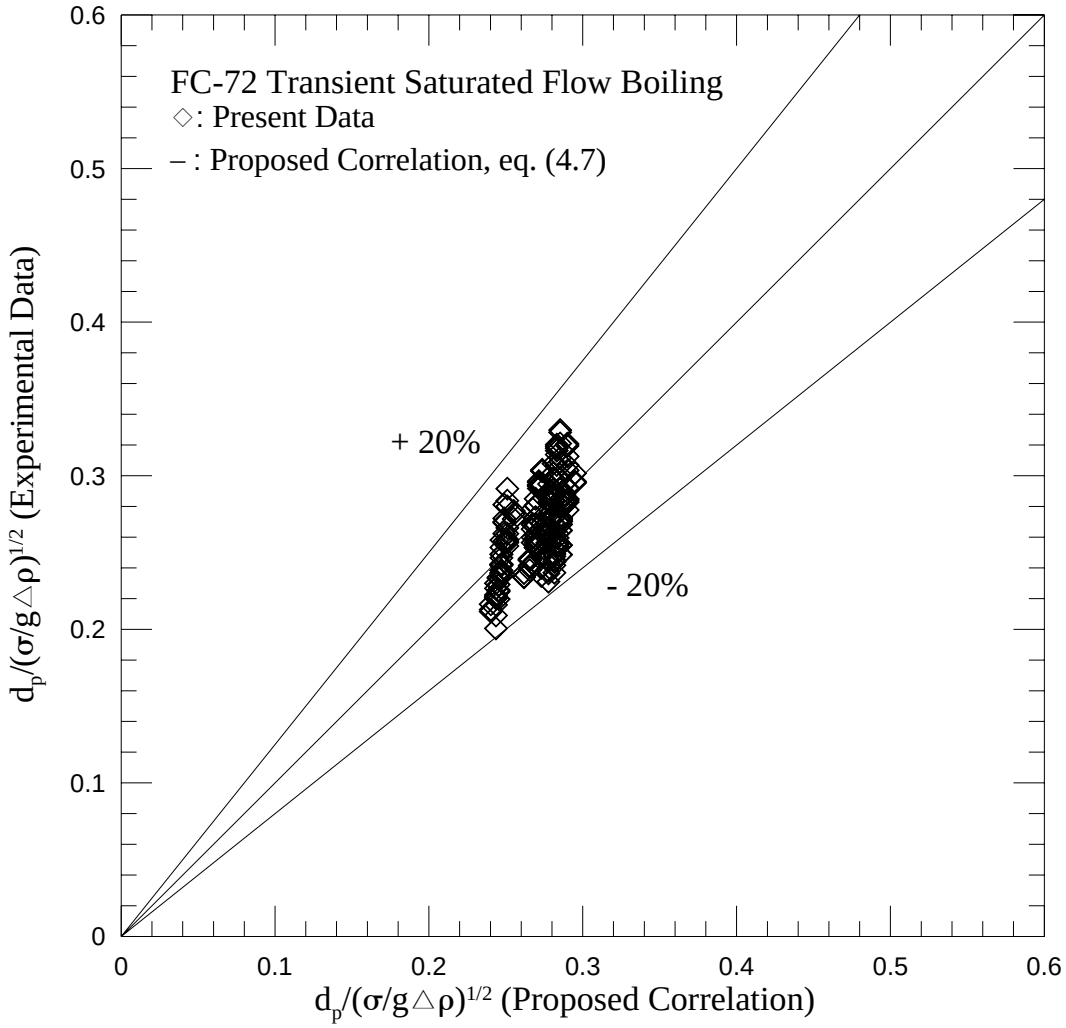

Fig. 4.96 Comparison of the measured data for mean bubble departure diameter for transient saturated flow boiling of FC-72 with the proposed correlation.

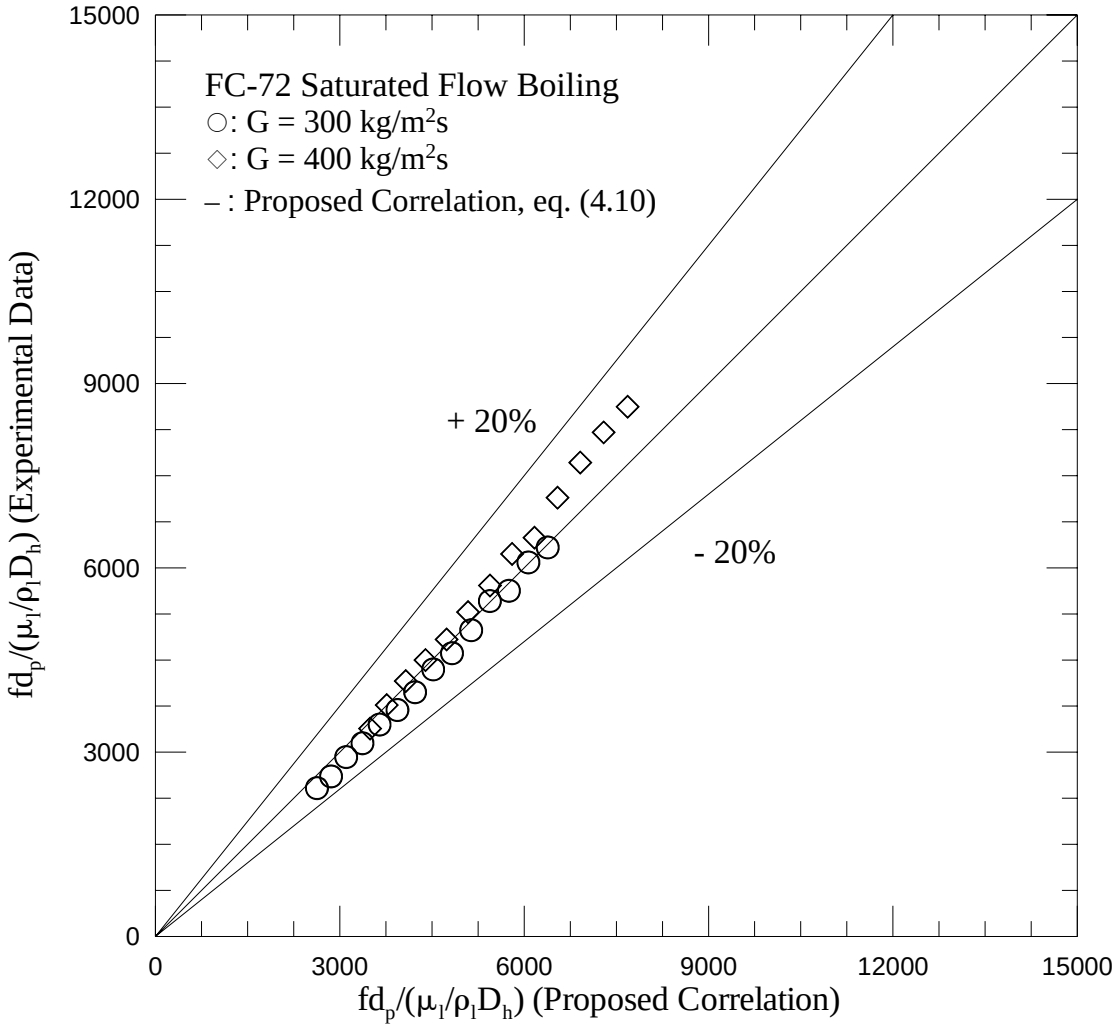

Fig. 4.97 Comparison of the measured data for mean bubble departure frequency for stable saturated flow boiling of FC-72 with the proposed correlation.

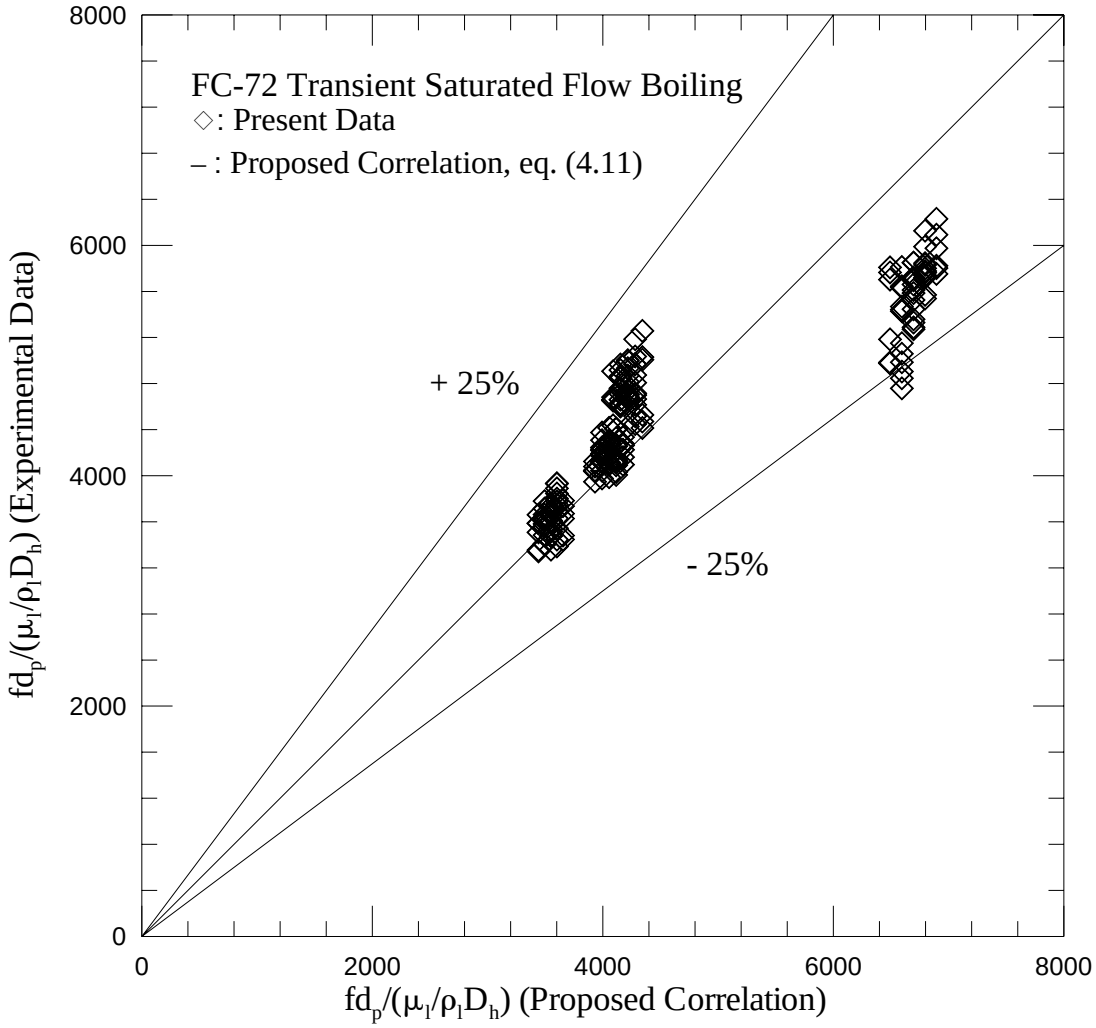

Fig. 4.98 Comparison of the measured data for mean bubble departure frequency for transient saturated flow boiling of FC-72 with the proposed correlation.

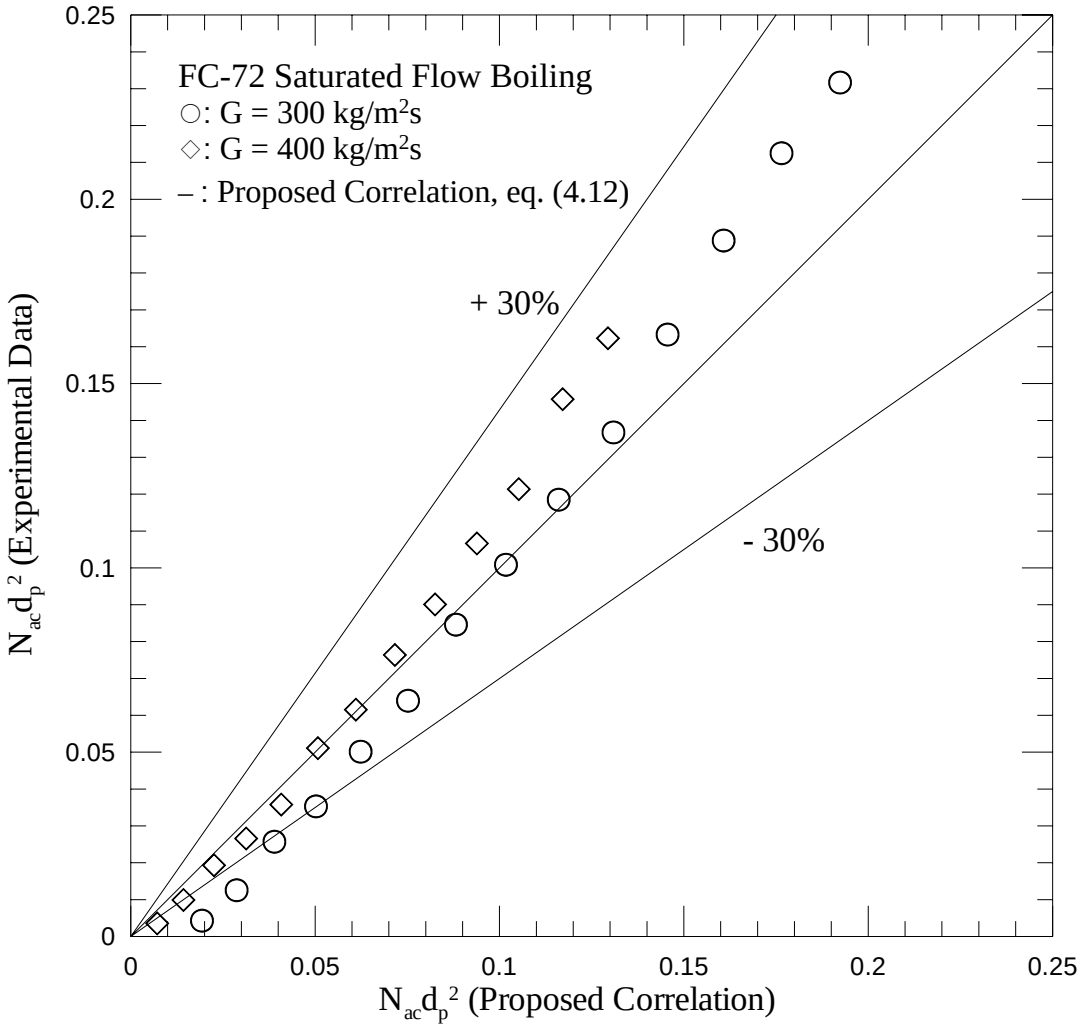

Fig. 4.99 Comparison of the measured data for mean active nucleation site density for stable saturated flow boiling of FC-72 with the proposed correlation.

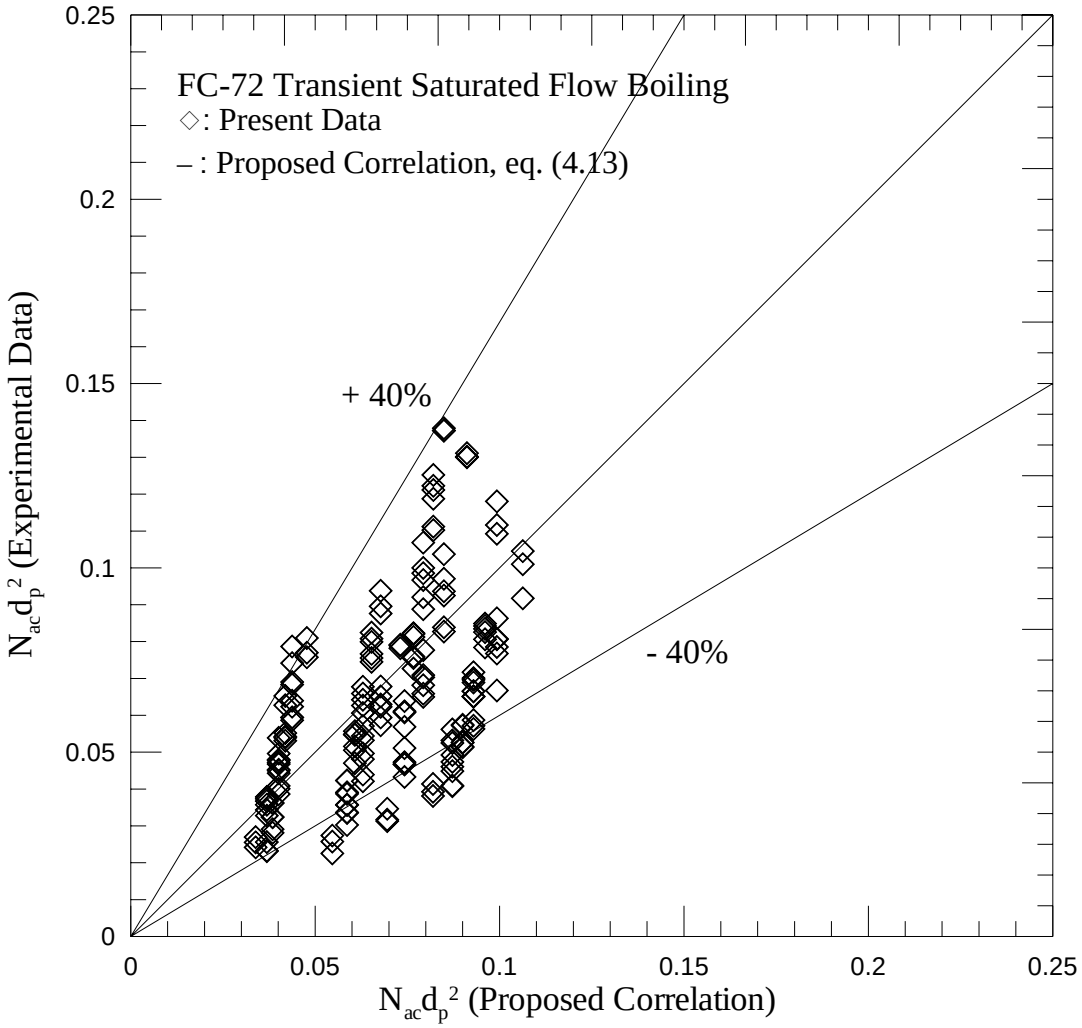

Fig. 4.100 Comparison of the measured data for mean active nucleation site density for transient saturated flow boiling of FC-72 with the proposed correlation.

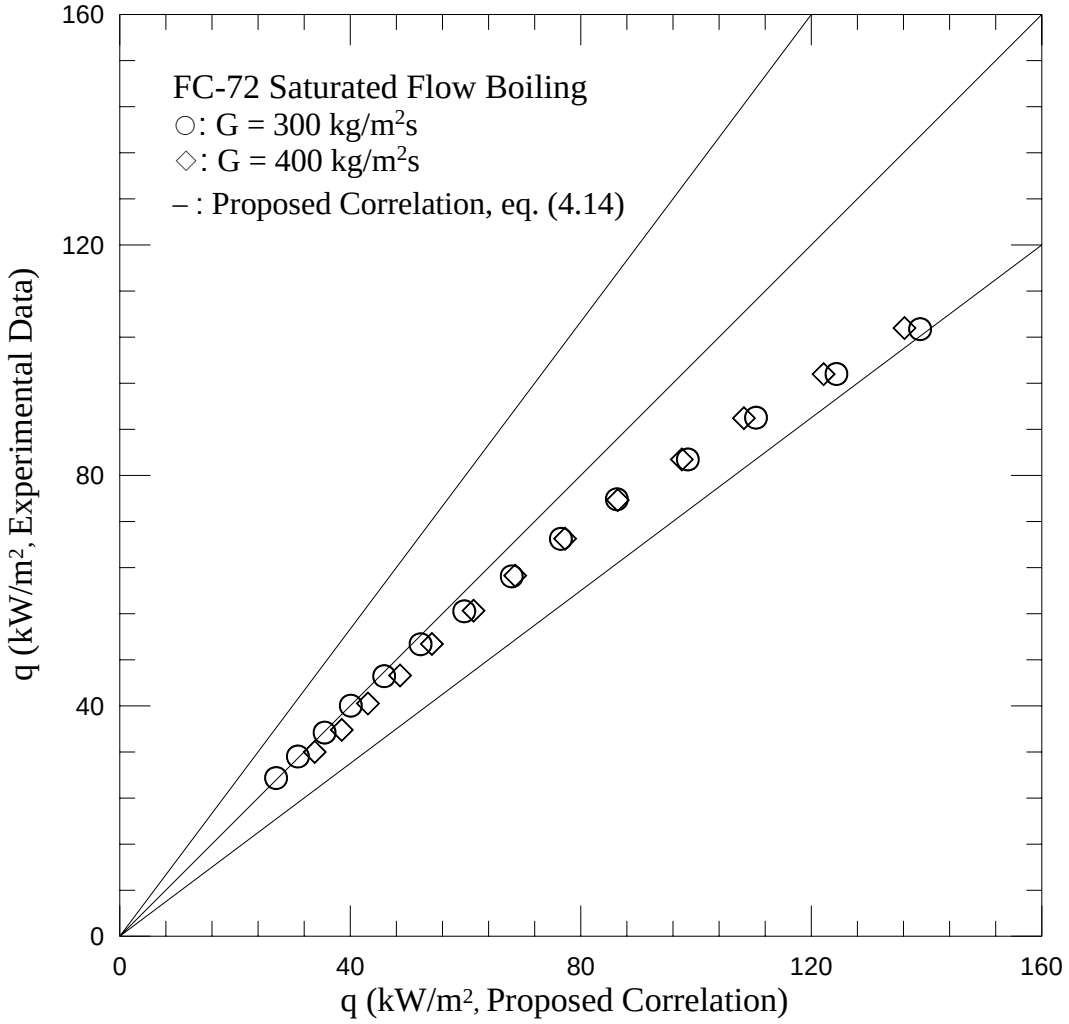

Fig. 4.101 Comparison of the measured data for boiling heat flux for stable saturated flow boiling of FC-72 with the proposed correlation.

CHAPTER 5

TRANSIENT SUBCOOLED FLOW BOILING OF FC-72 OVER A SMALL HEATED COPPER PLATE

The experimental data obtained in the second part of this study are presented in this chapter to illustrate how the FC-72 mass flux oscillation affects the transient subcooled flow boiling heat transfer of FC-72 over a small heated circular copper flat plate flush mounted on the bottom of a horizontal rectangular channel. The present experiments are carried out for the mean FC-72 mass flux fixed at 300 and 400 kg/m^2s, inlet liquid cooling of 5^oC and $10\ ^oC$, and imposed heat flux varying from 0.1 W/cm^2 to 10 W/cm^2. Besides, the amplitude of the coolant mass flux oscillation is set at 0%, 5% and 10% of the mean coolant mass flux. At the inlet of the test section the period of the mass flux oscillation is fixed at 10, 20 and 30 seconds. The coolant is at slightly subatmospheric pressure of 99 kPa with $T_{sat} = 55^oC$ for FC-72. In the following, the effects of the experimental parameters, namely, the mean level and the amplitude and period of the coolant mass flux oscillation, inlet coolant subcooling, imposed heat flux, on the transient FC-72 subcooled flow boiling heat transfer performance are examined in detail. Note that for the limiting case of 0% mass flux oscillation we have stable subcooled boiling of FC-72 in the test section. The heat transfer performance is presented in terms of the time variations of the space average surface temperature of the copper plate and boiling heat transfer coefficients. Besides, the photos of the boiling flow and the bubble departure diameter and frequency and active nucleation site density at selected time instants in a typical periodic cycle are presented.

5.1 Stable and Time-average Subcooled Flow Boiling Curves and Heat Transfer Coefficients

Effects of the mean coolant mass flux $\overline{G}$, inlet subcooling ΔT_{sub}, and the amplitude γ and period t_p of the coolant mass flux oscillation on the time-average boiling curves measured in the stable and transient FC-72 subcooled flow boiling are shown in Figures 5.1 - 5.4. Figure 5.1 shows the effects of the coolant mass flux oscillation on the measured time-average boiling curves for the stable and transient subcooled flow boiling for γ= 5% and t_p varied from 10s to 30s for ΔT_{sub} = 5^{o}C. The data for a higher γ of 10% are given in Figure 5.2. In Figures 5.3 and 5.4 the data for a higher inlet liquid subcooling of 10^{o}C are shown. These results indicate that for each boiling curve the space-average temperature of the copper plate increases gradually with the imposed heat flux from the subcooled temperature of the coolant at a low q to a certain value just slightly higher than the saturated temperature and no bubble nucleation is observed. The heat transfer in this region is completely due to the single-phase forced convection. With the continuing increase in the surface heat flux, bubbles begin to appear on the surface and the boiling curve is characterized by a sharp increase in the surface heat flux for a small rise in the temperature of the copper surface. We have onset of nucleate boiling (ONB) in the flow. A significant drop in the copper plate temperature occurs at ONB. The reason causing the sudden drop in the copper surface temperature at ONB is due to a significant increase in the wall heat transfer by the boiling processes. A close inspection of the data for the single-phase region further reveals that at a higher mass flux the temperature of the copper plate is somewhat lower for the same imposed heat flux. This obviously results from the increase in the single-phase convection heat transfer coefficient with the coolant mass flux. Note that except for the imposed heat flux slightly beyond that for ONB the amplitude and period of the coolant mass flux oscillation exhibit little effects on the

time-average boiling curves, suggesting that the dominance of the wall heat transfer by the fully developed nucleate boiling. However at a higher G the wall superheat and heat flux at ONB are substantially higher. This can be attributed to the fact that at a higher G more energy is needed for the vapor to nucleate from the cavities in the wall since the residence time of the coolant on the heated surface is shorter. A scrutiny of these data further suggests that the fully developed nucleate boiling prevails in the flow after ONB. It is worth to note that in the subcooled flow boiling significant temperature undershoot occurs at ONB. Besides, the temperature undershoot is smaller when the coolant mass flux oscillates at 5% and 10%. However, the effects of the period of the mass flux oscillation on the temperature are rather slight. Next, the effects of the inlet liquid subcooling on the time-average subcooled boiling curves are shown in Figures 5.5 – 5.11. The results indicate that during ONB a substantial increase in the temperature undershoot occurs when the inlet liquid subcooling is raised from 5^{o}C to 10 ^{o}C. Beyond ONB the effects of the inlet liquid subcooling on the time-average boiling curves are small.

We proceed to examine how the time-average subcooled flow boiling heat transfer coefficients $\overline{h}_{2\phi,sub}$ are affected by the FC-72 coolant mass flux oscillation. The results for the variations of $\overline{h}_{2\phi,sub}$ with the imposed surface heat flux presented in Figures 5.12 - 5.15 reveal that the mean level, amplitude and period of the coolant mass flux oscillation shows negligible influences on the time-average subcooled flow boiling heat transfer coefficients. However, for a given coolant mass flux the boiling heat transfer coefficient increases substantially with the imposed heat flux. For example, at $\triangle T_{sub}$ =5^{o}C and $\overline{G}$ =400 kg/m^{2}s, the subcooled boiling heat transfer coefficient for q =9.7 W/cm^2 is about 53.6% higher than that for q =5.0 W/cm^2 (Figure 5.12(a)). Moreover, the inlet liquid subcooling of the coolant also shows a significant effect on the time-average boiling heat transfer coefficient, as evident from

the data in Figures 5.16 – 5.22. Specifically, $\bar{h}_{2\phi,sub}$ is higher for a lower the inlet liquid subcooling.

5.2 Stable and Transient Subcooled Flow Boiling Heat Transfer Characteristics

The transient subcooled boiling heat transfer characteristics for FC-72 flow over the heated copper plate resulting from the temporal coolant mass flux oscillation are illustrated by presenting the time variations of the space-average heated surface temperature T_w and heat transfer coefficient $h_{2\phi}$ for various imposed heat fluxes and mass fluxes. For comparison purpose the results for T_w for the limiting cases of constant coolant mass fluxes are shown in Figure 5.23. These data for γ= 0% indicate that the fluctuations of the space average heated surface temperature with time for various q and G are relatively small. The subcooled boiling hence can be regarded as at a statistically stable state.

Now when the coolant mass flux oscillates periodically in time in a form of nearly a triangular wave, significant temporal oscillations in the space average heated surface temperature occur for the imposed heat flux slightly higher than that for the time average ONB, as evident from the data shown in Figures 5.24 -5.48 for the oscillation amplitude being 5% and 10% of the mean mass flux. Note that the temporal oscillation of the heated surface temperature is also periodic in time and is at the same frequency as the mass flux. Besides, the T_w oscillation gets slightly stronger for higher imposed heat flux and higher amplitude of the mass flux oscillation. Moreover, a longer period of the mass flux oscillation results in a larger amplitude of the T_w oscillation with $\triangle G$ being 10% of $\bar{G}$. Even in the single-phase forced convection for γ= 10% the space average heated surface temperature also oscillates

noticeably with time at a relatively low imposed heat flux with $q < \bar{q}_{ONB}$ (Figures 5.30 – 5.35). Here $\bar{q}_{ONB}$ is the time-average heat flux for ONB for the cases with the oscillating mass flux. A close inspection of the data given in Figures 5.24 – 5.35 further reveals that the T_w oscillation slightly lags the mass flux oscillation. Moreover for q substantially above $\bar{q}_{ONB}$, in the period of time at which the instantaneous mass flux is higher than the average level, the T_w is higher than the time-average level suggesting that the flow boiling heat transfer over the heated surface is poorer at a higher instantaneous G. But in the single-phase region the opposite is the case (Figures 5.30 – 5.35). The trend for the single-phase flow is apparently due to the better convection heat transfer for a higher mass flux. The somewhat unusual trend for the subcooled boiling flow requires more investigation into the associated bubble characteristics which will be examined later.

The measured temporal variations of the space average heated surface temperature for a higher inlet liquid subcooling of 10 ^{o}C are given in Figures 5.36 – 5.48. These results resemble that presented in Fugures 5.23 – 5.35 for $\triangle T_{sub}$ =5^{o}C except that at the higher inlet liquid subcooling T_w oscillates in a somewhat larger amplitude.

The corresponding time variations of the space-average subcooled flow boiling heat transfer coefficient affected by the coolant mass flux oscillation are shown in Fugures 5.49 – 5.60 for the inlet liquid subcooling of 5 ^{o}C. The results manifest that the flow boiling heat transfer coefficients also oscillate periodically in time and at the same frequency as the G oscillation. At a higher imposed heat flux and for the larger amplitude and longer period in the mass flux oscillation, the subcooled boiling heat transfer coefficients oscillate stronger. Besides in the period of time at which the mass flux is higher than the mean level, the boiling heat transfer coefficient is lower than

the time-average level. Note that at the higher inlet liquid subcoling of 10 ^{o}C the oscillation in the boiling heat transfer coefficient is stronger, as evident from the data shown in Figures 5.61 – 5.72. Moreover, the oscillation in $h_{2\phi}$ also lags slightly behind the mass flux oscillation.

In this transient oscillatory boiling flow the time variation of the coolant pressure at the inlet of the test section is also of interest in thermal-fluid design. These data are shown in Figures 5.73 - 5.96 for various cases. The results indicate that the inlet coolant pressure oscillates nearly in phase with the mass flux oscillation. Note that the inlet coolant pressure oscillation becomes more irregular for the cases with a longer period of the mass flux oscillation and a higher average mass flux. Besides, at the higher inlet liquid subcooling of 10^{o}C the oscillation in the inlet coolant pressure is stronger. Finally, the quantitative data evaluated from the above results are summarized in Tables 5.1 and 5.2 for the relative oscillation amplitudes of the space average heated surface temperature and boiling heat transfer coefficient $A_{T_w}/\Delta\bar{T}_{sat}$ and $A_{h2\varphi}/\bar{h}_{2\varphi}$ at various imposed heat fluxes and the amplitude and period of the coolant mass flux oscillation.

5.3 Transient Bubble Characteristics in Subcooled Flow Boiling

To elucidate the transient FC-72 subcooled flow boiling heat transfer characteristics affected by the mass flux oscillation, the data for the bubble characteristics obtained from the present flow visualization are examined in the following. The top views of the boiling flow in a small region around the geometric center of the heated surface for various coolant mass fluxes and imposed heat fluxes are shown in Figs. 5.97 – 5.146 for the transient subcooled flow boiling. In the flow visualization we note that as the wall superheat exceeds that for the boiling incipience, the vapor bubbles

generated from the heated plate begin to appear. At first, the bubble characteristics for the limiting cases of constant mass fluxes are illustrated by the photos in Figures 5.97 for $\triangle T_{sub}$ =5^{o}C and 5.122 for $\triangle T_{sub}$ =10^{o}C for the stable subcooled flow boiling. In the beginning, tiny bubbles are observed in the active nucleation sites. The tiny bubbles keep growing until their diameters reach to a certain size and they detach from the active nucleation sites immediately. Then they slide along the heating surface for some distance. The processes of bubble growth and departure are nearly regular and the bubbles are nearly spherical at low imposed heat flux. The formation, growth, and detachment processes of the bubbles on the heated copper plate obviously depend on the flow and thermal conditions and on the geometry of the cavities.

Next, the bubble characteristics in the transient flow boiling are illustrated by presenting the photos of the subcooled boiling flow at eight selected time instants in a typical periodic cycle in Figures 5.98 – 5.121 for $\triangle T_{sub}$ =5^{o}C and in Figures 5.123 – 5.146 for $\triangle T_{sub}$ =10^{o}C. In these figures the symbol " $t=t_o$ " signifies the time instant at which the instantaneous mass flux is at the mean level and starts to increase with time. The results indicate that for given imposed heat flux and inlet liquid subcooling and fixed mean level, amplitude and period of the mass flux oscillation the bubbles get smaller and become more dispersed in the period of time in which the instantaneous mass flux increases. The opposite processes take place when the instantaneous mass flux decreases with time. These changes of the bubble characteristics with the instantaneous mass flux become more significant for an increase in the amplitude of the mass flux oscillation (Figures 5.98 and 5.110 and Figures 5.99 and 5.111) and for a higher imposed heat flux. It is of interest to note that the mean level of the mass flux oscillation exhibits larger influences on the bubble characteristics in the transient flow boiling, as evident by comparing Figures 5.99 and 5.100. Besides, the bubble characteristics are only affected slightly by the period of the mass flux oscillation.

Finally, it should be mentioned that in the subcooled flow boiling with $\triangle T_{sub}$ =5^{o}C and 10^{o}C the bubble coalescence is less significant than the saturated flow boiling.

To quantify the bubble characteristics, the measured data for the time variations of the space-average bubble departure diameter and frequency and active nucleation site density in a typical periodic cycle are shown in Figures 5.147 – 5.200 for various experimental parameters. The results in Figures 5.147 and 5.174 indicate that the mean size of the bubbles departing from the heated surface is somewhat smaller for the mass flux raised from 300 to 400 kg/m^{2}s in stable subcooled flow boiling. It reflects the fact that the coolant at a higher mass flux and hence at a higher speed tends to sweep the bubbles more quickly away from the heating surface. Now as the coolant mass flux oscillates, the bubble departure diameter varies significantly with time (Figures 5.147(b) - (c) and 5.174(b) - (c)). More specifically, the size of the departing bubbles decreases in the first and fourth quarters of the periodic cycle in which the instantaneous mass flux increases with time. While in the second and third quarters of the cycle an opposite process is noted since the instantaneous mass flux decreases with time. Besides, at a higher imposed heat flux the departing bubbles are larger. Similar trend is noted in Figures 5.148 – 5.150 and 5.175 – 5.177. Comparing the results in Figure 5.147 with Figure 5.148 and Figure 5.149 with Figure 5.150 indicates that at the larger amplitude of the mass flux oscillation the effects of the imposed heat flux on the bubble departure diameter are slightly smaller. Figures 5.151 – 5.154 and 5.178 – 5.181 indicate that the bubble departure diameters are only affected slightly by the period of the mass flux oscillation. At the small amplitude of the mass flux oscillation of 5% the bubble departure diameters are slightly larger than that at the large amplitude of the mass flux oscillation of 10% (Figures 5.155 and 5.182).

Next, the data for the variations of the space-average bubble departure frequency

with time for various cases are shown in Figures 5.156 – 5.159 for $\triangle T_{sub}$ =5^{o}C and Figures 5.183 – 5.186 for $\triangle T_{sub}$ =10^{o}C. In the stable flow boiling the results in Figures 5.156(a) and 5.183(a) indicate that the increase in the bubble departure frequency with the imposed heat flux and coolant mass flux is clearly seen. The increase of f with G is ascribed again to the higher drag on the bubbles still attaching to the heated surface by the liquid coolant moving at a higher speed for a higher G. This, in turn, causes an earlier departure of the bubbles from the surface, resulting in a higher departure frequency. For an oscillation mass flux the bubbles depart from the heated surface at a slightly faster rate in the first and fourth quarters of the periodic cycle in which the coolant mass flux rises with time. Apparently, in the second and third quarters of the cycle in which G decreases with time the bubble departing rate reduces slightly. It is also observed that the mean bubble departure frequency increases noticeably with the imposed heat flux. It should be pointed out that the time variations of the bubble departure frequency are somewhat weaker than the bubble departure diameter. Figures 5.160 – 5.163 and 5.187 – 5.190 indicate that the bubble departure frequencies are only affected slightly by the period of the mass flux oscillation. At the large amplitude of the mass flux oscillation of 10% the bubble departure frequencies are slightly higher than that at the small amplitude of the mass flux oscillation of 5% (Figures 5.164 and 5.191).

Finally, the space-average active nucleation site density on the heated surface affected by the coolant mass flux oscillation is illustrated in Figures 5.165 – 5.168 for $\triangle T_{sub}$ =5^{o}C and Figures 5.192 – 5.195 for $\triangle T_{sub}$ =10^{o}C. The results Figures 5.165(a) and 5.192(a) indicate that in stable flow boiling the active nucleation site density increases substantially with the imposed heat flux. But the increase is also significant for the mass flux reduced from 400 to 300 kg/m^{2}s. Note that in transient flow boiling the active nucleation site density decreases with time in the first and fourth quarters of

the periodic cycle in which G increases. The reverse process appears in the second and third quarters of the cycle in which the coolant decelerates. At a higher amplitude of the mass flux oscillation the temporal variations of N_{ac} is stronger (Figures 5.166, 5.168, 5.193 and 5.195). The effects of the period of the mass flux oscillation are weaker. Figures 5.169 – 5.172 and 5.196 – 5.199 indicate that the active nucleation site density is only affected slightly by the period of the mass flux oscillation. At the large amplitude of the mass flux oscillation of 10% the active nucleation site densities are less than that at the small amplitude of the mass flux oscillation of 5% (Figures 5.173 and 5.200).

5.4 Correlation Equations

According to the present experimental data, empirical correlations for the space-average bubble departure diameter in FC-72 stable and transient subcooled flow boiling on the heated circular copper flat plate flush mounted on the bottom of the rectangular channel estimated from the present flow visualization are proposed as

$$\frac{d_p}{\sqrt{\sigma/g\cdot\Delta\rho}} = \frac{0.37\cdot(\rho_l/\rho_v)^{1.32}}{\overline{Re_D}^{0.2}\cdot[Ja' + \frac{0.6\cdot(\rho_l/\rho_v)^{0.9}}{\overline{Bo}^{0.3}\overline{Re_D}^{0.1}}]} \quad \text{for stable flow boiling} \tag{5.1}$$

where $\overline{Re_D}$ and $\overline{Bo}$ are the mean Reynolds and Boiling numbers respectively. They are defined as

$$\overline{Re_D} = \frac{\bar{G}\cdot D}{\mu_l} \tag{5.2}$$

$$\overline{Bo} = \frac{q''}{\bar{G}\cdot i_{lv}} \tag{5.3}$$

and

$$\frac{d_p}{\sqrt{\sigma/g\cdot\Delta\rho}} = \frac{0.37\cdot(\rho_l/\rho_v)^{1.29}}{Re_D^{0.2}\cdot[Ja' + \frac{0.6\cdot(\rho_l/\rho_v)^{0.9}}{Bo^{0.3}Re_D^{0.1}}]} \quad \text{for transient flow boiling} \tag{5.4}$$

where Re_D and Bo are respectively the instantaneous Reynolds and Boiling numbers. They are defined as

$$Re_D = \frac{G\cdot D}{\mu_l} \tag{5.5}$$

$$Bo = \frac{q''}{G \cdot i_{lv}} \tag{5.6}$$

Here Ja' is the modified Jacob number based on the coolant inlet subcooled temperature ΔT_{sub} which is defined as

$$Ja' = \frac{\rho_l \cdot c_{pl} \cdot \Delta T_{sub}}{\rho_v \cdot i_{lv}} \tag{5.7}$$

where $G(=\bar{G}+\Delta G)$ is the instantaneous coolant mass flux, $\bar{G}$ is the average coolant mass flux, ΔG is the amplitude of the mass flux oscillation, c_{pl} is the liquid specific heat, ρ_l is the liquid density, and D is the copper diameter. Figures 5.201 and 5.202 show that the present experimental data fall within ± 15 % and ± 20 % of the correlations given in Equations (5.1) and (5.4). In addition, empirical equations are provided to correlate the data for the space-average bubble departure frequency as

$$\frac{f \cdot d_p}{\mu_l/\rho_l \cdot D_h} = 0.65\overline{Re_D}^{1.4} \cdot Ja'^{-0.3} \cdot \overline{Bo}^{0.5} \quad \text{for stable flow boiling} \tag{5.8}$$

and

$$\frac{f \cdot d_p}{\mu_l/\rho_l \cdot D_h} = 0.63 Re_D^{1.41} \cdot Ja'^{-0.3} \cdot Bo^{0.54} \quad \text{for transient flow boiling} \tag{5.9}$$

Figures 4.203 and 4.204 reveal that the present experimental data for $f \cdot d_p$ can be correlated with the deviation less than ± 25 % by the above two equations. Moreover, empirical correlations for the space-average active nucleation site density in the FC-72 subcooled flow boiling deduced from the present flow visualization are proposed as

$$N_{ac} \cdot d_p^{\,2} = -0.09 + (80 \cdot \overline{Bo}^{0.8} \cdot \overline{Re_D}^{-0.15} \cdot Ja'^{-0.05}) \quad \text{for stable flow boiling} \tag{5.10}$$

and

$$N_{ac} \cdot d_p^{\,2} = -0.09 + (68 \cdot Bo^{0.8} \cdot Re_D^{-0.15} \cdot Ja'^{-0.05}) \quad \text{for transient flow boiling} \tag{5.11}$$

The comparisons in Figs. 4.205 and 4.206 show that more than 80 % of the present experimental data fall within ± 30 % and ± 40 % of the correlation given in Equations (5.10) and (5.11). Finally, the total heat flux input to the stable boiling flow q_t is considered to be roughly composed of two parts: one resulting from the bubble

nucleation q_b and another due to the single phase forced convection q_c. Thus

$$q_t = q_b + q_c \tag{5.12}$$

Here q_b and q_c can be individually calculated from the quantitative data for the bubble characteristics examined in section 5.3 and single phase liquid forced convection as

$$q_b = \rho_v \cdot V_v \cdot f \cdot N_{ac} \cdot i_{lv} \tag{5.13}$$

where ρ_v is the vapor density, V_v is the vapor volume of the mean departing bubble defined as $\frac{4\pi}{3}(\frac{d_p}{2})^3$, f is the space-average bubble departure frequency, N_{ac} is the space-average active nucleation site density, i_{lv} is the enthalpy of vaporization, and

$$q_c = E \cdot \bar{h}_{1\phi} \cdot \Delta T_{sat} \tag{5.14}$$

where E is an enhancement factor added to account for the agitating motion of the bubbles which can enhance the single phase liquid convection heat transfer. From the experimental data, E can be empirically correlated as

$$E = 4.5 \cdot N_{conf}{}^{0.5} \cdot \overline{Fr_l}^{0.15} \cdot (1 + 280 \cdot \overline{Bo})^2 \quad \text{for stable flow boiling} \tag{5.15}$$

Here $\overline{Fr_l}$ is the Froude number and N_{conf} is the Confinement number. They are respectively defined as

$$N_{conf} = \frac{(\sigma/g \cdot \Delta\rho)^{0.5}}{D_h} \tag{5.16}$$

and

$$\overline{Fr_l} = \frac{\bar{G}^2}{\rho_l{}^2 \cdot g \cdot D_h} \tag{5.17}$$

where g is the acceleration due to gravity, D_h is the hydraulic diameter of the test section, and ΔT_{sat} (= T_w - T_{sat}) is the wall superheat. The results given in Figure 5.207 indicate that the present data can be correlated with the deviation less than $\pm$ 25% by the empirical correlation given in Equations (5.12) - (5.17).

Table 5.1 Relative amplitudes of heated surface temperature and heat transfer coefficient oscillations in transient oscillatory subcooled flow boiling at $\Delta T_{sub} = 5^{o}C$ for various imposed heat fluxes and the amplitudes and periods of the coolant mass flux oscillation.

$\Delta G/\bar{G}$	t_p (sec)	$\bar{G}$ =300 kg/m^{2}s			$\bar{G}$ =400 kg/m^{2}s		
		q(W/cm^2)	$A_{T_w}/\Delta\bar{T}_{sat}$	$A_{h_{2\rho}}/\bar{h}_{2\rho}$	q(W/cm^2)	$A_{T_w}/\Delta\bar{T}_{sat}$	$A_{h_{2\rho}}/\bar{h}_{2\rho}$
±5%	10	4.98	0.0147	0.0114	5.55	0.0158	0.0123
		6.16	0.0162	0.0128	6.78	0.0160	0.0126
		8.19	0.0144	0.0116	8.17	0.0183	0.0147
		9.69	0.0145	0.0119	9.67	0.0159	0.0130
	20	4.96	0.0208	0.0160	5.46	0.0291	0.0226
		6.10	0.0188	0.0150	6.72	0.0267	0.0211
		8.17	0.0192	0.0155	8.11	0.0284	0.0229
		9.67	0.0213	0.0173	9.62	0.0286	0.0234
	30	4.95	0.0177	0.0137	5.48	0.0304	0.0235
		6.12	0.0193	0.0151	6.71	0.0306	0.0242
		8.15	0.0206	0.0165	8.10	0.0293	0.0236
		9.65	0.0225	0.0183	9.62	0.0272	0.0222
±10%	10	5.50	0.0280	0.0219	5.50	0.0287	0.0224
		6.78	0.0283	0.0226	6.73	0.0327	0.0260
		8.14	0.0309	0.0250	8.12	0.0360	0.0292
		9.64	0.0289	0.0237	9.63	0.0347	0.0285
	20	5.45	0.0329	0.0256	5.02	0.0297	0.0230
		6.70	0.0351	0.0279	6.78	0.0430	0.0313
		8.10	0.0358	0.0289	8.19	0.0432	0.0352
		9.61	0.0346	0.0284	9.70	0.0443	0.0366
	30	5.48	0.0338	0.0264	4.88	0.0375	0.0292
		6.72	0.0384	0.0305	6.72	0.0459	0.0368
		8.11	0.0378	0.0306	8.12	0.0476	0.0389
		9.62	0.0378	0.0309	9.63	0.0516	0.0426

Table 5.2 Relative amplitudes of heated surface temperature and heat transfer coefficient oscillations in transient oscillatory subcooled flow boiling at $\Delta T_{sub} = 10^{o}C$ for various imposed heat fluxes and the amplitudes and periods of the coolant mass flux oscillation.

$\Delta G/\bar{G}$	t_p (sec)	$\bar{G}$ =300 kg/m^{2}s			$\bar{G}$ =400 kg/m^{2}s		
		q(W/cm^2)	$A_{T_w}/\Delta\bar{T}_{sat}$	$A_{h_{2\rho}}/\bar{h}_{2\rho}$	q(W/cm^2)	$A_{T_w}/\Delta\bar{T}_{sat}$	$A_{h_{2\rho}}/\bar{h}_{2\rho}$
±5%	10	5.48	0.0221	0.0139	6.13	0.0157	0.0090
		6.72	0.0243	0.0158	7.39	0.0275	0.0151
		8.12	0.0244	0.0165	8.81	0.0252	0.0170
		9.60	0.0250	0.0172	10.36	0.0246	0.0170
	20	5.54	0.0306	0.0193	6.04	0.0230	0.0147
		6.67	0.0280	0.0183	7.35	0.0259	0.0170
		8.05	0.0306	0.0206	8.78	0.0285	0.0194
		9.56	0.0307	0.0211	10.37	0.0277	0.0192
	30	5.98	0.0329	0.0209	5.96	0.0259	0.0167
		7.29	0.0300	0.0197	7.28	0.0284	0.0191
		8.74	0.0297	0.0202	8.73	262	0.0179
		10.32	0.0265	0.0184	10.30	0.0288	0.0200
±10%	10	5.50	0.0389	0.0244	5.58	0.0247	0.0154
		6.69	0.0415	0.0270	6.82	0.0356	0.0231
		8.10	0.0445	0.0299	8.22	0.0397	0.0266
		9.61	0.0470	0.0320	9.75	0.0404	0.0277
	20	5.49	0.0543	0.0339	5.47	0.0220	0.0136
		6.67	0.0613	0.0397	6.70	0.0462	0.0296
		8.06	0.0612	0.0407	8.08	0.0529	0.0353
		9.56	0.0584	0.0400	9.58	0.0584	0.0402
	30	5.47	0.0609	0.0382	5.44	0.0249	0.0154
		6.67	0.0656	0.0426	6.72	0.0551	0.0356
		8.05	0.0676	0.0452	8.07	0.0527	0.0350
		9.55	0.0624	0.0429	9.61	0.0565	0.0387

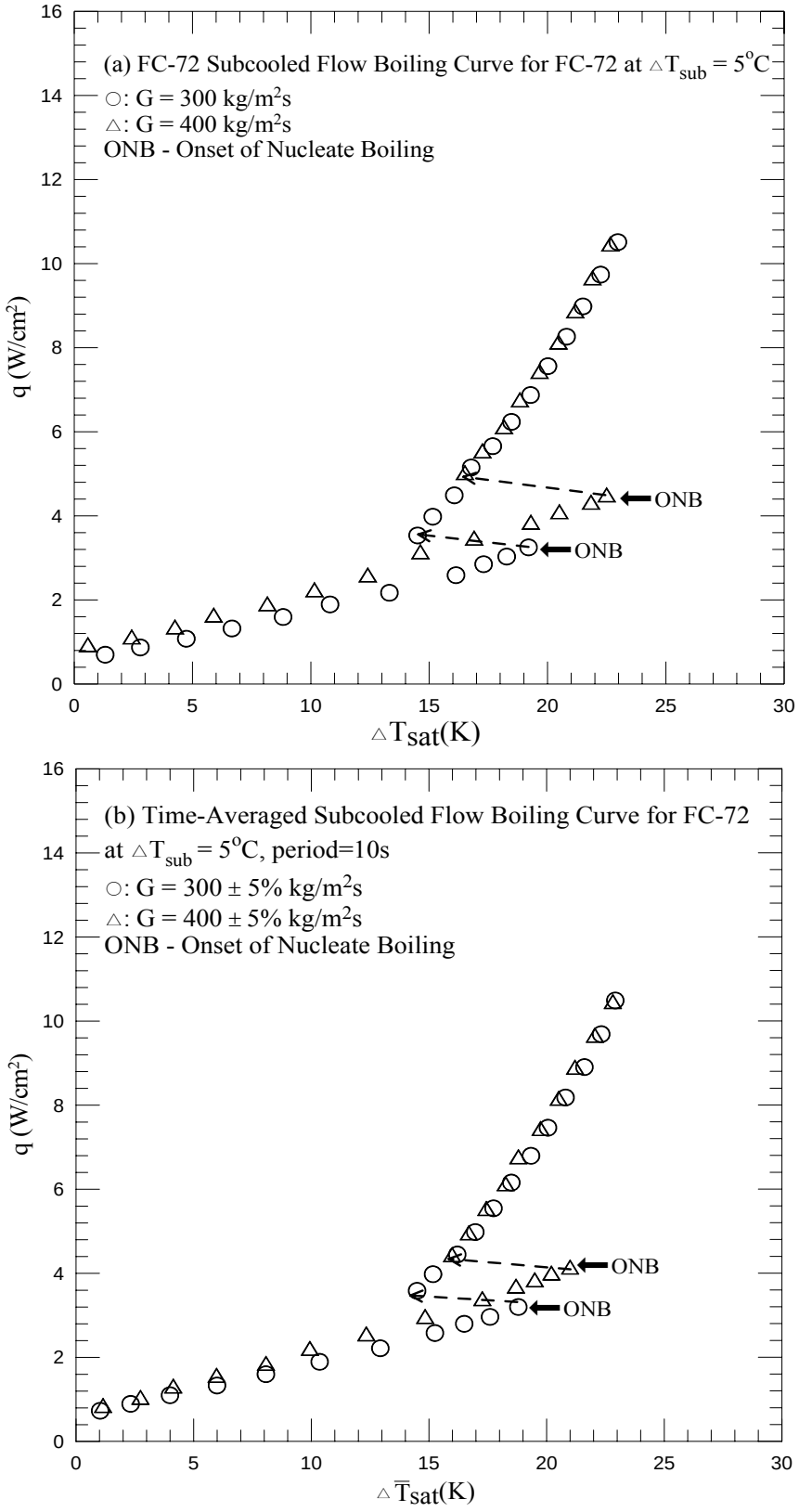

Fig. 5.1 Time-average flow boiling curves for various coolant mass fluxes for stable subcooled flow boiling (a) and transient subcooled flow boiling at $\triangle T_{sub}$ =5°C for t_p=10 sec (b), 20 sec (c) and 30 sec (d).

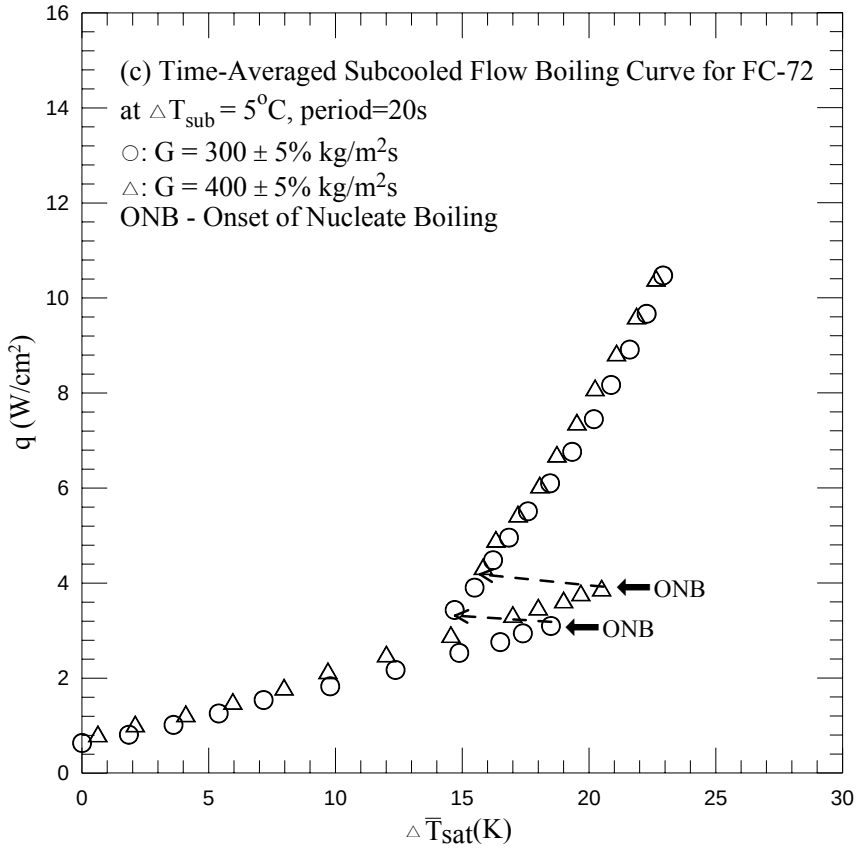

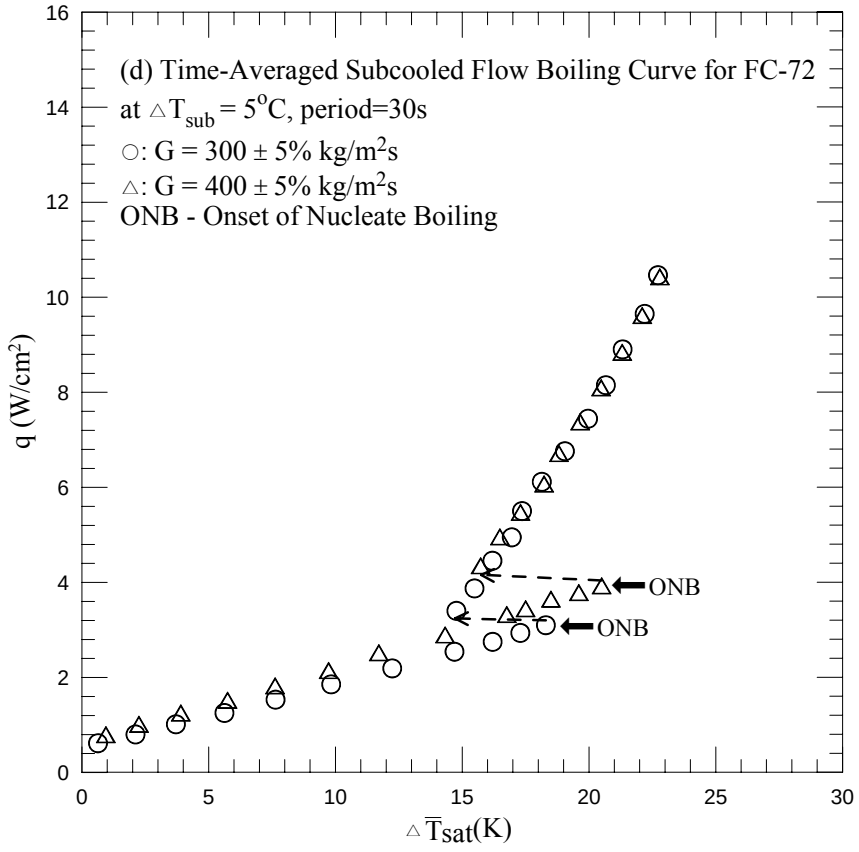

Fig. 5.1 Continued.

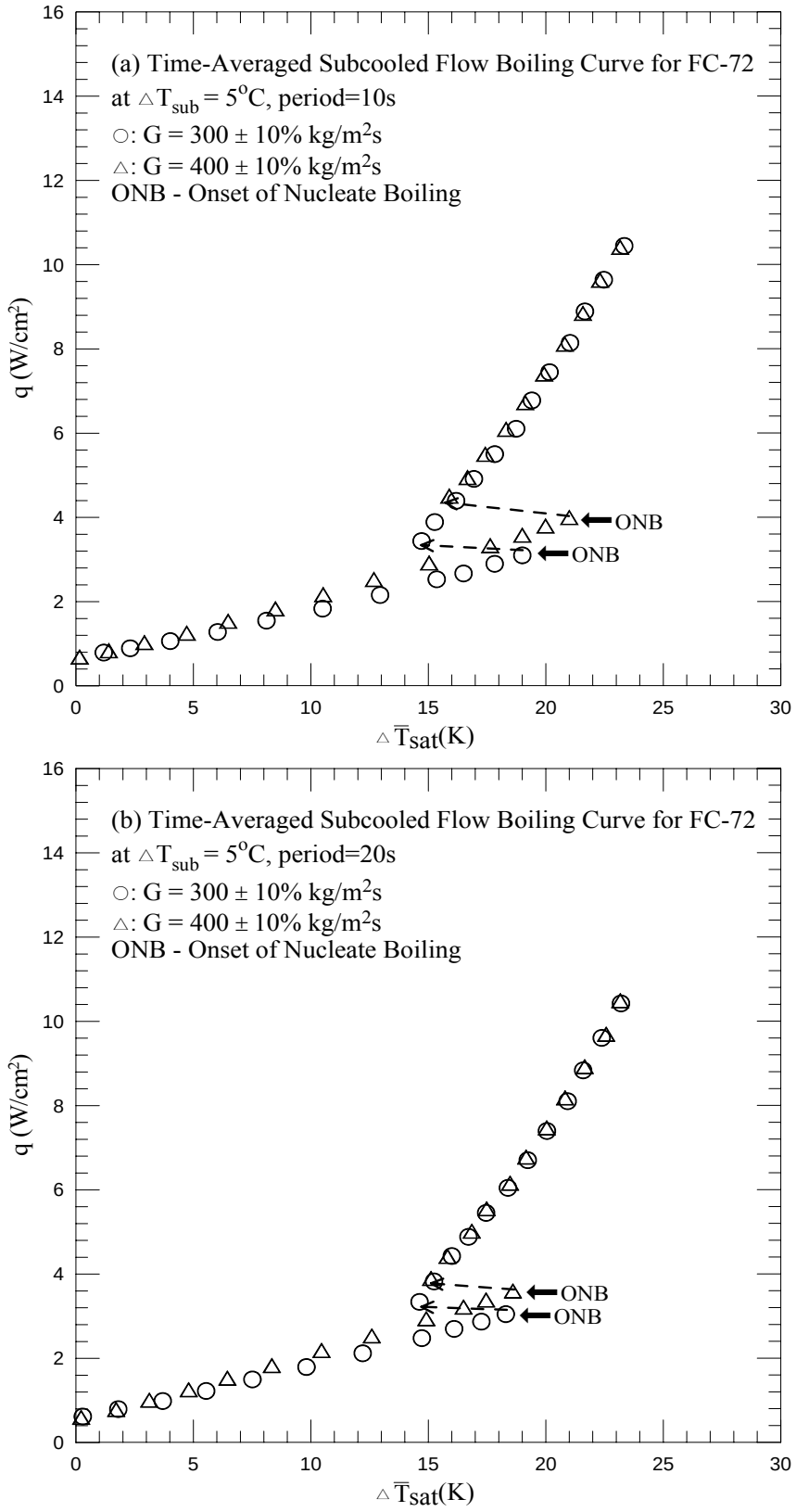

Fig. 5.2 Time-average flow boiling curves for various coolant mass fluxes for transient subcooled flow boiling at $\triangle T_{sub}$ =5°C for t_p=10 sec (a), 20 sec (b) and 30 sec (c).

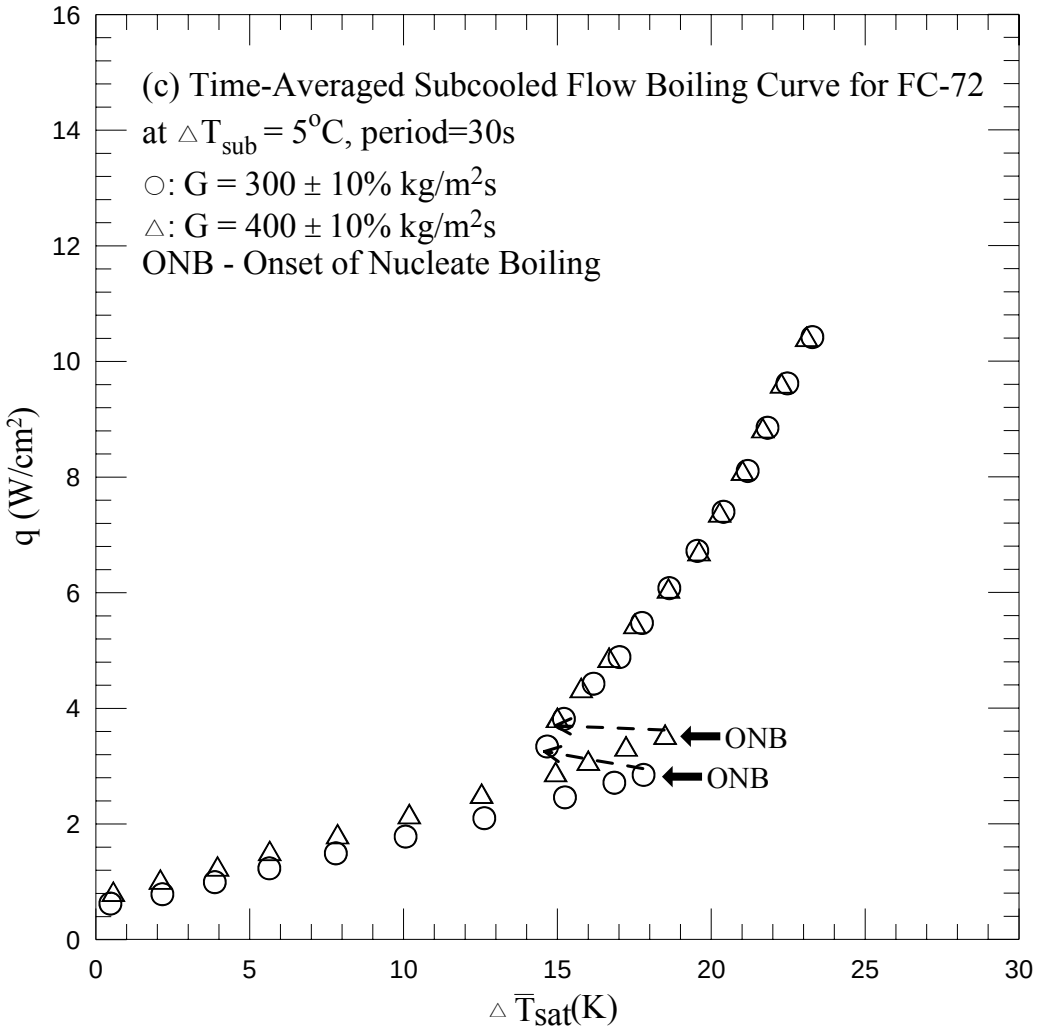

Fig. 5.2 Continued.

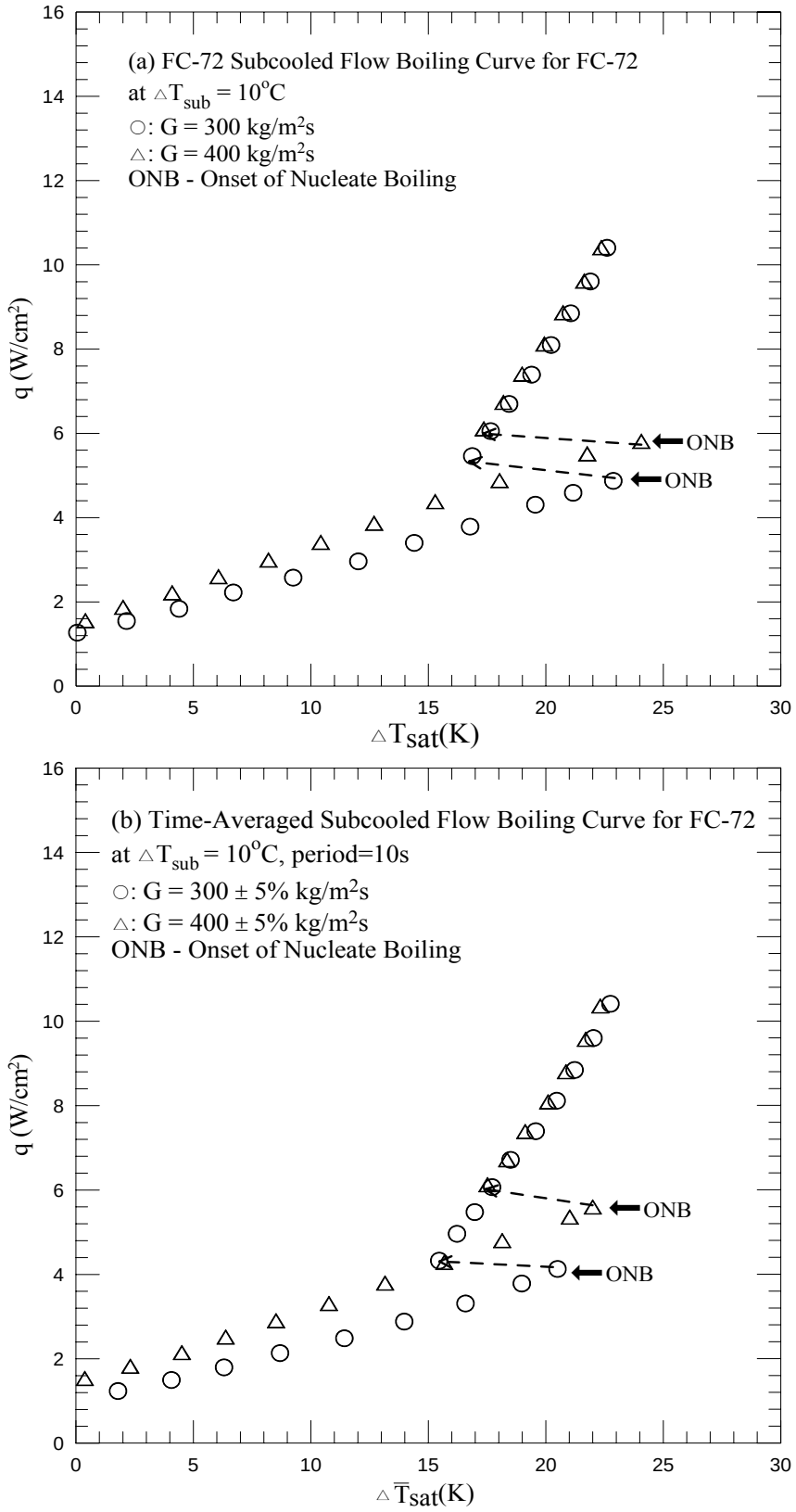

Fig. 5.3 Time-average flow boiling curves for various coolant mass fluxes for stable subcooled flow boiling (a) and transient subcooled flow boiling at $\triangle T_{sub}$ =10°C for t_p=10 sec (b), 20 sec (c) and 30 sec (d).

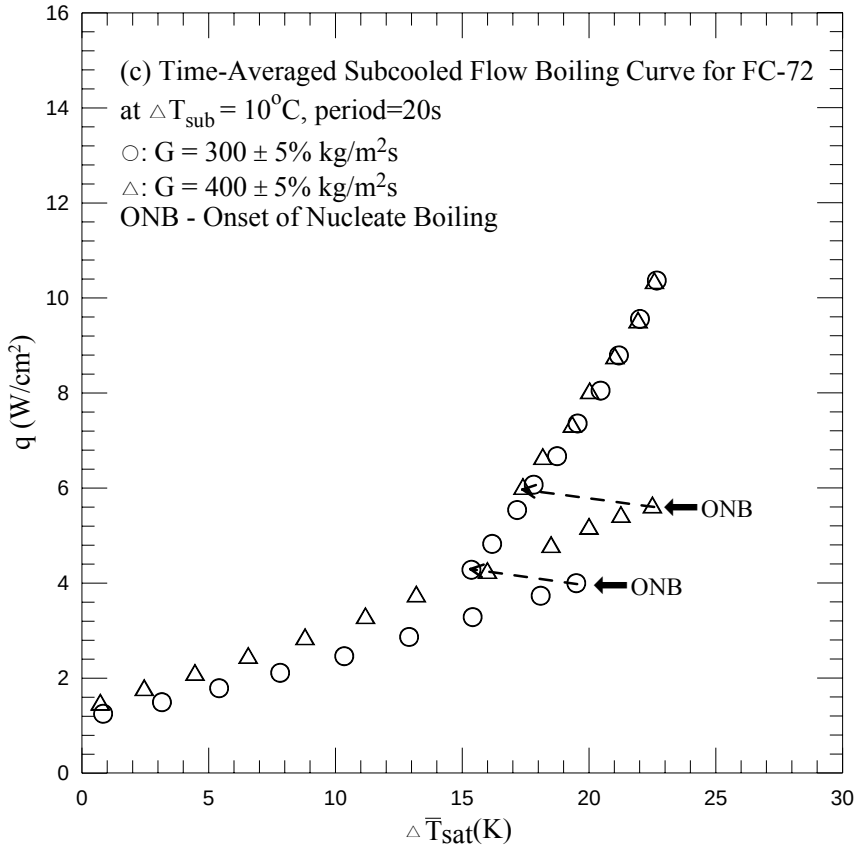

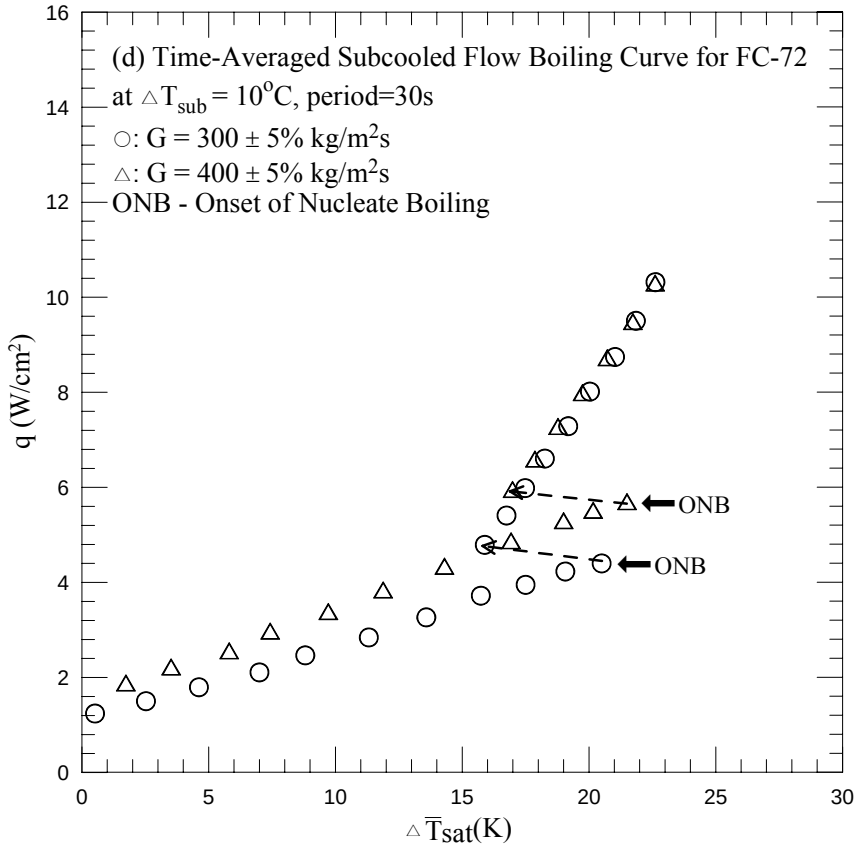

Fig. 5.3 Continued.

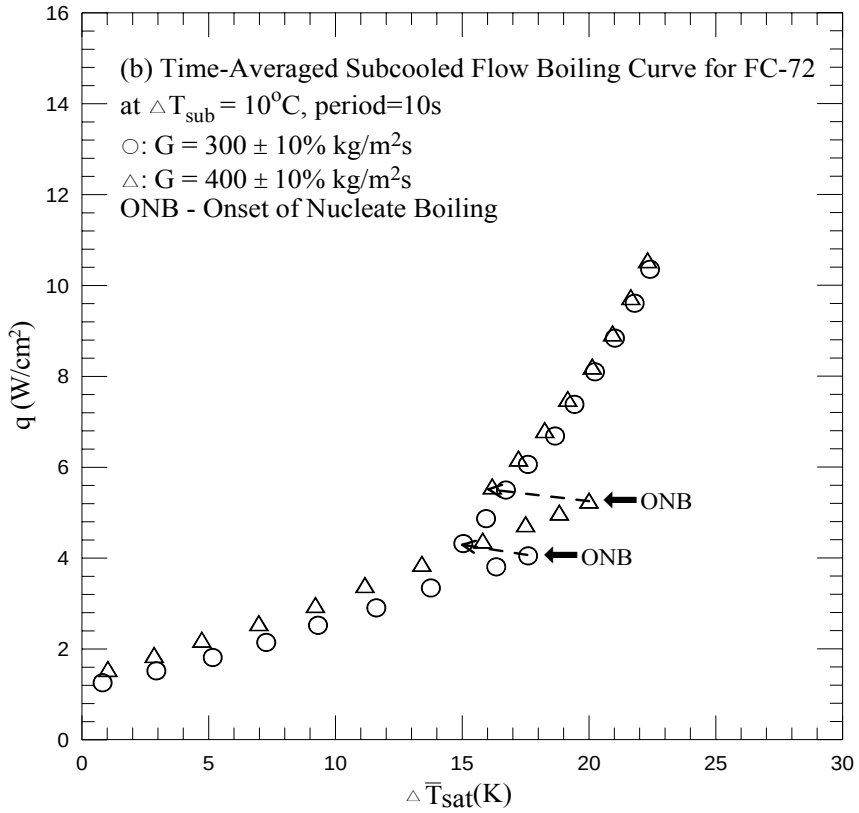

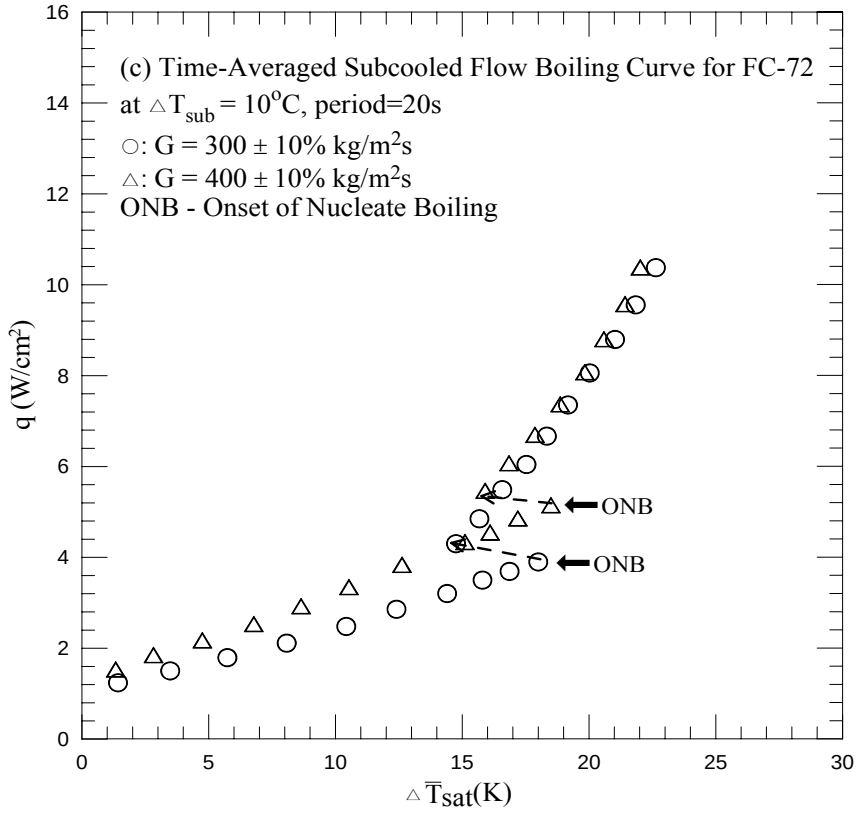

Fig. 5.4 Time-average flow boiling curves for various coolant mass fluxes for transient subcooled flow boiling at $\triangle T_{sub}$ =10°C for t_p=10 sec (a), 20 sec (b) and 30 sec (c).

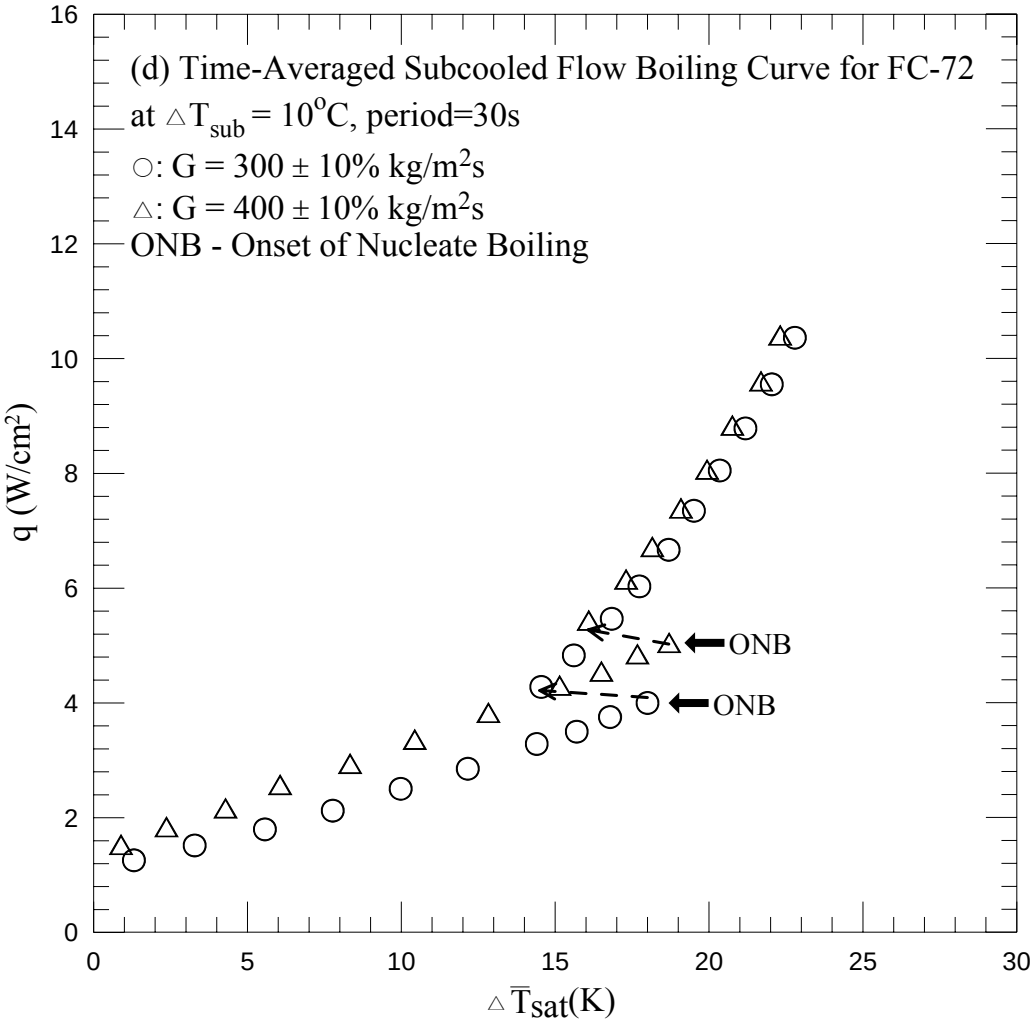

Fig. 5.4 Continued.

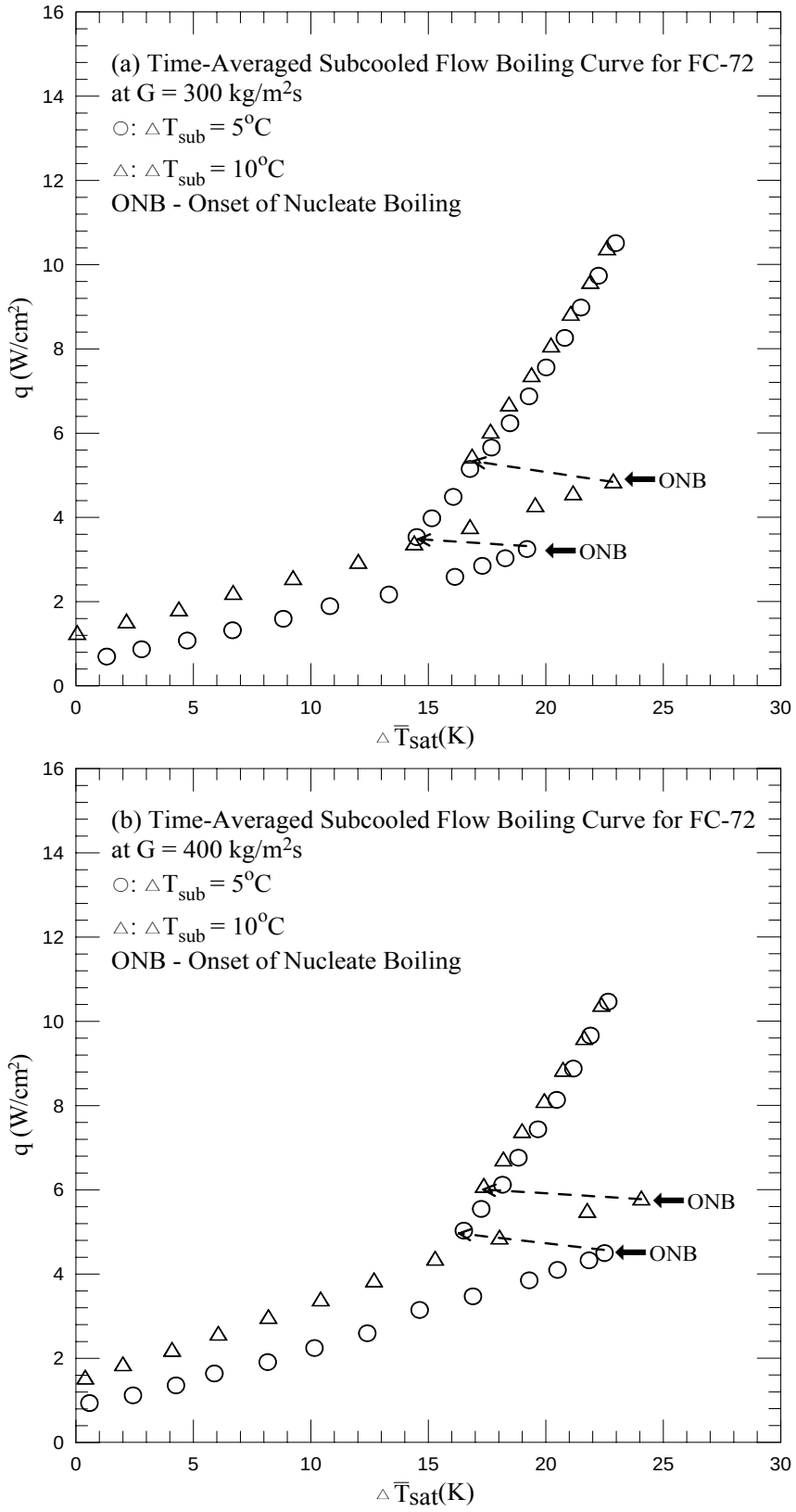

Fig. 5.5 Time-average flow boiling curves for various inlet subcoolings for stable subcooled flow boiling at (a) G=300 kg/m^{2}s and (b) G=400 kg/m^{2}s.

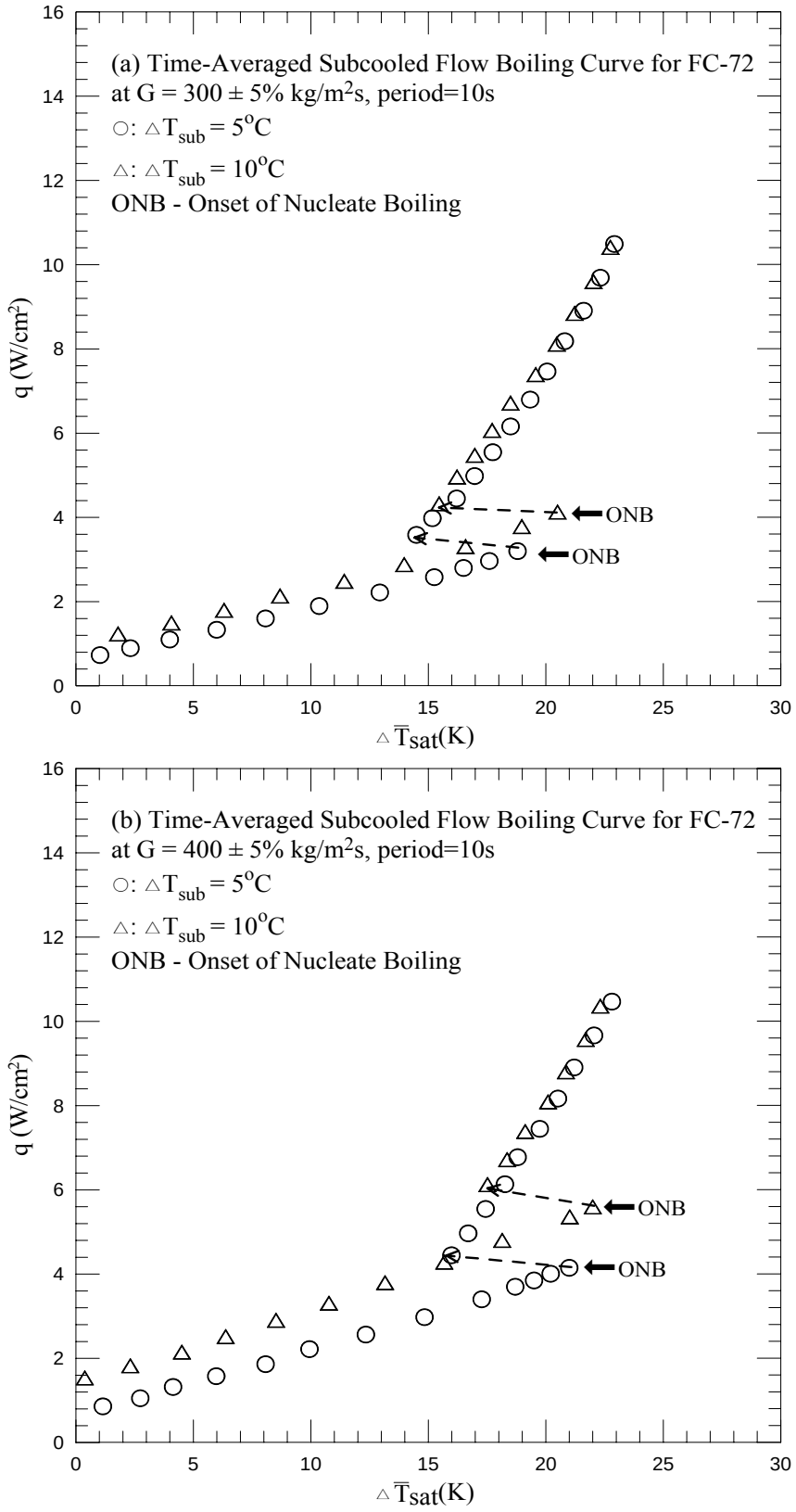

Fig. 5.6 Time-average flow boiling curves for various inlet subcoolings for transient subcooled flow boiling at (a) G=300±5% kg/m^{2}s and (b) G=400±5% kg/m^{2}s at t_p=10 sec.

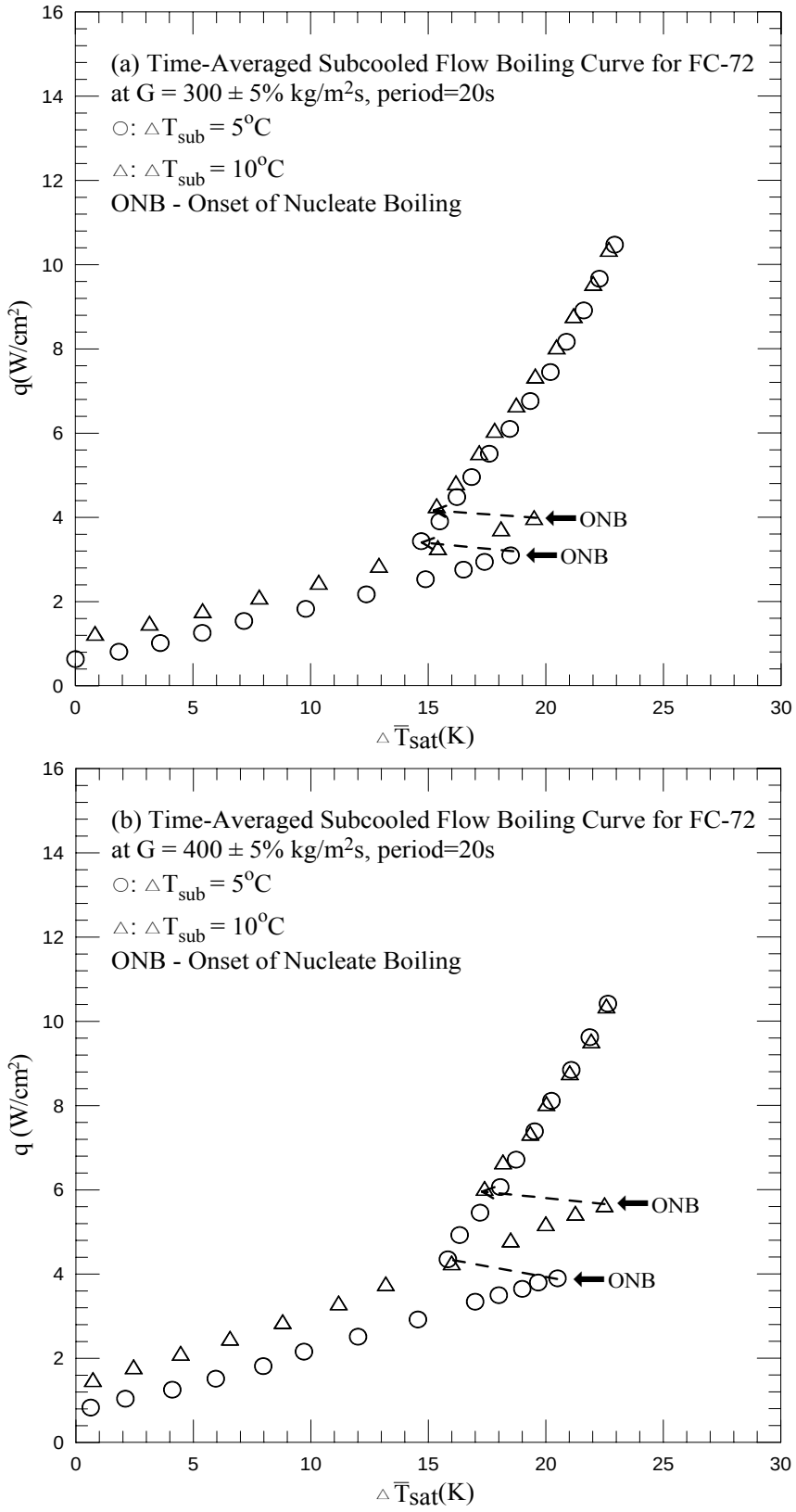

Fig. 5.7 Time-average flow boiling curves for various inlet subcoolings for transient subcooled flow boiling at (a) G=300±5% kg/m^{2}s and (b) G=400±5% kg/m^{2}s at t_p=20 sec.

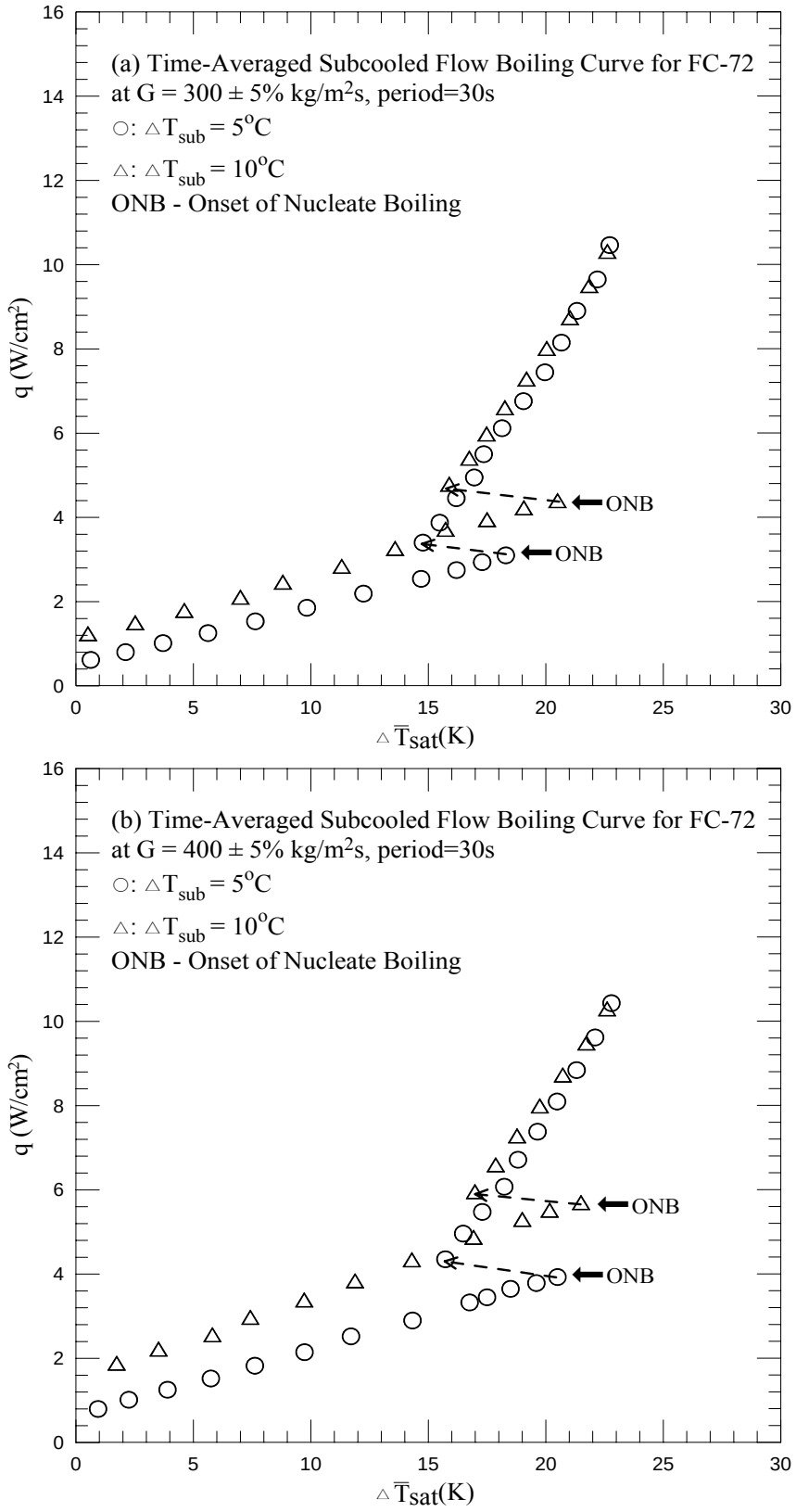

Fig. 5.8 Time-average flow boiling curves for various inlet subcoolings for transient subcooled flow boiling at (a) G=300±5% kg/m^{2}s and (b) G=400±5% kg/m^{2}s at t_p=30 sec.

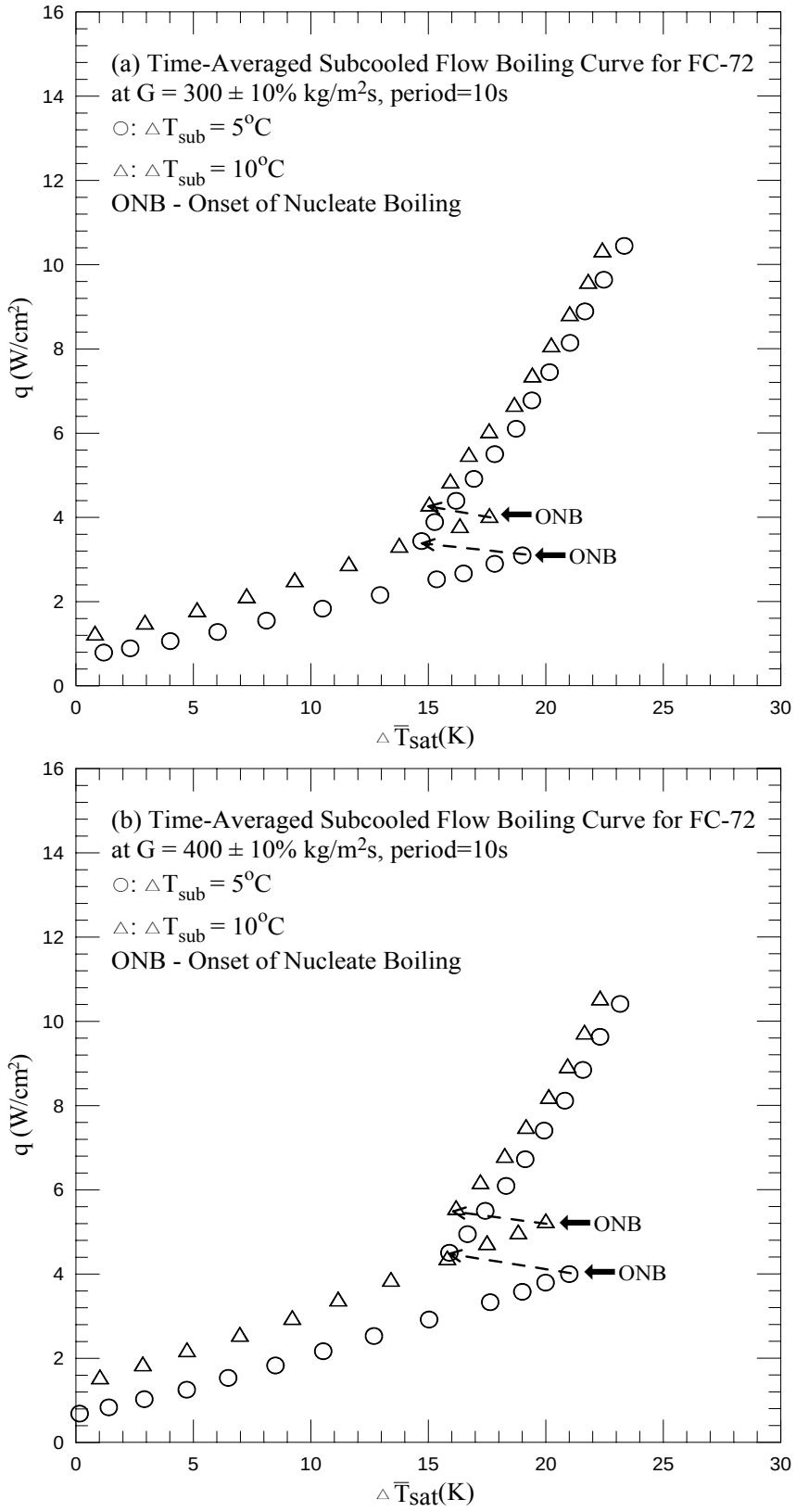

Fig. 5.9 Time-average flow boiling curves for various inlet subcoolings for transient subcooled flow boiling at (a) G=300±10% kg/m^{2}s and (b) G=400±10% kg/m^{2}s at t_p=10 sec.

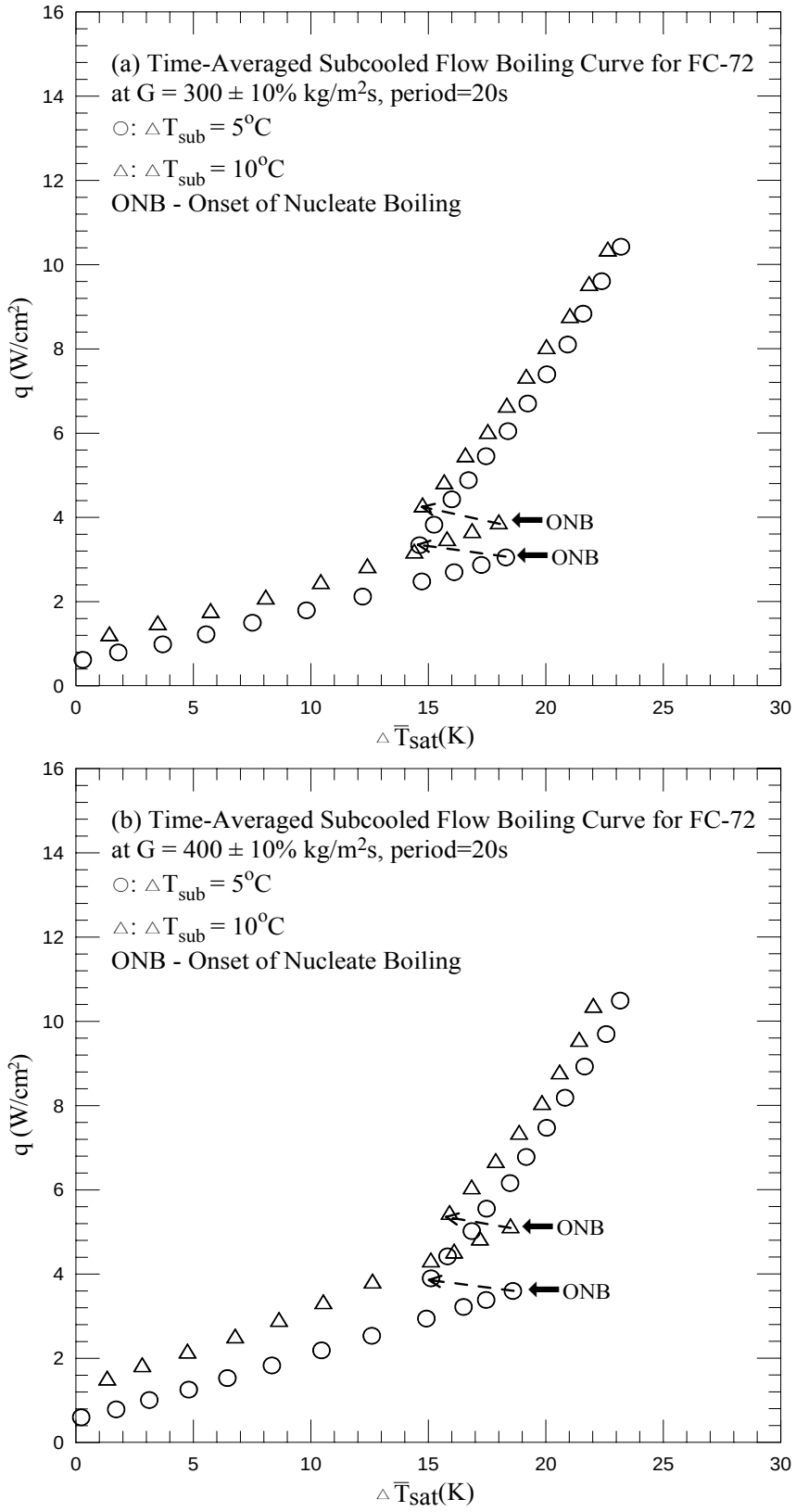

Fig. 5.10 Time-average flow boiling curves for various inlet subcoolings for transient subcooled flow boiling at (a) G=300±10% kg/m^{2}s and (b) G=400±10% kg/m^{2}s at t_p=20 sec.

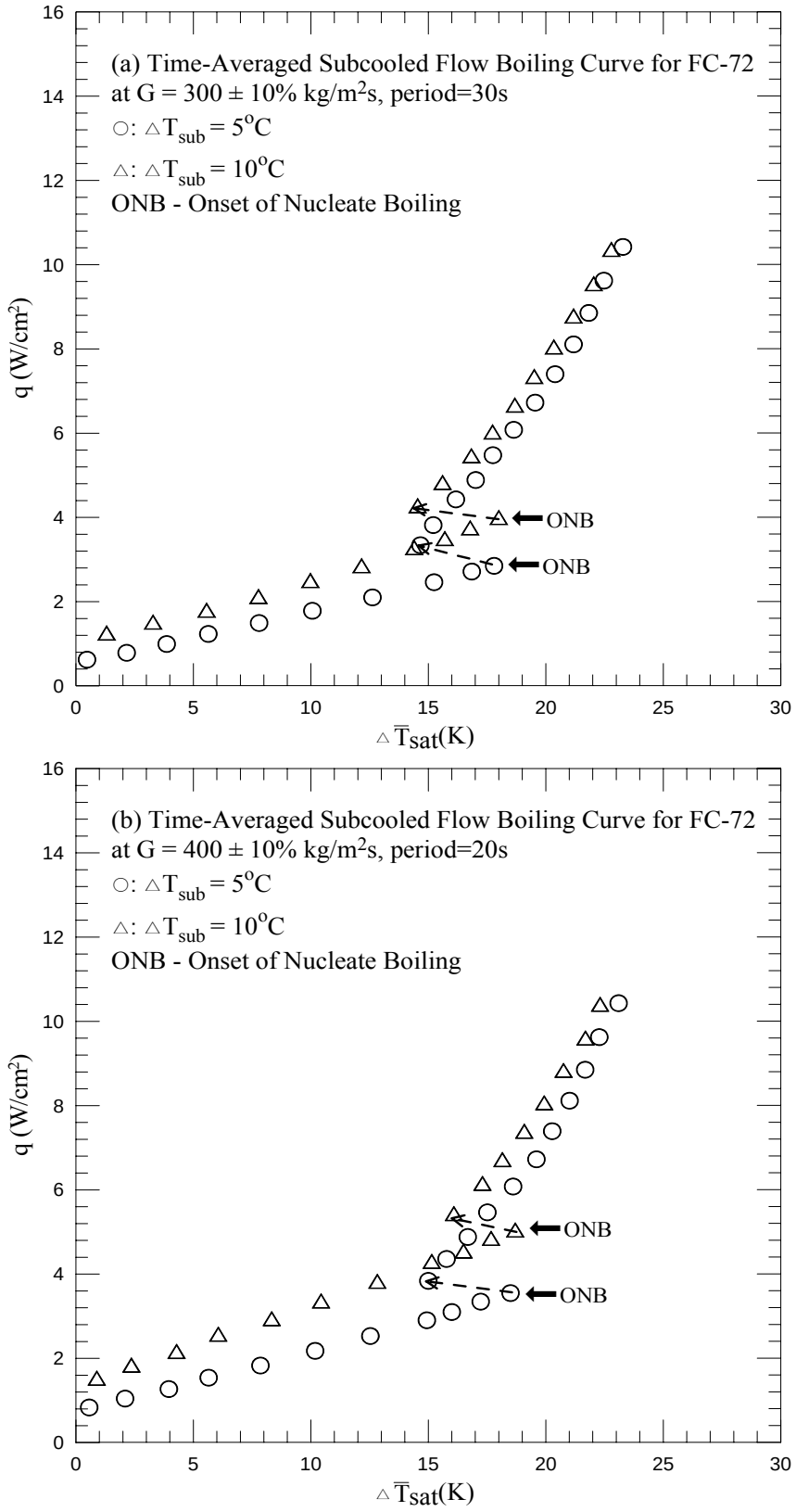

Fig. 5.11 Time-average flow boiling curves for various inlet subcoolings for transient subcooled flow boiling at (a) G=300±10% kg/m^{2}s and (b) G=400±10% kg/m^{2}s at t_p=30 sec.

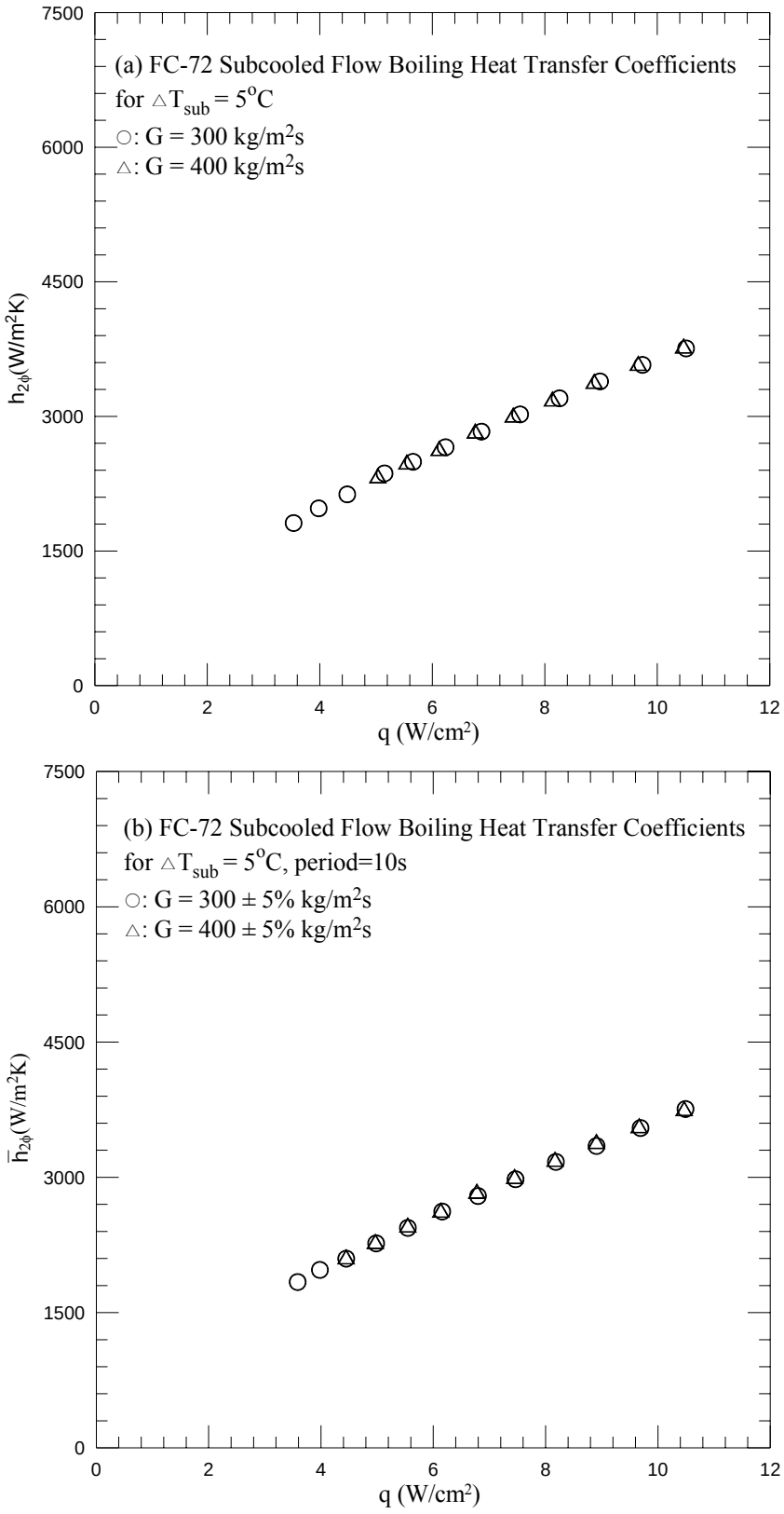

Fig. 5.12 Time-average flow boiling heat transfer coefficients for various coolant mass fluxes for stable subcooled flow boiling (a) and transient subcooled flow boiling at ΔT_{sub} =5°C for t_p=10 sec (b), 20 sec (c) and 30 sec (d).

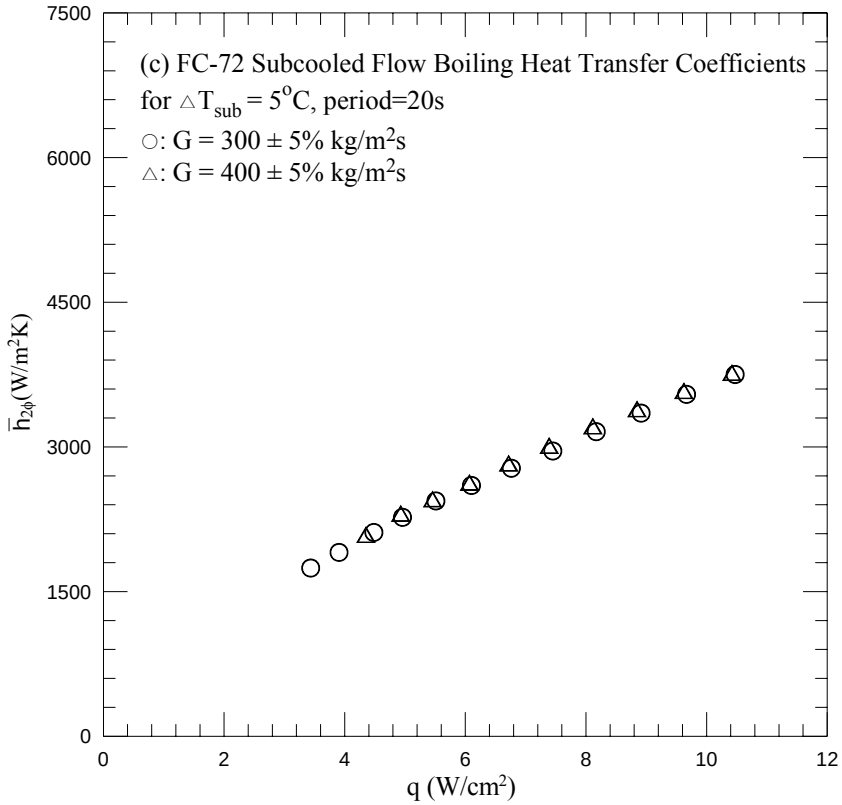

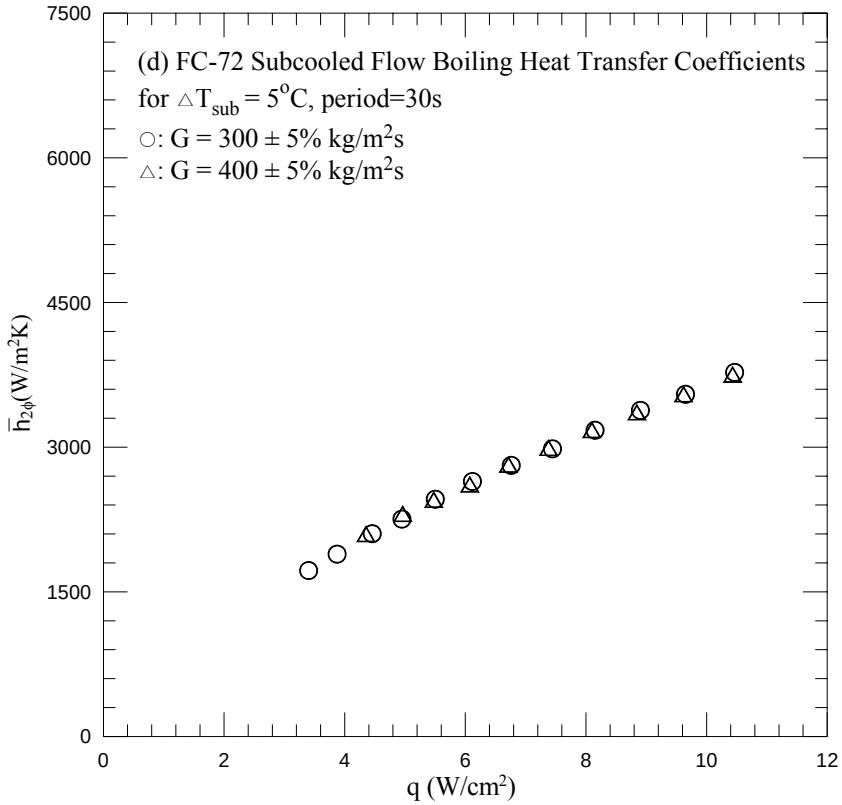

Fig. 5.12 Continued.

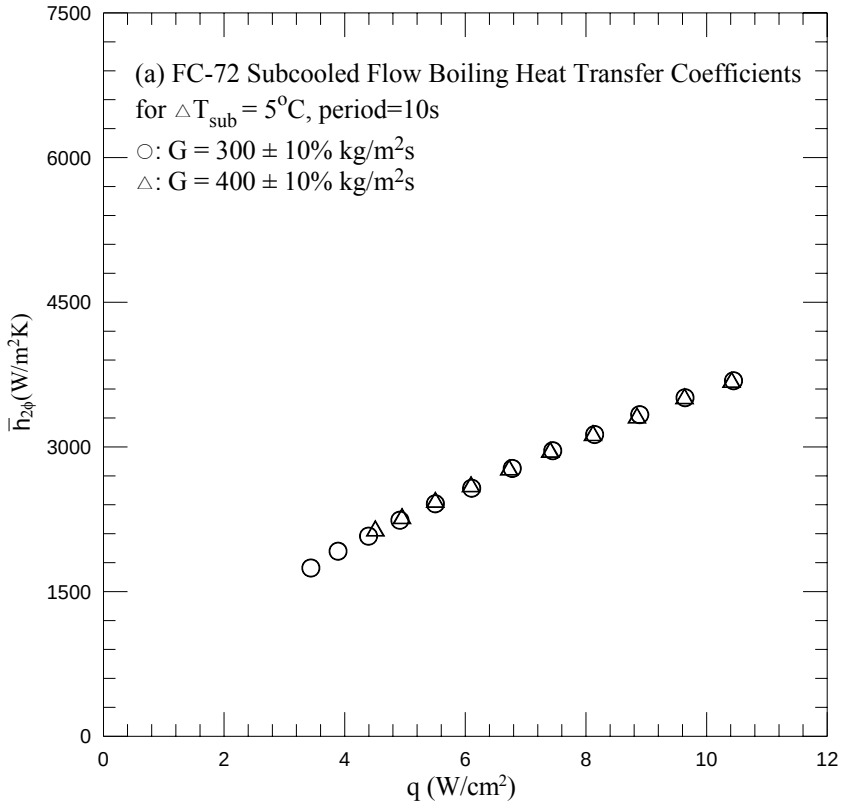

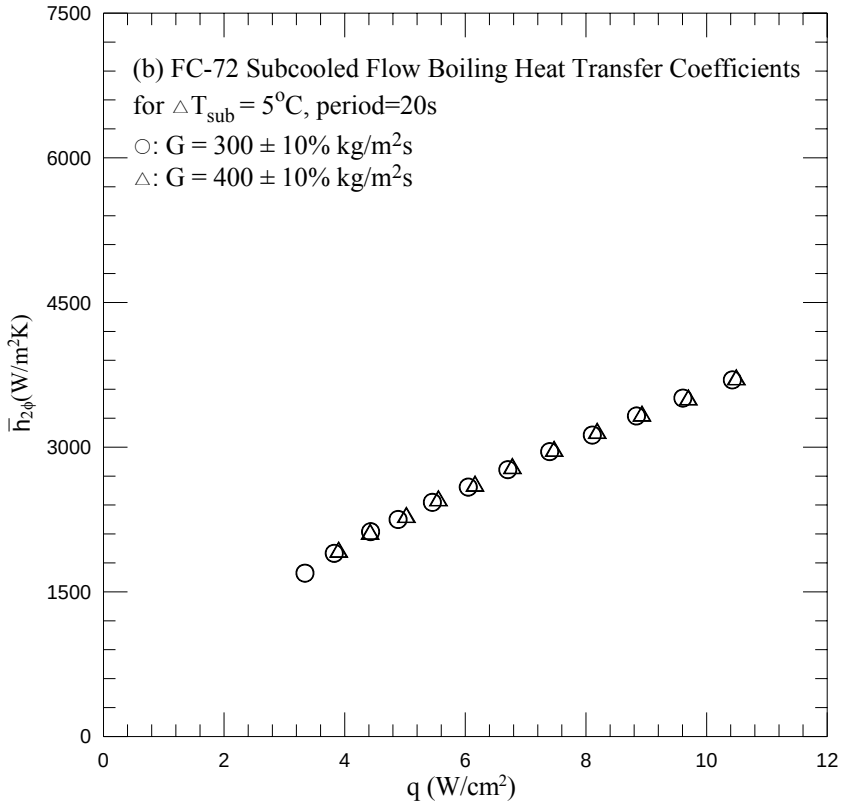

Fig. 5.13 Time-average flow boiling heat transfer coefficients for various coolant mass fluxes for transient subcooled flow boiling at ΔT_{sub} =5°C for t_p=10 sec (a), 20 sec (b) and 30 sec (c).

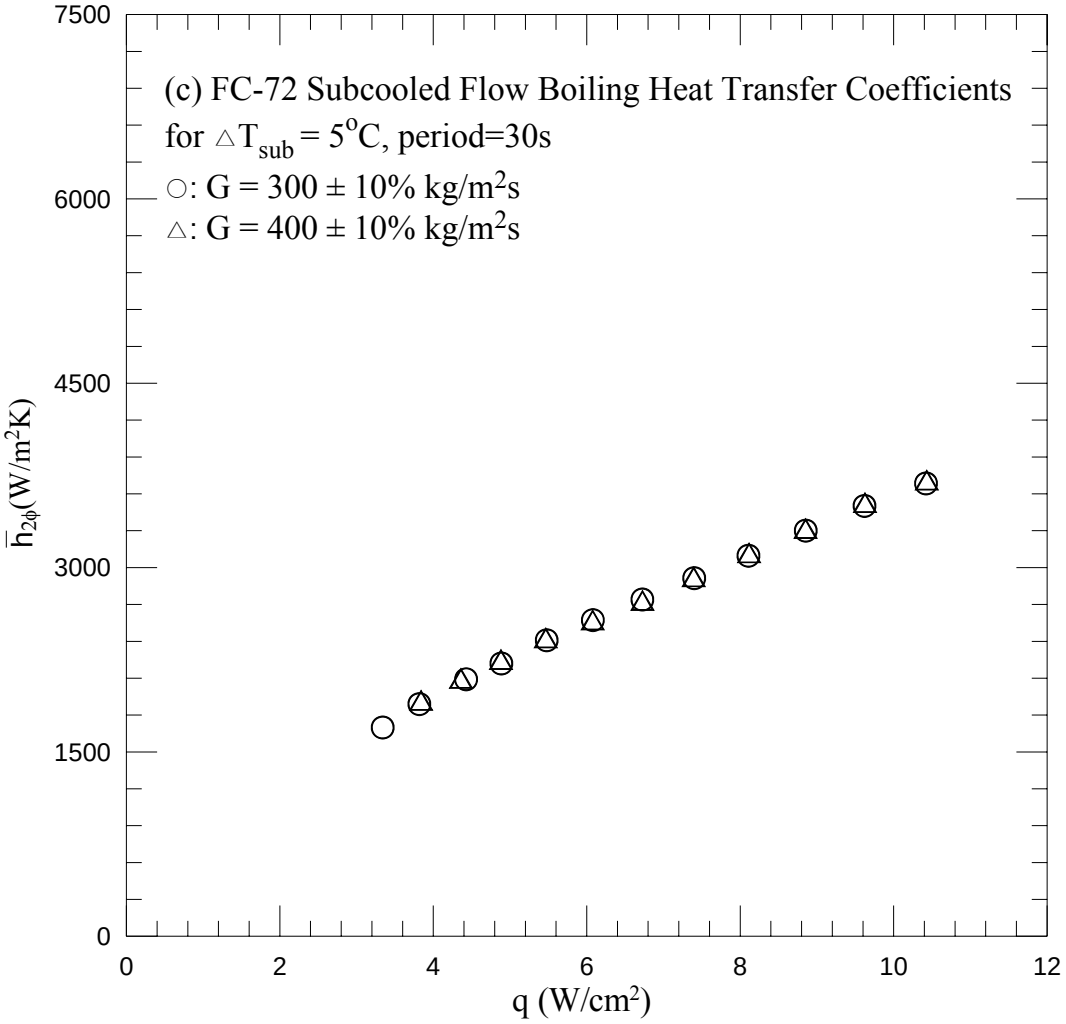

Fig. 5.13 Continued.

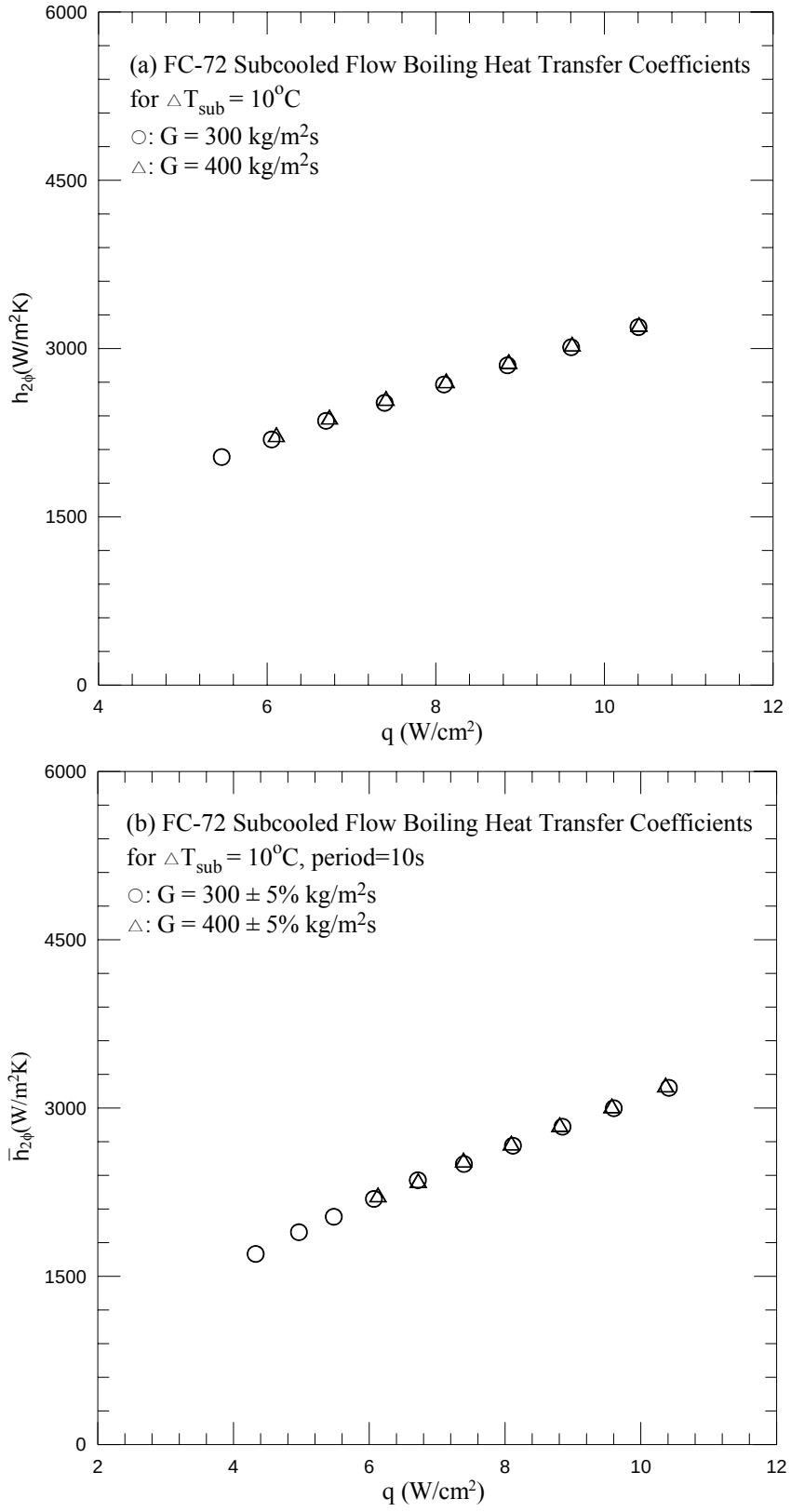

Fig. 5.14 Time-average flow boiling heat transfer coefficients for various coolant mass fluxes for stable subcooled flow boiling (a) and transient subcooled flow boiling at ΔT_{sub} =10°C for t_p=10 sec (b), 20 sec (c) and 30 sec (d).

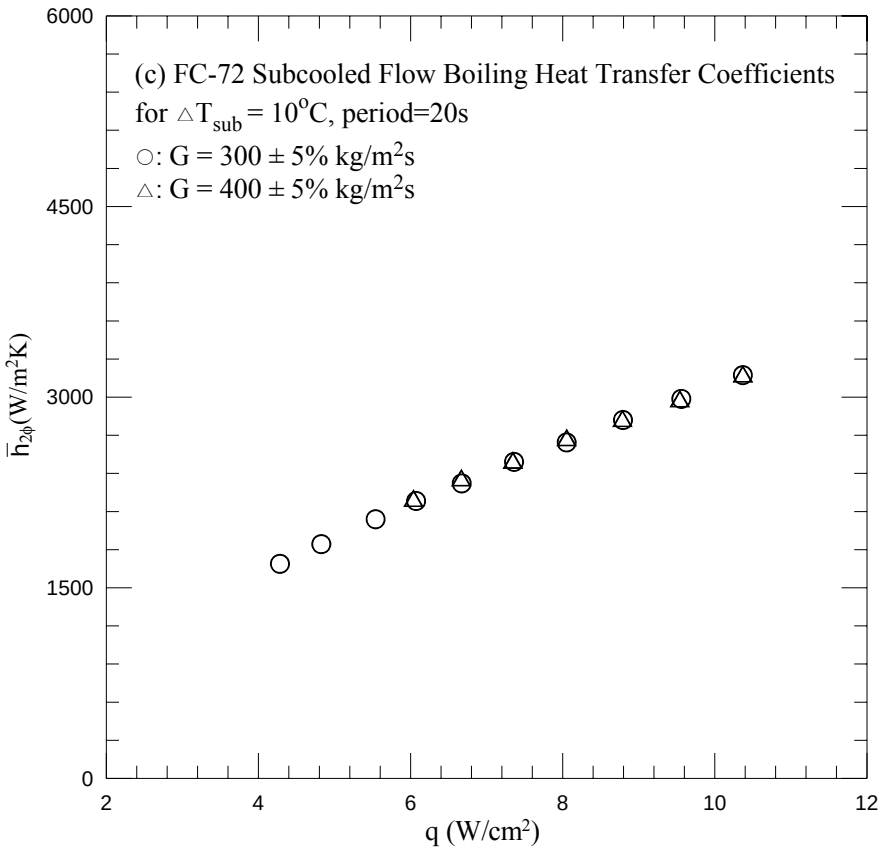

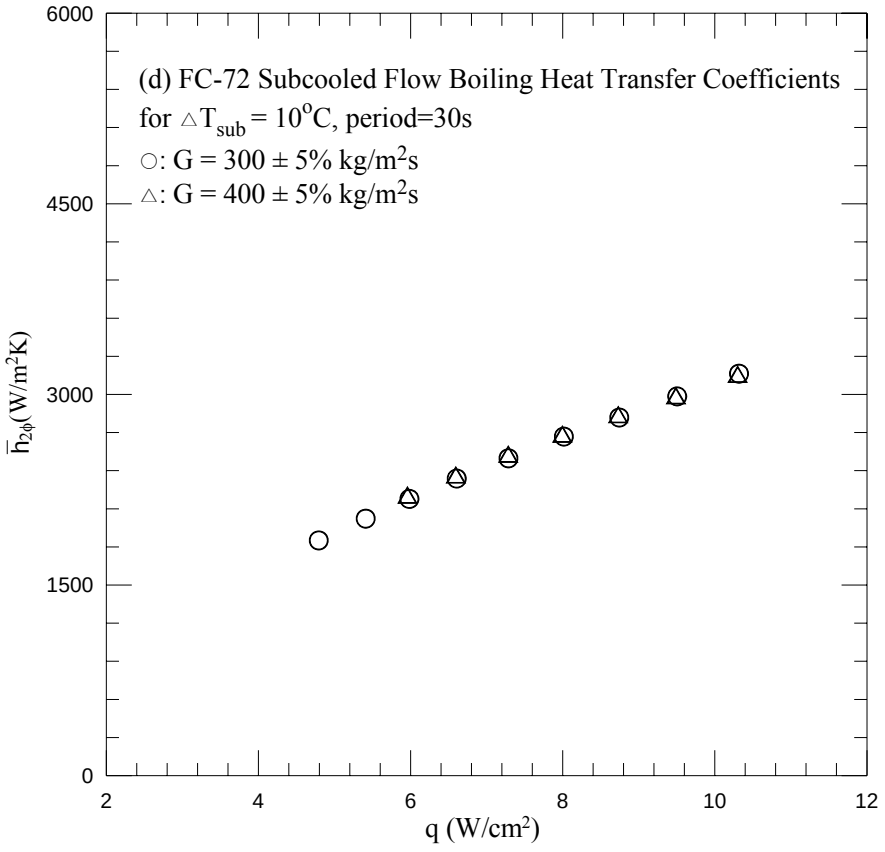

Fig. 5.14 Continued.

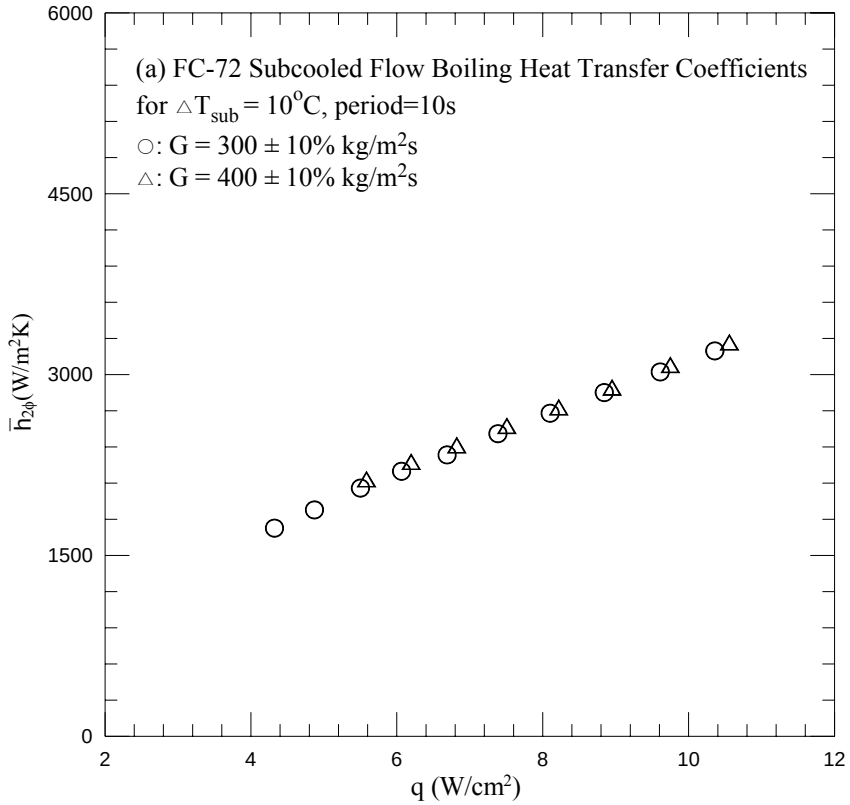

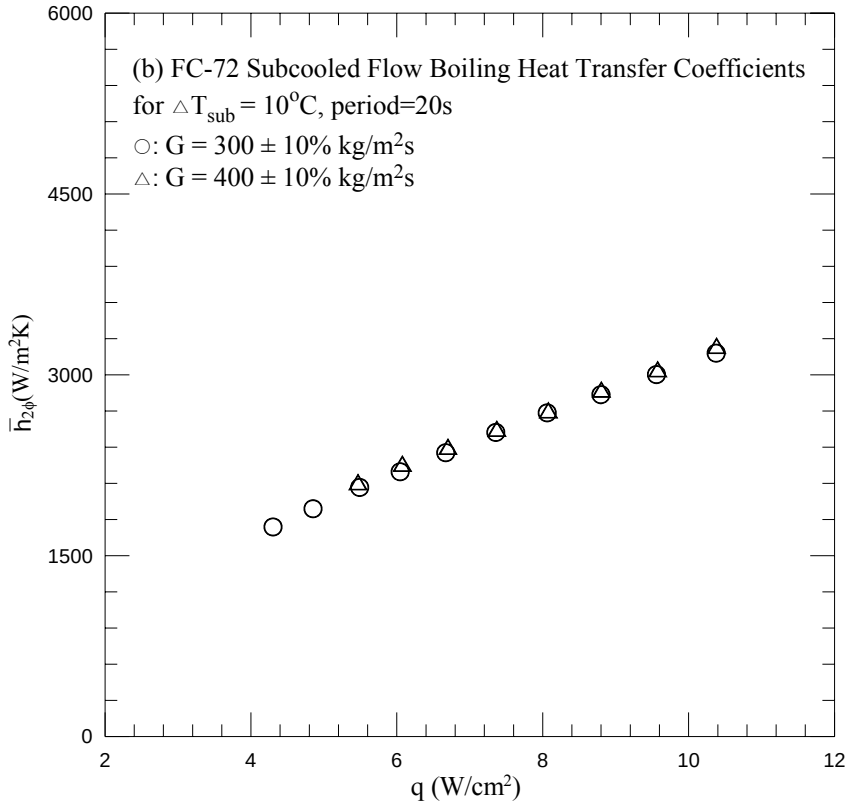

Fig. 5.15 Time-average flow boiling heat transfer coefficients for various coolant mass fluxes for transient subcooled flow boiling at ΔT_{sub} =10°C for t_p=10 sec (a), 20 sec (b) and 30 sec (c).

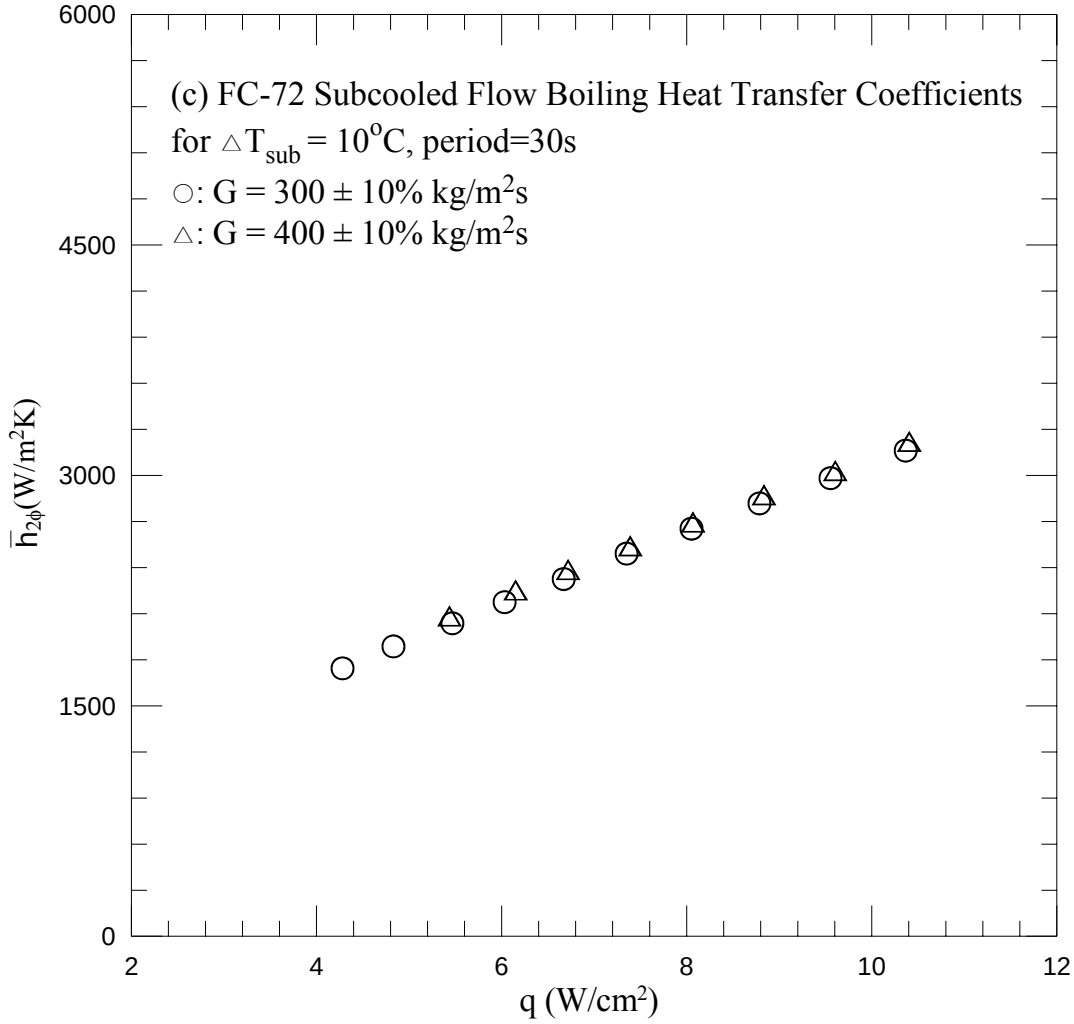

Fig. 5.15 Continued.

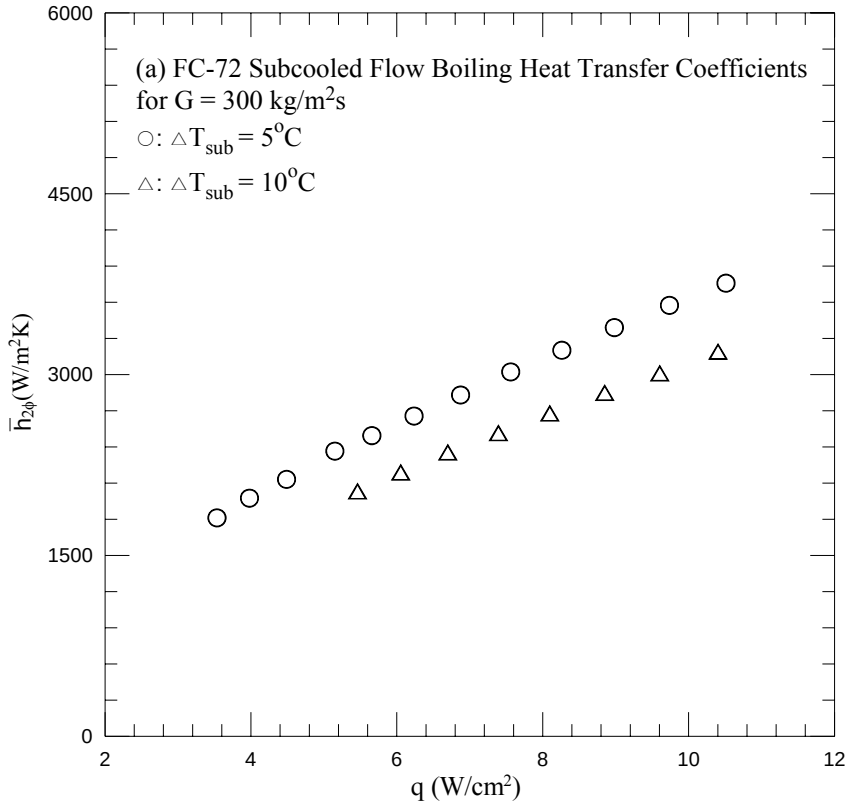

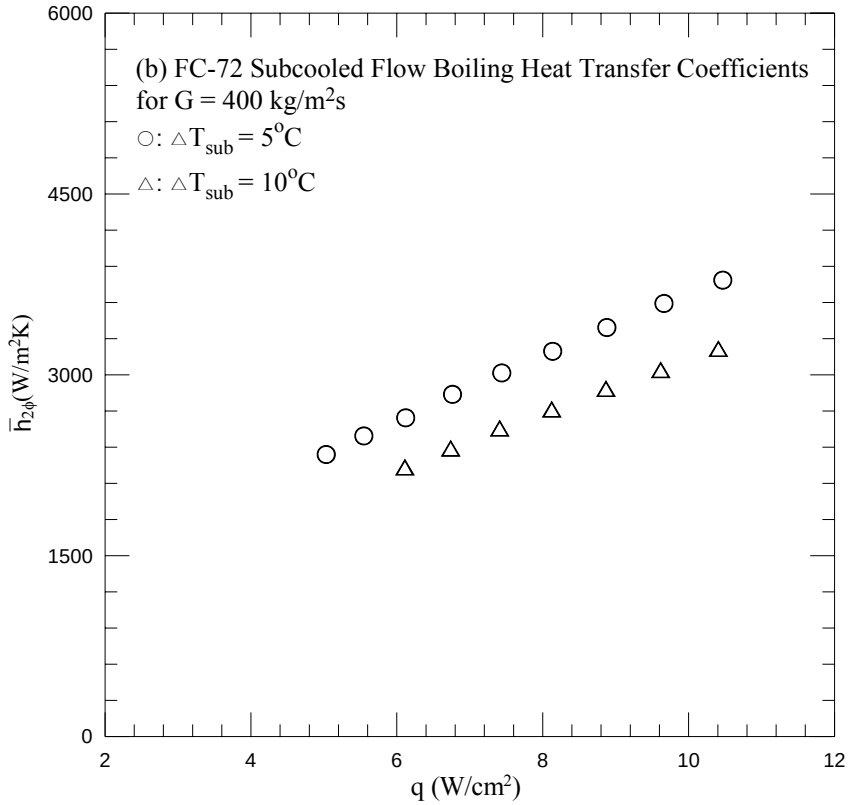

Fig. 5.16 Time-average flow boiling heat transfer coefficients for various inlet subcoolings for stable subcooled flow boiling at (a) G=300 kg/m^{2}s and (b) G=400 kg/m^{2}s.

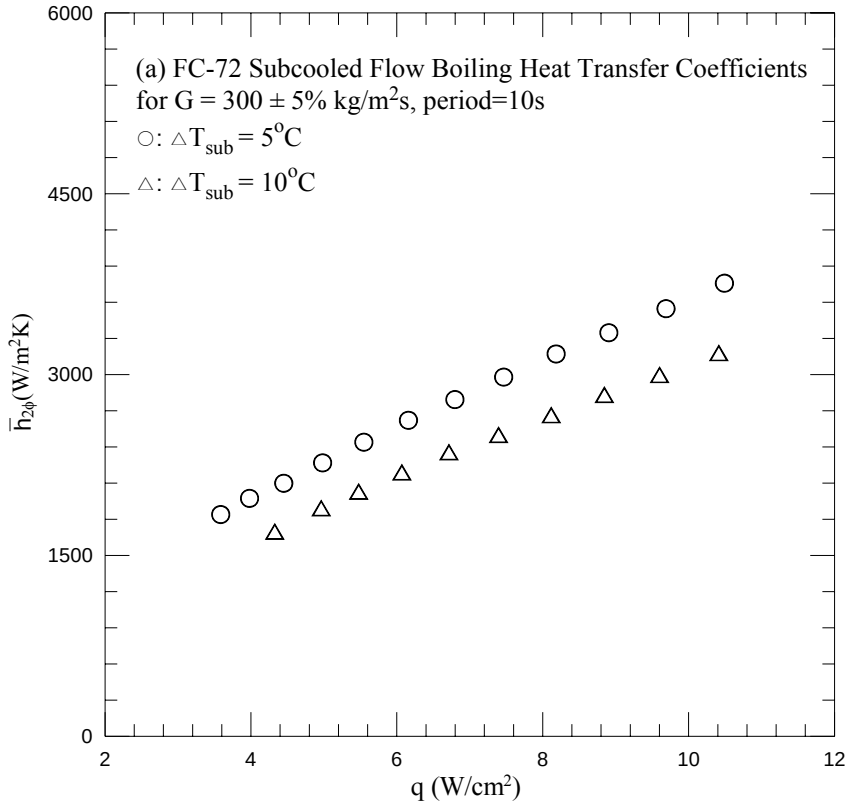

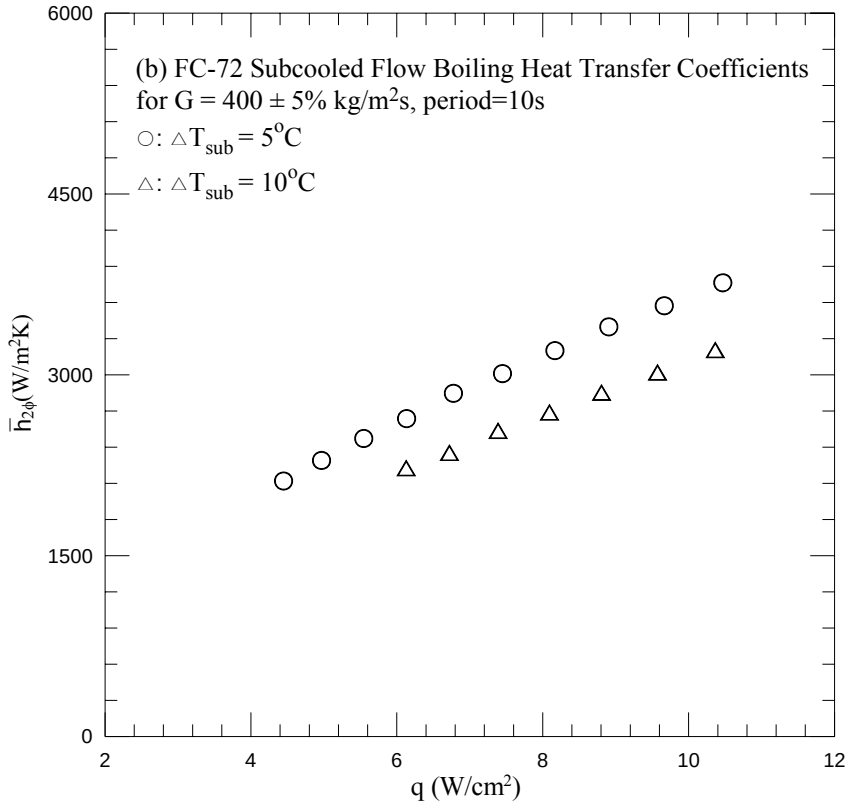

Fig. 5.17 Time-average flow boiling heat transfer coefficients for various inlet subcoolings for stable subcooled flow boiling at (a) G=300±5% kg/m^{2}s and (b) G=400±5% kg/m^{2}s at t_p=10 sec.

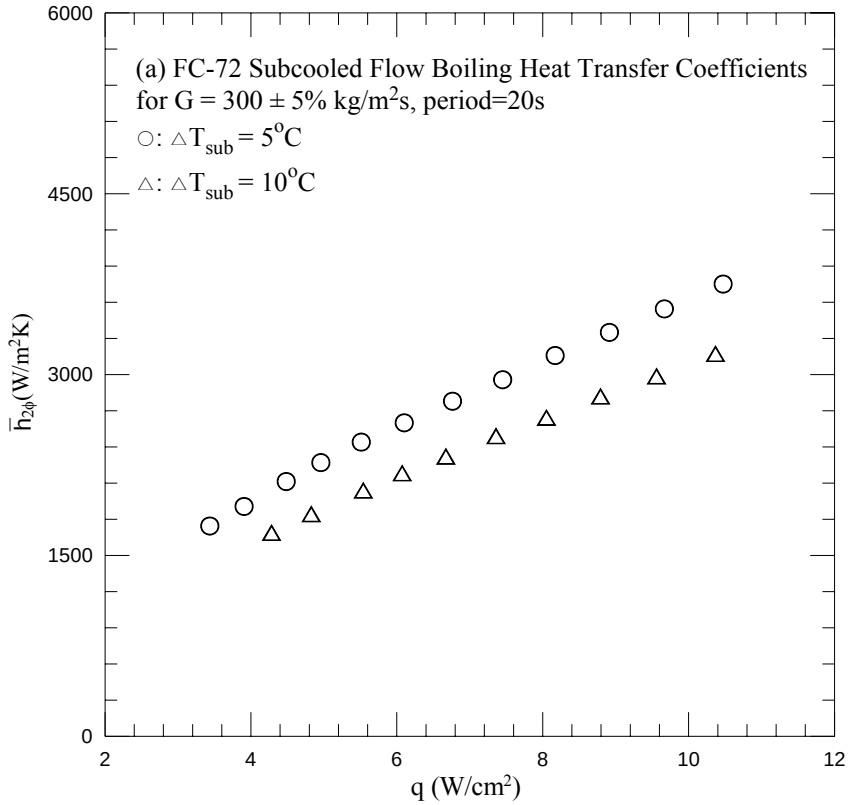

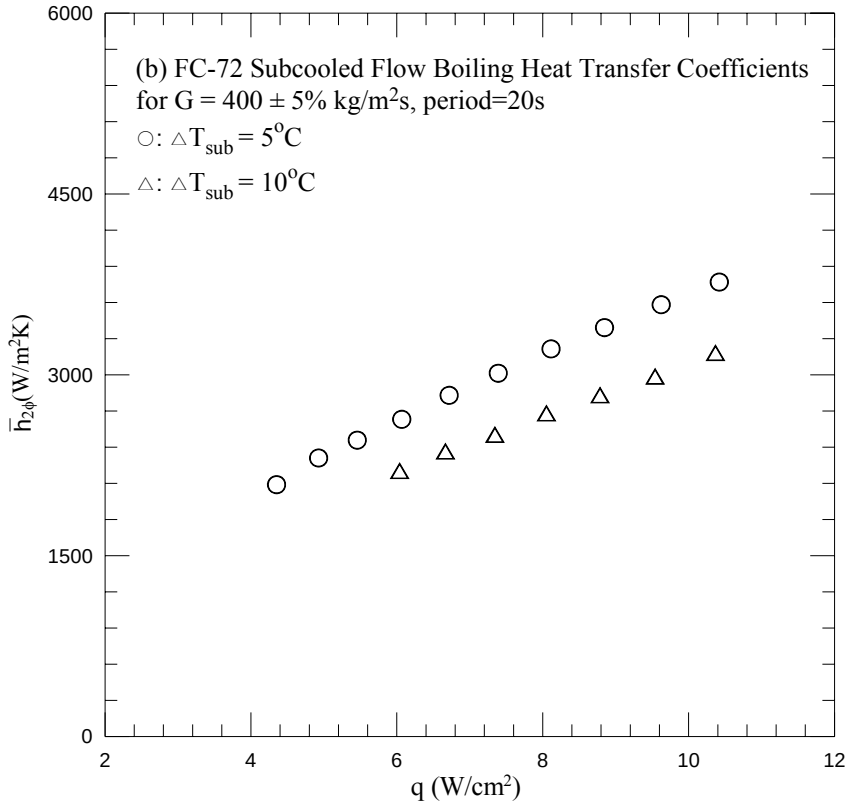

Fig. 5.18 Time-average flow boiling heat transfer coefficients for various inlet subcoolings for stable subcooled flow boiling at (a) G=300±5% kg/m^{2}s and (b) G=400±5% kg/m^{2}s at t_p=20 sec.

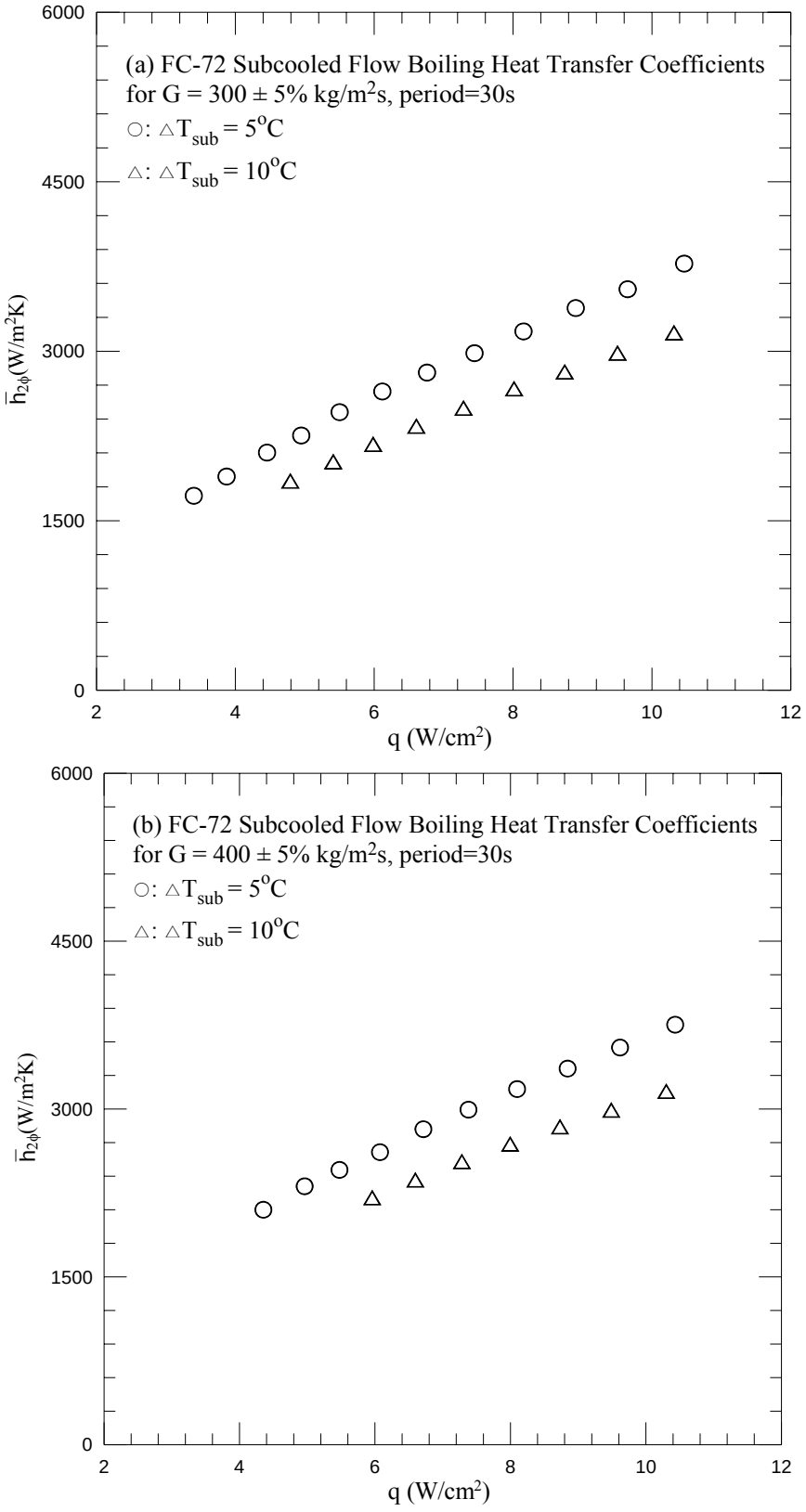

Fig. 5.19 Time-average flow boiling heat transfer coefficients for various inlet subcoolings for stable subcooled flow boiling at (a) G=300±5% kg/m^{2}s and (b) G=400±5% kg/m^{2}s at t_p=30 sec.

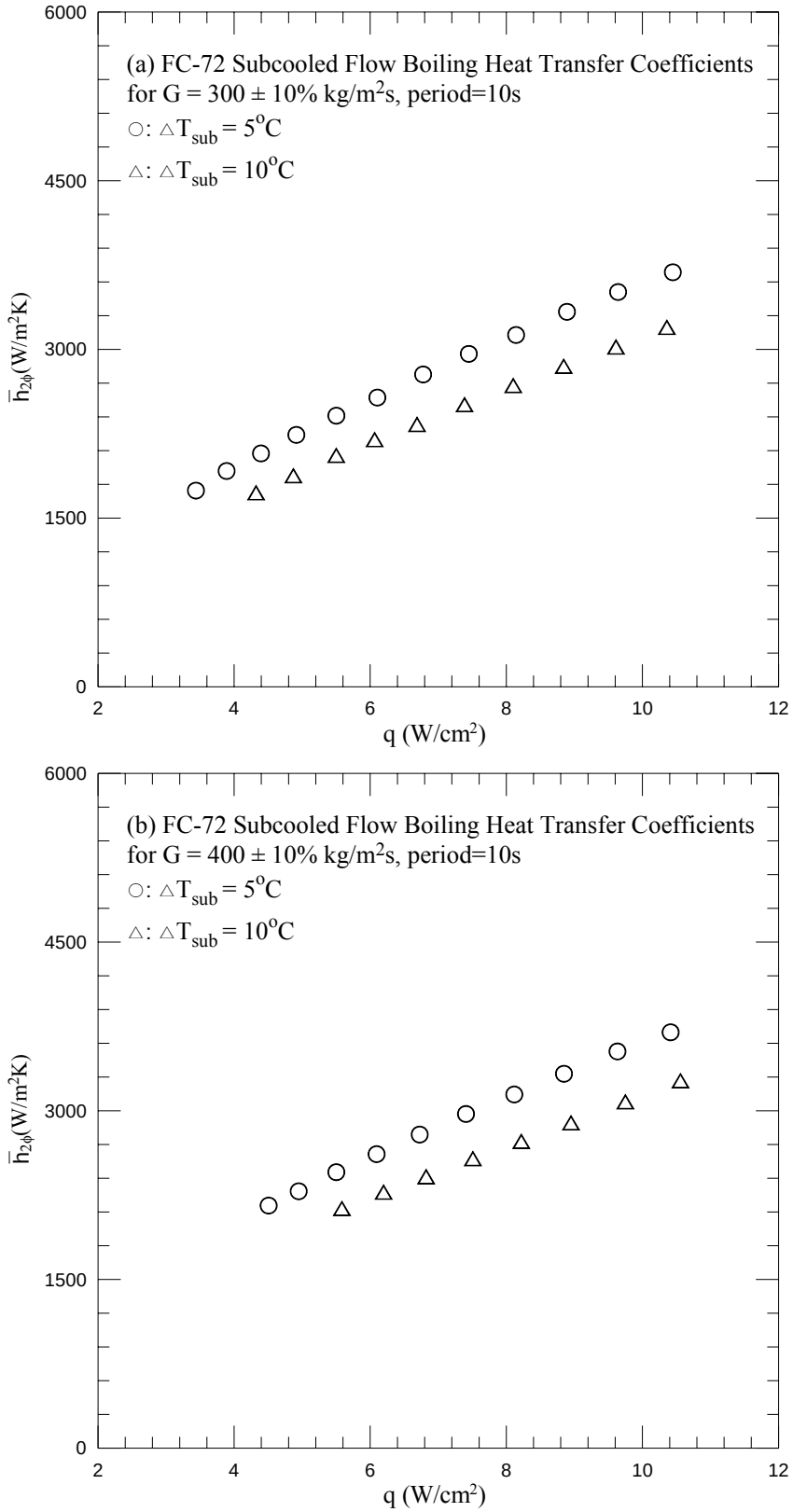

Fig. 5.20 Time-average flow boiling heat transfer coefficients for various inlet subcoolings for stable subcooled flow boiling at (a) G=300±10% kg/m^{2}s and (b) G=400±10% kg/m^{2}s at t_p=10 sec.

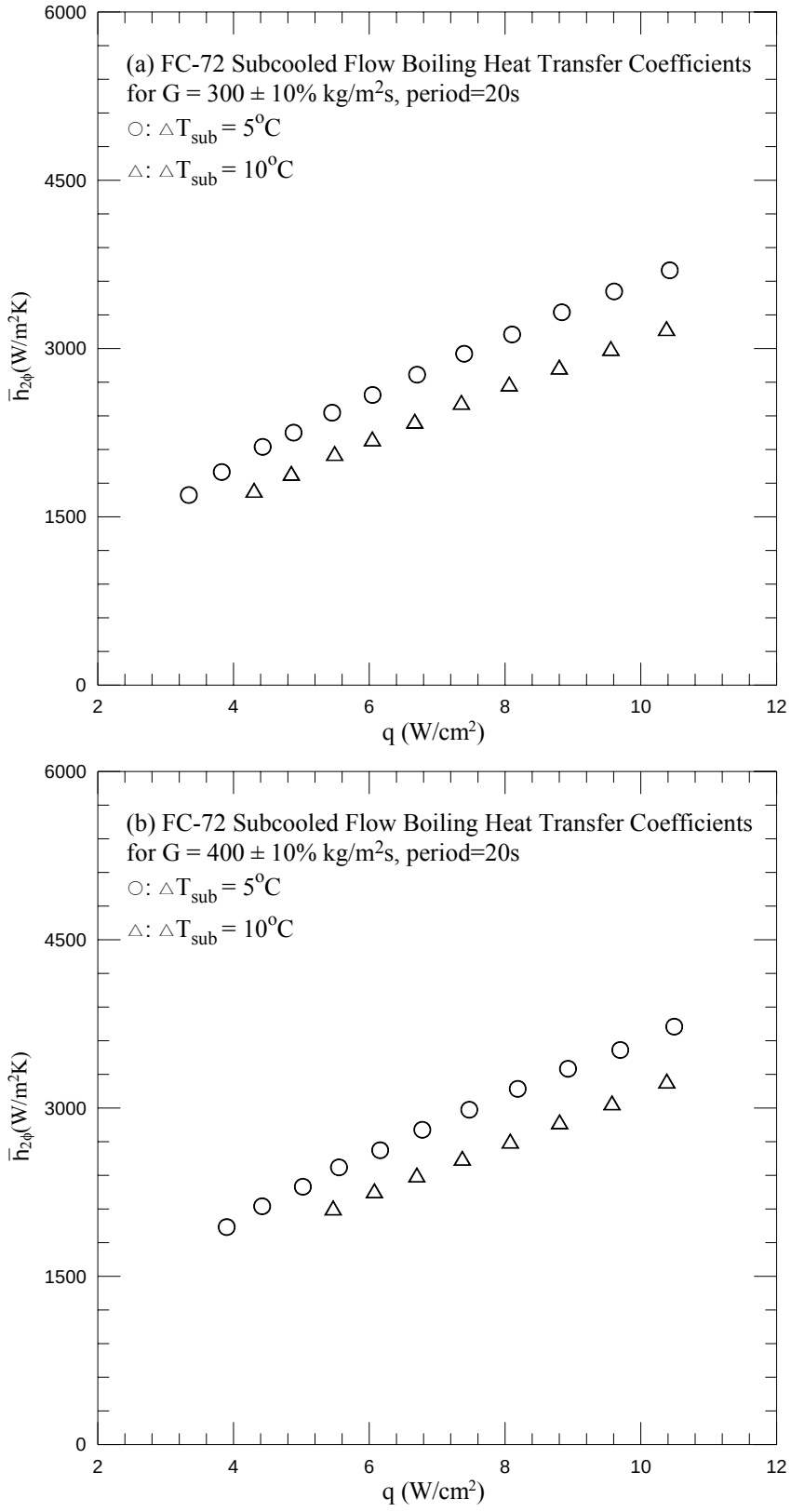

Fig. 5.21 Time-average flow boiling heat transfer coefficients for various inlet subcoolings for stable subcooled flow boiling at (a) G=300±10% kg/m^{2}s and (b) G=400±10% kg/m^{2}s at t_p=20 sec.

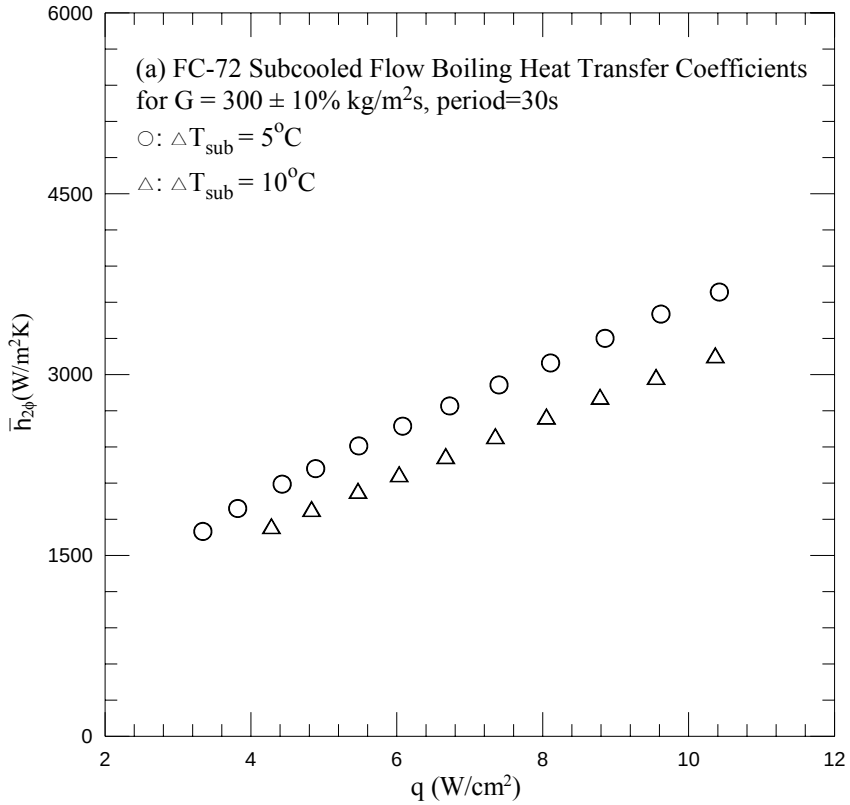

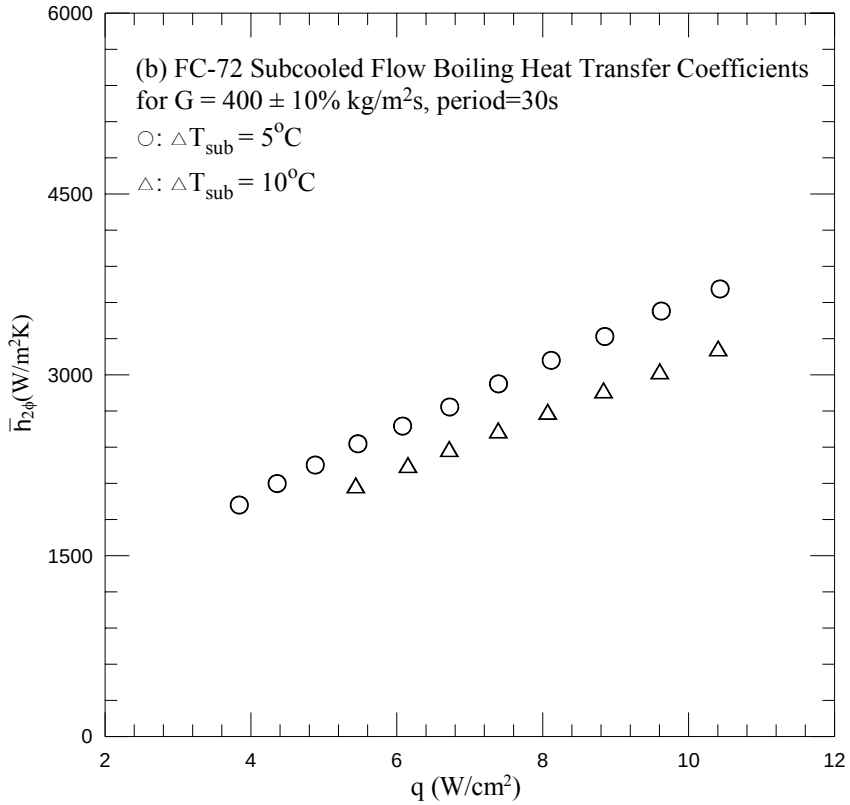

Fig. 5.22 Time-average flow boiling heat transfer coefficients for various inlet subcoolings for stable subcooled flow boiling at (a) G=300±10% kg/m^{2}s and (b) G=400±10% kg/m^{2}s at t_p=30 sec.

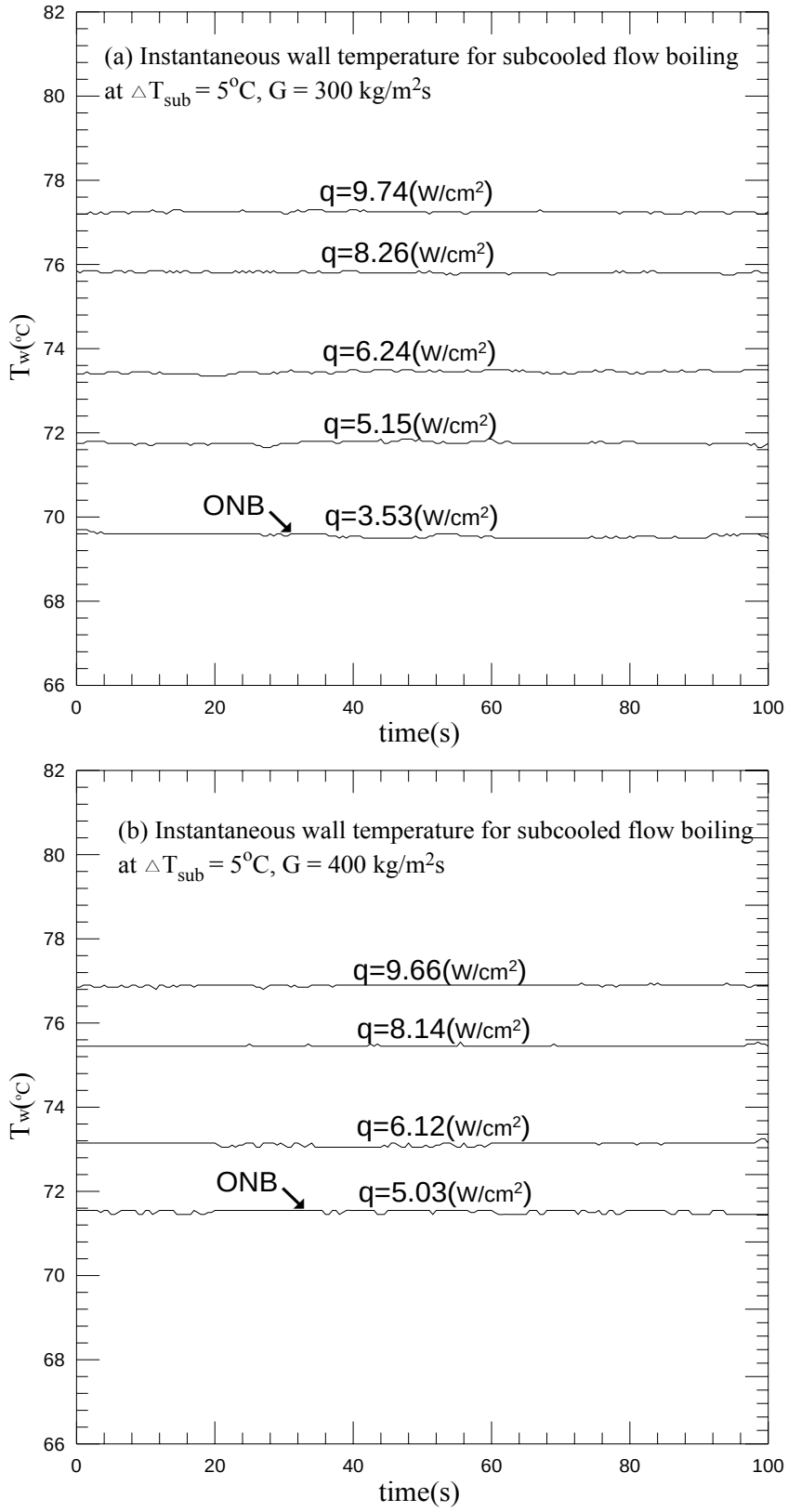

Fig. 5.23 Time variations of the copper plate temperature in stable subcooled flow boiling for various imposed heat fluxes for ΔT_{sub} =5°C at (a) G=300 kg/m^{2}s and (b) G=400 kg/m^{2}s.

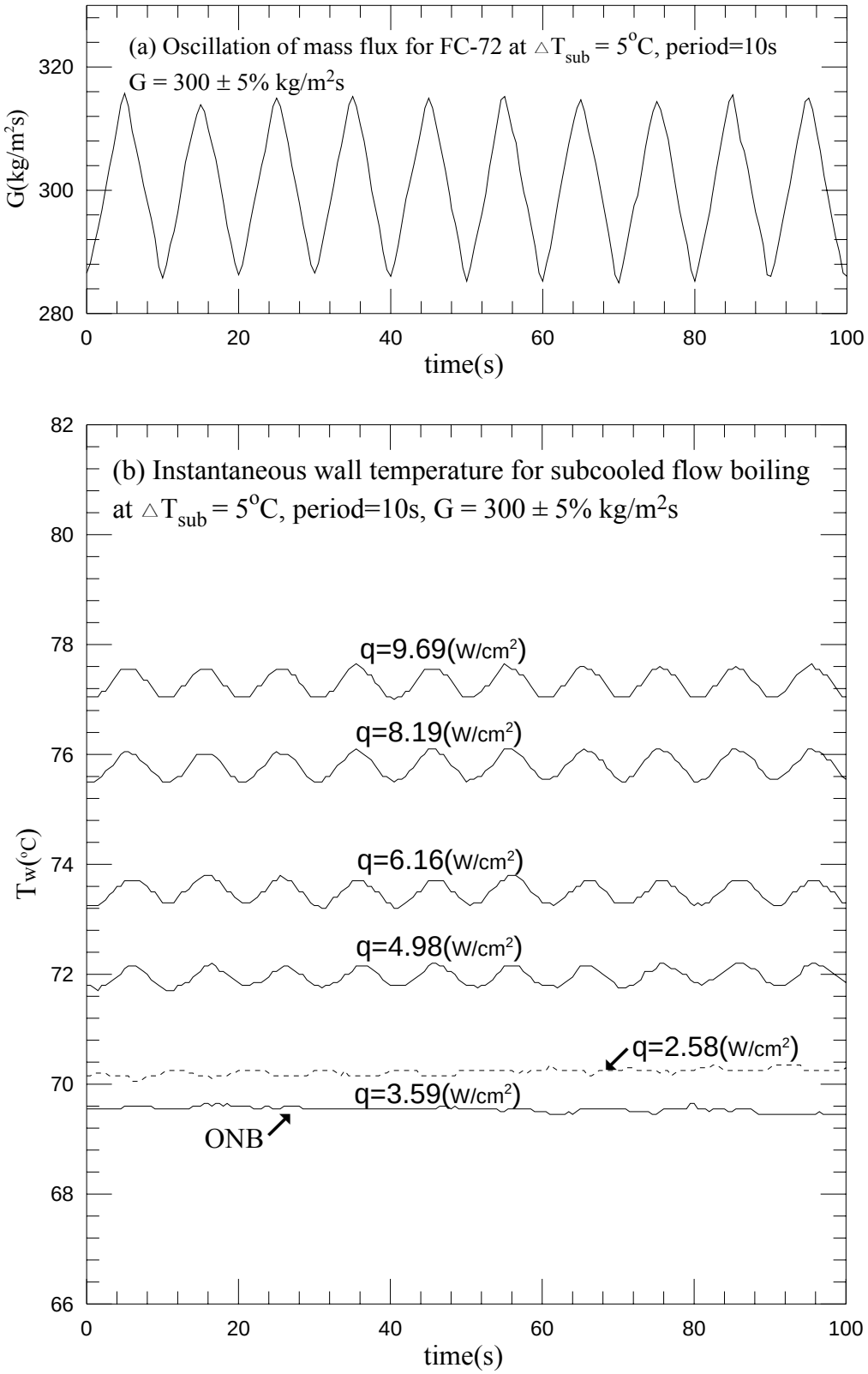

Fig. 5.24 Time variations of (a) imposed coolant mass flux and (b) copper plate temperature in transient oscillatory subcooled flow boiling for various imposed heat fluxes for G=300±5% kg/m^{2}s with t_p =10 sec.($\overline{q}_{ONB}$ =3.59 w/cm^2 at G =300 kg/m^{2}s)

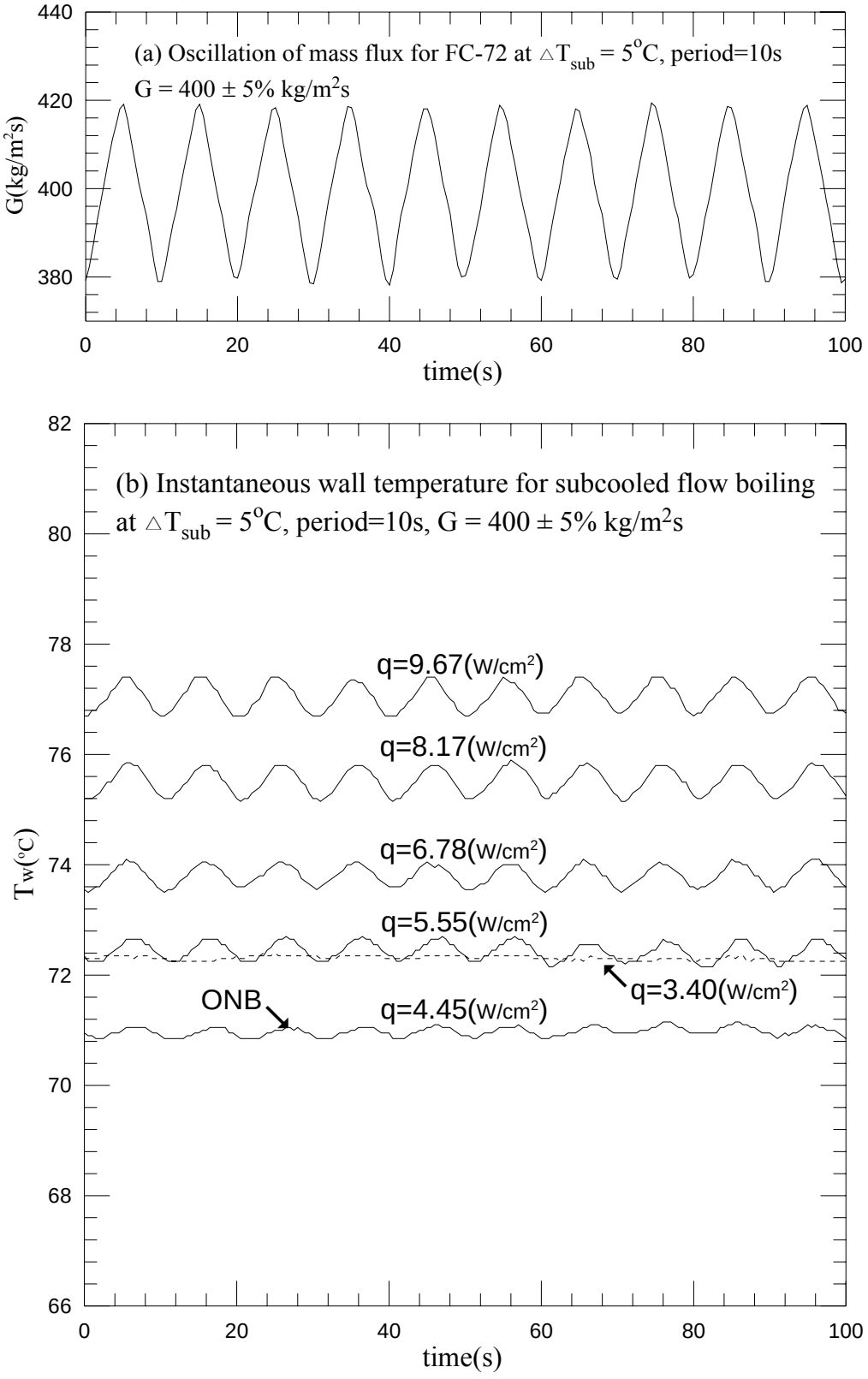

Fig. 5.25 Time variations of (a) imposed coolant mass flux and (b) copper plate temperature in transient oscillatory subcooled flow boiling for various imposed heat fluxes for G=400±5% kg/m^{2}s with t_p =10 sec.($\overline{q}_{ONB}$ =4.45 w/cm^2 at G =400 kg/m^{2}s)

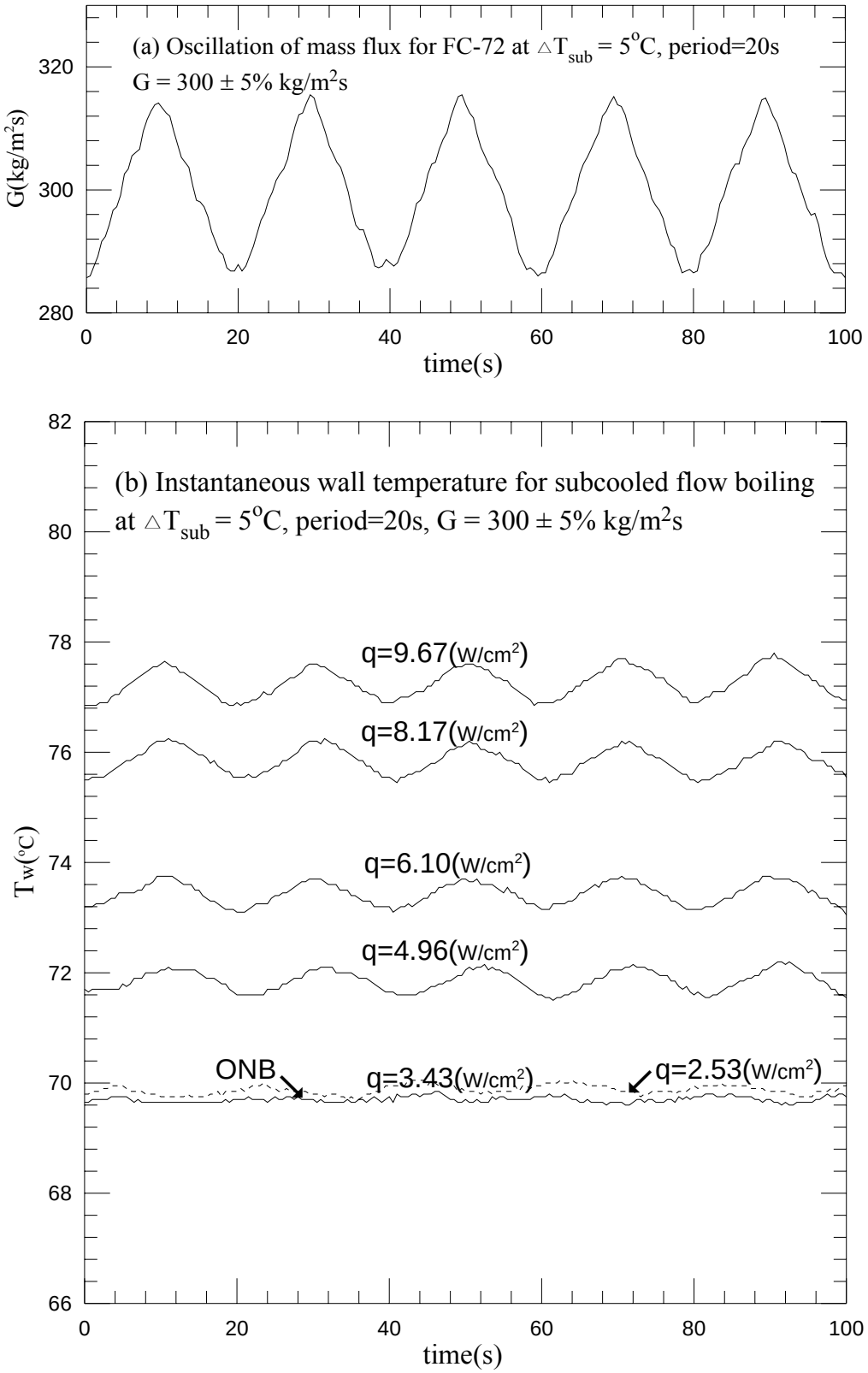

Fig. 5.26 Time variations of (a) imposed coolant mass flux and (b) copper plate temperature in transient oscillatory subcooled flow boiling for various imposed heat fluxes for G=300±5% kg/m^{2}s with t_p =20 sec.($\overline{q}_{ONB}$ =3.43 w/cm^2 at G =300 kg/m^{2}s)

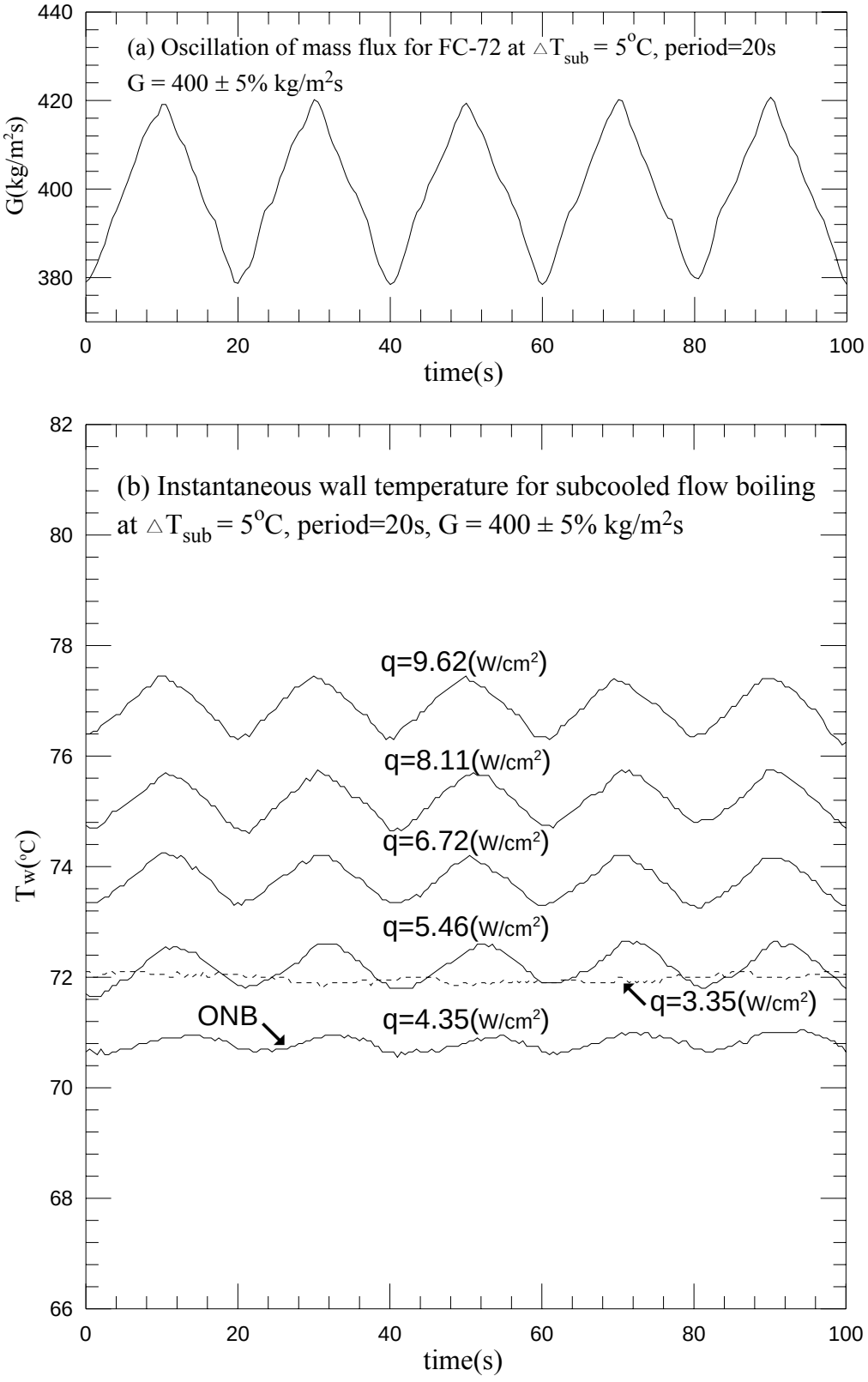

Fig. 5.27 Time variations of (a) imposed coolant mass flux and (b) copper plate temperature in transient oscillatory subcooled flow boiling for various imposed heat fluxes for G=400±5% kg/m^{2}s with t_p =20 sec.($\overline{q}_{ONB}$ =4.35 w/cm^2 at G =400 kg/m^{2}s)

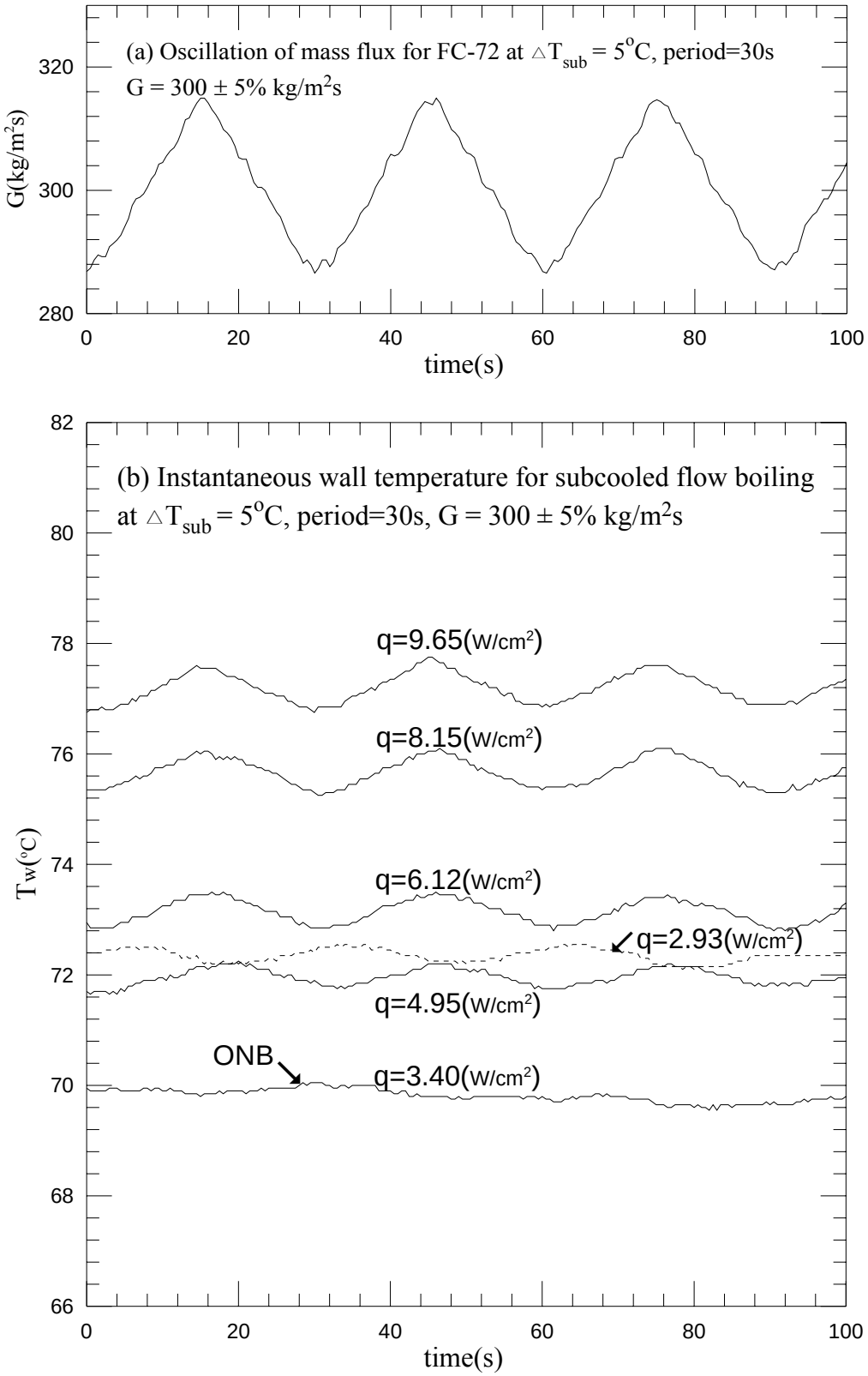

Fig. 5.28 Time variations of (a) imposed coolant mass flux and (b) copper plate temperature in transient oscillatory subcooled flow boiling for various imposed heat fluxes for G=300±5% kg/m^{2}s with t_p =30 sec.($\overline{q}_{ONB}$ =3.40 w/cm^2 at G =300 kg/m^{2}s)

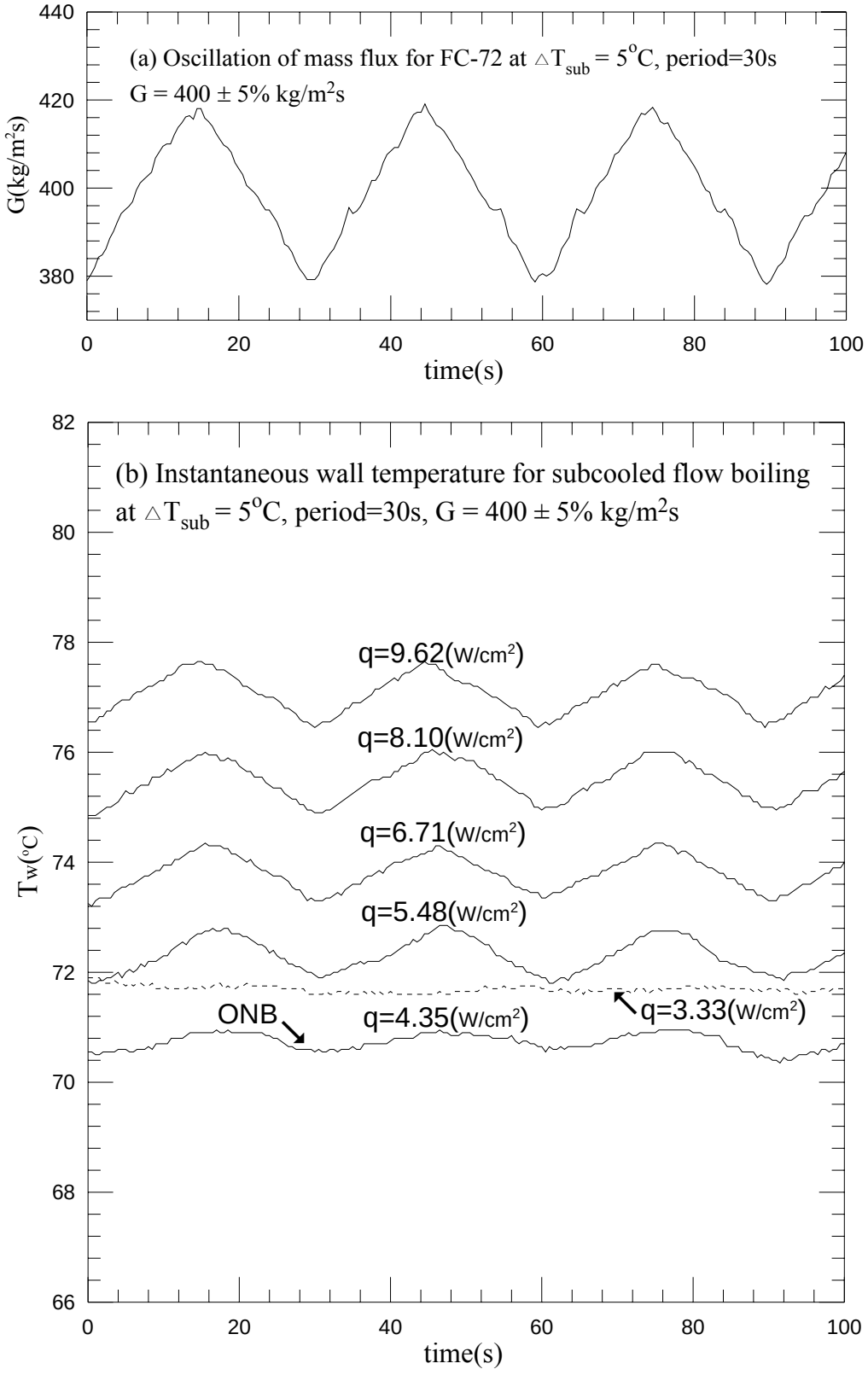

Fig. 5.29 Time variations of (a) imposed coolant mass flux and (b) copper plate temperature in transient oscillatory subcooled flow boiling for various imposed heat fluxes for G=400±5% kg/m^{2}s with t_p =30 sec.($\overline{q}_{ONB}$ =4.35 w/cm^2 at G =400 kg/m^{2}s)

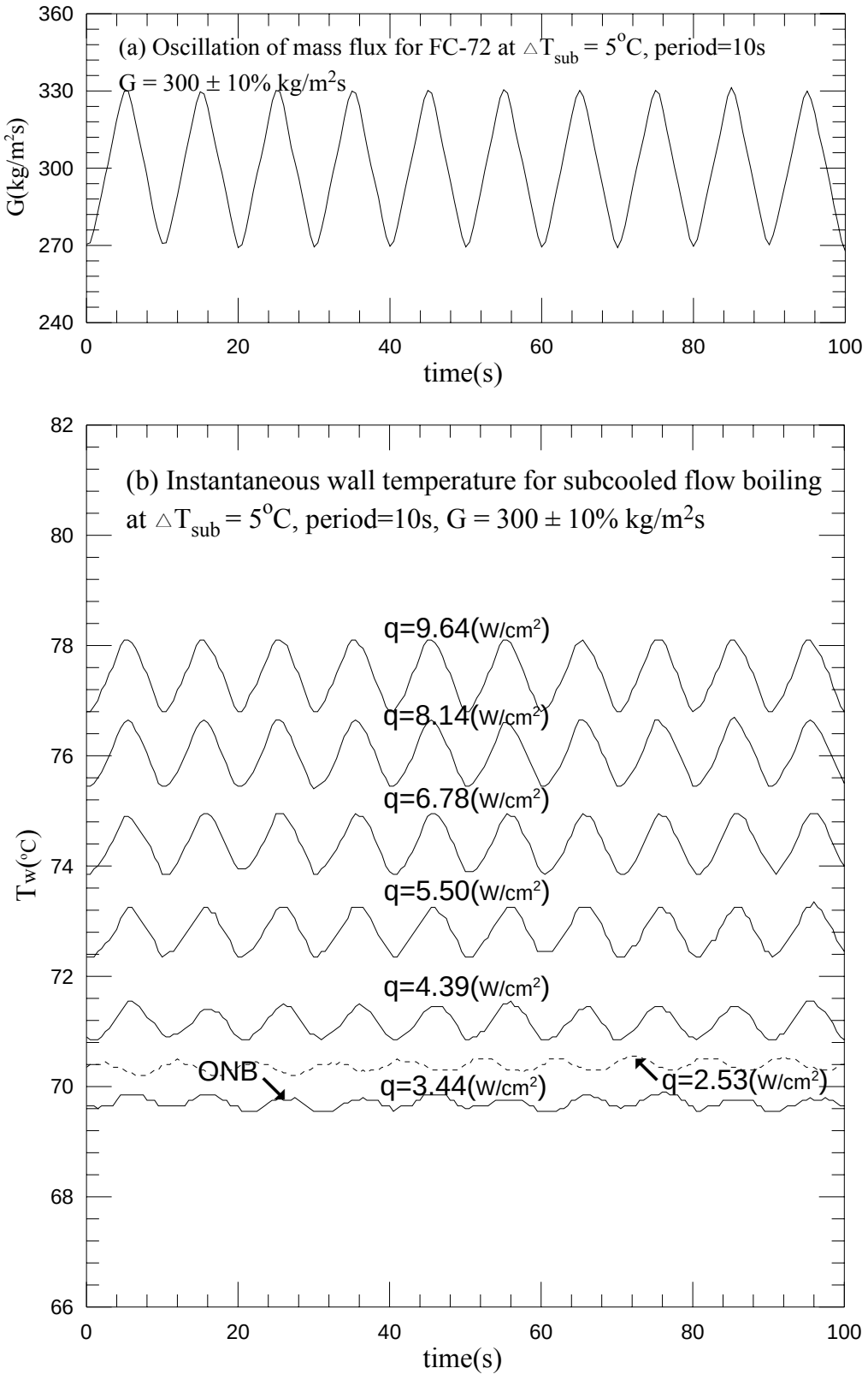

Fig. 5.30 Time variations of (a) imposed coolant mass flux and (b) copper plate temperature in transient oscillatory subcooled flow boiling for various imposed heat fluxes for G=300±10% kg/m^{2}s with t_p =10 sec.($\bar{q}_{ONB}$ =3.44 w/cm^2 at G =300 kg/m^{2}s)

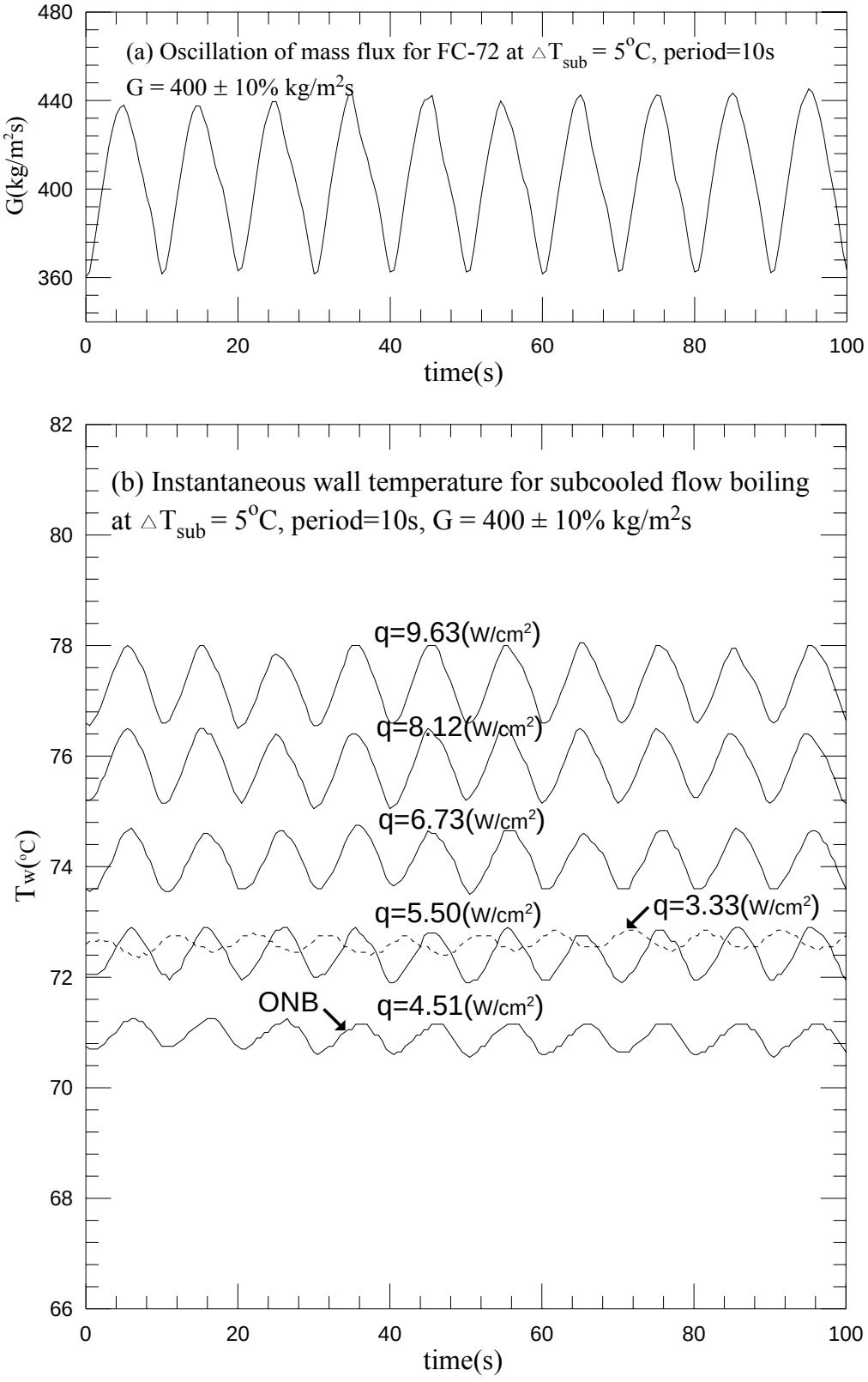

Fig. 5.31 Time variations of (a) imposed coolant mass flux and (b) copper plate temperature in transient oscillatory subcooled flow boiling for various imposed heat fluxes for G=400±10% kg/m^{2}s with t_p=10 sec.($\bar{q}_{ONB}$ =4.51 w/cm^2 at G =400 kg/m^{2}s)

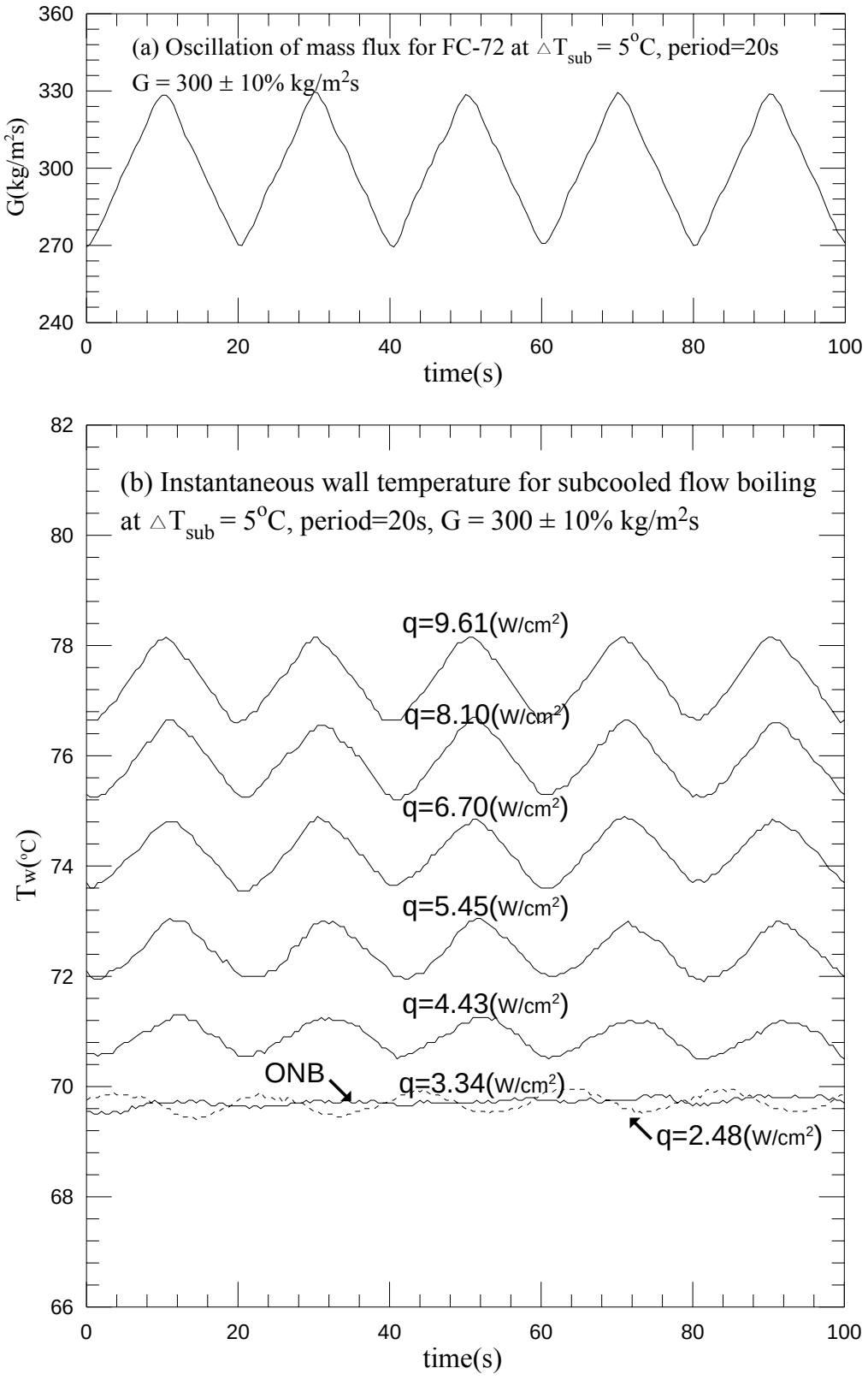

Fig. 5.32 Time variations of (a) imposed coolant mass flux and (b) copper plate temperature in transient oscillatory subcooled flow boiling for various imposed heat fluxes for G=300±10% kg/m^{2}s with t_p =20 sec.($\bar{q}_{ONB}$ =3.34 w/cm^2 at G =300 kg/m^{2}s)

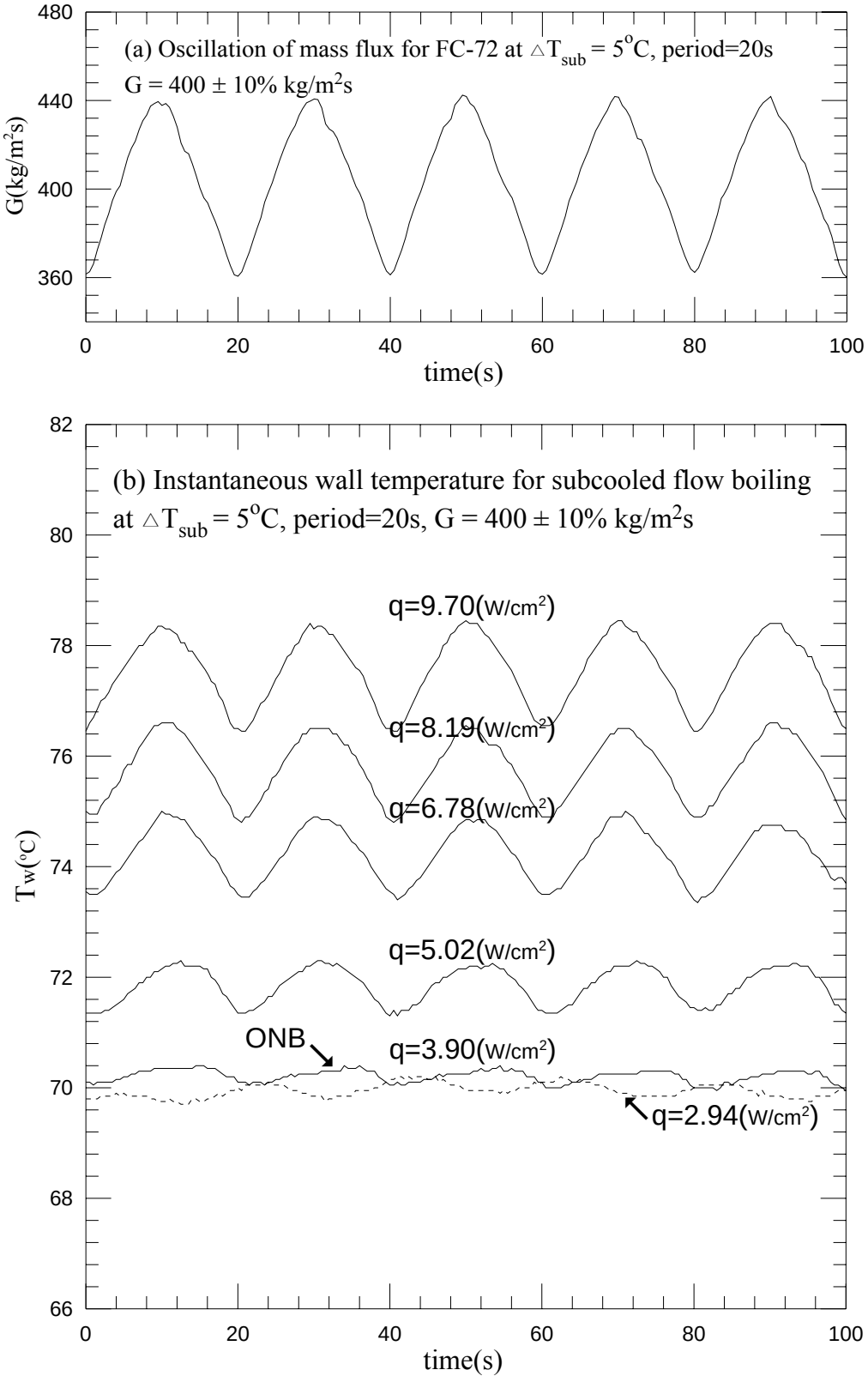

Fig. 5.33 Time variations of (a) imposed coolant mass flux and (b) copper plate temperature in transient oscillatory subcooled flow boiling for various imposed heat fluxes for G=400±10% kg/m^{2}s with t_p =20 sec.($\bar{q}_{ONB}$ =3.90 w/cm^2 at G =400 kg/m^{2}s)

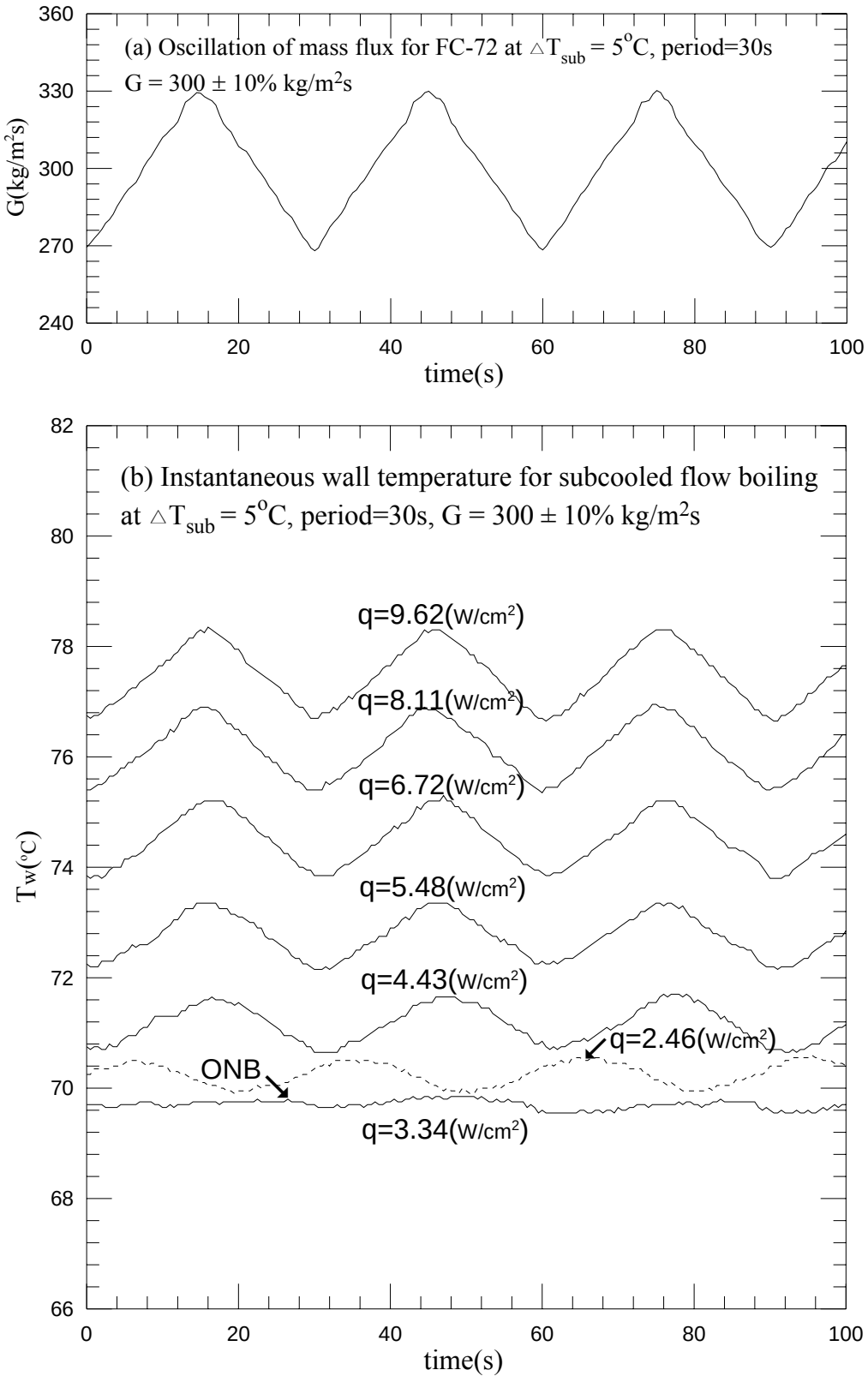

Fig. 5.34 Time variations of (a) imposed coolant mass flux and (b) copper plate temperature in transient oscillatory subcooled flow boiling for various imposed heat fluxes for G=300±10% kg/m^{2}s with t_p =30 sec.($\overline{q}_{ONB}$ =3.34 w/cm^2 at G =300 kg/m^{2}s)

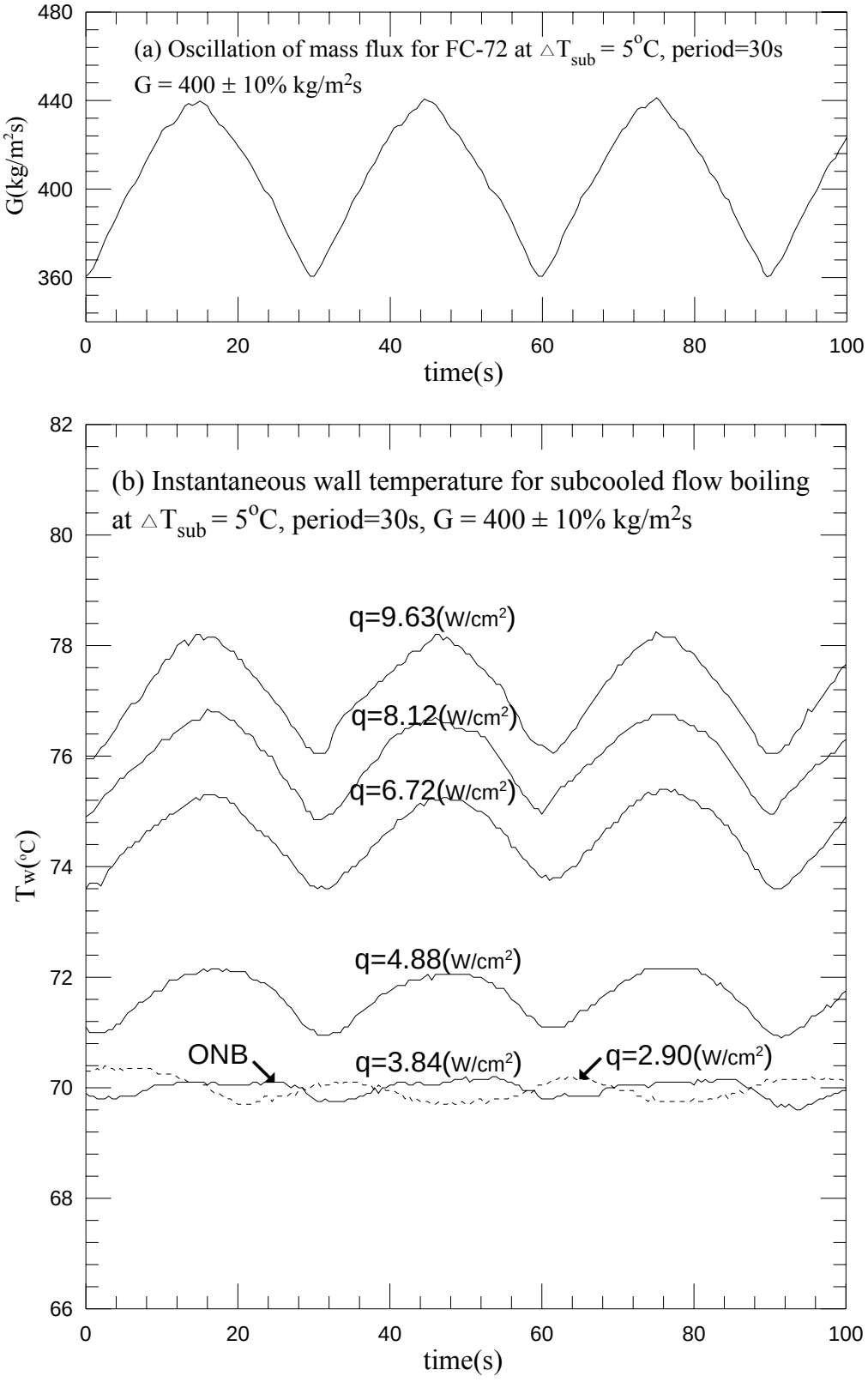

Fig. 5.35 Time variations of (a) imposed coolant mass flux and (b) copper plate temperature in transient oscillatory subcooled flow boiling for various imposed heat fluxes for G=400±10% kg/m^{2}s with t_p =30 sec.($\bar{q}_{ONB}$ =3.84 w/cm^2 at G =400 kg/m^{2}s)

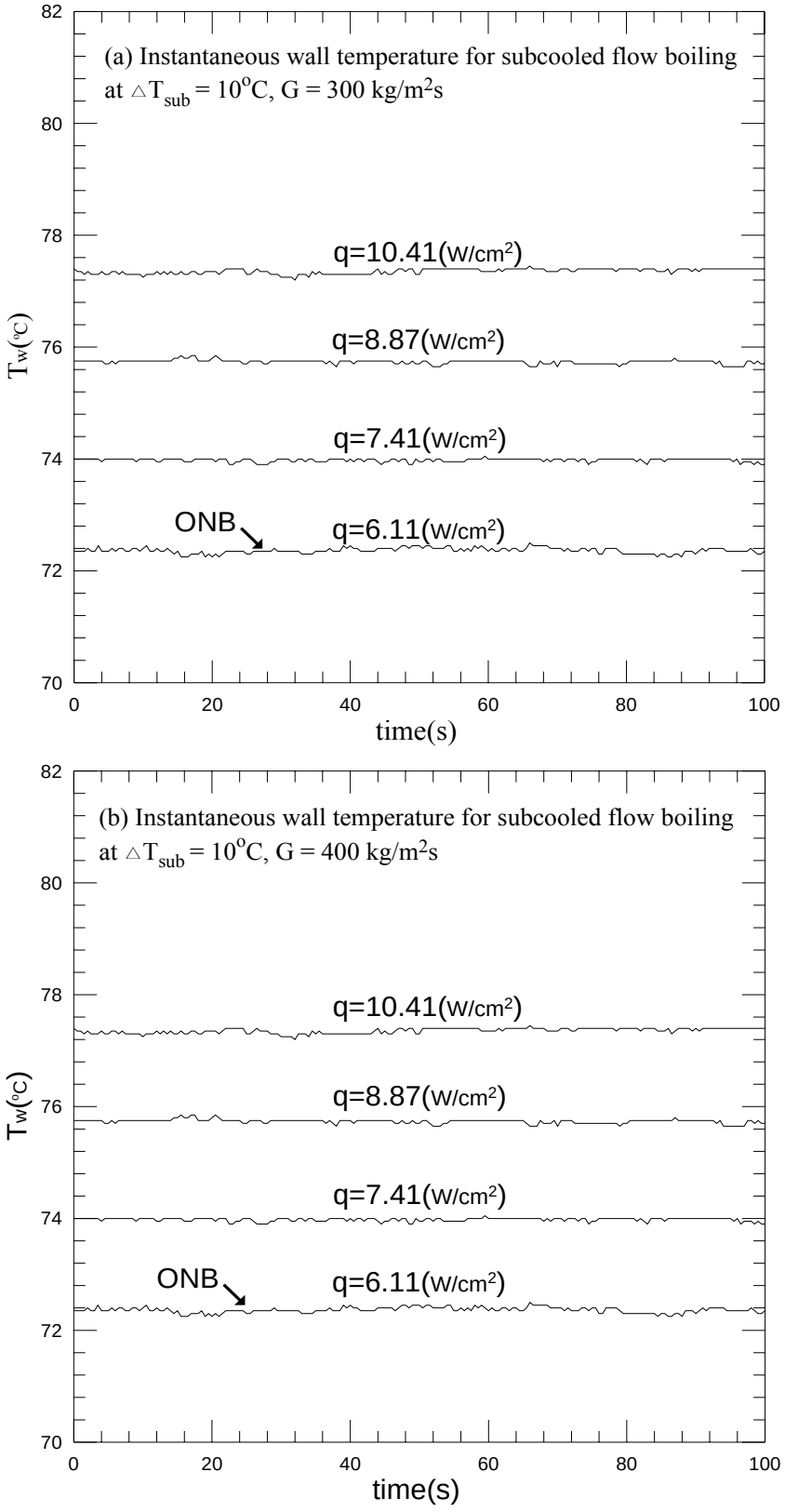

Fig. 5.36 Time variations of the copper plate temperature in stable subcooled flow boiling for various imposed heat fluxes for $\triangle T_{in}$=10°C at (a) G=300 kg/m^{2}s and (b) G=400 kg/m^{2}s.

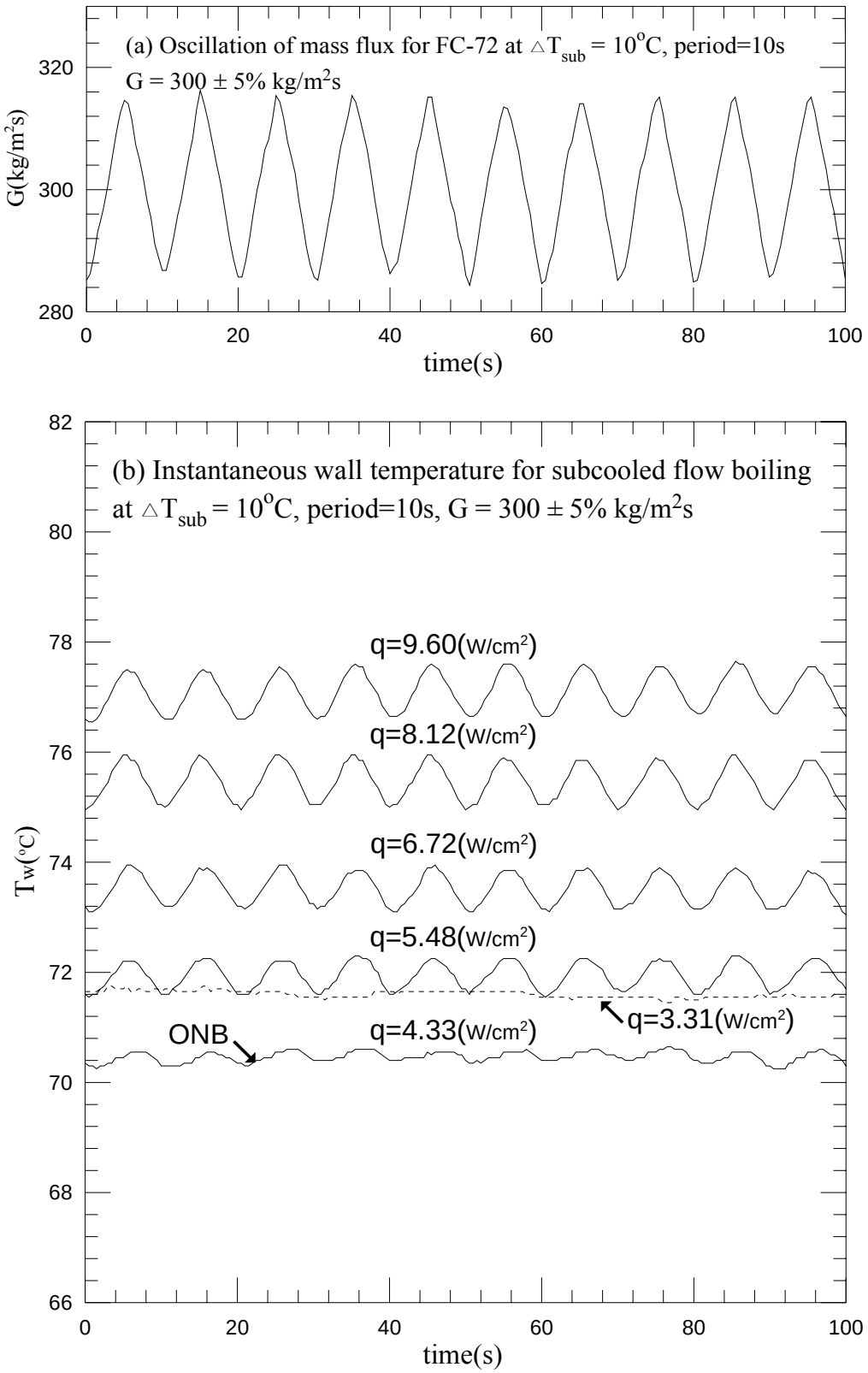

Fig. 5.37 Time variations of (a) imposed coolant mass flux and (b) copper plate temperature in transient oscillatory subcooled flow boiling for various imposed heat fluxes for G=300±5% kg/m^{2}s with t_p=10 sec.($\overline{q}_{ONB}$ =4.33 w/cm^2 at G =300 kg/m^{2}s)

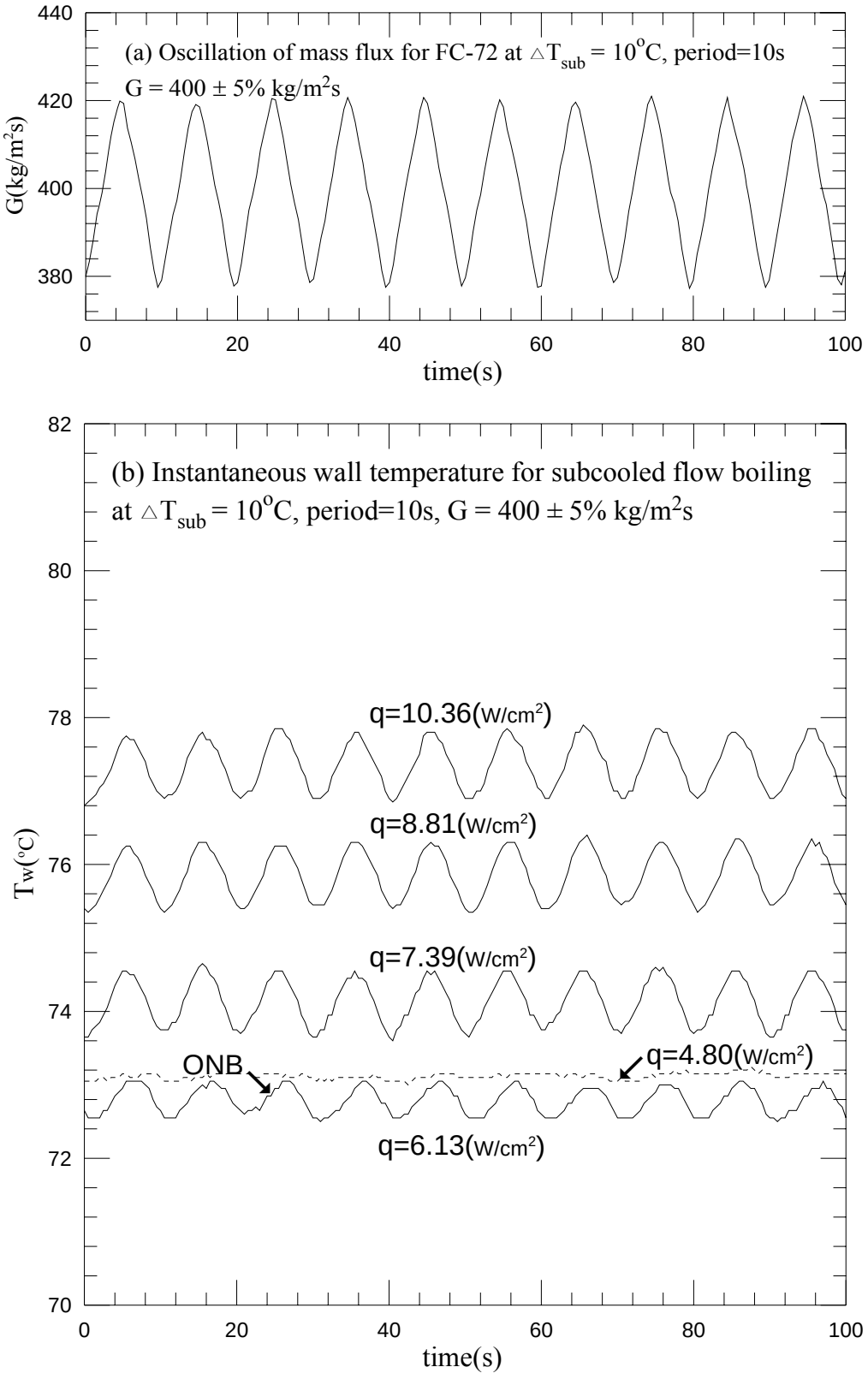

Fig. 5.38 Time variations of (a) imposed coolant mass flux and (b) copper plate temperature in transient oscillatory subcooled flow boiling for various imposed heat fluxes for G=400±5% kg/m^{2}s with t_p=10 sec.($\overline{q}_{ONB}$ =6.13 w/cm^2 at G =400 kg/m^{2}s)

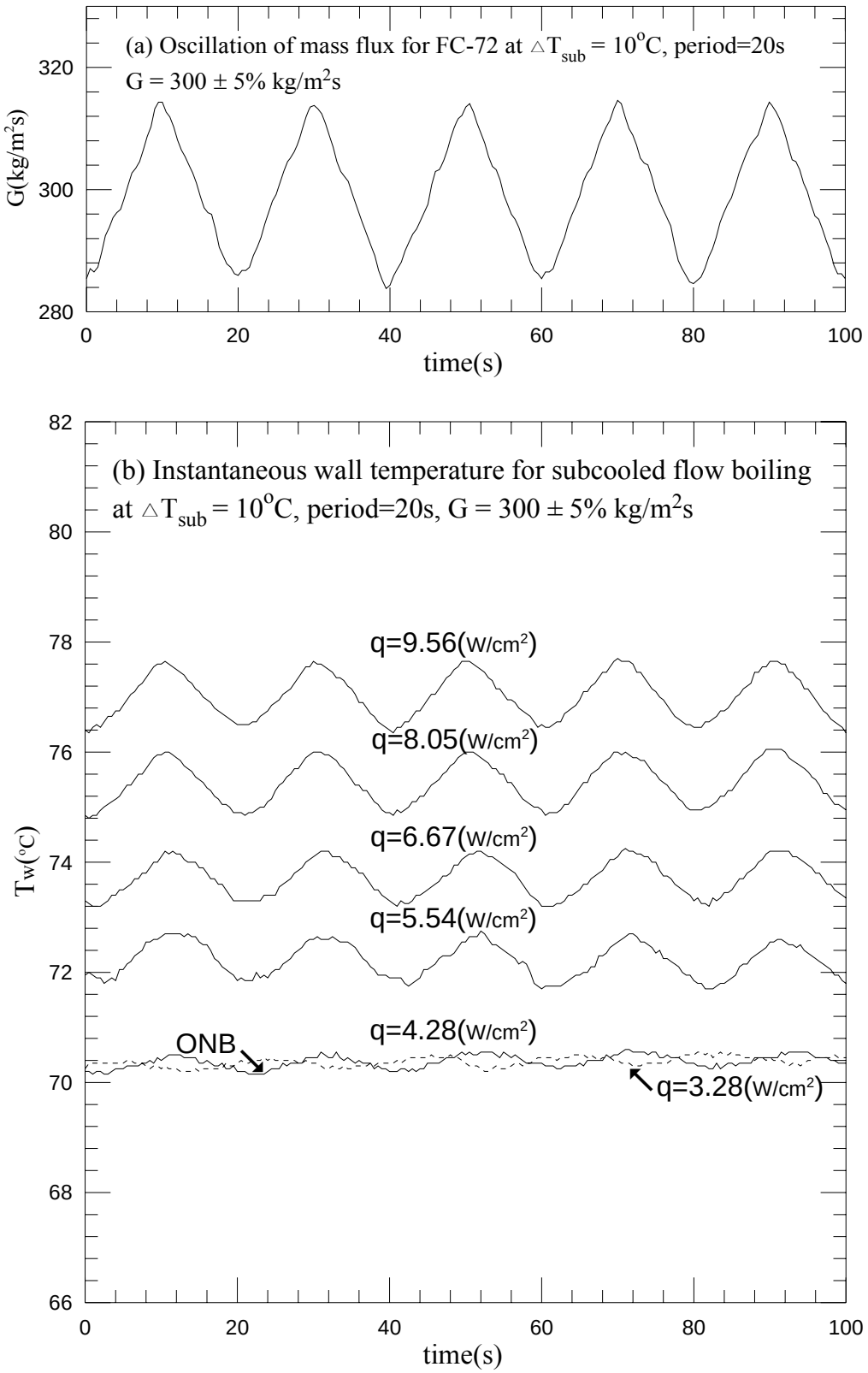

Fig. 5.39 Time variations of (a) imposed coolant mass flux and (b) copper plate temperature in transient oscillatory subcooled flow boiling for various imposed heat fluxes for G=300±5% kg/m^{2}s with t_p =20 sec.($\overline{q}_{ONB}$ =4.28 w/cm^2 at G =300 kg/m^{2}s)

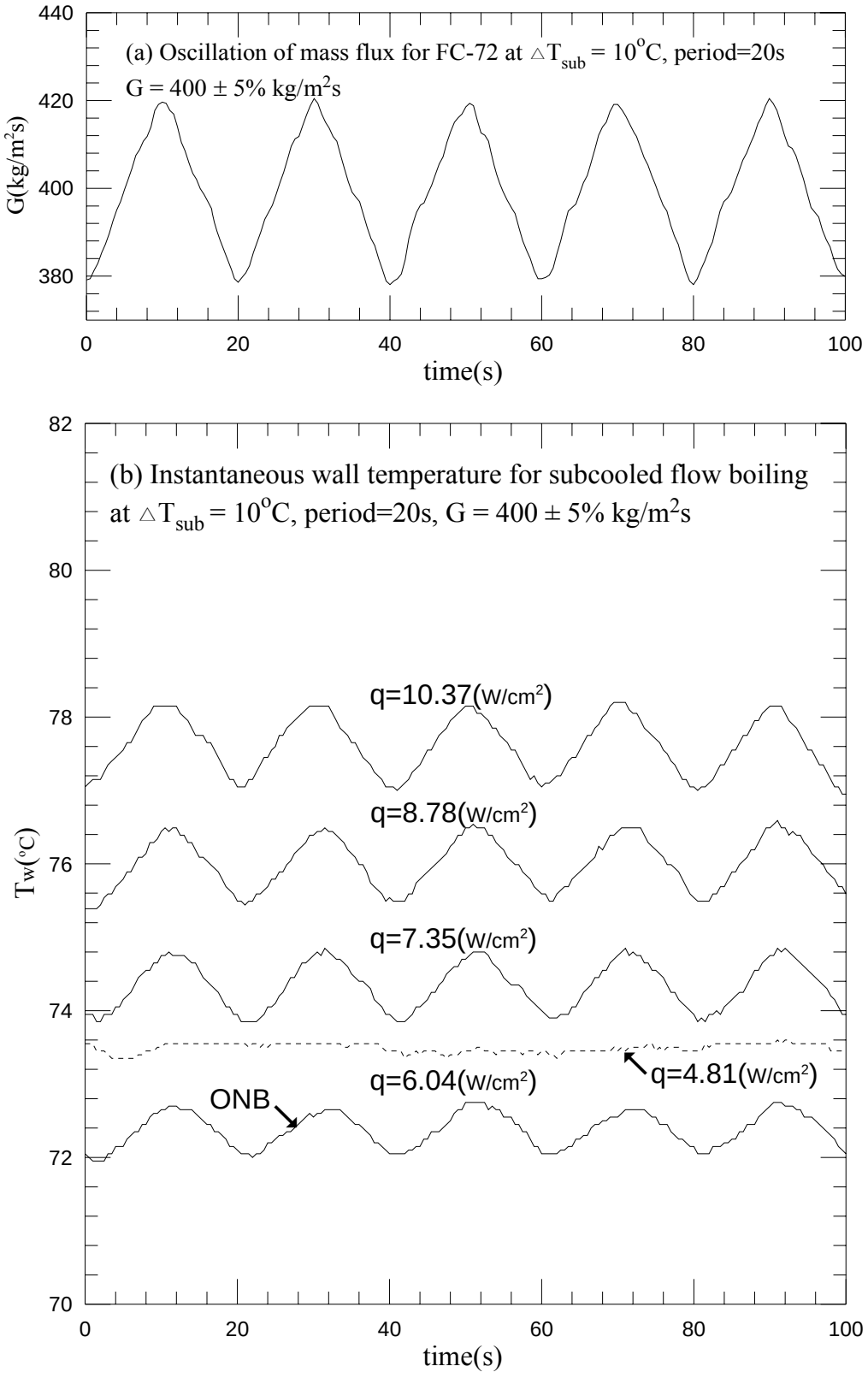

Fig. 5.40 Time variations of (a) imposed coolant mass flux and (b) copper plate temperature in transient oscillatory subcooled flow boiling for various imposed heat fluxes for G=400±5% kg/m^{2}s with t_p =20 sec.($\overline{q}_{ONB}$ =6.04 w/cm^2 at G =400 kg/m^{2}s)

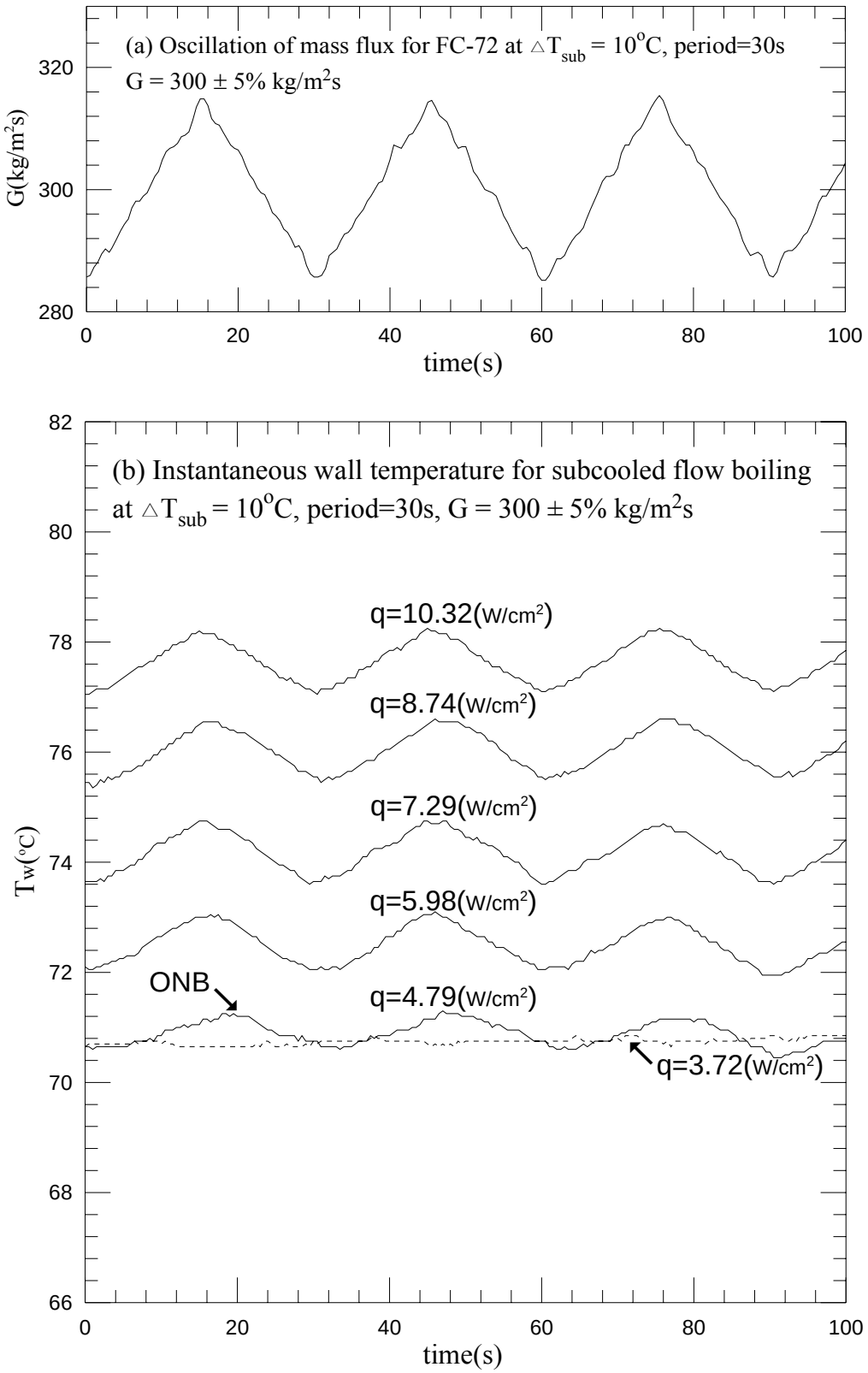

Fig. 5.41 Time variations of (a) imposed coolant mass flux and (b) copper plate temperature in transient oscillatory subcooled flow boiling for various imposed heat fluxes for G=300±5% kg/m^{2}s with t_p =30 sec.($\overline{q}_{ONB}$ =4.79 w/cm^2 at G =300 kg/m^{2}s)

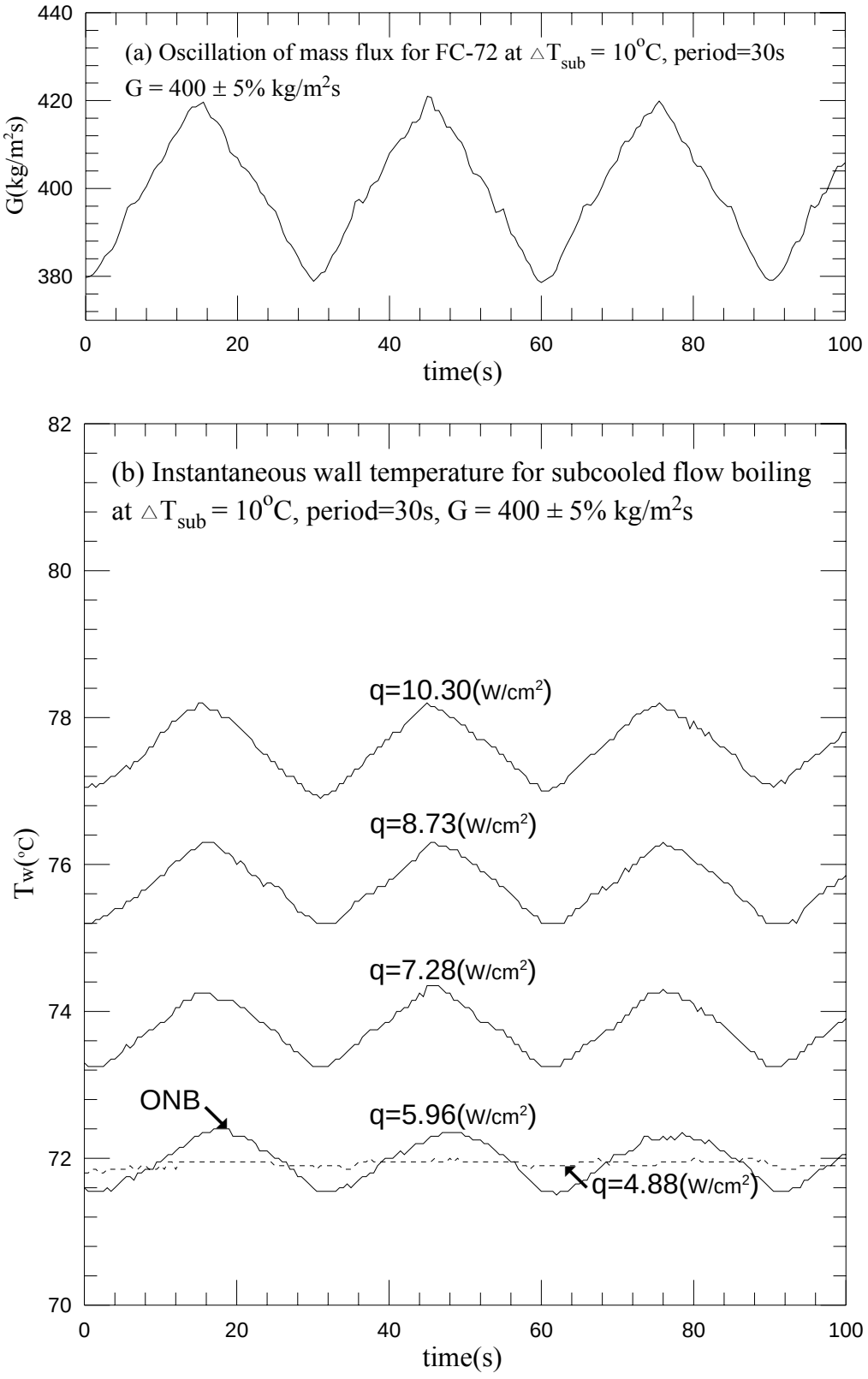

Fig. 5.42 Time variations of (a) imposed coolant mass flux and (b) copper plate temperature in transient oscillatory subcooled flow boiling for various imposed heat fluxes for G=400±5% kg/m^{2}s with t_p =30 sec.($\overline{q}_{ONB}$ =5.96 w/cm^2 at G =400 kg/m^{2}s)

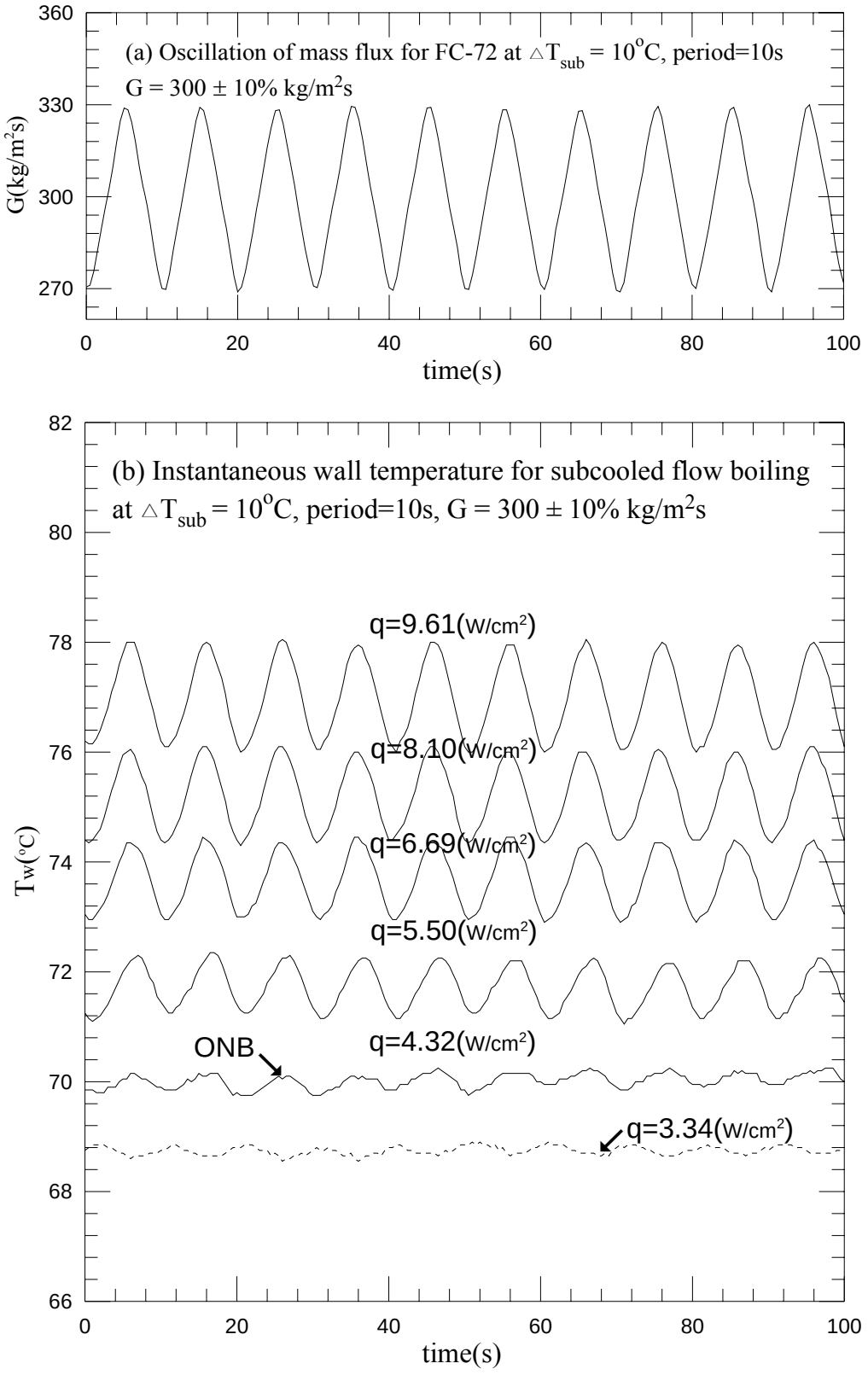

Fig. 5.43 Time variations of (a) imposed coolant mass flux and (b) copper plate temperature in transient oscillatory subcooled flow boiling for various imposed heat fluxes for G=300±10% kg/m^{2}s with t_p=10 sec.($\bar{q}_{ONB}$ =4.32 w/cm^2 at G =300 kg/m^{2}s)

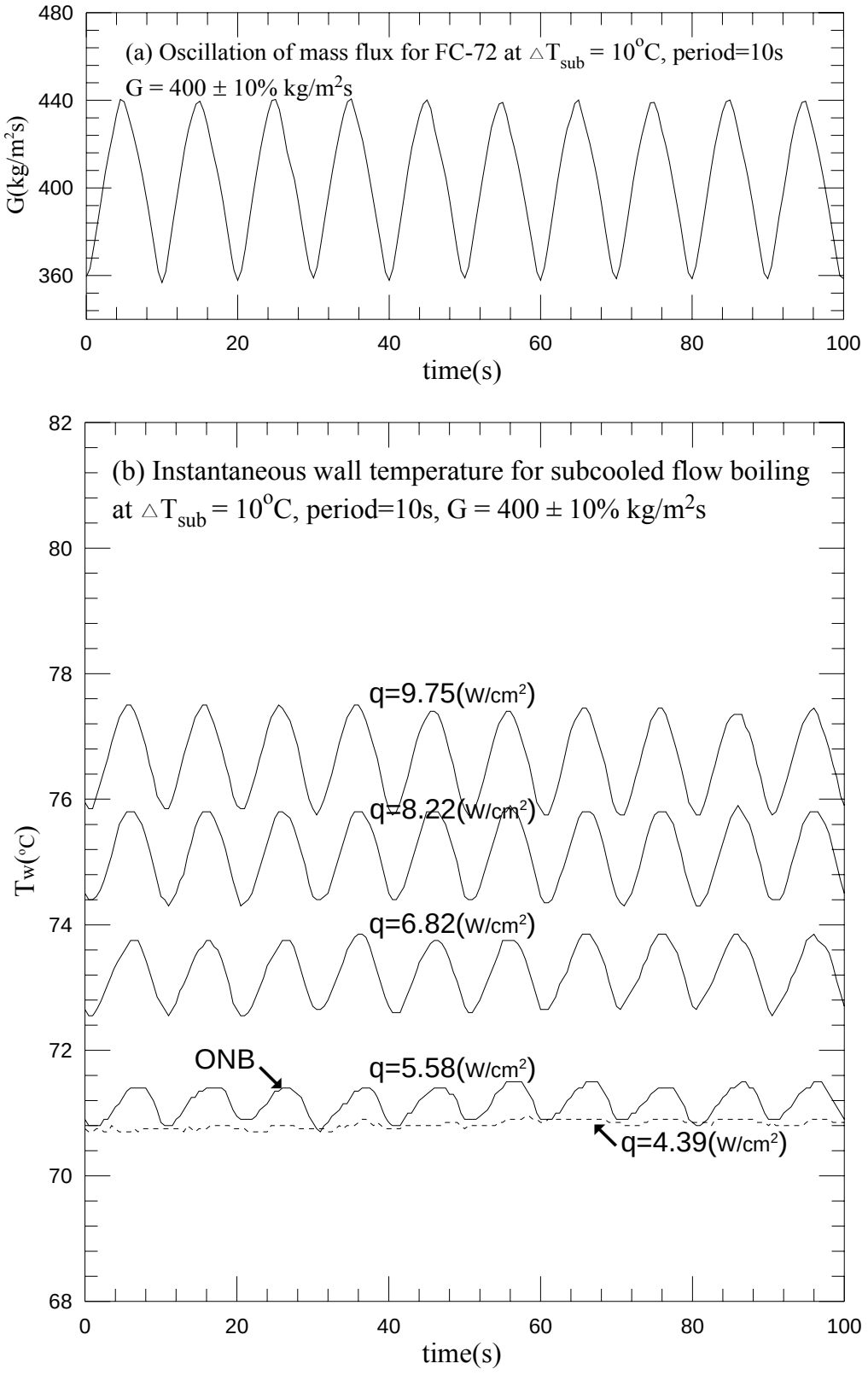

Fig. 5.44 Time variations of (a) imposed coolant mass flux and (b) copper plate temperature in transient oscillatory subcooled flow boiling for various imposed heat fluxes for G=400±10% kg/m^{2}s with t_p=10 sec.($\bar{q}_{ONB}$ =5.58 w/cm^2 at G =400 kg/m^{2}s)

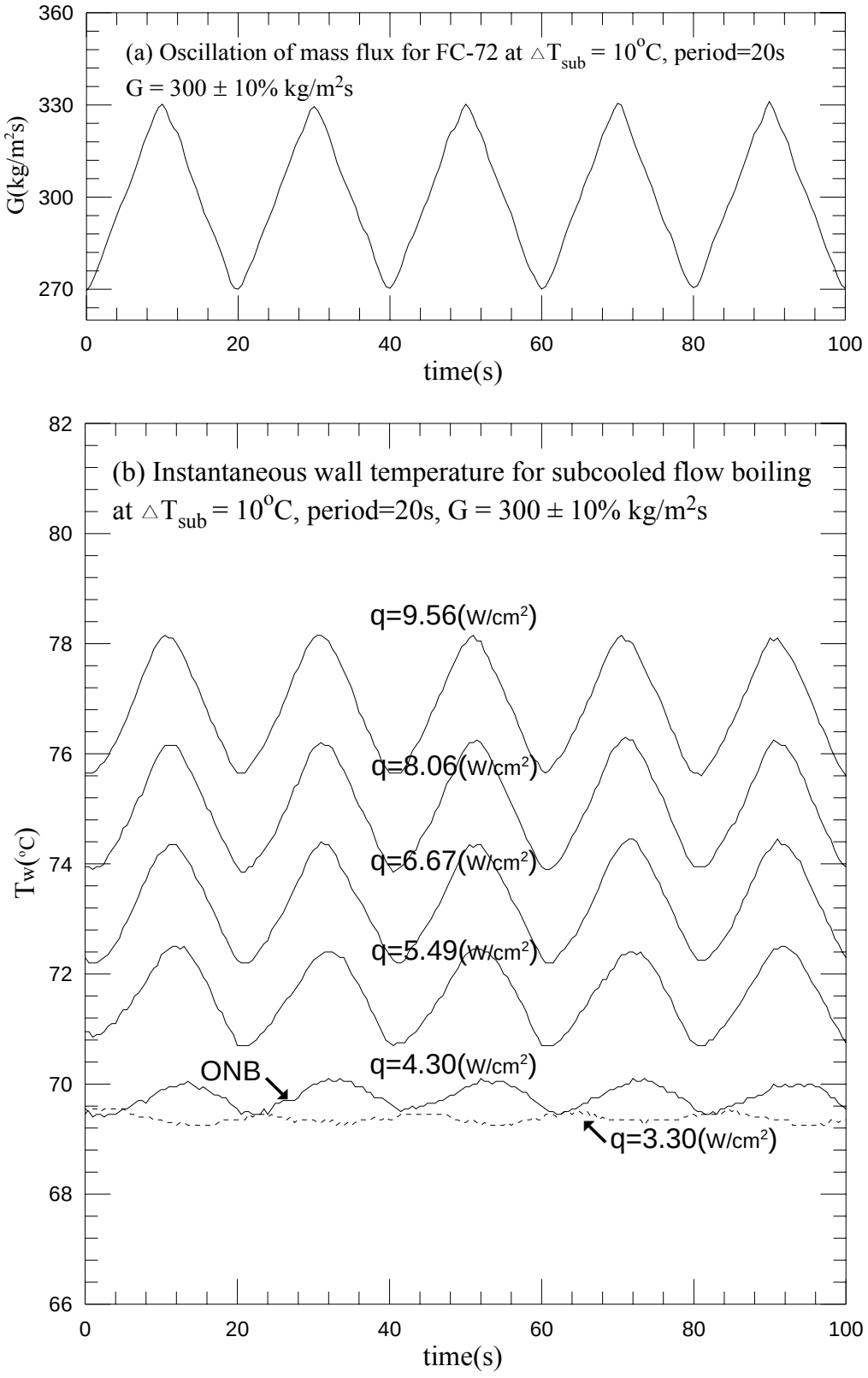

Fig. 5.45 Time variations of (a) imposed coolant mass flux and (b) copper plate temperature in transient oscillatory subcooled flow boiling for various imposed heat fluxes for G=300±10% kg/m^{2}s with t_p =20 sec.($\overline{q}_{ONB}$ =4.30 w/cm^2 at G =300 kg/m^{2}s)

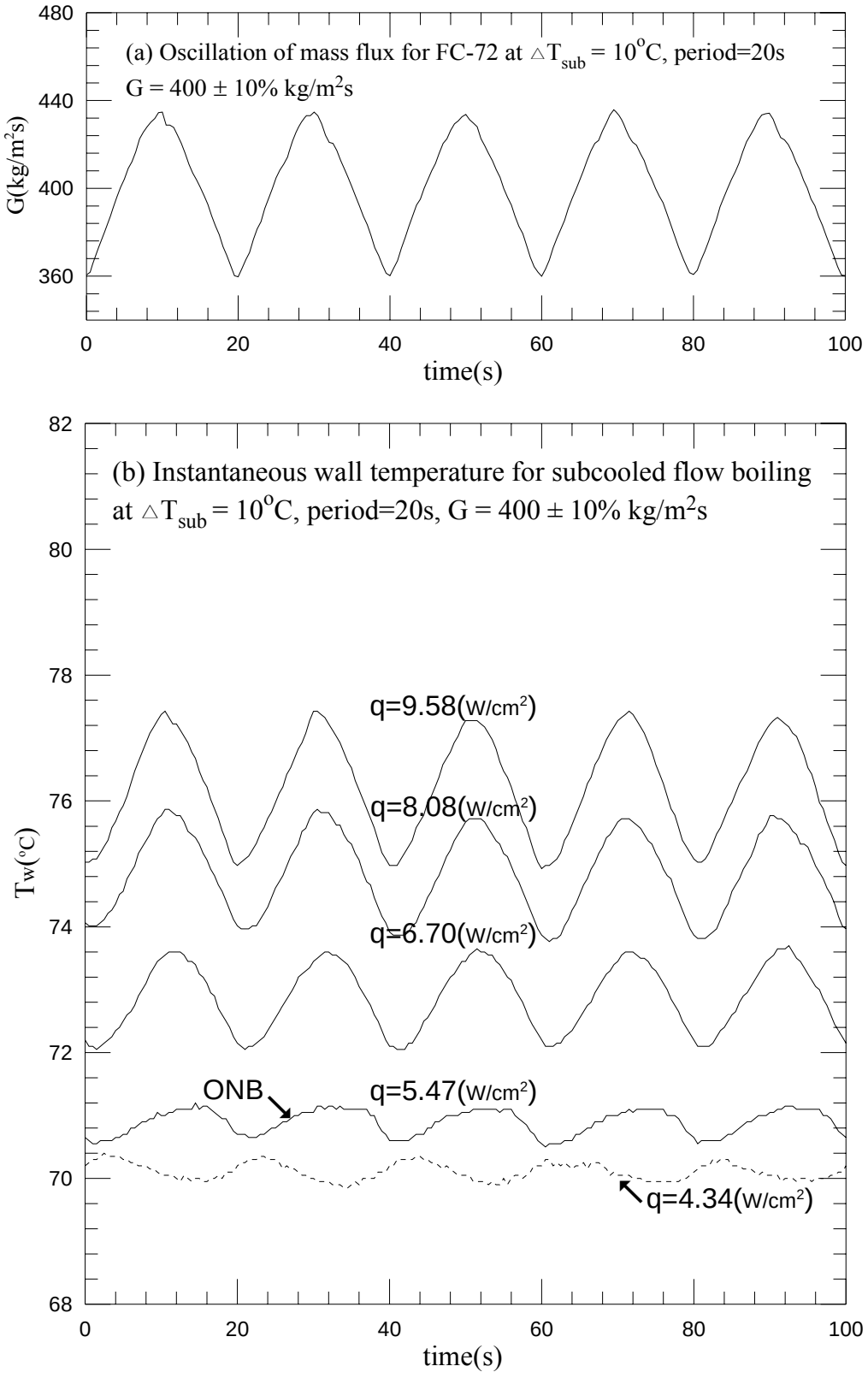

Fig. 5.46 Time variations of (a) imposed coolant mass flux and (b) copper plate temperature in transient oscillatory subcooled flow boiling for various imposed heat fluxes for G=400±10% kg/m^{2}s with t_p =20 sec.($\bar{q}_{ONB}$ =5.47 w/cm^2 at G =400 kg/m^{2}s)

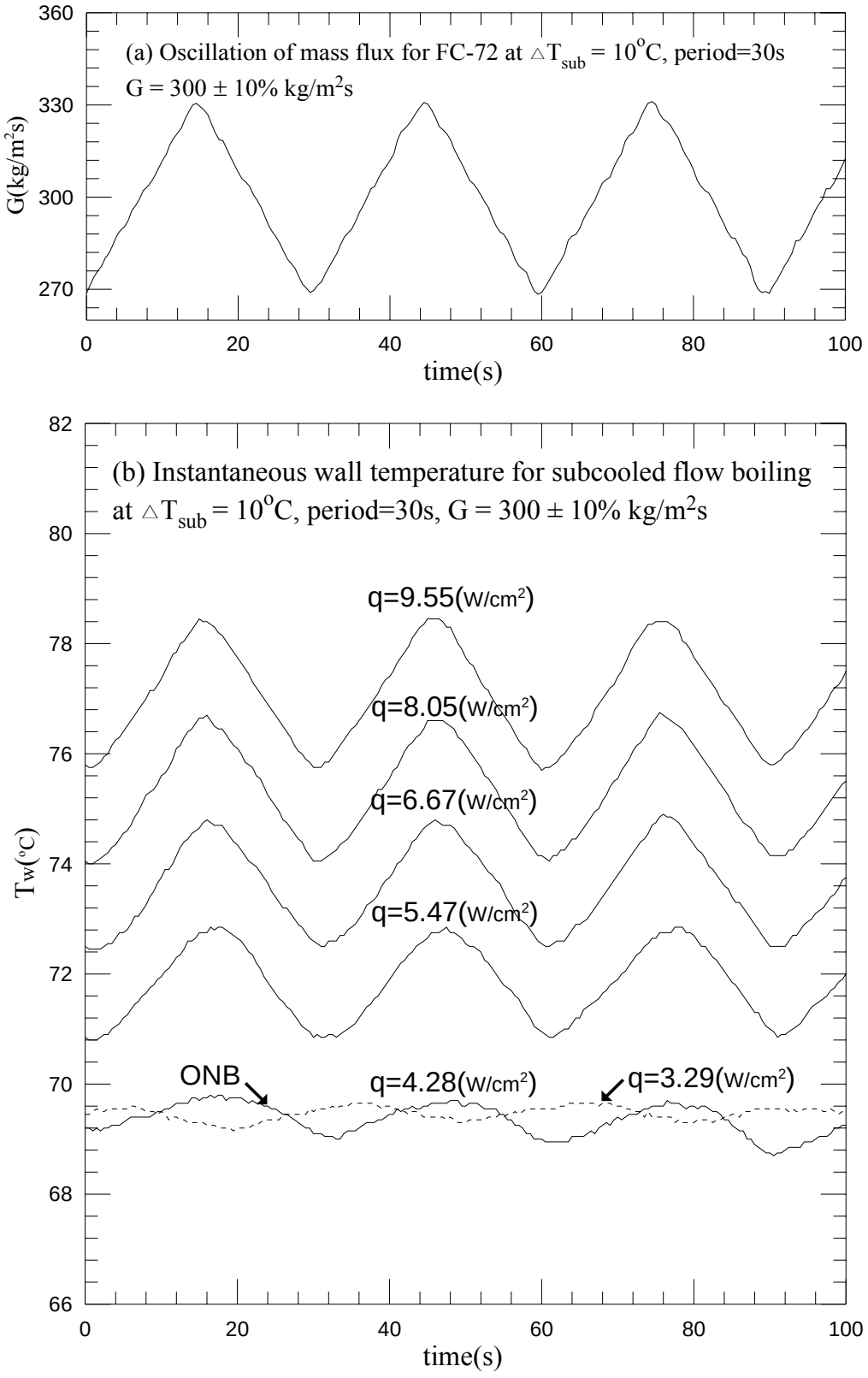

Fig. 5.47 Time variations of (a) imposed coolant mass flux and (b) copper plate temperature in transient oscillatory subcooled flow boiling for various imposed heat fluxes for G=300±10% kg/m^{2}s with t_p =30 sec.($\overline{q}_{ONB}$ =4.28 w/cm^2 at G =300 kg/m^{2}s)

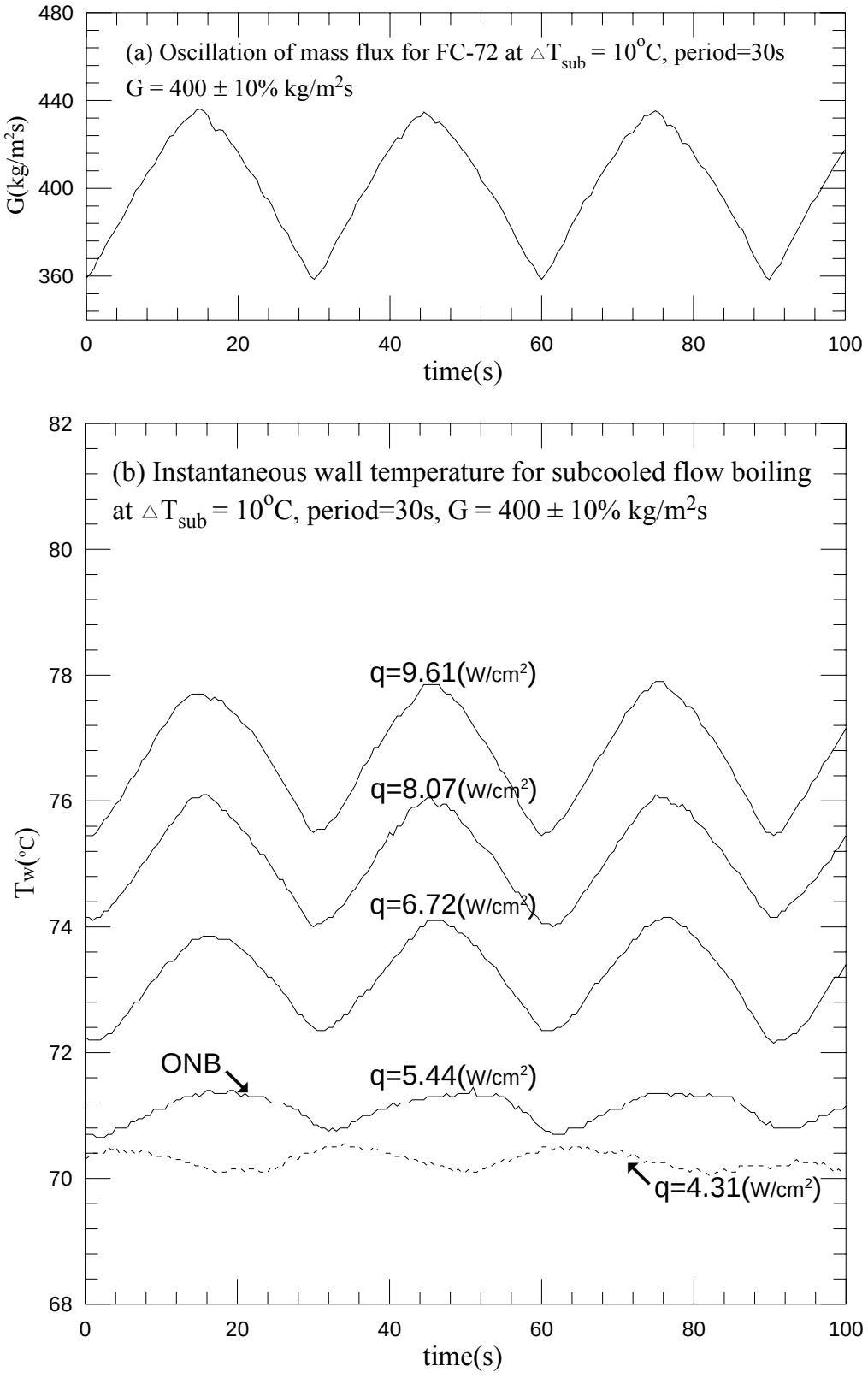

Fig. 5.48 Time variations of (a) imposed coolant mass flux and (b) copper plate temperature in transient oscillatory subcooled flow boiling for various imposed heat fluxes for G=400±10% kg/m^{2}s with t_p =30 sec.($\bar{q}_{ONB}$ =5.44 w/cm^2 at G =400 kg/m^{2}s)

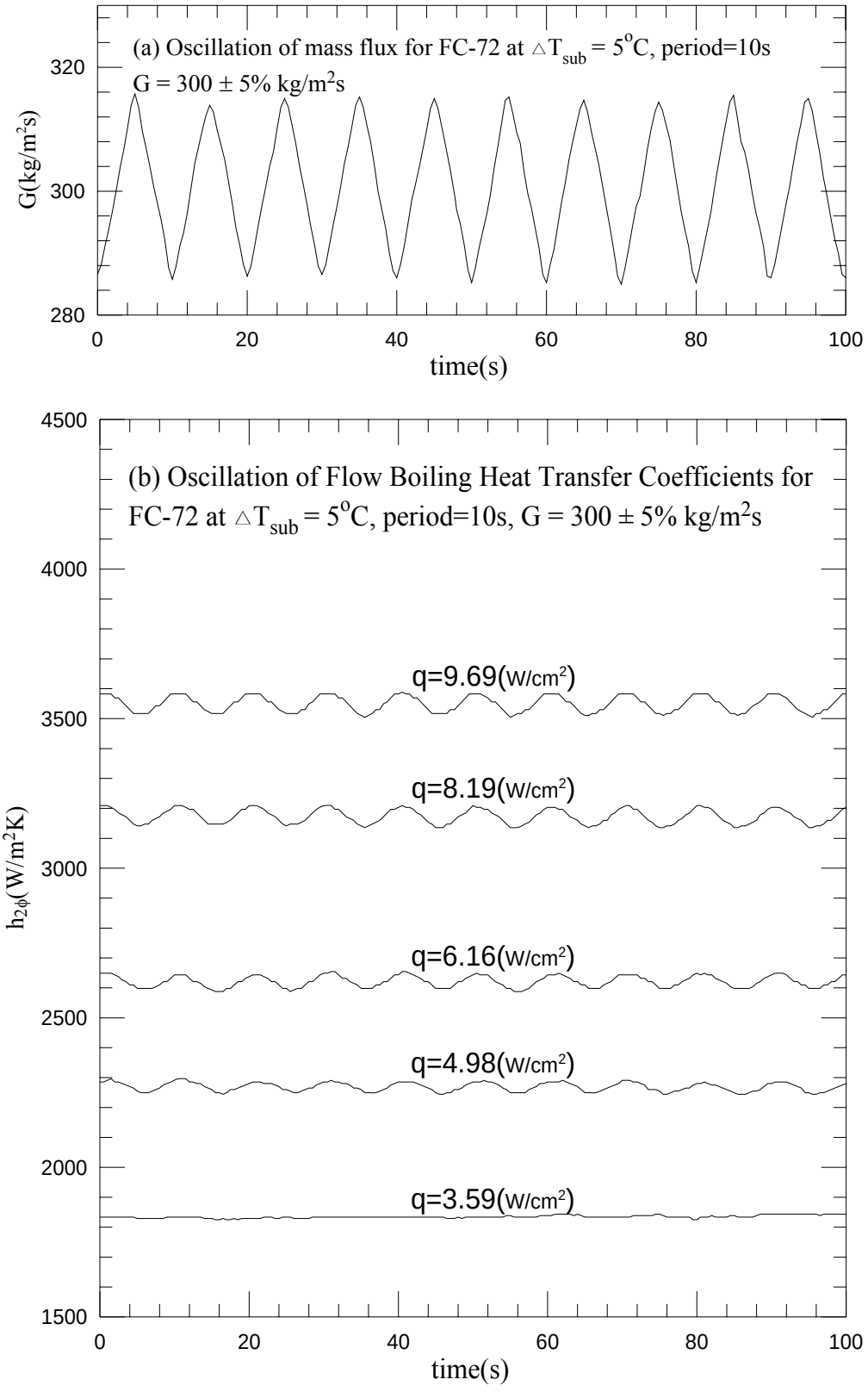

Fig. 5.49 Time variations of (a) imposed coolant mass flux and (b) flow boiling heat transfer coefficients in transient oscillatory subcooled flow boiling for various imposed heat fluxes for G=300±5% kg/m^{2}s with t_p=10 sec.

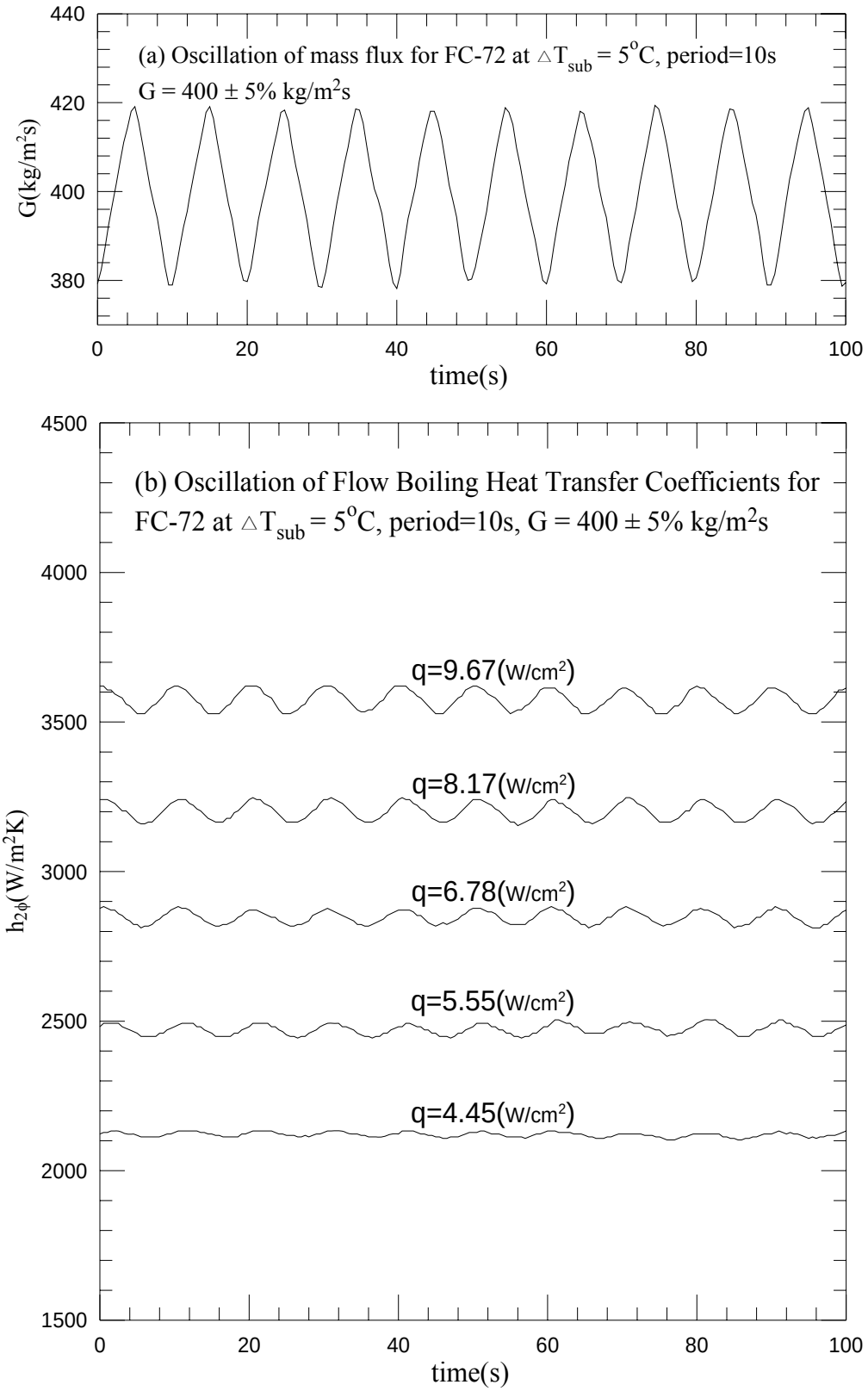

Fig. 5.50 Time variations of (a) imposed coolant mass flux and (b) flow boiling heat transfer coefficients in transient oscillatory subcooled flow boiling for various imposed heat fluxes for G=400±5% kg/m^{2}s with t_p=10 sec.

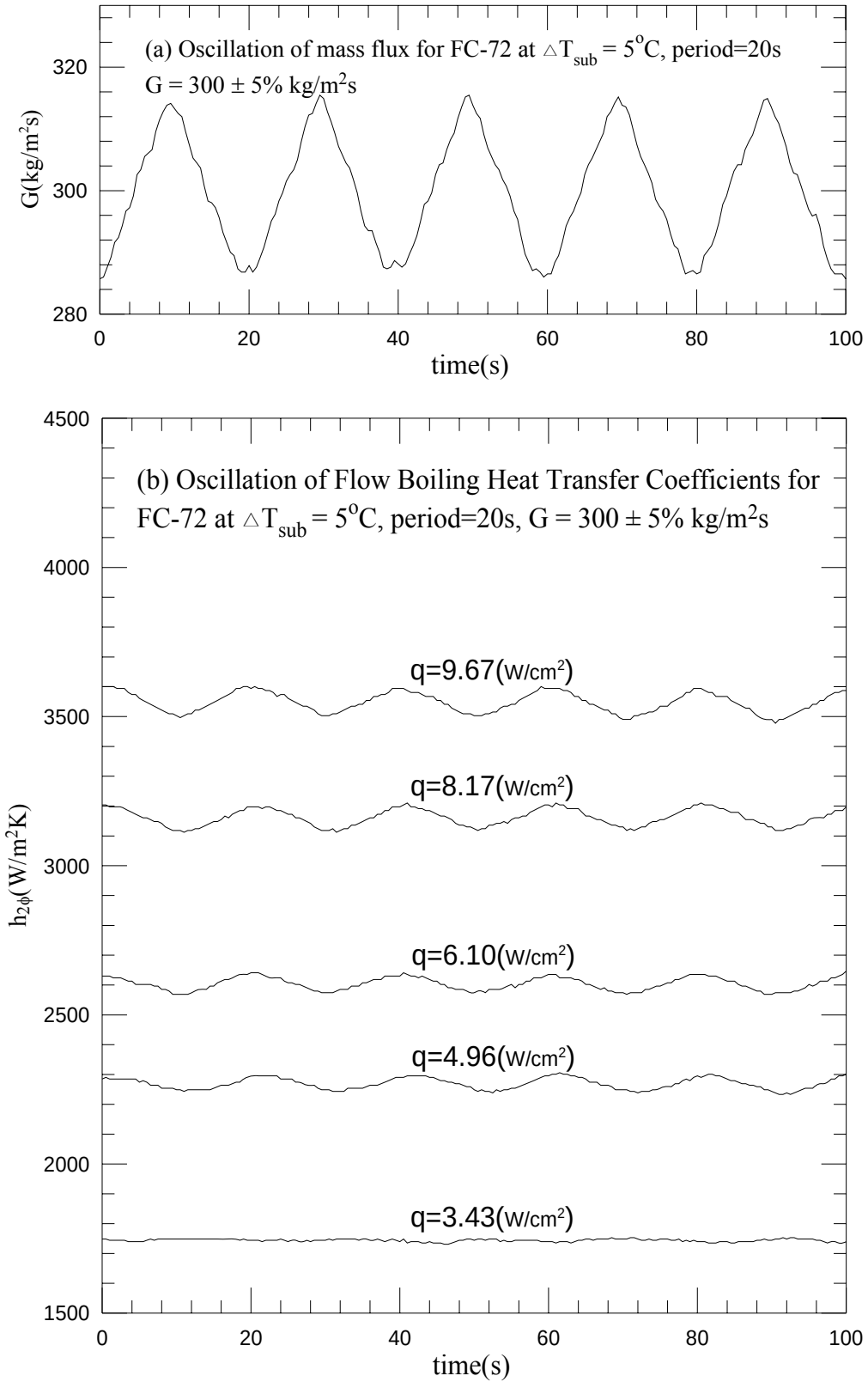

Fig. 5.51 Time variations of (a) imposed coolant mass flux and (b) flow boiling heat transfer coefficients in transient oscillatory subcooled flow boiling for various imposed heat fluxes for G=300±5% kg/m^{2}s with t_p=20 sec.

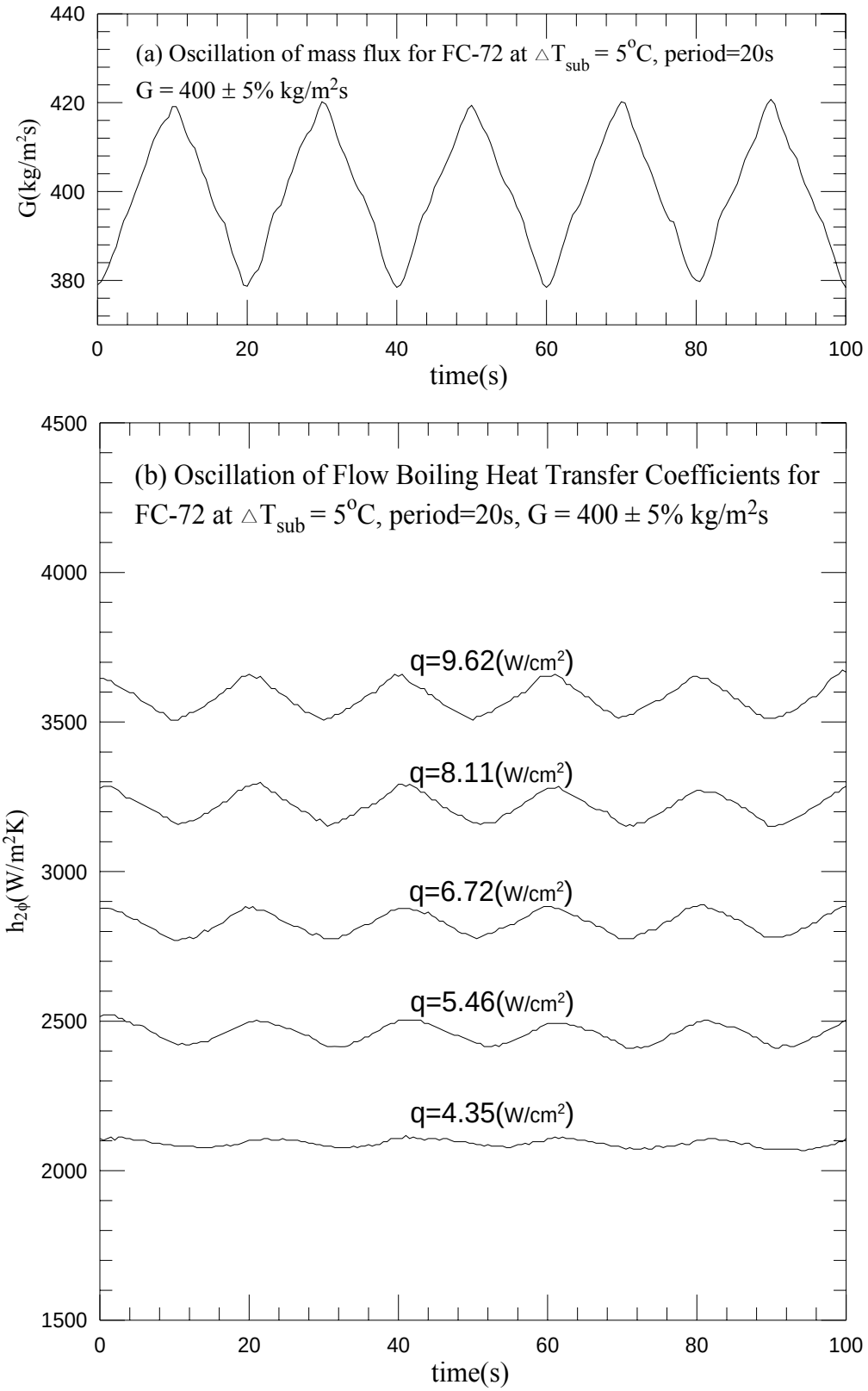

Fig. 5.52 Time variations of (a) imposed coolant mass flux and (b) flow boiling heat transfer coefficients in transient oscillatory subcooled flow boiling for various imposed heat fluxes for G=400±5% kg/m^{2}s with t_p=20 sec.

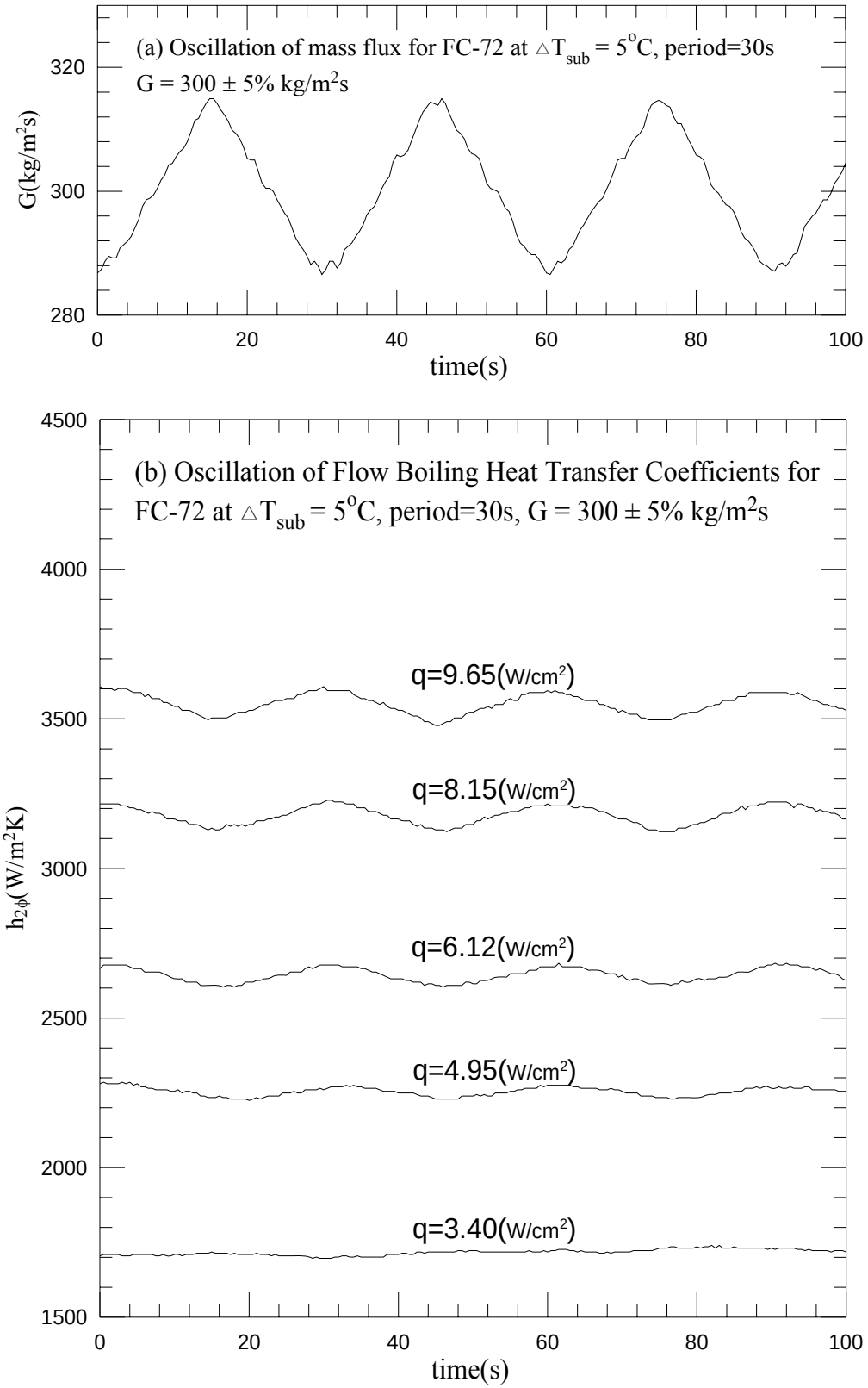

Fig. 5.53 Time variations of (a) imposed coolant mass flux and (b) flow boiling heat transfer coefficients in transient oscillatory subcooled flow boiling for various imposed heat fluxes for G=300±5% kg/m^{2}s with t_p=30 sec.

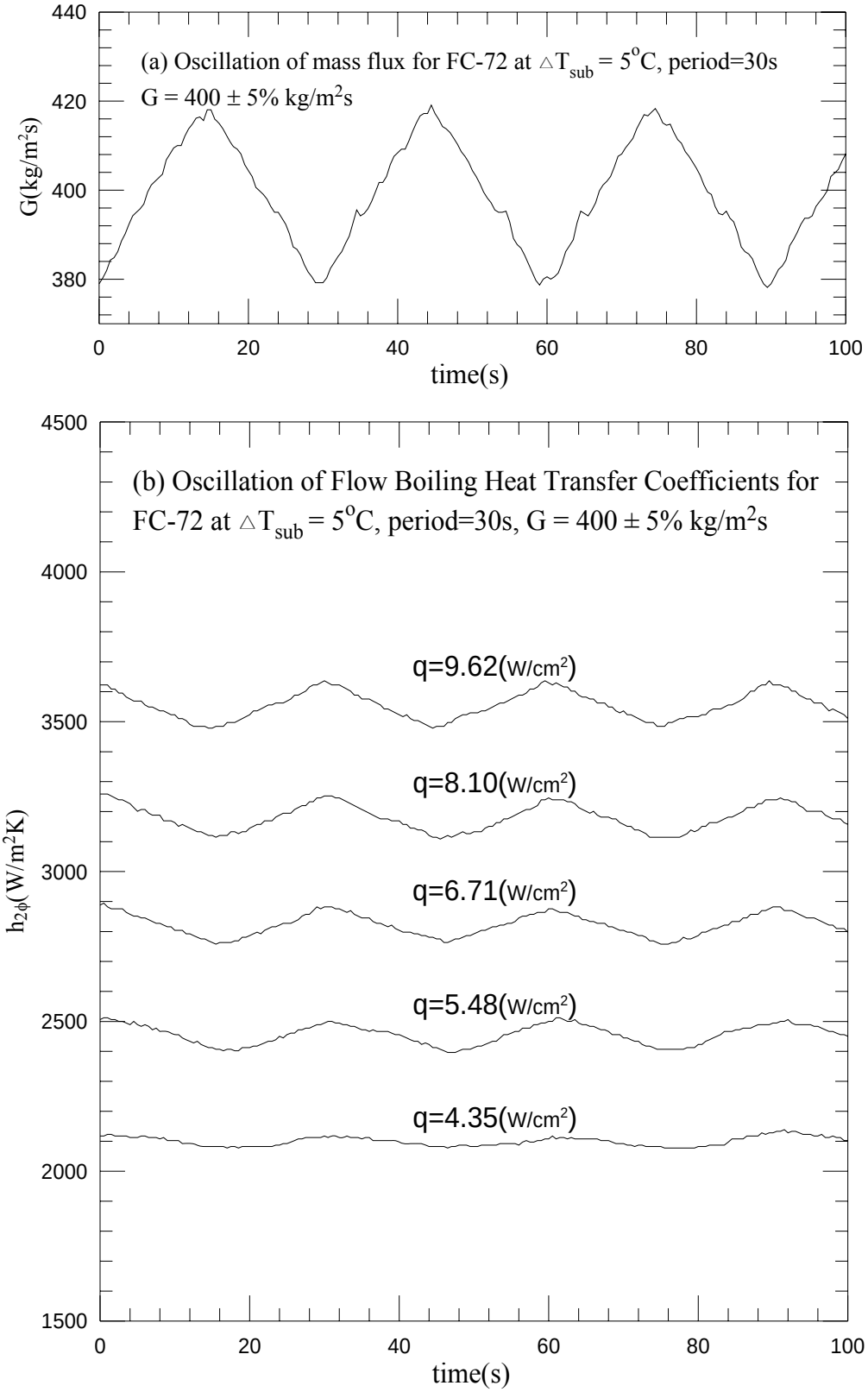

Fig. 5.54 Time variations of (a) imposed coolant mass flux and (b) flow boiling heat transfer coefficients in transient oscillatory subcooled flow boiling for various imposed heat fluxes for G=400±5% kg/m^{2}s with t_p=30 sec.

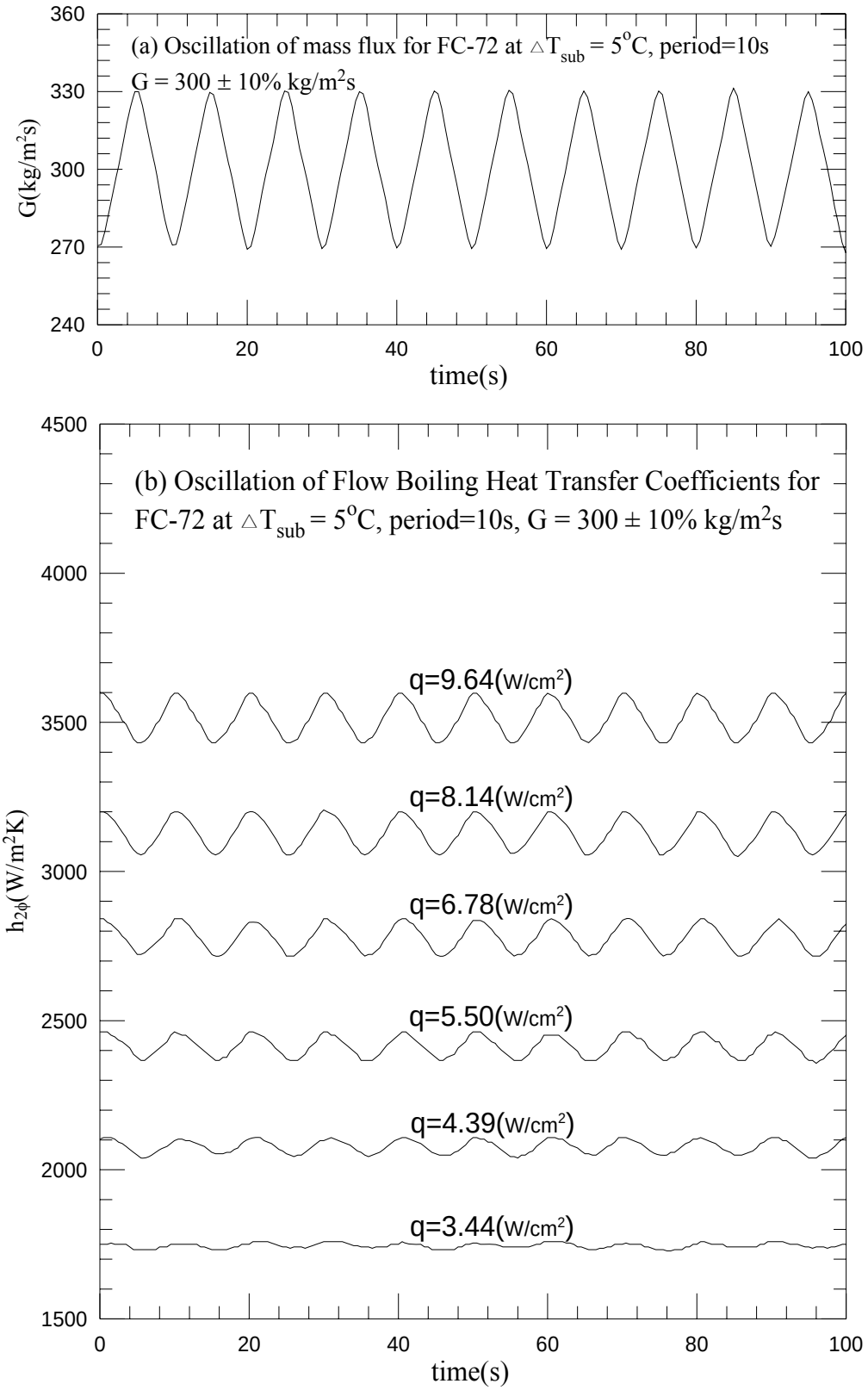

Fig. 5.55 Time variations of (a) imposed coolant mass flux and (b) flow boiling heat transfer coefficients in transient oscillatory subcooled flow boiling for various imposed heat fluxes for G=300±10% kg/m^{2}s with t_p=10 sec.

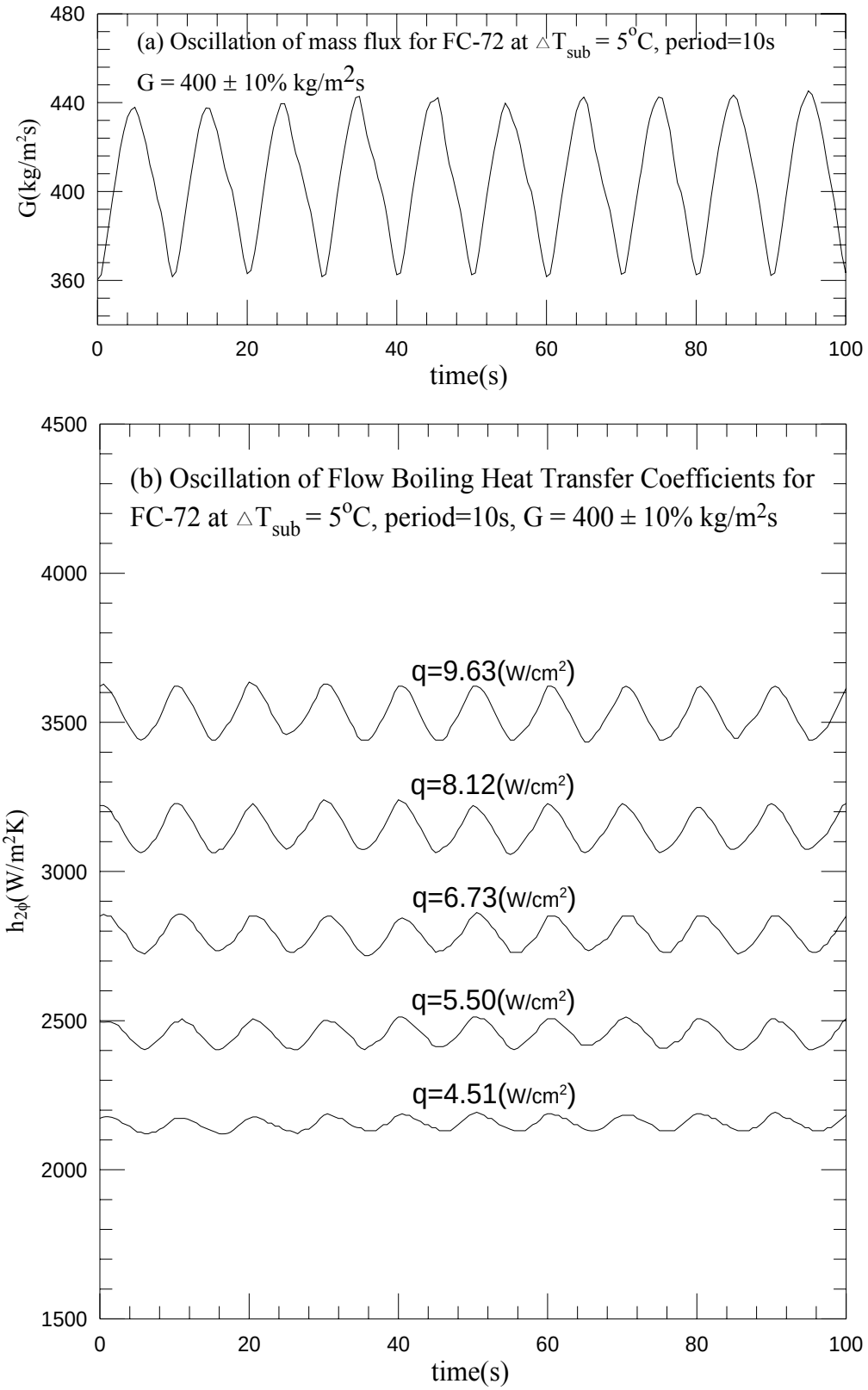

Fig. 5.56 Time variations of (a) imposed coolant mass flux and (b) flow boiling heat transfer coefficients in transient oscillatory subcooled flow boiling for various imposed heat fluxes for G=400±10% kg/m^{2}s with t_p=10 sec.

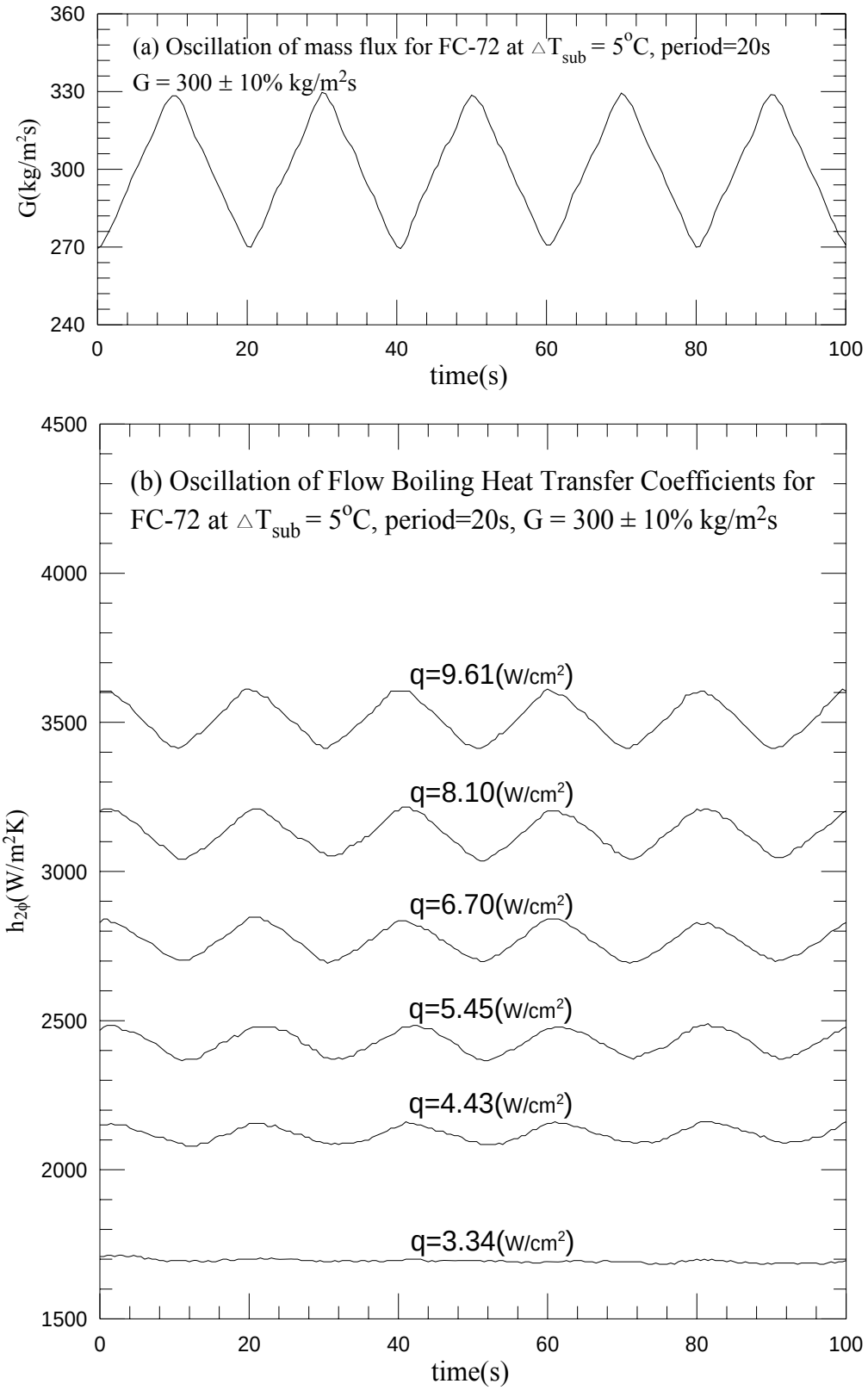

Fig. 5.57 Time variations of (a) imposed coolant mass flux and (b) flow boiling heat transfer coefficients in transient oscillatory subcooled flow boiling for various imposed heat fluxes for G=300±10% kg/m^{2}s with t_p=20 sec.

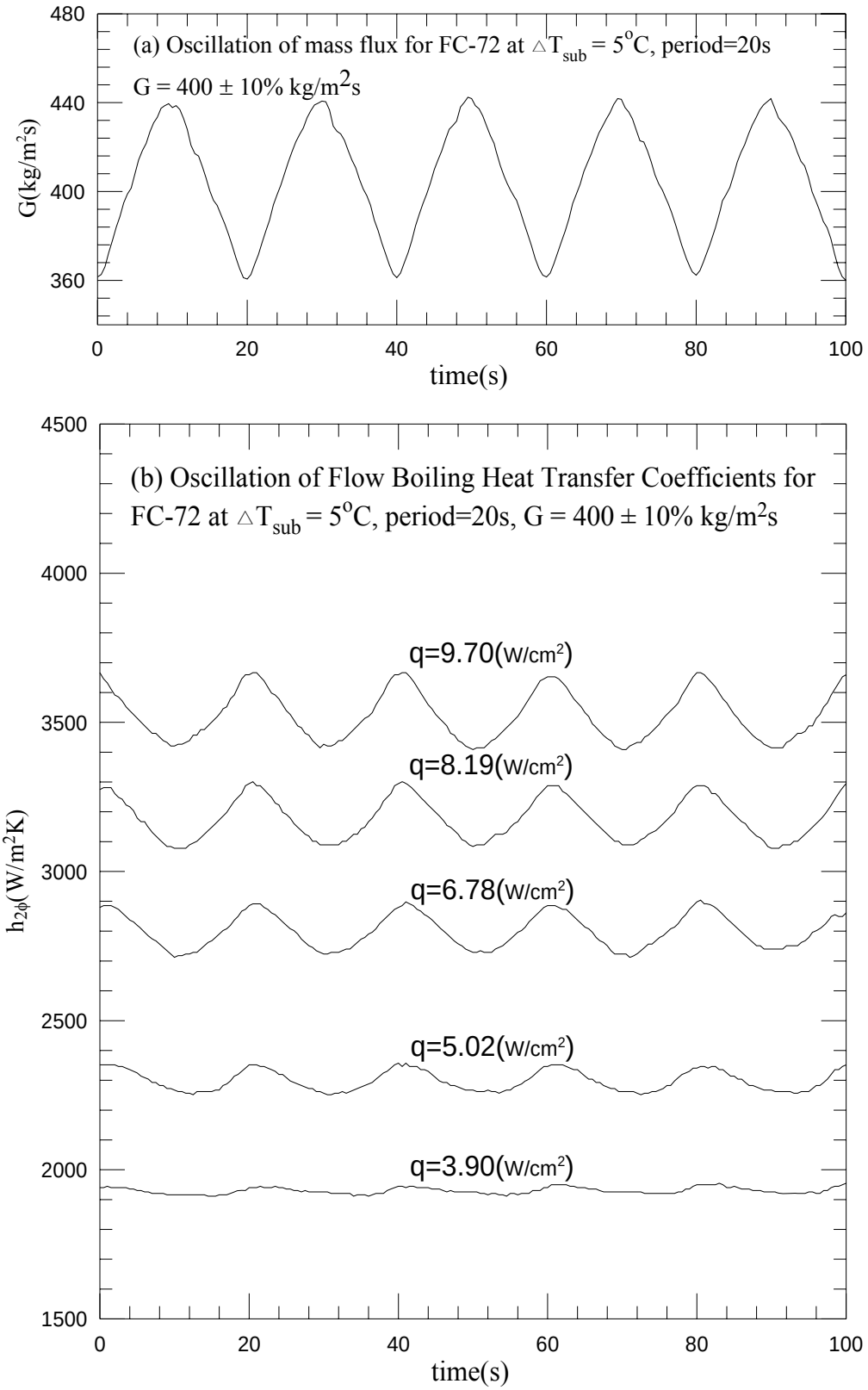

Fig. 5.58 Time variations of (a) imposed coolant mass flux and (b) flow boiling heat transfer coefficients in transient oscillatory subcooled flow boiling for various imposed heat fluxes for G=400±10% kg/m^{2}s with t_p=20 sec.

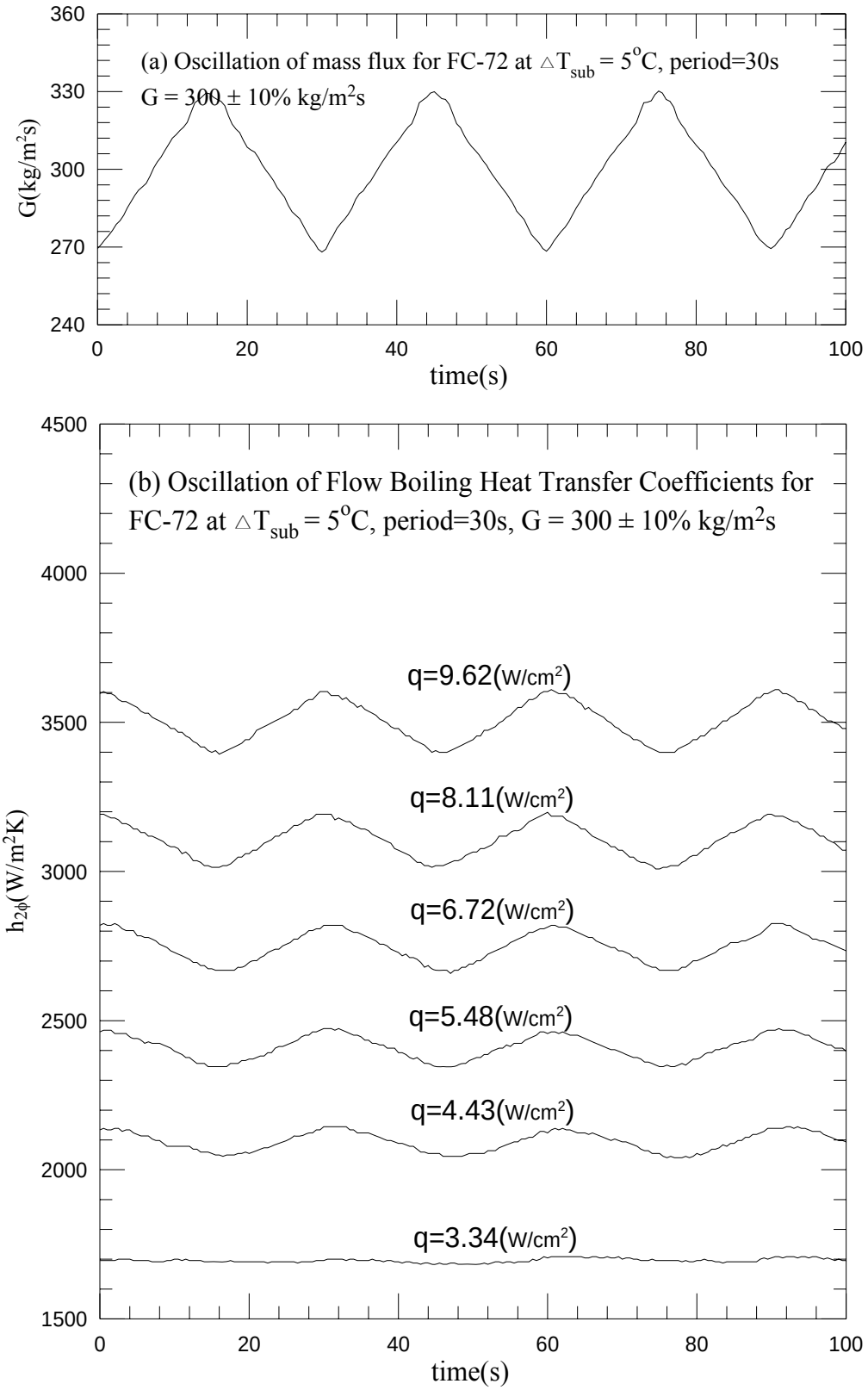

Fig. 5.59 Time variations of (a) imposed coolant mass flux and (b) flow boiling heat transfer coefficients in transient oscillatory subcooled flow boiling for various imposed heat fluxes for G=300±10% kg/m^{2}s with t_p=30 sec.

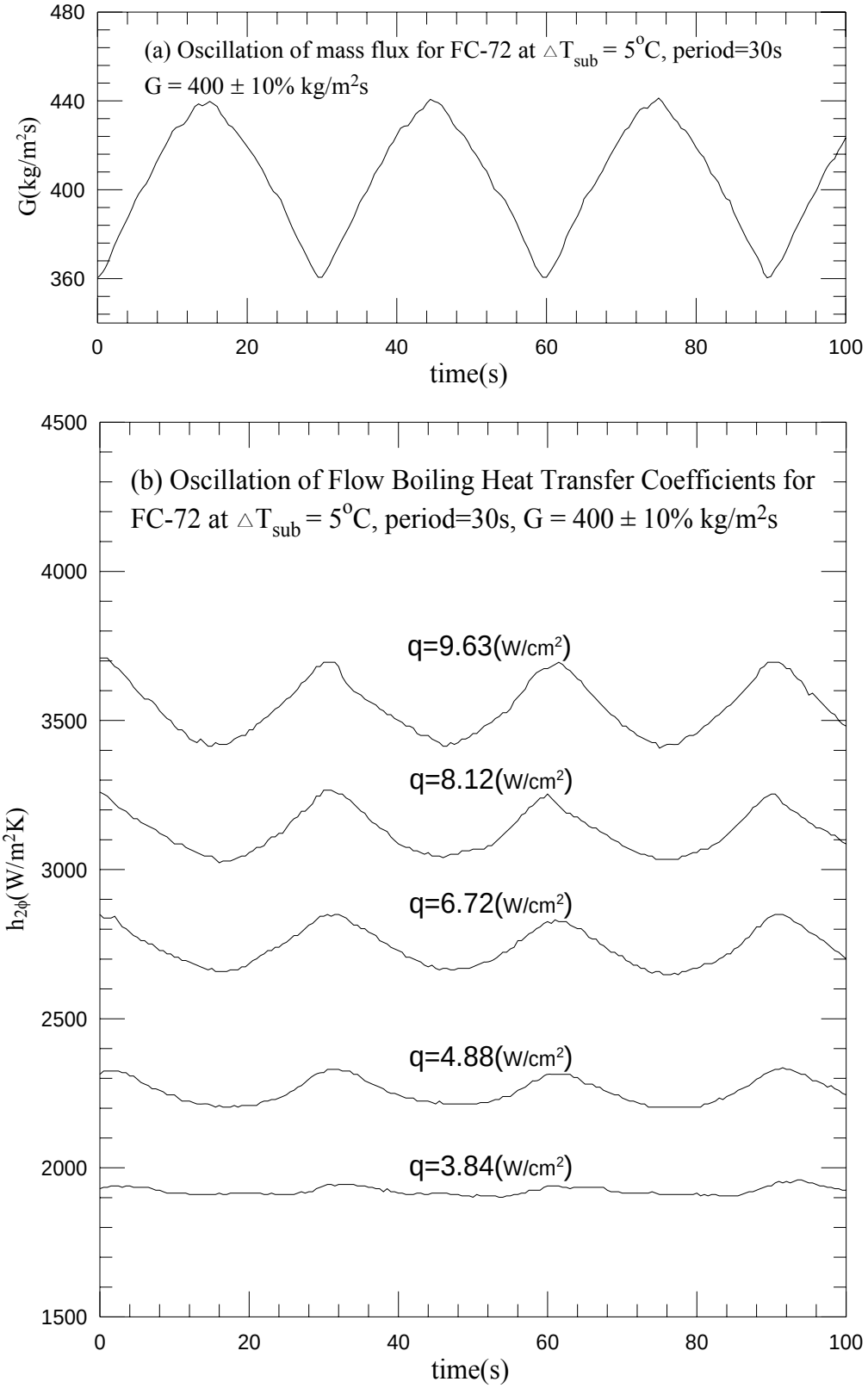

Fig. 5.60 Time variations of (a) imposed coolant mass flux and (b) flow boiling heat transfer coefficients in transient oscillatory subcooled flow boiling for various imposed heat fluxes for G=400±10% kg/m^{2}s with t_p=30 sec.

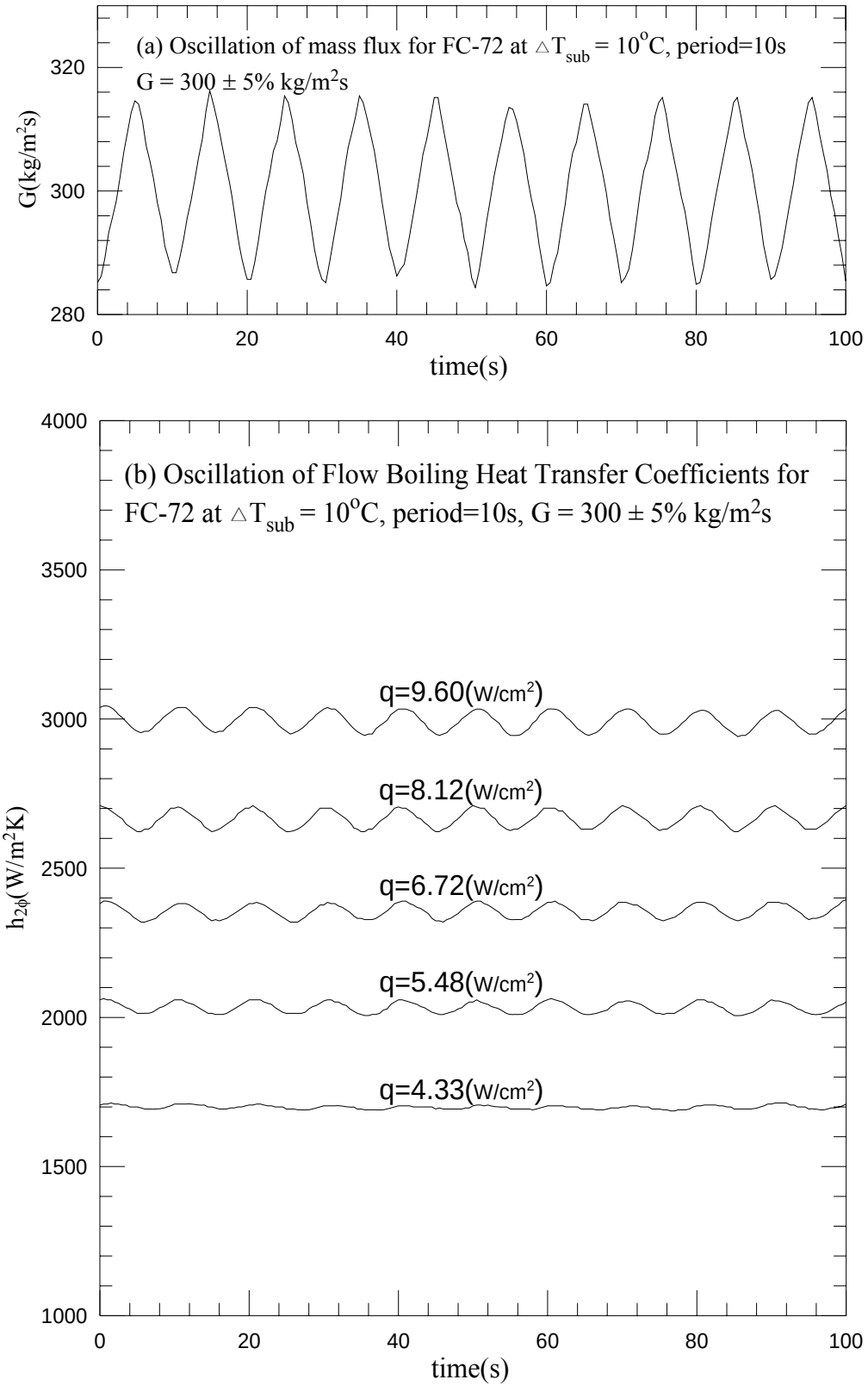

Fig. 5.61 Time variations of (a) imposed coolant mass flux and (b) flow boiling heat transfer coefficients in transient oscillatory subcooled flow boiling for various imposed heat fluxes for G=300±5% kg/m^{2}s with t_p=10 sec.

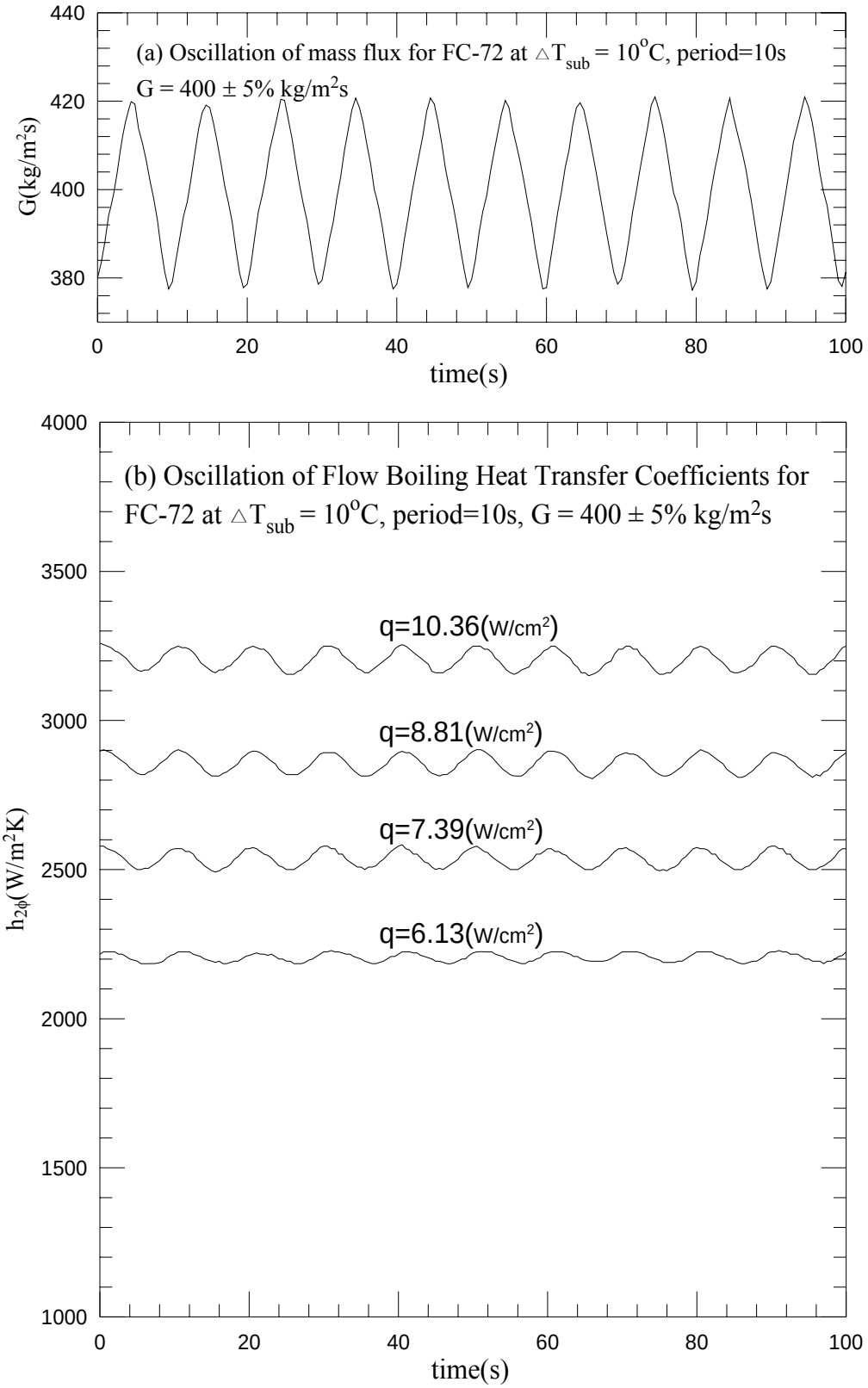

Fig. 5.62 Time variations of (a) imposed coolant mass flux and (b) flow boiling heat transfer coefficients in transient oscillatory subcooled flow boiling for various imposed heat fluxes for G=400±5% kg/m^{2}s with t_p=10 sec.

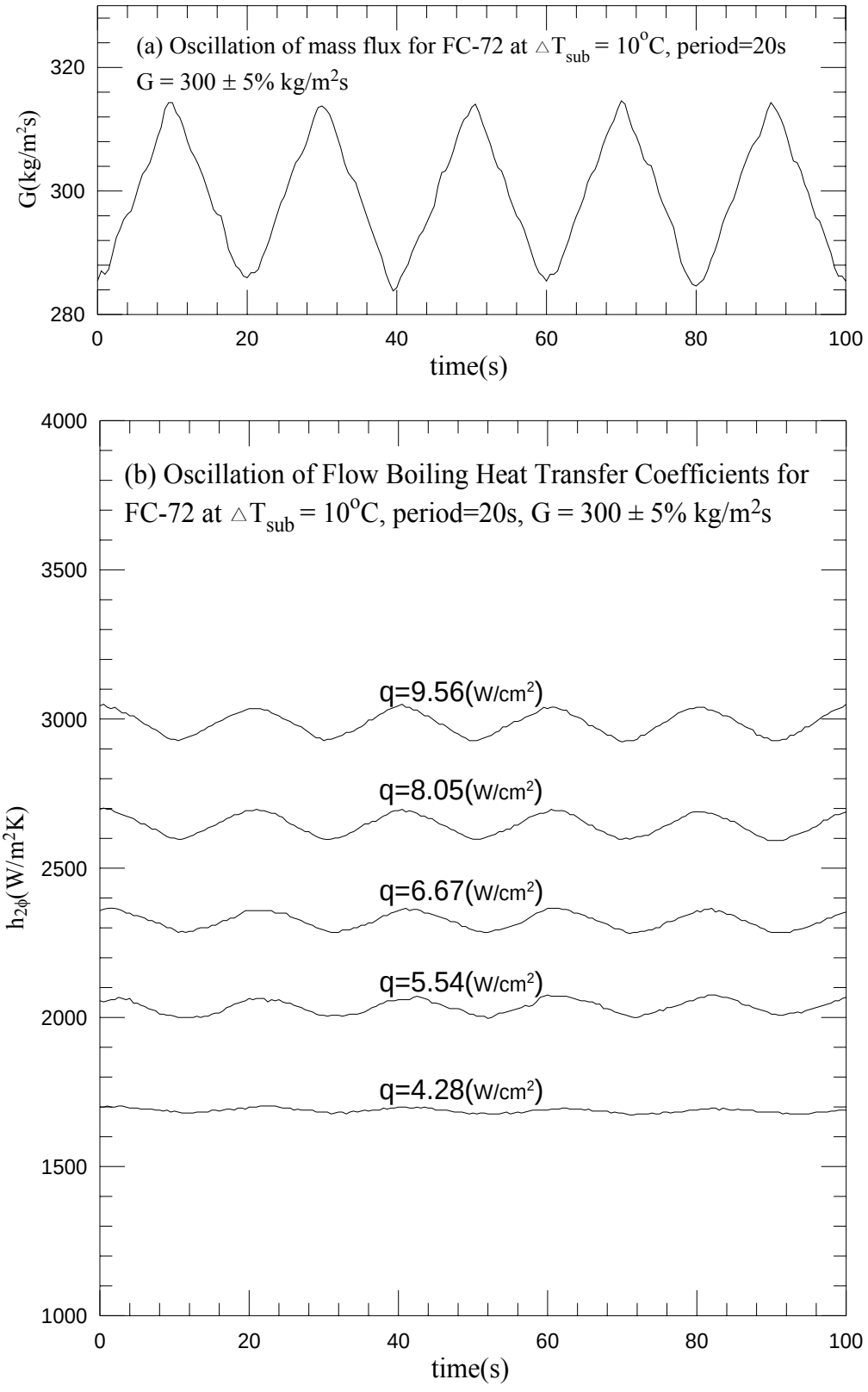

Fig. 5.63 Time variations of (a) imposed coolant mass flux and (b) flow boiling heat transfer coefficients in transient oscillatory subcooled flow boiling for various imposed heat fluxes for G=300±5% kg/m^{2}s with t_p=20 sec.

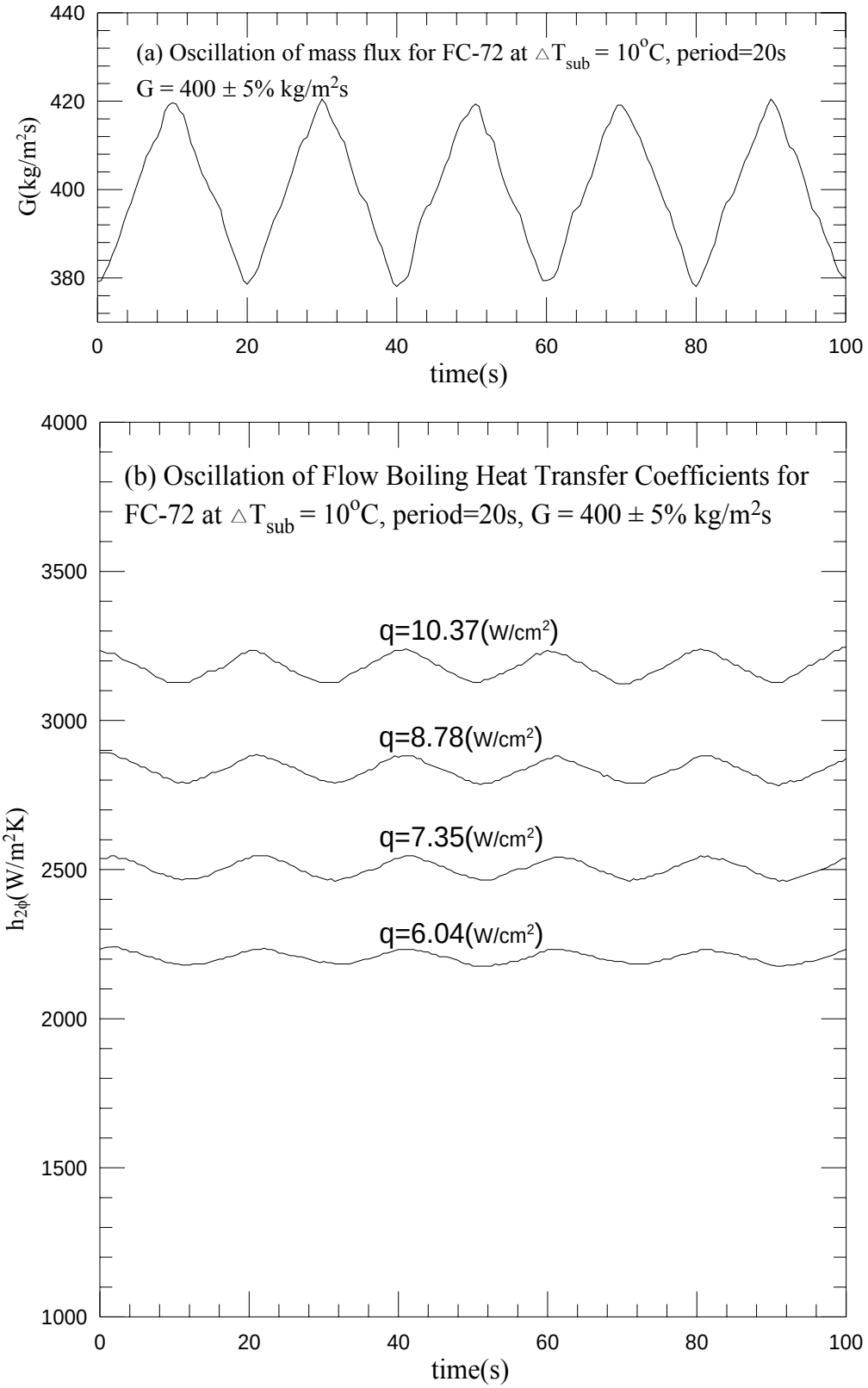

Fig. 5.64 Time variations of (a) imposed coolant mass flux and (b) flow boiling heat transfer coefficients in transient oscillatory subcooled flow boiling for various imposed heat fluxes for G=400±5% kg/m^{2}s with t_p=20 sec.

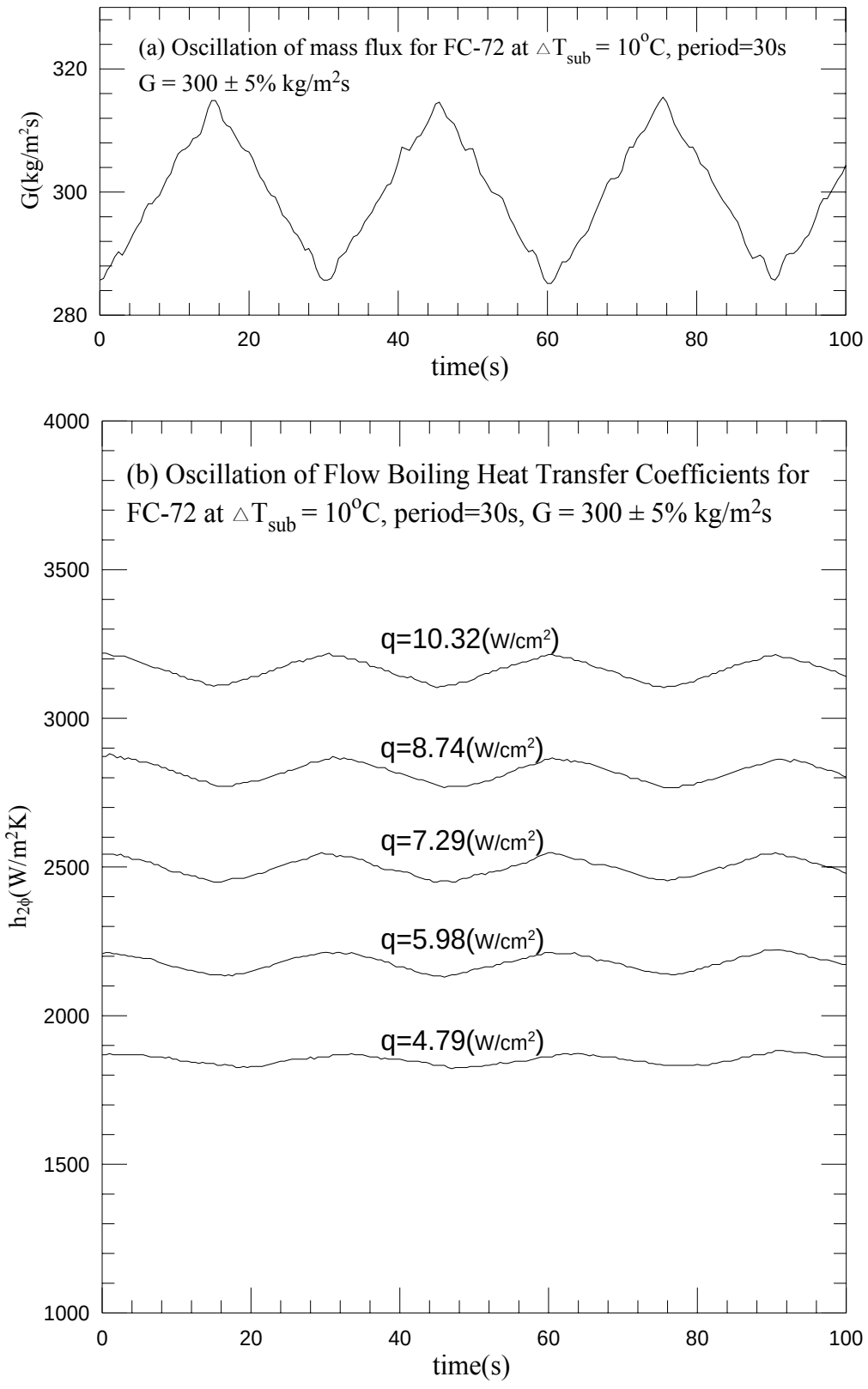

Fig. 5.65 Time variations of (a) imposed coolant mass flux and (b) flow boiling heat transfer coefficients in transient oscillatory subcooled flow boiling for various imposed heat fluxes for G=300±5% kg/m^{2}s with t_p=30 sec.

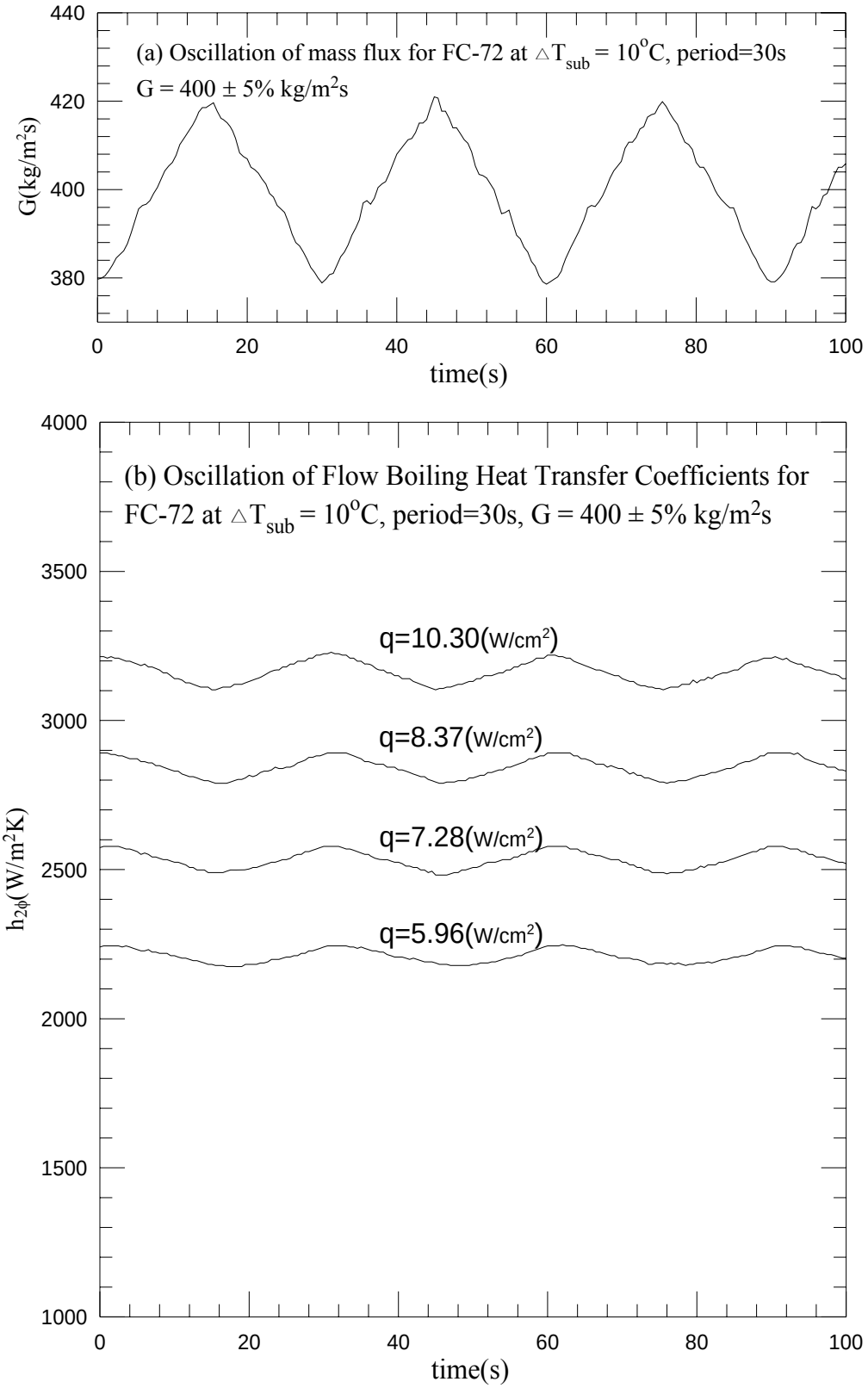

Fig. 5.66 Time variations of (a) imposed coolant mass flux and (b) flow boiling heat transfer coefficients in transient oscillatory subcooled flow boiling for various imposed heat fluxes for G=400±5% kg/m^{2}s with t_p=30 sec.

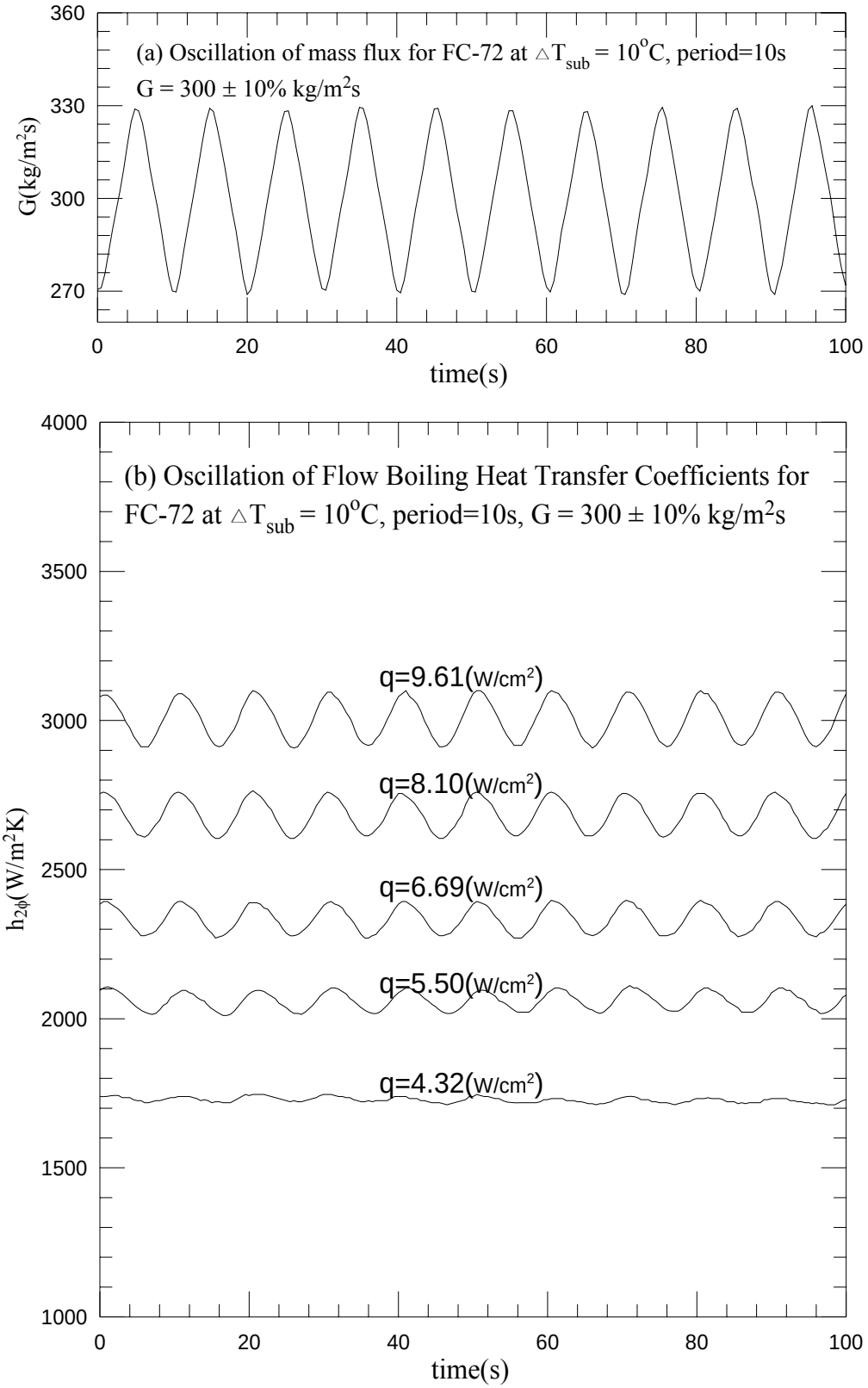

Fig. 5.67 Time variations of (a) imposed coolant mass flux and (b) flow boiling heat transfer coefficients in transient oscillatory subcooled flow boiling for various imposed heat fluxes for G=300±10% kg/m^{2}s with t_p=10 sec.

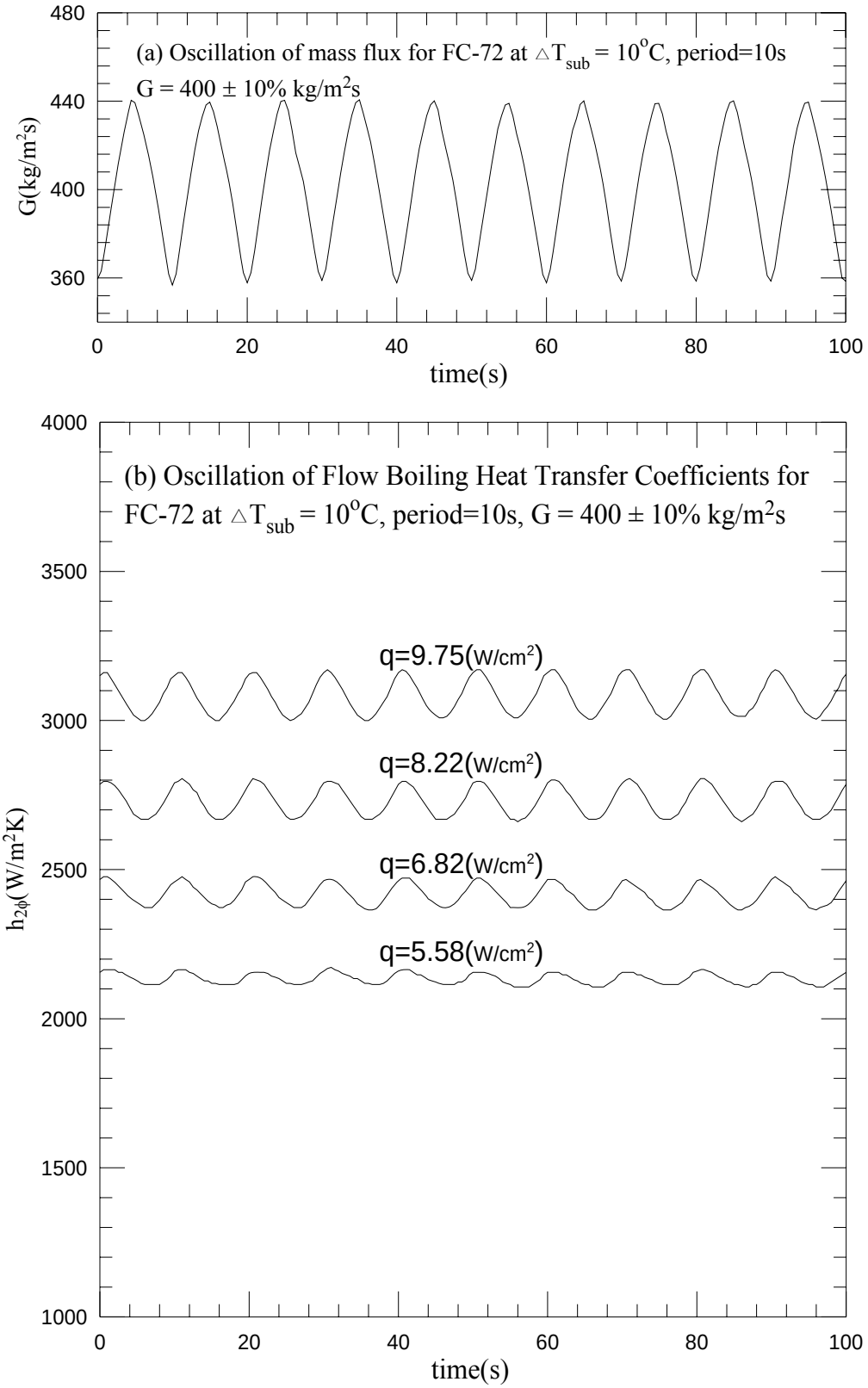

Fig. 5.68 Time variations of (a) imposed coolant mass flux and (b) flow boiling heat transfer coefficients in transient oscillatory subcooled flow boiling for various imposed heat fluxes for G=400±10% kg/m^{2}s with t_p=10 sec.

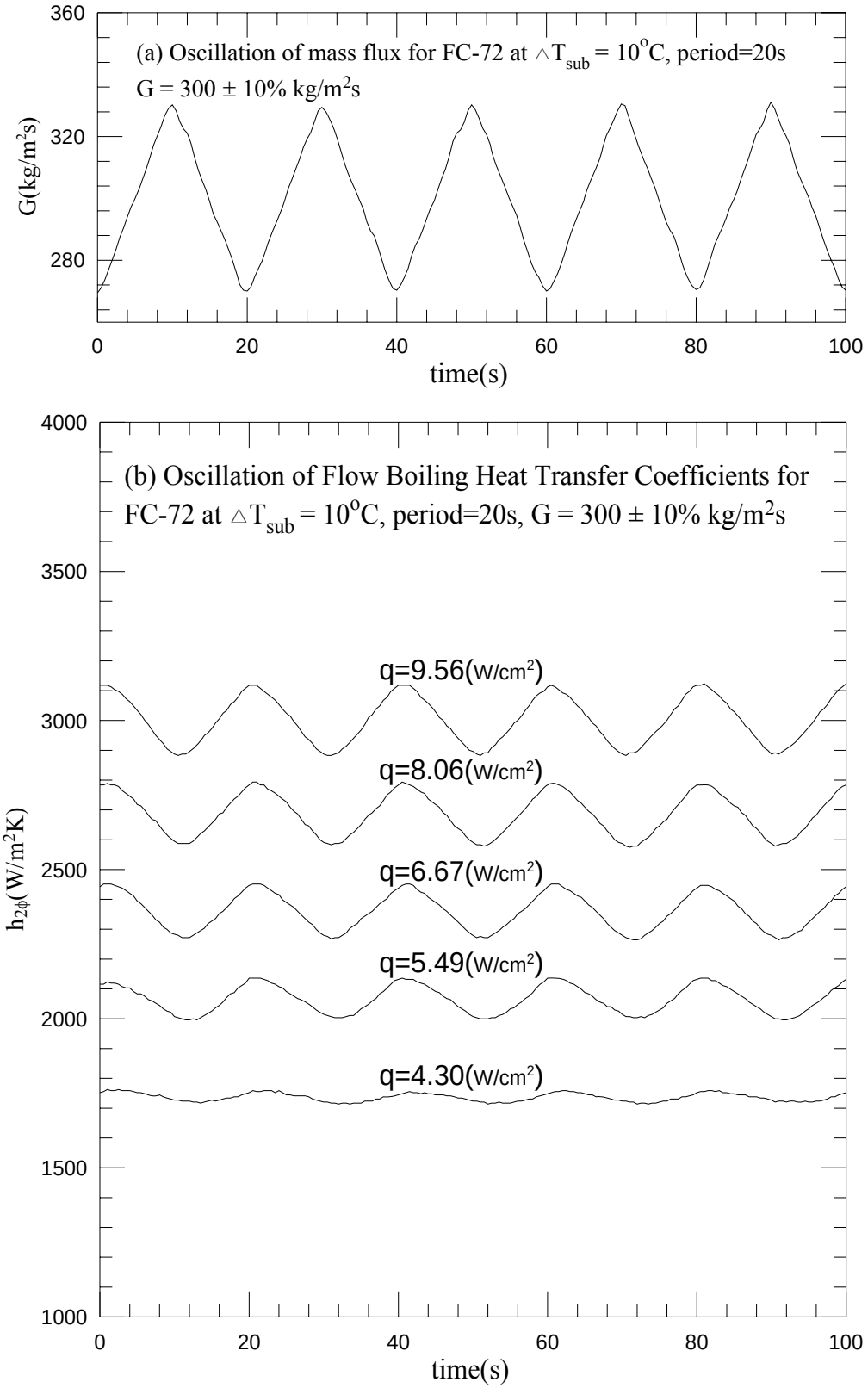

Fig. 5.69 Time variations of (a) imposed coolant mass flux and (b) flow boiling heat transfer coefficients in transient oscillatory subcooled flow boiling for various imposed heat fluxes for G=300±10% kg/m^{2}s with t_p=20 sec.

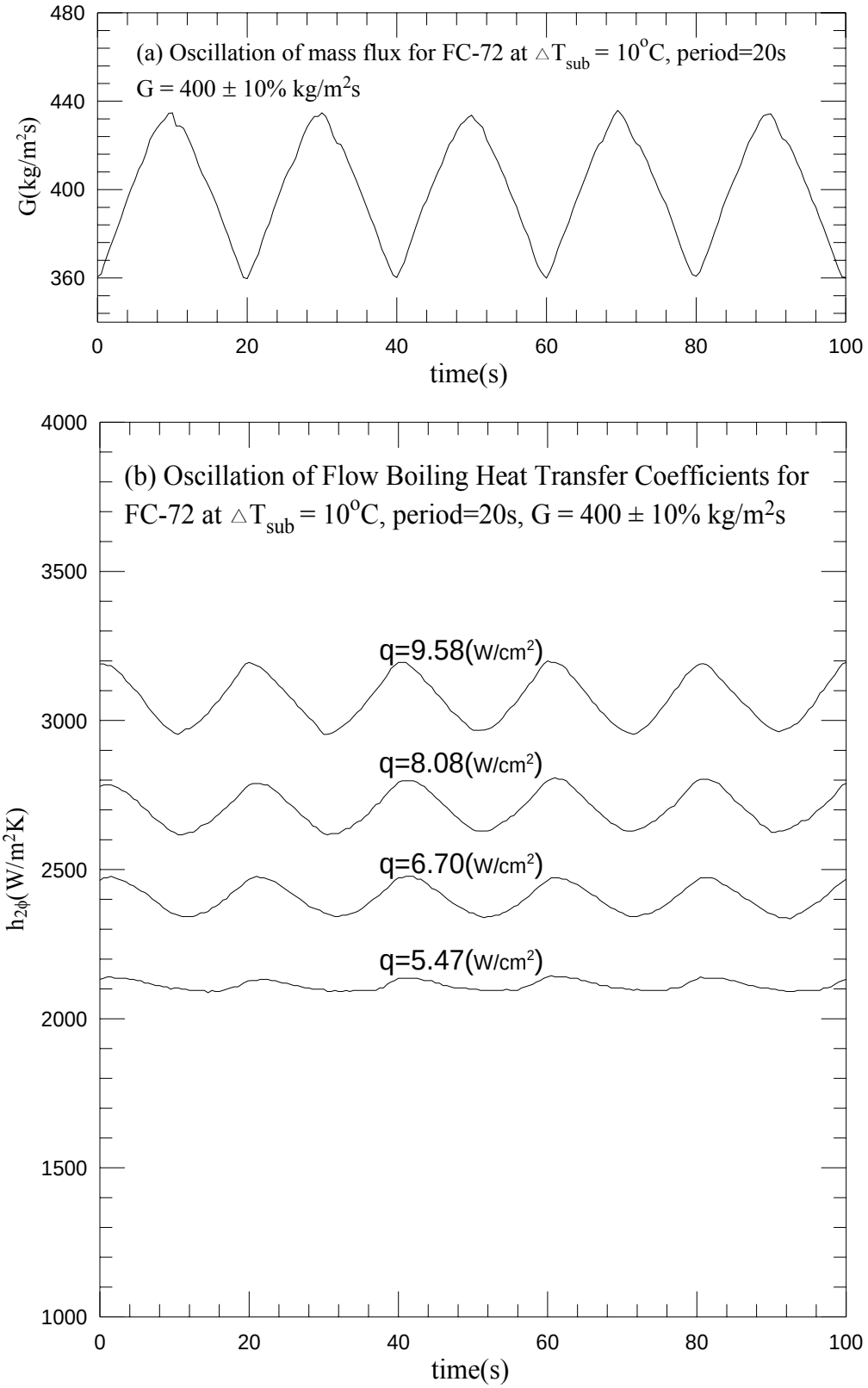

Fig. 5.70 Time variations of (a) imposed coolant mass flux and (b) flow boiling heat transfer coefficients in transient oscillatory subcooled flow boiling for various imposed heat fluxes for G=400±10% kg/m^{2}s with t_p=20 sec.

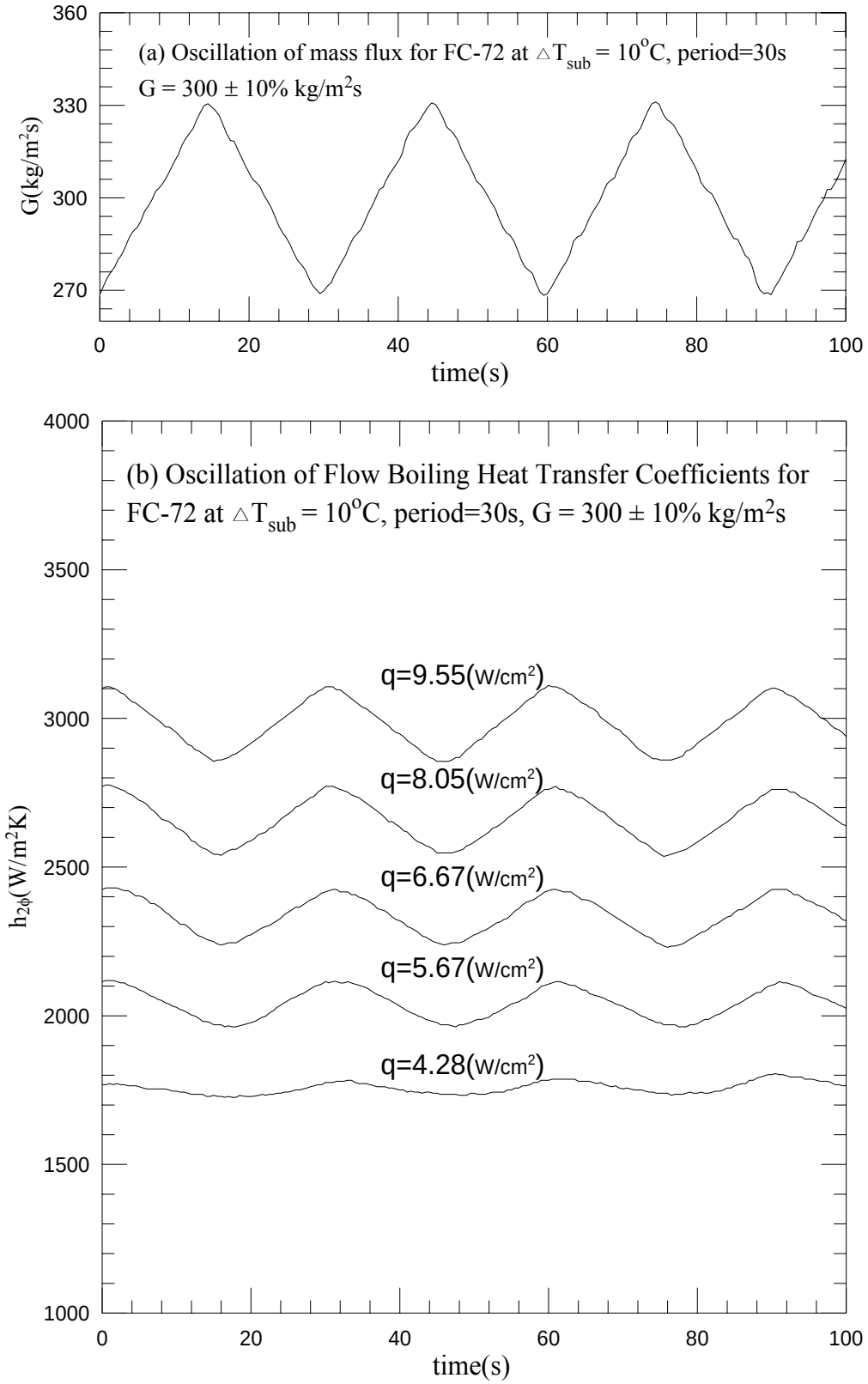

Fig. 5.71 Time variations of (a) imposed coolant mass flux and (b) flow boiling heat transfer coefficients in transient oscillatory subcooled flow boiling for various imposed heat fluxes for G=300±10% kg/m^{2}s with t_p=30 sec.

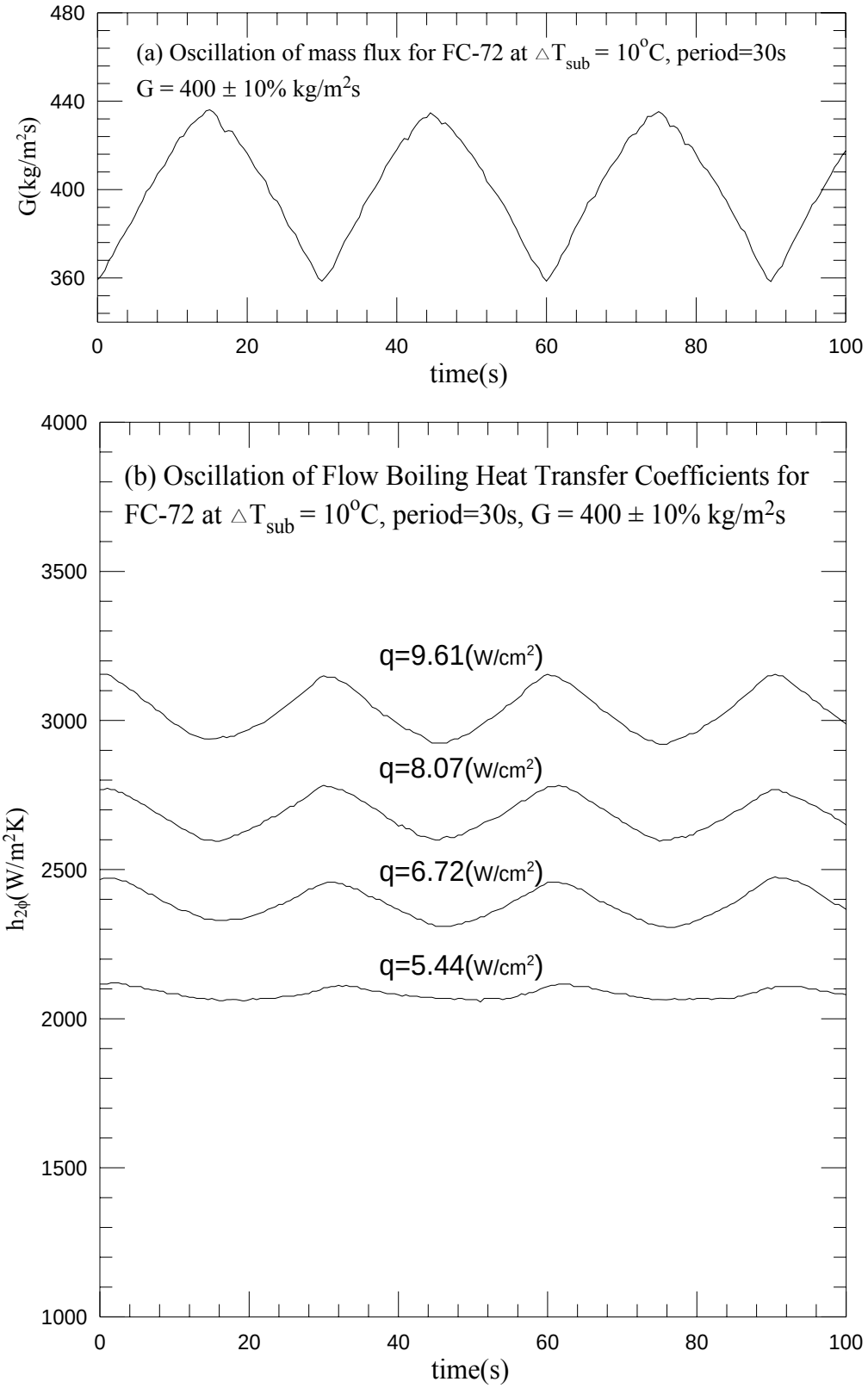

Fig. 5.72 Time variations of (a) imposed coolant mass flux and (b) flow boiling heat transfer coefficients in transient oscillatory subcooled flow boiling for various imposed heat fluxes for G=400±10% kg/m^{2}s with t_p=30 sec.

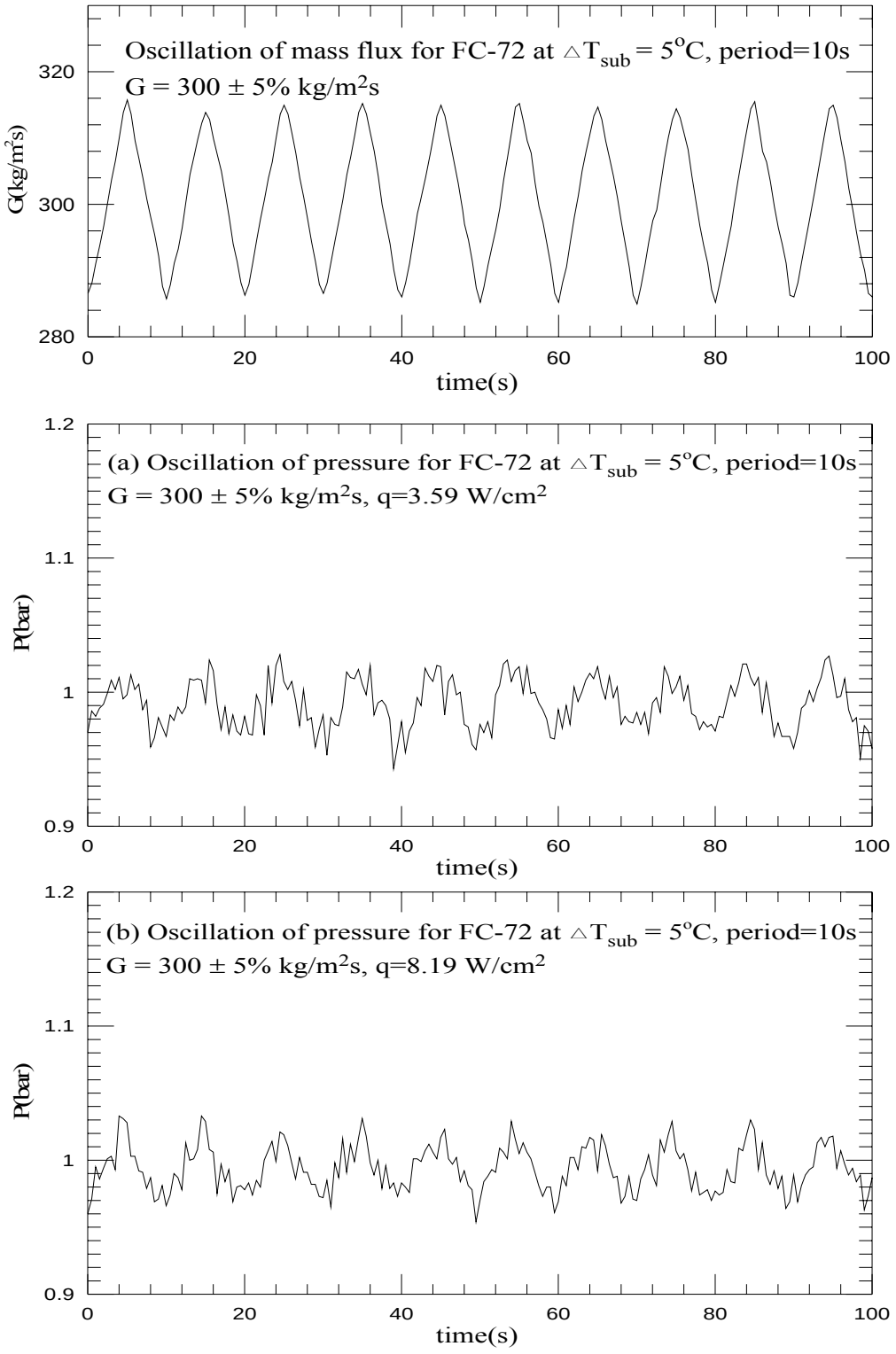

Fig.5.73 Time variations of coolant mass flux and inlet pressure in transient oscillatory subcooled flow boiling for various imposed heat fluxes at (a) q=3.59 W/cm^2 and (b) q=8.19 W/cm^2 for G=300±5% kg/m^{2}s with t_p=10 sec.

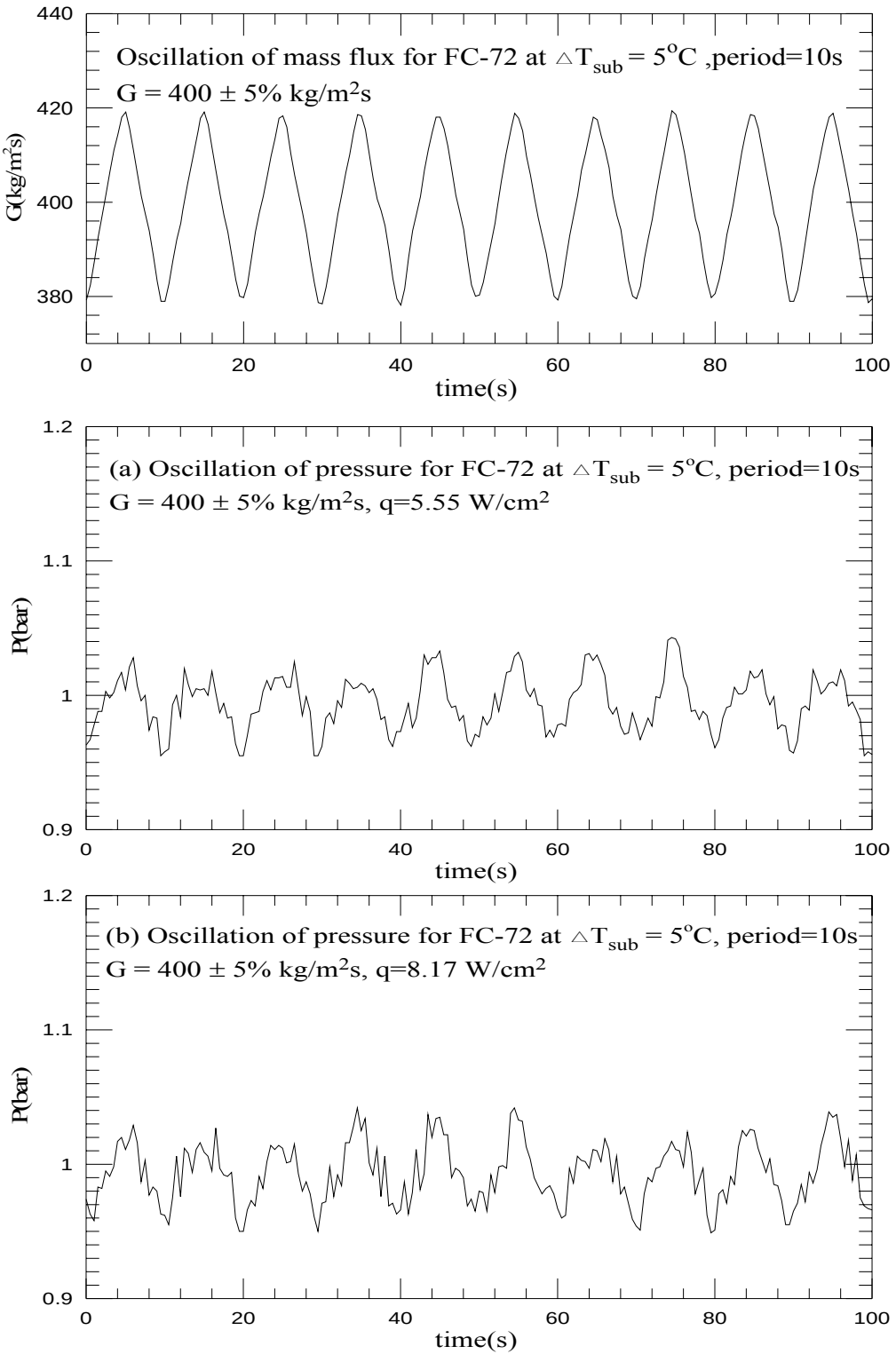

Fig.5.74 Time variations of coolant mass flux and inlet pressure in transient oscillatory subcooled flow boiling for various imposed heat fluxes at (a) q=5.55 W/cm^2 and (b) q=8.17 W/cm^2 for G=400±5% kg/m^{2}s with t_p=10 sec.

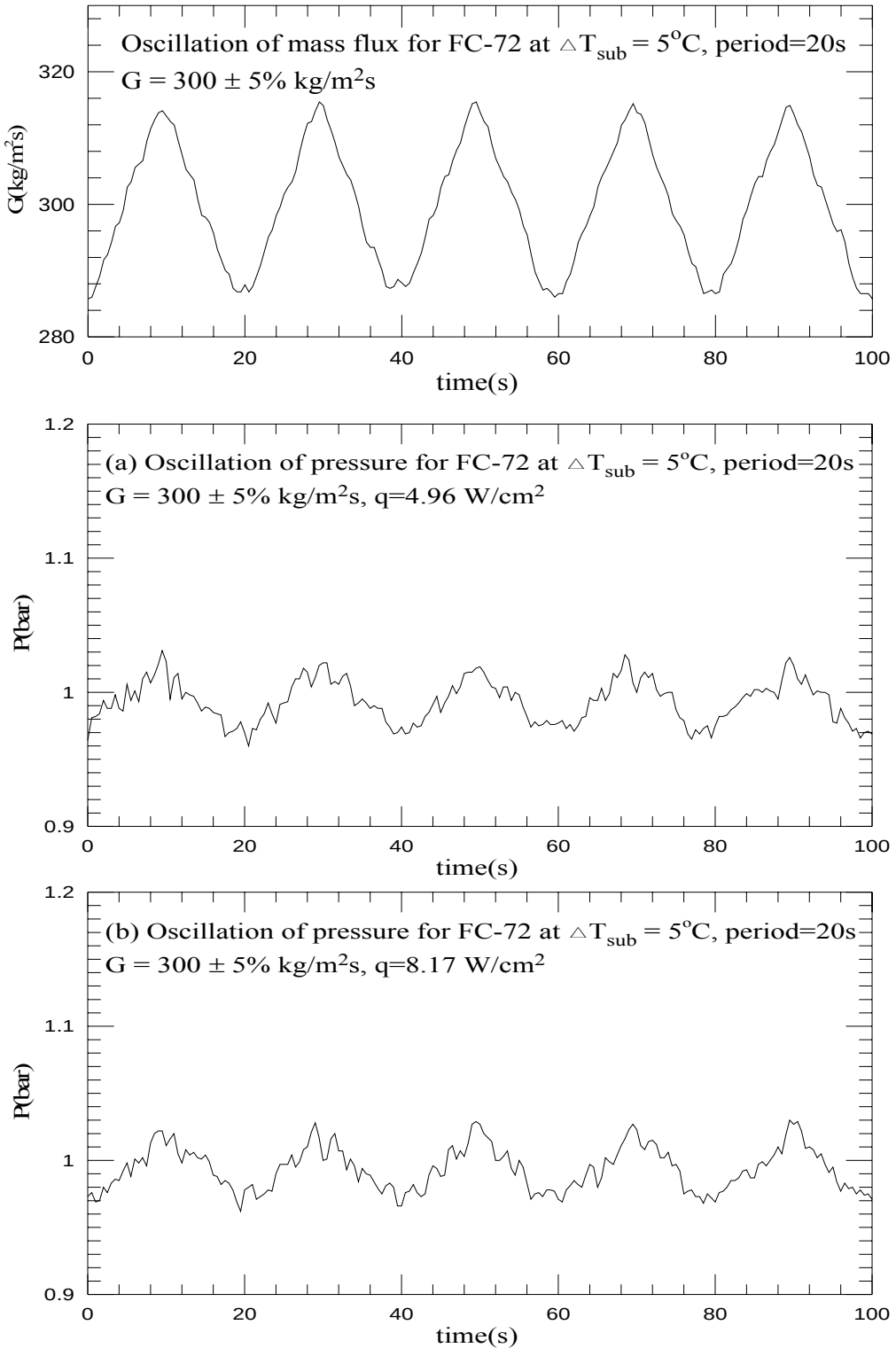

Fig.5.75 Time variations of coolant mass flux and inlet pressure in transient oscillatory subcooled flow boiling for various imposed heat fluxes at (a) q=4.96 W/cm^2 and (b) q=8.17 W/cm^2 for G=300±5% kg/m^{2}s with t_p=20 sec.

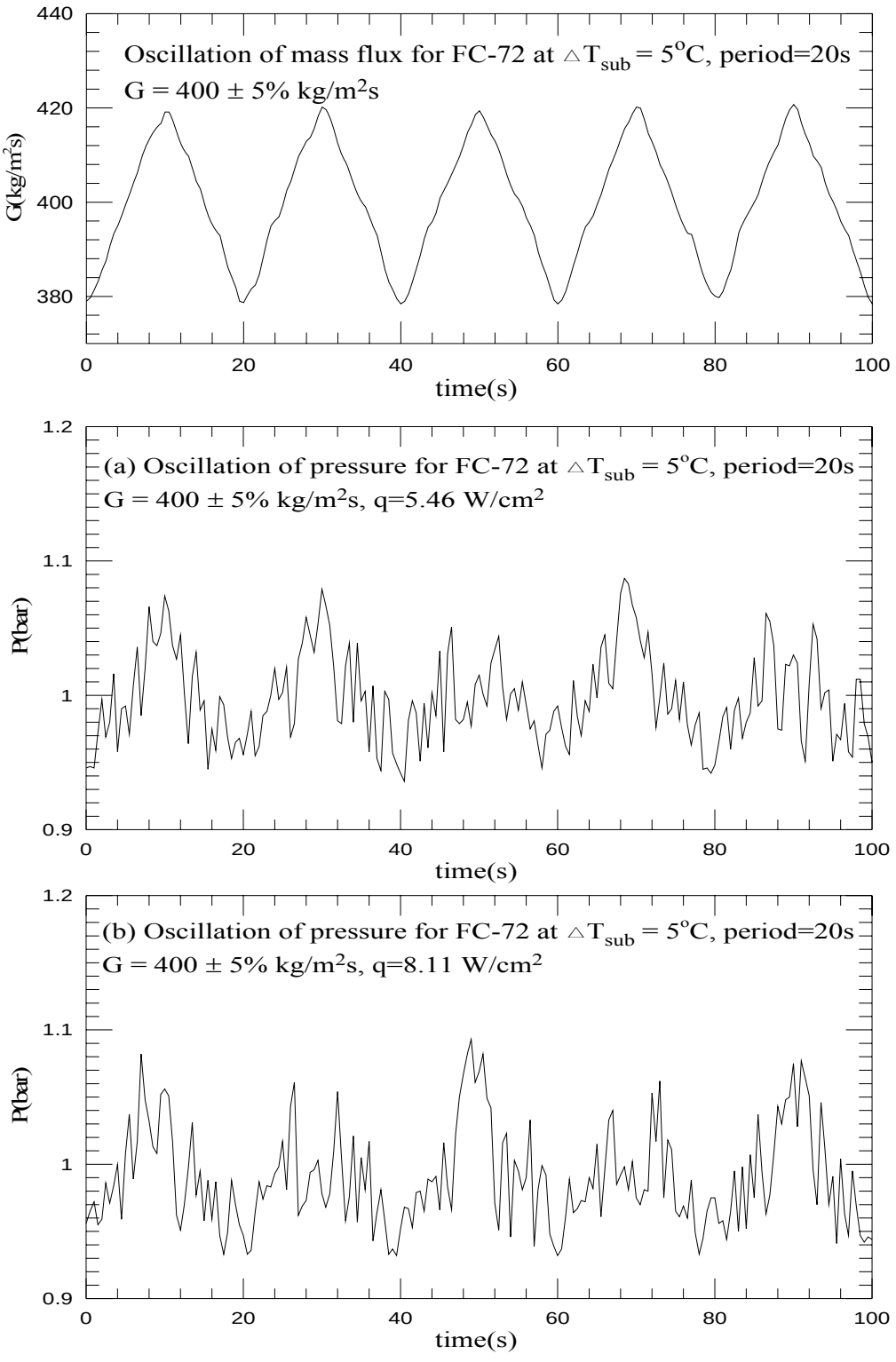

Fig.5.76 Time variations of coolant mass flux and inlet pressure in transient oscillatory subcooled flow boiling for various imposed heat fluxes at (a) q=5.46 W/cm^2 and (b) q=8.11 W/cm^2 for G=400±5% kg/m^{2}s with t_p=20 sec.

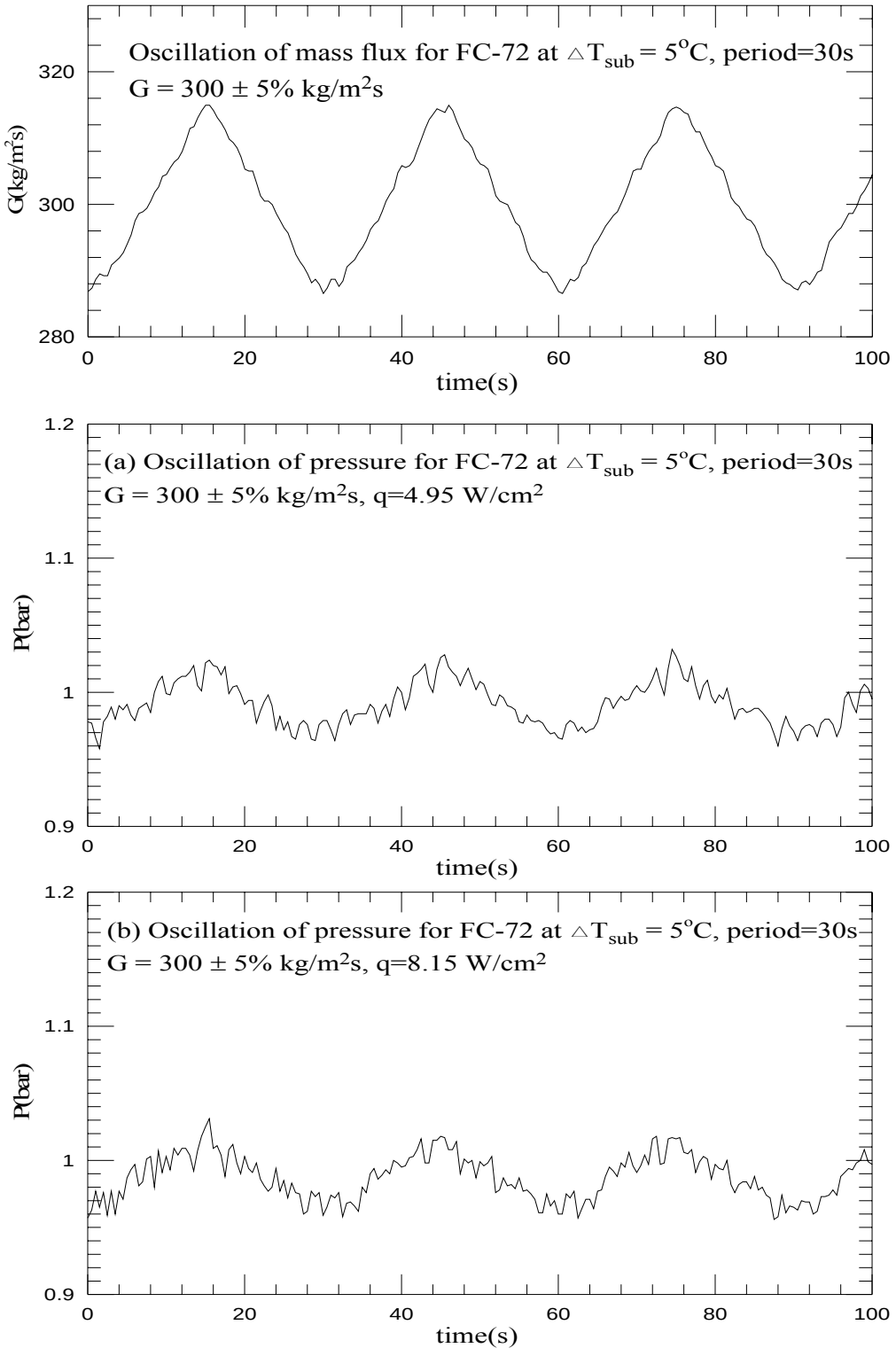

Fig.5.77 Time variations of coolant mass flux and inlet pressure in transient oscillatory subcooled flow boiling for various imposed heat fluxes at (a) q=4.95 W/cm^2 and (b) q=8.15 W/cm^2 for G=300±5% kg/m^{2}s with t_p=30 sec.

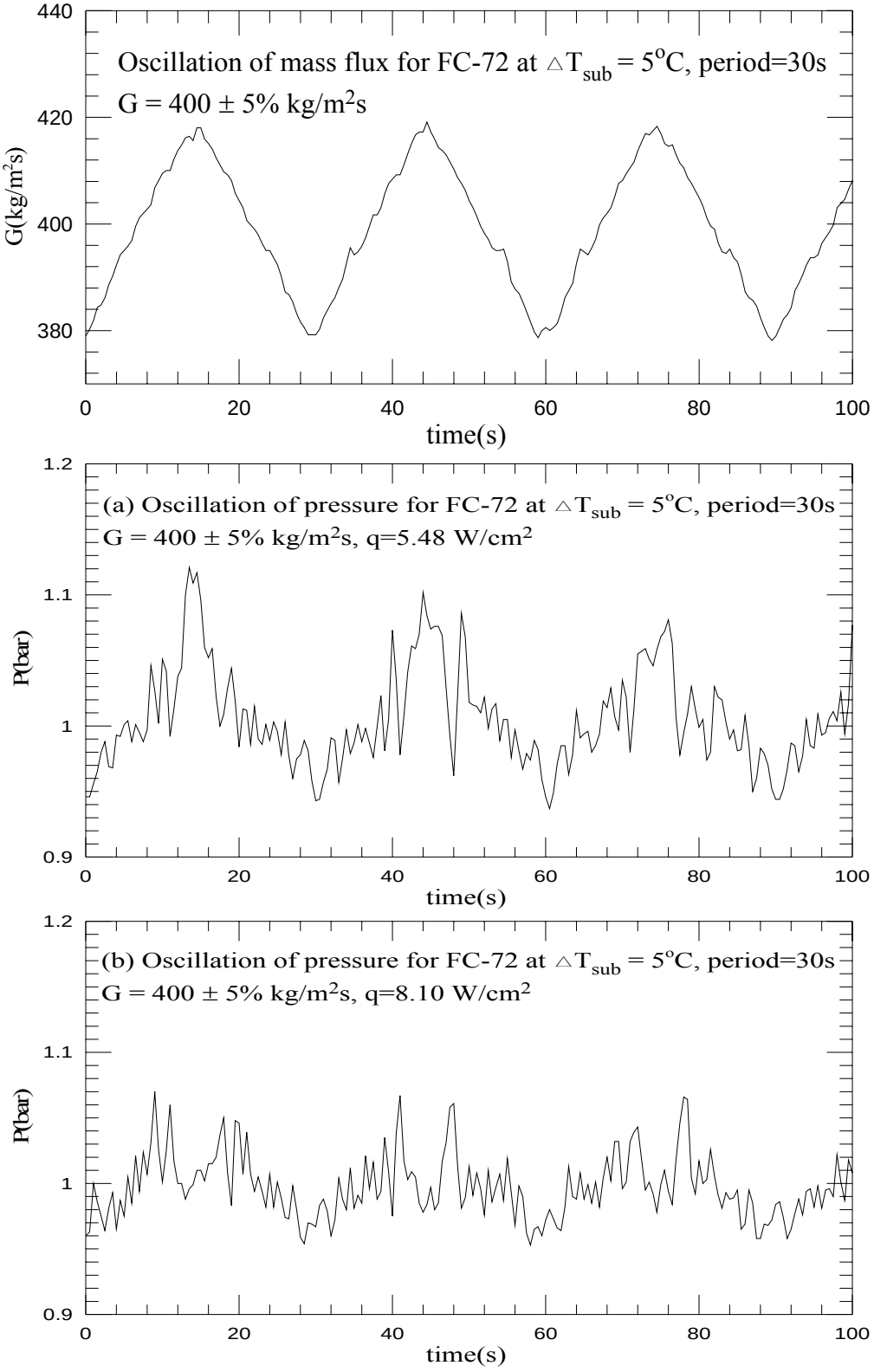

Fig.5.78 Time variations of coolant mass flux and inlet pressure in transient oscillatory subcooled flow boiling for various imposed heat fluxes at (a) q=5.48 W/cm^2 and (b) q=8.10 W/cm^2 for G=400±5% kg/m^{2}s with t_p=30 sec.

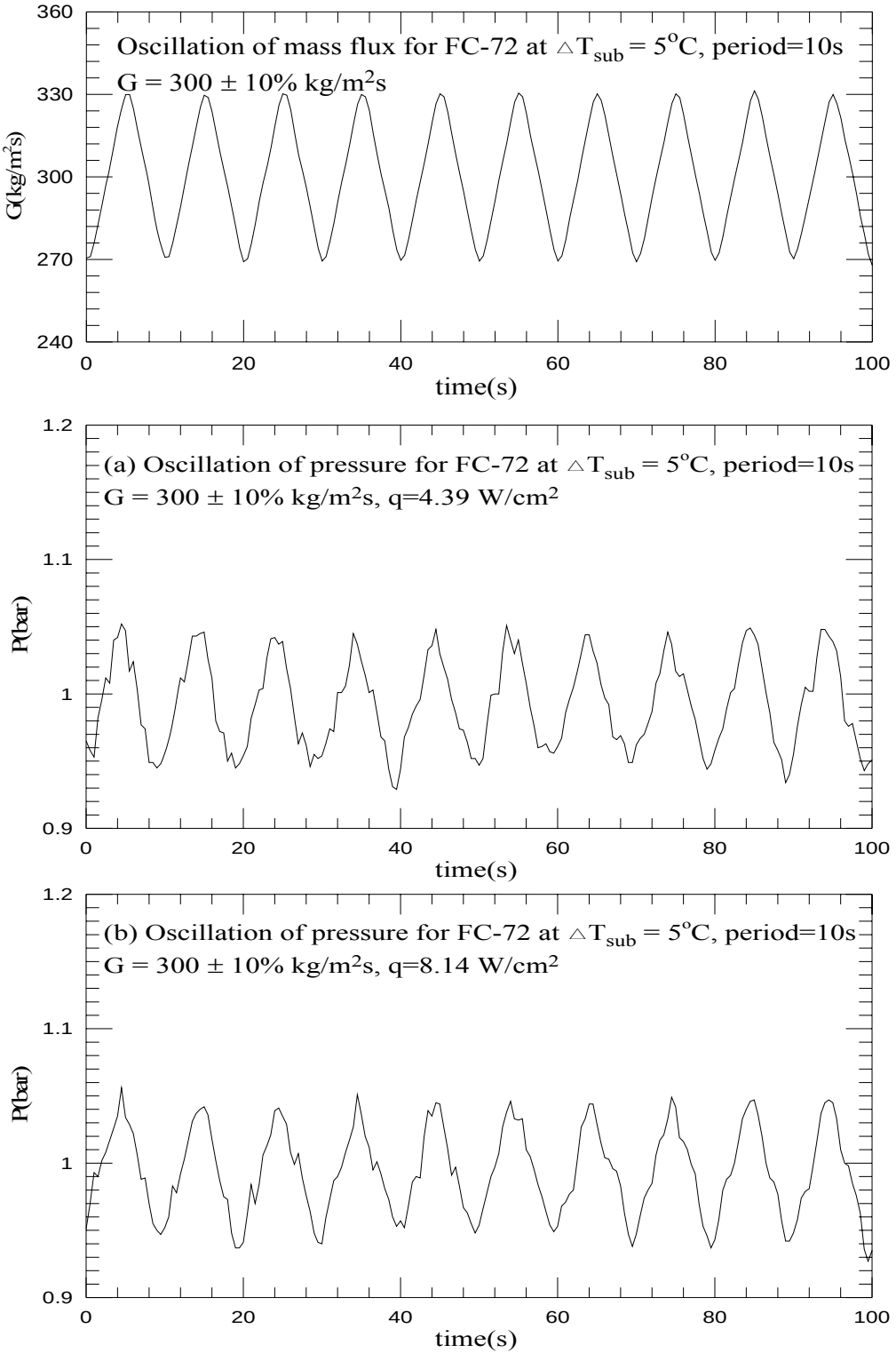

Fig.5.79 Time variations of coolant mass flux and inlet pressure in transient oscillatory subcooled flow boiling for various imposed heat fluxes at (a) q=4.39 W/cm^2 and (b) q=8.14 W/cm^2 for G=300±10% kg/m^{2}s with t_p=10 sec.

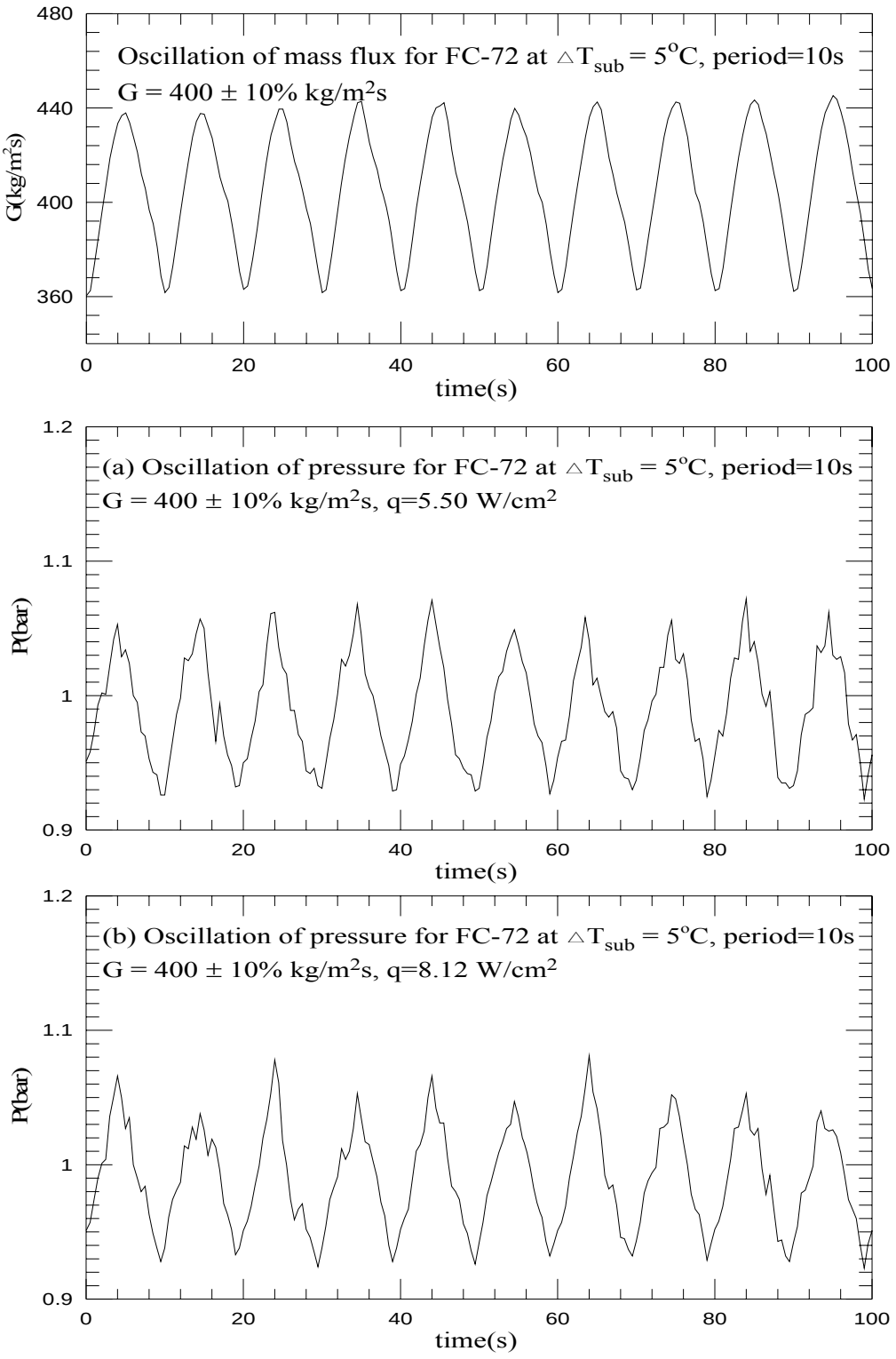

Fig.5.80 Time variations of coolant mass flux and inlet pressure in transient oscillatory subcooled flow boiling for various imposed heat fluxes at (a) q=5.50 W/cm^2 and (b) q=8.12 W/cm^2 for G=400±10% kg/m^{2}s with t_p=10 sec.

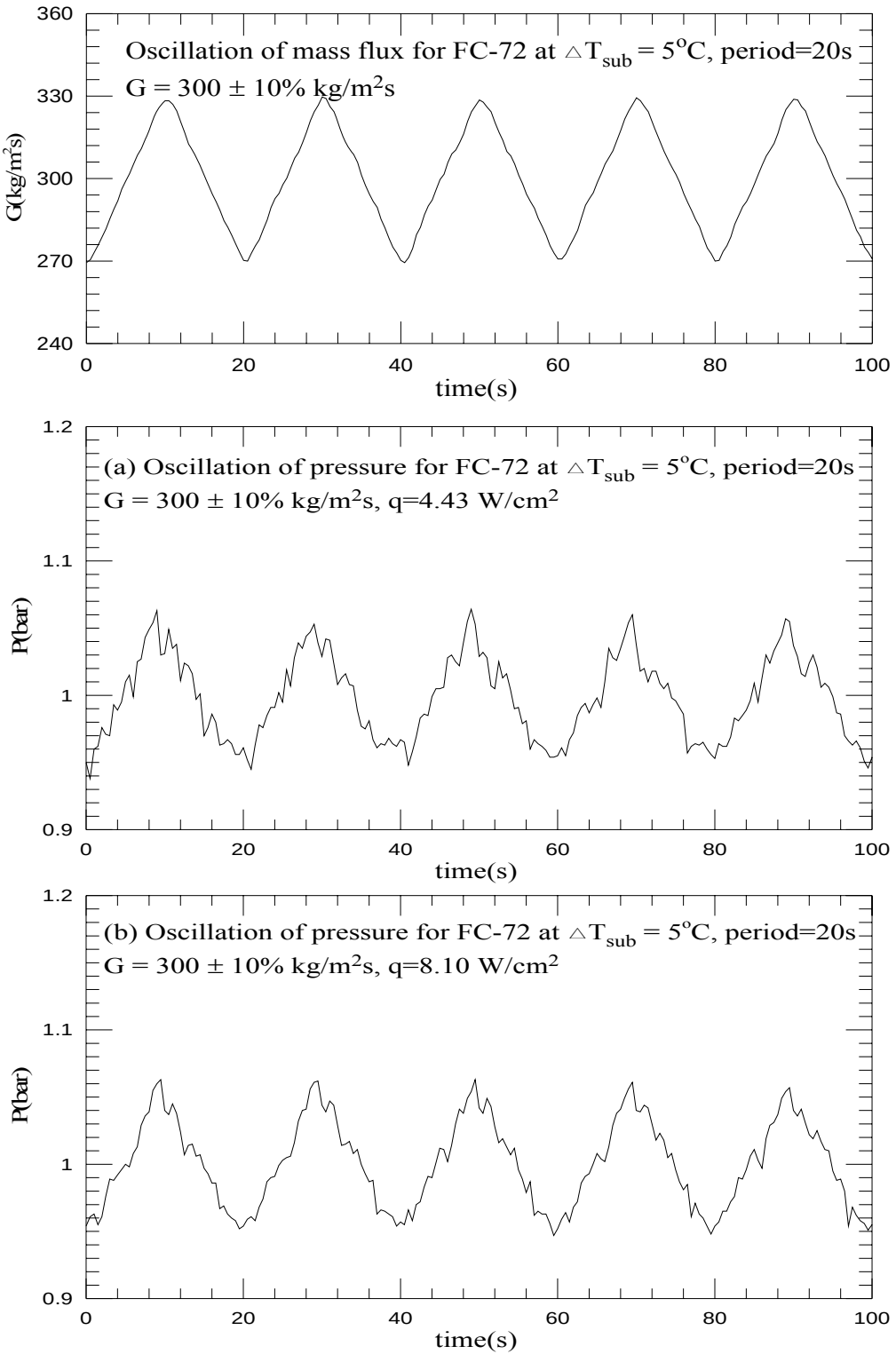

Fig.5.81 Time variations of coolant mass flux and inlet pressure in transient oscillatory subcooled flow boiling for various imposed heat fluxes at (a) q=4.43 W/cm^2 and (b) q=8.10 W/cm^2 for G=300±10% kg/m^{2}s with t_p=20 sec.

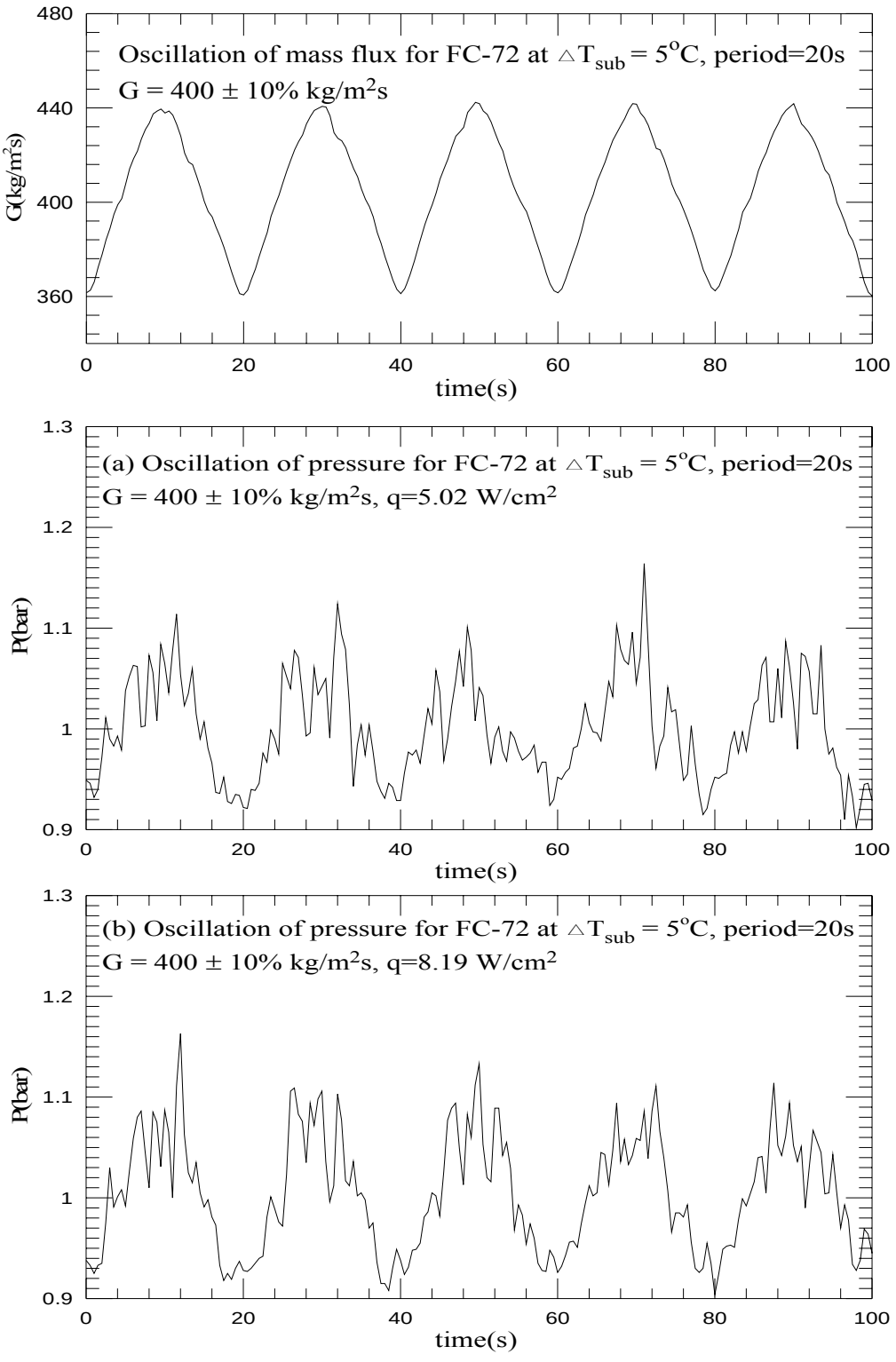

Fig.5.82 Time variations of coolant mass flux and inlet pressure in transient oscillatory subcooled flow boiling for various imposed heat fluxes at (a) q=5.02 W/cm^2 and (b) q=8.19 W/cm^2 for G=400±10% kg/m^{2}s with t_p=20 sec.

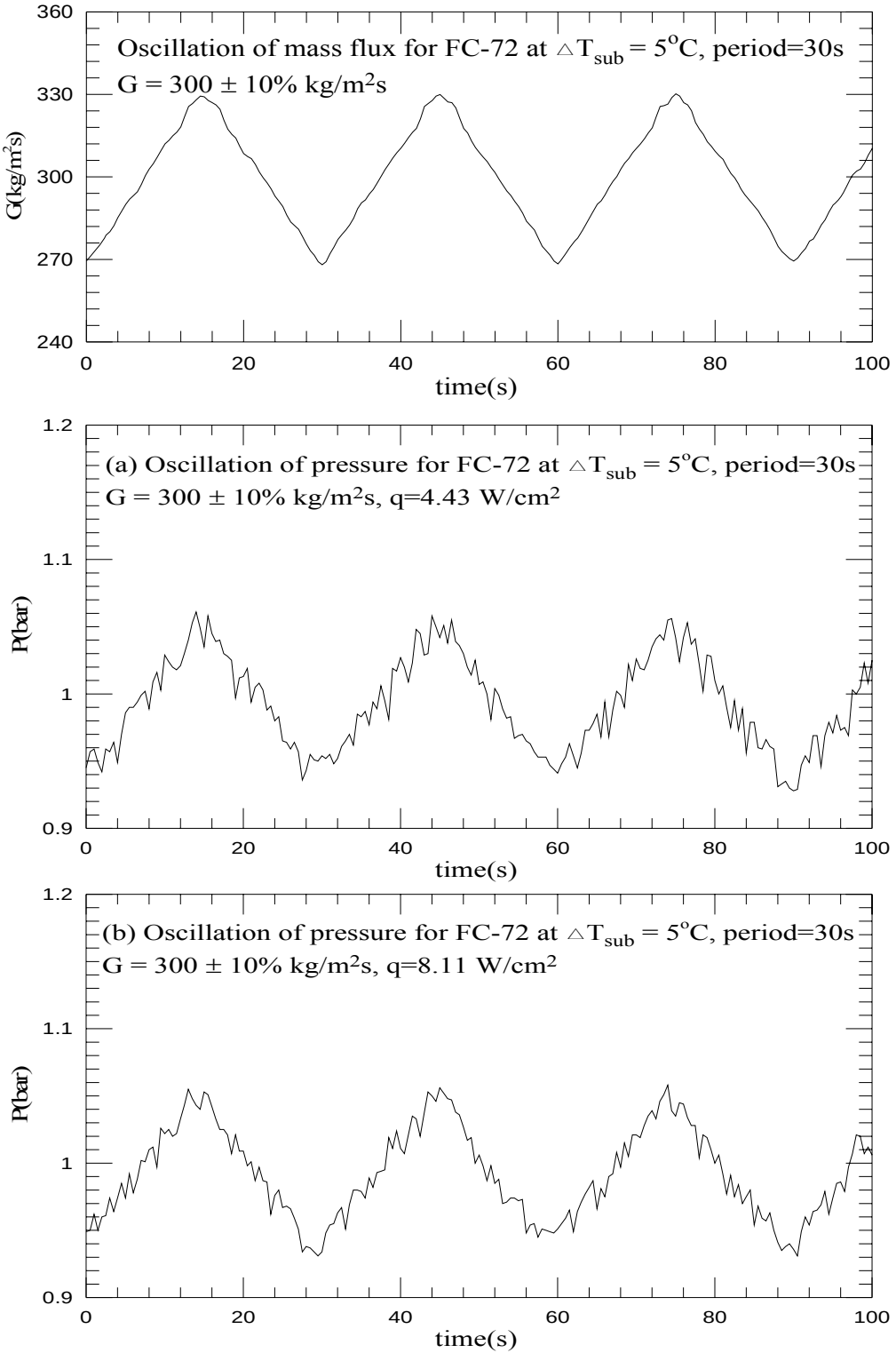

Fig.5.83 Time variations of coolant mass flux and inlet pressure in transient oscillatory subcooled flow boiling for various imposed heat fluxes at (a) q=4.43 W/cm^2 and (b) q=8.11 W/cm^2 for G=300±10% kg/m^{2}s with t_p=30 sec.

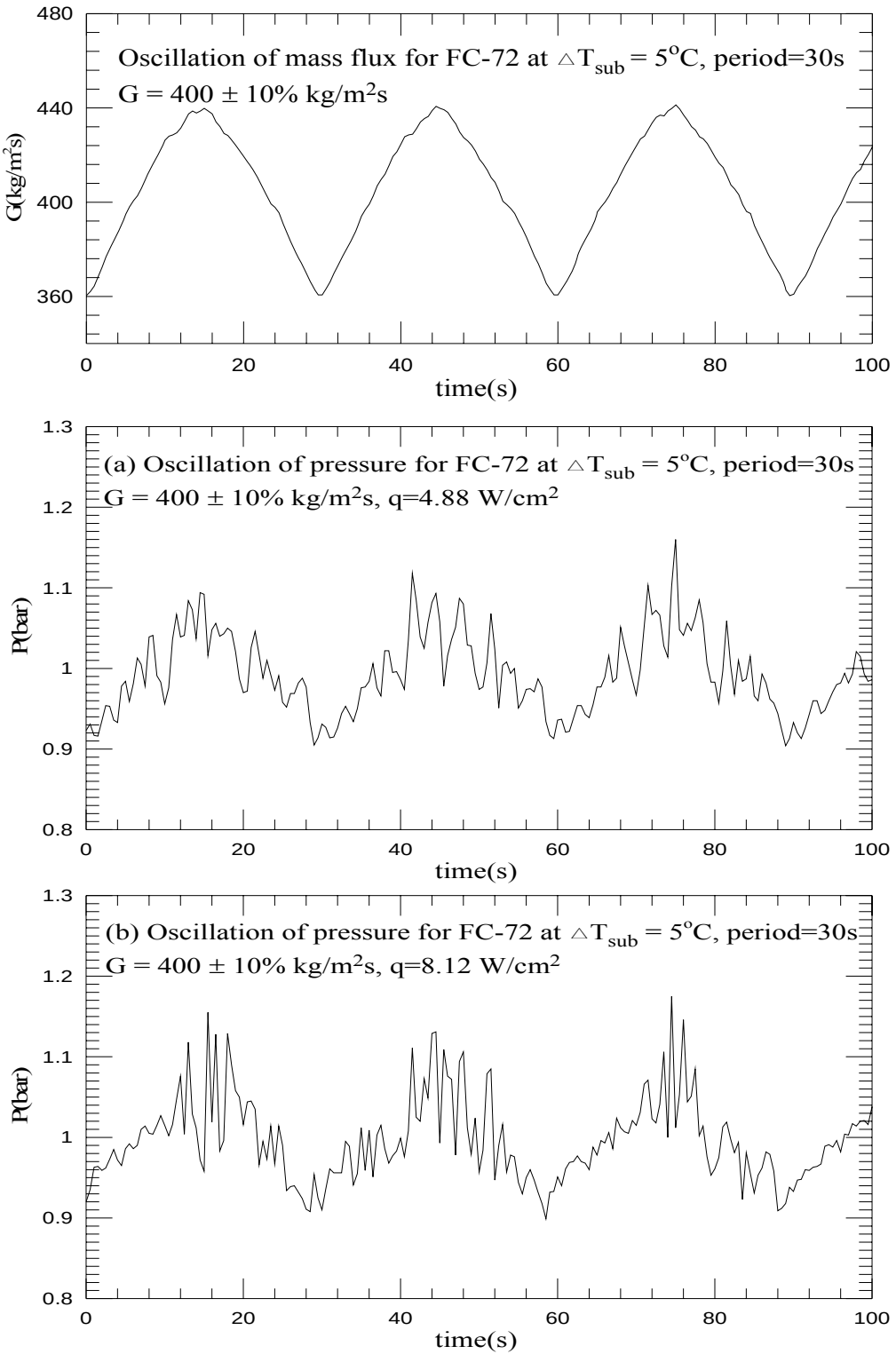

Fig.5.84 Time variations of coolant mass flux and inlet pressure in transient oscillatory subcooled flow boiling for various imposed heat fluxes at (a) q=4.88 W/cm^2 and (b) q=8.12 W/cm^2 for G=400±10% kg/m^{2}s with t_p=30 sec.

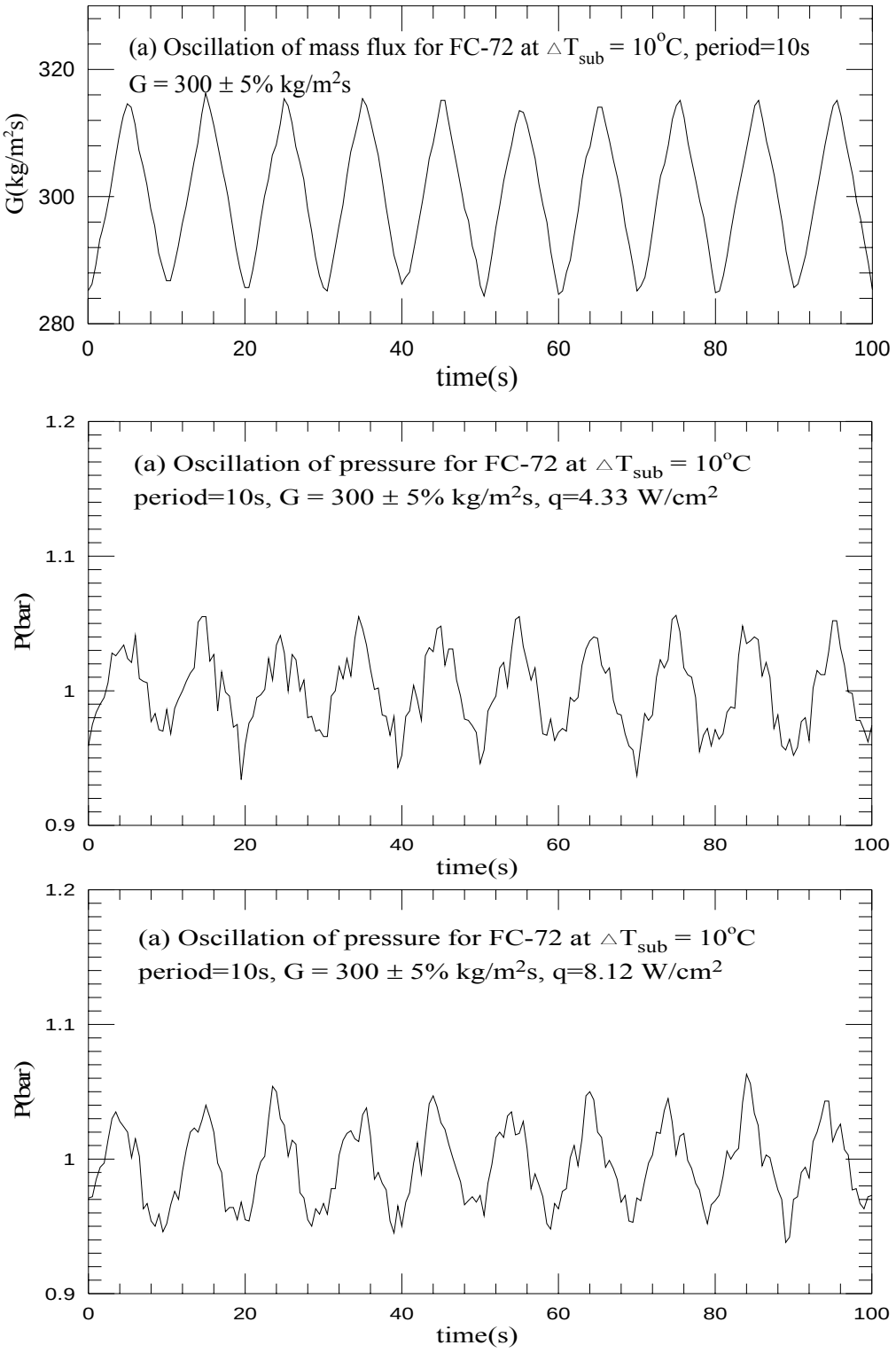

Fig.5.85 Time variations of coolant mass flux and inlet pressure in transient oscillatory subcooled flow boiling for various imposed heat fluxes at (a) q=4.33 W/cm^2 and (b) q=8.12 W/cm^2 for G=300±5% kg/m^{2}s with t_p=10 sec.

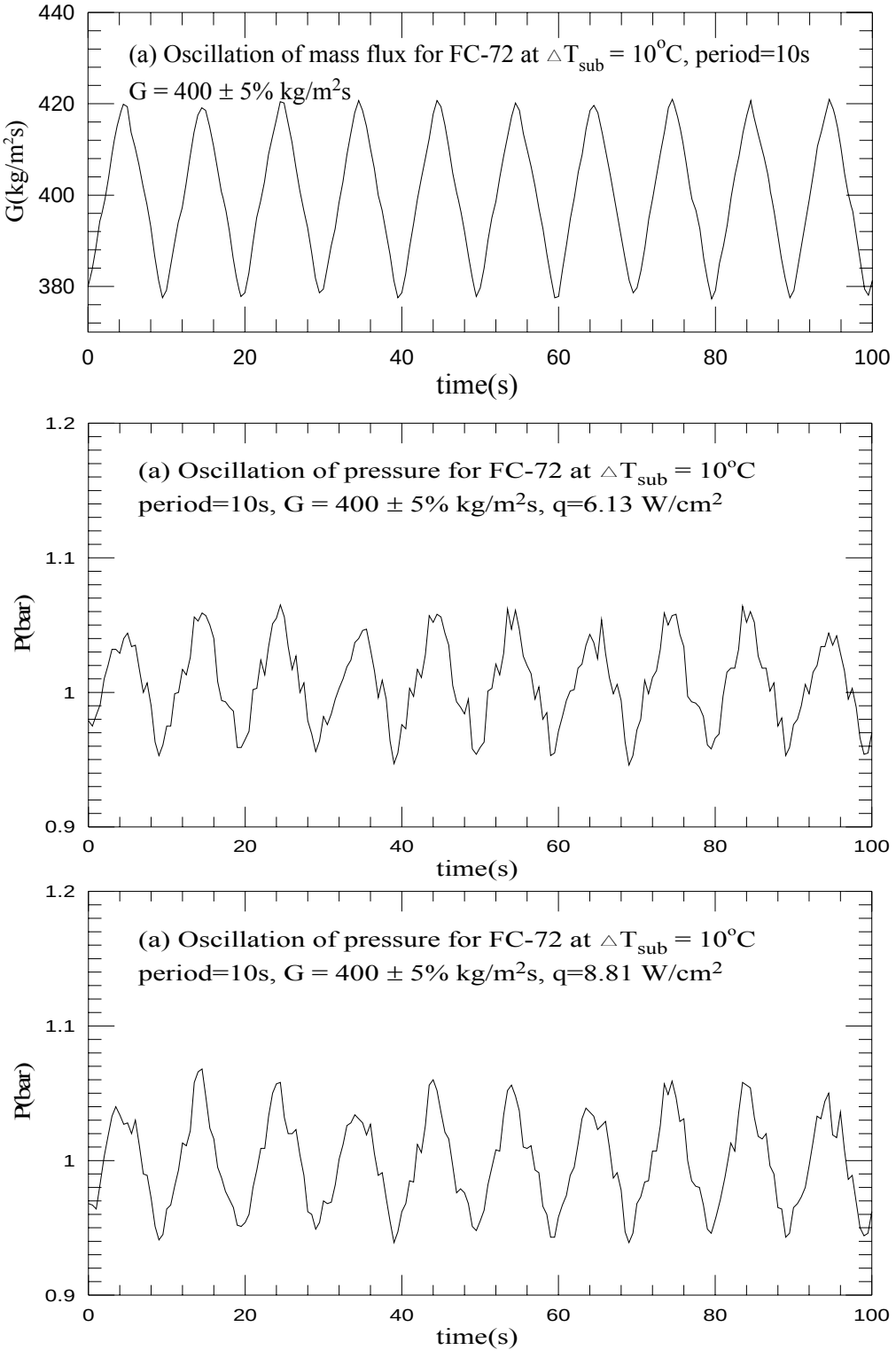

Fig.5.86 Time variations of coolant mass flux and inlet pressure in transient oscillatory subcooled flow boiling for various imposed heat fluxes at (a) q=6.13 W/cm^2 and (b) q=8.81 W/cm^2 for G=400±5% kg/m^{2}s with t_p=10 sec.

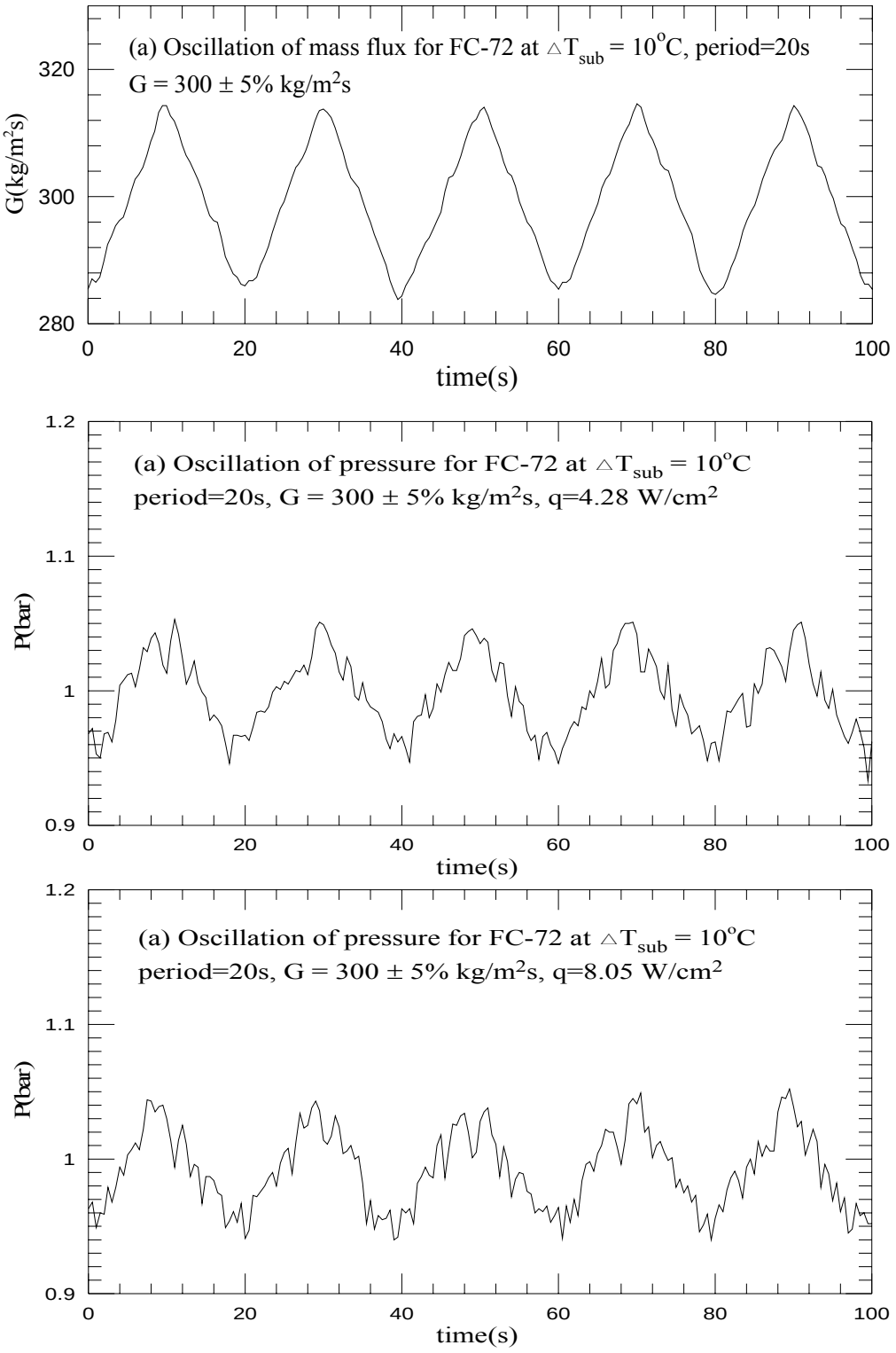

Fig.5.87 Time variations of coolant mass flux and inlet pressure in transient oscillatory subcooled flow boiling for various imposed heat fluxes at (a) q=4.28 W/cm^2 and (b) q=8.05 W/cm^2 for G=300±5% kg/m^{2}s with t_p=20 sec.

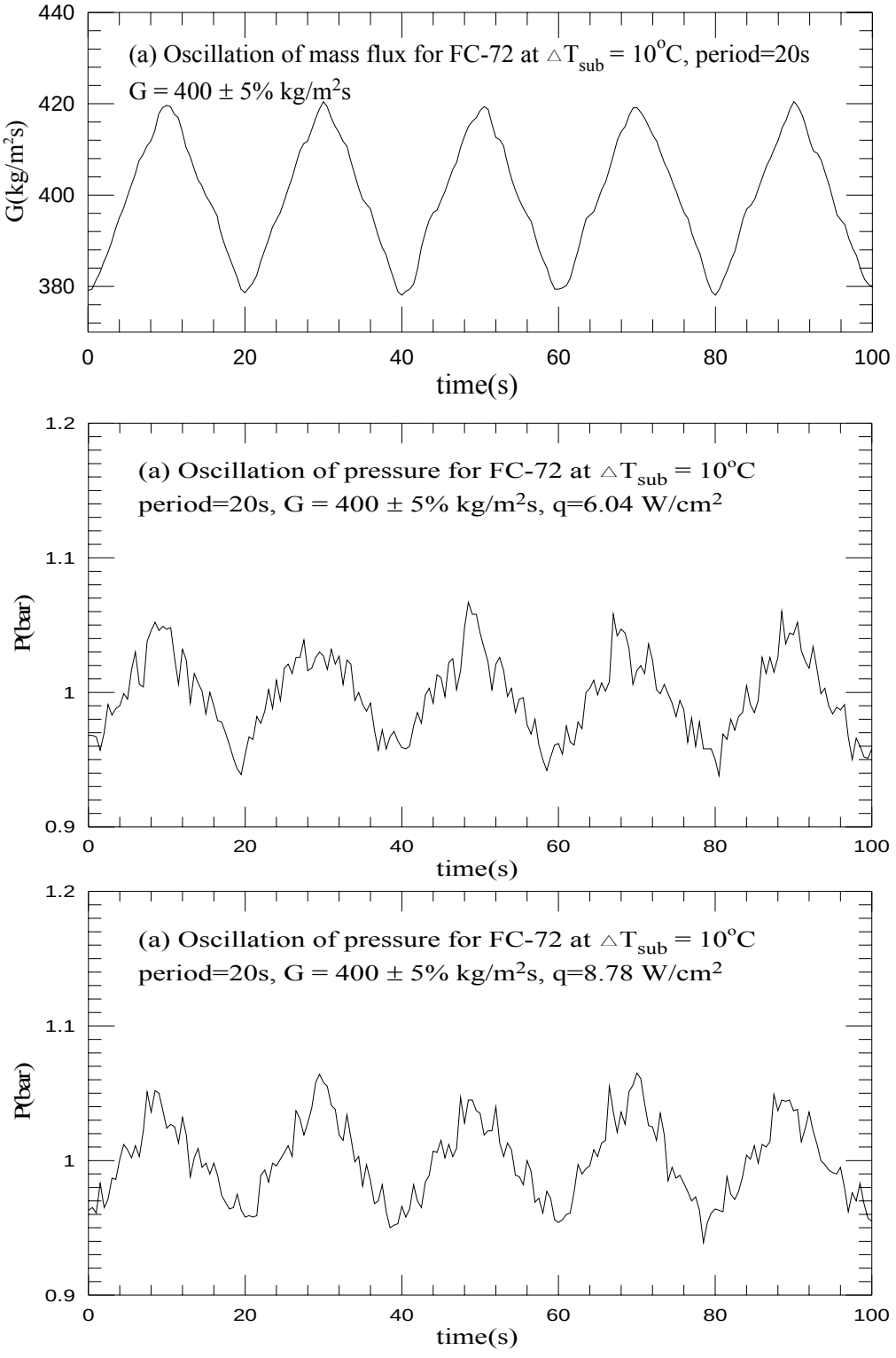

Fig.5.88 Time variations of coolant mass flux and inlet pressure in transient oscillatory subcooled flow boiling for various imposed heat fluxes at (a) q=6.04 W/cm^2 and (b) q=8.78 W/cm^2 for G=400±5% kg/m^{2}s with t_p=20 sec.

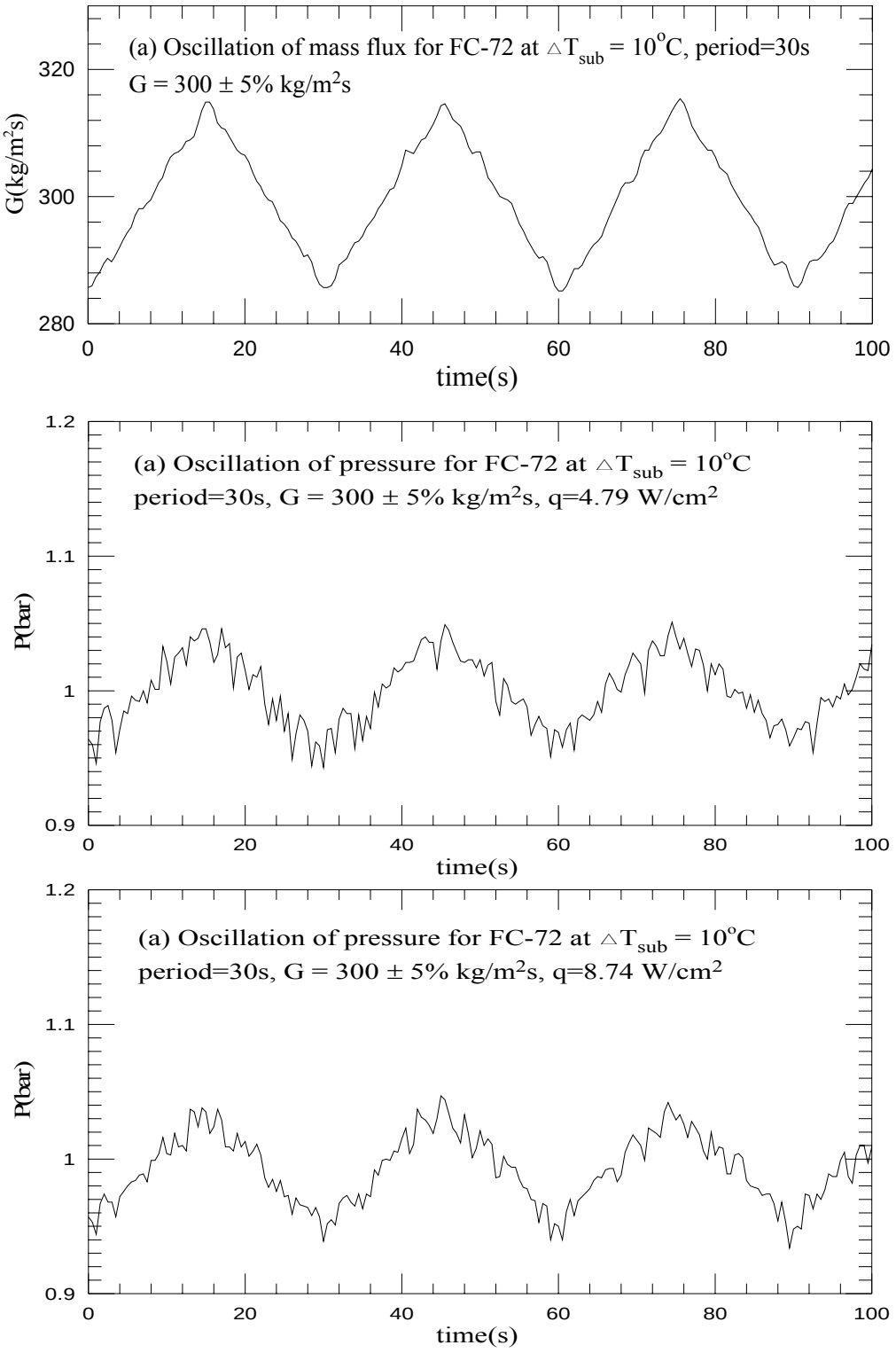

Fig.5.89 Time variations of coolant mass flux and inlet pressure in transient oscillatory subcooled flow boiling for various imposed heat fluxes at (a) q=4.79 W/cm^2 and (b) q=8.74 W/cm^2 for G=300±5% kg/m^{2}s with t_p=30 sec.

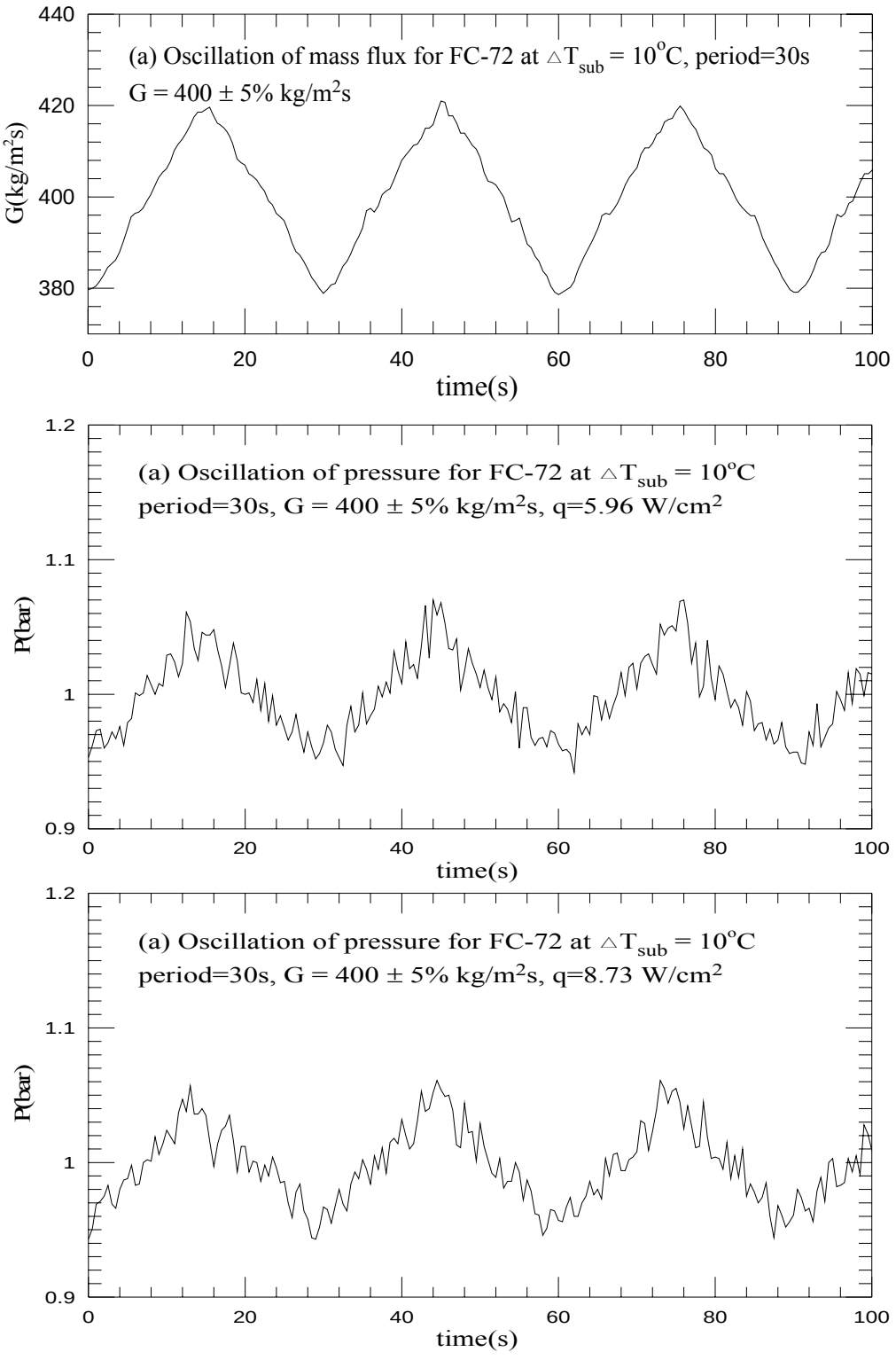

Fig.5.90 Time variations of coolant mass flux and inlet pressure in transient oscillatory subcooled flow boiling for various imposed heat fluxes at (a) q=5.96 W/cm^2 and (b) q=8.73 W/cm^2 for G=400±5% kg/m^{2}s with t_p=30 sec.

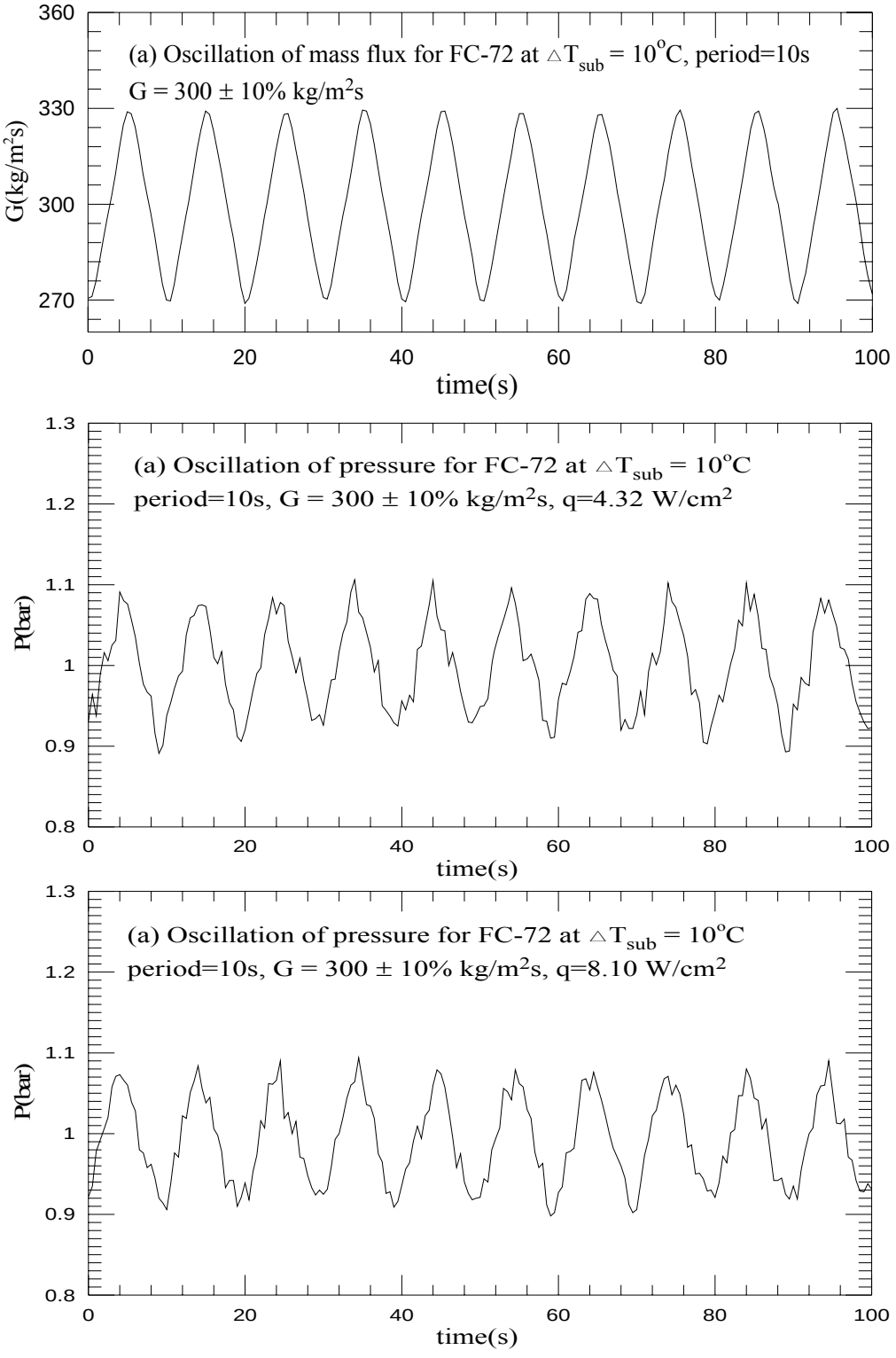

Fig.5.91 Time variations of coolant mass flux and inlet pressure in transient oscillatory subcooled flow boiling for various imposed heat fluxes at (a) q=4.32 W/cm^2 and (b) q=8.10 W/cm^2 for G=300±10% kg/m^{2}s with t_p=10 sec.

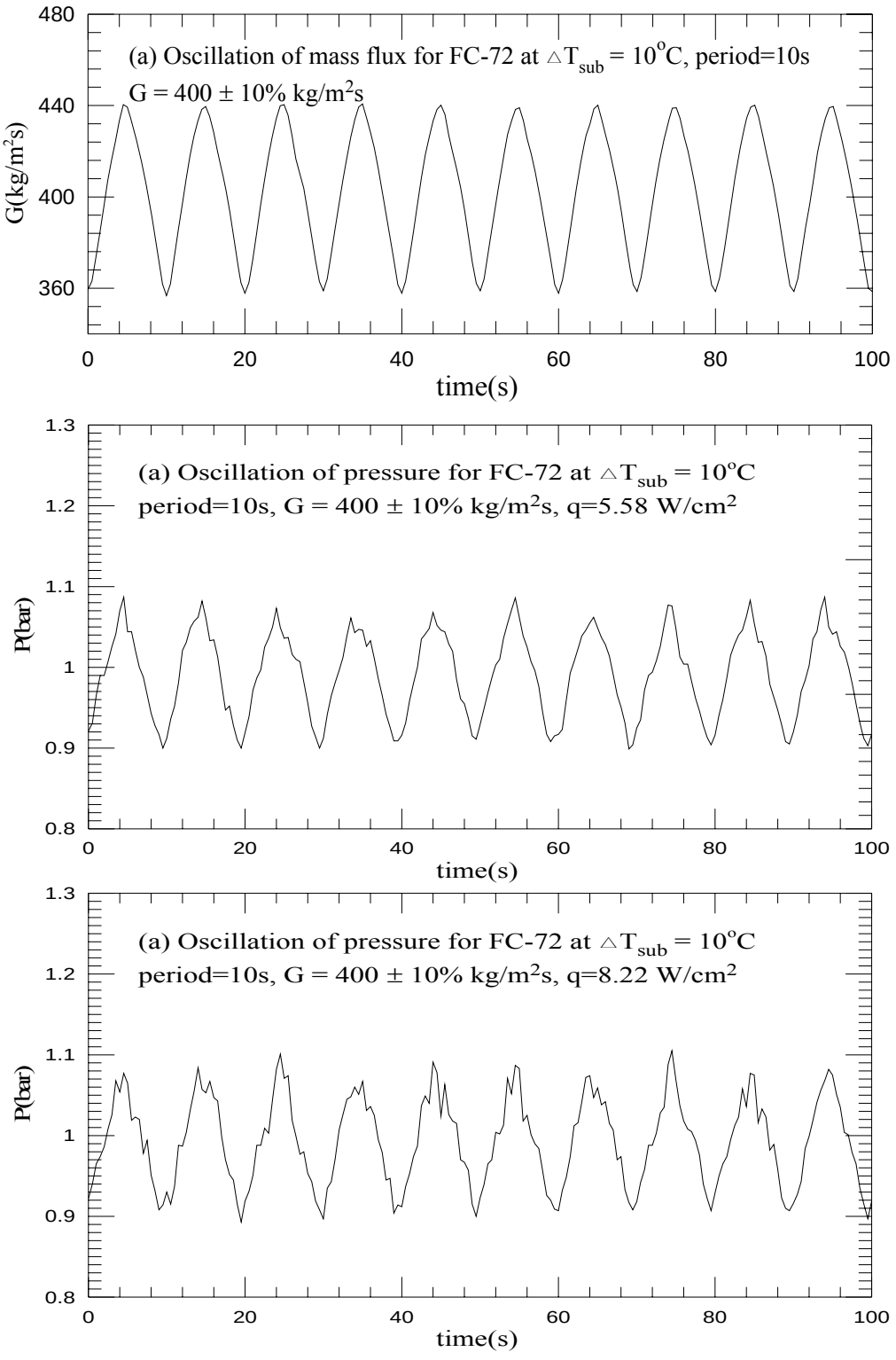

Fig.5.92 Time variations of coolant mass flux and inlet pressure in transient oscillatory subcooled flow boiling for various imposed heat fluxes at (a) q=5.58 W/cm^2 and (b) q=8.22 W/cm^2 for G=400±10% kg/m^{2}s with t_p=10 sec.

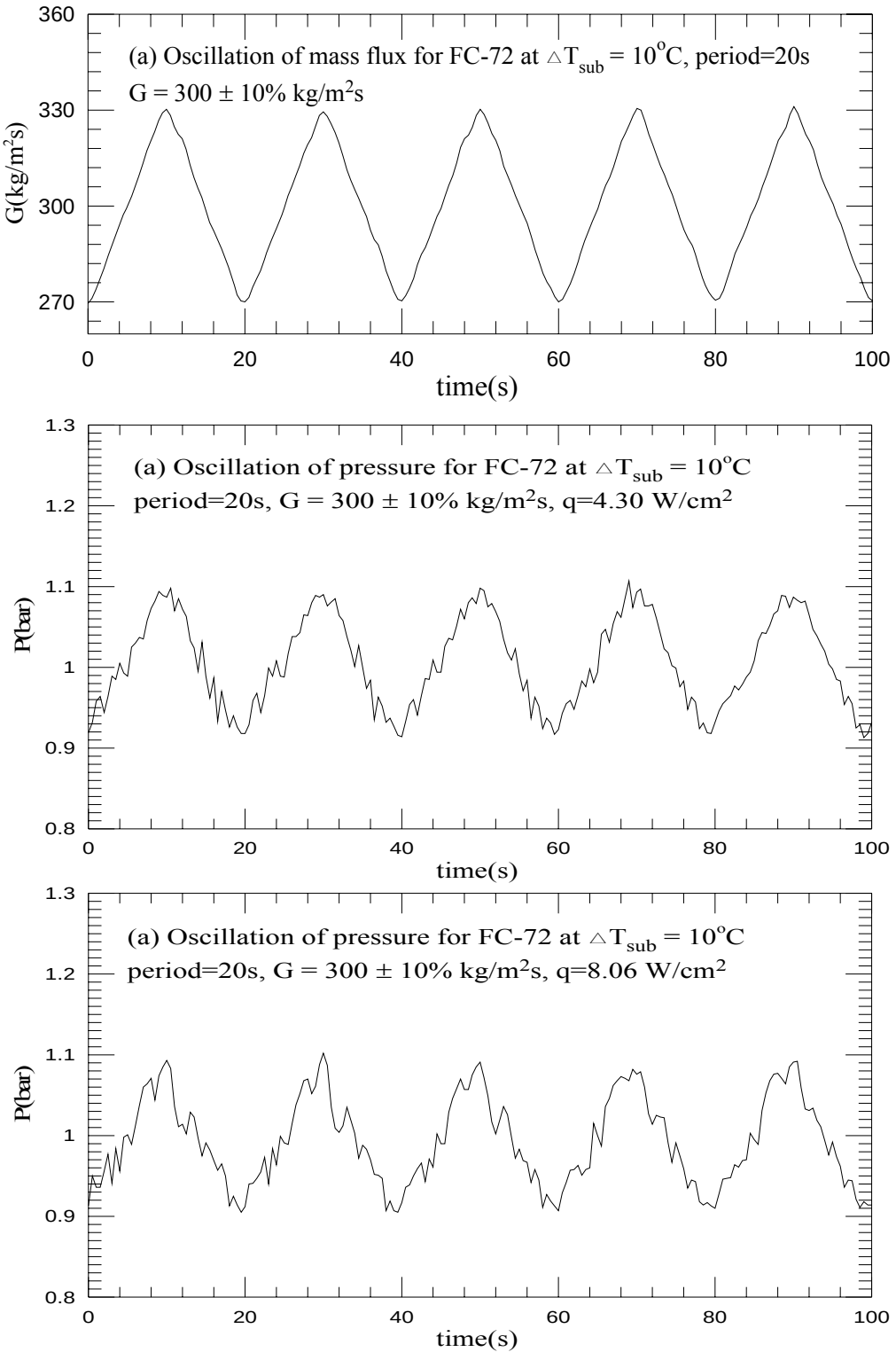

Fig.5.93 Time variations of coolant mass flux and inlet pressure in transient oscillatory subcooled flow boiling for various imposed heat fluxes at (a) q=4.30 W/cm^2 and (b) q=8.06 W/cm^2 for G=300±10% kg/m^{2}s with t_p=20 sec.

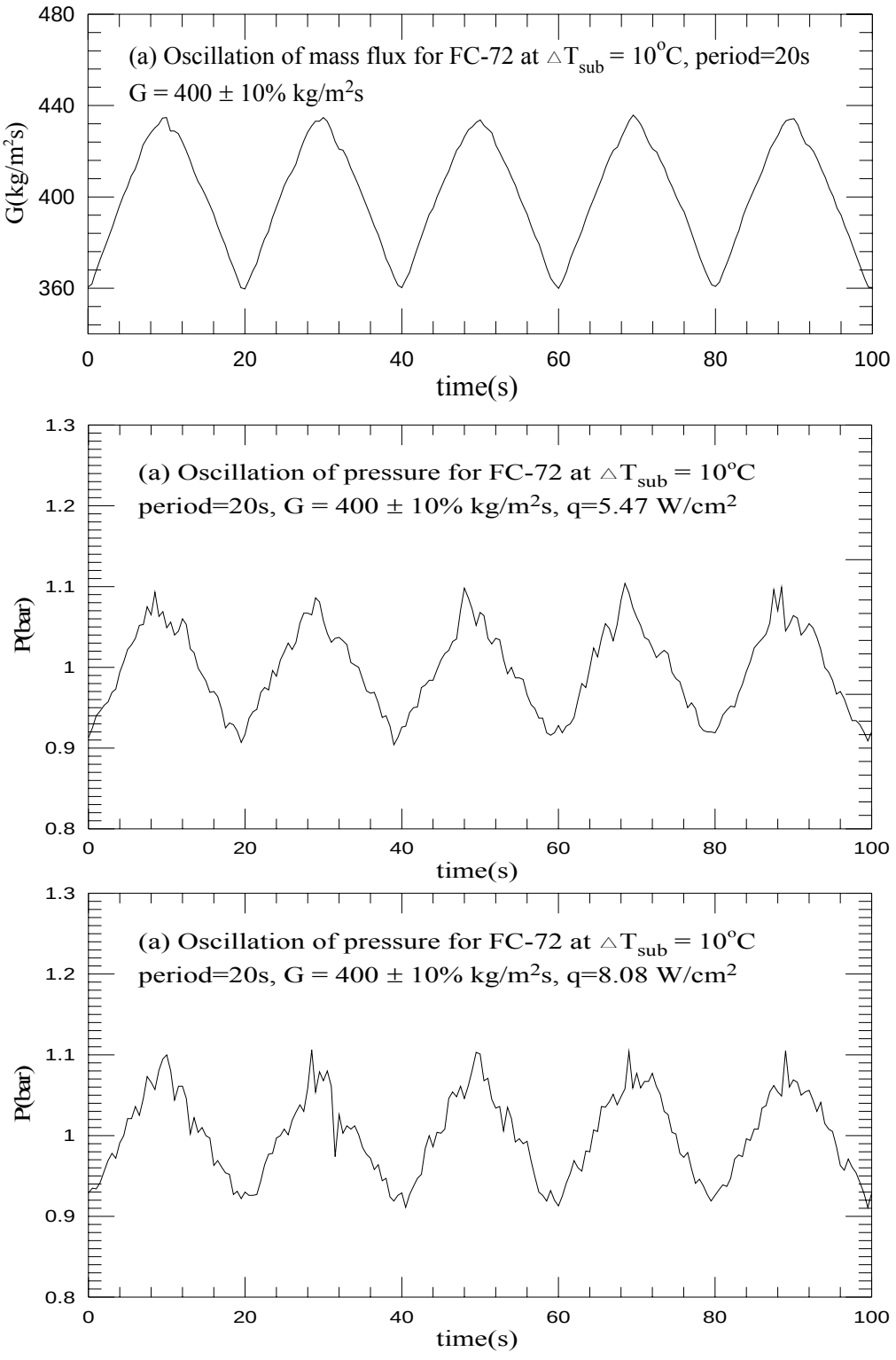

Fig.5.94 Time variations of coolant mass flux and inlet pressure in transient oscillatory subcooled flow boiling for various imposed heat fluxes at (a) q=5.47 W/cm^2 and (b) q=8.08 W/cm^2 for G=400±10% kg/m^{2}s with t_p=20 sec.

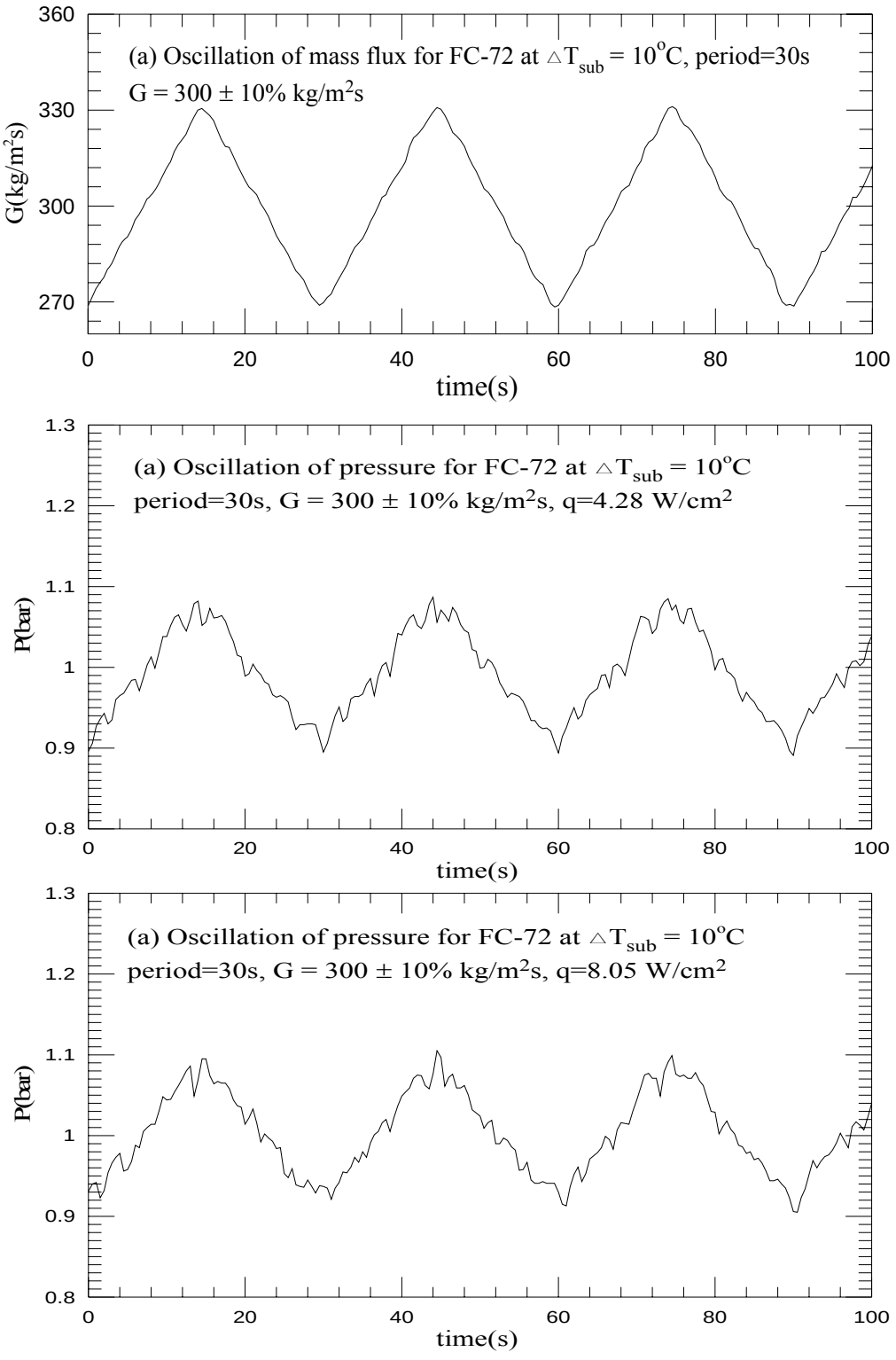

Fig.5.95 Time variations of coolant mass flux and inlet pressure in transient oscillatory subcooled flow boiling for various imposed heat fluxes at (a) q=4.28 W/cm^2 and (b) q=8.05 W/cm^2 for G=300±10% kg/m^{2}s with t_p=30 sec.

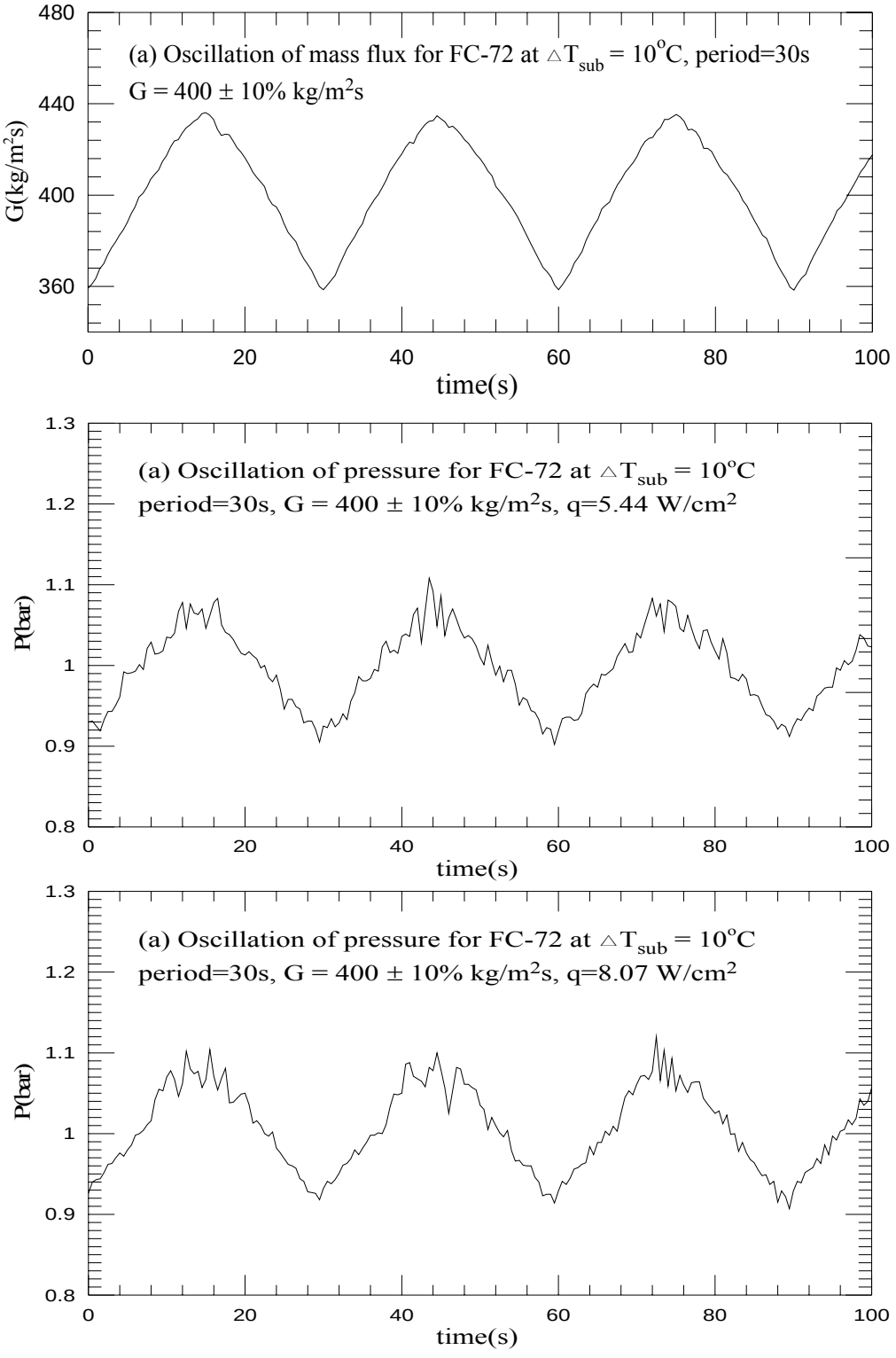

Fig.5.96 Time variations of coolant mass flux and inlet pressure in transient oscillatory subcooled flow boiling for various imposed heat fluxes at (a) q=5.44 W/cm^2 and (b) q=8.07 W/cm^2 for G=400±10% kg/m^{2}s with t_p=30 sec.

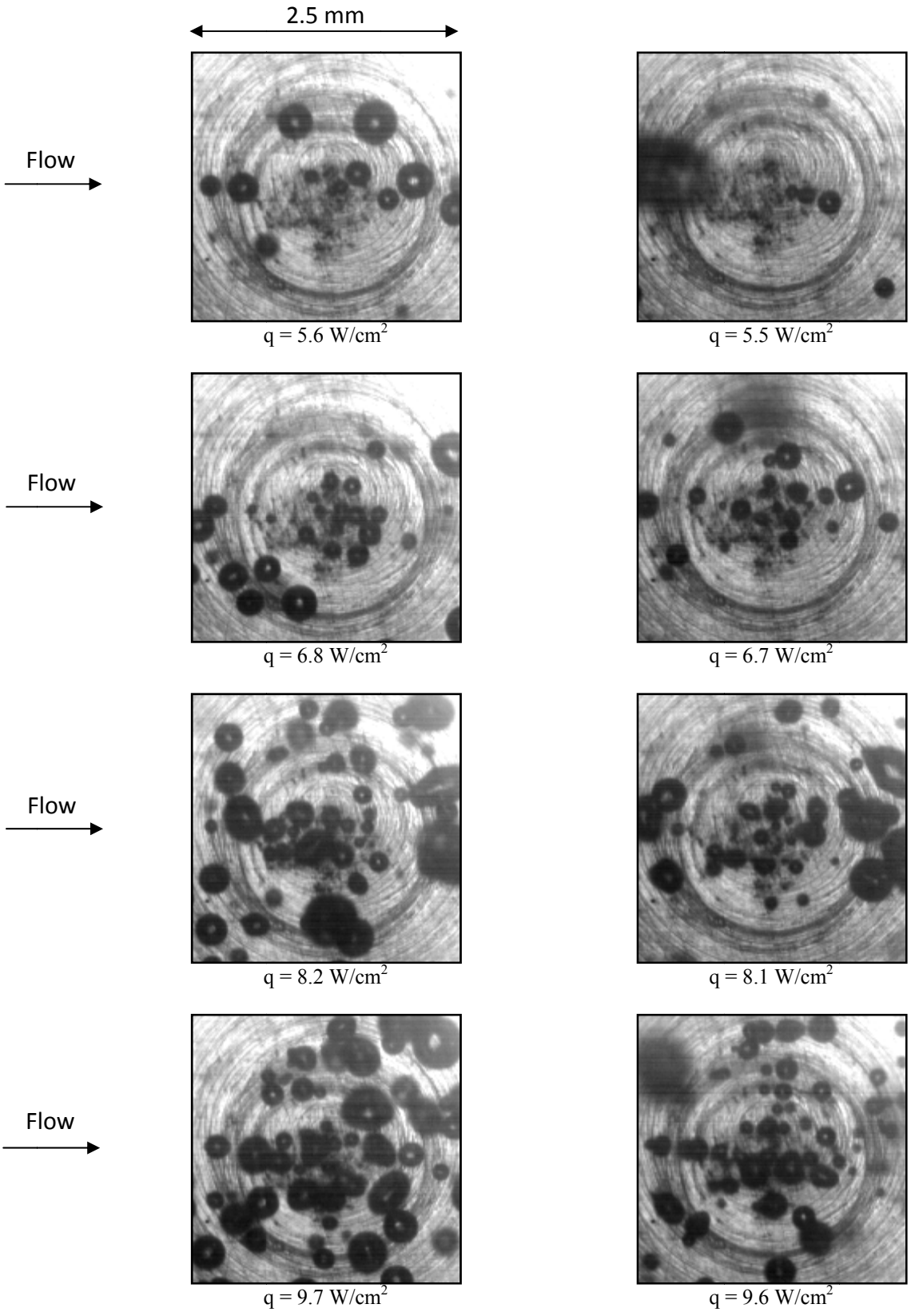

(a) G = 300 kg/m^{2}s (b) G = 400 kg/m^{2}s

Fig.5.97 Photos of stable subcooled boiling flow at certain time instants for various imposed heat fluxes at ΔT_{sub}= 5^{o}C for (a) G =300 kg/m^{2}s and (b) G =400 kg/m^{2}s.

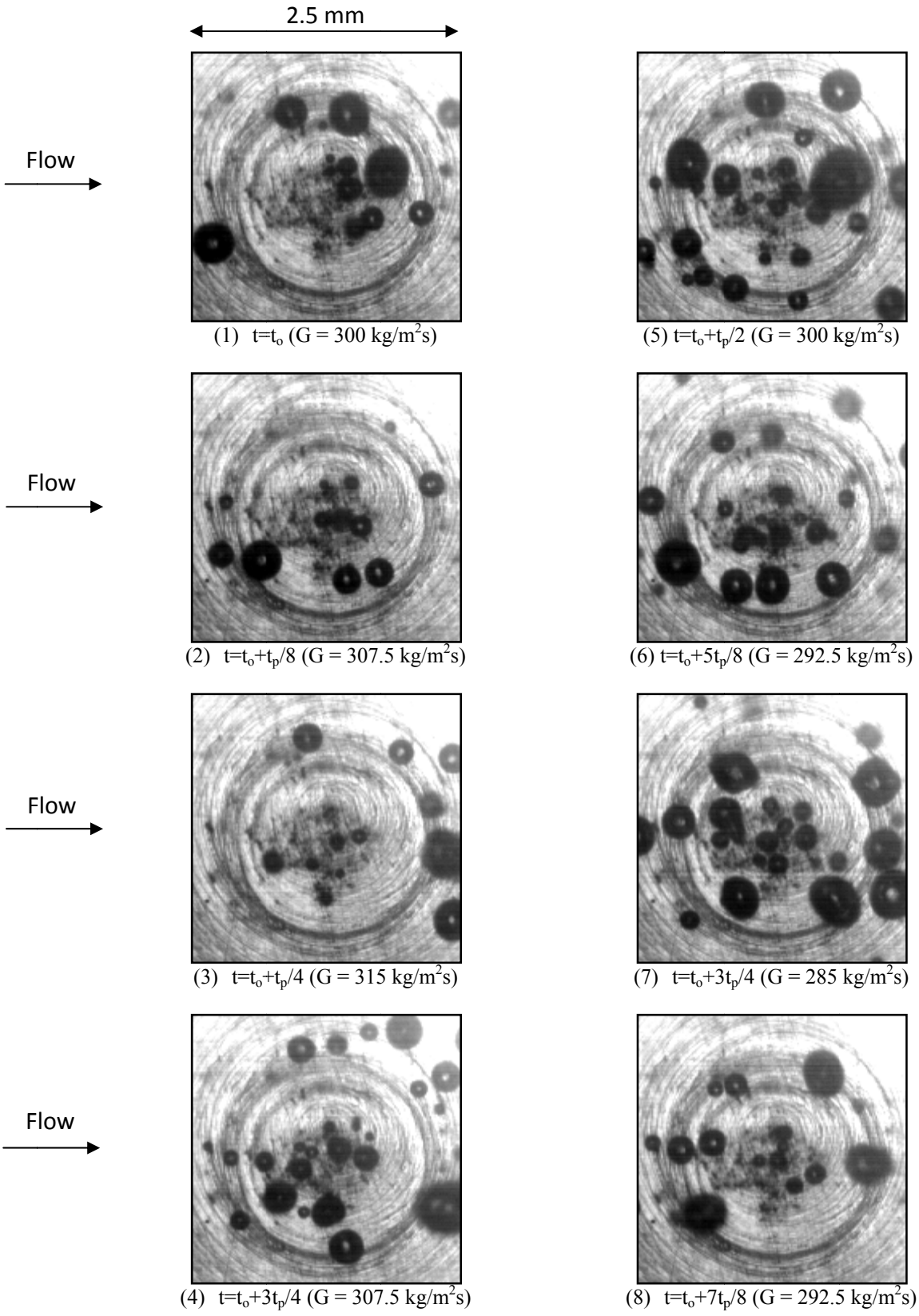

Fig.5.98 Photos of transient oscillatory subcooled flow boiling flow at certain time instants for various imposed mass fluxes for q=6.2 W/cm^2 and ΔT_{sub}= 5^{o}C at G=300±5% kg/m^{2}s with oscillation t_p=10s.

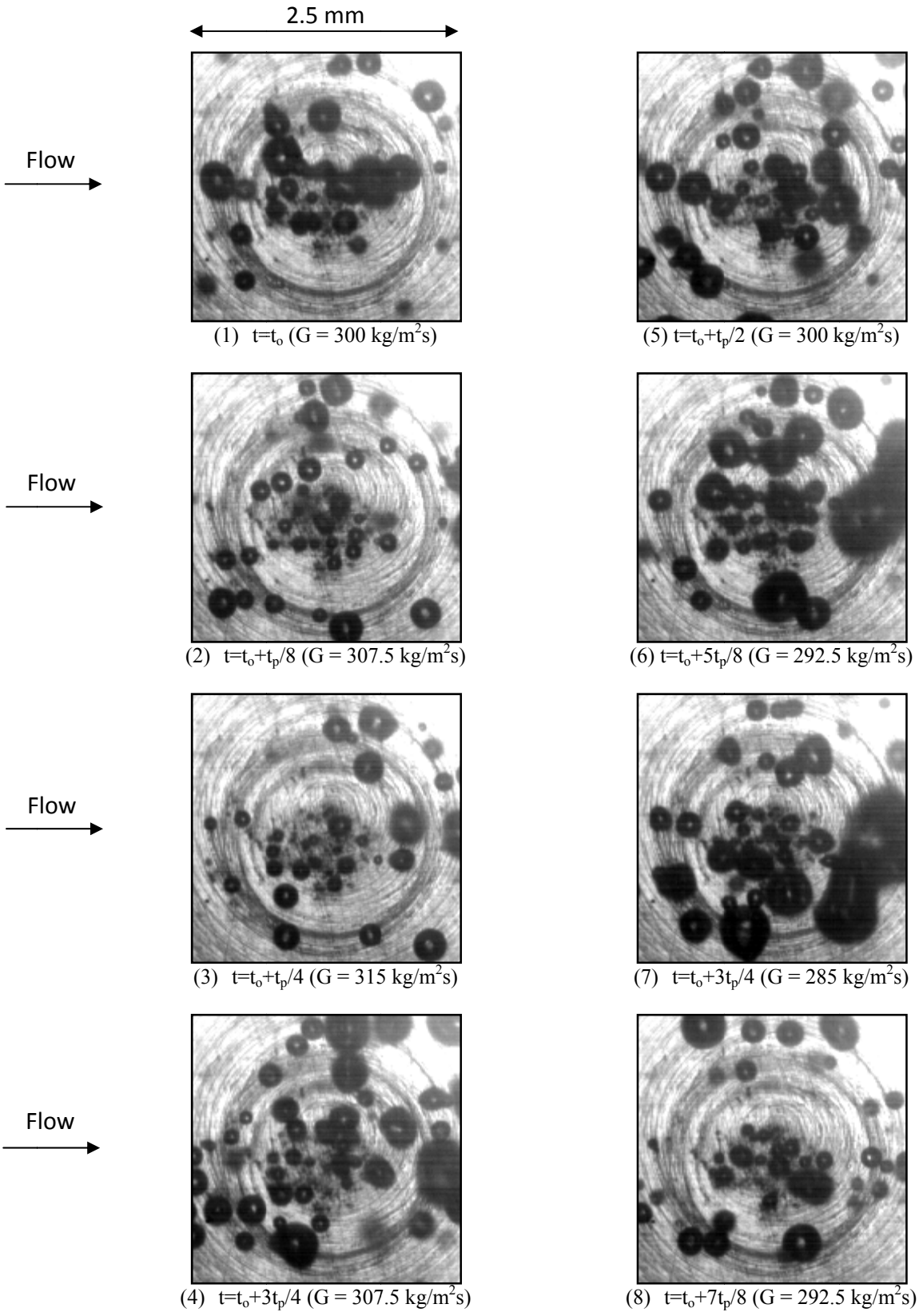

Fig.5.99 Photos of transient oscillatory subcooled flow boiling flow at certain time instants for various imposed mass fluxes for q=7.5 W/cm^2 and ΔT_{sub}= 5^{o}C at G=300±5% kg/m^{2}s with oscillation t$_p$=10s.

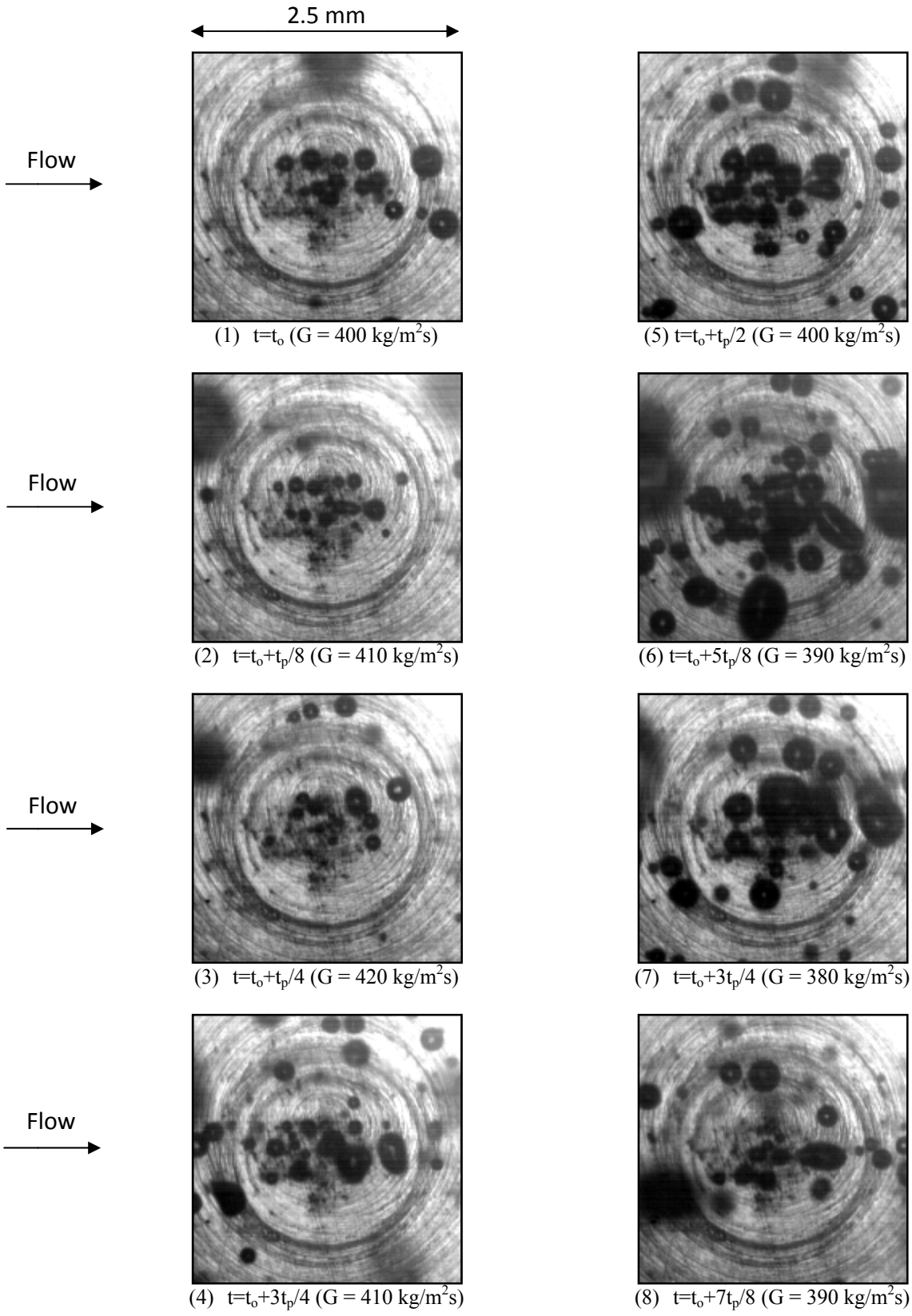

Fig.5.100 Photos of transient oscillatory subcooled flow boiling flow at certain time instants for various imposed mass fluxes for q=7.5 W/cm^2 and ΔT_{sub}= 5^{o}C at G=400±5% kg/m^{2}s with oscillation t_p=10s.

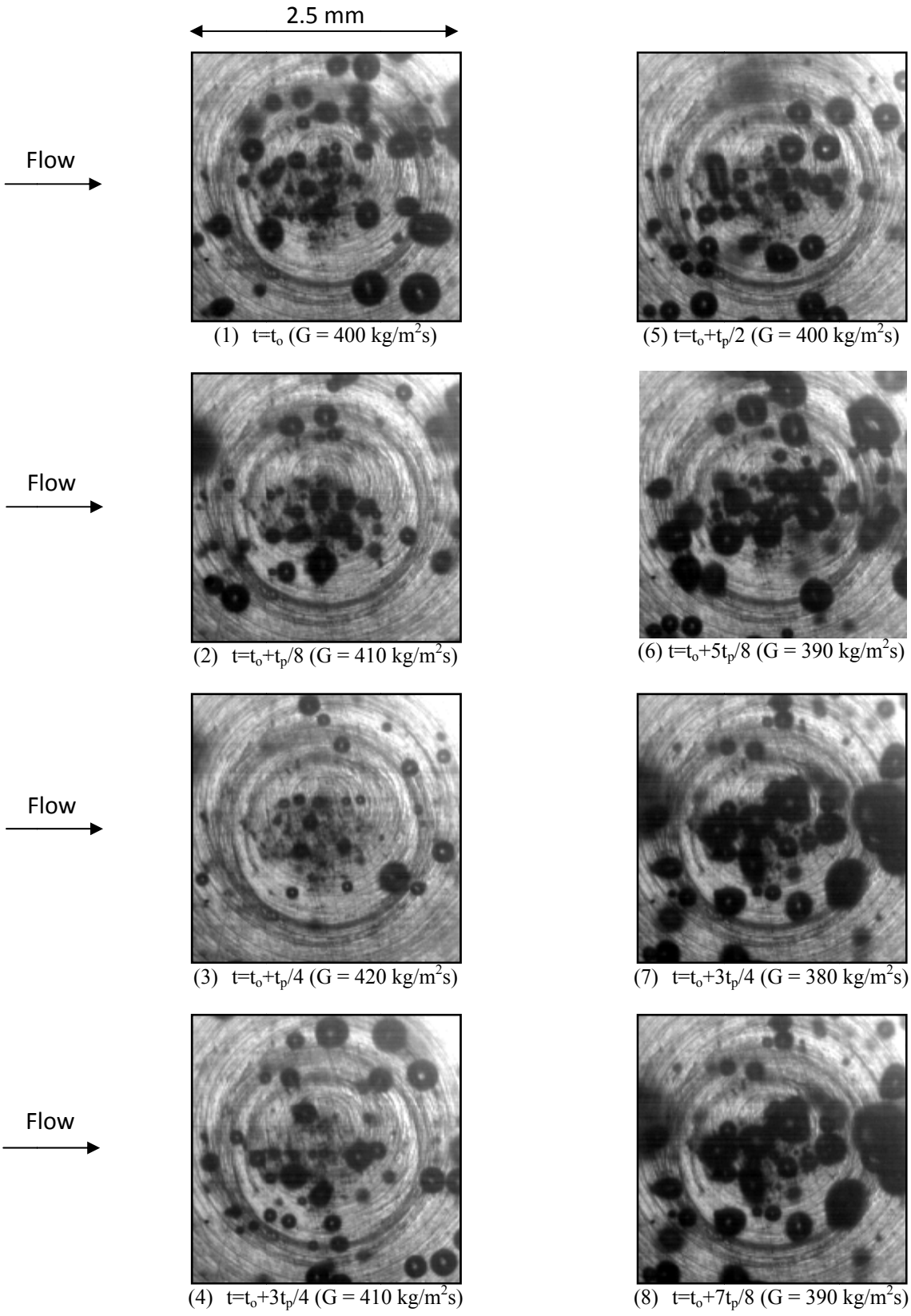

Fig.5.101 Photos of transient oscillatory subcooled flow boiling flow at certain time instants for various imposed mass fluxes for q=8.9 W/cm^2 and ΔT_{sub}= 5^{o}C at G=400±5% kg/m^{2}s with oscillation t_p=10s.

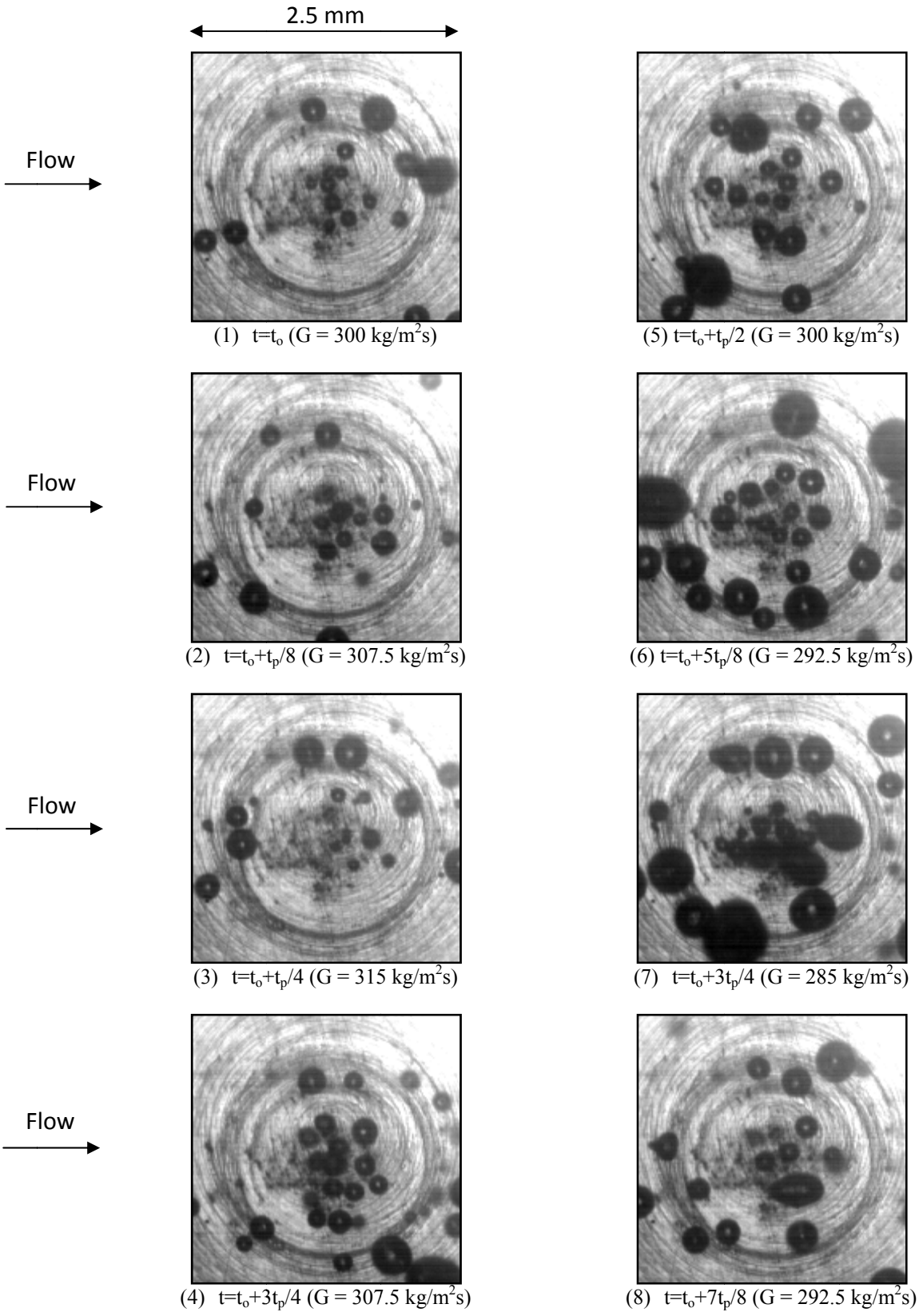

Fig.5.102 Photos of transient oscillatory subcooled flow boiling flow at certain time instants for various imposed mass fluxes for q=6.1 W/cm^2 and ΔT_{sub}= 5^{o}C at G=300±5% kg/m^{2}s with oscillation t_p=20s.

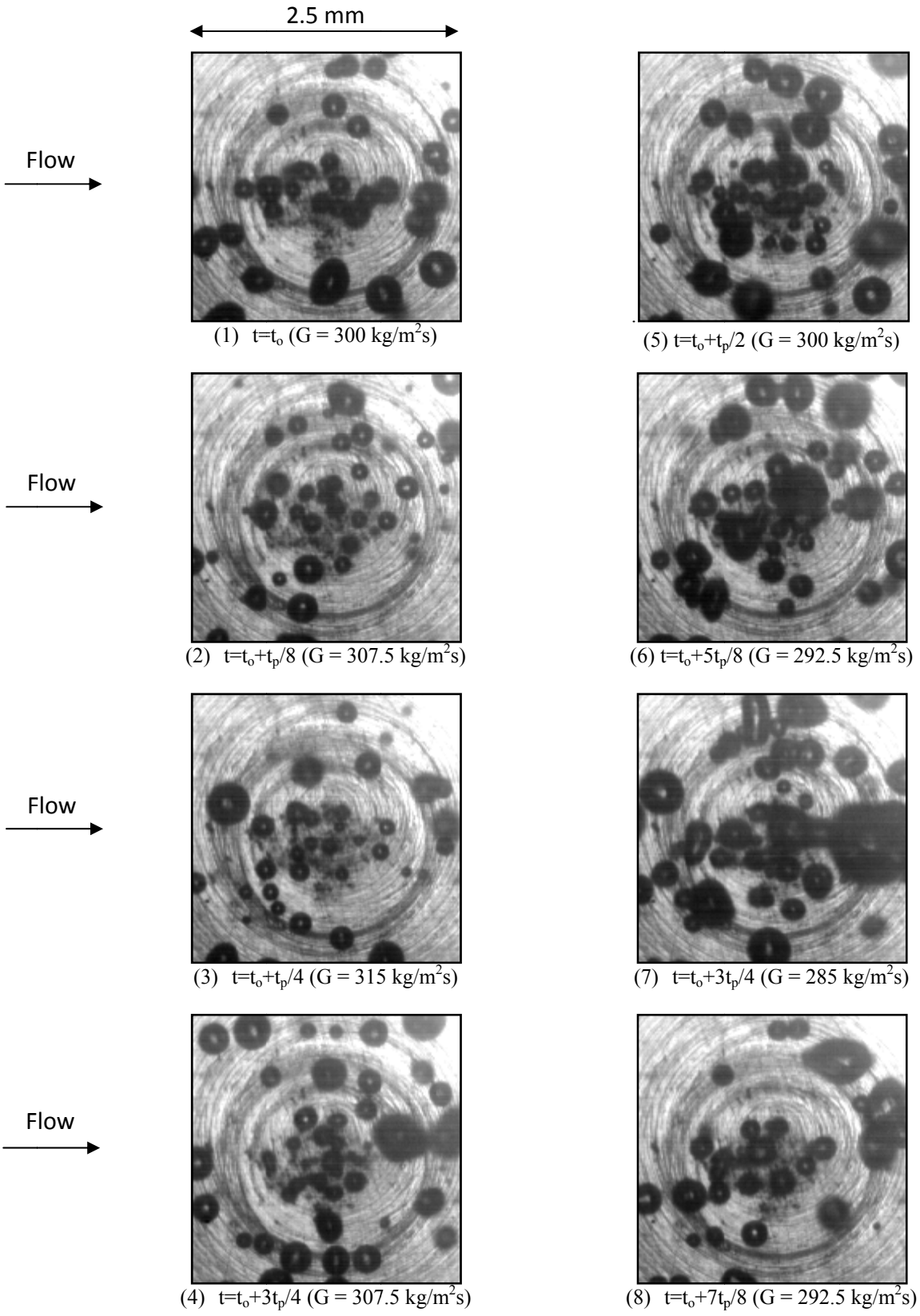

Fig.5.103 Photos of transient oscillatory subcooled flow boiling flow at certain time instants for various imposed mass fluxes for q=7.5 W/cm^2 and ΔT_{sub}= 5^{o}C at G=300±5% kg/m^{2}s with oscillation t$_p$=20s.

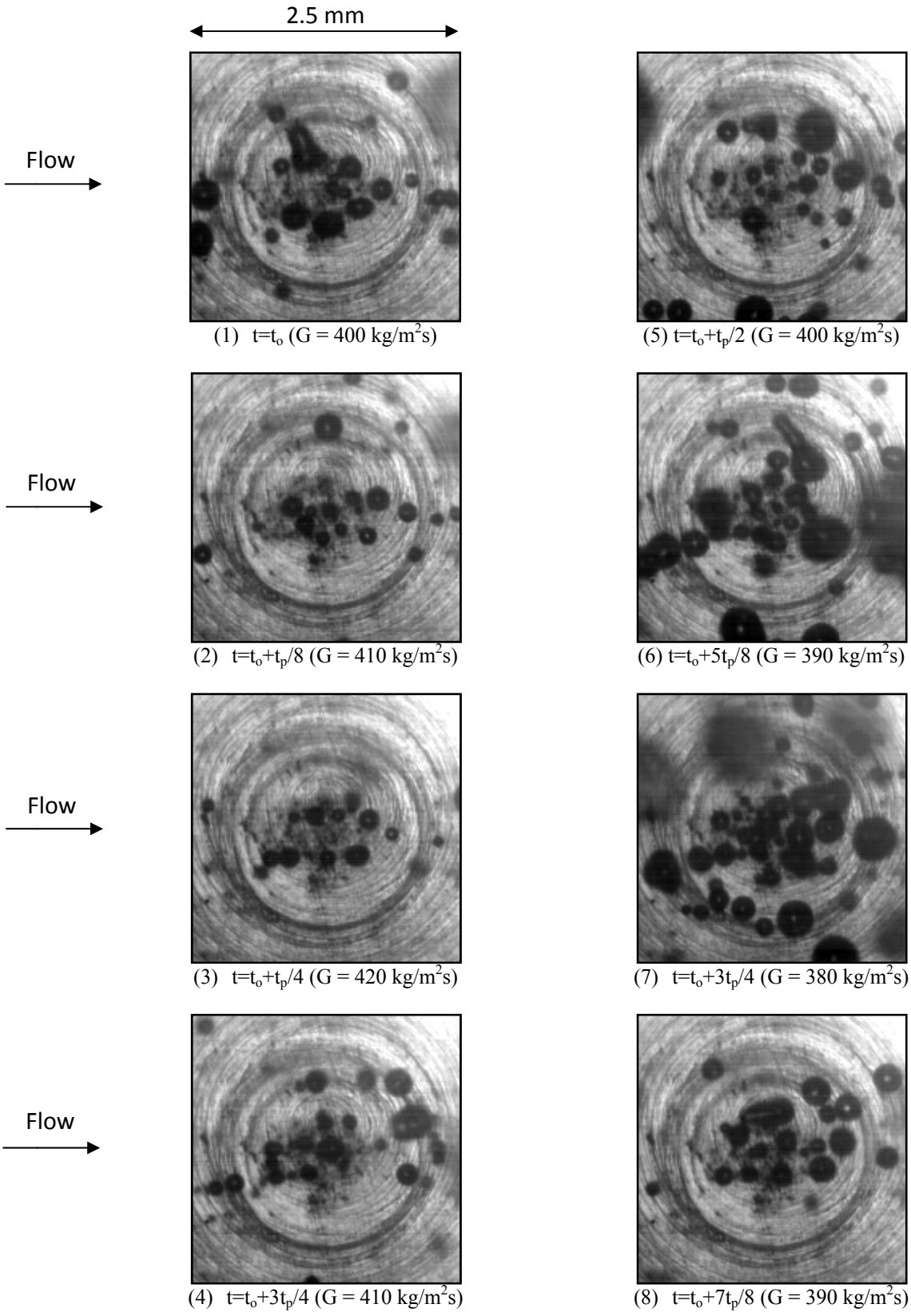

Fig.5.104 Photos of transient oscillatory subcooled flow boiling flow at certain time instants for various imposed mass fluxes for q=7.4 W/cm^2 and ΔT_{sub}= 5^{o}C at G=400±5% kg/m^{2}s with oscillation t_p=20s.

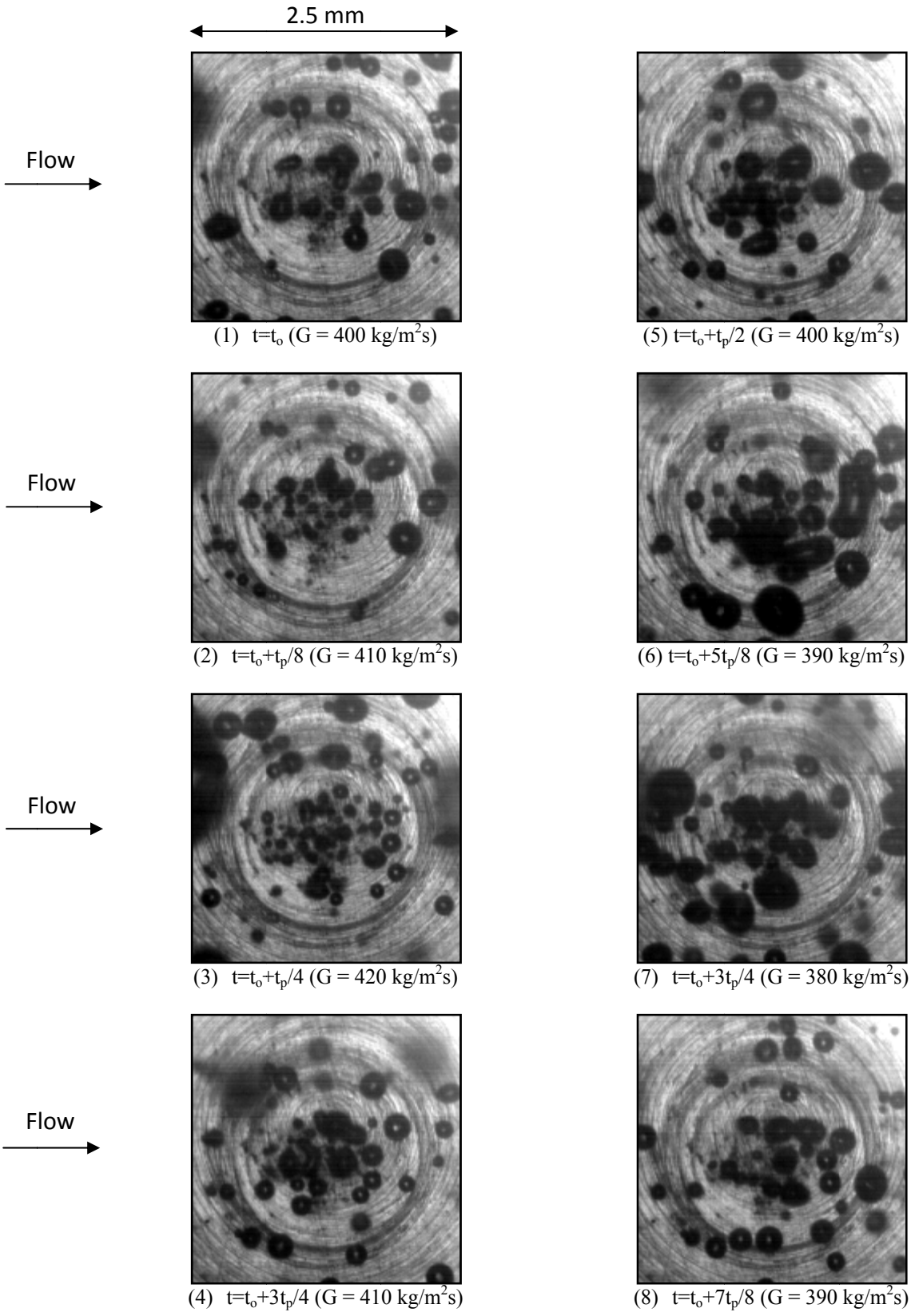

Fig.5.105 Photos of transient oscillatory subcooled flow boiling flow at certain time instants for various imposed mass fluxes for q=8.9 W/cm^2 and ΔT_{sub}= 5^{o}C at G=400±5% kg/m^{2}s with oscillation t_p=20s.

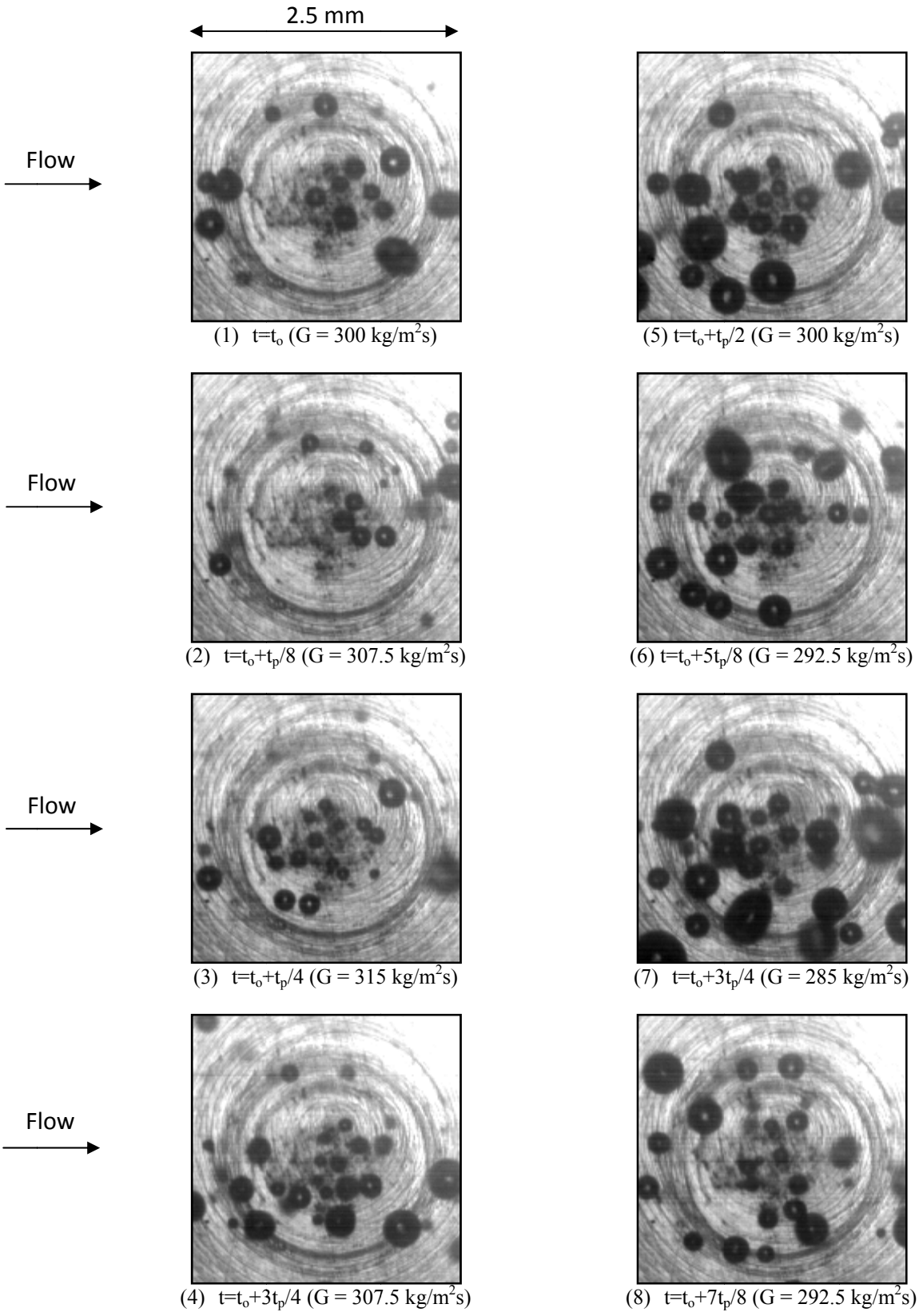

Fig.5.106 Photos of transient oscillatory subcooled flow boiling flow at certain time instants for various imposed mass fluxes for q=6.1 W/cm^2 and ΔT_{sub}= 5^{o}C at G=300±5% kg/m^{2}s with oscillation t_p=30s.

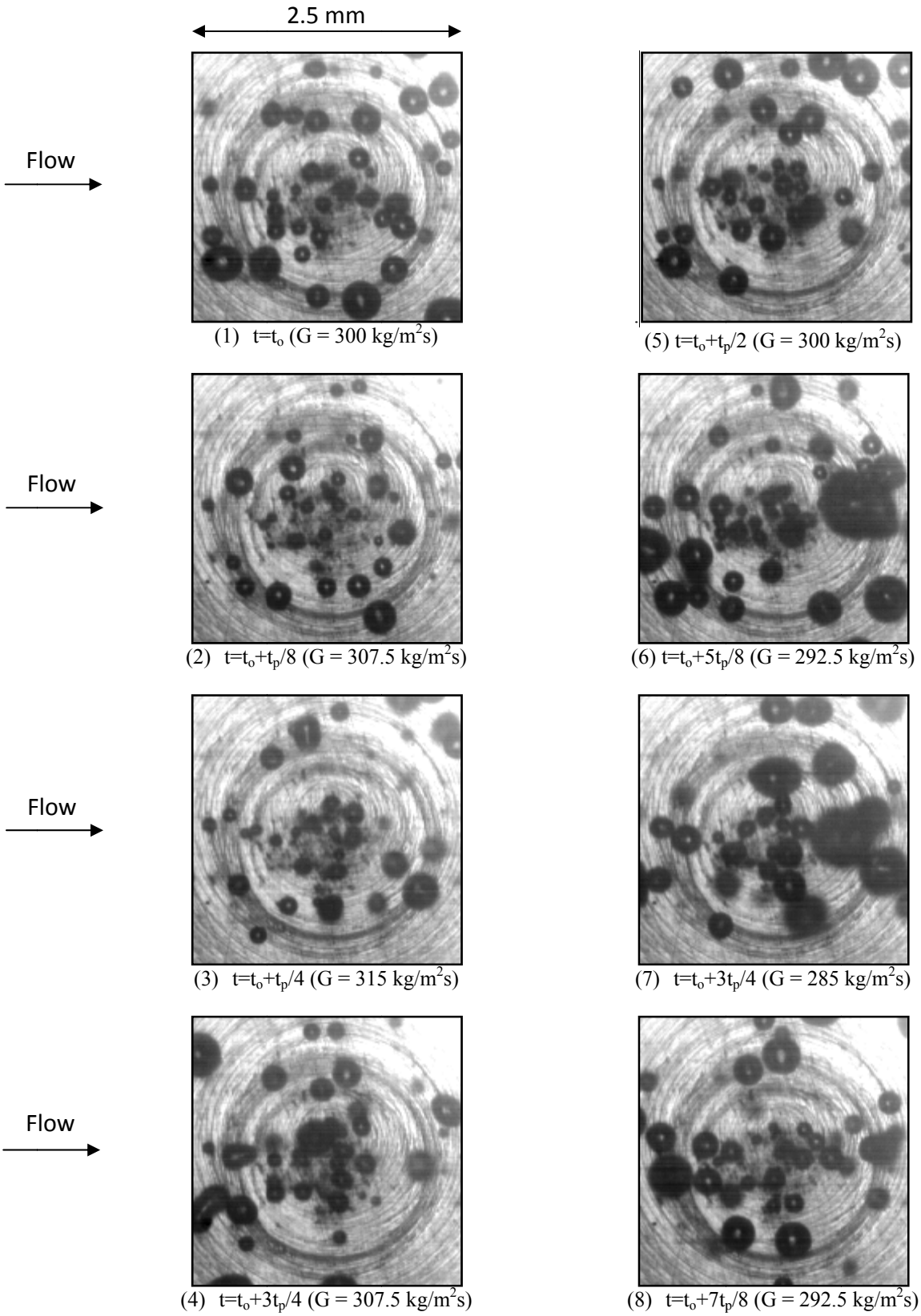

Fig.5.107 Photos of transient oscillatory subcooled flow boiling flow at certain time instants for various imposed mass fluxes for q=7.4 W/cm^2 and ΔT_{sub}= 5^{o}C at G=300±5% kg/m^{2}s with oscillation t$_p$=30s.

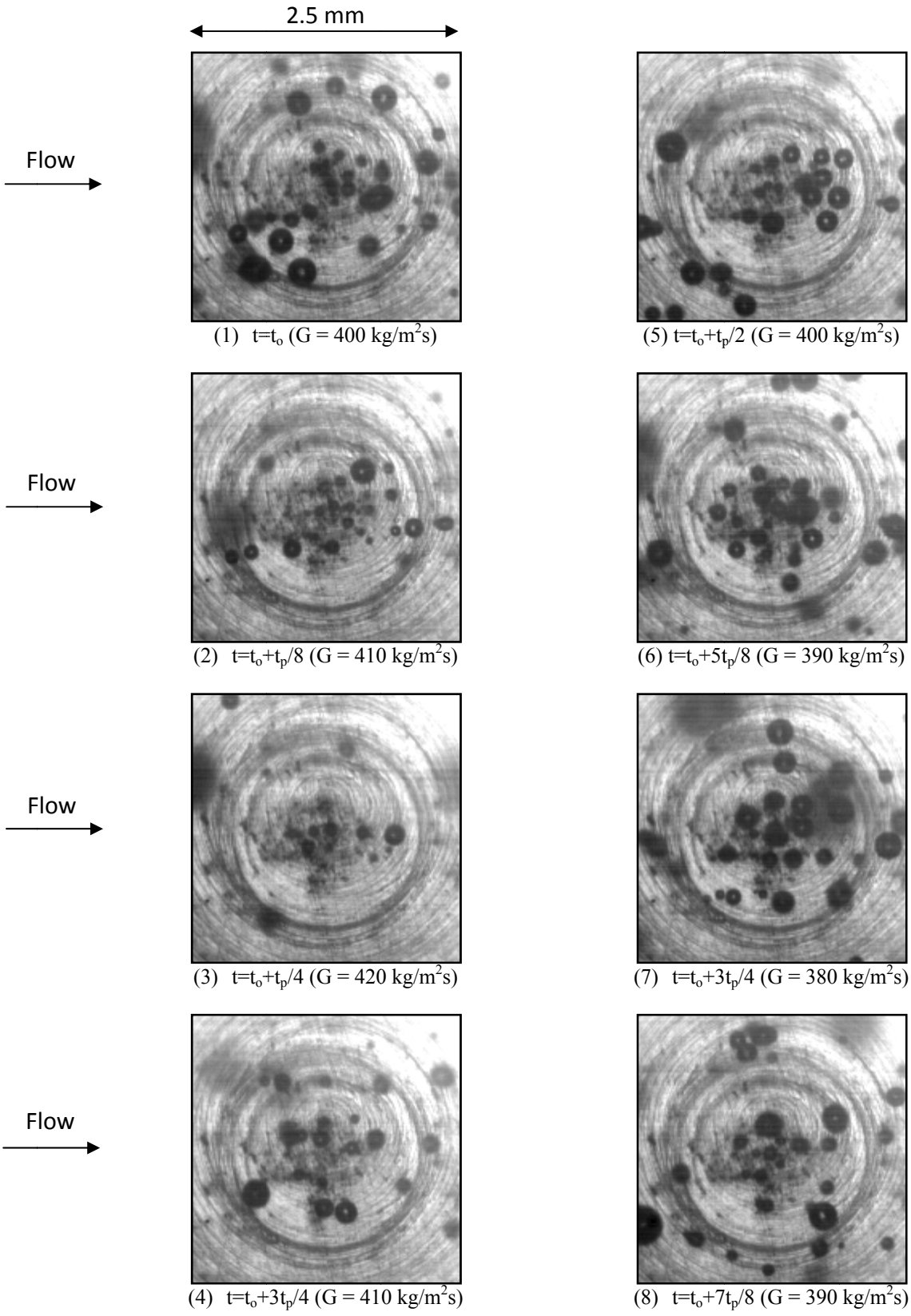

Fig.5.108 Photos of transient oscillatory subcooled flow boiling flow at certain time instants for various imposed mass fluxes for q=7.4 W/cm^2 and ΔT_{sub}= 5^{o}C at G=400±5% kg/m^{2}s with oscillation t_p=30s.

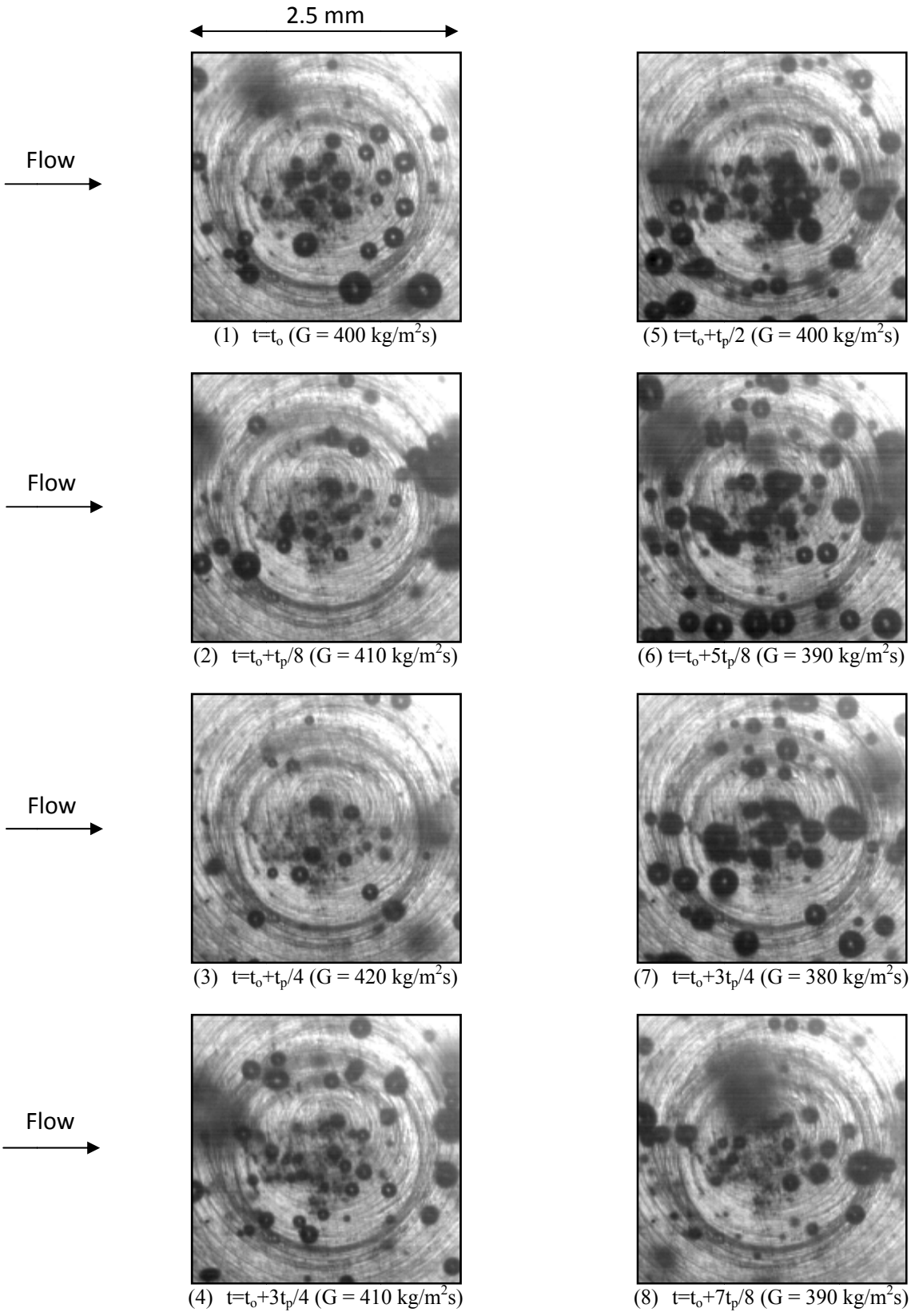

Fig.5.109 Photos of transient oscillatory subcooled flow boiling flow at certain time instants for various imposed mass fluxes for q=8.8 W/cm^2 and ΔT_{sub}= 5^{o}C at G=400±5% kg/m^{2}s with oscillation t_p=30s.

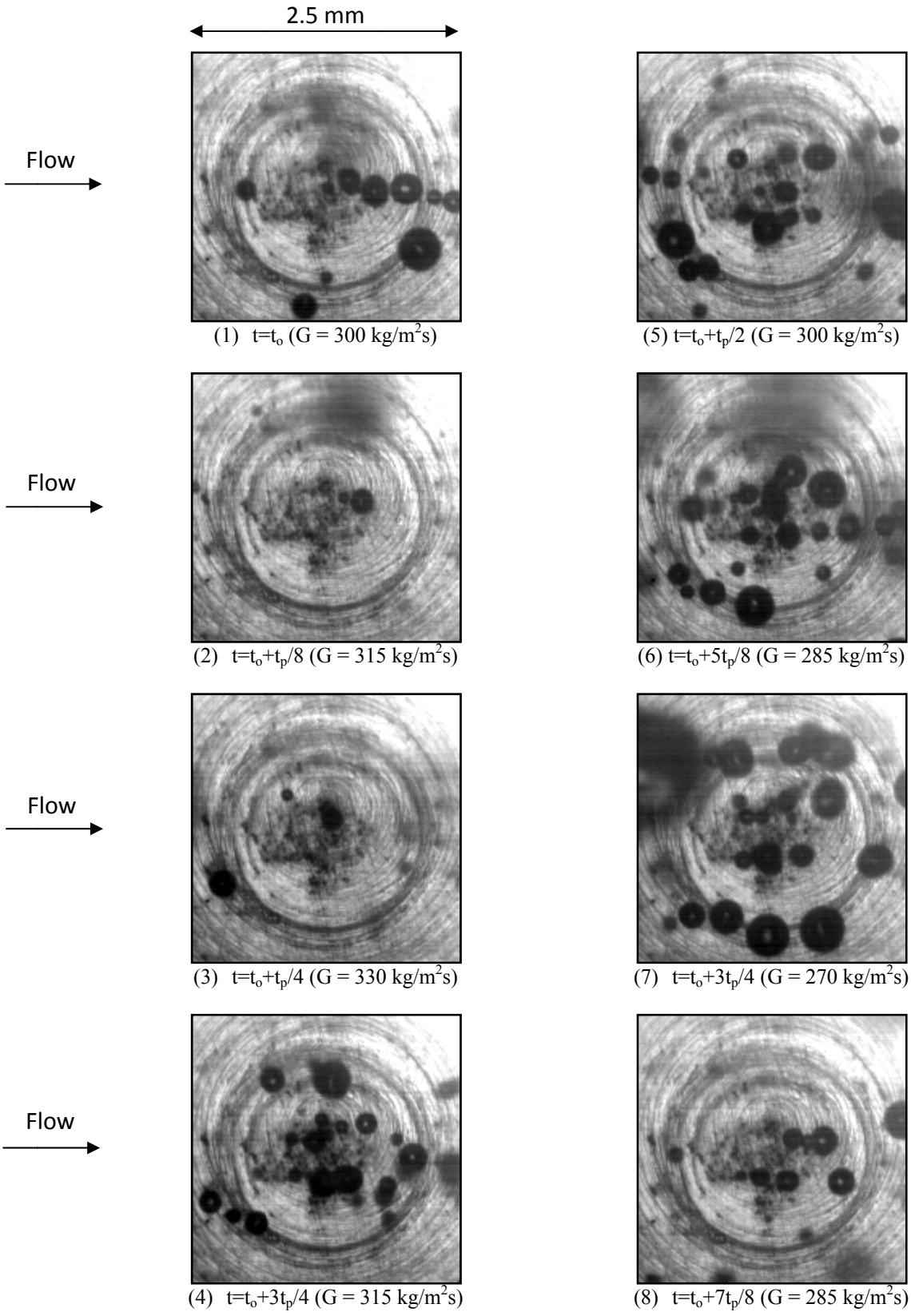

Fig.5.110 Photos of transient oscillatory subcooled flow boiling flow at certain time instants for various imposed mass fluxes for q=6.1 W/cm^2 and ΔT_{sub}= 5^{o}C at G=300±10% kg/m^{2}s with oscillation t_p=10s.

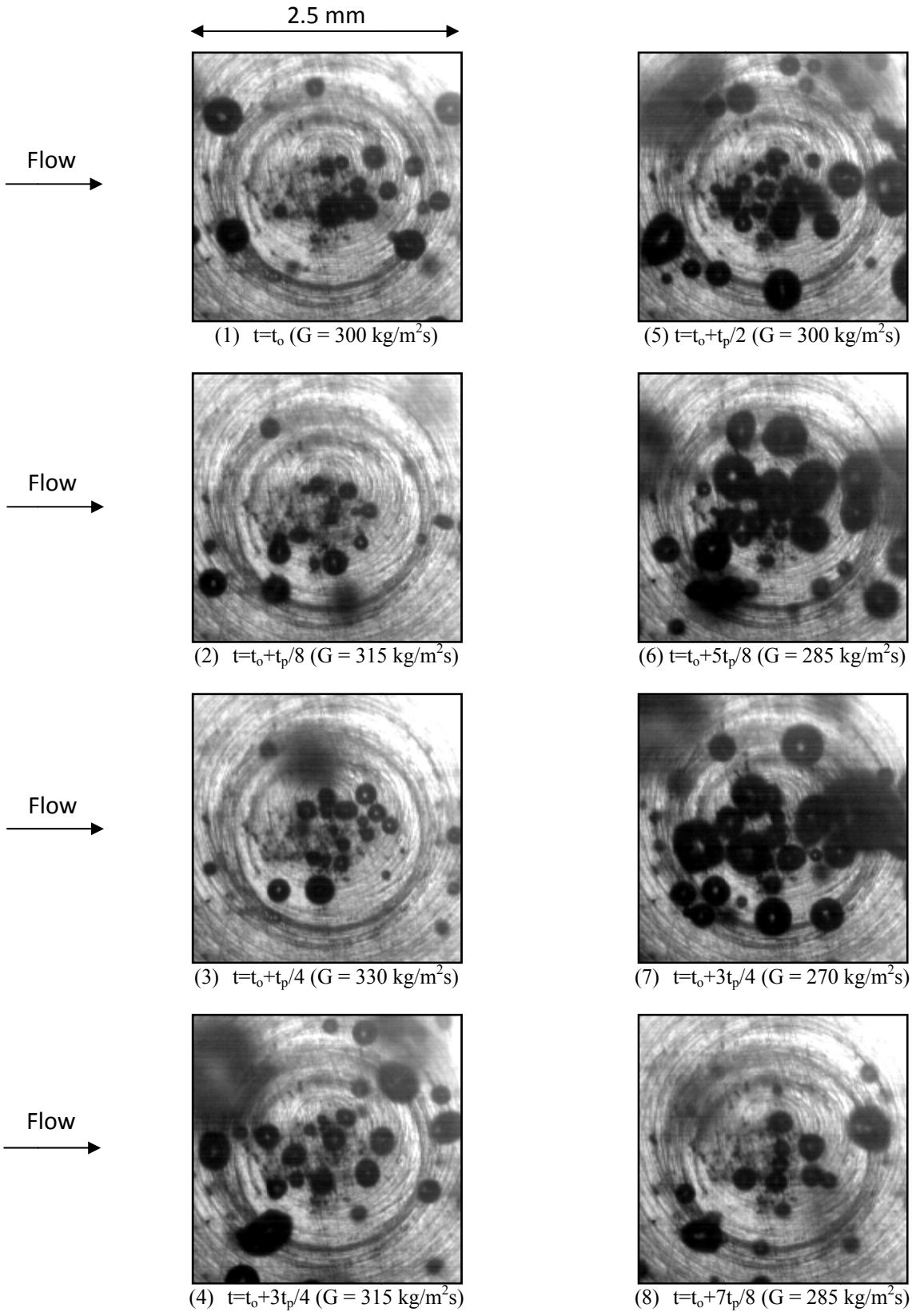

Fig.5.111 Photos of transient oscillatory subcooled flow boiling flow at certain time instants for various imposed mass fluxes for q=7.4 W/cm^2 and ΔT_{sub}= 5^{o}C at G=300±10% kg/m^{2}s with oscillation t_p=10s.

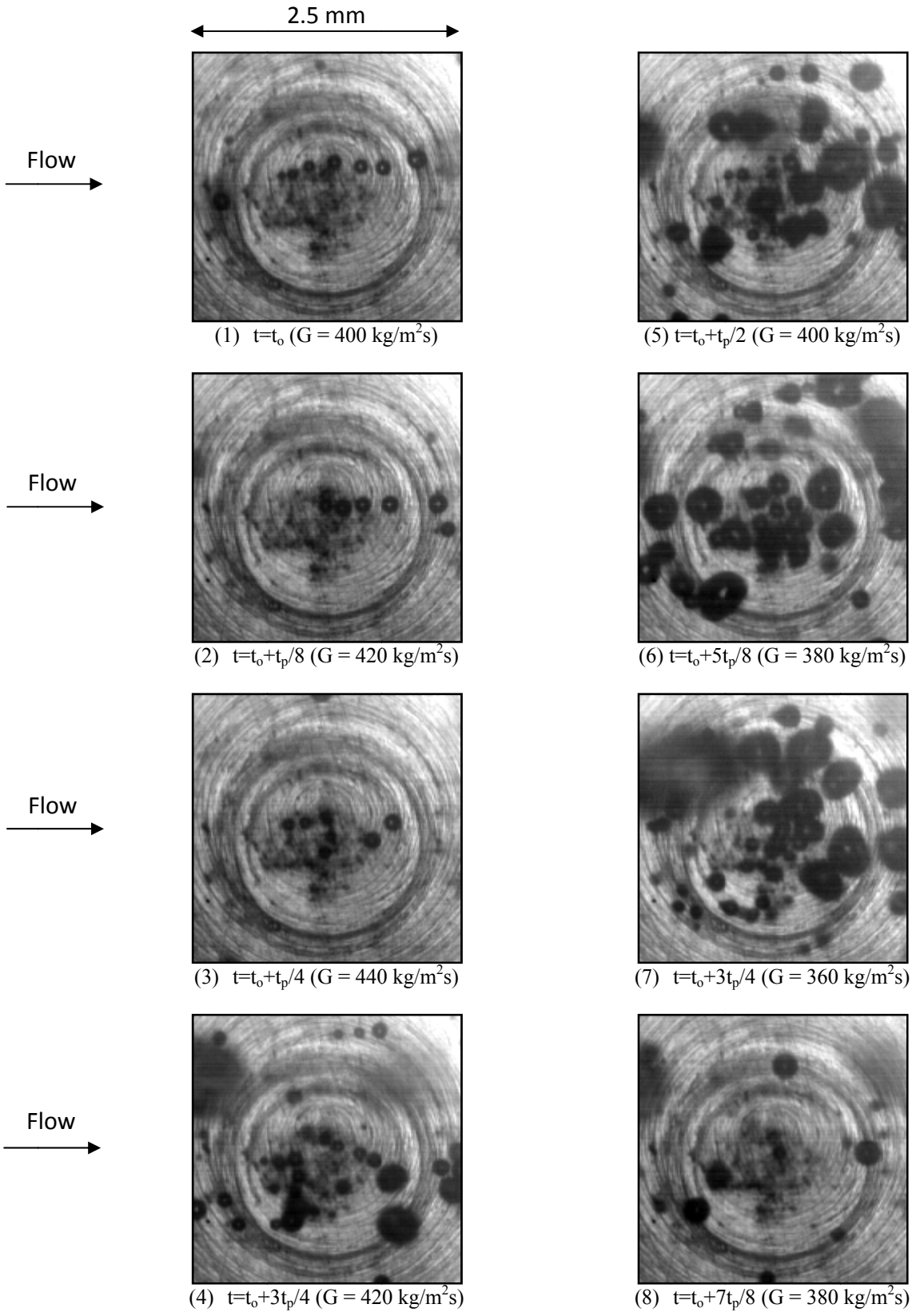

Fig.5.112 Photos of transient oscillatory subcooled flow boiling flow at certain time instants for various imposed mass fluxes for q=7.4 W/cm^2 and ΔT_{sub}= 5^{o}C at G=400±10% kg/m^{2}s with oscillation t_p=10s.

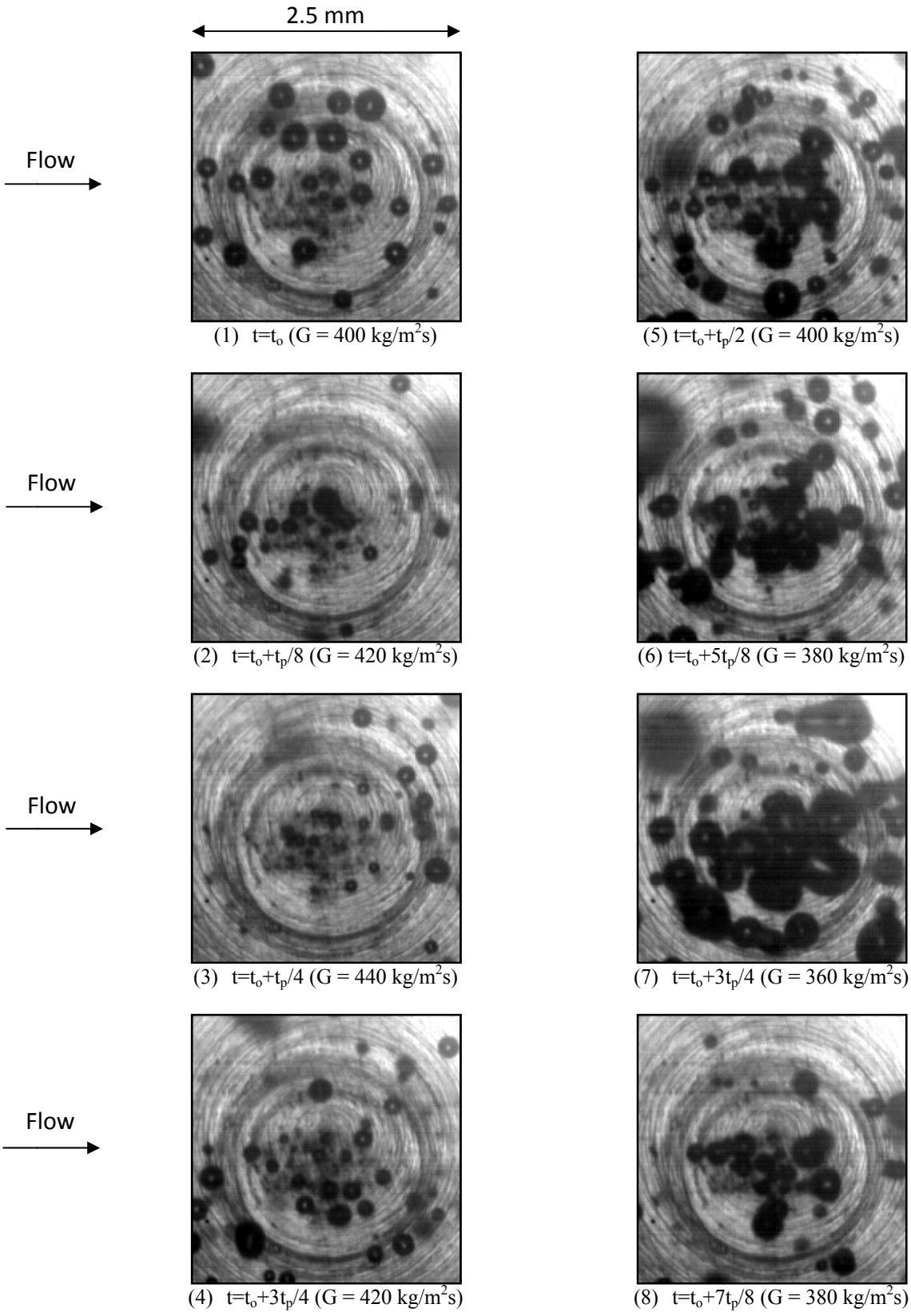

Fig.5.113 Photos of transient oscillatory subcooled flow boiling flow at certain time instants for various imposed mass fluxes for q=8.8 W/cm^2 and ΔT_{sub}= 5^{o}C at G=400±10% kg/m^{2}s with oscillation t_p=10s.

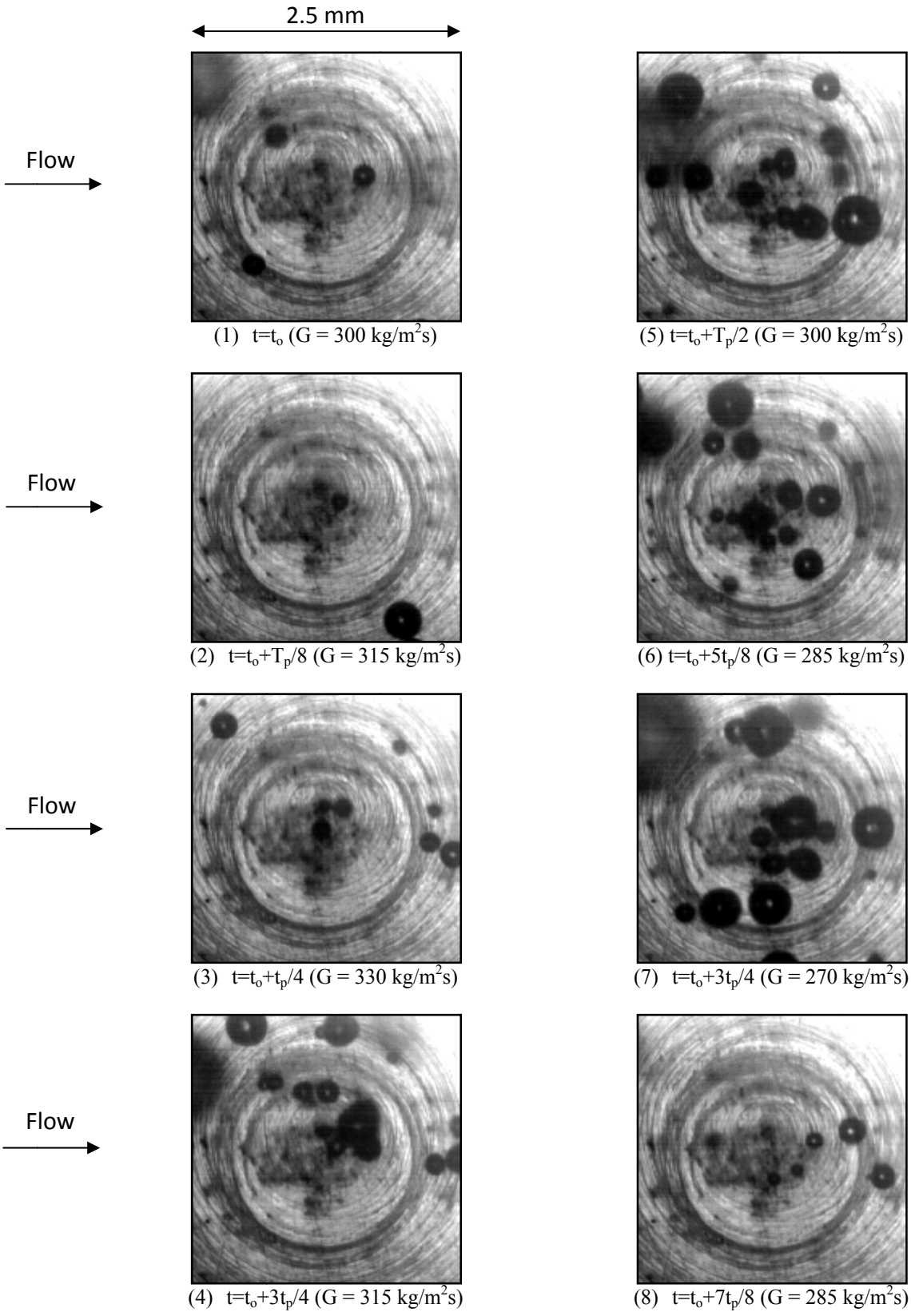

Fig.5.114 Photos of transient oscillatory subcooled flow boiling flow at certain time instants for various imposed mass fluxes for q=6.0 W/cm^2 and ΔT_{sub}= 5^{o}C at G=300±10% kg/m^{2}s with oscillation t_p=20s.

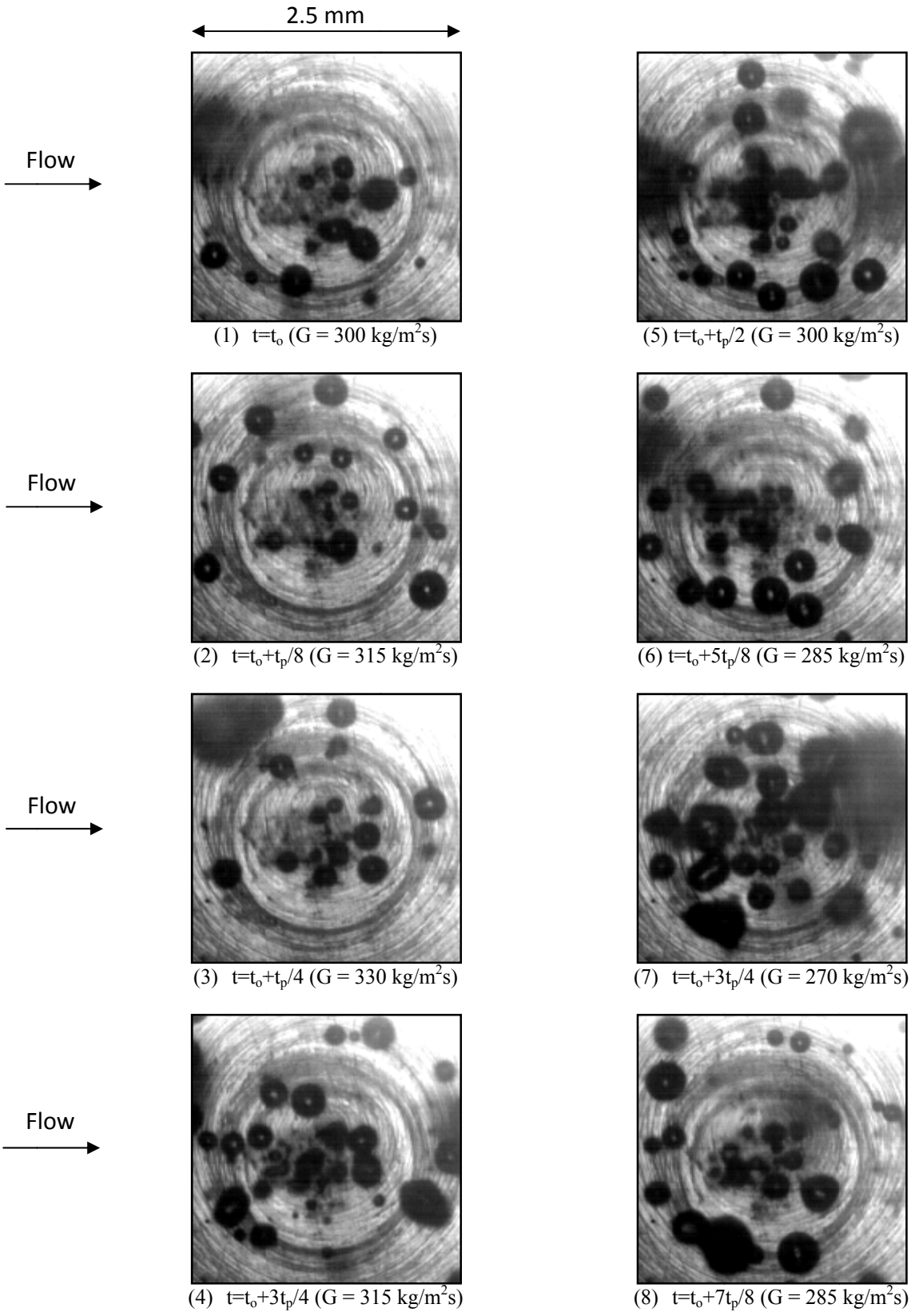

Fig.5.115 Photos of transient oscillatory subcooled flow boiling flow at certain time instants for various imposed mass fluxes for q=7.4 W/cm^2 and ΔT_{sub}= 5^{o}C at G=300±10% kg/m^{2}s with oscillation t_p=20s.

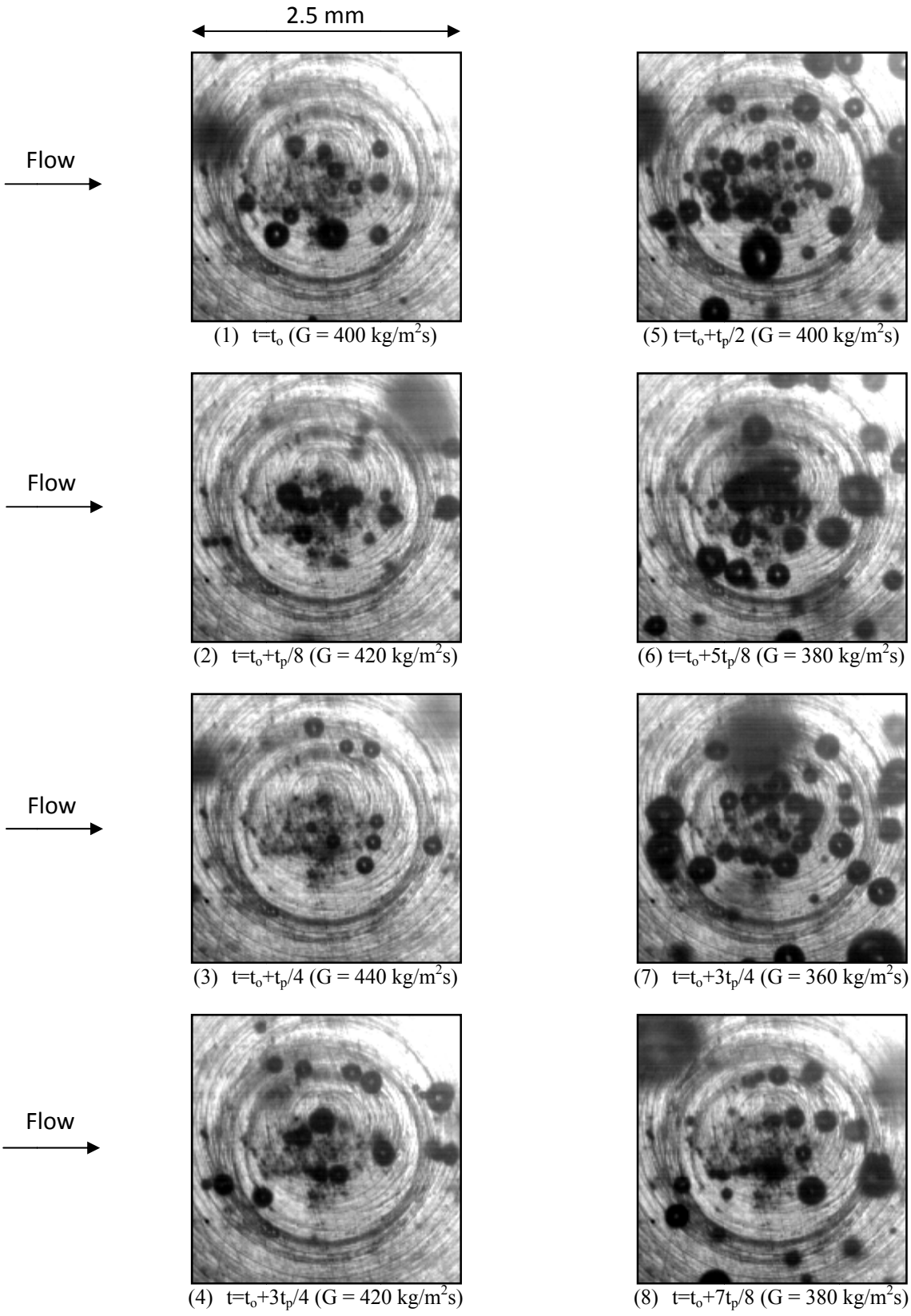

Fig.5.116 Photos of transient oscillatory subcooled flow boiling flow at certain time instants for various imposed mass fluxes for q=7.5 W/cm^2 and ΔT_{sub}= 5^{o}C at G=400±10% kg/m^{2}s with oscillation t_p=20s.

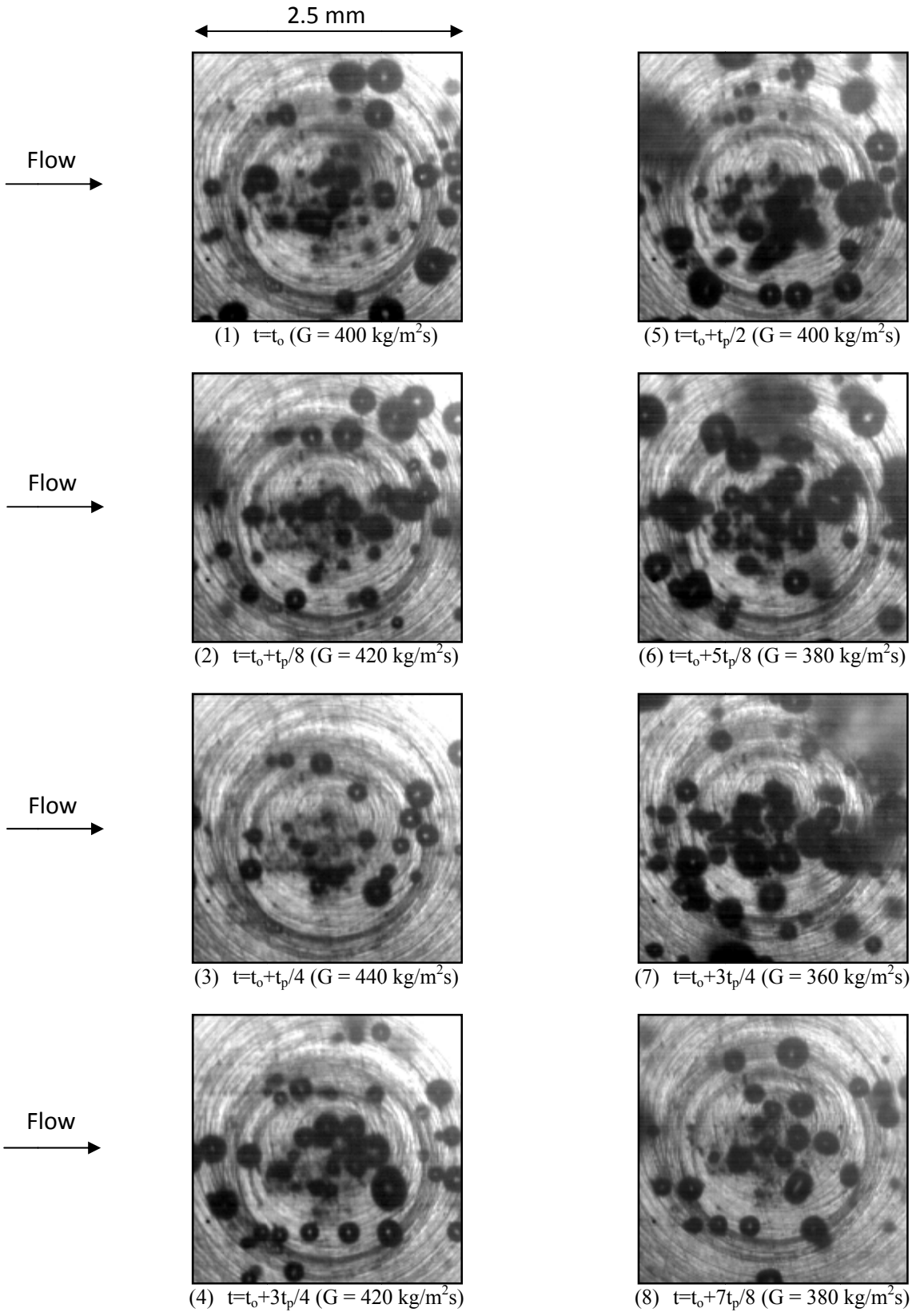

Fig.5.117 Photos of transient oscillatory subcooled flow boiling flow at certain time instants for various imposed mass fluxes for q=8.9 W/cm^2 and ΔT_{sub}= 5^{o}C at G=400±10% kg/m^{2}s with oscillation t_p=20s.

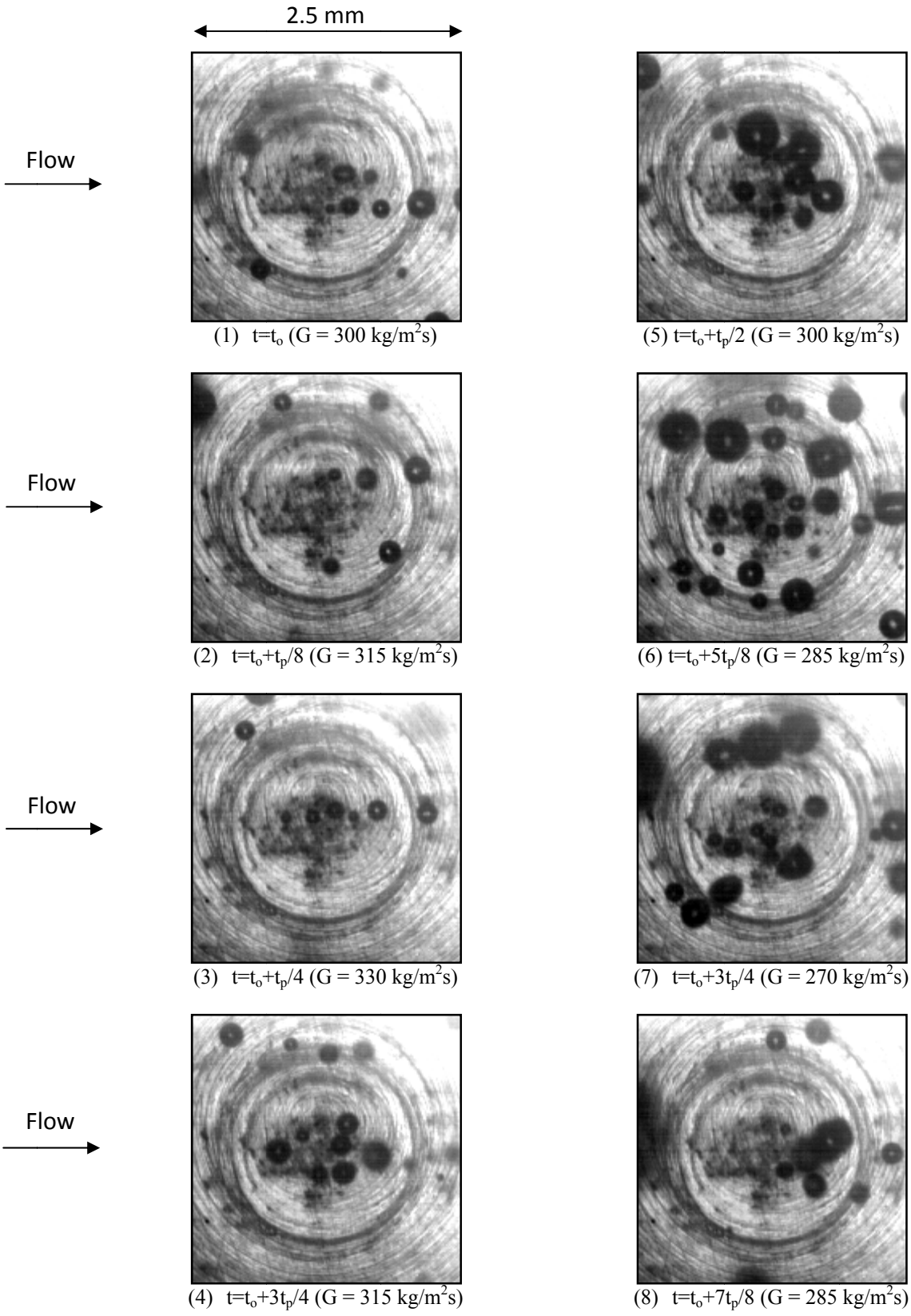

Fig.5.118 Photos of transient oscillatory subcooled flow boiling flow at certain time instants for various imposed mass fluxes for q=6.1 W/cm^2 and ΔT_{sub}= 5^{o}C at G=300±10% kg/m^{2}s with oscillation t_p=30s.

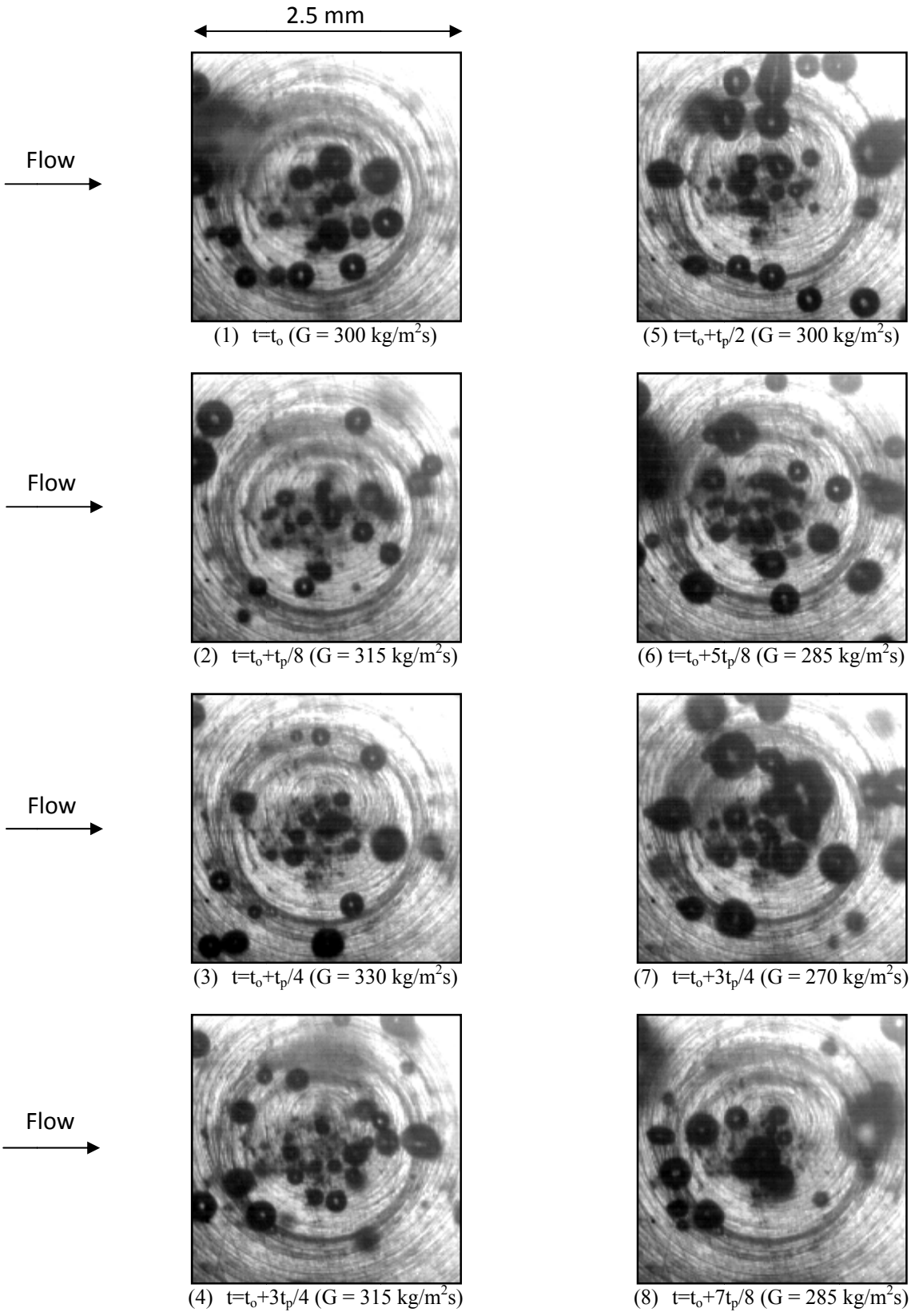

Fig.5.119 Photos of transient oscillatory subcooled flow boiling flow at certain time instants for various imposed mass fluxes for q=7.4 W/cm^2 and ΔT_{sub}= 5^{o}C at G=300±10% kg/m^{2}s with oscillation t_p=30s.

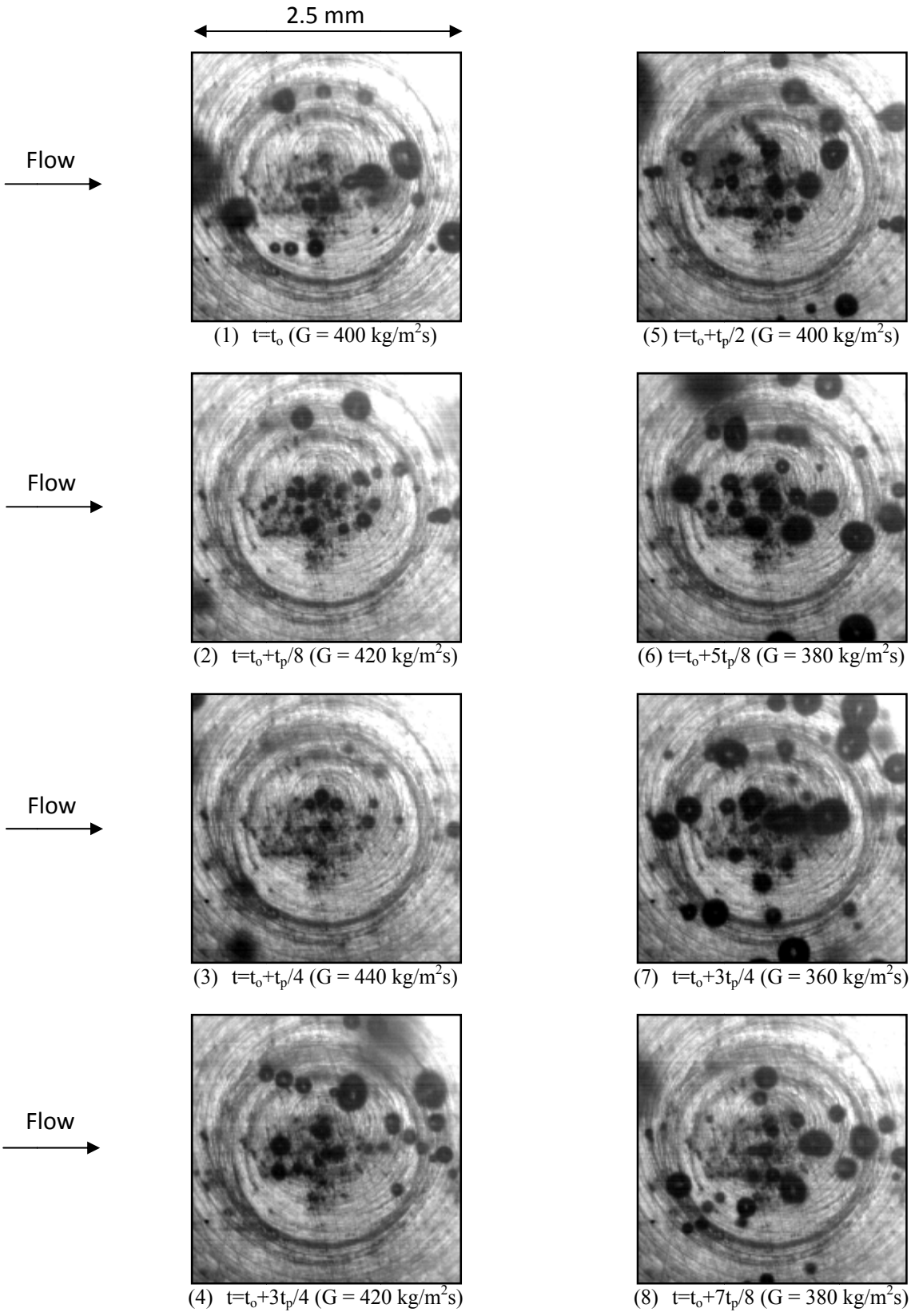

Fig.5.120 Photos of transient oscillatory subcooled flow boiling flow at certain time instants for various imposed mass fluxes for q=7.4 W/cm^2 and ΔT_{sub}= 5^{o}C at G=400±10% kg/m^{2}s with oscillation t_p=30s.

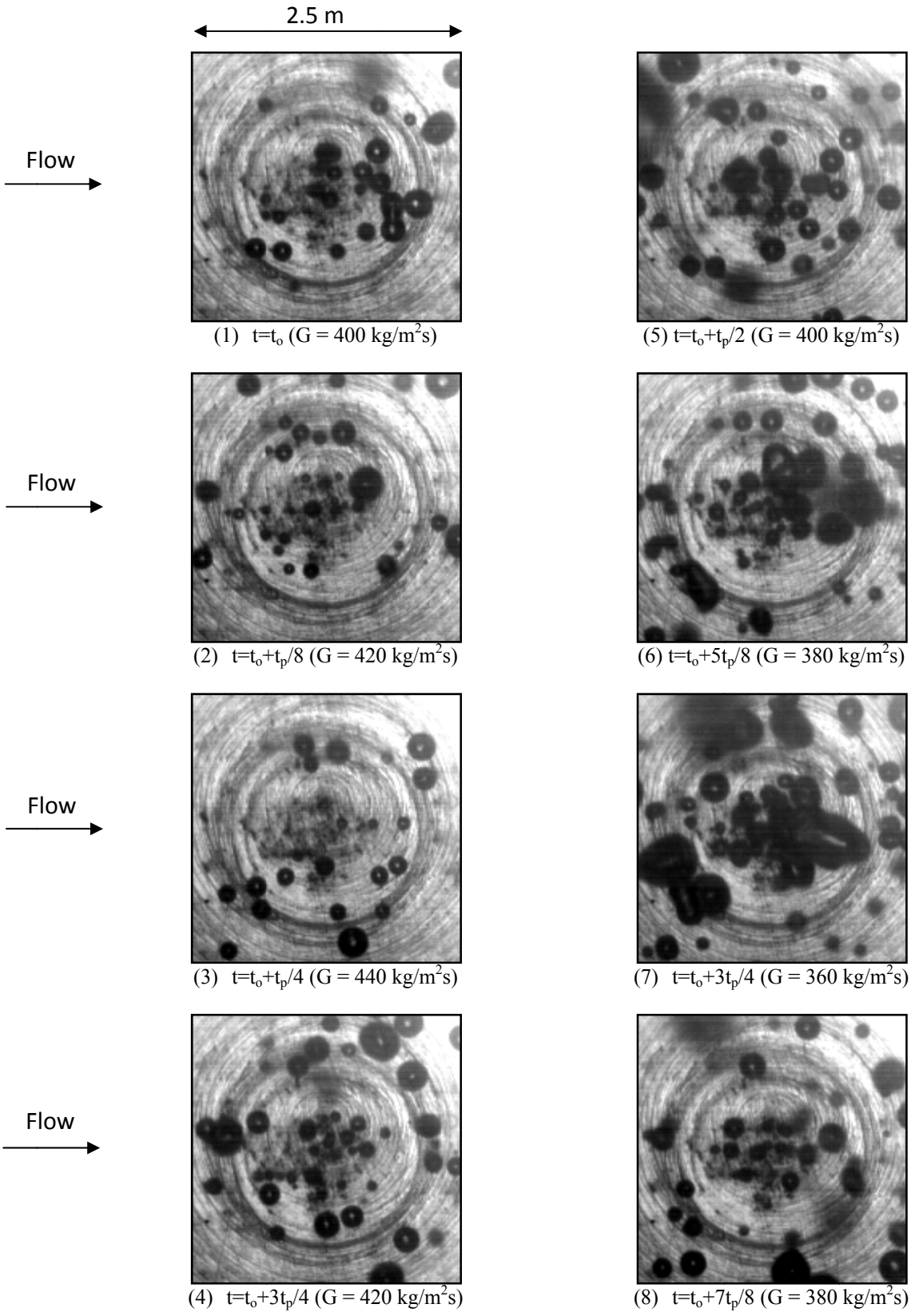

Fig.5.121 Photos of transient oscillatory subcooled flow boiling flow at certain time instants for various imposed mass fluxes for q=8.9 W/cm^2 and ΔT_{sub}= 5^{o}C at G=400±10% kg/m^{2}s with oscillation t$_p$=30s.

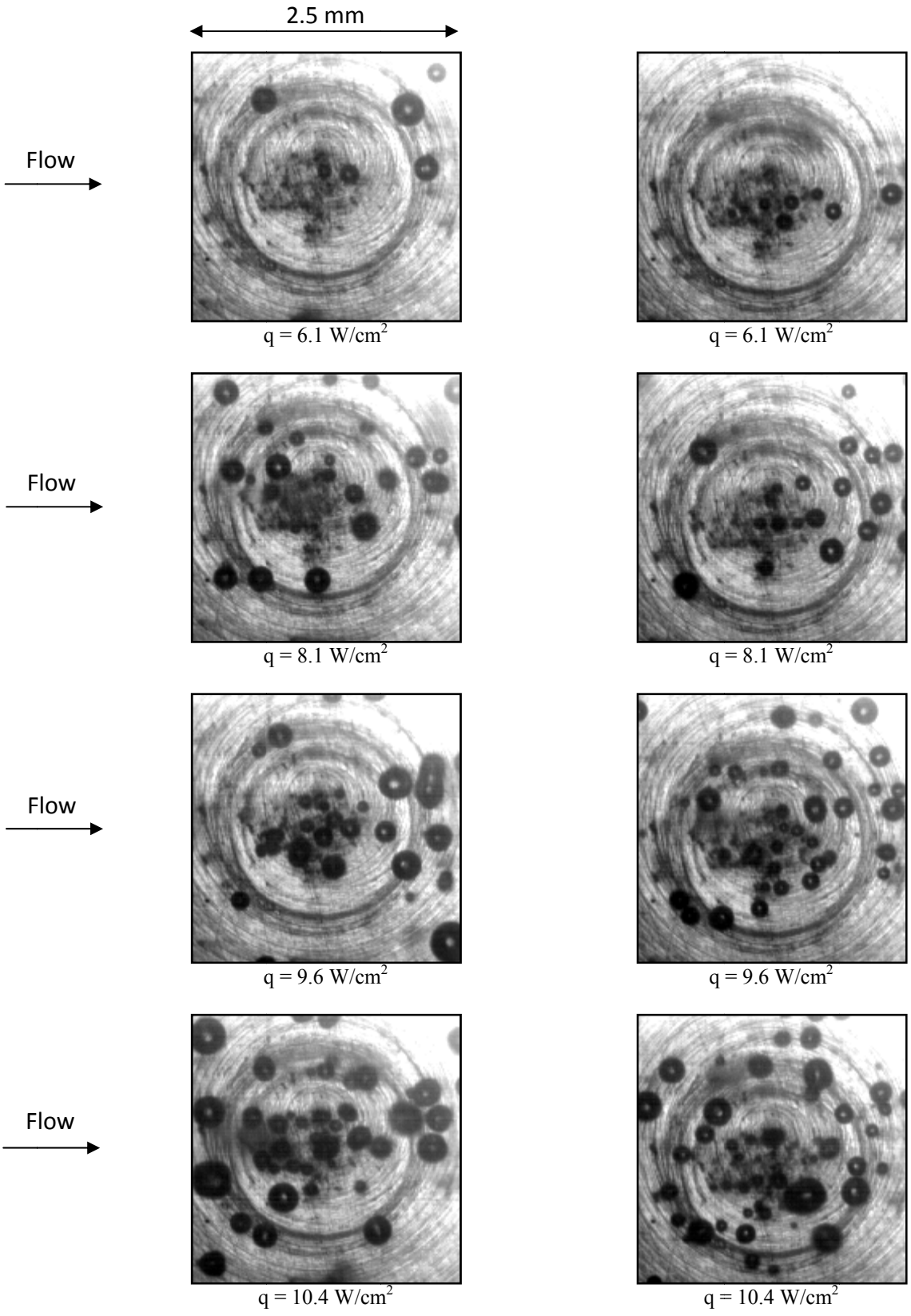

Fig.5.122 Photos of stable subcooled boiling flow at certain time instants for various imposed heat fluxes at ΔT_{sub}= 10^{o}C for (a) G =300 kg/m^{2}s and (b) G =400 kg/m^{2}s.

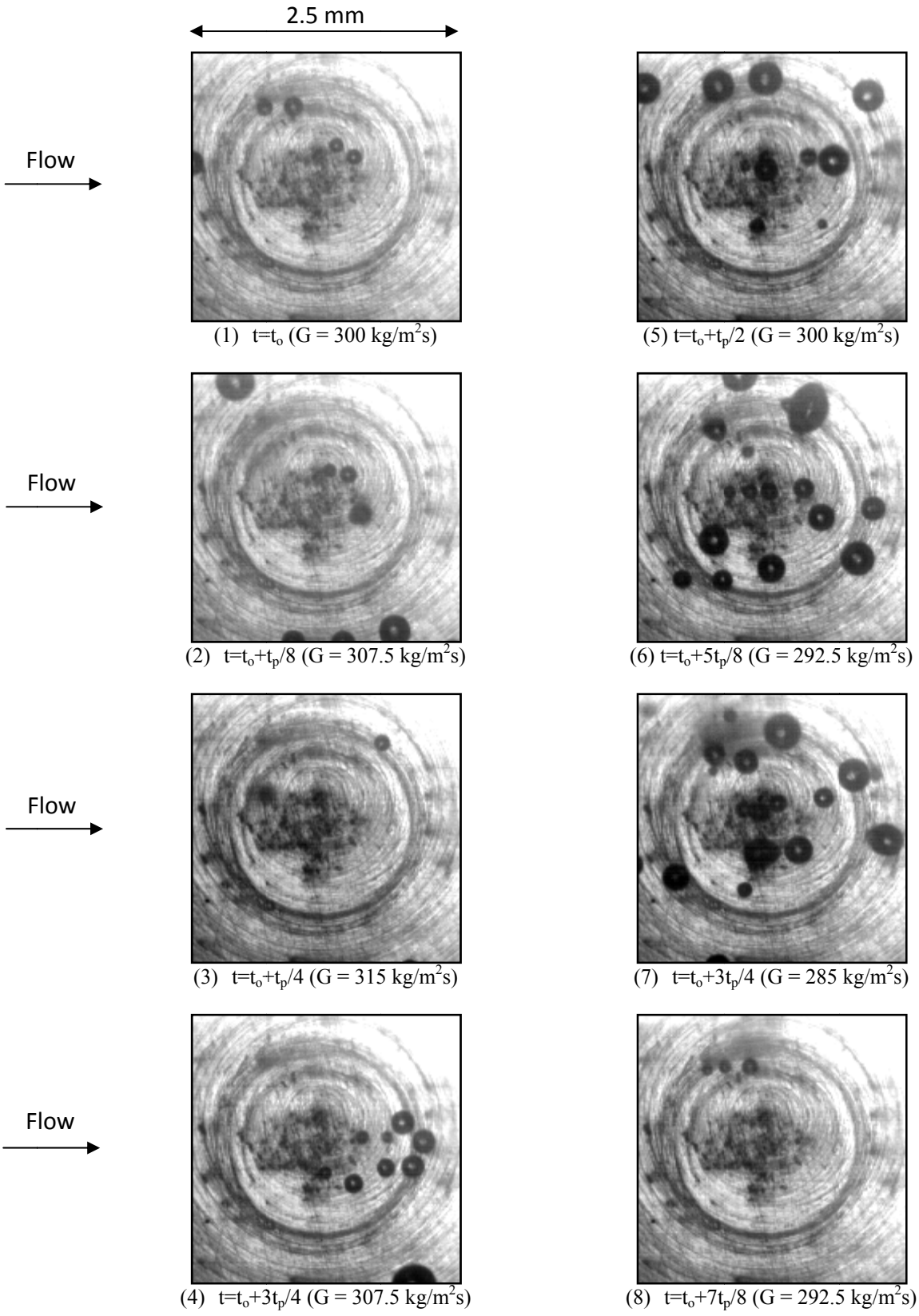

Fig.5.123 Photos of transient oscillatory subcooled flow boiling flow at certain time instants for various imposed mass fluxes for q=6.7 W/cm^2 and ΔT_{sub}= 10^{o}C at G=300±5% kg/m^{2}s with oscillation t_p=10s.

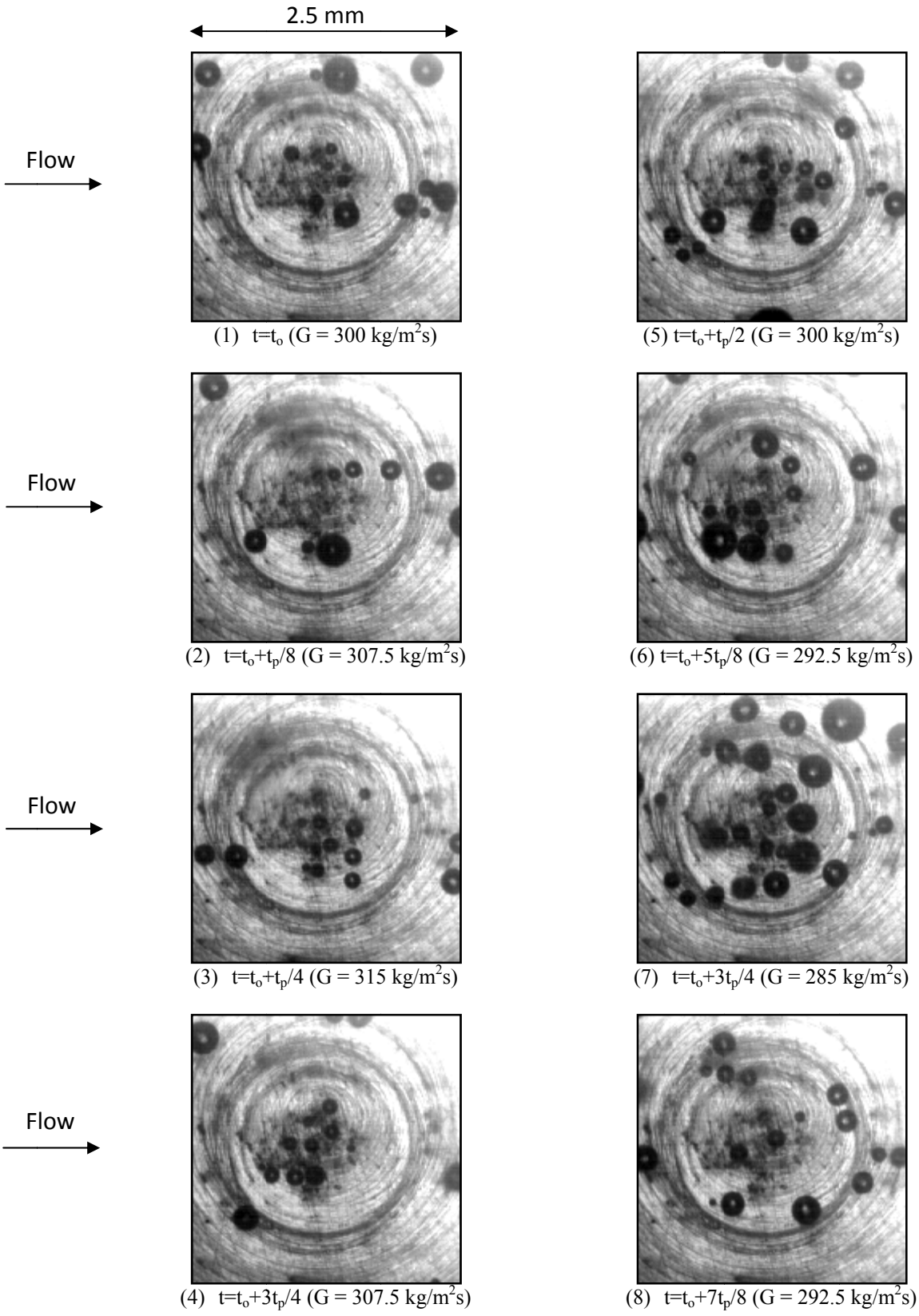

Fig.5.124 Photos of transient oscillatory subcooled flow boiling flow at certain time instants for various imposed mass fluxes for q=8.1 W/cm^2 and ΔT_{sub}= 10^{o}C at G=300±5% kg/m^{2}s with oscillation t_p=10s.

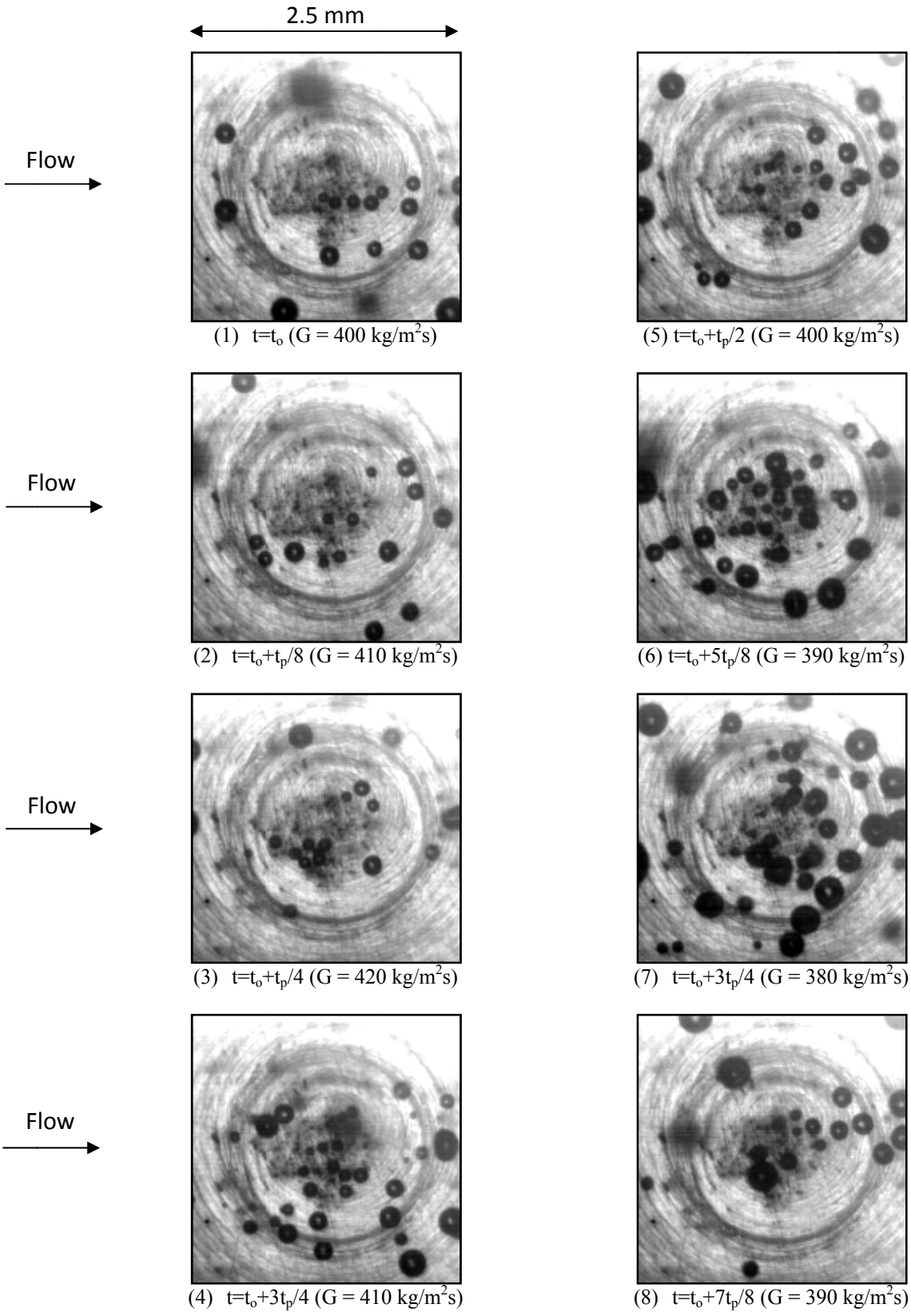

Fig.5.125 Photos of transient oscillatory subcooled flow boiling flow at certain time instants for various imposed mass fluxes for q=8.1 W/cm^2 and ΔT_{sub}= 10^{o}C at G=400±5% kg/m^{2}s with oscillation t$_p$=10s.

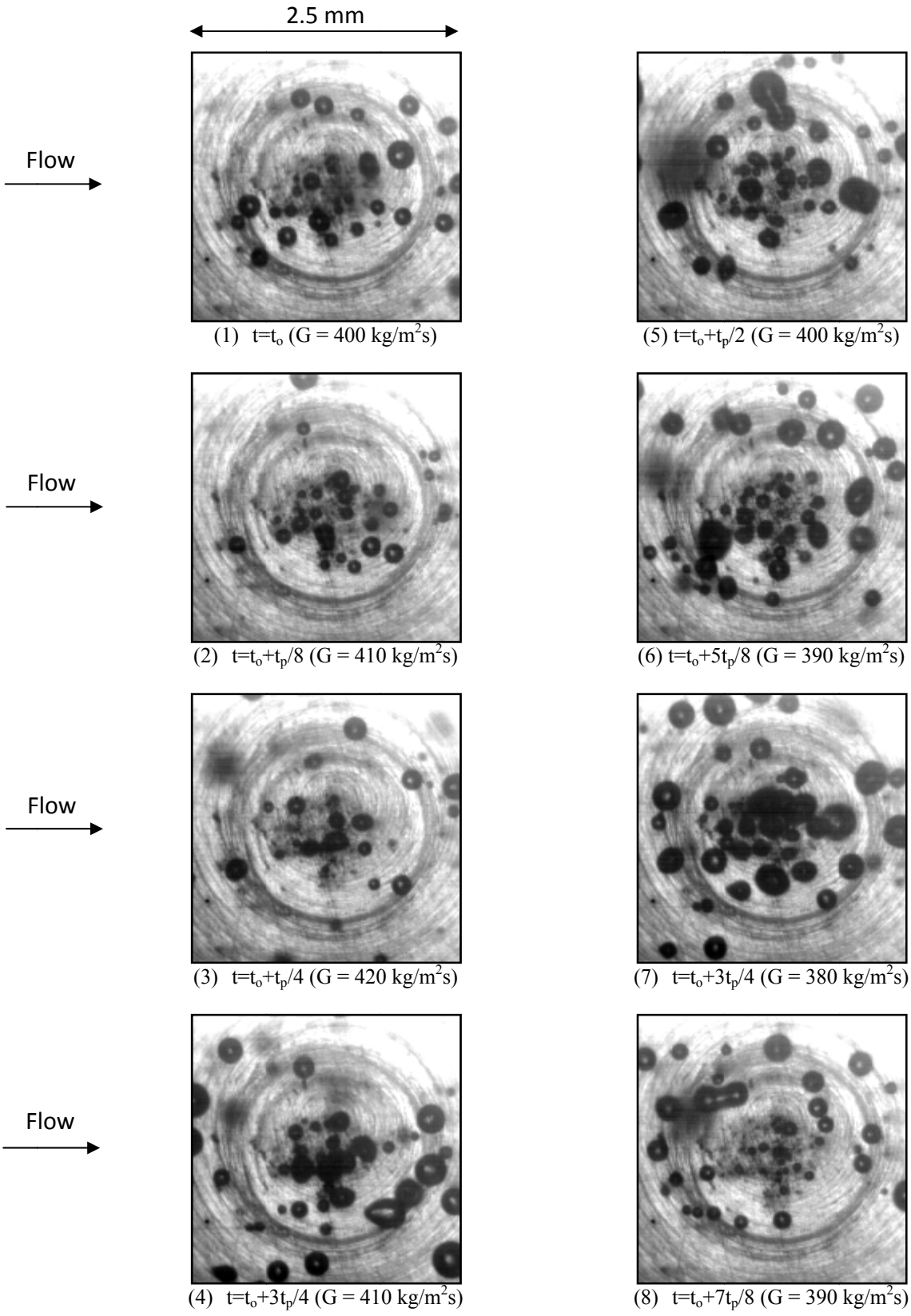

Fig.5.126 Photos of transient oscillatory subcooled flow boiling flow at certain time instants for various imposed mass fluxes for q=9.6 W/cm^2 and ΔT_{sub}= 10^{o}C at G=400±5% kg/m^{2}s with oscillation t$_p$=10s.

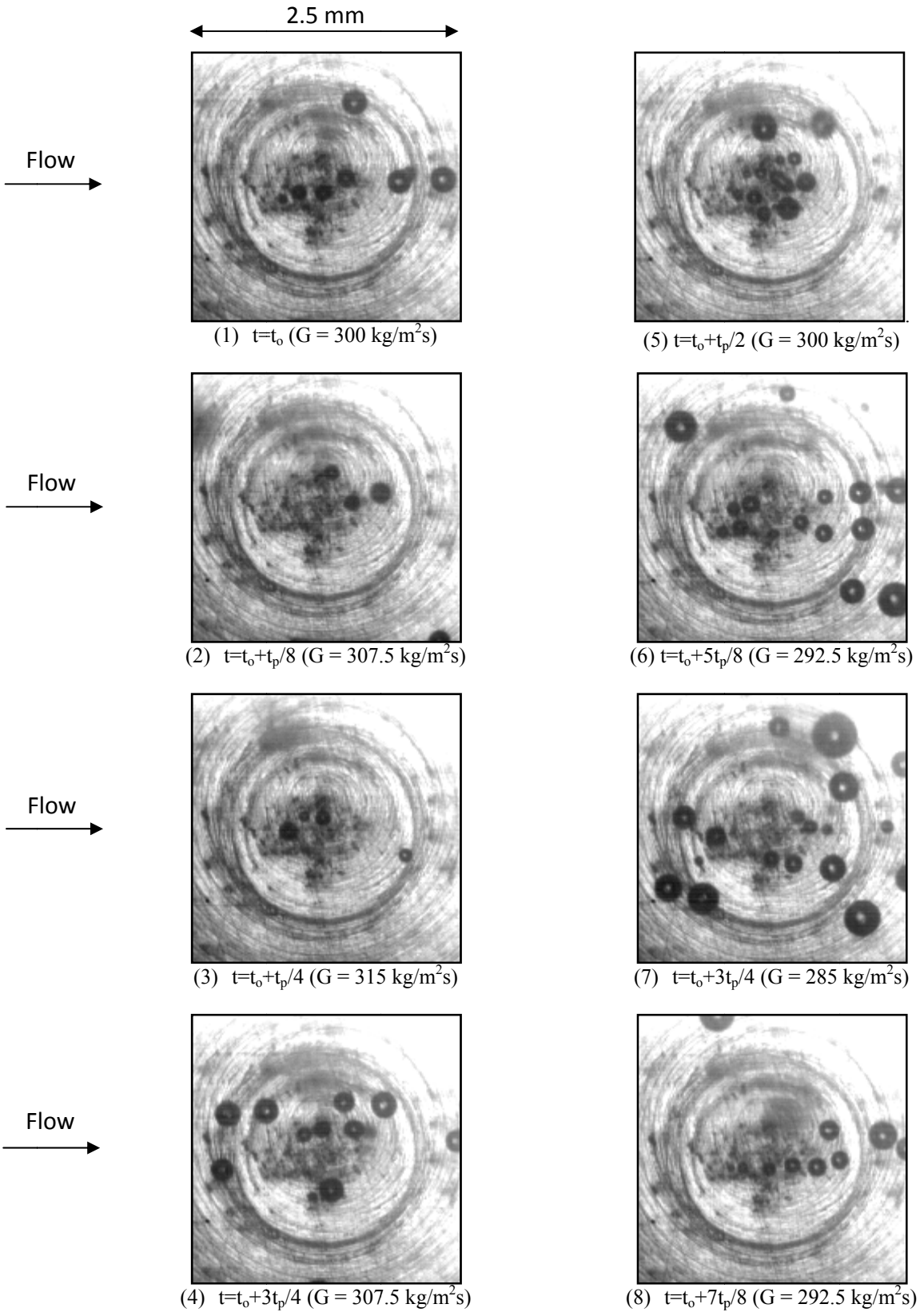

Fig.5.127 Photos of transient oscillatory subcooled flow boiling flow at certain time instants for various imposed mass fluxes for q=6.7 W/cm^2 and ΔT_{sub}= 10^{o}C at G=300±5% kg/m^{2}s with oscillation t_p=20s.

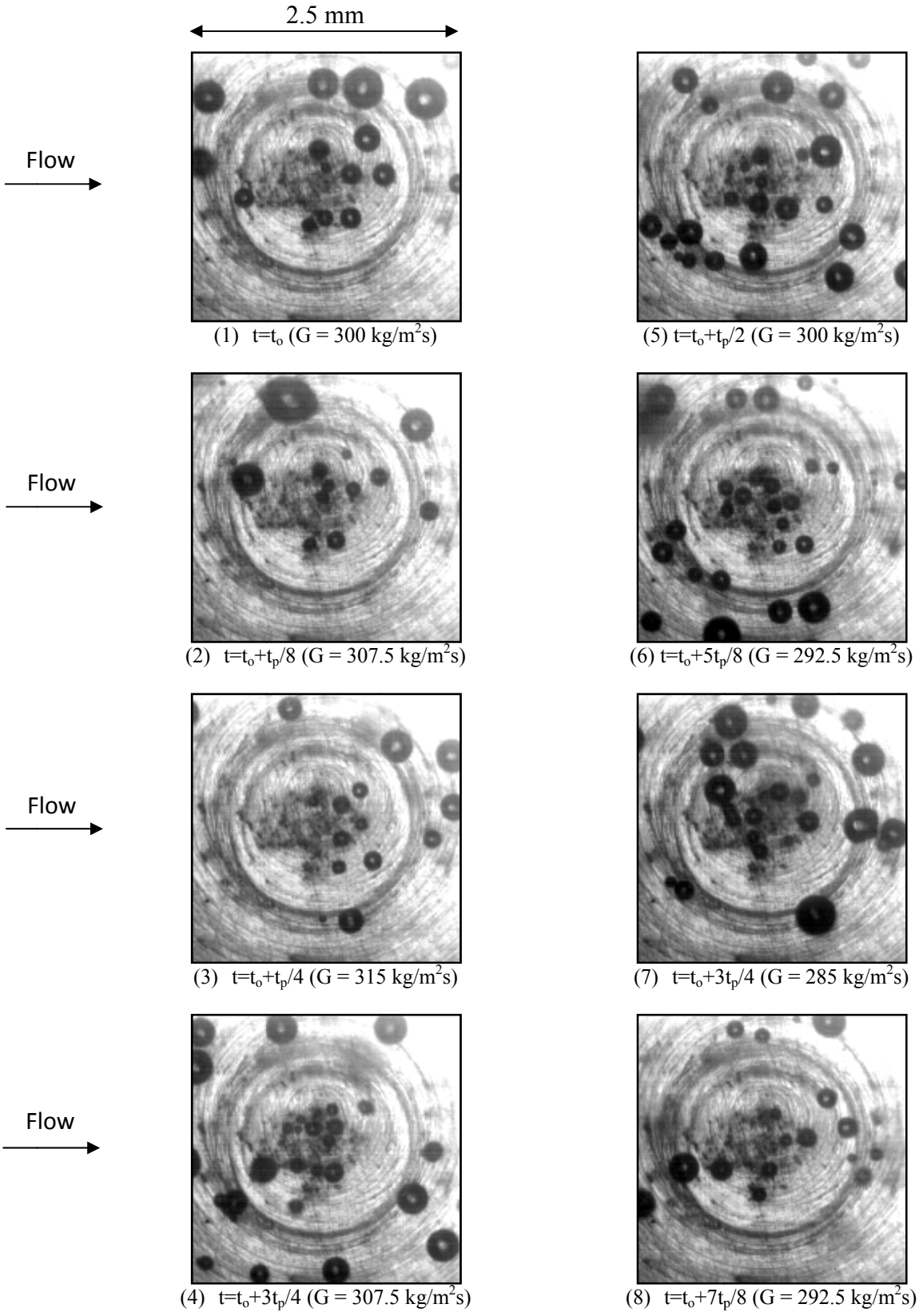

Fig.5.128 Photos of transient oscillatory subcooled flow boiling flow at certain time instants for various imposed mass fluxes for q=8.1 W/cm^2 and ΔT_{sub}= 10^{o}C at G=300±5% kg/m^{2}s with oscillation t$_p$=20s.

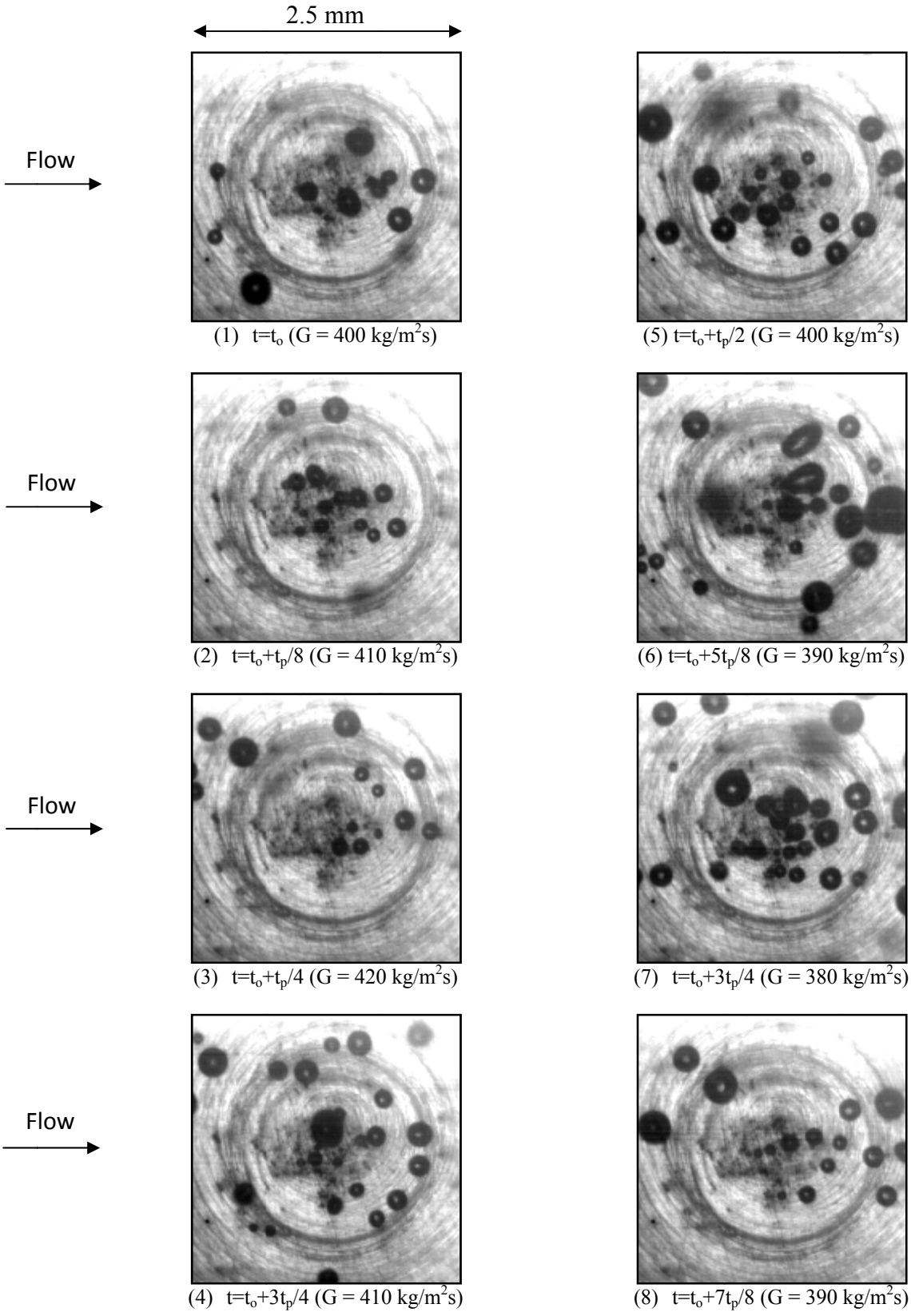

Fig.5.129 Photos of transient oscillatory subcooled flow boiling flow at certain time instants for various imposed mass fluxes for q=8.1 W/cm^2 and ΔT_{sub}= 10^{o}C at G=400±5% kg/m^{2}s with oscillation t_p=20s.

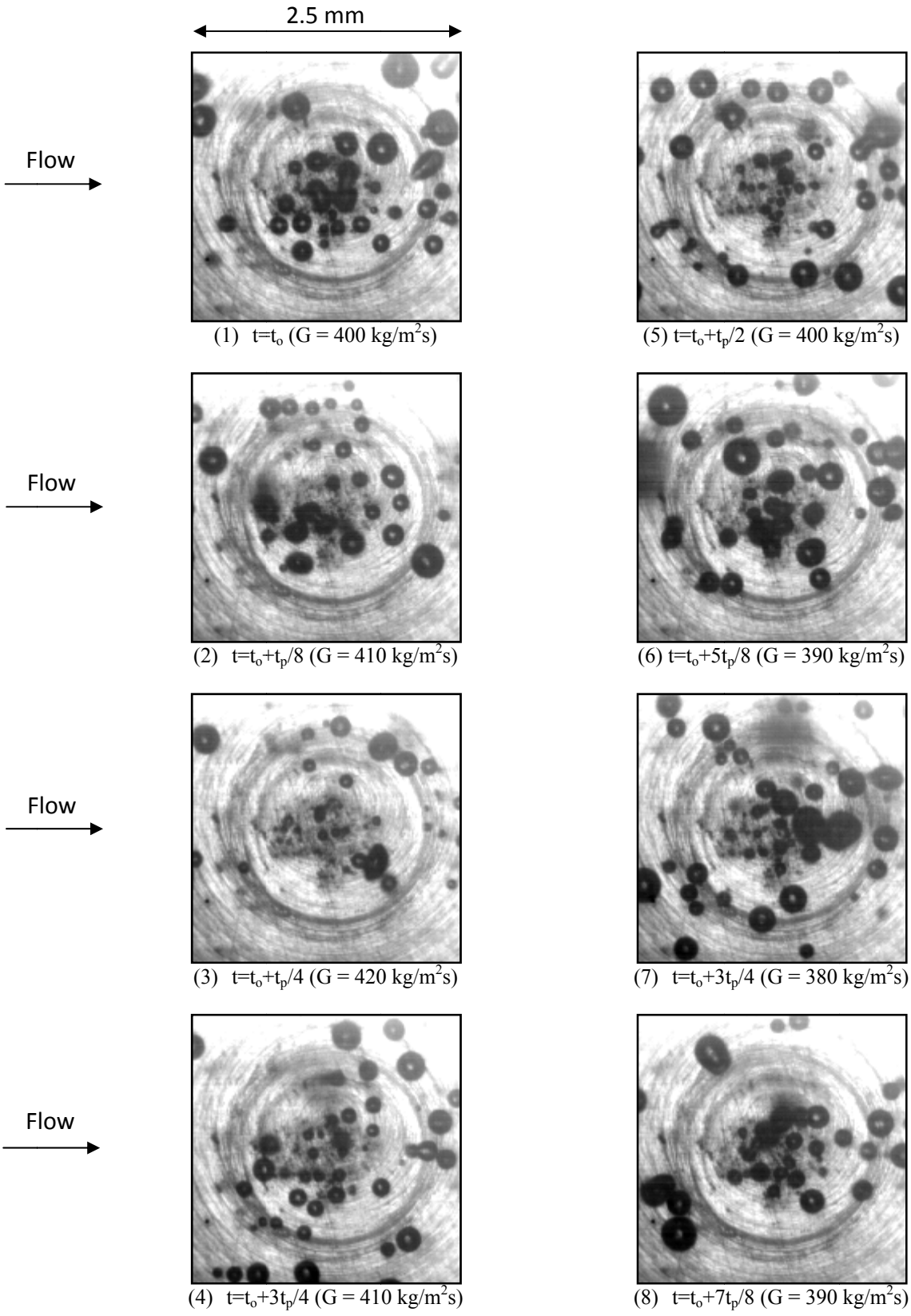

Fig.5.130 Photos of transient oscillatory subcooled flow boiling flow at certain time instants for various imposed mass fluxes for q=9.5 W/cm^2 and ΔT_{sub}= 10^{o}C at G=400±5% kg/m^{2}s with oscillation t$_p$=20s.

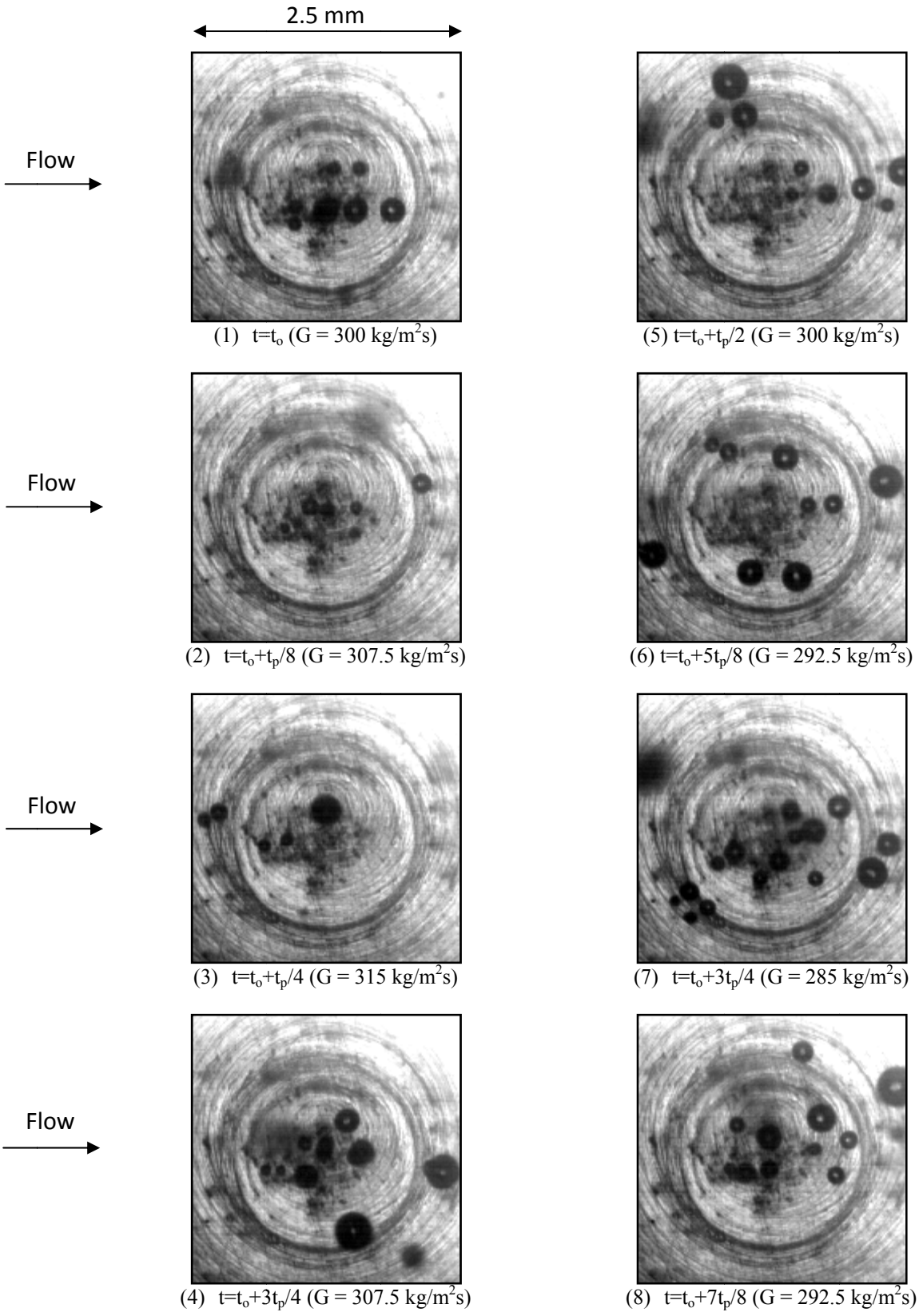

Fig.5.131 Photos of transient oscillatory subcooled flow boiling flow at certain time instants for various imposed mass fluxes for q=6.6 W/cm^2 and ΔT_{sub}= 10^{o}C at G=300±5% kg/m^{2}s with oscillation t_p=30s.

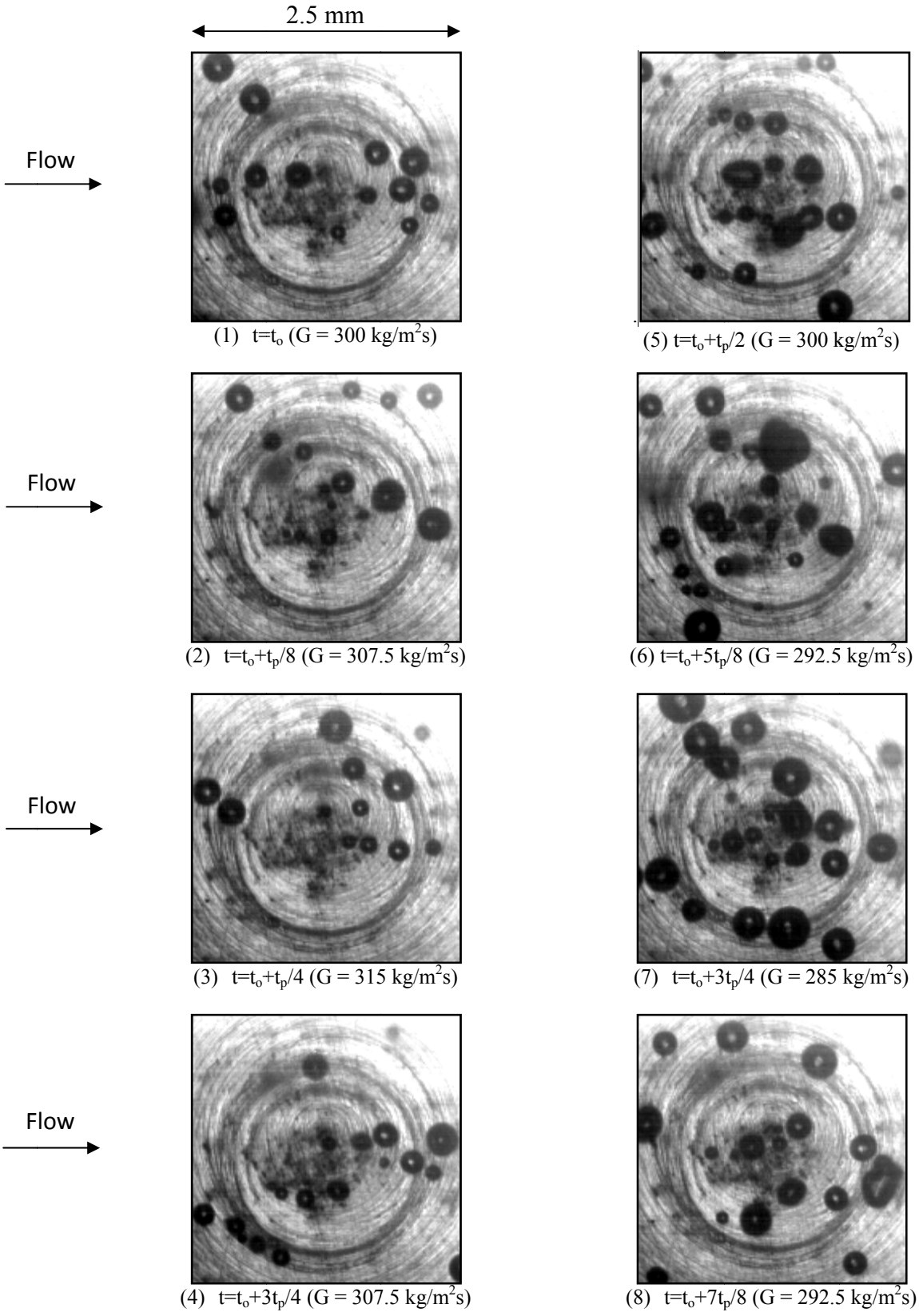

Fig.5.132 Photos of transient oscillatory subcooled flow boiling flow at certain time instants for various imposed mass fluxes for q=8.0 W/cm^2 and ΔT_{sub}= 10^{o}C at G=300±5% kg/m^{2}s with oscillation t_p=30s.

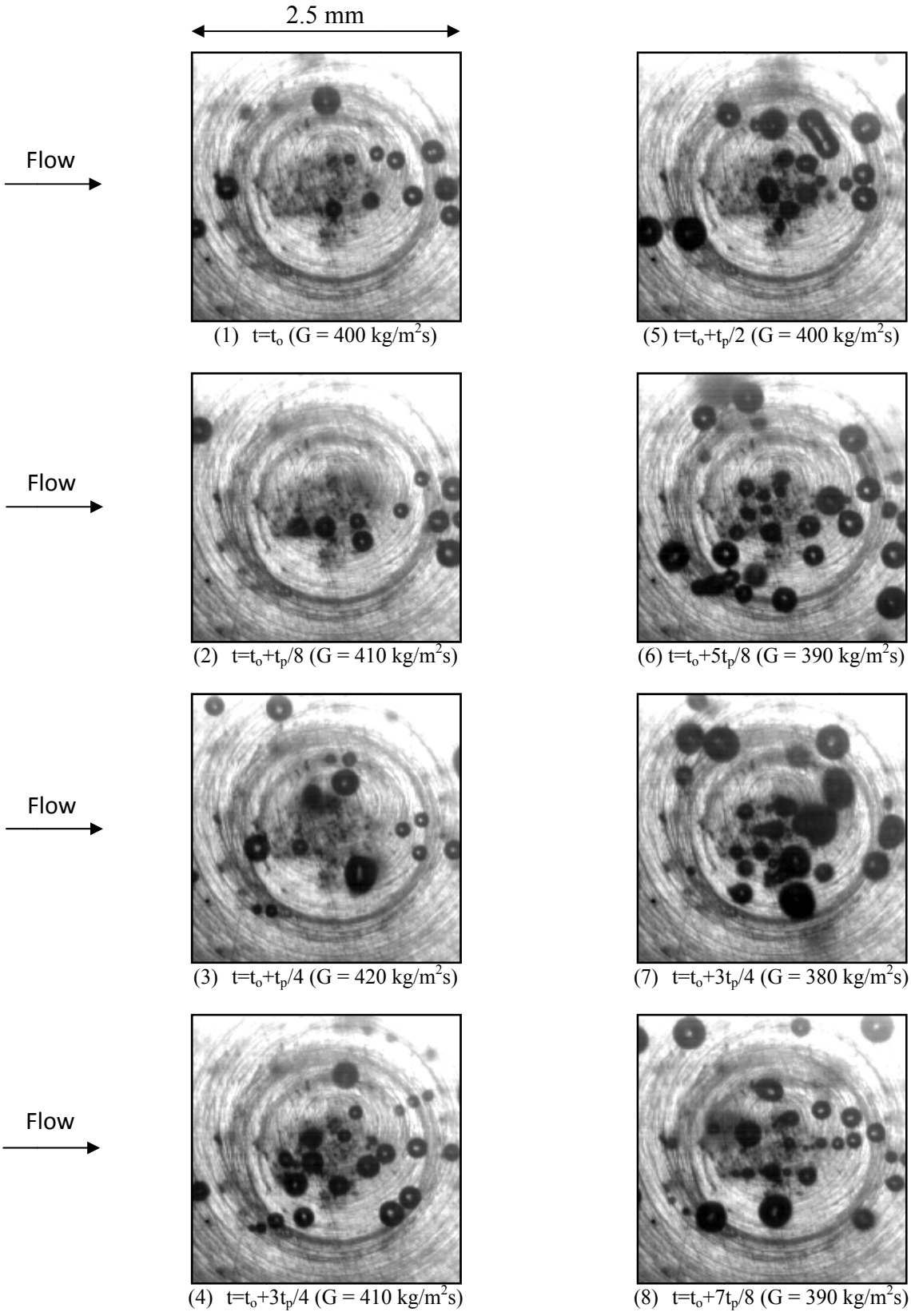

Fig.5.133 Photos of transient oscillatory subcooled flow boiling flow at certain time instants for various imposed mass fluxes for q=8.0 W/cm^2 and ΔT_{sub}= 10^{o}C at G=400±5% kg/m^{2}s with oscillation t_p=30s.

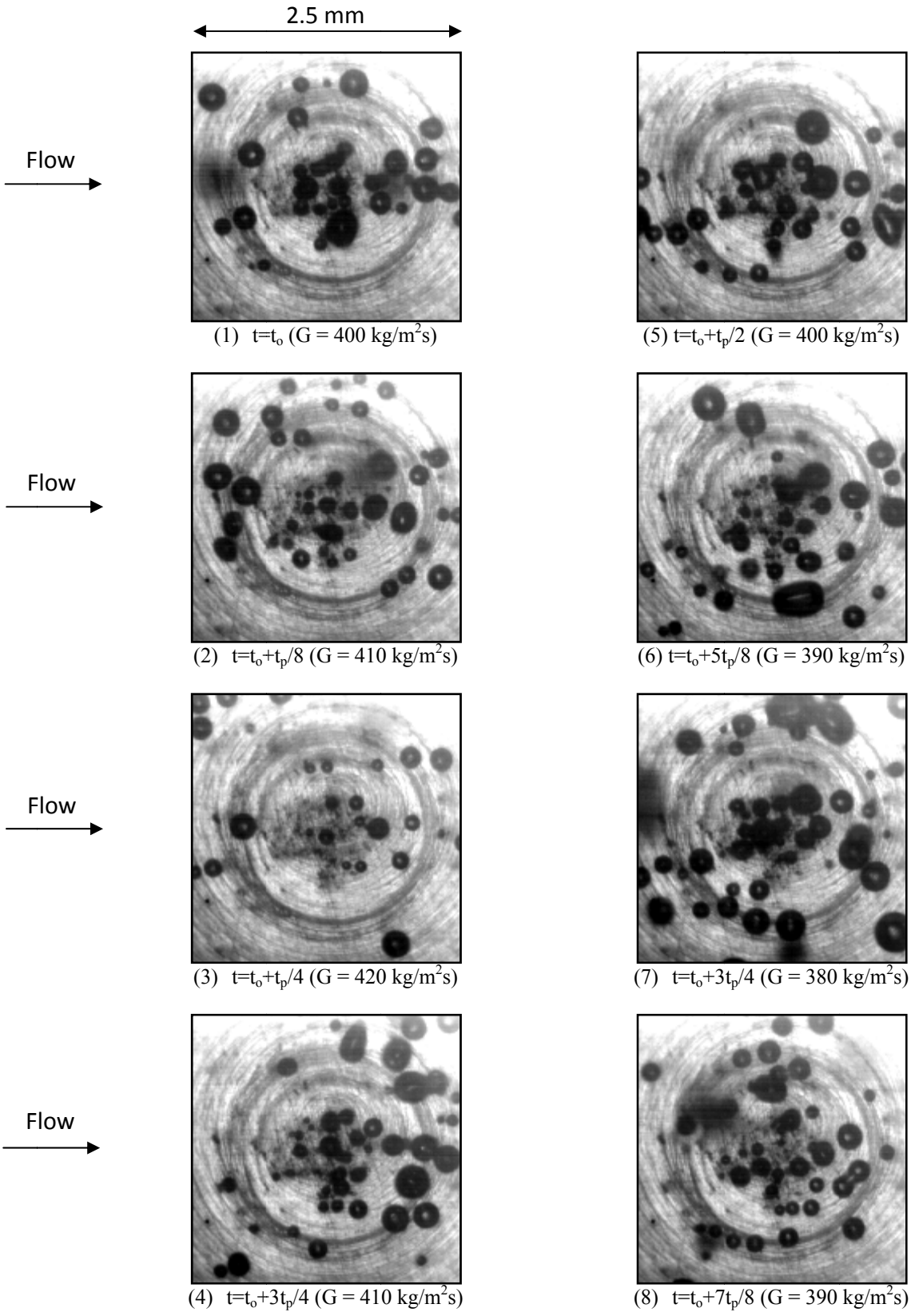

Fig.5.134 Photos of transient oscillatory subcooled flow boiling flow at certain time instants for various imposed mass fluxes for q=9.5 W/cm^2 and ΔT_{sub}= 10^{o}C at G=400±5% kg/m^{2}s with oscillation t_p=30s.

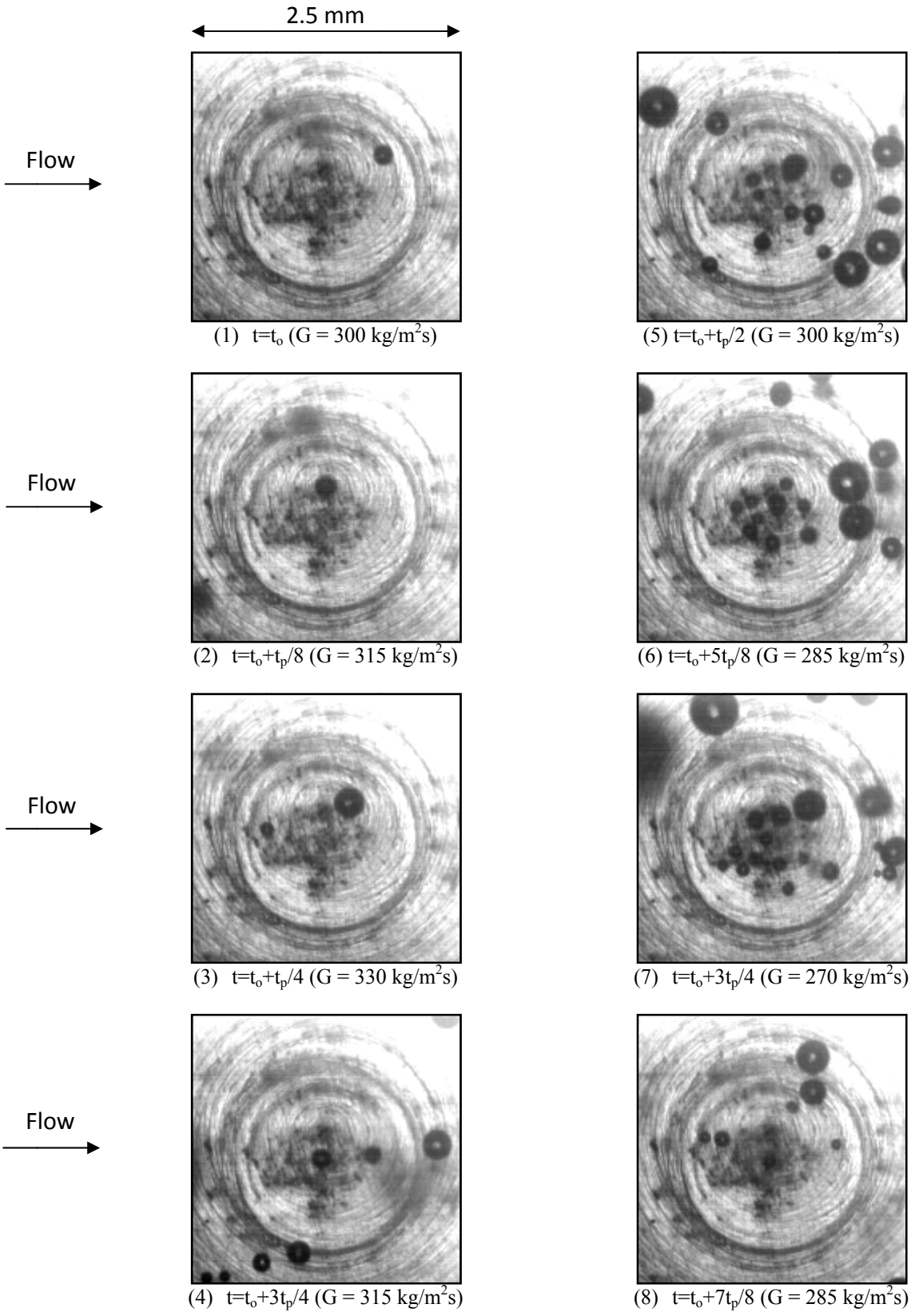

Fig.5.135 Photos of transient oscillatory subcooled flow boiling flow at certain time instants for various imposed mass fluxes for q=6.7 W/cm^2 and ΔT_{sub}= 10^{o}C at G=300±10% kg/m^{2}s with oscillation t_p=10s.

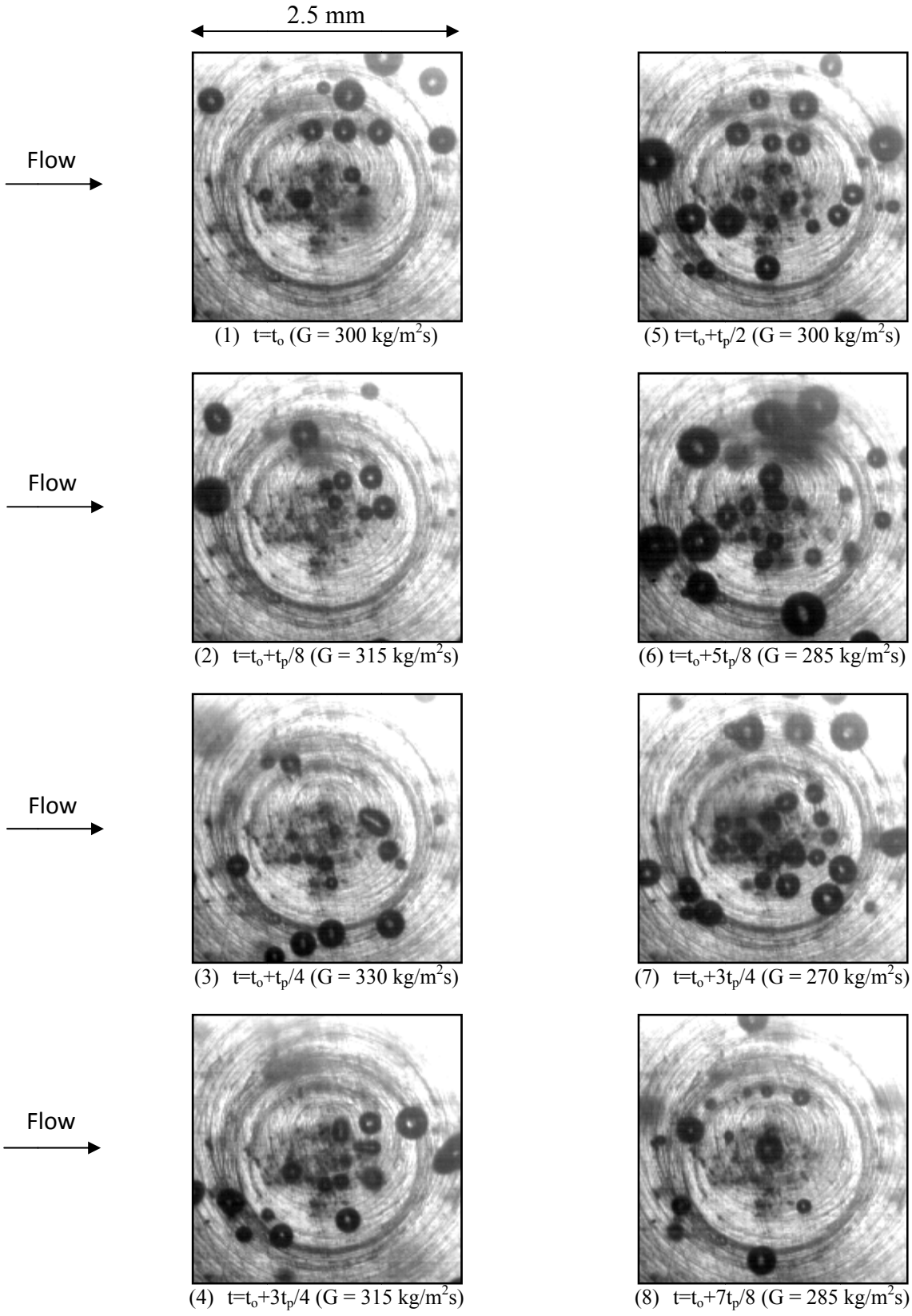

Fig.5.136 Photos of transient oscillatory subcooled flow boiling flow at certain time instants for various imposed mass fluxes for q=8.1 W/cm^2 and ΔT_{sub}= 10^{o}C at G=300±10% kg/m^{2}s with oscillation t_p=10s.

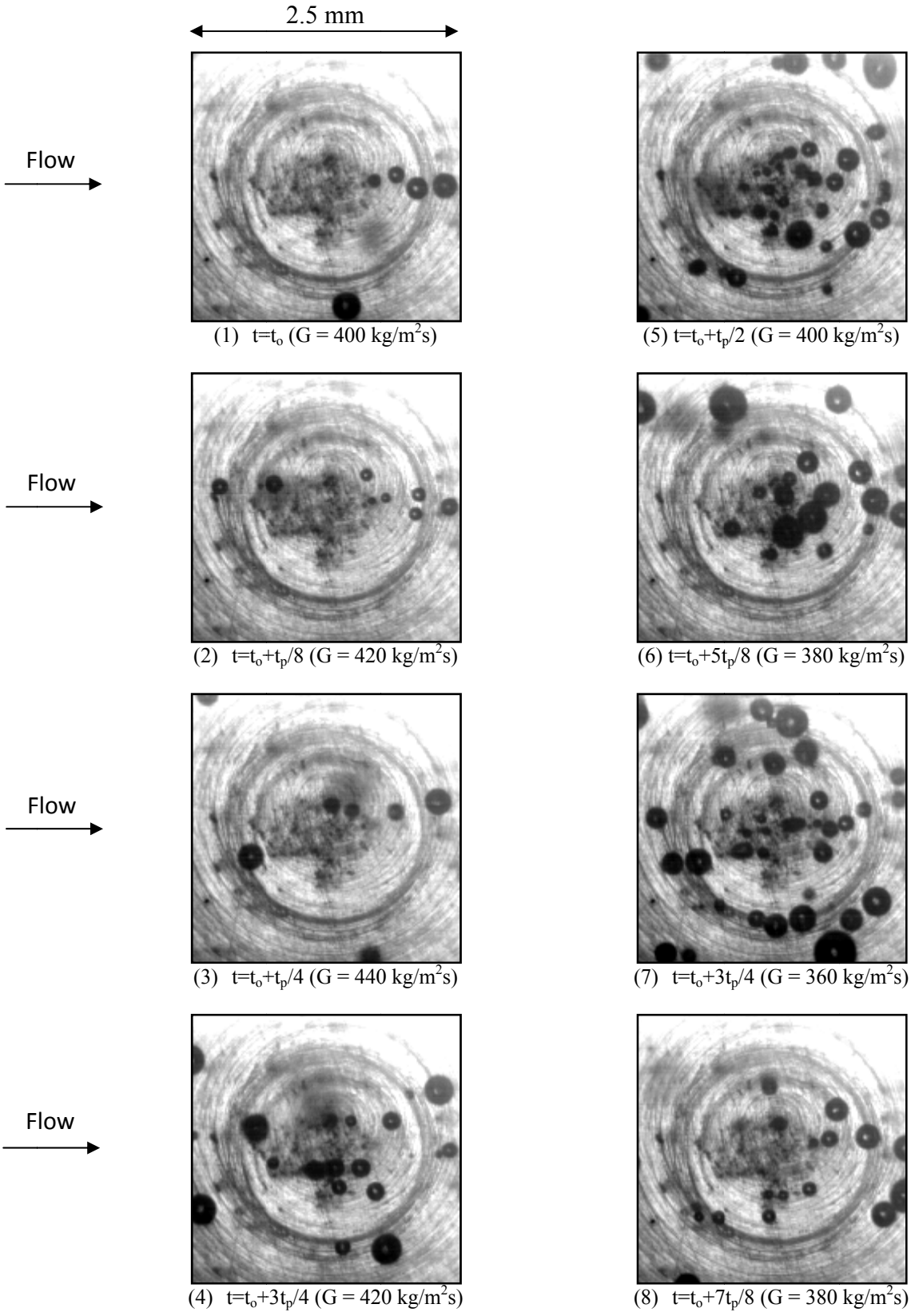

Fig.5.137 Photos of transient oscillatory subcooled flow boiling flow at certain time instants for various imposed mass fluxes for q=8.2 W/cm^2 and ΔT_{sub}= 10^{o}C at G=400±10% kg/m^{2}s with oscillation t$_p$=10s.

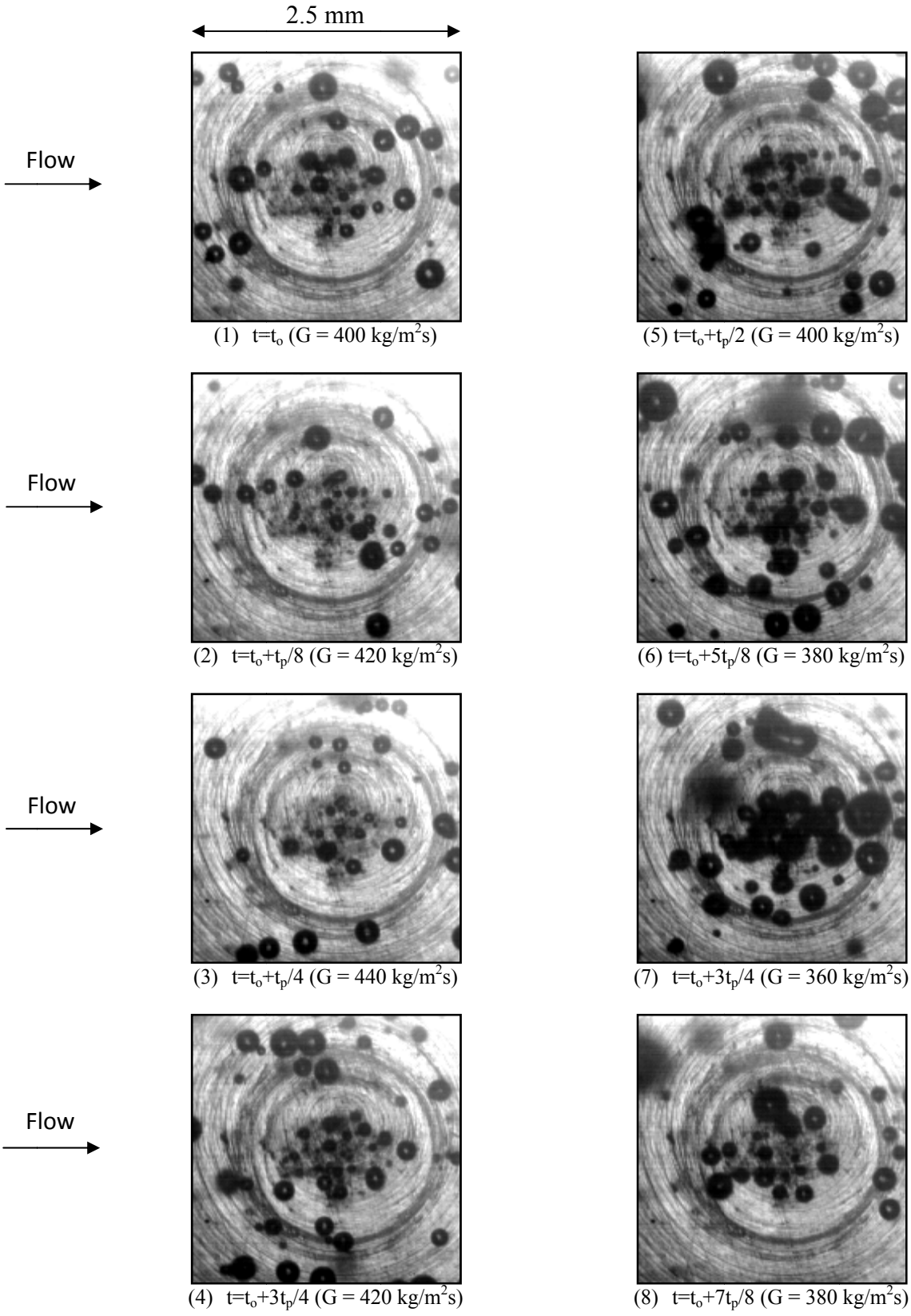

Fig.5.138 Photos of transient oscillatory subcooled flow boiling flow at certain time instants for various imposed mass fluxes for q=9.7 W/cm^2 and ΔT_{sub}= 10^{o}C at G=400±10% kg/m^{2}s with oscillation t$_p$=10s.

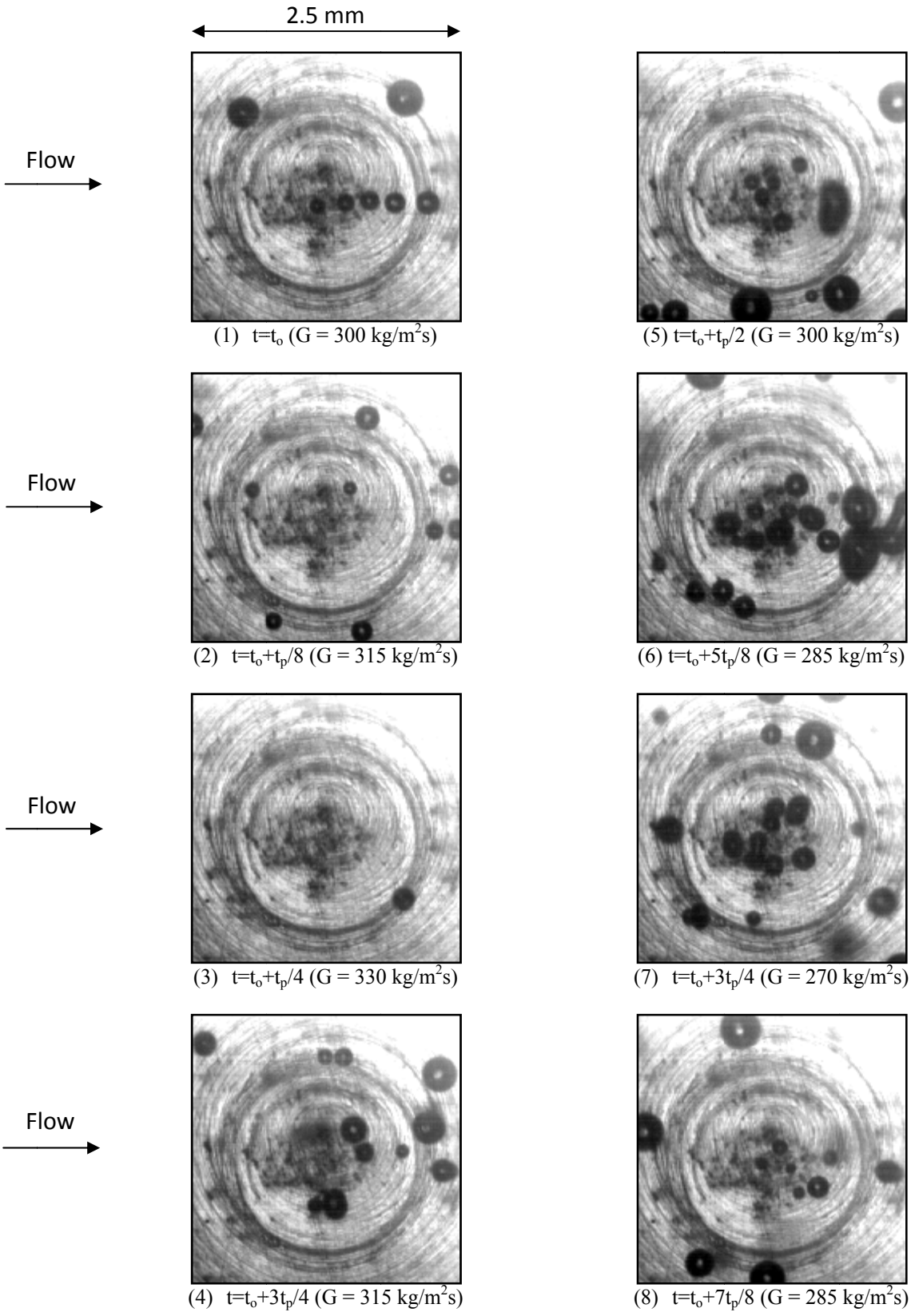

Fig.5.139 Photos of transient oscillatory subcooled flow boiling flow at certain time instants for various imposed mass fluxes for q=6.7 W/cm^2 and ΔT_{sub}= 10^{o}C at G=300±10% kg/m^{2}s with oscillation t_p=20s.

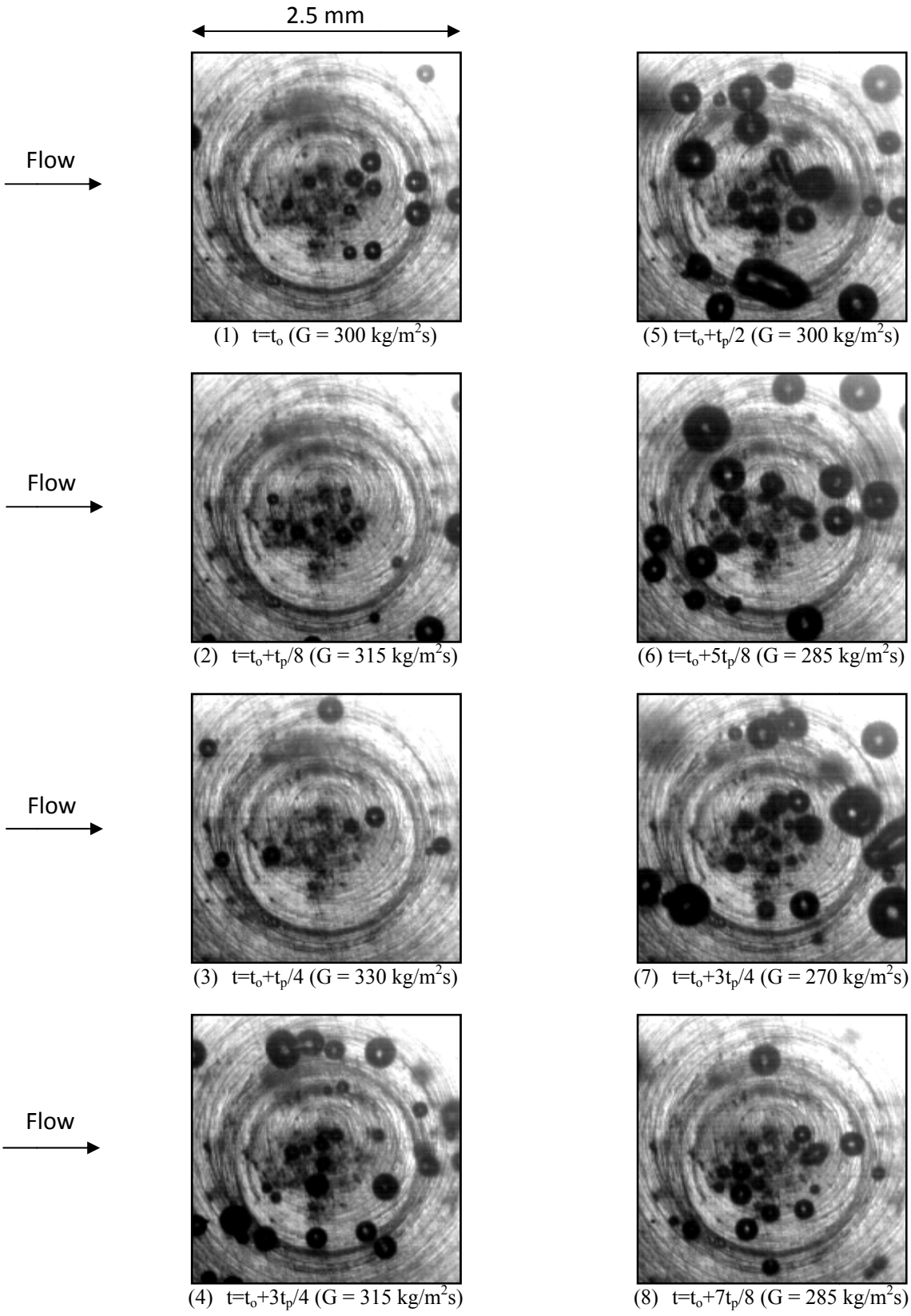

Fig.5.140 Photos of transient oscillatory subcooled flow boiling flow at certain time instants for various imposed mass fluxes for q=8.1 W/cm^2 and ΔT_{sub}= 10^{o}C at G=300±10% kg/m^{2}s with oscillation t_p=20s.

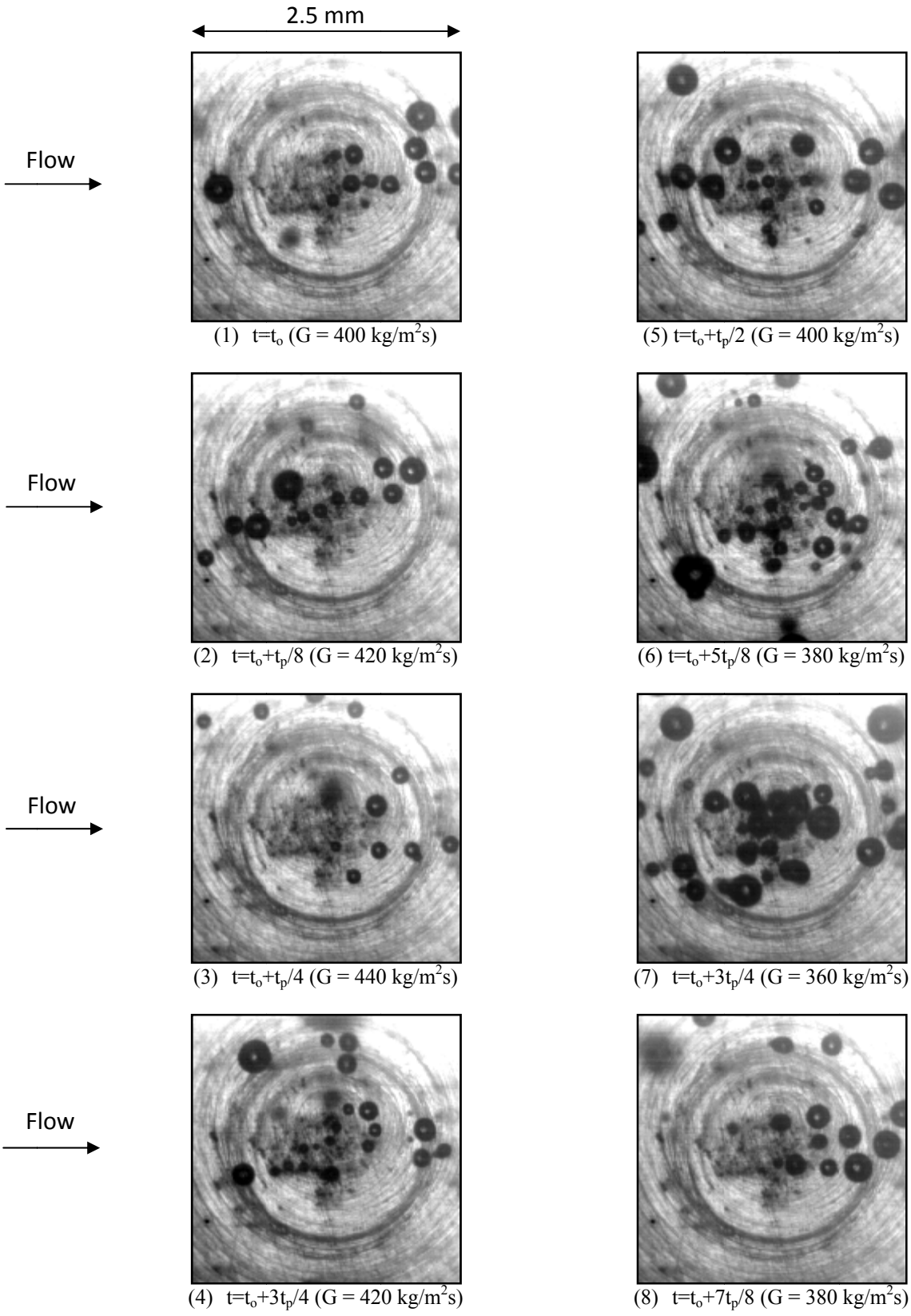

Fig.5.141 Photos of transient oscillatory subcooled flow boiling flow at certain time instants for various imposed mass fluxes for q=8.1 W/cm^2 and ΔT_{sub}= 10^{o}C at G=400±10% kg/m^{2}s with oscillation t_p=20s.

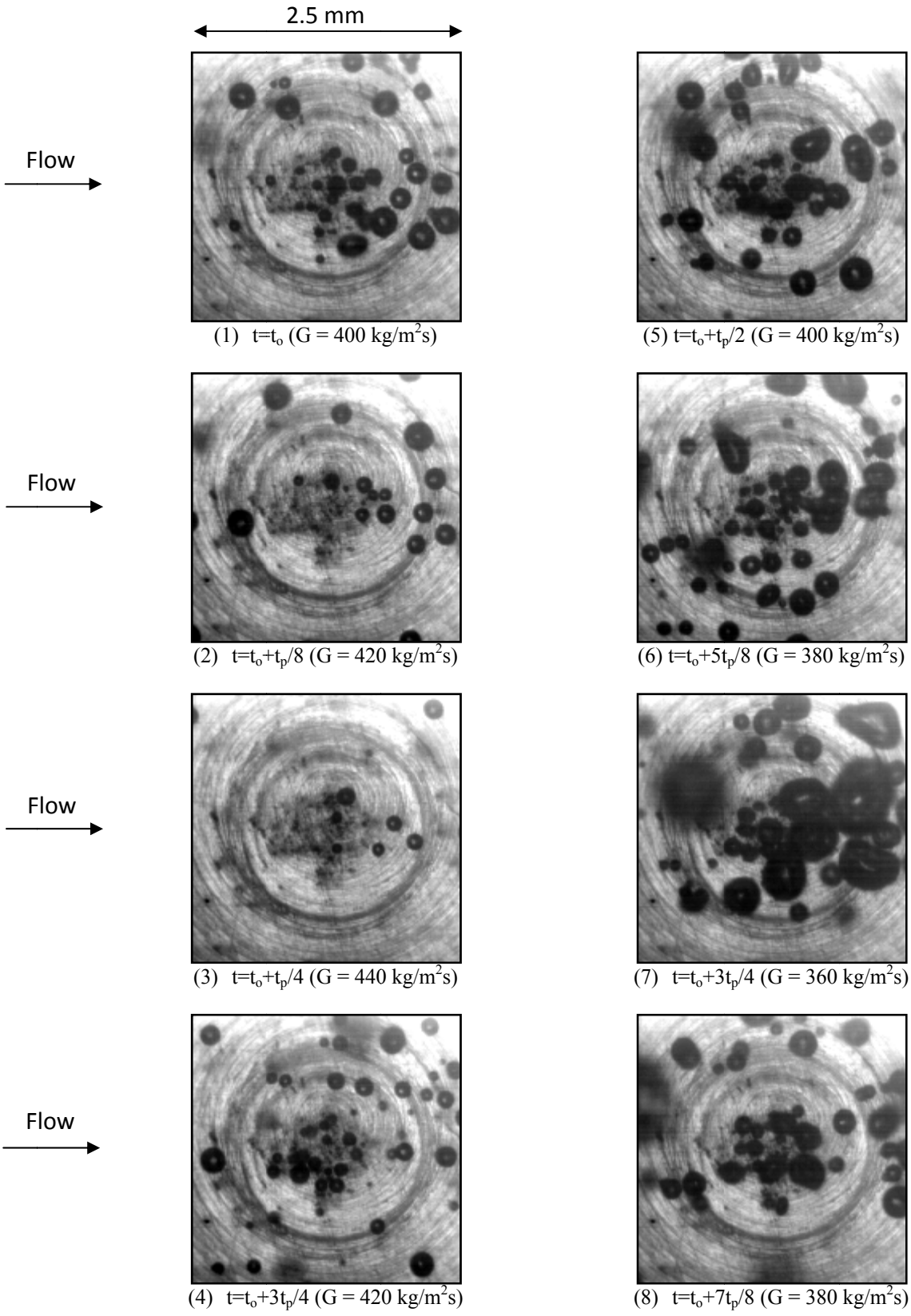

Fig.5.142 Photos of transient oscillatory subcooled flow boiling flow at certain time instants for various imposed mass fluxes for q=9.6 W/cm^2 and ΔT_{sub}= 10^{o}C at G=400±10% kg/m^{2}s with oscillation t$_p$=20s.

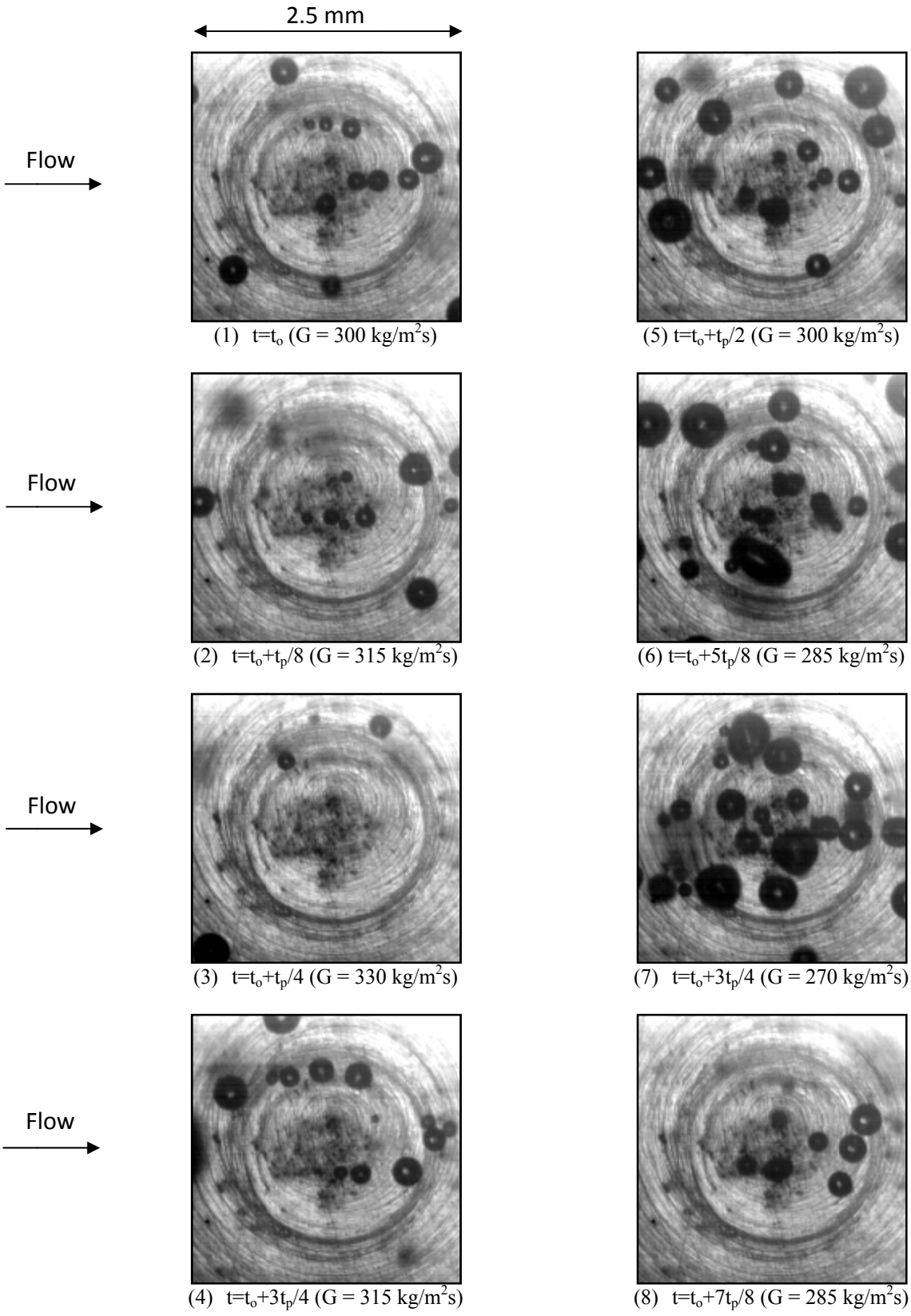

Fig.5.143 Photos of transient oscillatory subcooled flow boiling flow at certain time instants for various imposed mass fluxes for q=6.7 W/cm^2 and ΔT_{sub}= 10^{o}C at G=300±10% kg/m^{2}s with oscillation t_p=30s.

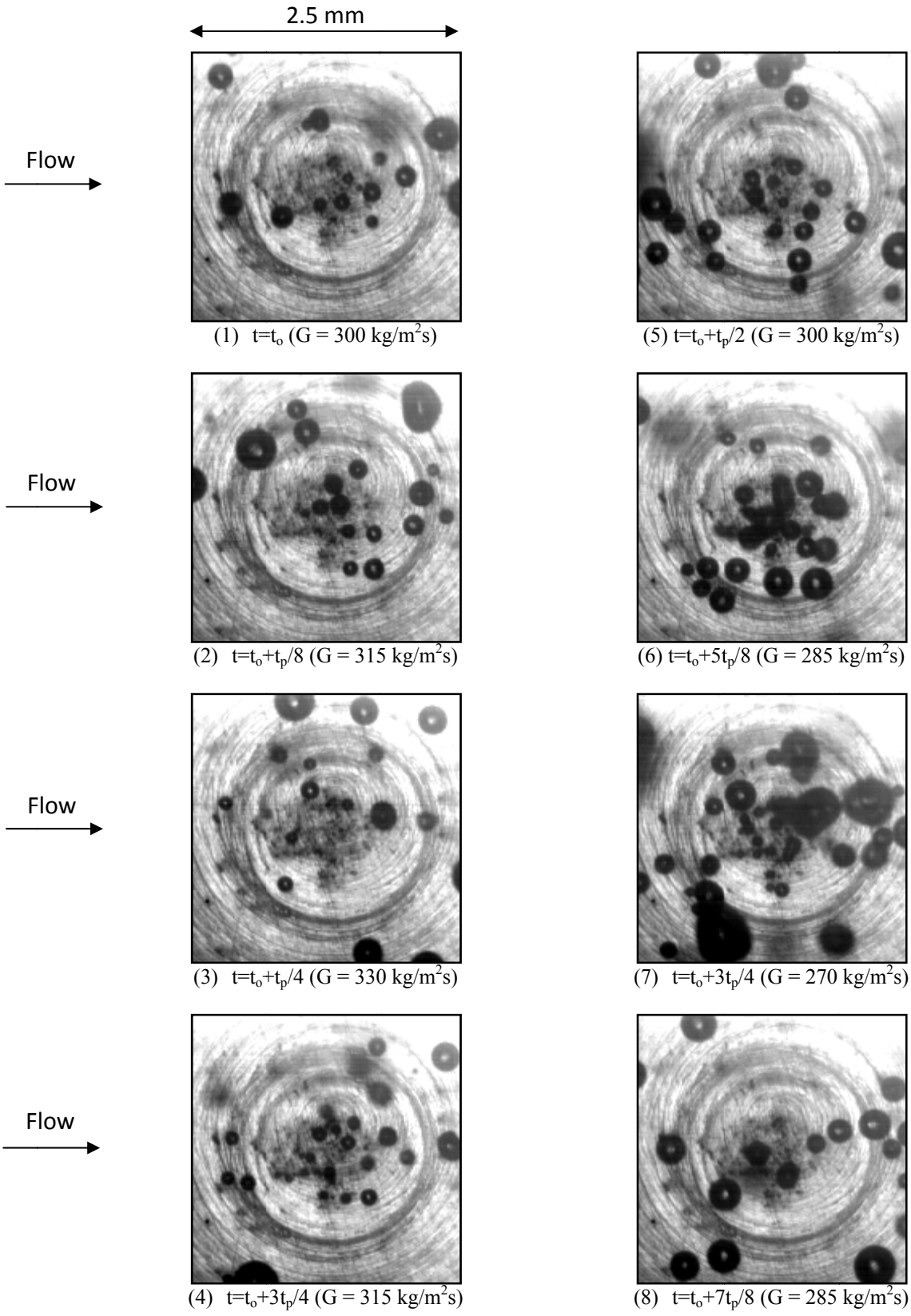

Fig.5.144 Photos of transient oscillatory subcooled flow boiling flow at certain time instants for various imposed mass fluxes for q=8.1 W/cm^2 and ΔT_{sub}= 10^{o}C at G=300±10% kg/m^{2}s with oscillation t_p=30s.

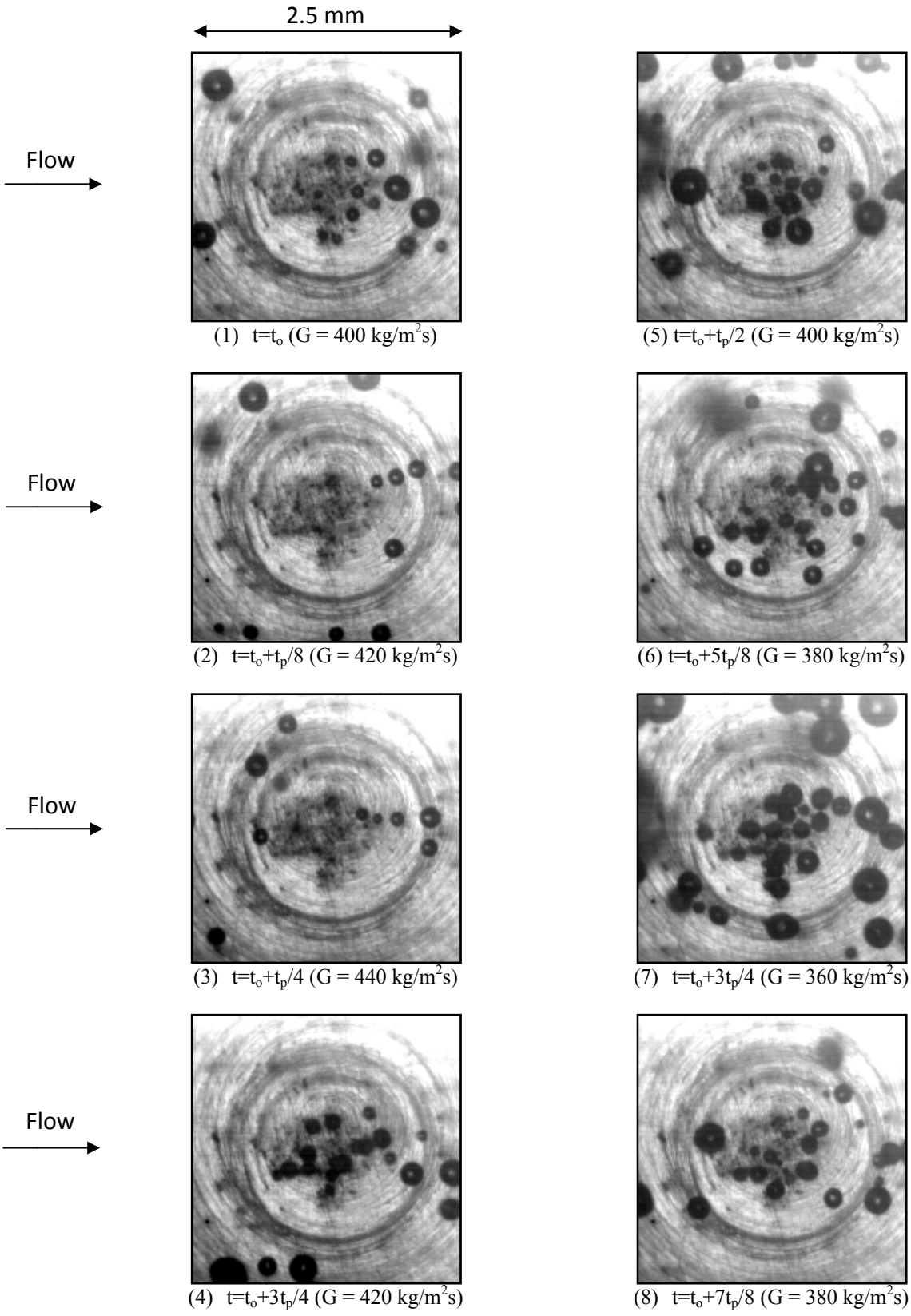

Fig.5.145 Photos of transient oscillatory subcooled flow boiling flow at certain time instants for various imposed mass fluxes for q=8.1 W/cm^2 and ΔT_{sub}= 10^{o}C at G=400±10% kg/m^{2}s with oscillation t_p=30s.

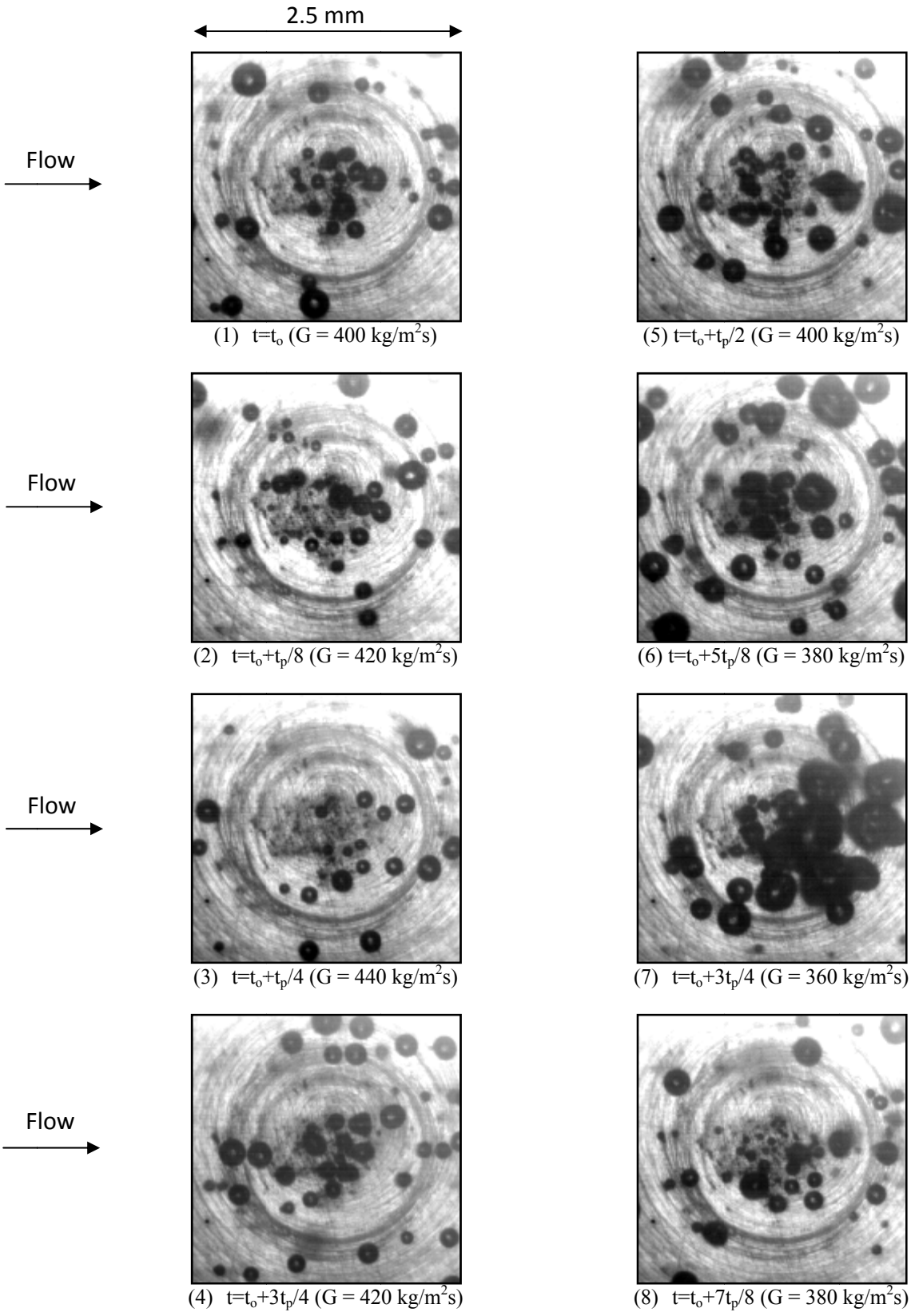

Fig.5.146 Photos of transient oscillatory subcooled flow boiling flow at certain time instants for various imposed mass fluxes for q=9.6 W/cm^2 and ΔT_{sub}= 10^{o}C at G=400±10% kg/m^{2}s with oscillation t$_p$=30s.

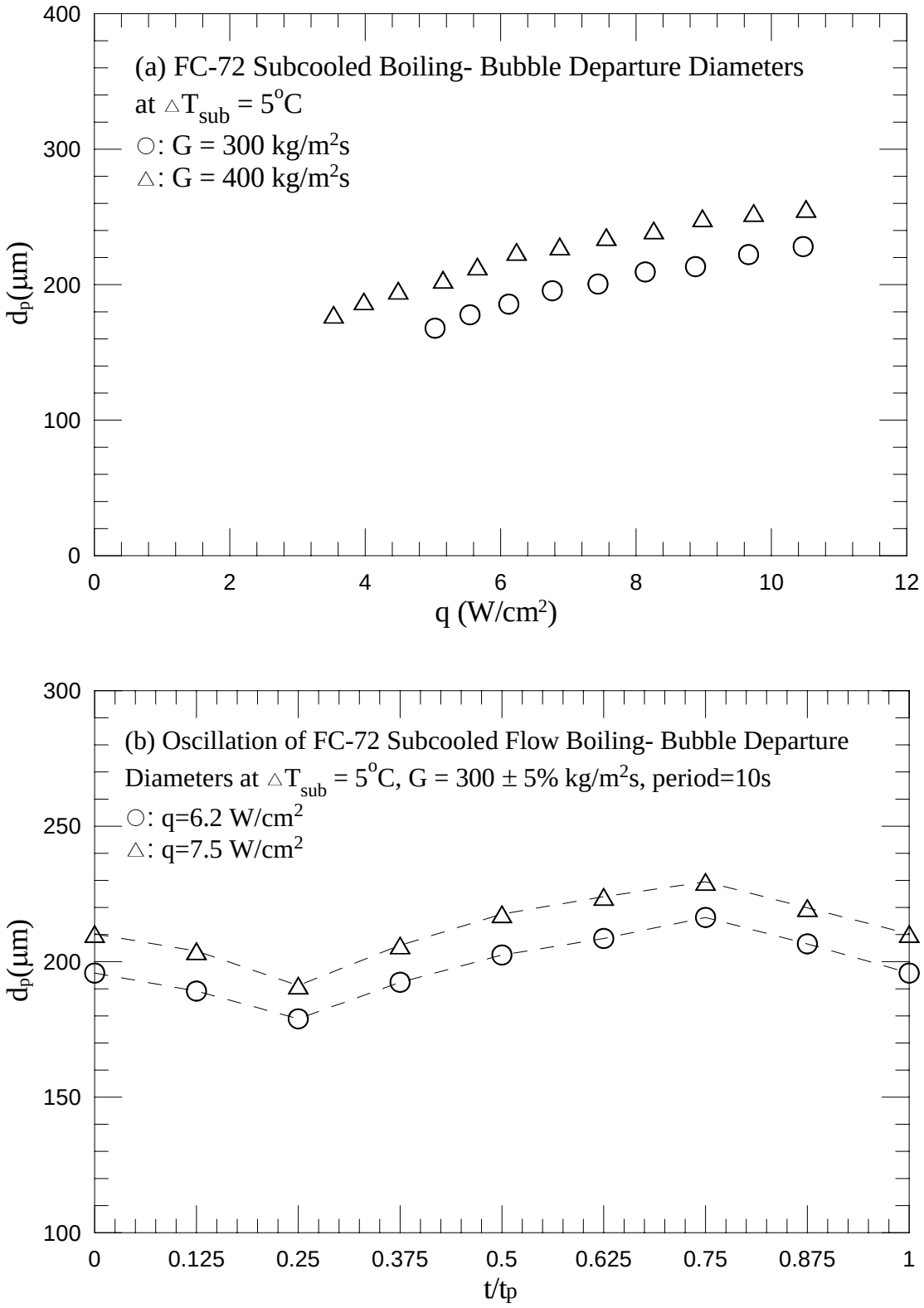

Fig. 5.147 Mean bubble departure diameters for various coolant mass fluxes for stable subcooled flow boiling (a) and various imposed heat fluxes for transient subcooled flow boiling for G=300±5% kg/m^{2}s and ΔT_{sub} =5°C with t_p=10 sec (b), 20sec (c) and 30 sec (d).

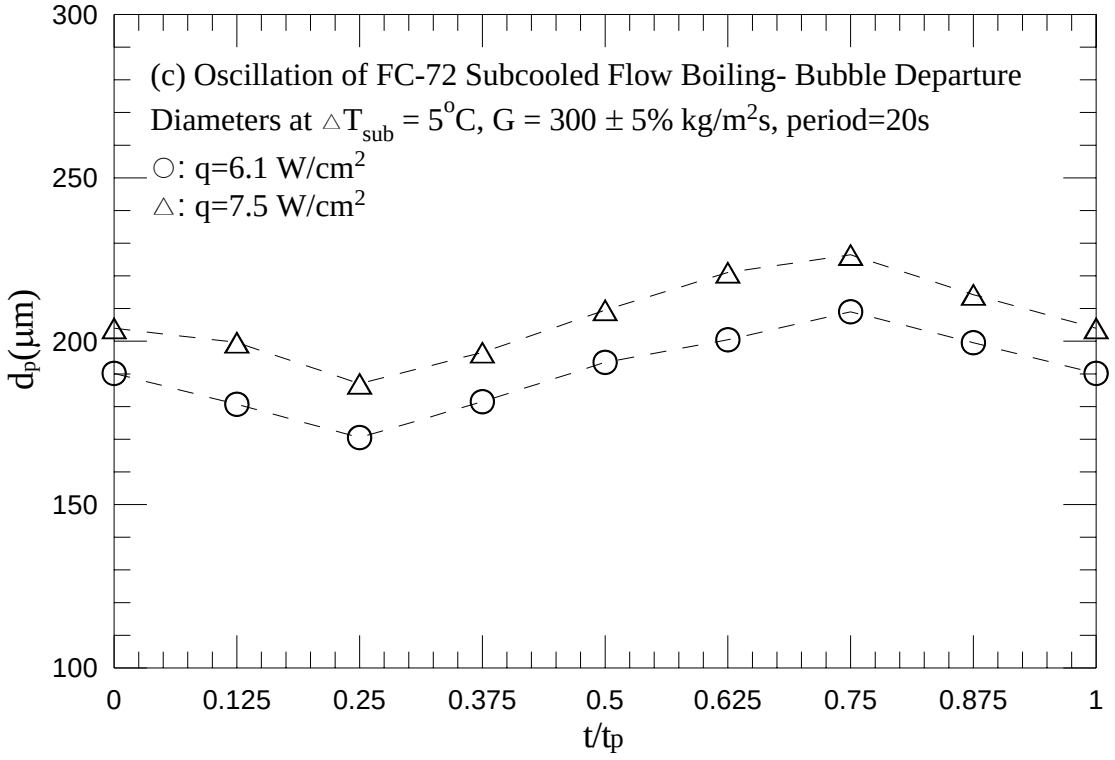

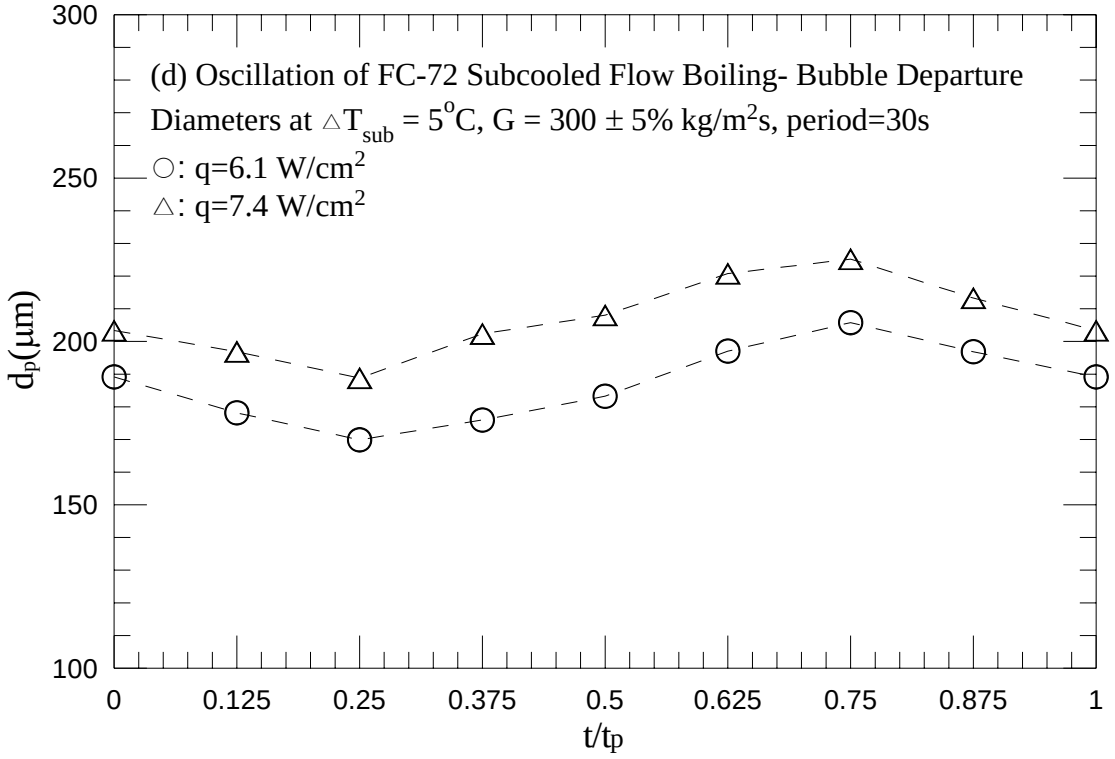

Fig. 5.147 Continued.

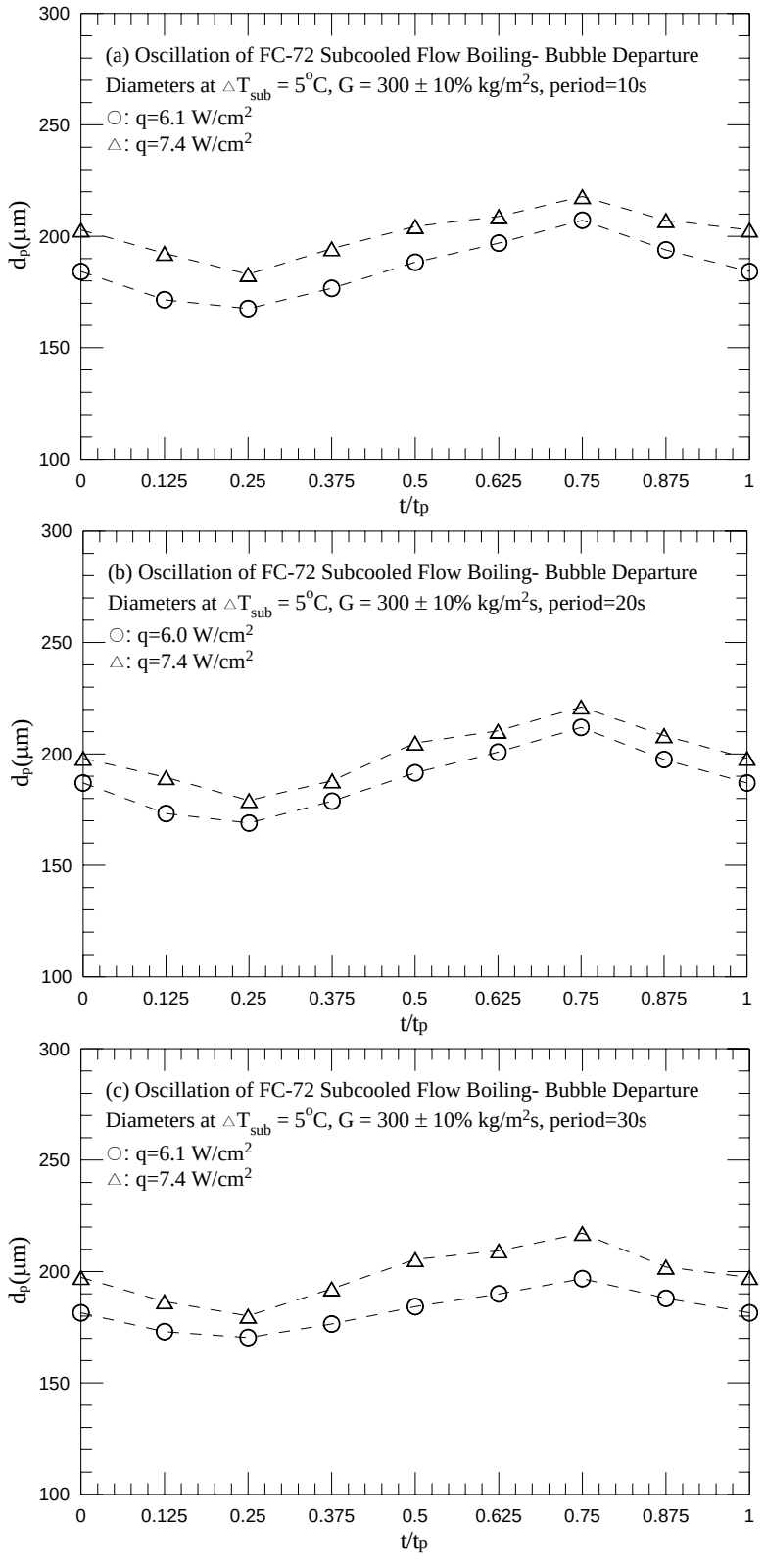

Fig. 5.148 Mean bubble departure diameters for various imposed heat fluxes for transient subcooled flow boiling for G=300±10% kg/m^{2}s and ΔT_{sub} =5°C with t_p=10 sec (a), 20sec (b) and 30 sec (c).

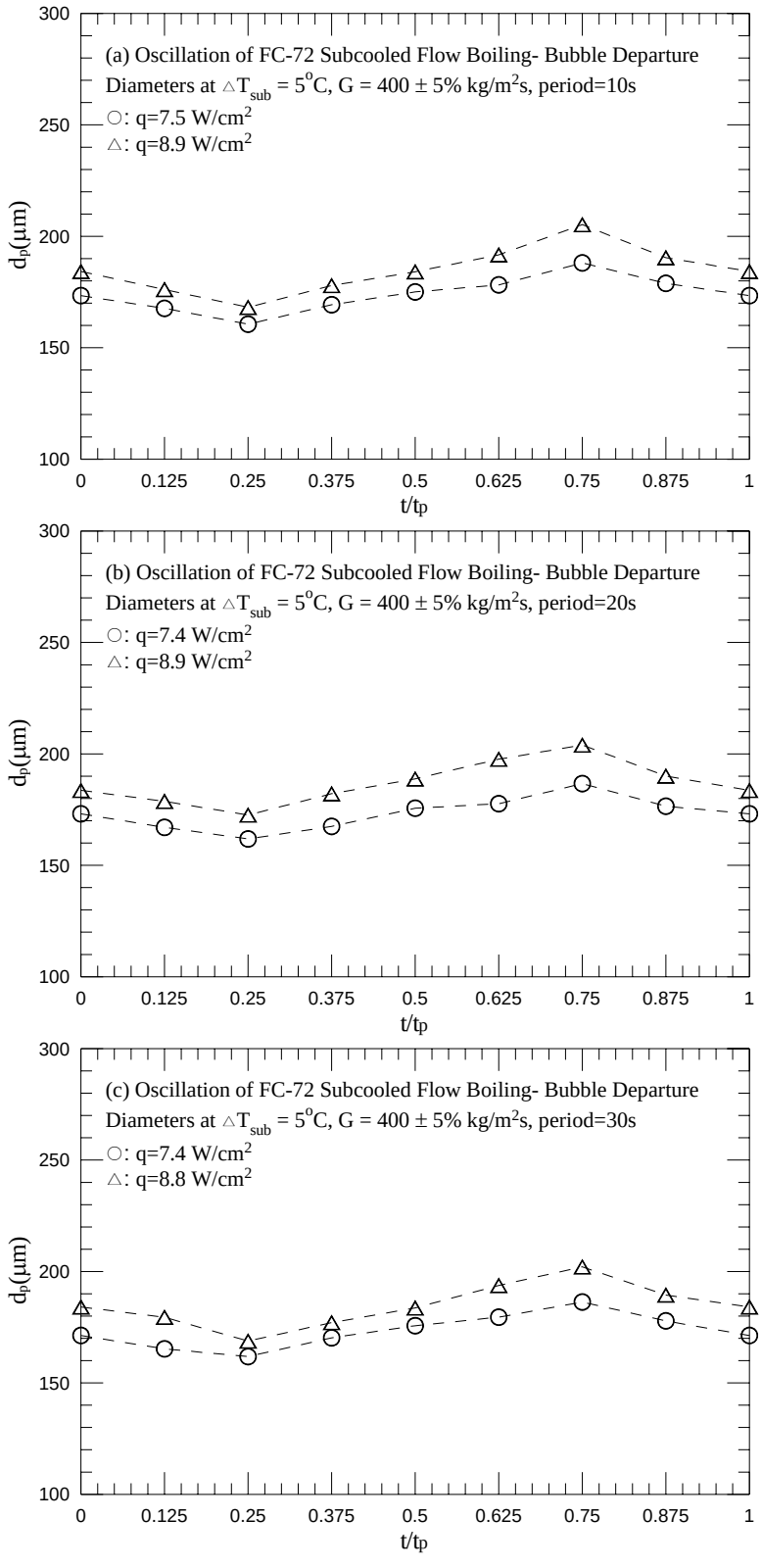

Fig. 5.149 Mean bubble departure diameters for various imposed heat fluxes for transient subcooled flow boiling for G=400±5% kg/m^{2}s and ΔT_{sub} =5°C with t_p=10 sec (a), 20sec (b) and 30 sec (c).

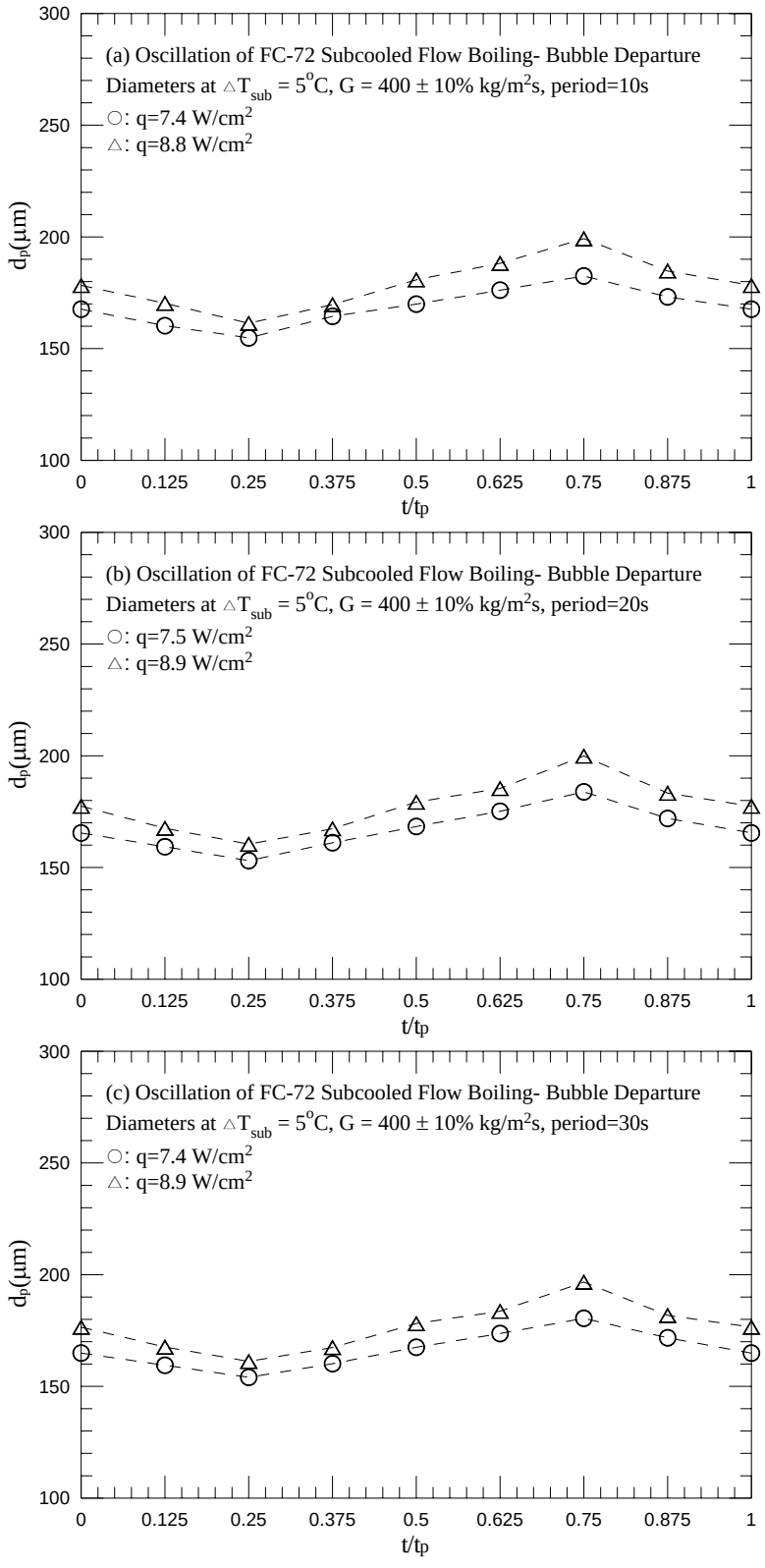

Fig. 5.150 Mean bubble departure diameters for various imposed heat fluxes for transient subcooled flow boiling for G=400±10% kg/m^{2}s and ΔT_{sub} =5°C with t_p=10 sec (a), 20sec (b) and 30 sec (c).

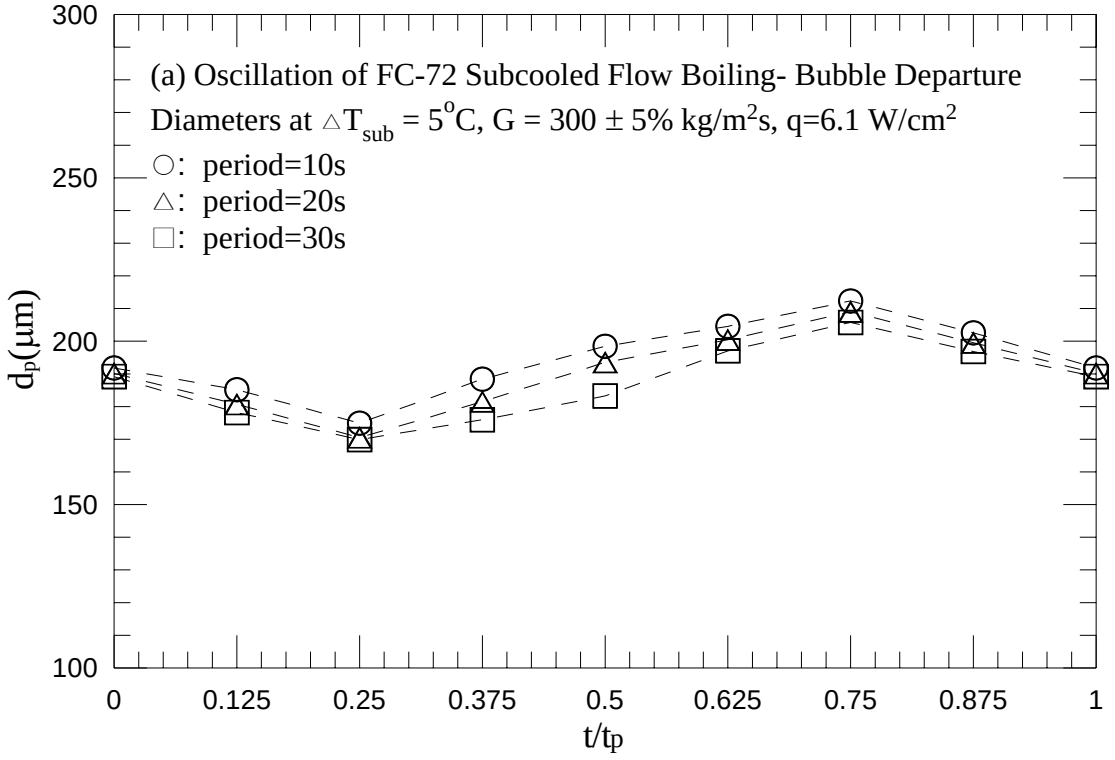

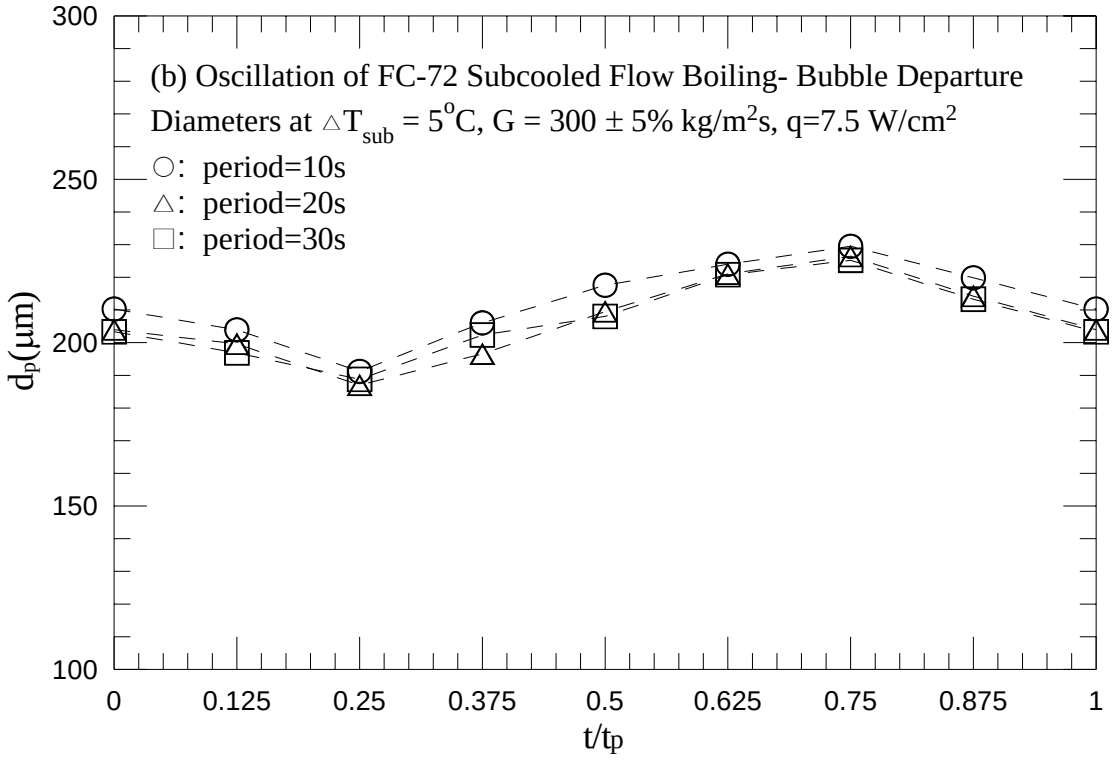

Fig. 5.151 Mean bubble departure diameters for various period of mass flux oscillation for transient subcooled flow boiling for G=300±5% kg/m^{2}s and ΔT_{sub} =5°C with (a) q=6.1 W/cm^2 and (b) q=7.5 W/cm^2.

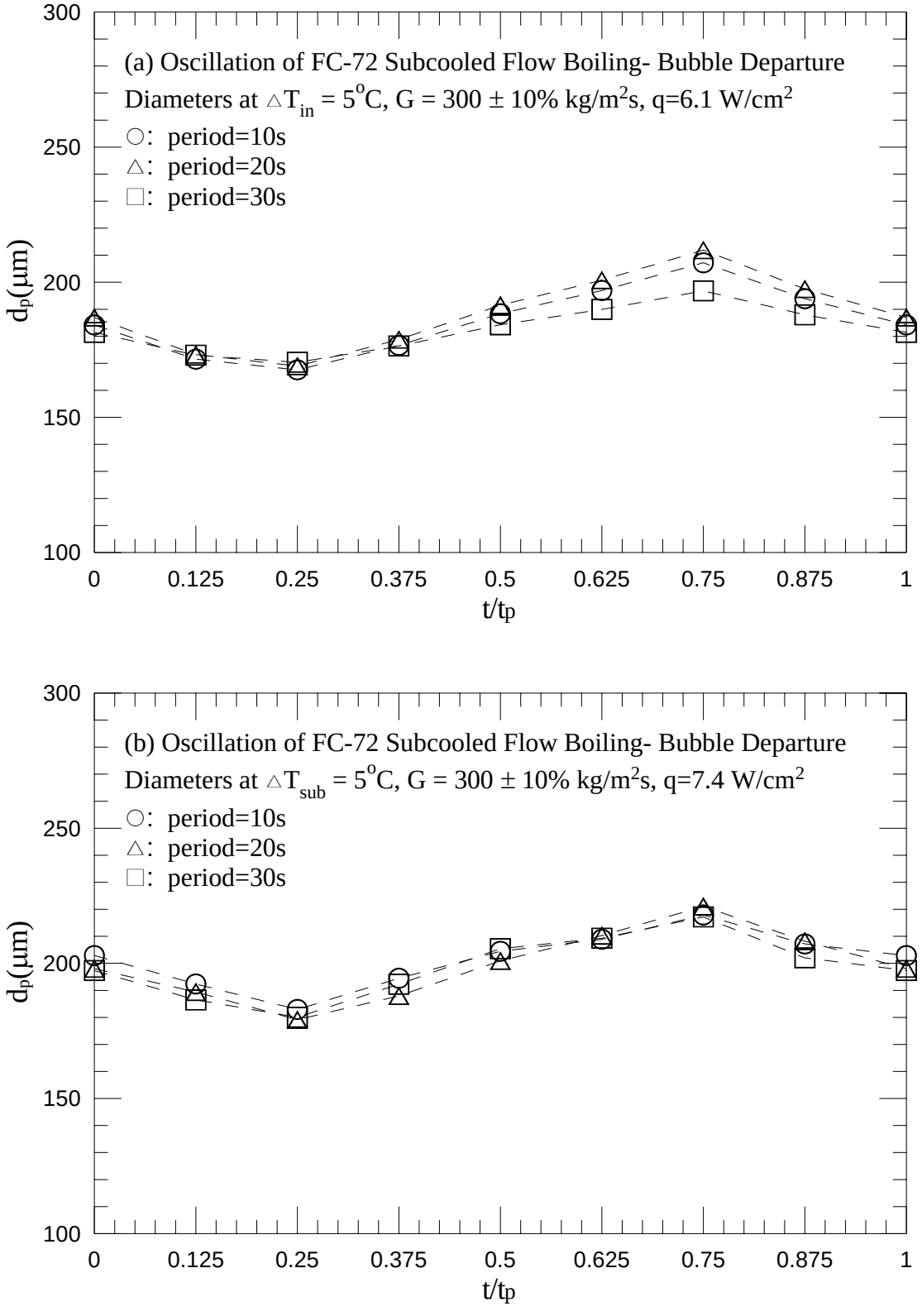

Fig. 5.152 Mean bubble departure diameters for various period of mass flux oscillation for transient subcooled flow boiling for G=300±10% kg/m^{2}s and ΔT_{sub} =5°C with (a) q=6.1 W/cm^2 and (b) q=7.4 W/cm^2.

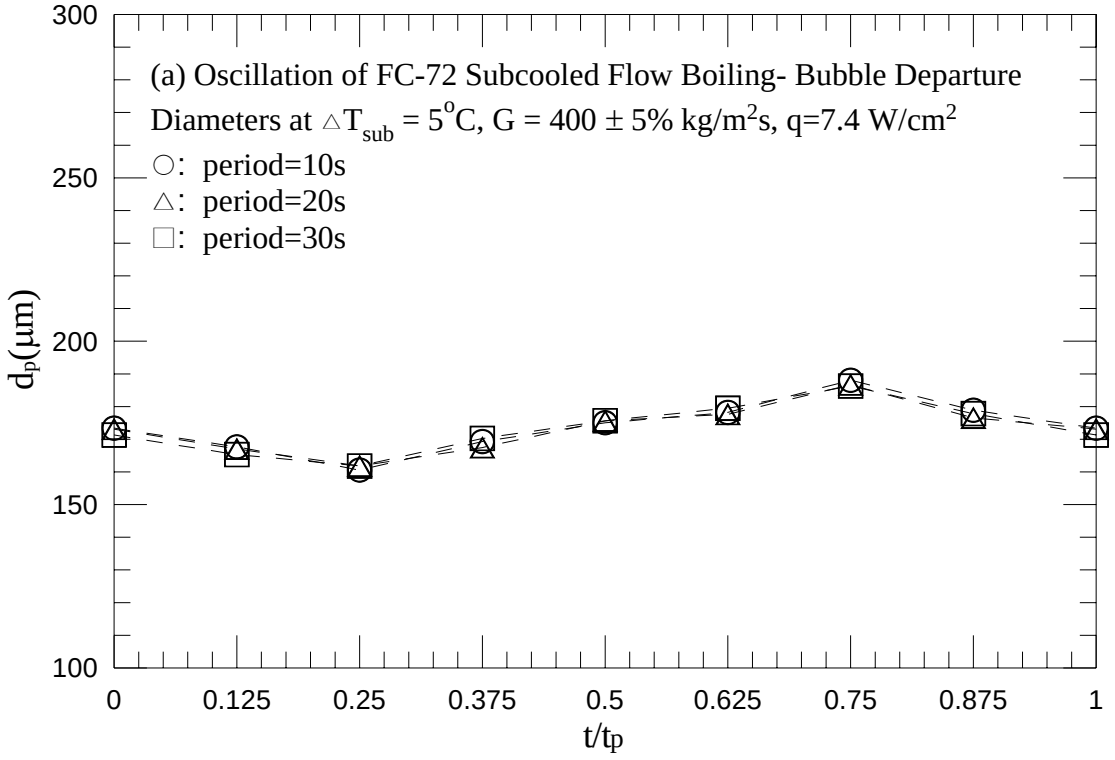

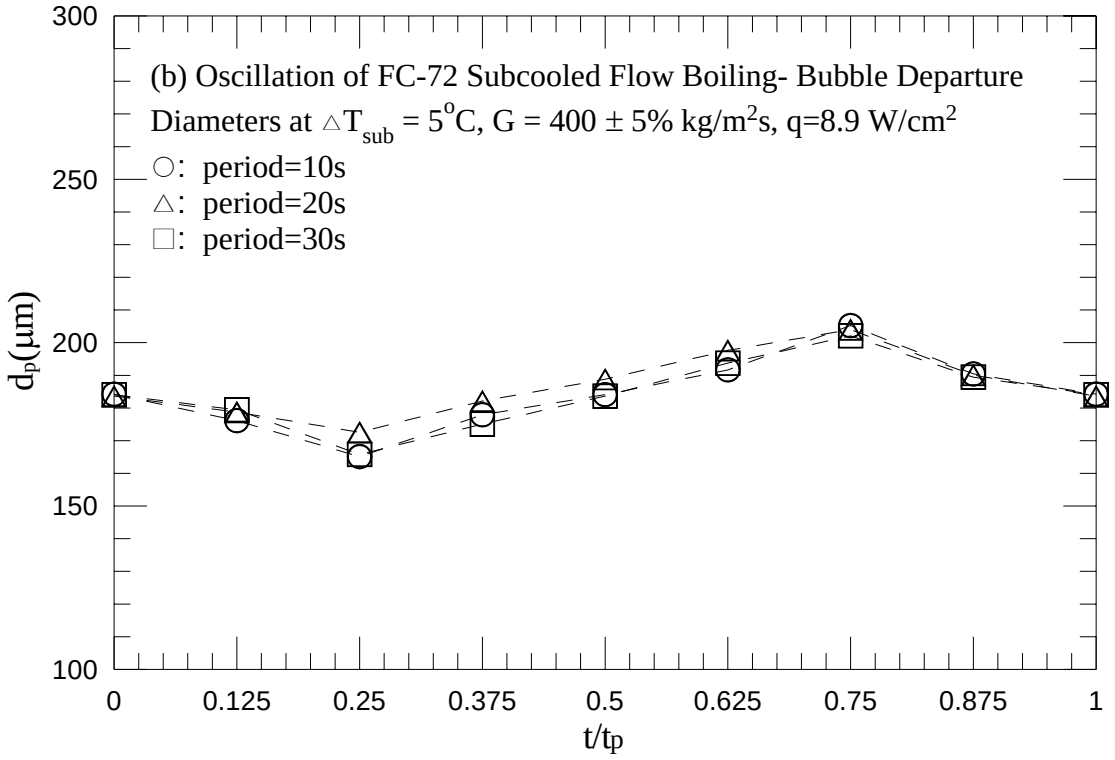

Fig. 5.153 Mean bubble departure diameters for various period of mass flux oscillation for transient subcooled flow boiling for G=400±5% kg/m^{2}s and ΔT_{sub} =5°C with (a) q=7.4 W/cm^2 and (b) q=8.9 W/cm^2.

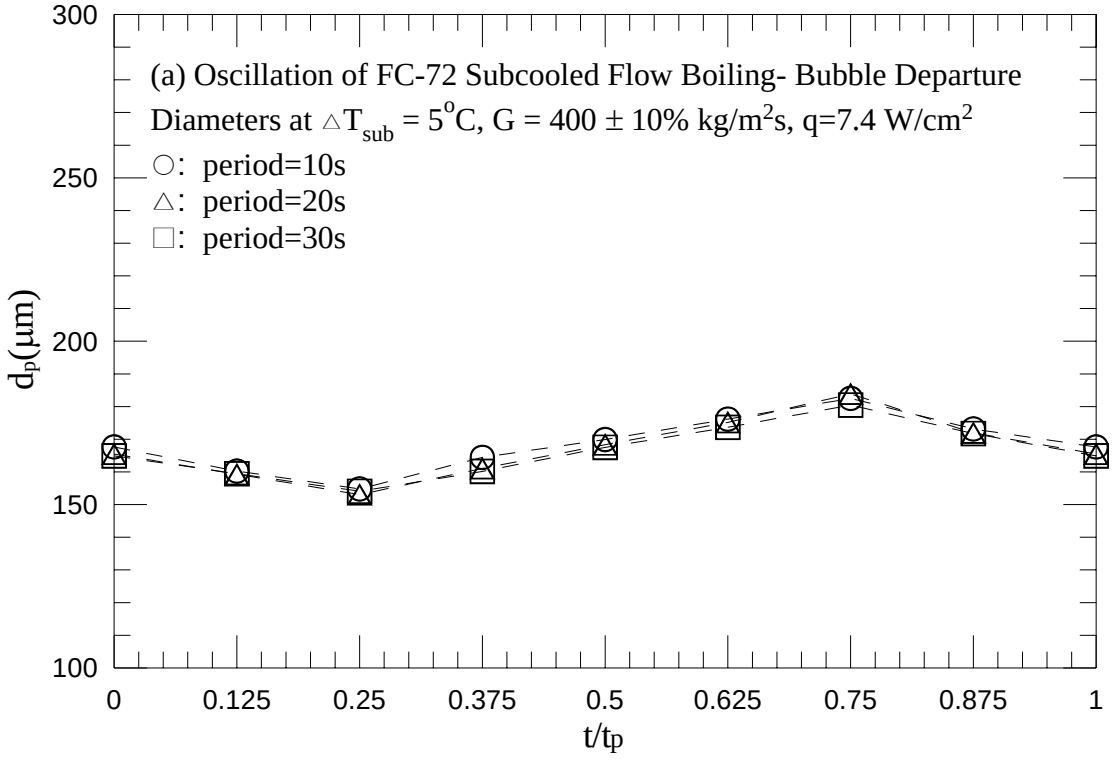

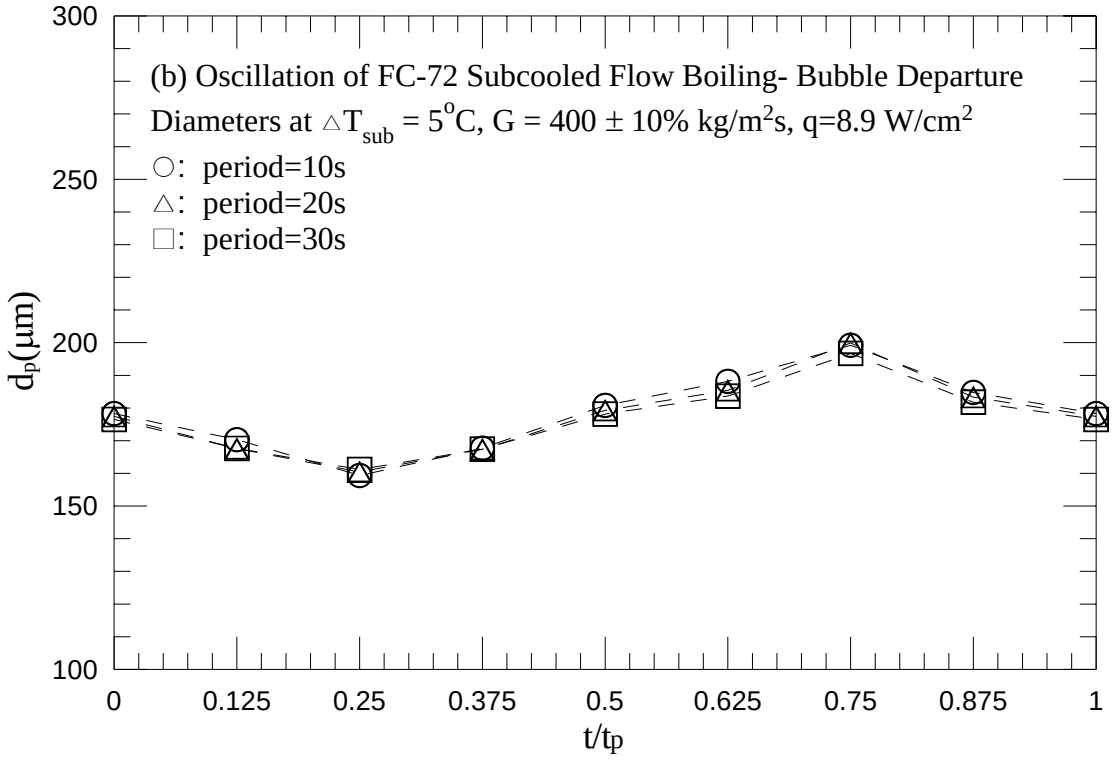

Fig. 5.154 Mean bubble departure diameters for various period of mass flux oscillation for transient subcooled flow boiling for G=400±10% kg/m^{2}s and ΔT_{sub} =5°C with (a) q=7.4 W/cm^2 and (b) q=8.9 W/cm^2.

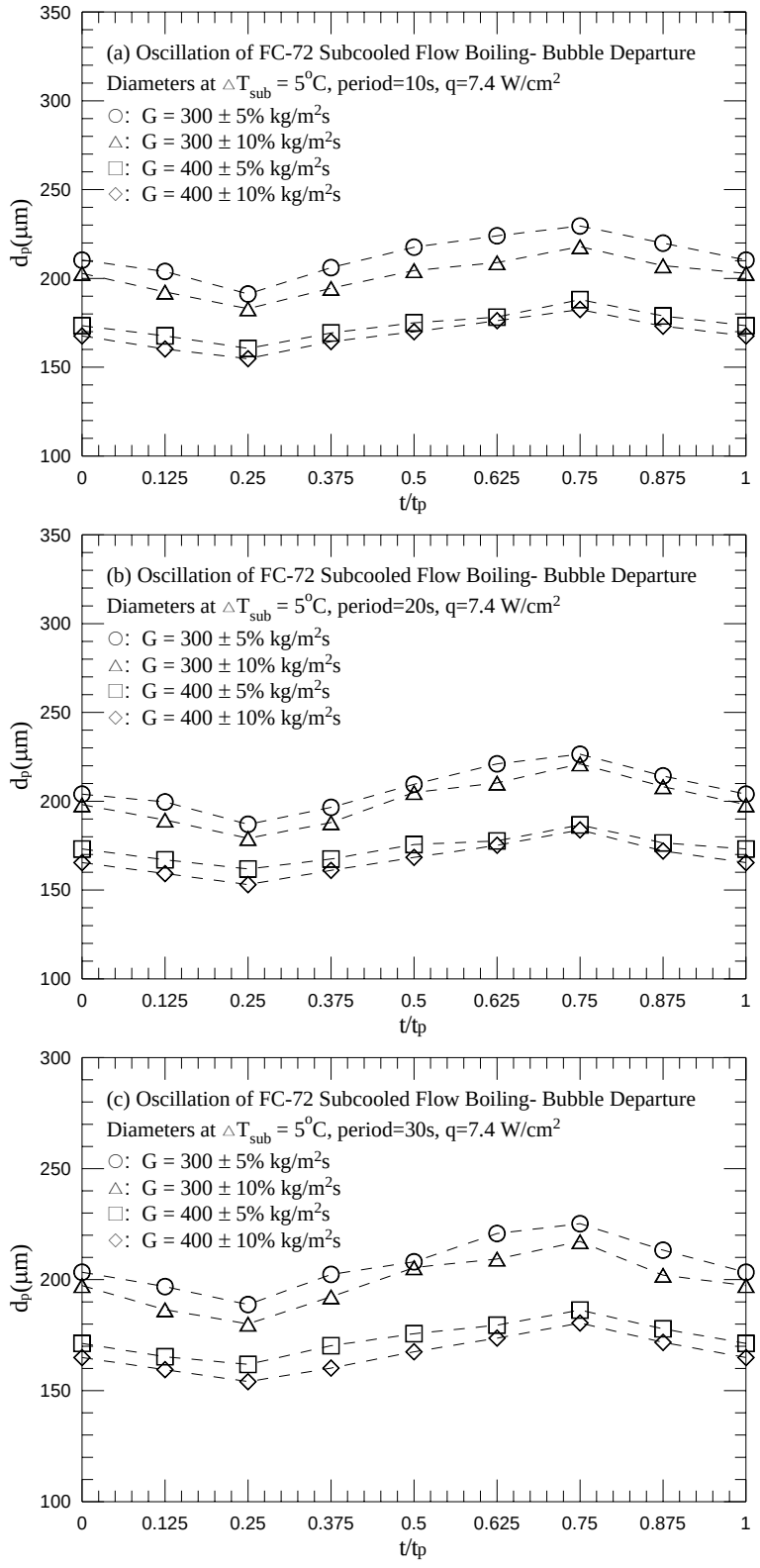

Fig. 5.155 Mean bubble departure diameters for various amplitudes of the mass fluxes oscillation for transient subcooled flow boiling for q=7.4 W/cm^2 and ΔT_{sub} =5^{o}C with period=10 sec (a), 20 sec (b), and 30 sec (c).

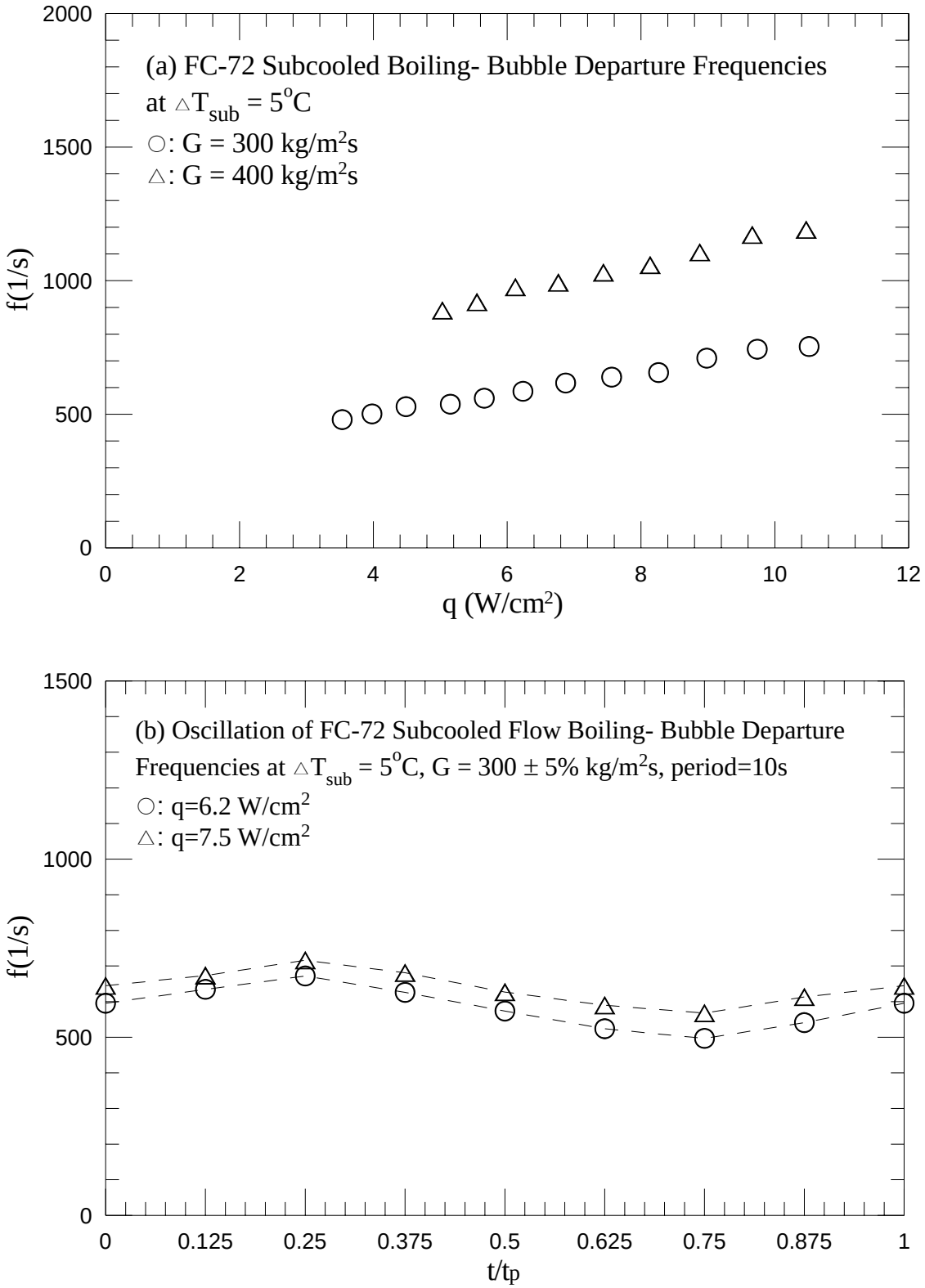

Fig. 5.156 Mean bubble departure frequencies for various coolant mass fluxes for stable subcooled flow boiling (a) and various imposed heat fluxes for transient subcooled flow boiling for G=300±5% kg/m^{2}s and ΔT_{sub} =5°C with t_p=10 sec (b), 20sec (c) and 30 sec (d).

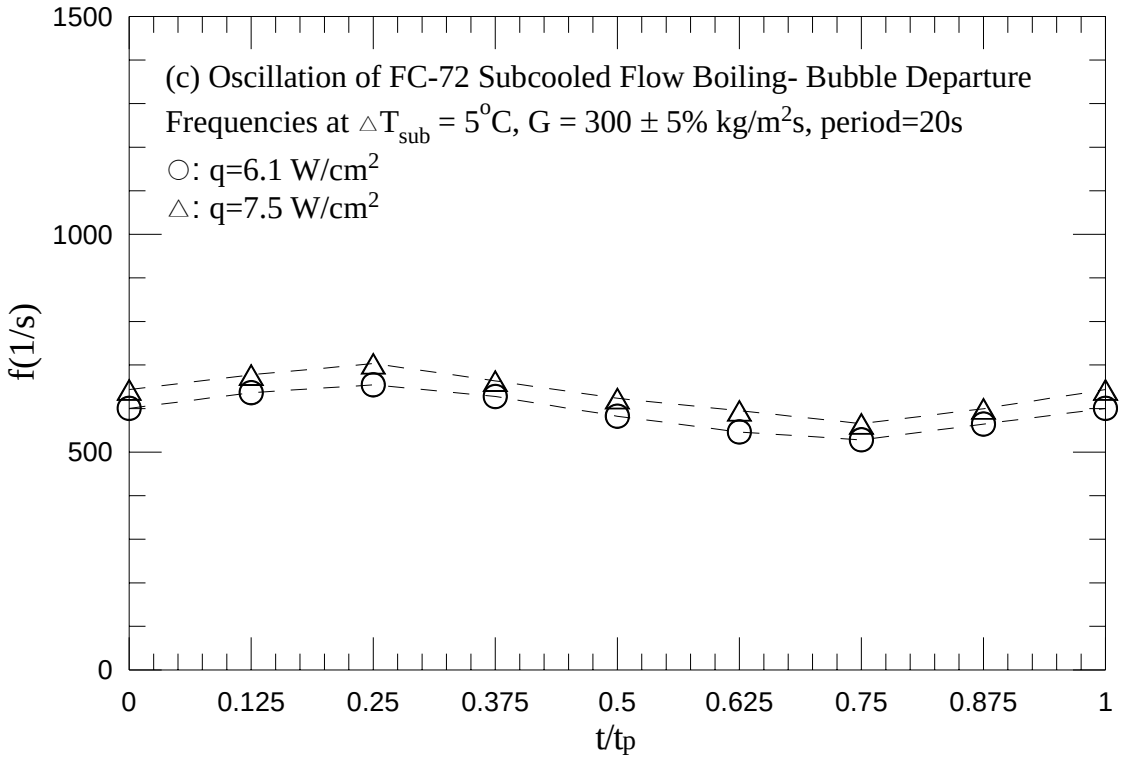

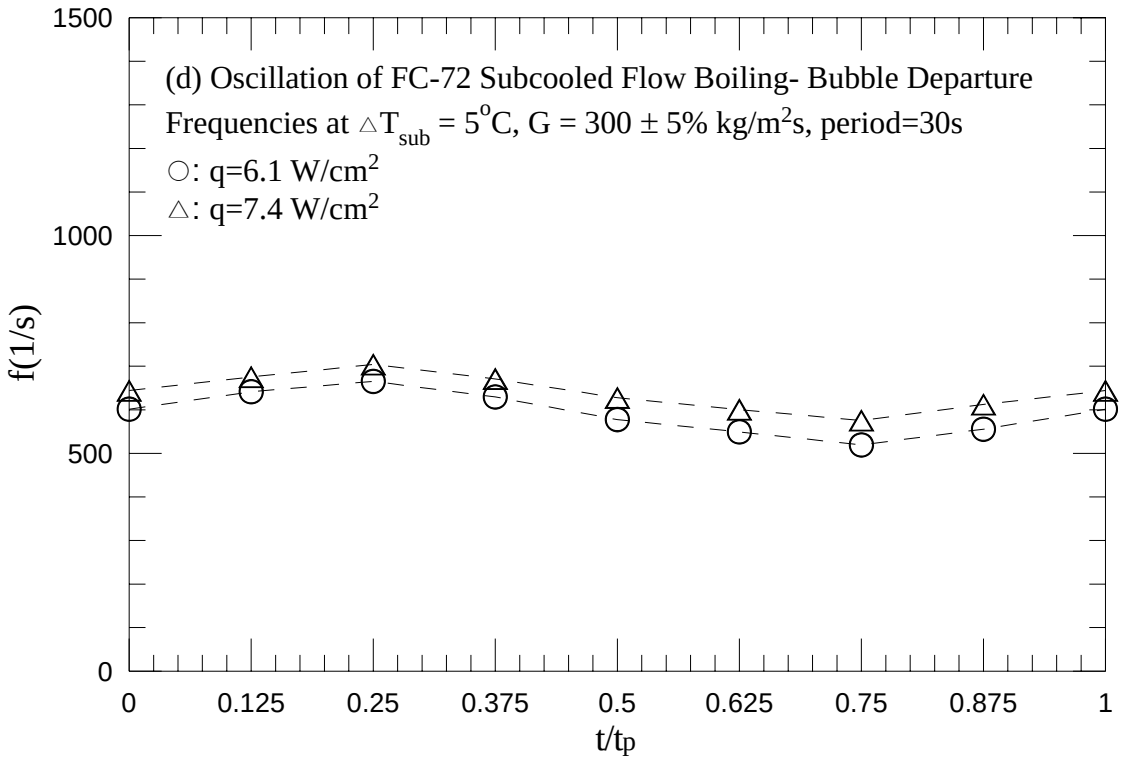

Fig. 5.156 Continued.

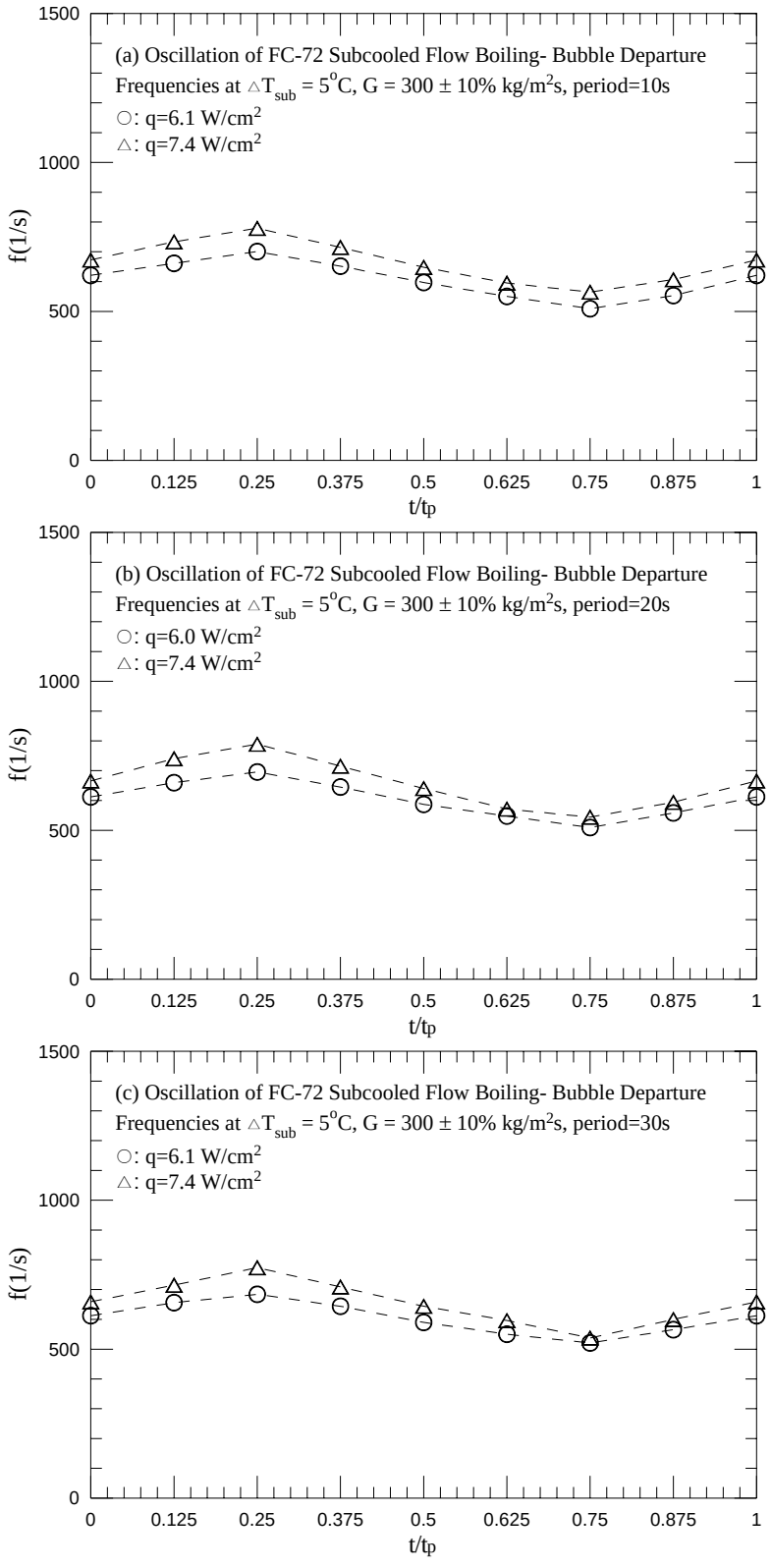

Fig. 5.157 Mean bubble departure frequencies for various imposed heat fluxes for transient subcooled flow boiling for G=300±10% kg/m^{2}s and ΔT_{sub} =5°C with t_p=10 sec (a), 20sec (b) and 30 sec (c).

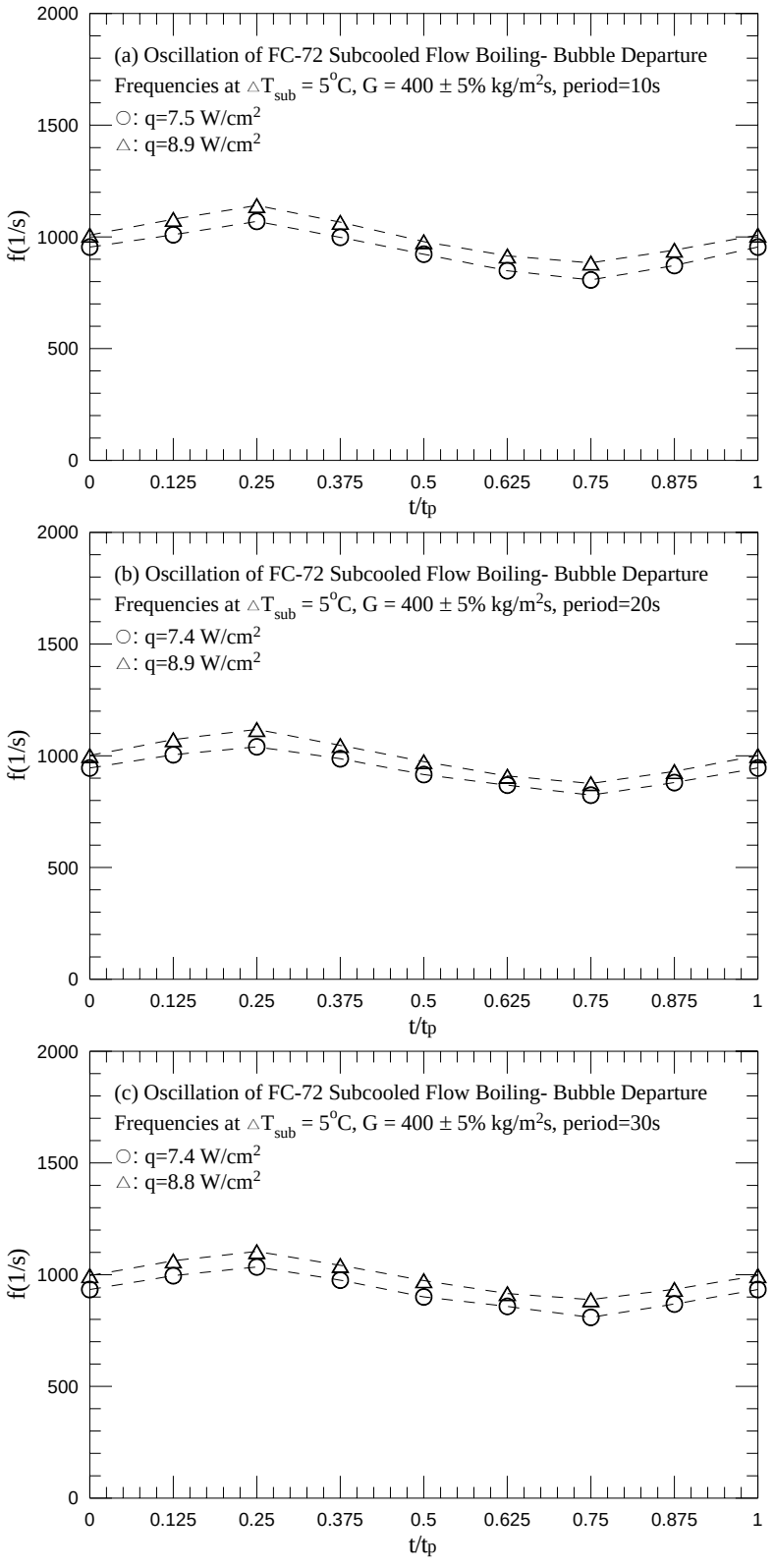

Fig. 5.158 Mean bubble departure frequencies for various imposed heat fluxes for transient subcooled flow boiling for G=400±5% kg/m^{2}s and ΔT_{sub} =5°C with t_p=10 sec (a), 20sec (b) and 30 sec (c).

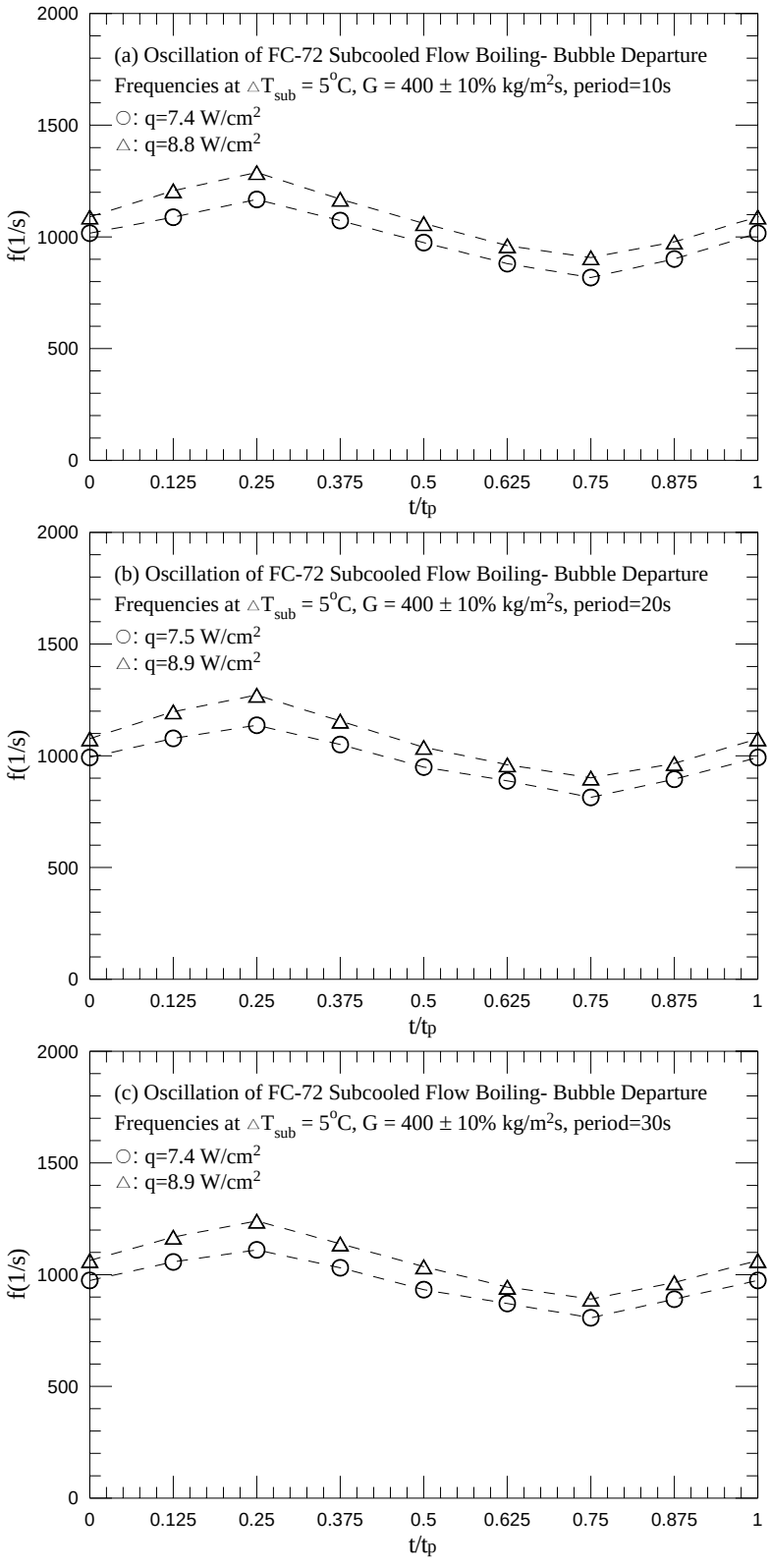

Fig. 5.159 Mean bubble departure frequencies for various imposed heat fluxes for transient subcooled flow boiling for G=400±10% kg/m^{2}s and ΔT_{sub} =5°C with t_p=10 sec (a), 20sec (b) and 30 sec (c).

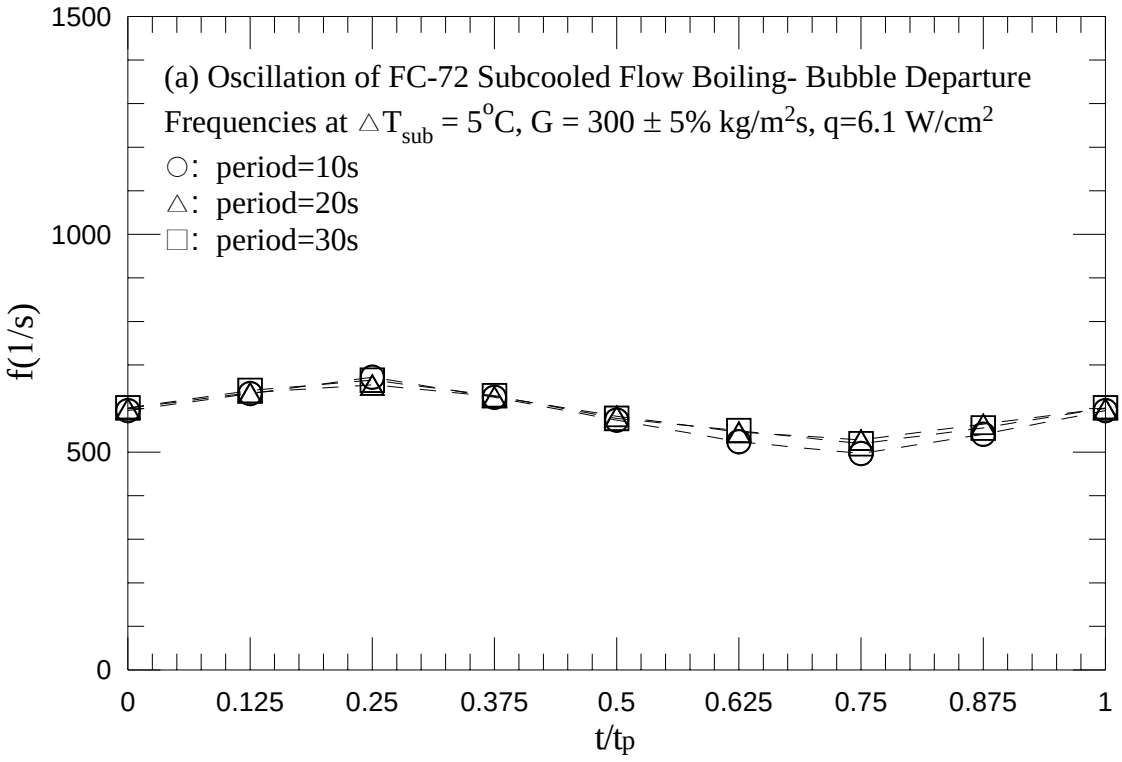

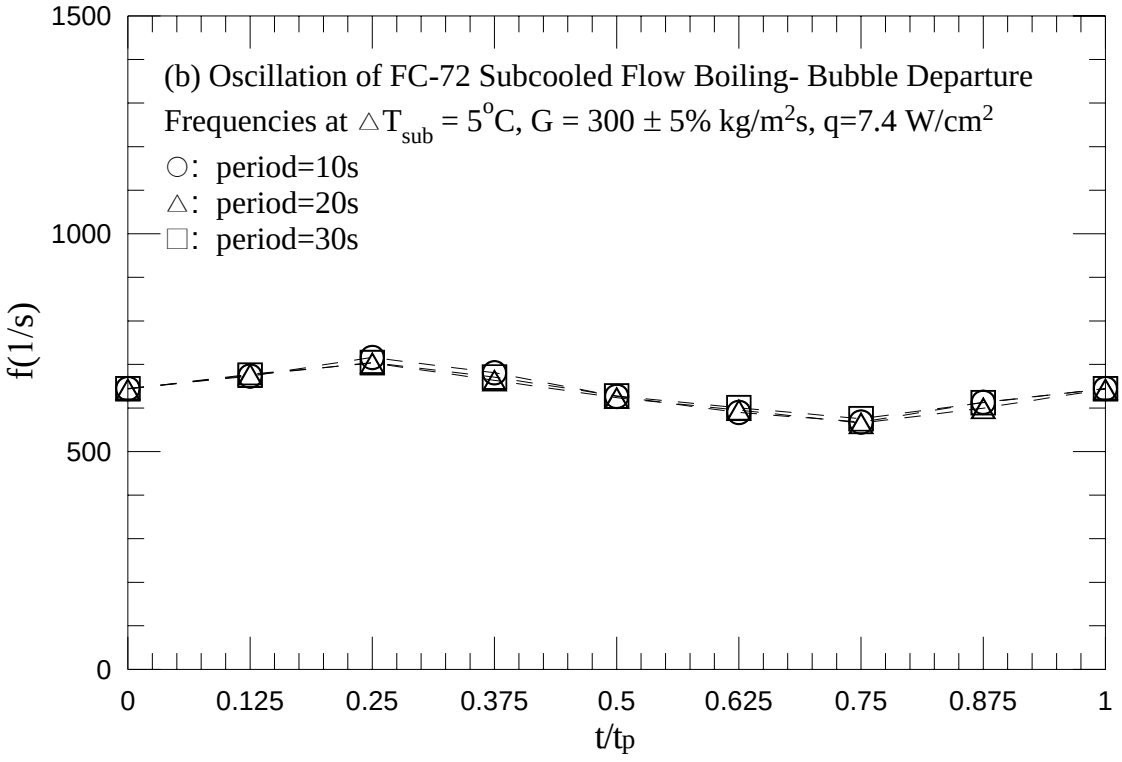

Fig. 5.160 Mean bubble departure frequencies for various periods of mass flux oscillation for transient subcooled flow boiling for G=300±5% kg/m^{2}s and ΔT_{sub} =5°C with (a) q=6.1 W/cm^2 and (b) q=7.4 W/cm^2.

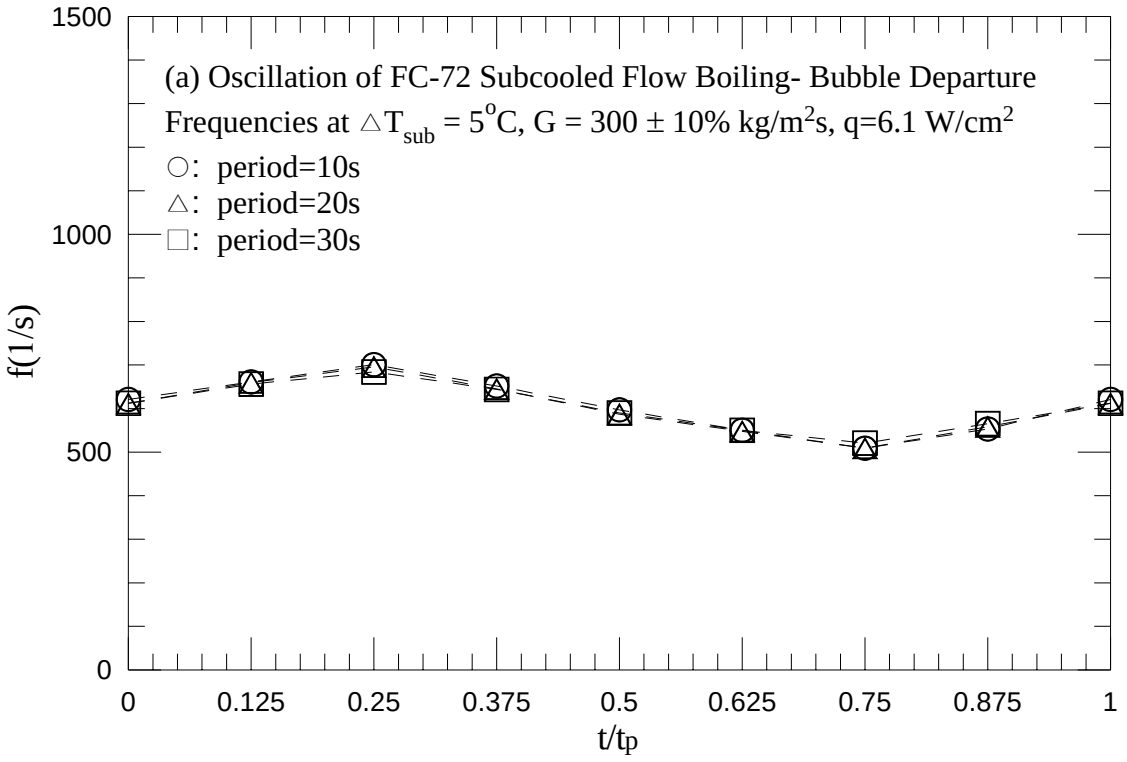

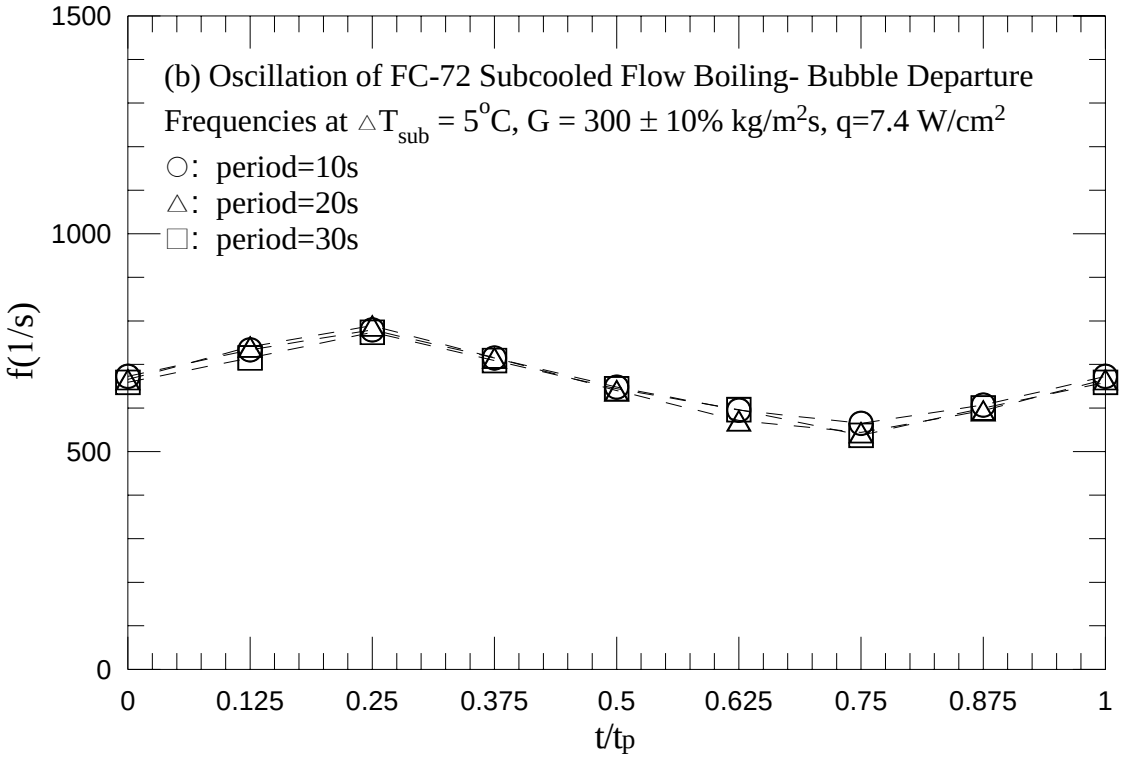

Fig. 5.161 Mean bubble departure frequencies for various periods of mass flux oscillation for transient subcooled flow boiling for G=300±10% kg/m^{2}s and ΔT_{sub} =5°C with (a) q=6.1 W/cm^2 and (b) q=7.4 W/cm^2.

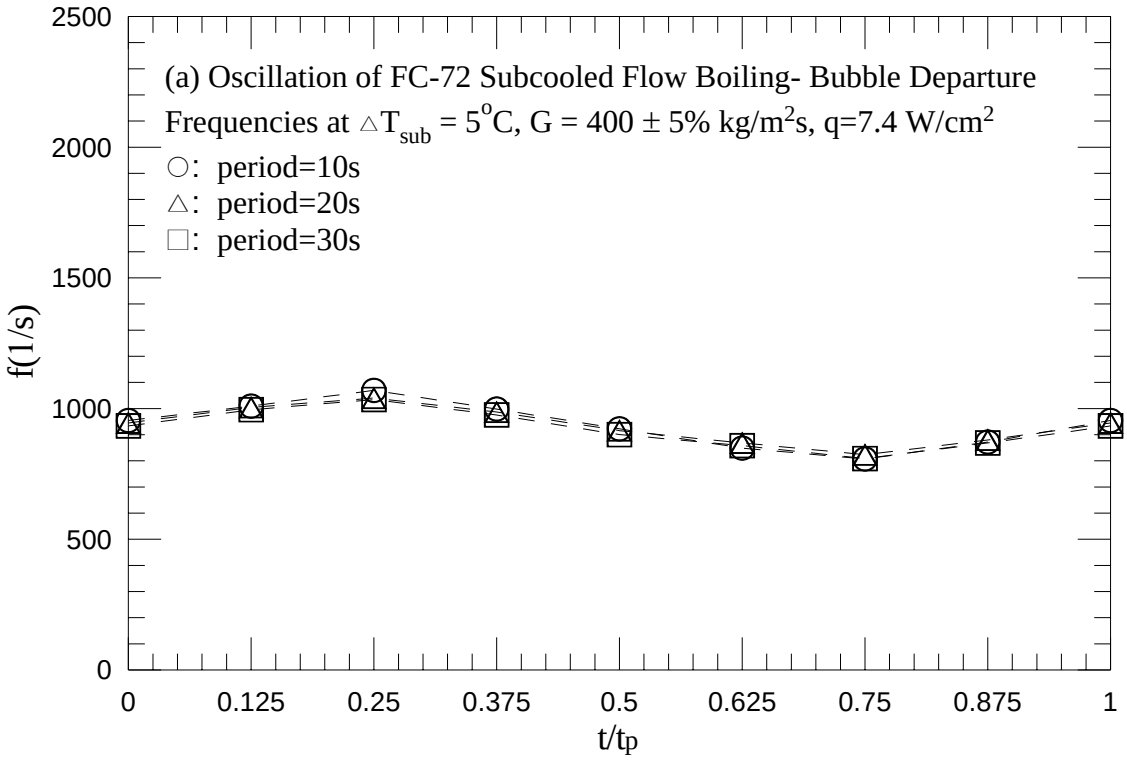

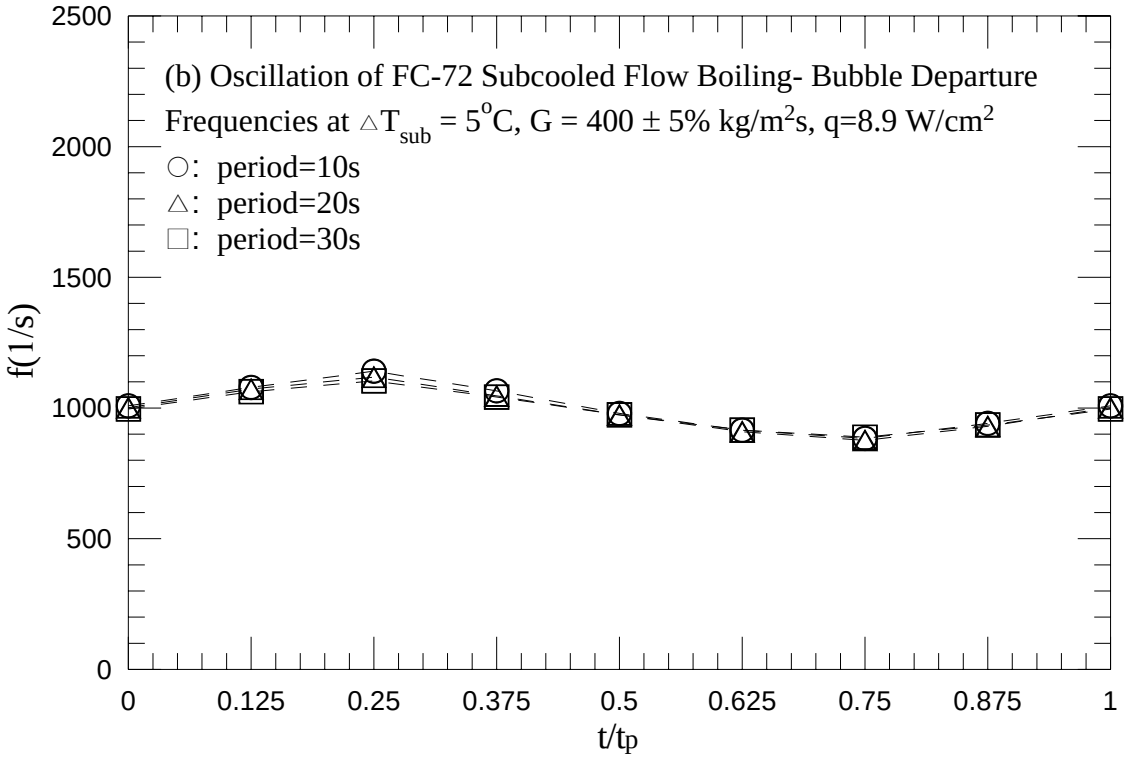

Fig. 5.162 Mean bubble departure frequencies for various periods of mass flux oscillation for transient subcooled flow boiling for G=400±5% kg/m^{2}s and ΔT_{sub} =5°C with (a) q=7.4 W/cm^2 and (b) q=8.9 W/cm^2.

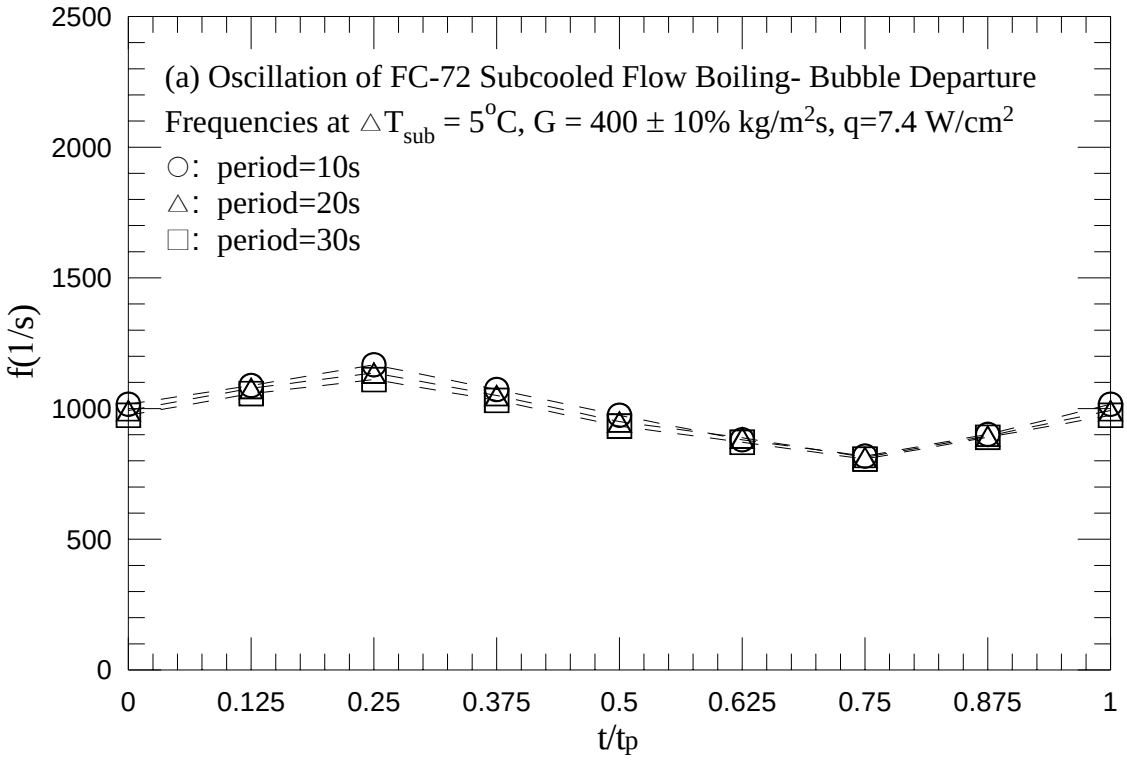

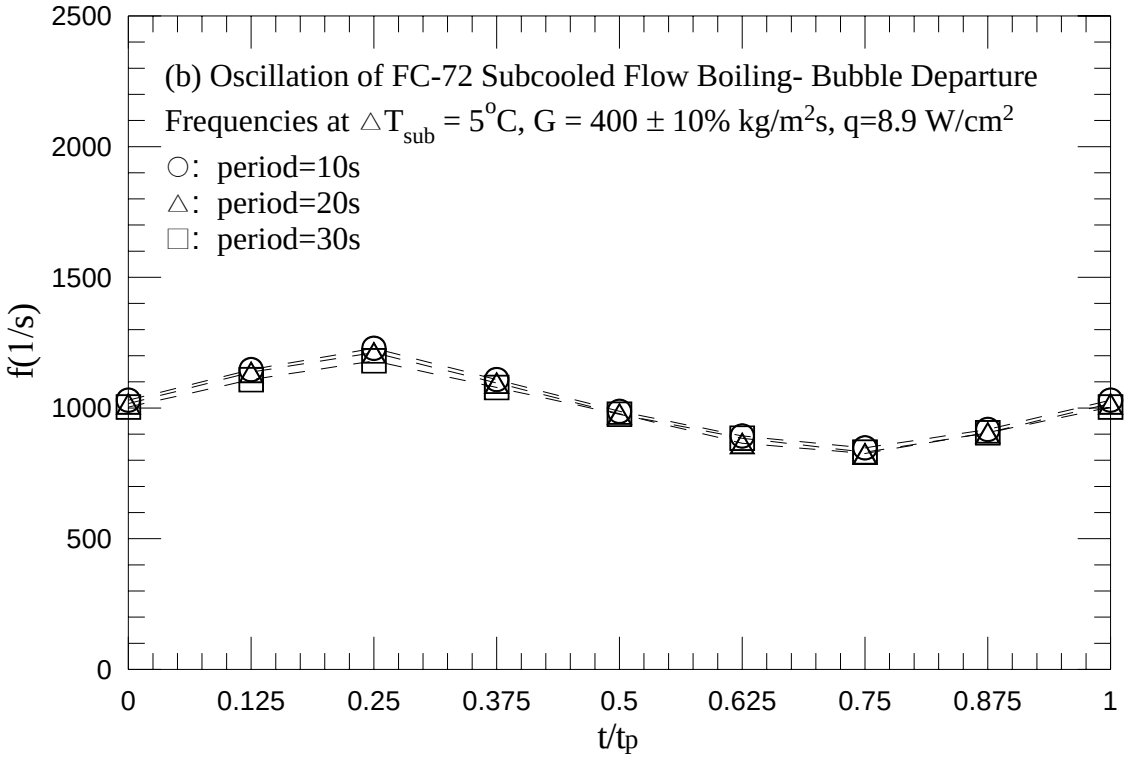

Fig. 5.163 Mean bubble departure frequencies for various periods of mass flux oscillation for transient subcooled flow boiling for G=400±10% kg/m^{2}s and ΔT_{sub} =5°C with (a) q=7.4 W/cm^2 and (b) q=8.9 W/cm^2.

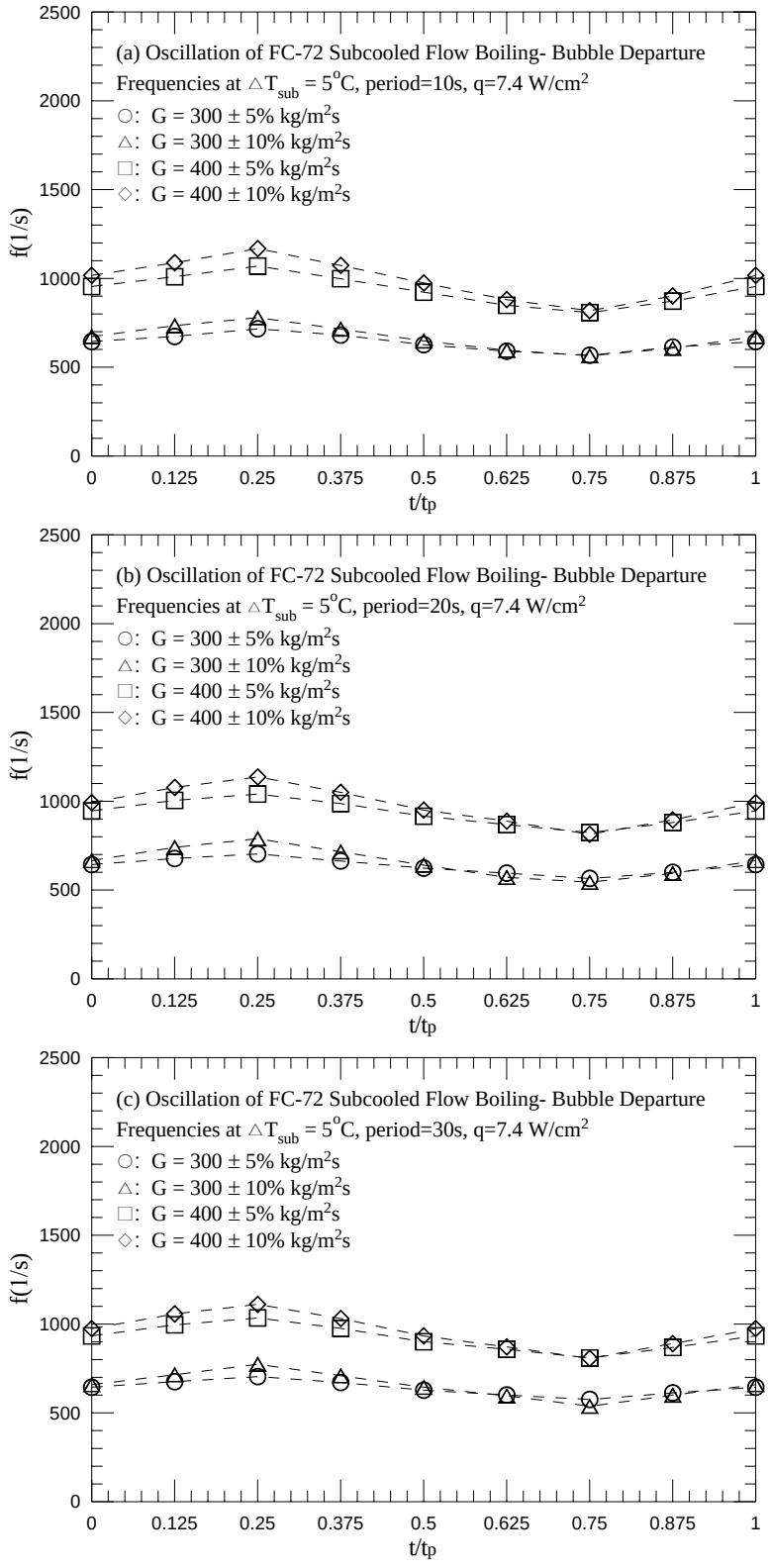

Fig. 5.164 Mean bubble departure frequencies for various amplitudes of the mass fluxes oscillation for transient subcooled flow boiling for q=7.4 W/cm^2 and ΔT_{sub} =5^{o}C with period=10 sec (a), 20 sec (b), and 30 sec (c).

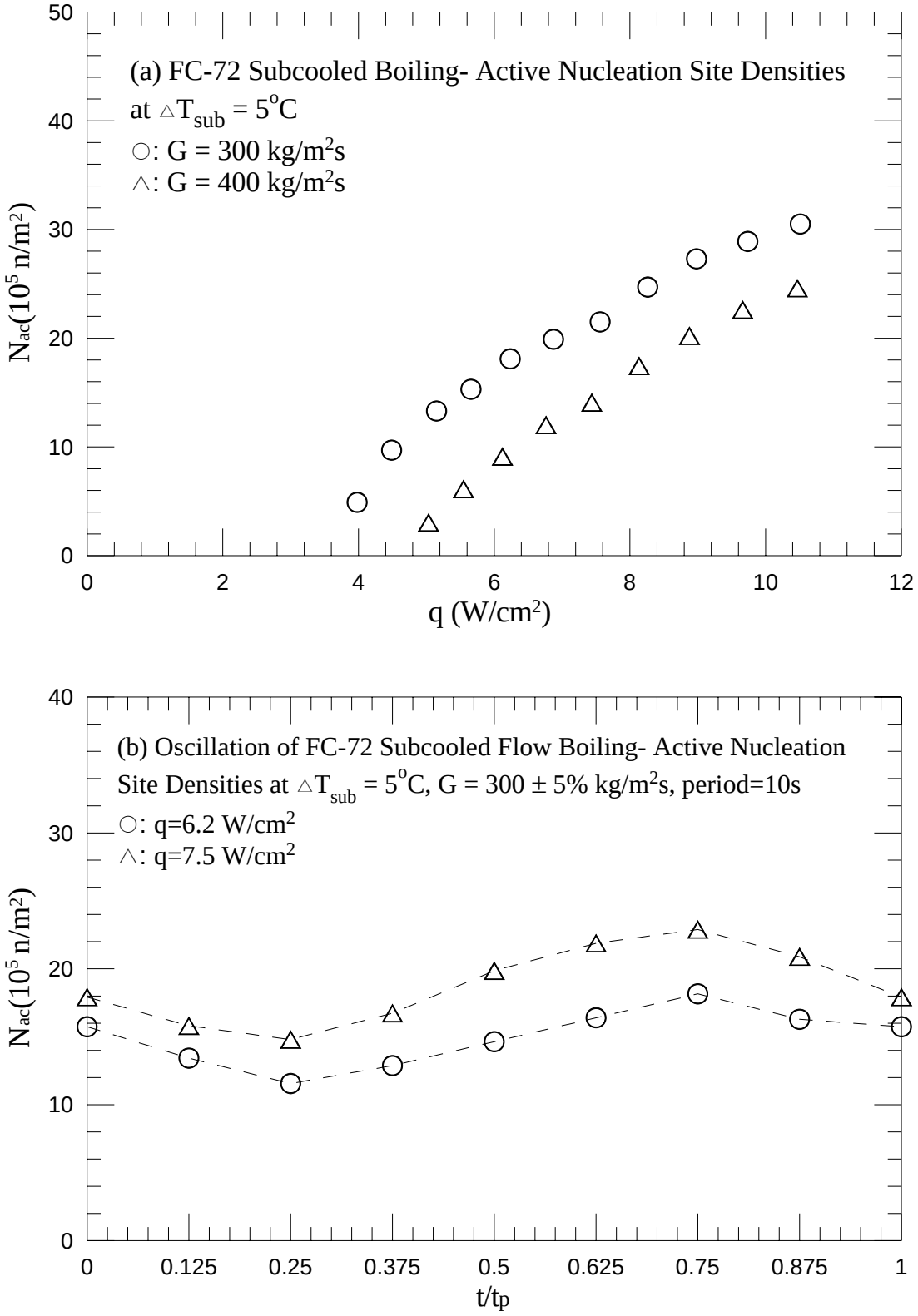

Fig. 5.165 Mean active nucleation site densities for various coolant mass fluxes for stable subcooled flow boiling (a) and various imposed heat fluxes for transient subcooled flow boiling for G=300±5% kg/m^{2}s and ΔT_{sub} =5°C with t_p=10 sec (b), 20sec (c) and 30 sec (d).

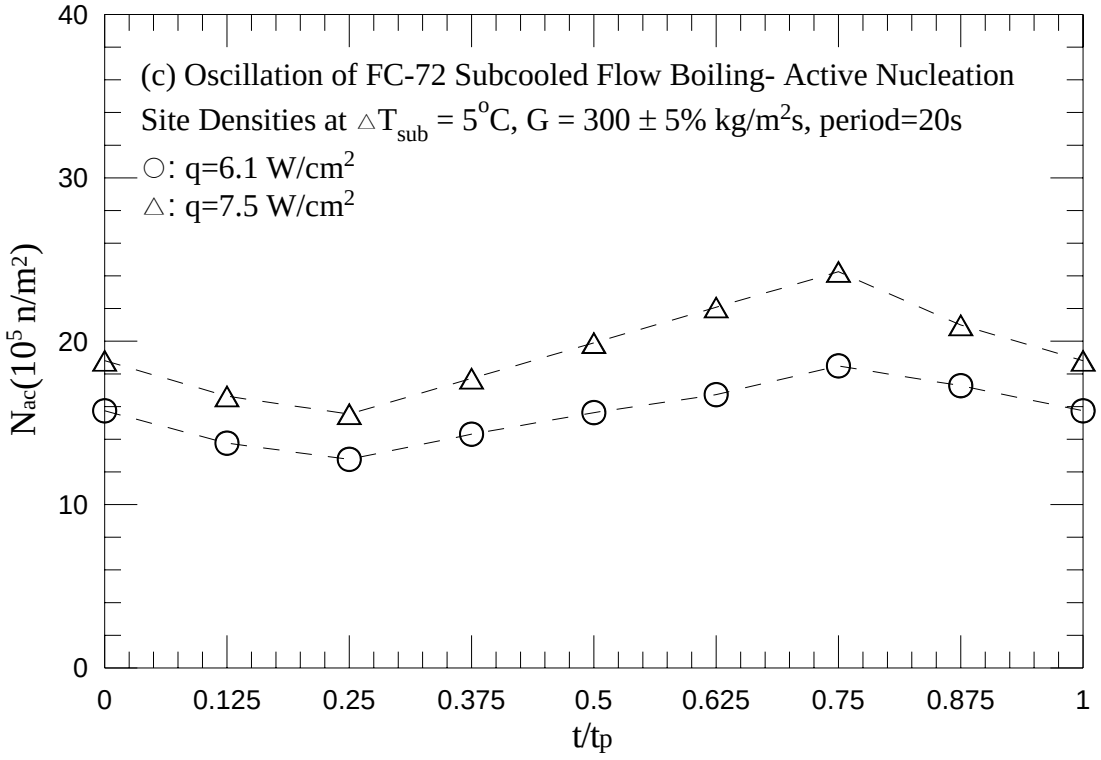

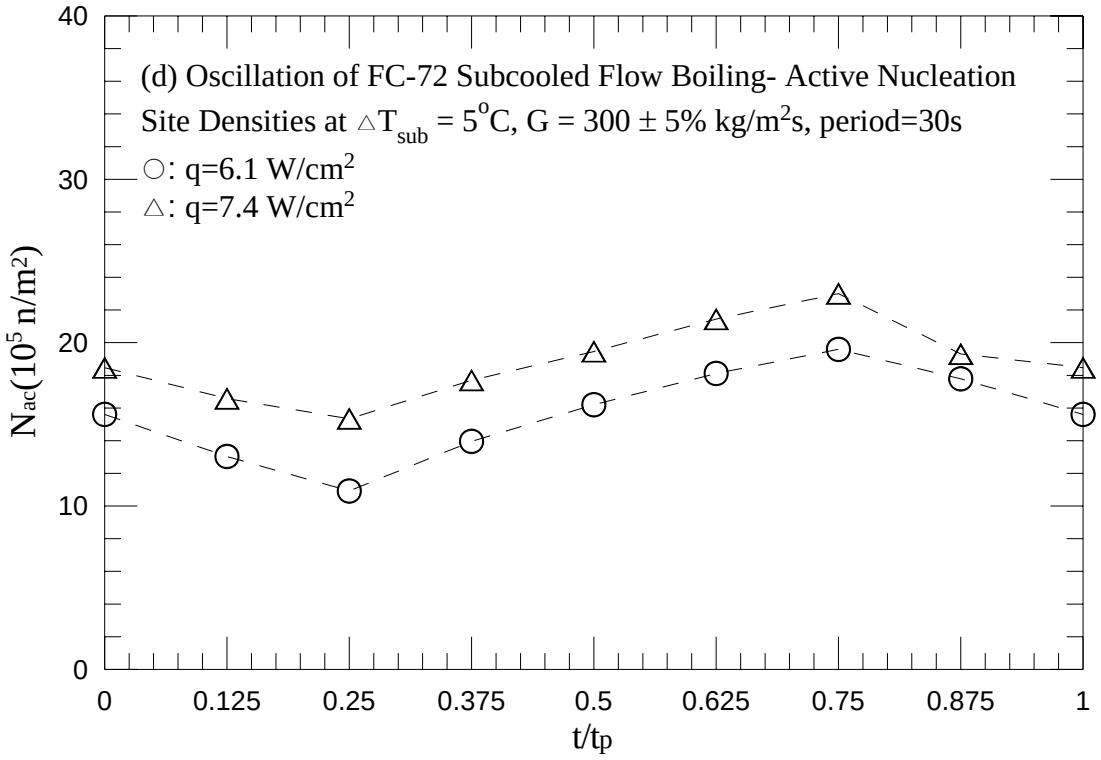

Fig. 5.165 Continued.

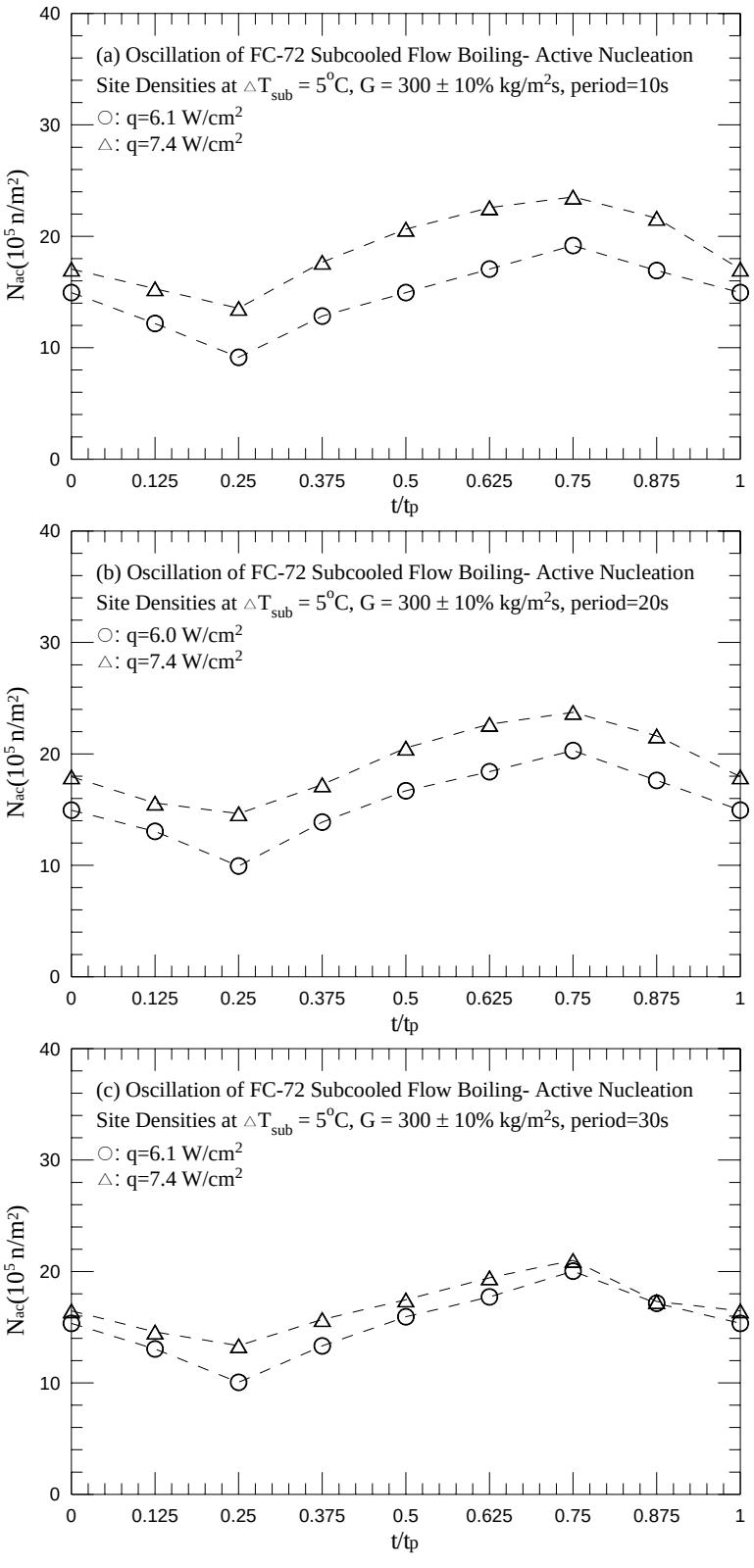

Fig. 5.166 Mean active nucleation site densities for various imposed heat fluxes for transient subcooled flow boiling for G=300±10% kg/m^{2}s and ΔT_{sub} =5°C with t_p=10 sec (a), 20sec (b) and 30 sec (c).

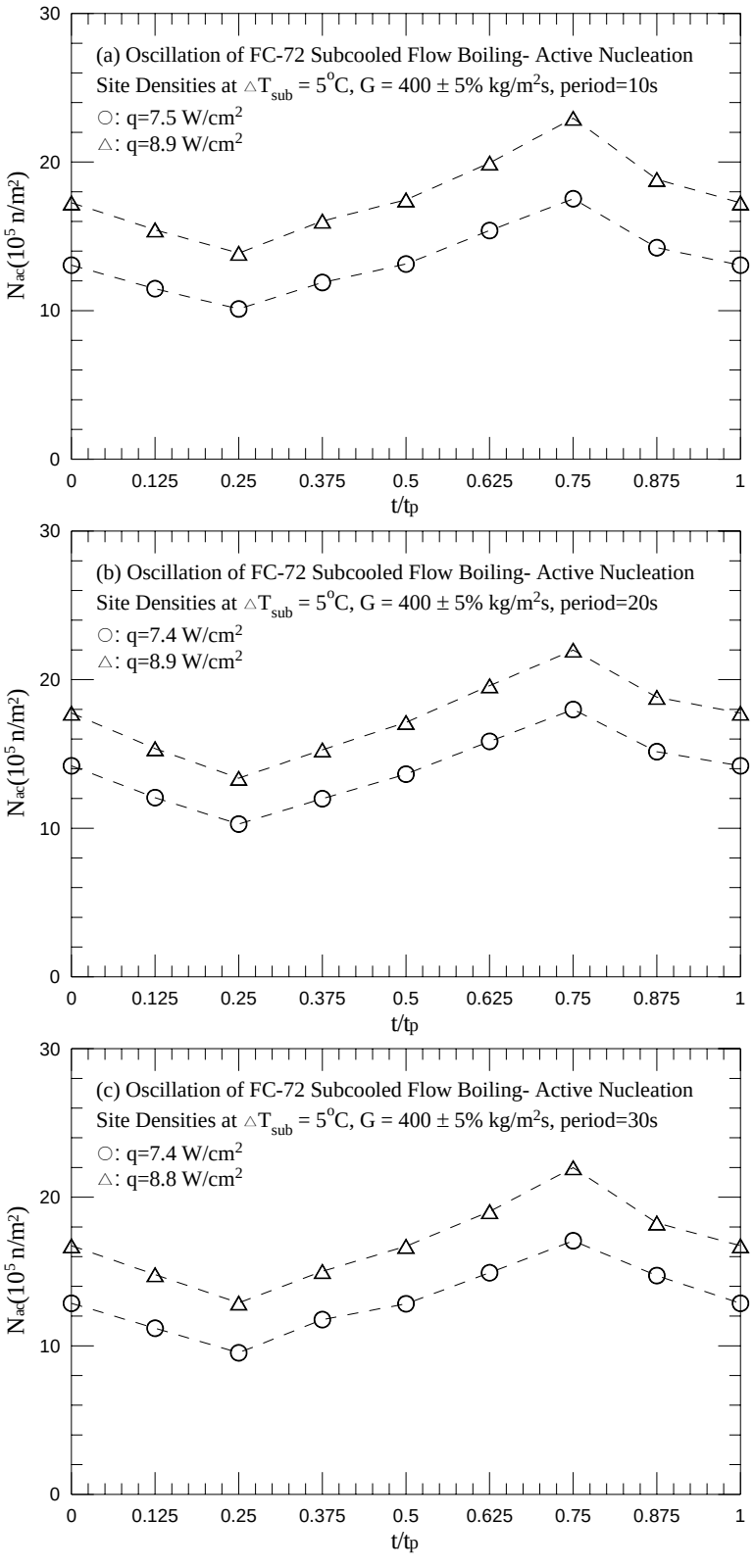

Fig. 5.167 Mean active nucleation site densities for various imposed heat fluxes for transient subcooled flow boiling for G=400±5% kg/m^{2}s and ΔT_{sub} =5°C with t_p=10 sec (a), 20sec (b) and 30 sec (c).

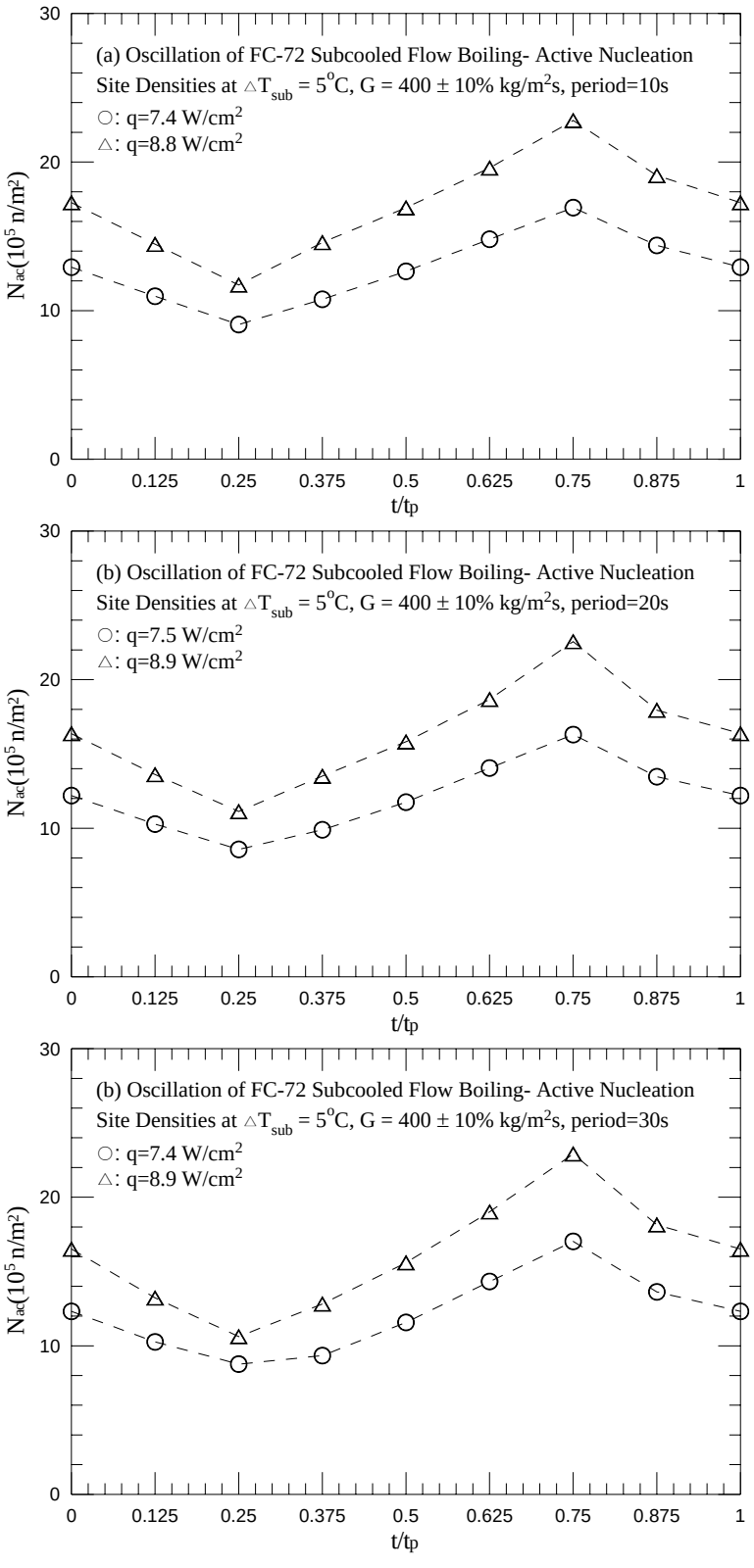

Fig. 5.168 Mean active nucleation site densities for various imposed heat fluxes for transient subcooled flow boiling for G=400±10% kg/m^{2}s and ΔT_{sub} =5^{o}C with t_p=10 sec (a), 20sec (b) and 30 sec (c).

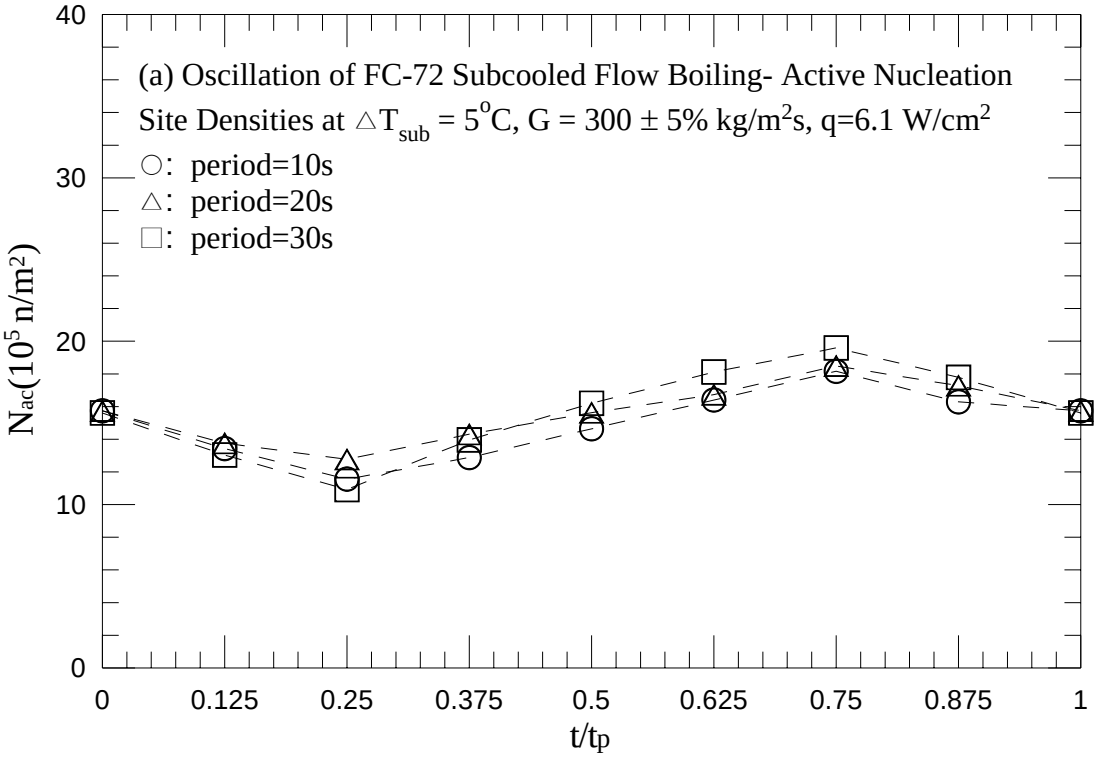

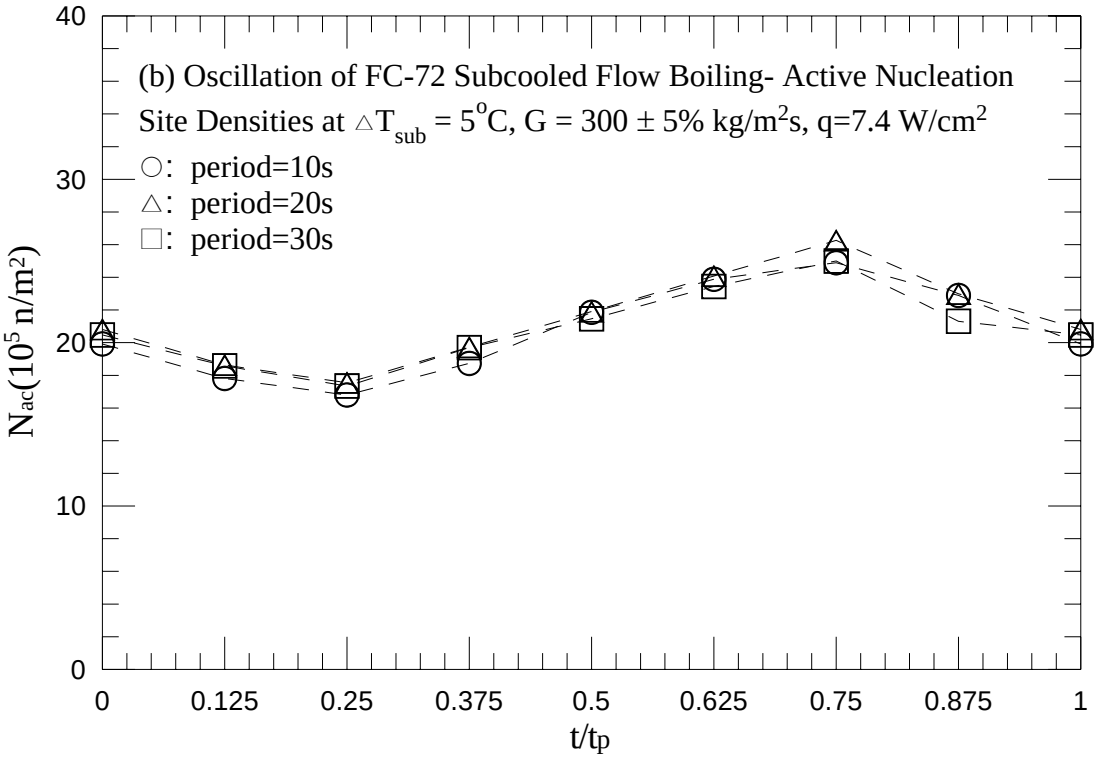

Fig. 5.169 Mean active nucleation site densities for various periods of mass flux oscillation for transient subcooled flow boiling for G=300±5% kg/m^{2}s and ΔT_{sub} =5°C with (a) q=6.1 W/cm^2 and (b) q=7.4 W/cm^2.

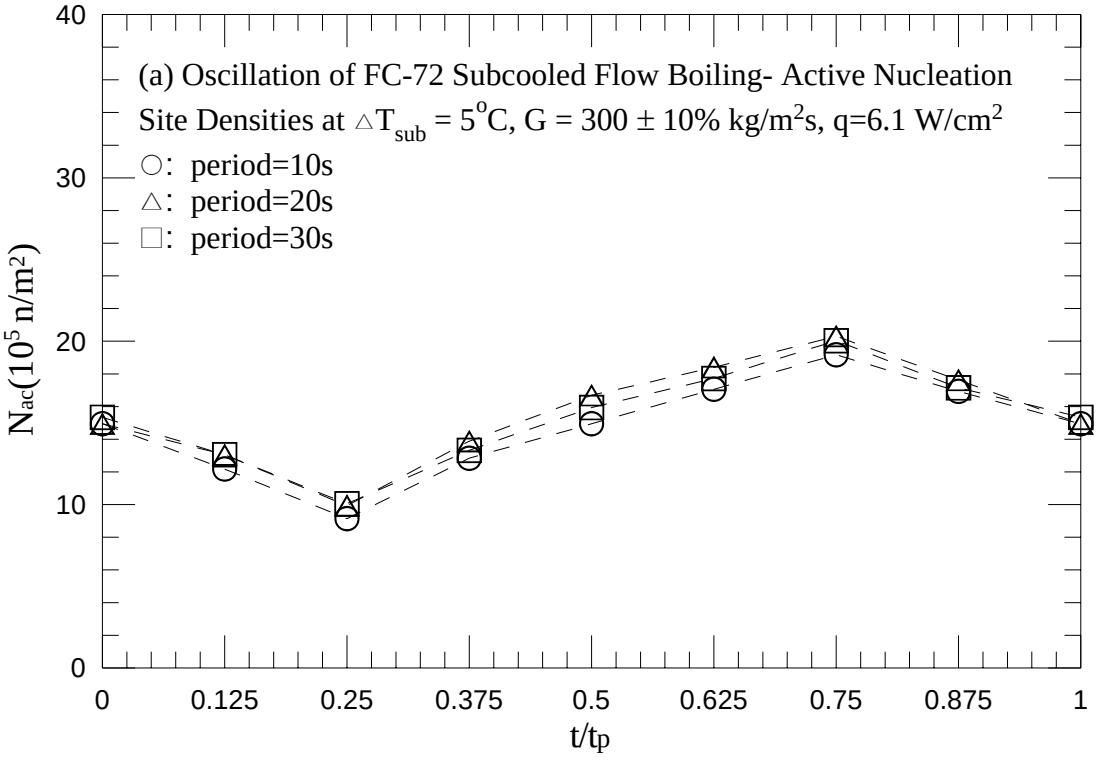

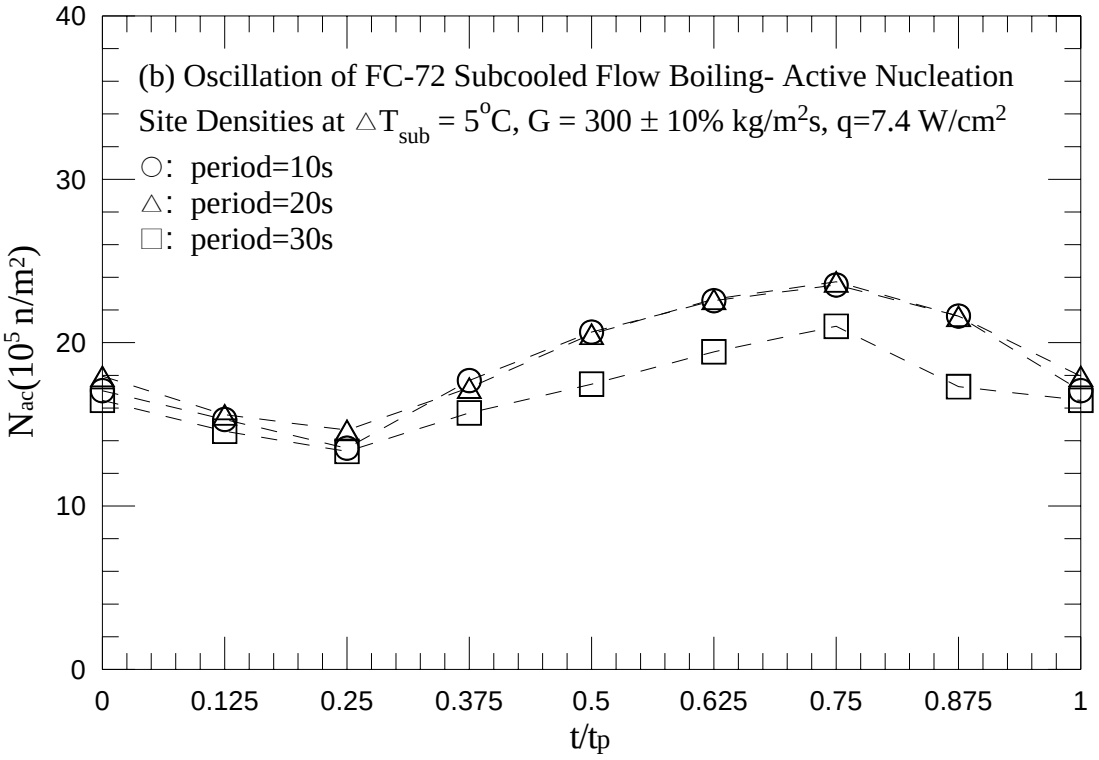

Fig. 5.170 Mean active nucleation site densities for various periods of mass flux oscillation for transient subcooled flow boiling for G=300±10% kg/m^{2}s and ΔT_{sub} =5°C with (a) q=6.1 W/cm^2 and (b) q=7.4 W/cm^2.

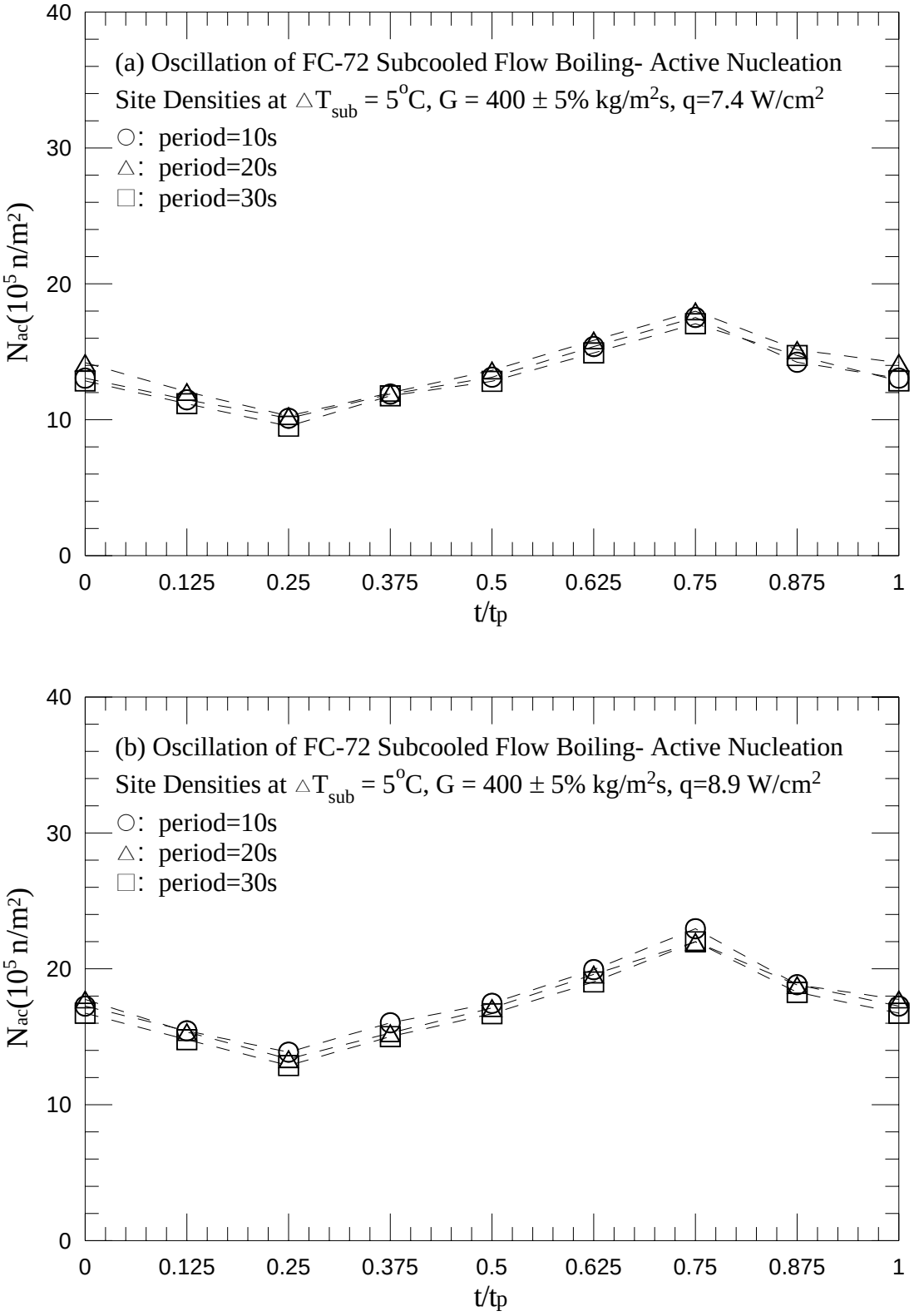

Fig. 5.171 Mean active nucleation site densities for various periods of mass flux oscillation for transient subcooled flow boiling for G=400±5% kg/m^{2}s and ΔT_{sub} =5°C with (a) q=7.4 W/cm^2 and (b) q=8.9 W/cm^2.

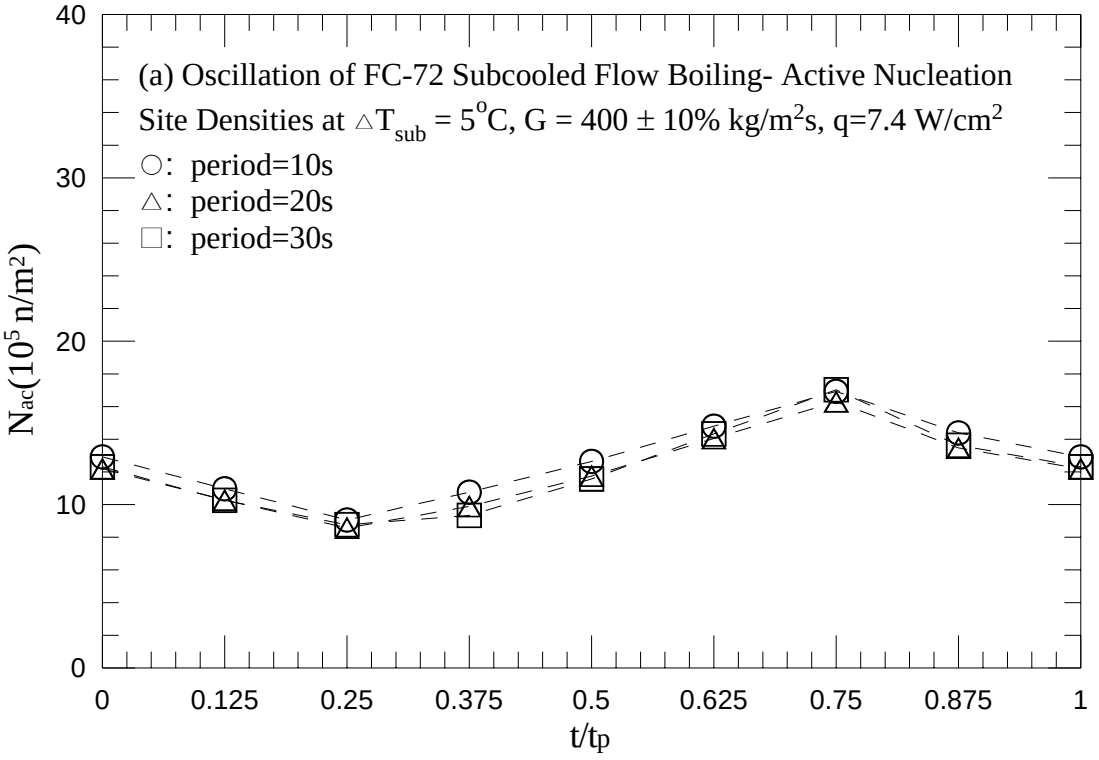

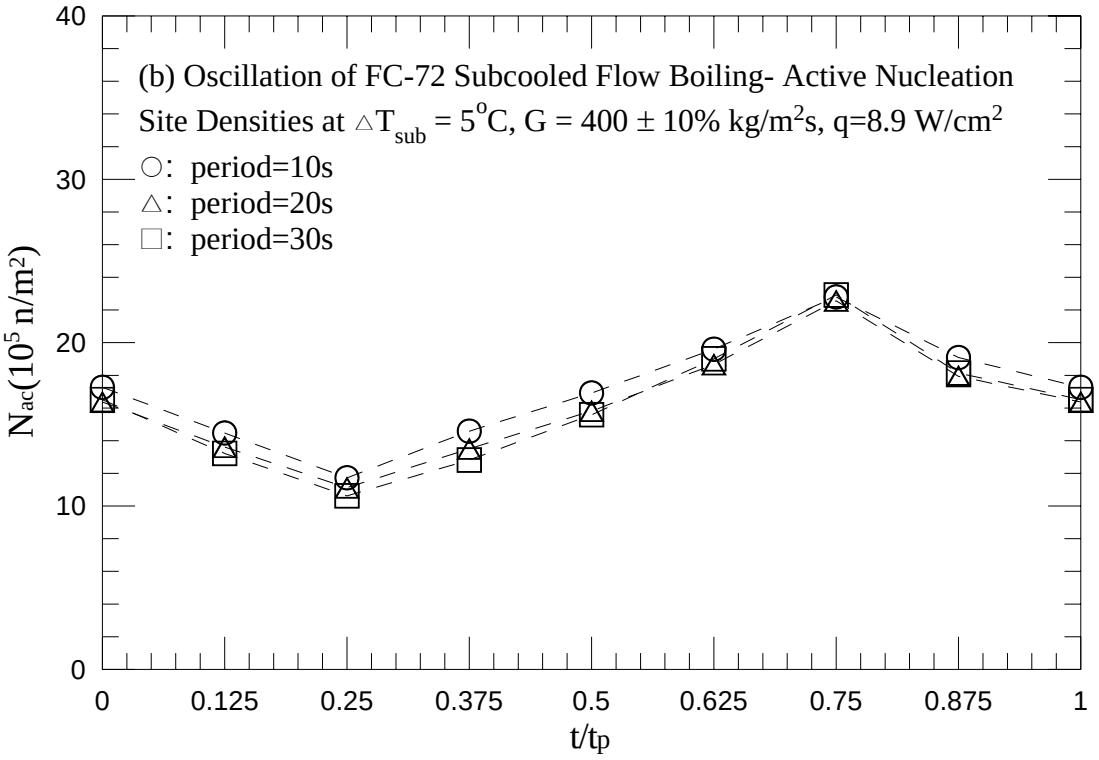

Fig. 5.172 Mean active nucleation site densities for various periods of mass flux oscillation for transient subcooled flow boiling for G=400±10% kg/m^{2}s and ΔT_{sub} =5°C with (a) q=7.4 W/cm^2 and (b) q=8.9 W/cm^2.

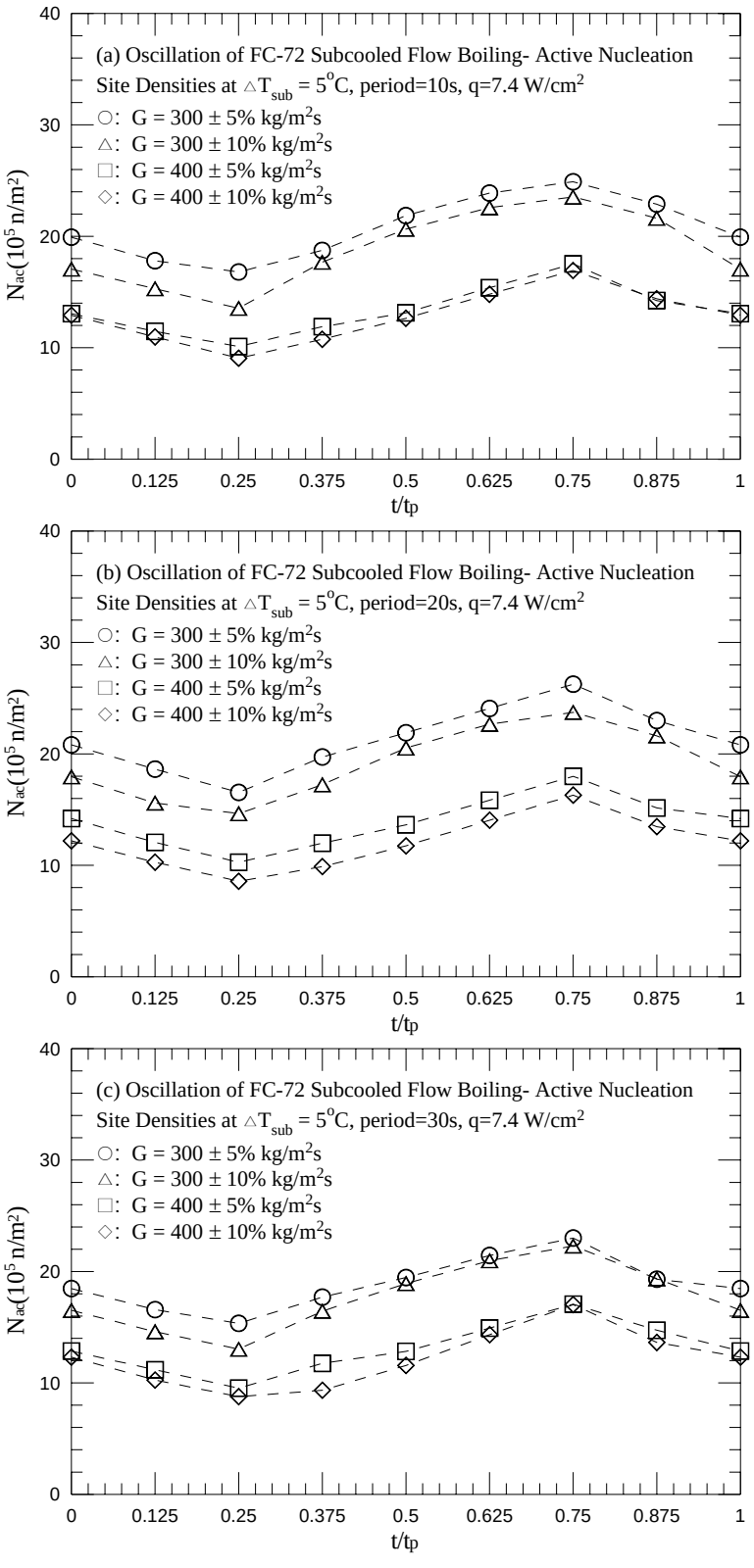

Fig. 5.173 Mean active nucleation site densities for various amplitudes of the mass fluxes oscillation for transient subcooled flow boiling for q=7.4 and ΔT_{sub} =5°C W/cm^2 with period=10 sec (a), 20 sec (b), and 30 sec (c).

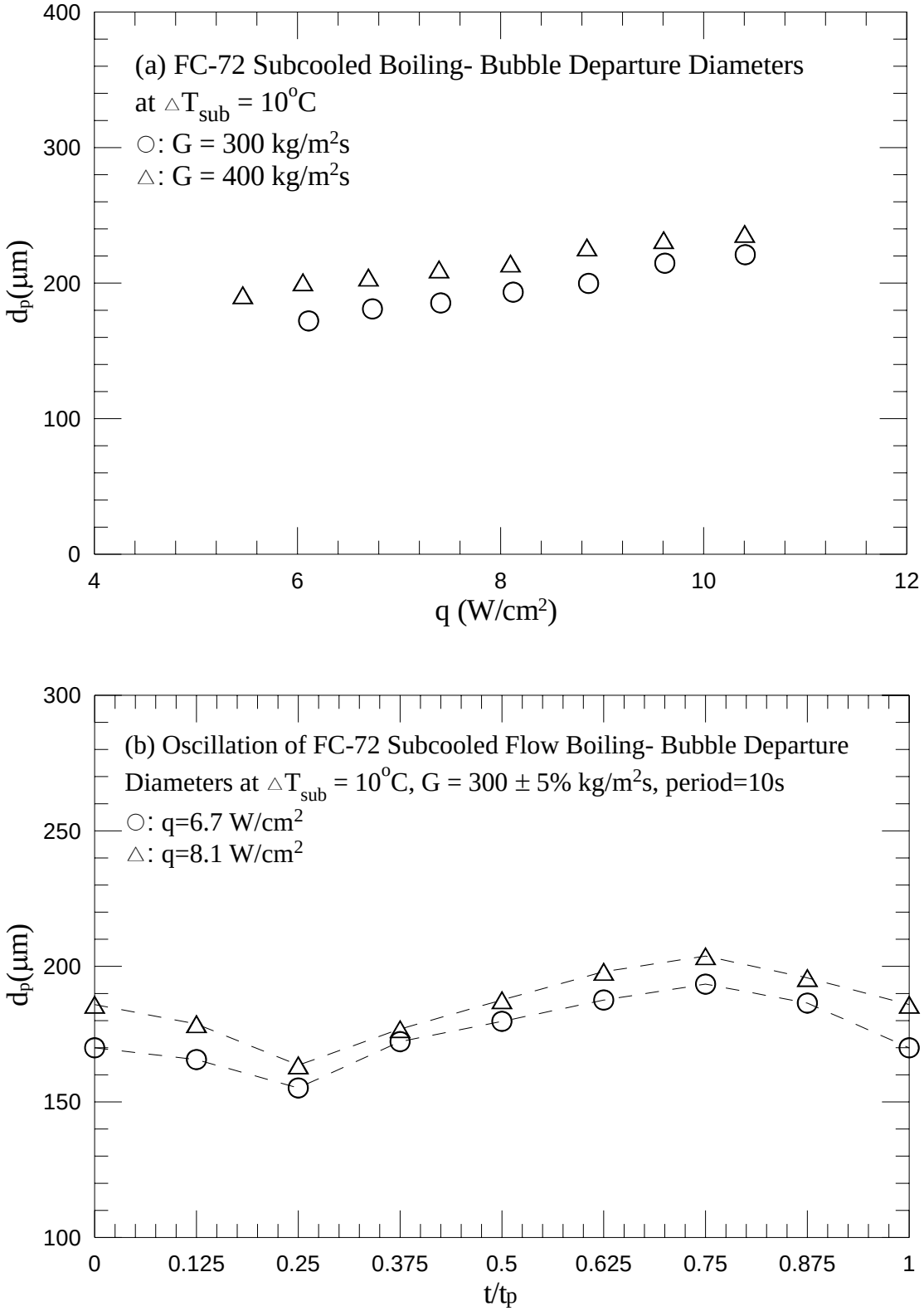

Fig. 5.174 Mean bubble departure diameters for various coolant mass fluxes for stable subcooled flow boiling (a) and various imposed heat fluxes for transient subcooled flow boiling for G=300±5% kg/m^{2}s and ΔT_{sub} =10°C with t_p=10 sec (b), 20sec (c) and 30 sec (d).

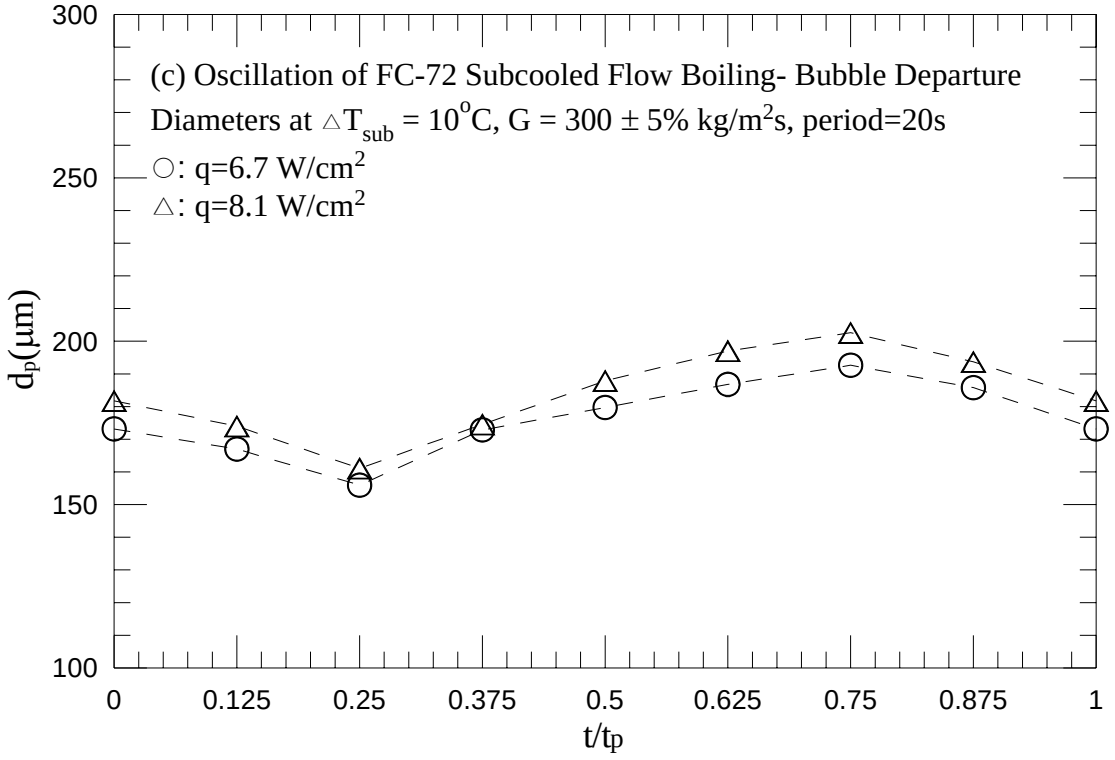

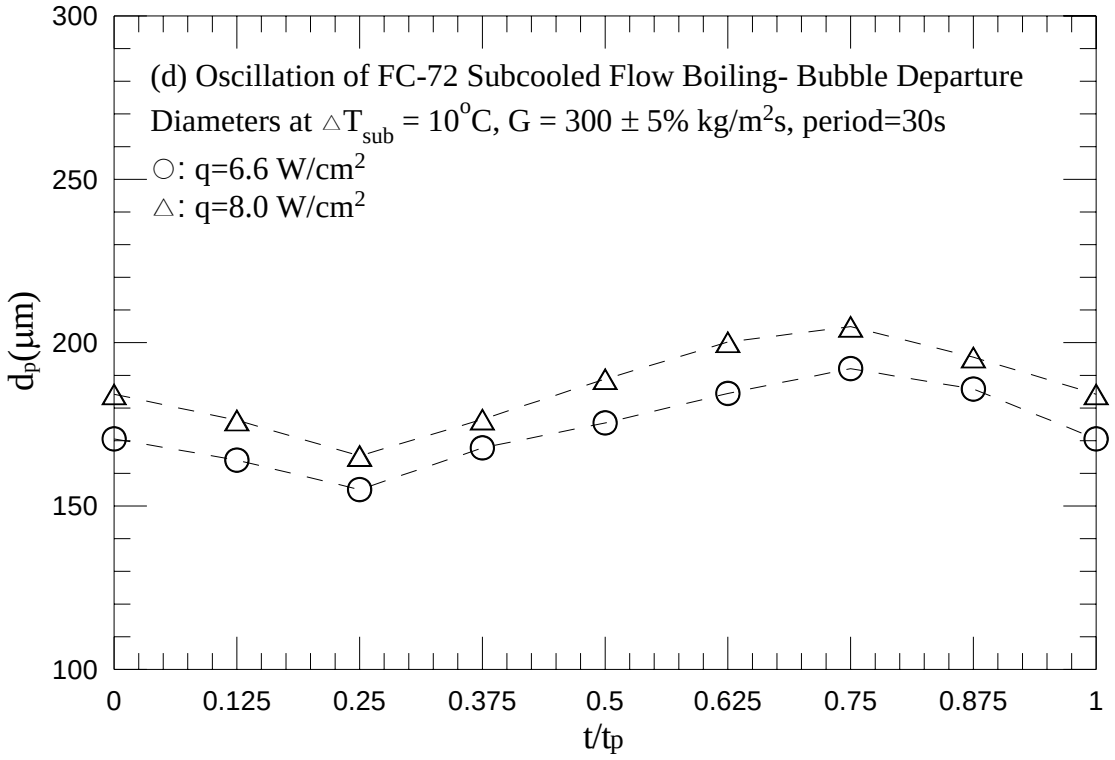

Fig. 5.174 Continued.

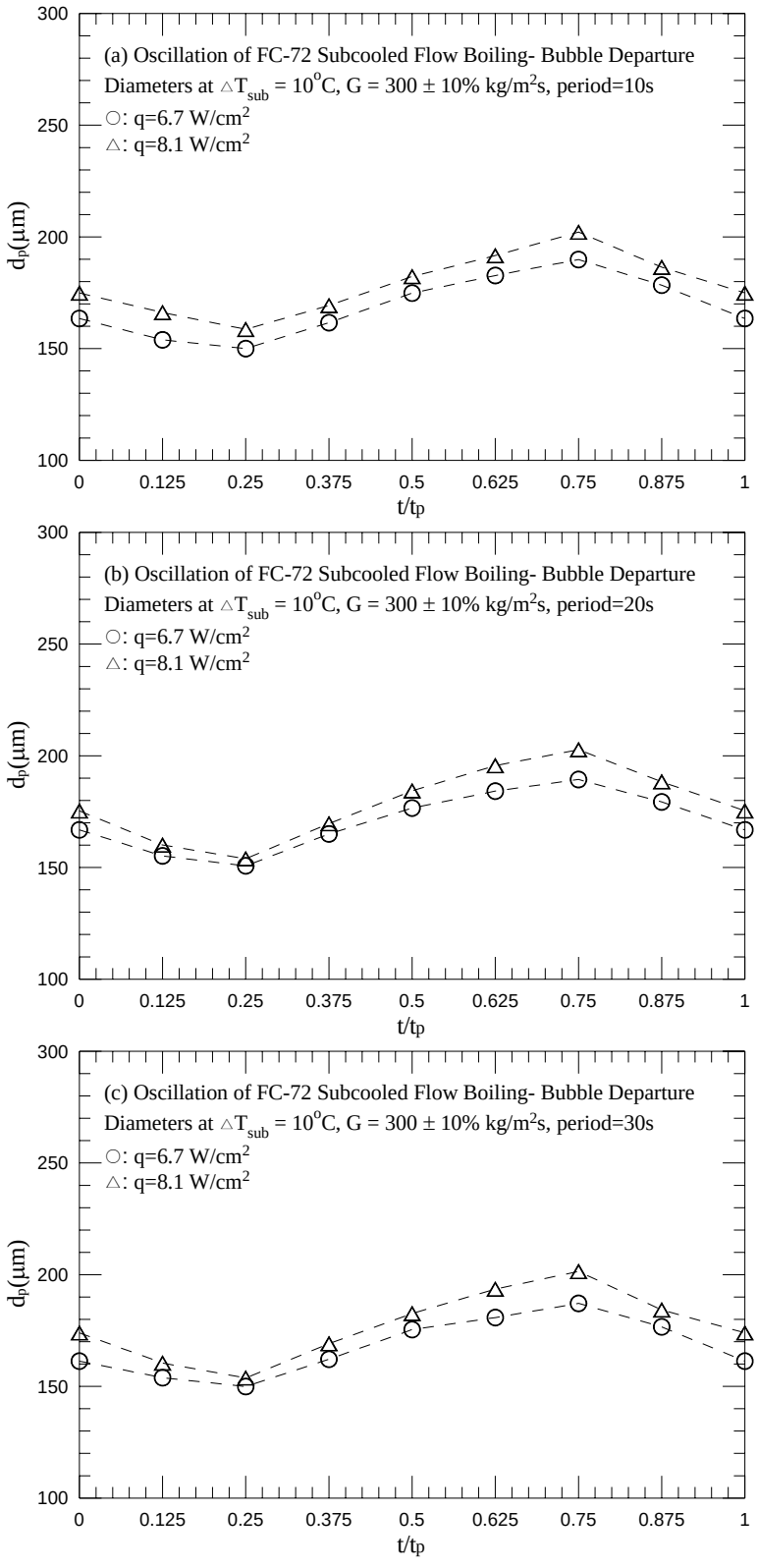

Fig. 5.175 Mean bubble departure diameters for various imposed heat fluxes for transient subcooled flow boiling for G=300±10% kg/m^{2}s and ΔT_{sub} =10^{o}C with t_p=10 sec (a), 20sec (b) and 30 sec (c).

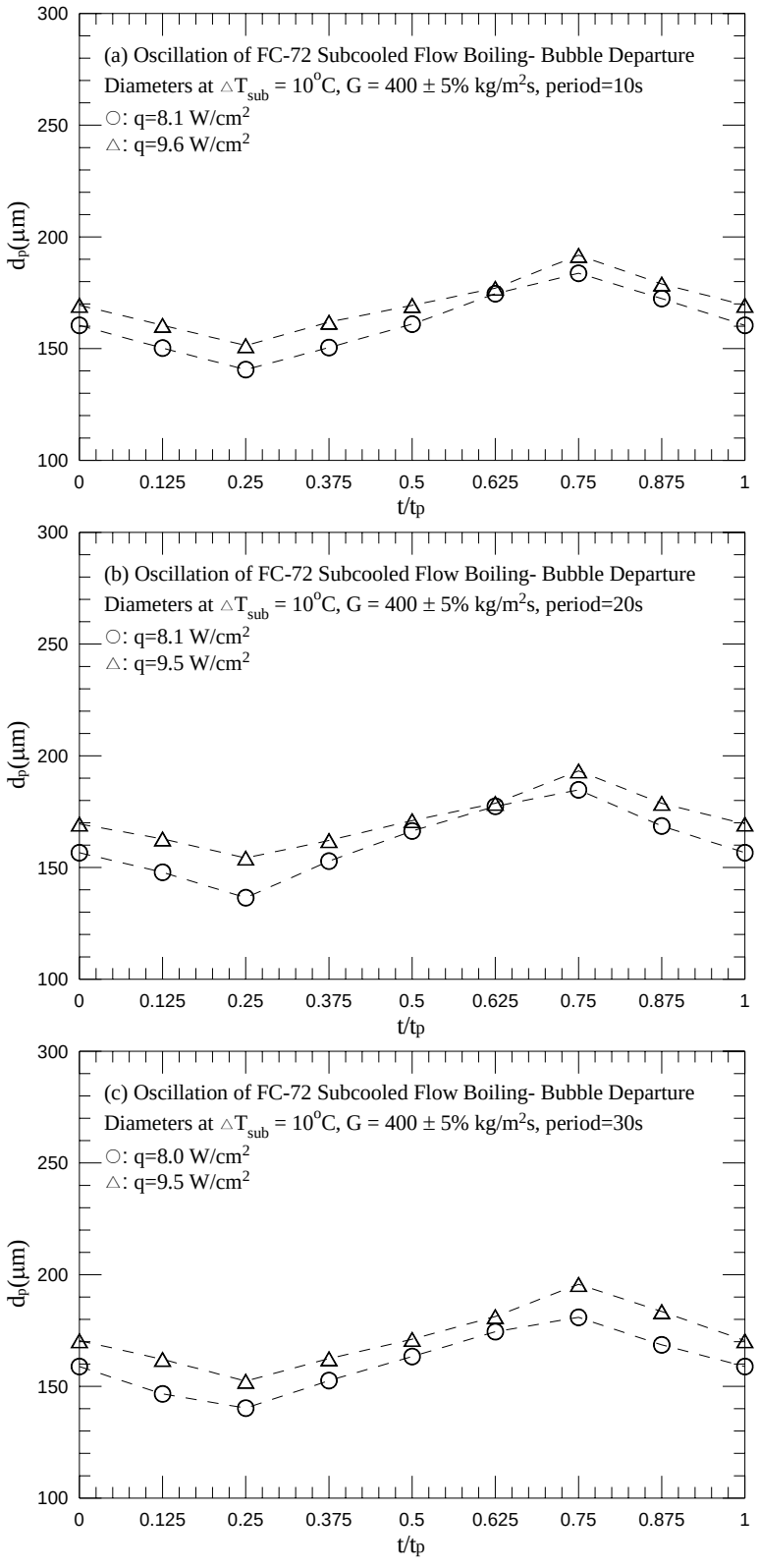

Fig. 5.176 Mean bubble departure diameters for various imposed heat fluxes for transient subcooled flow boiling for G=400±5% kg/m^{2}s and ΔT_{sub} =10^{o}C with t_p=10 sec (a), 20sec (b) and 30 sec (c).

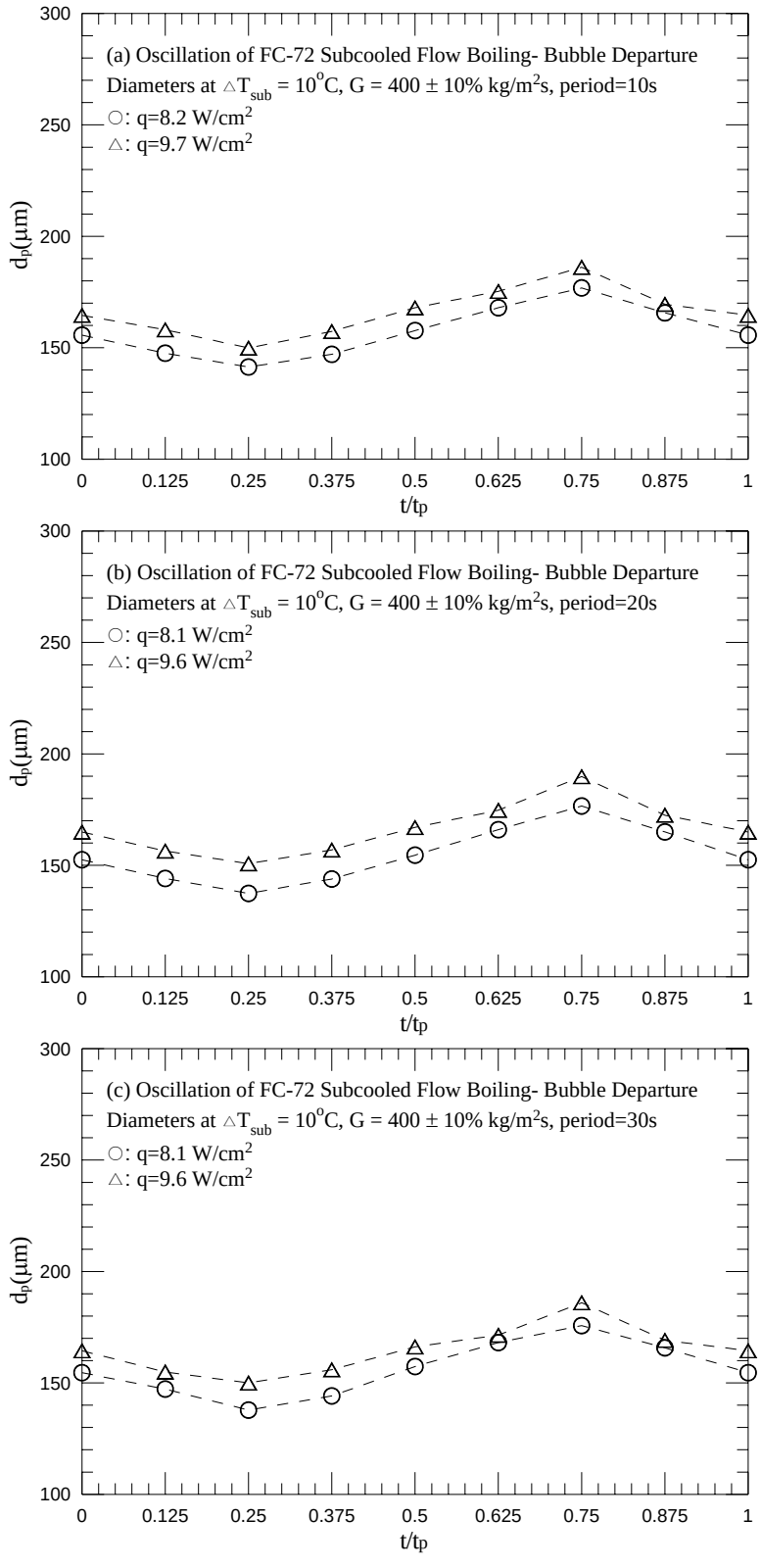

Fig. 5.177 Mean bubble departure diameters for various imposed heat fluxes for transient subcooled flow boiling for G=400±10% kg/m^{2}s and ΔT_{sub} =10°C with t_p=10 sec (a), 20sec (b) and 30 sec (c).

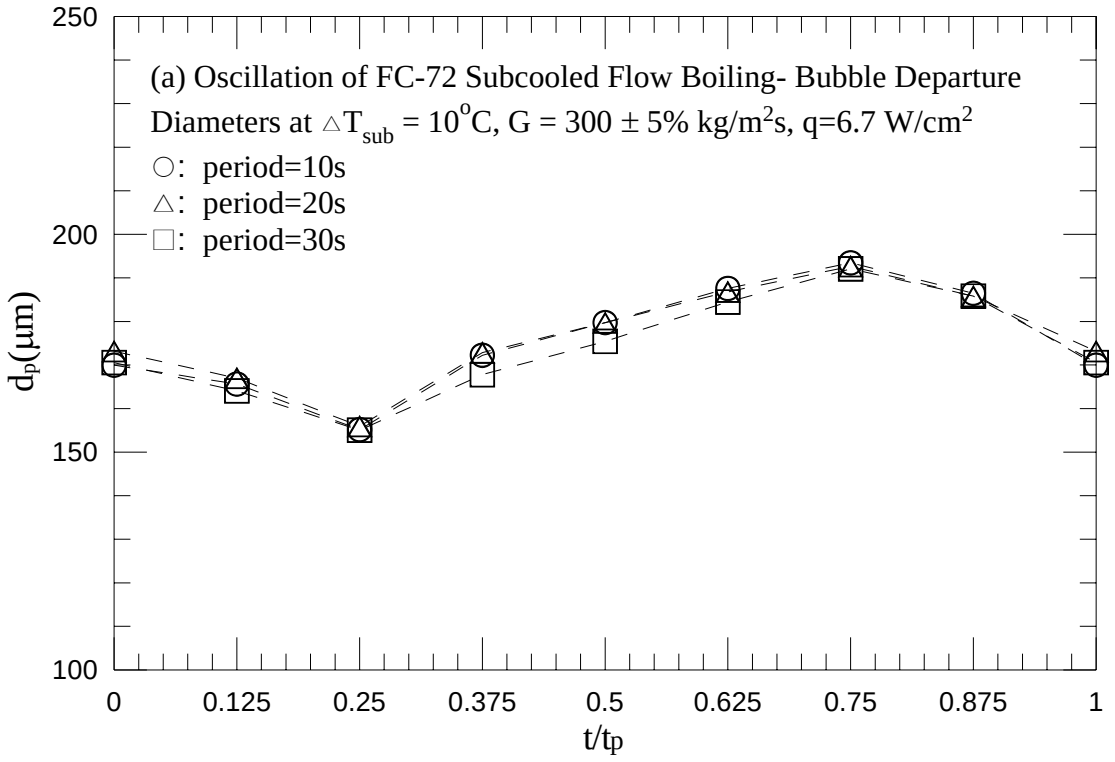

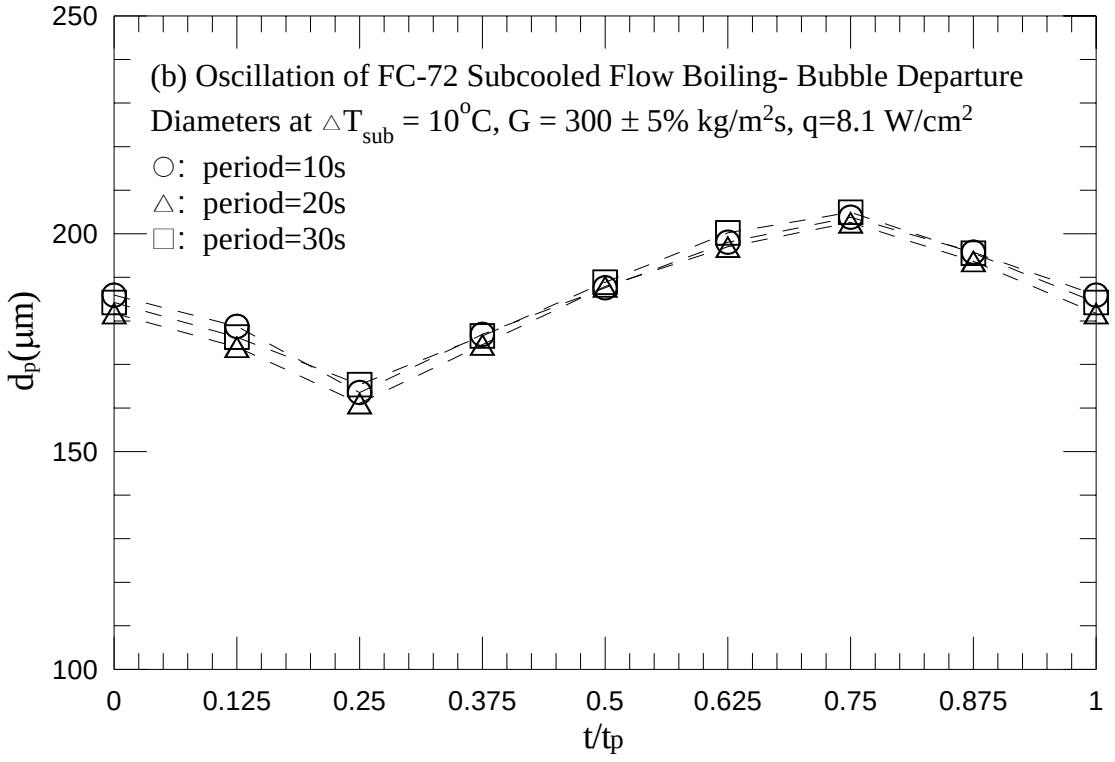

Fig. 5.178 Mean bubble departure diameters for various period of mass flux oscillation for transient subcooled flow boiling for G=300±5% kg/m^{2}s and ΔT_{sub} =10°C with (a) q=6.7 W/cm^2 and (b) q=8.1 W/cm^2.

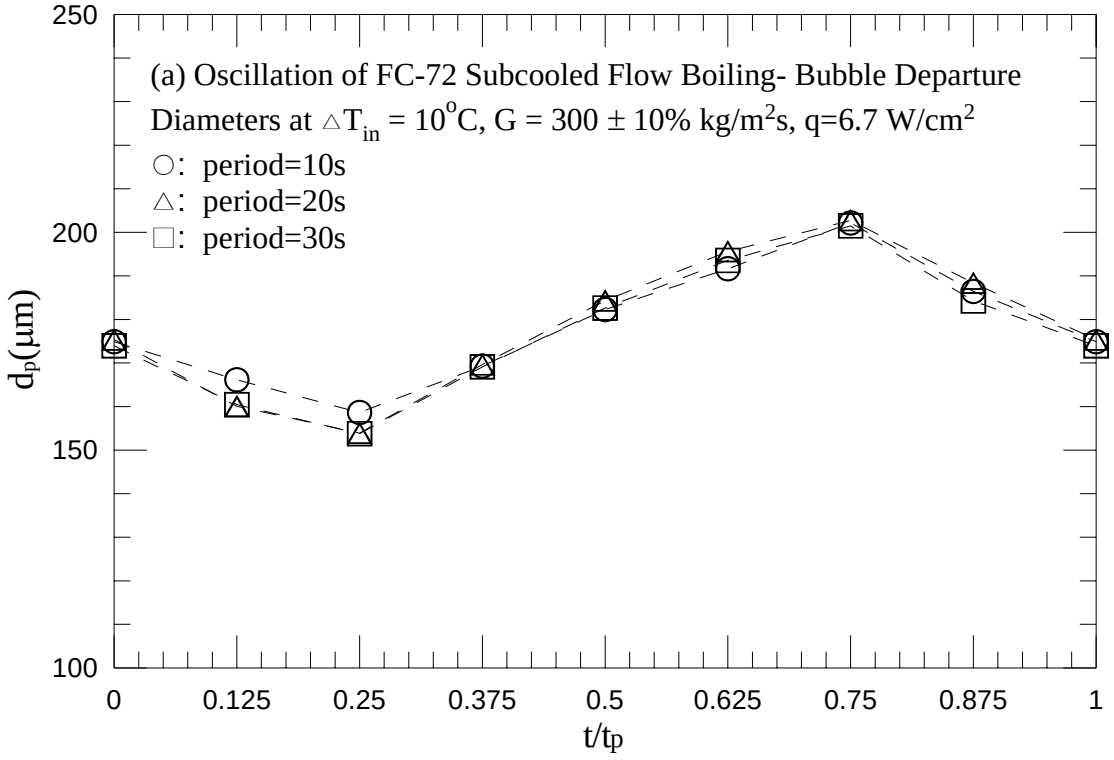

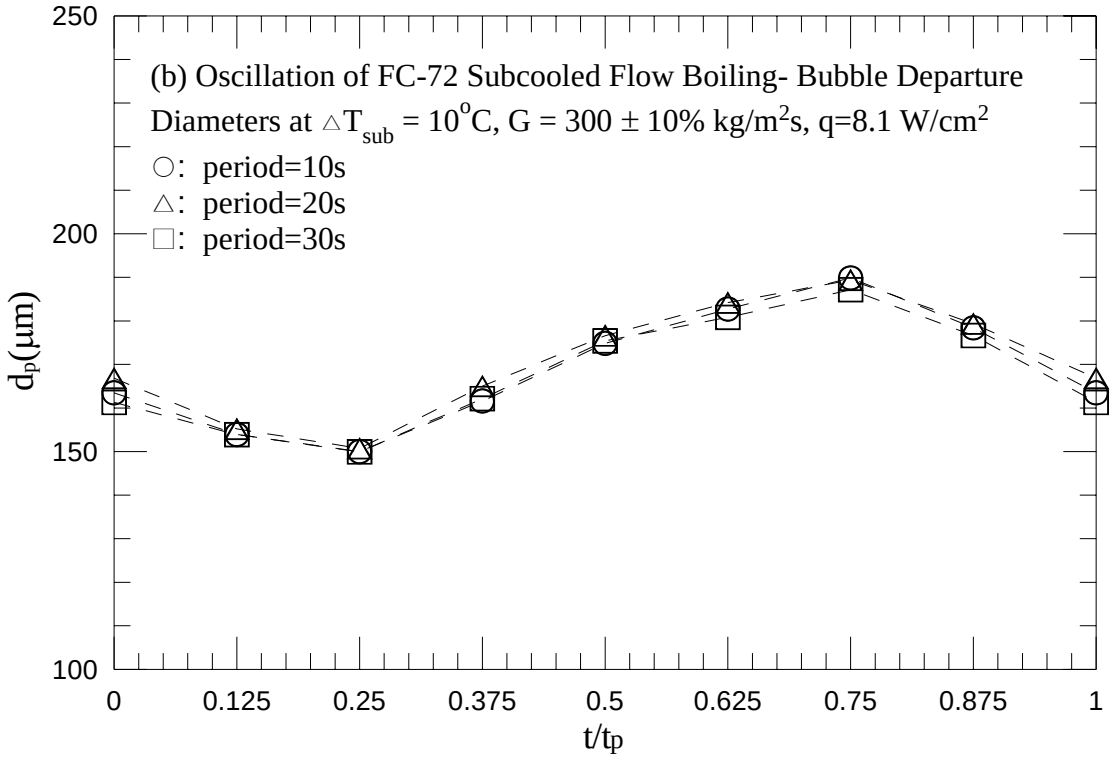

Fig. 5.179 Mean bubble departure diameters for various period of mass flux oscillation for transient subcooled flow boiling for G=300±10% kg/m^{2}s and ΔT_{sub} =10°C with (a) q=6.7 W/cm^2 and (b) q=8.1 W/cm^2.

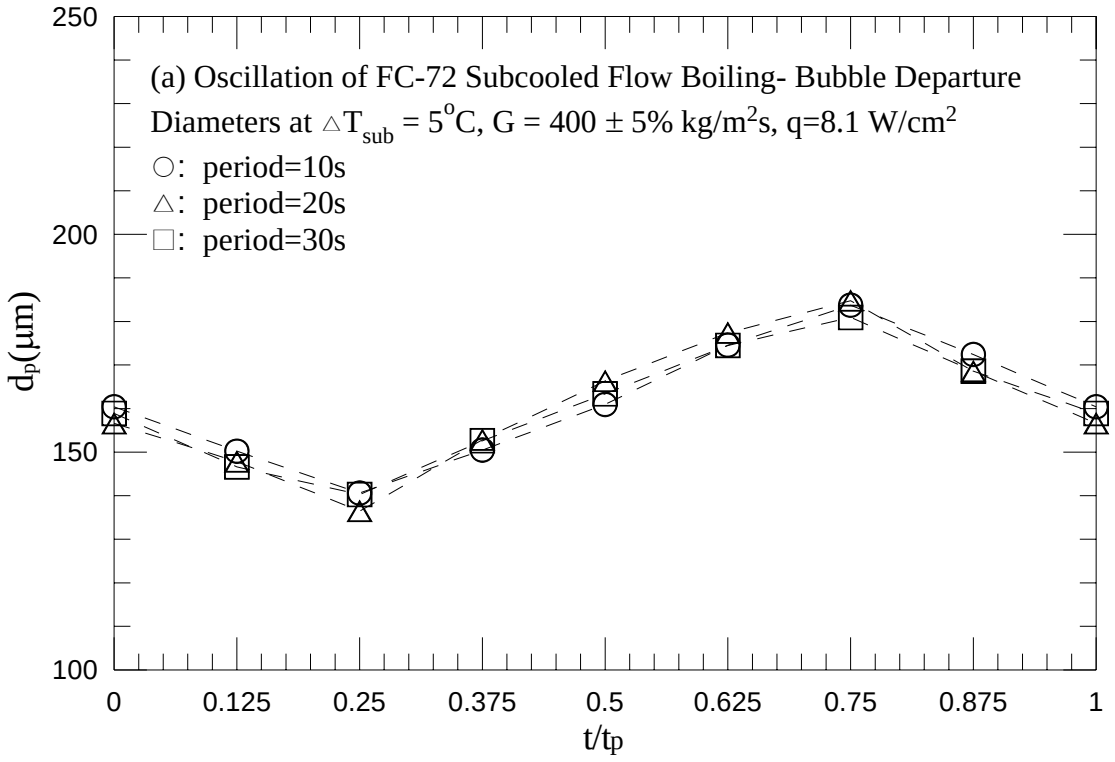

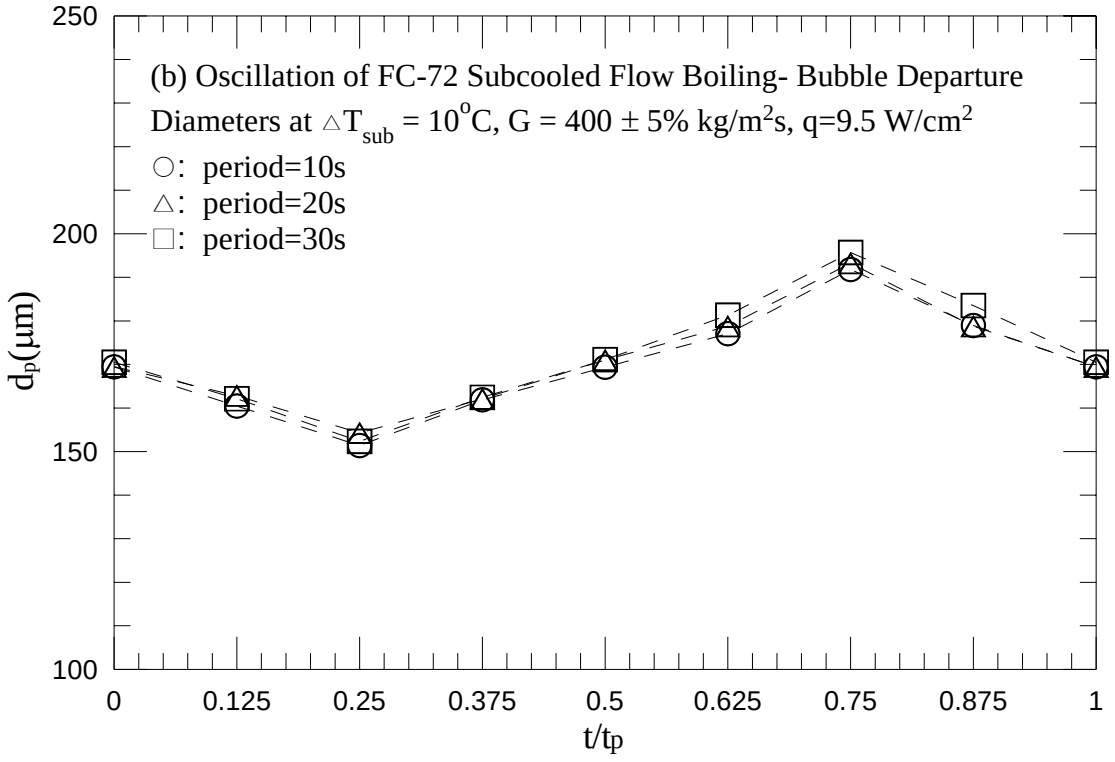

Fig. 5.180 Mean bubble departure diameters for various period of mass flux oscillation for transient subcooled flow boiling for G=400±5% kg/m^{2}s and ΔT_{sub} =10°C with (a) q=8.1 W/cm^2 and (b) q=9.5 W/cm^2.

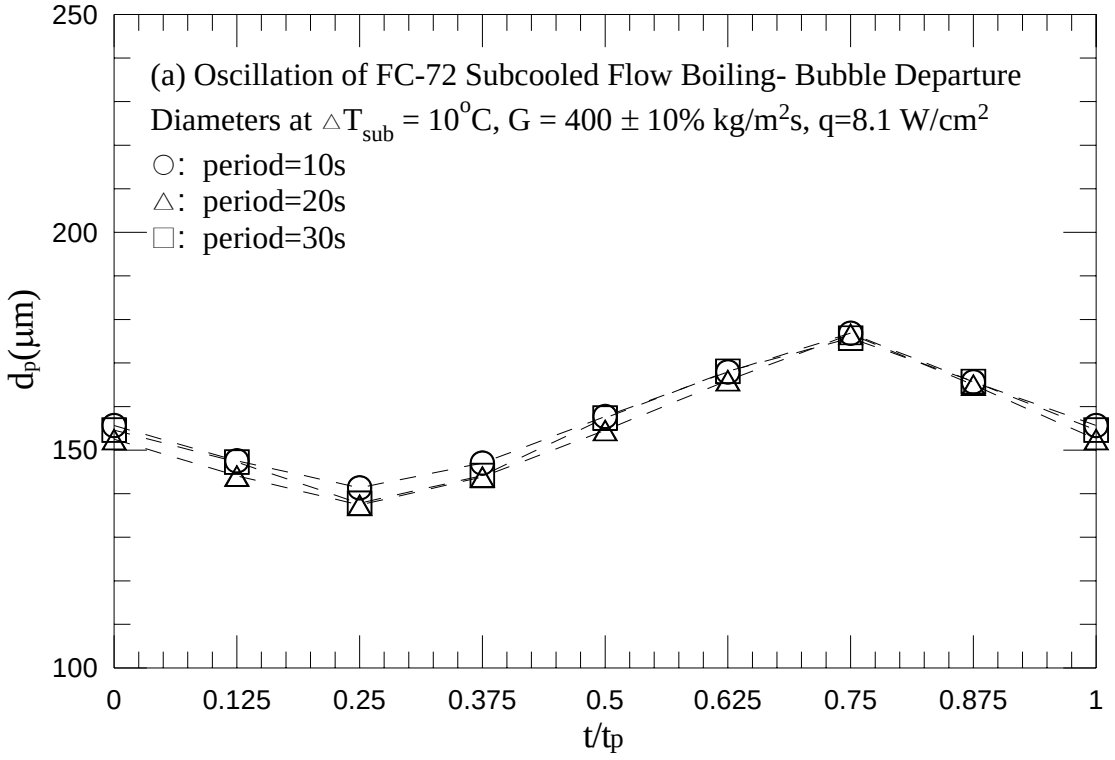

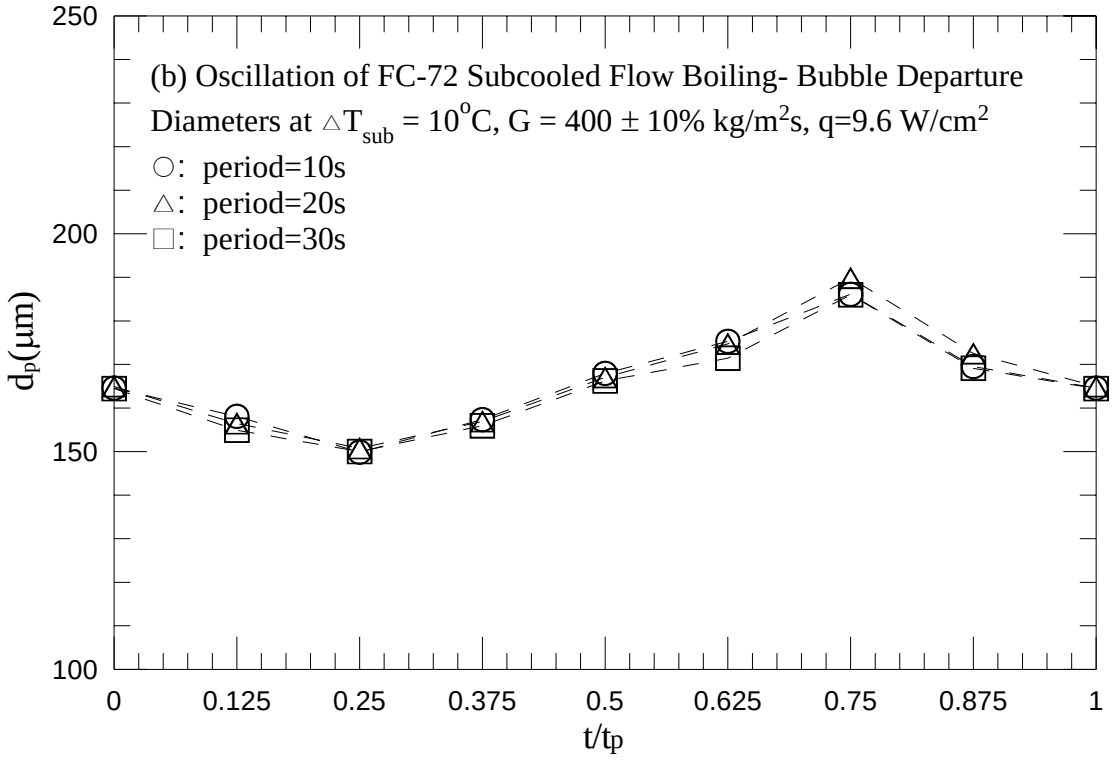

Fig. 5.181 Mean bubble departure diameters for various period of mass flux oscillation for transient subcooled flow boiling for G=400±10% kg/m^{2}s and ΔT_{sub} =10°C with (a) q=8.1 W/cm^2 and (b) q=9.6 W/cm^2.

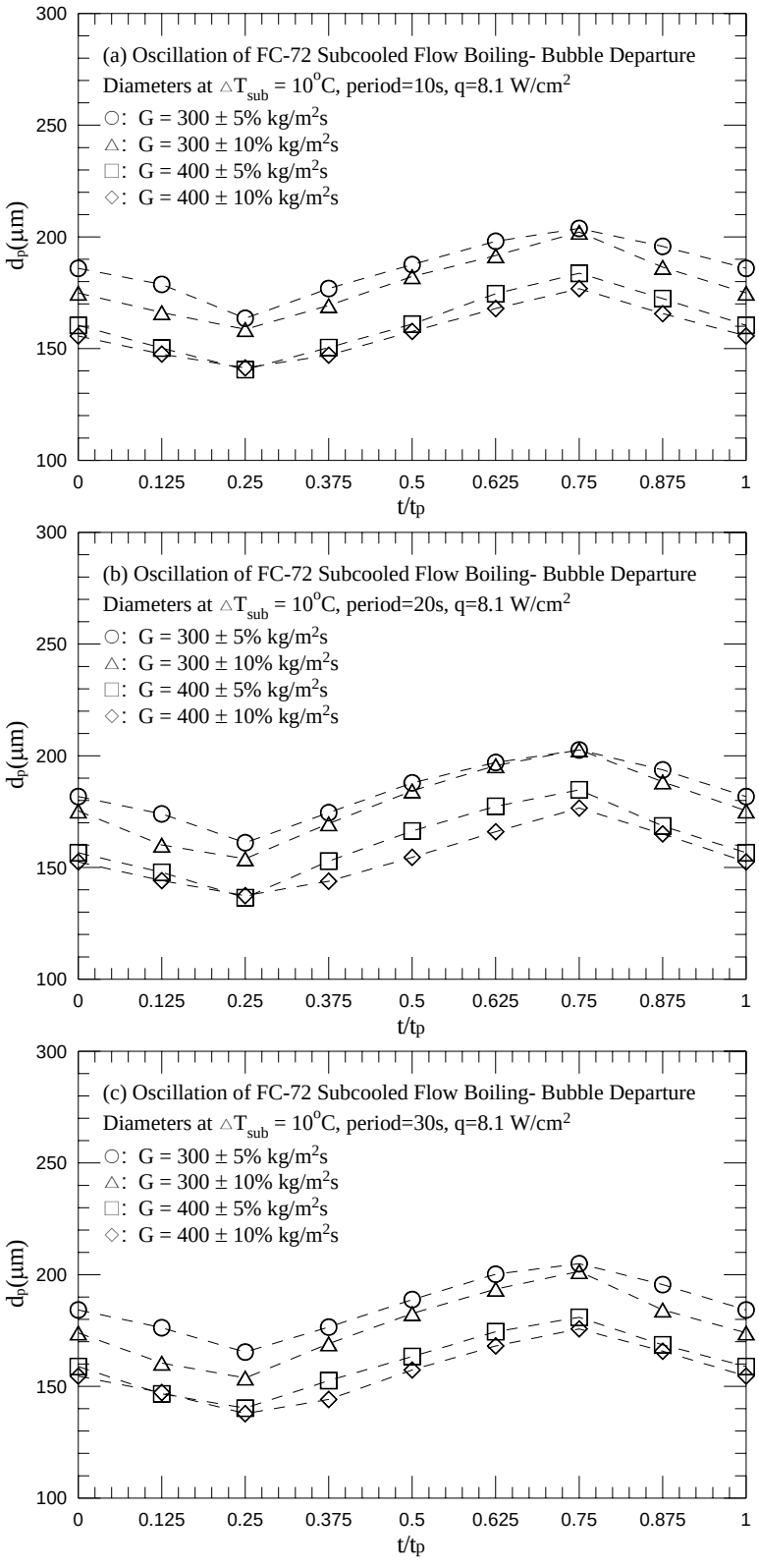

Fig. 5.182 Mean bubble departure diameters for various amplitudes of the mass fluxes oscillation for transient subcooled flow boiling for q=8.1 W/cm^2 and ΔT_{sub} =10^{o}C with period=10 sec (a), 20 sec (b), and 30 sec (c).

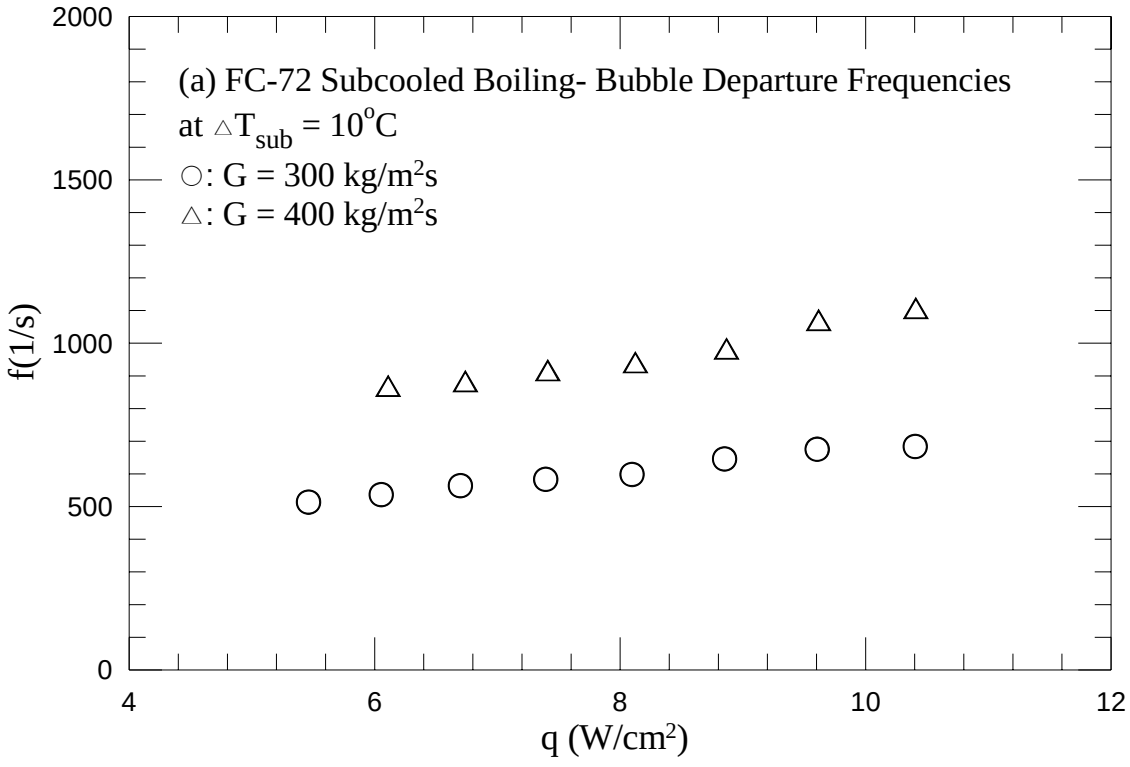

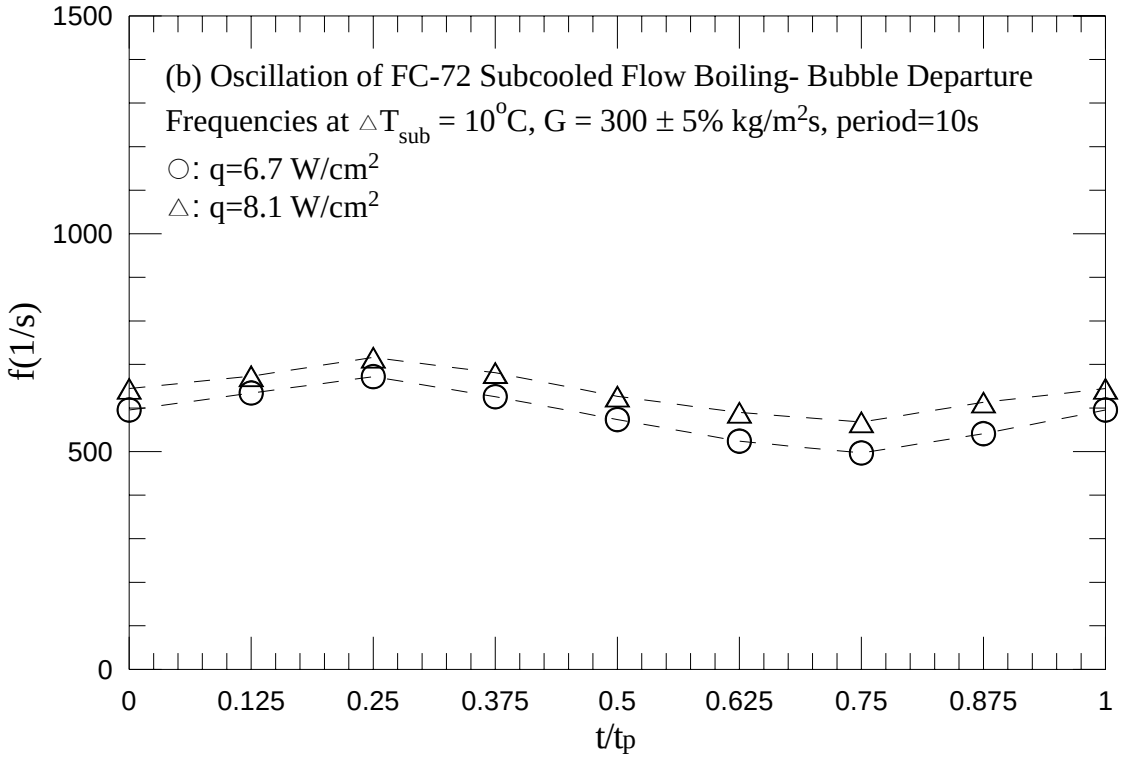

Fig. 5.183 Mean bubble departure frequencies for various coolant mass fluxes for stable subcooled flow boiling (a) and various imposed heat fluxes for transient subcooled flow boiling for G=300±5% kg/m^{2}s and ΔT_{sub} =10°C with t_p=10 sec (b), 20sec (c) and 30 sec (d).

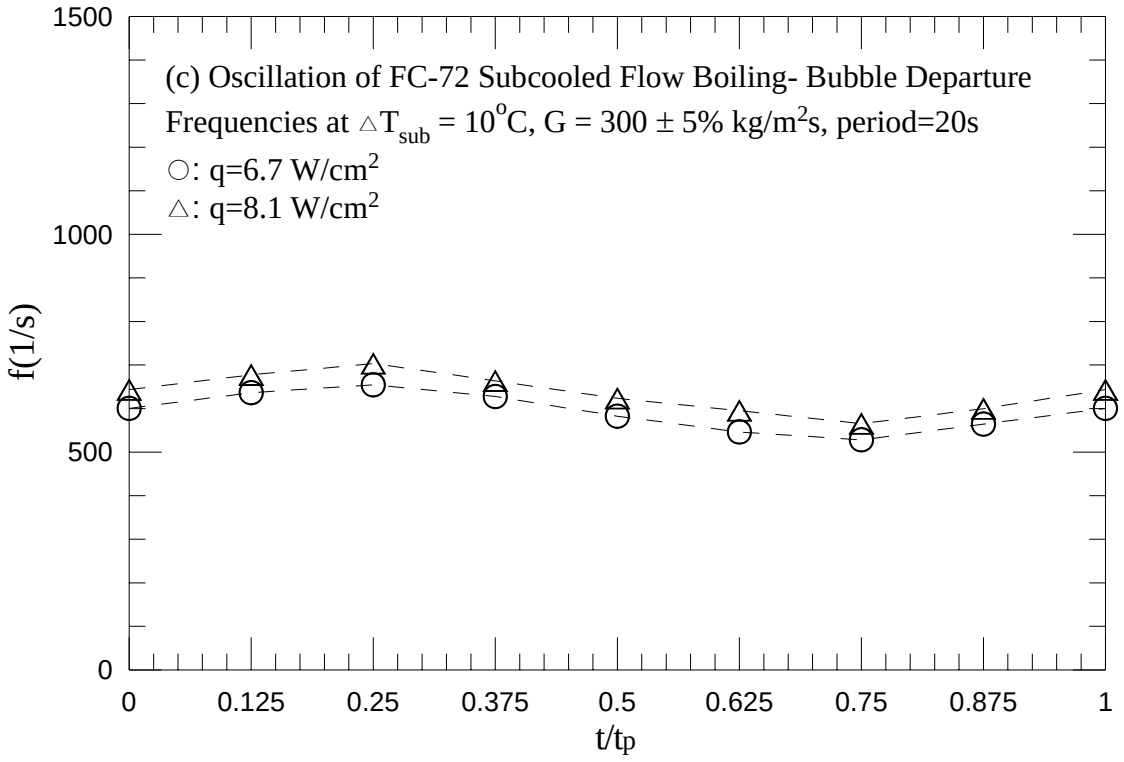

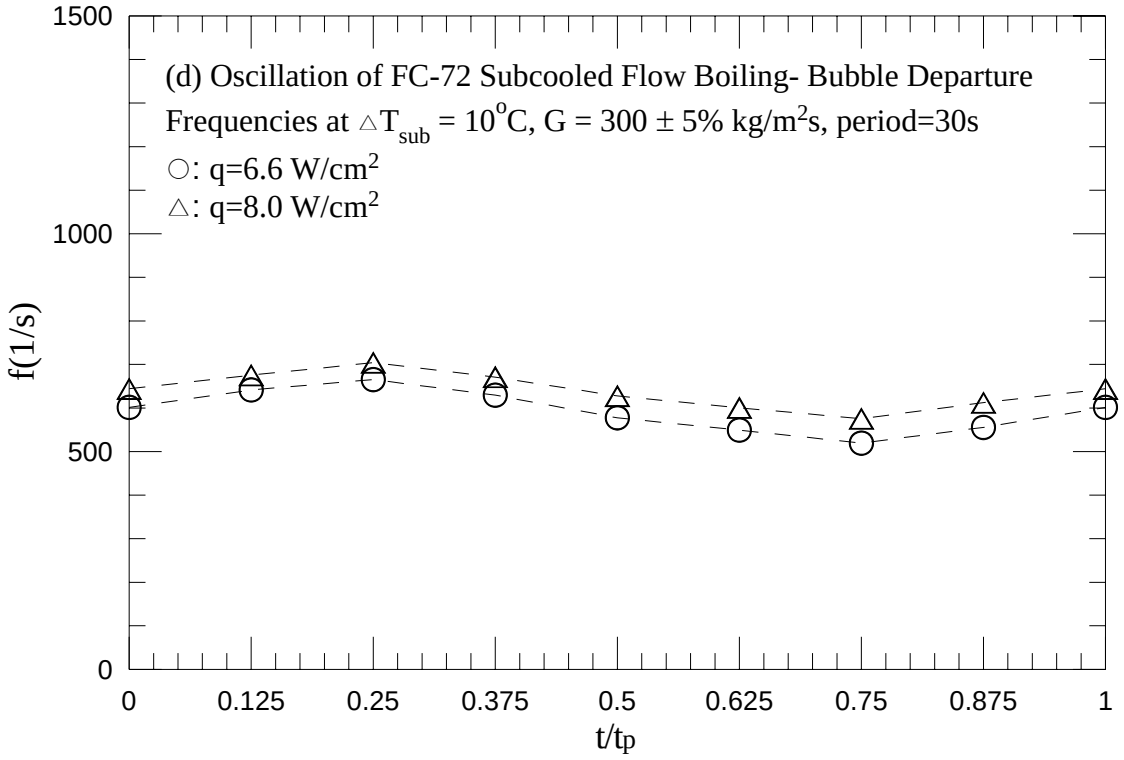

Fig. 5.183 Continued.

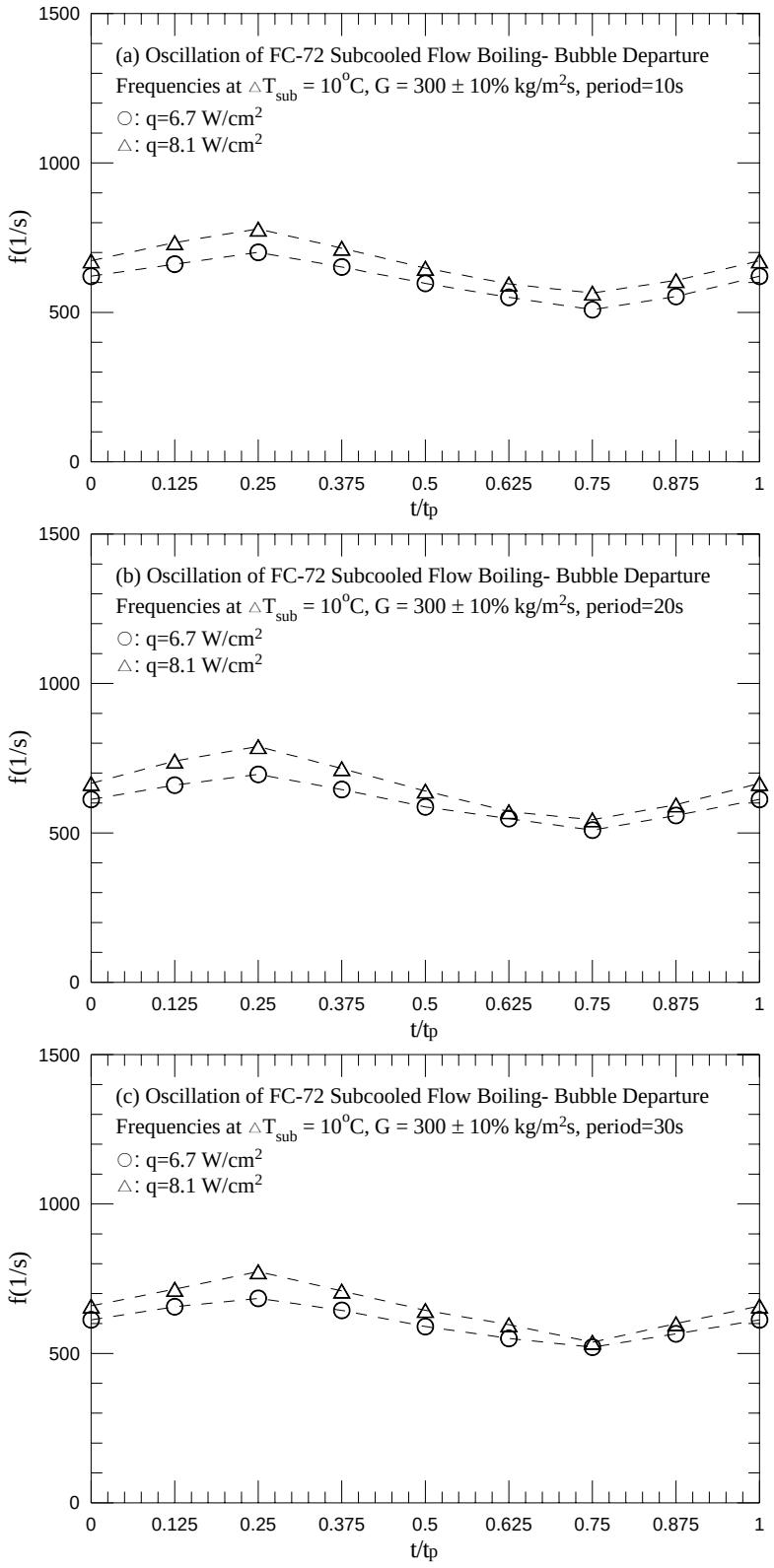

Fig. 5.184 Mean bubble departure frequencies for various imposed heat fluxes for transient subcooled flow boiling for G=300±10% kg/m^{2}s and ΔT_{sub} =10°C with t_p=10 sec (a), 20sec (b) and 30 sec (c).

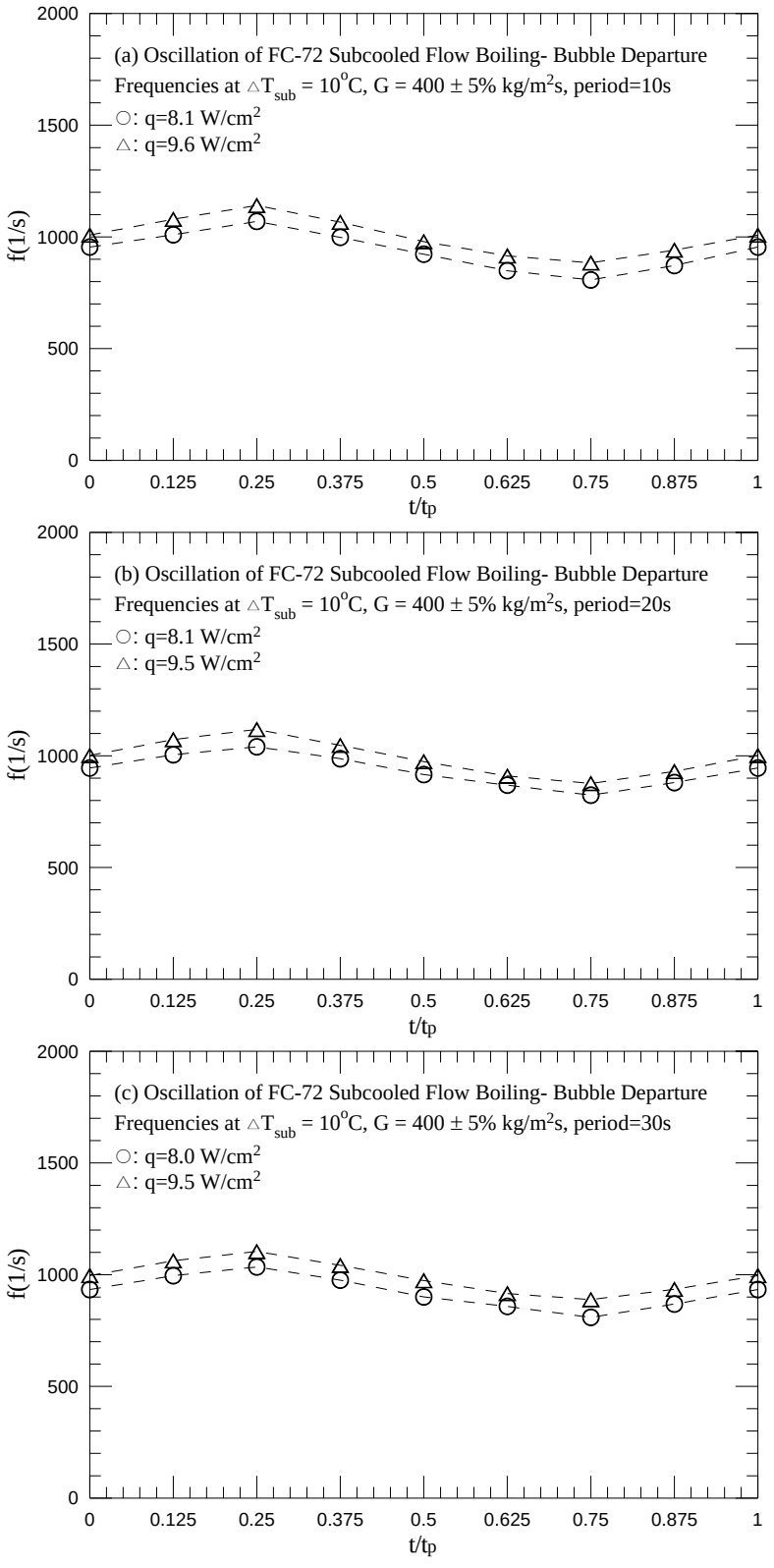

Fig. 5.185 Mean bubble departure frequencies for various imposed heat fluxes for transient subcooled flow boiling for G=400±5% kg/m^{2}s and ΔT_{sub} =10^{o}C with t_p=10 sec (a), 20sec (b) and 30 sec (c).

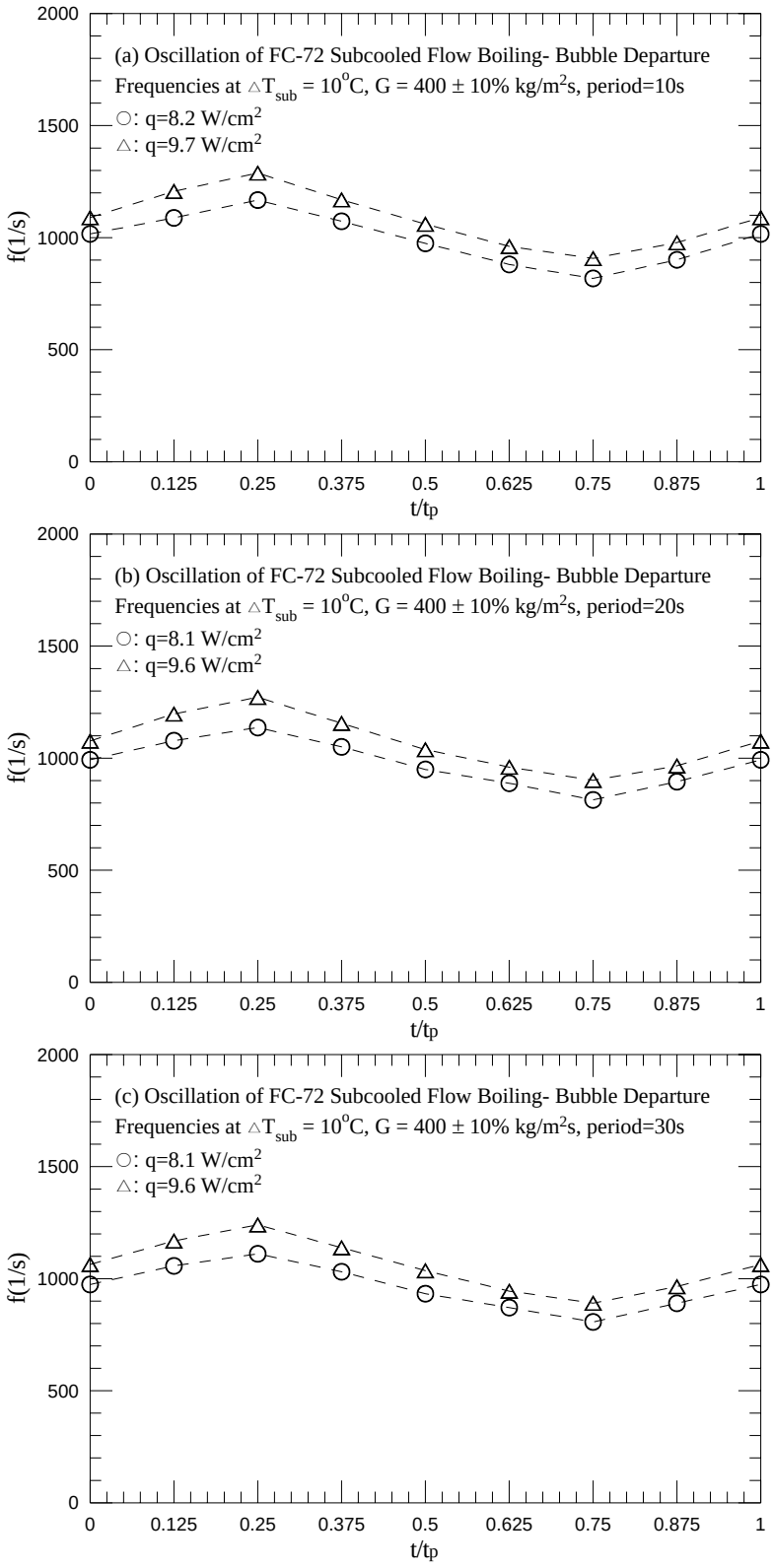

Fig. 5.186 Mean bubble departure frequencies for various imposed heat fluxes for transient subcooled flow boiling for G=400±10% kg/m^{2}s and ΔT_{sub} =10°C with t_p=10 sec (a), 20sec (b) and 30 sec (c).

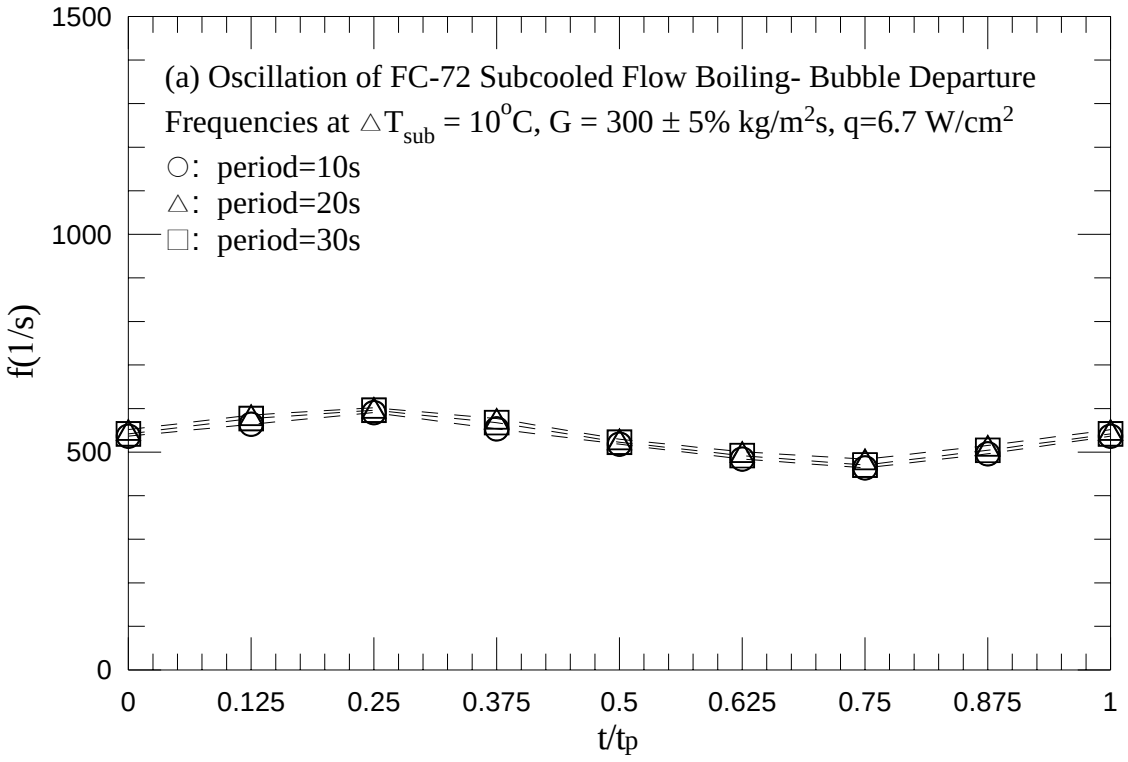

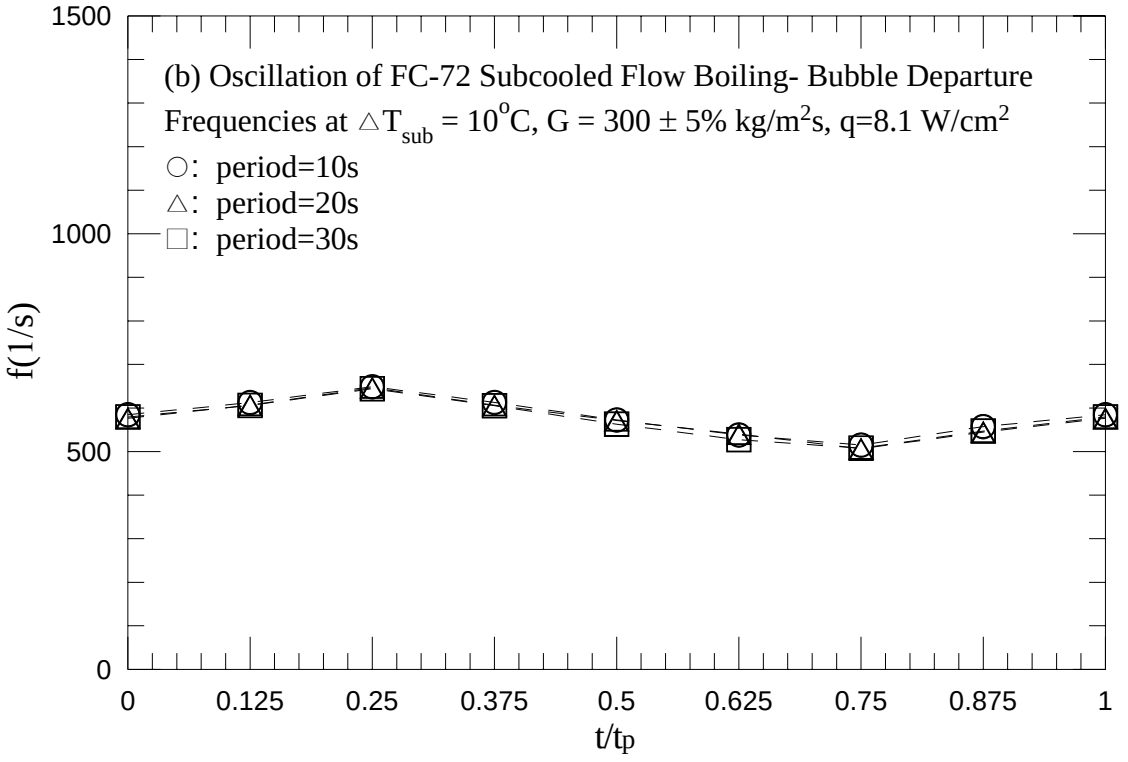

Fig. 5.187 Mean bubble departure frequencies for various periods of mass flux oscillation for transient subcooled flow boiling for G=300±5% kg/m^{2}s and ΔT_{sub} =10°C with (a) q=6.7 W/cm^2 and (b) q=8.1 W/cm^2.

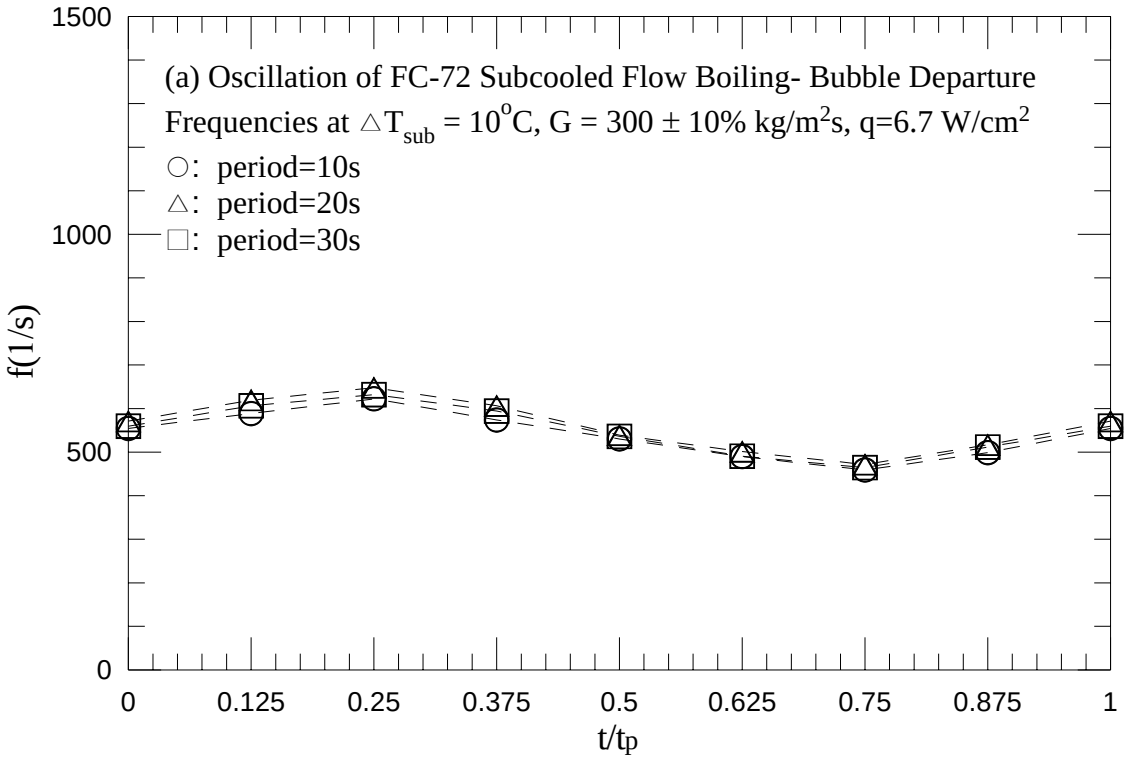

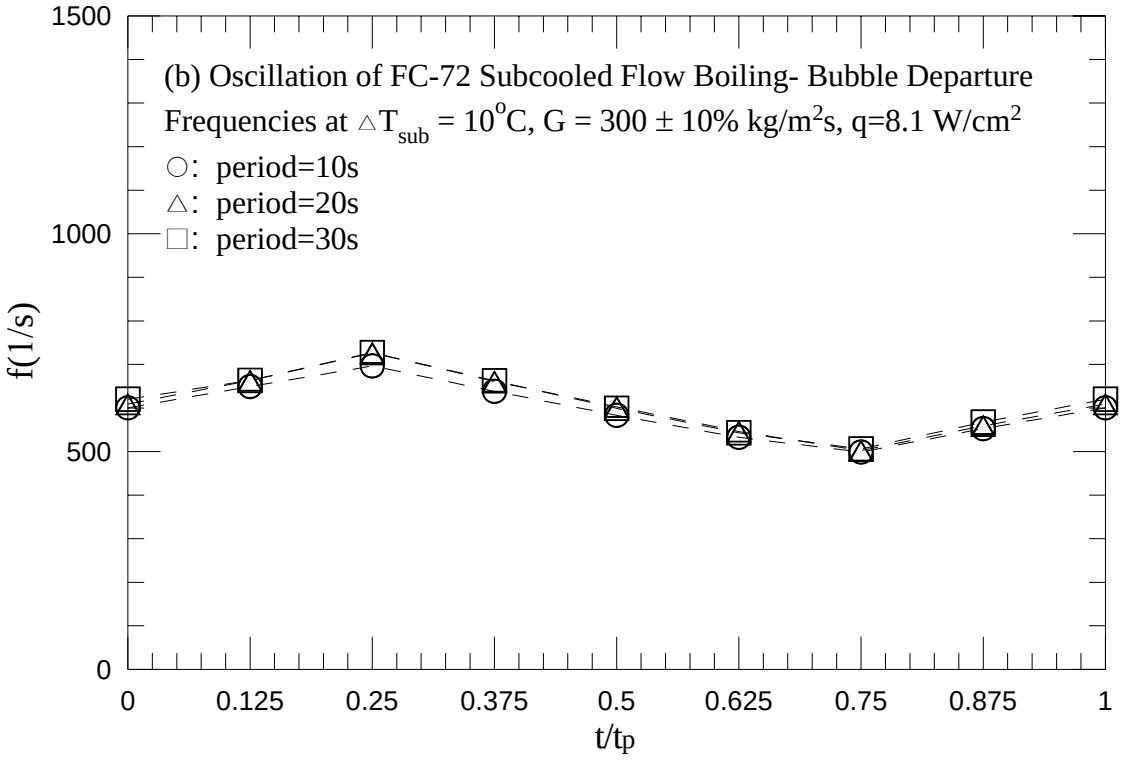

Fig. 5.188 Mean bubble departure frequencies for various periods of mass flux oscillation for transient subcooled flow boiling for G=300±10% kg/m^{2}s and ΔT_{sub} =10°C with (a) q=6.7 W/cm^2 and (b) q=8.1 W/cm^2.

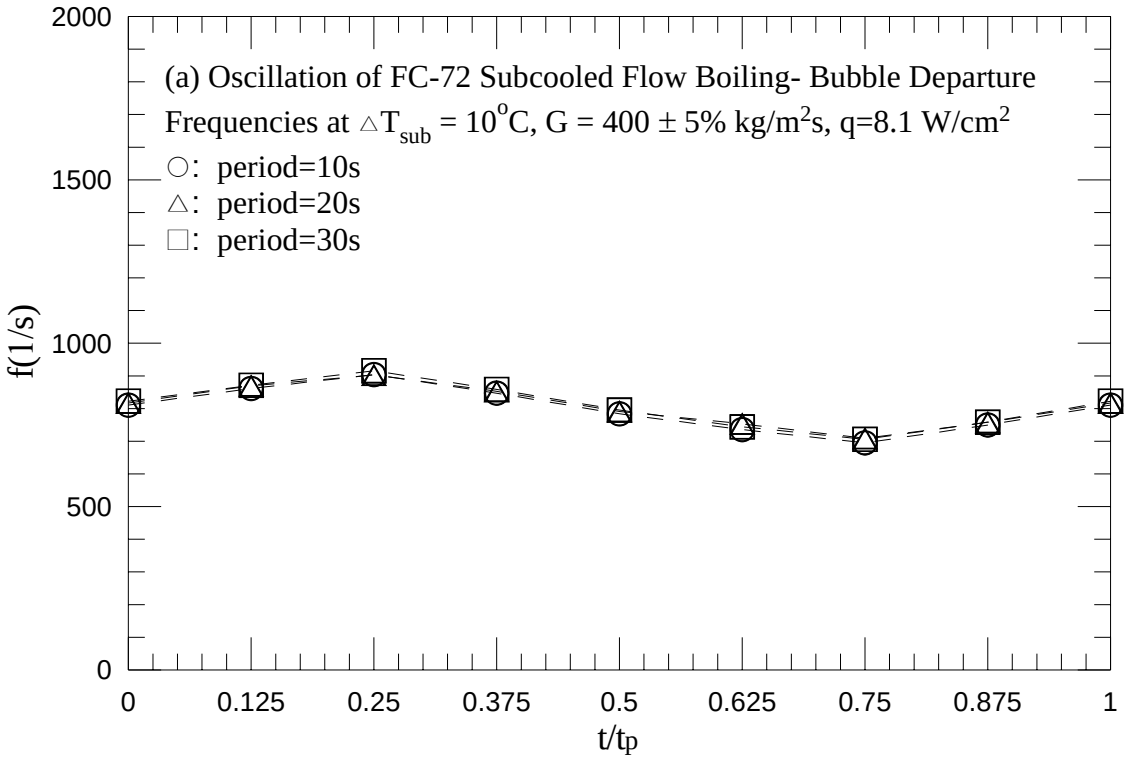

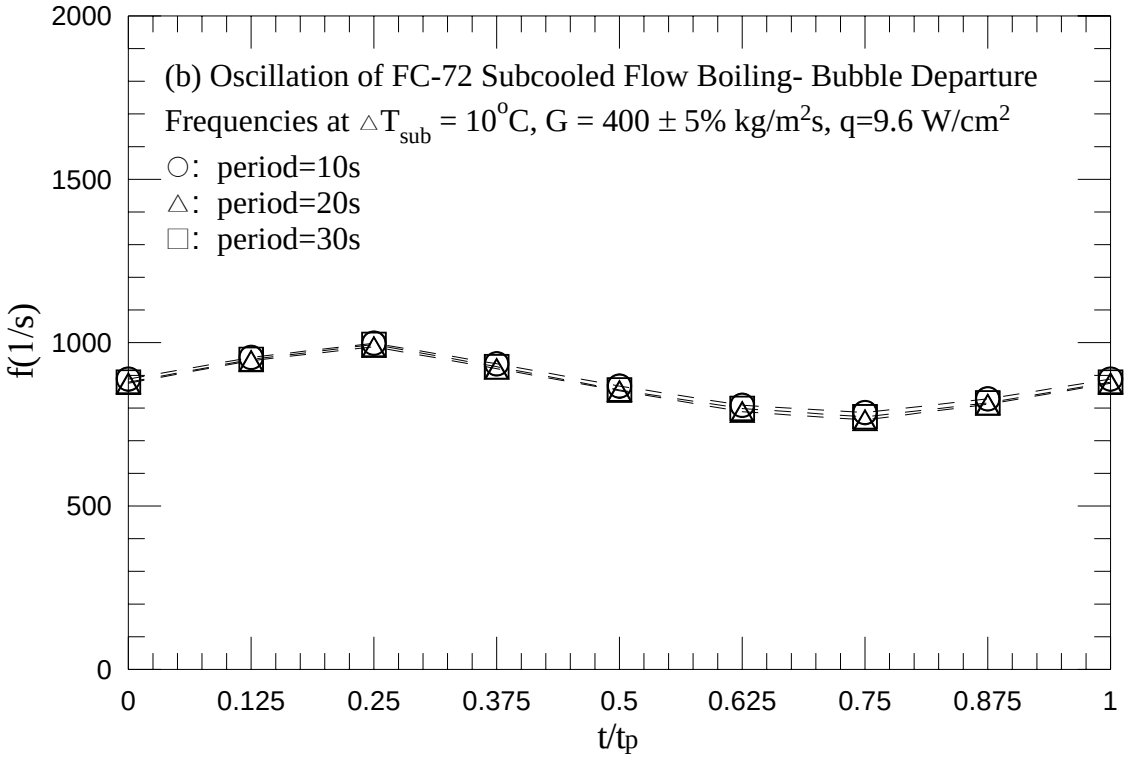

Fig. 5.189 Mean bubble departure frequencies for various periods of mass flux oscillation for transient subcooled flow boiling for G=400±5% kg/m^{2}s and ΔT_{sub} =10°C with (a) q=8.1 W/cm^2 and (b) q=9.6 W/cm^2.

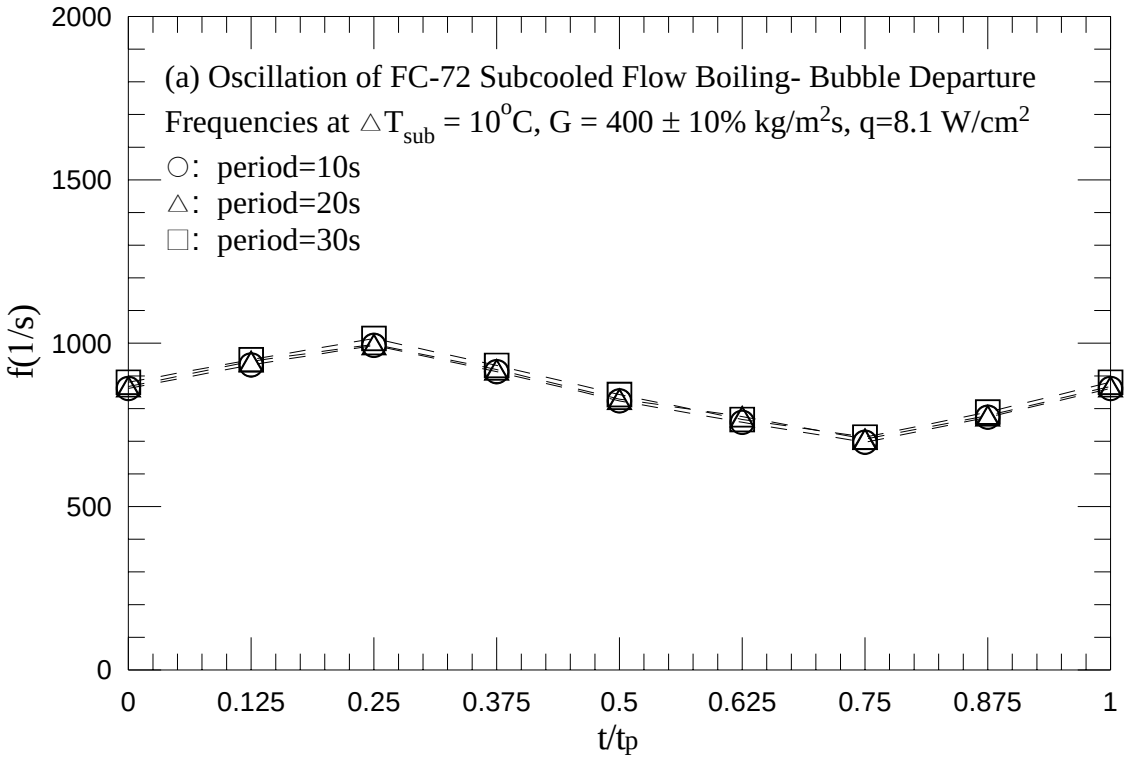

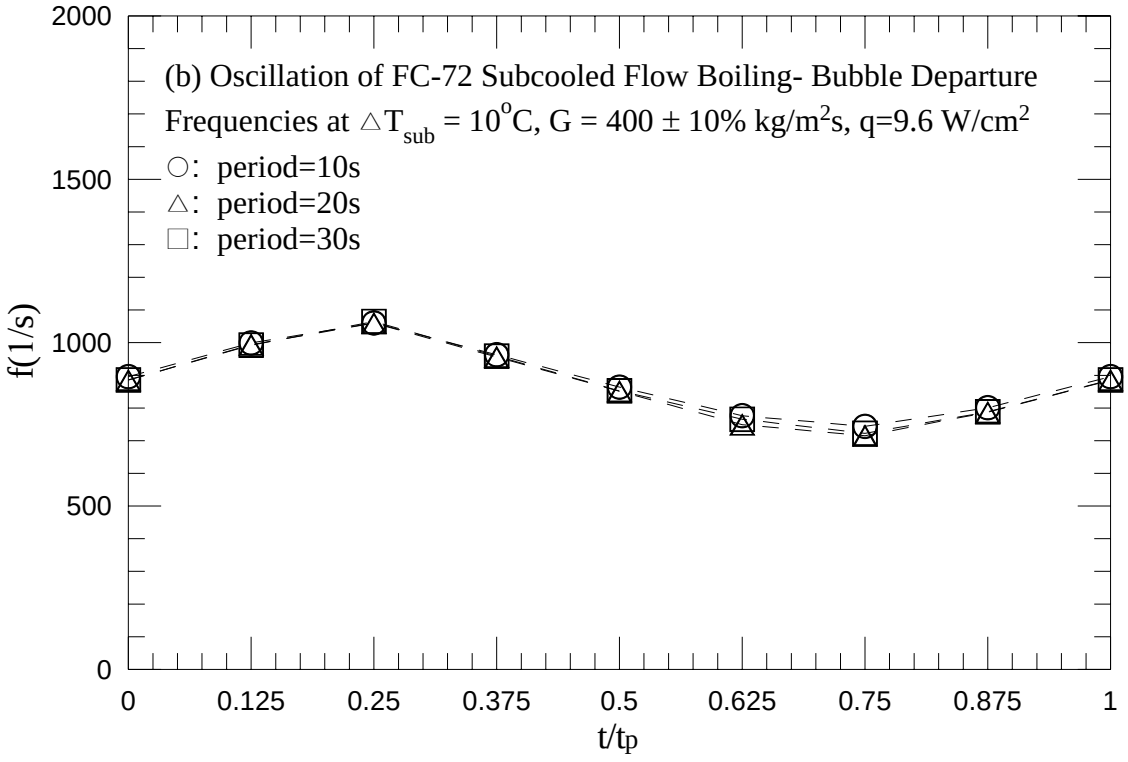

Fig. 5.190 Mean bubble departure frequencies for various periods of mass flux oscillation for transient subcooled flow boiling for G=400±10% kg/m^{2}s and ΔT_{sub} =10°C with (a) q=8.1 W/cm^2 and (b) q=9.6 W/cm^2.

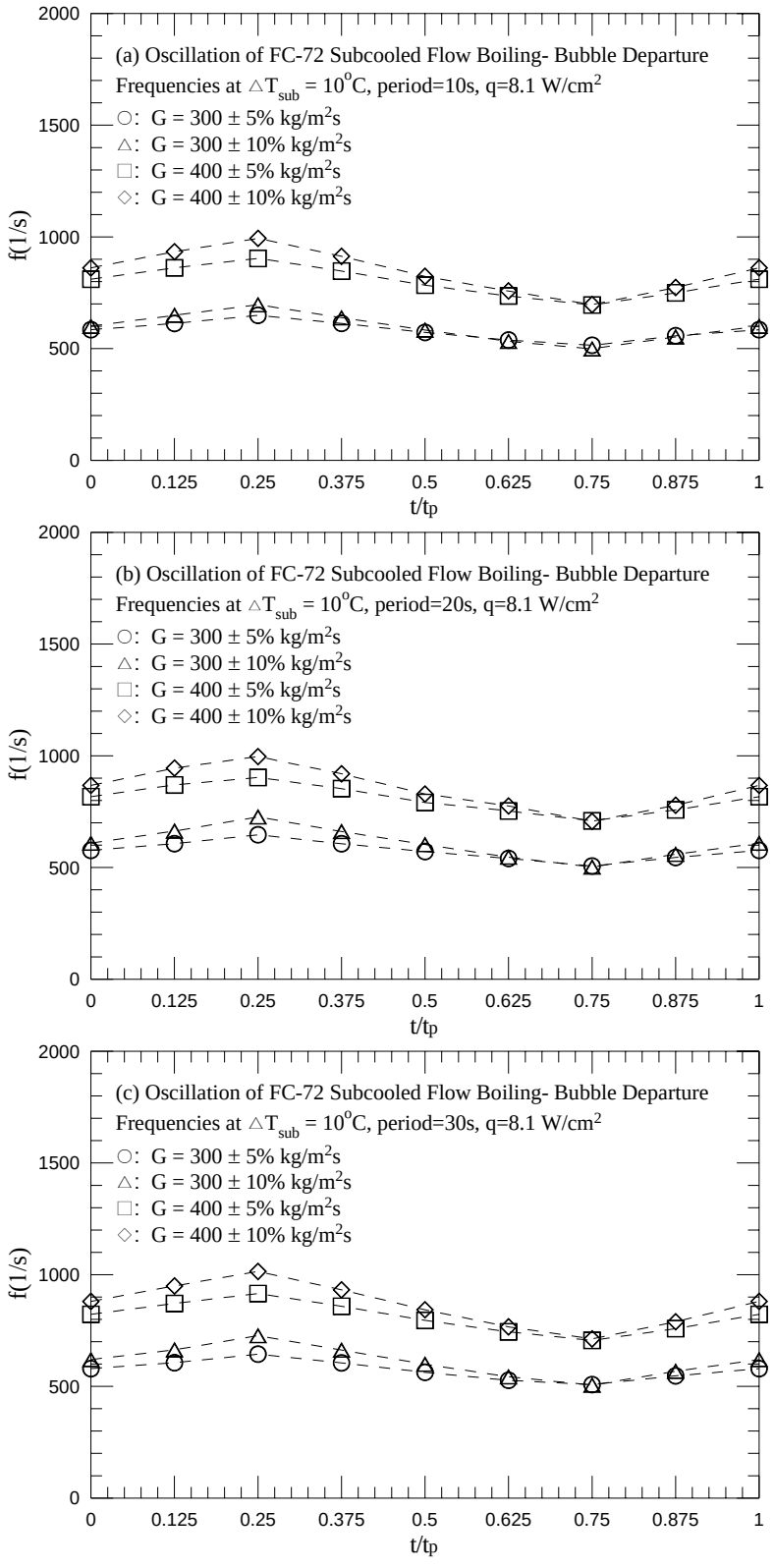

Fig. 5.191 Mean bubble departure frequencies for various amplitudes of the mass fluxes oscillation for transient subcooled flow boiling for q=8.1 W/cm^2 and ΔT_{sub} =10^{o}C with period=10 sec (a), 20 sec (b), and 30 sec (c).

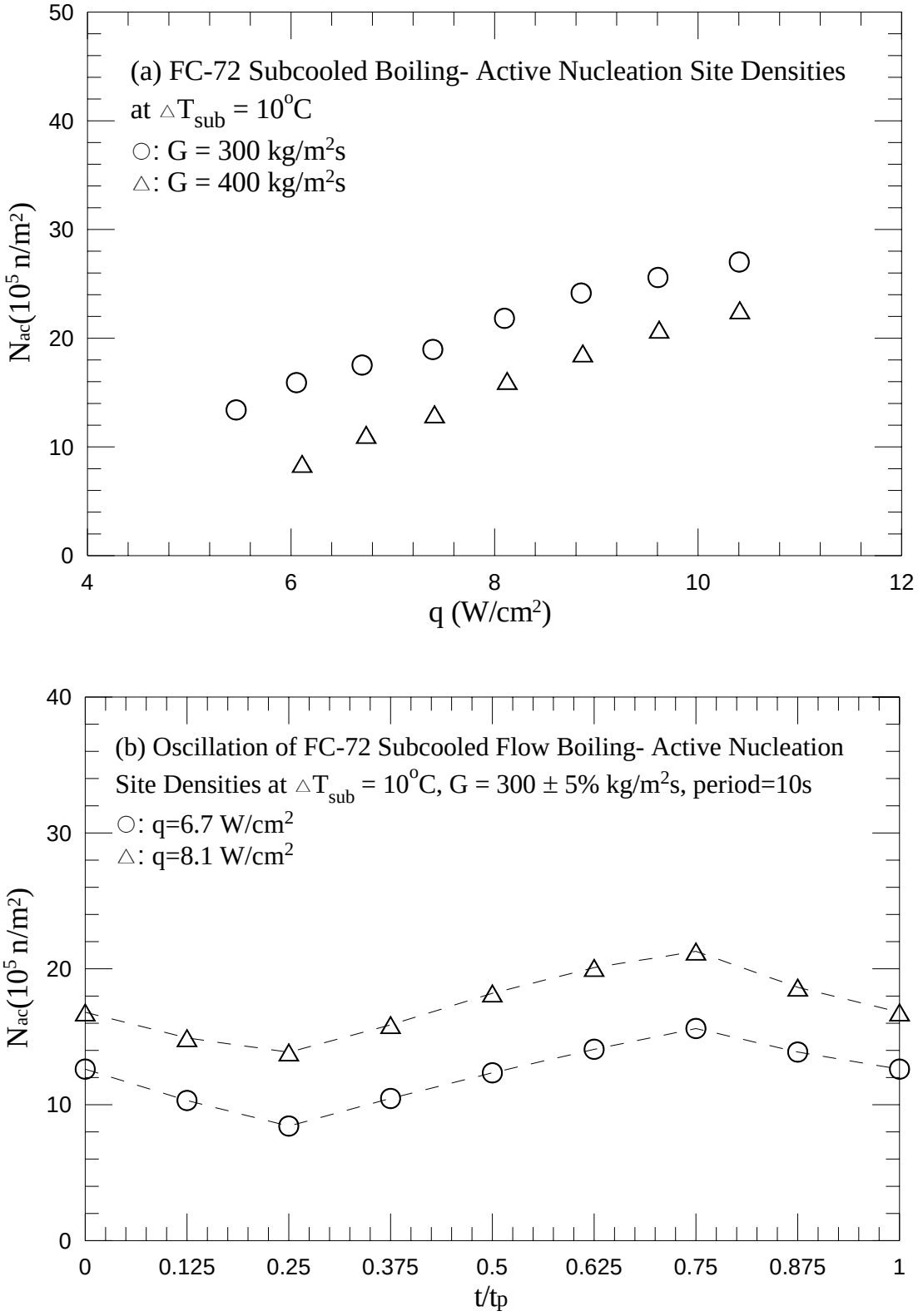

Fig. 5.192 Mean active nucleation site densities for various coolant mass fluxes for stable subcooled flow boiling (a) and various imposed heat fluxes for transient subcooled flow boiling for G=300±5% kg/m^{2}s and ΔT_{sub} =10°C with t_p=10 sec (b), 20sec (c) and 30 sec (d).

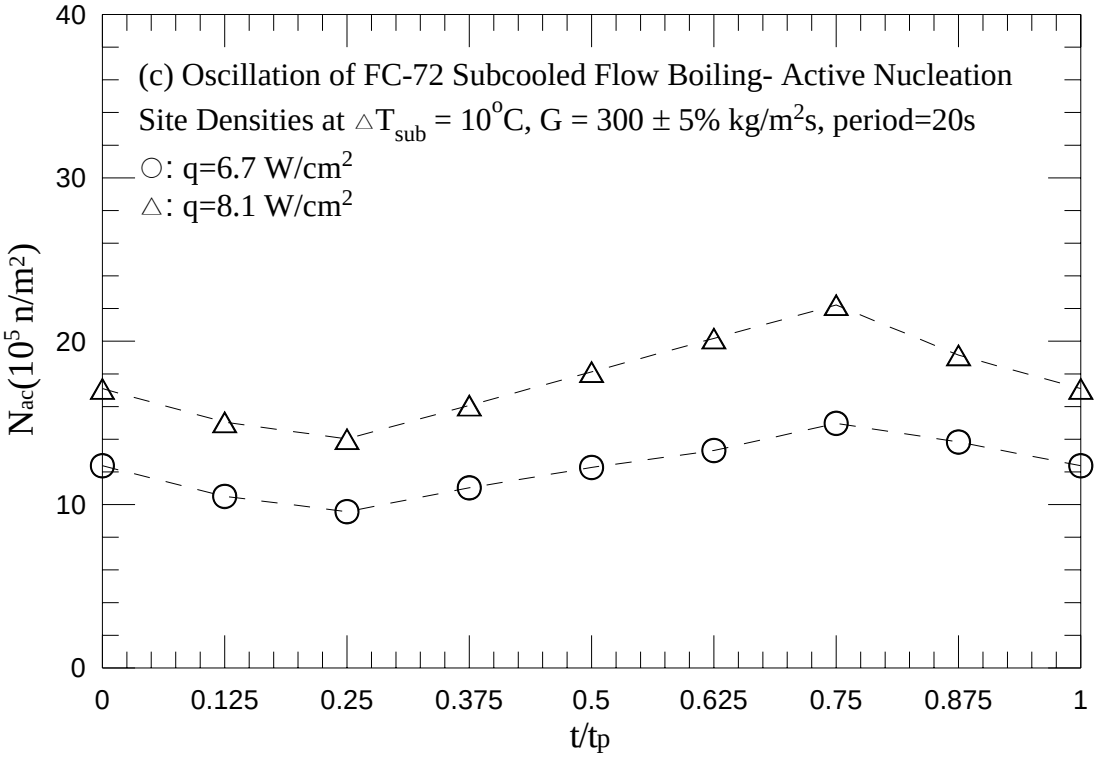

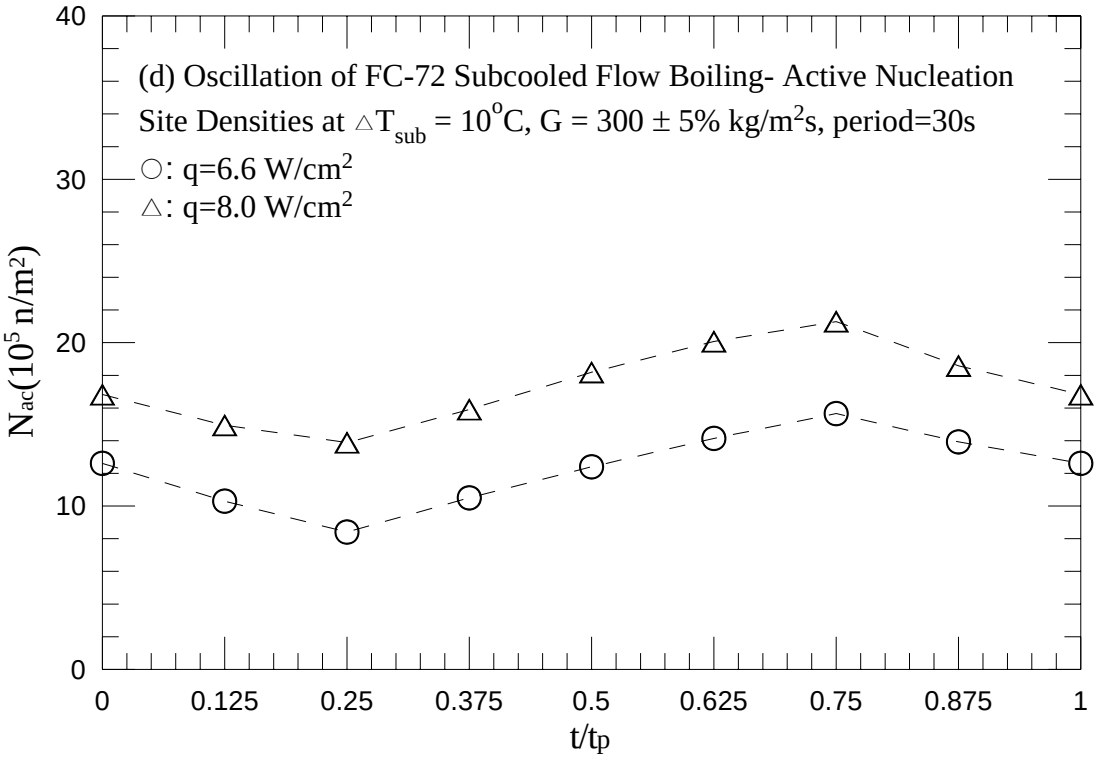

Fig. 5.192 Continued.

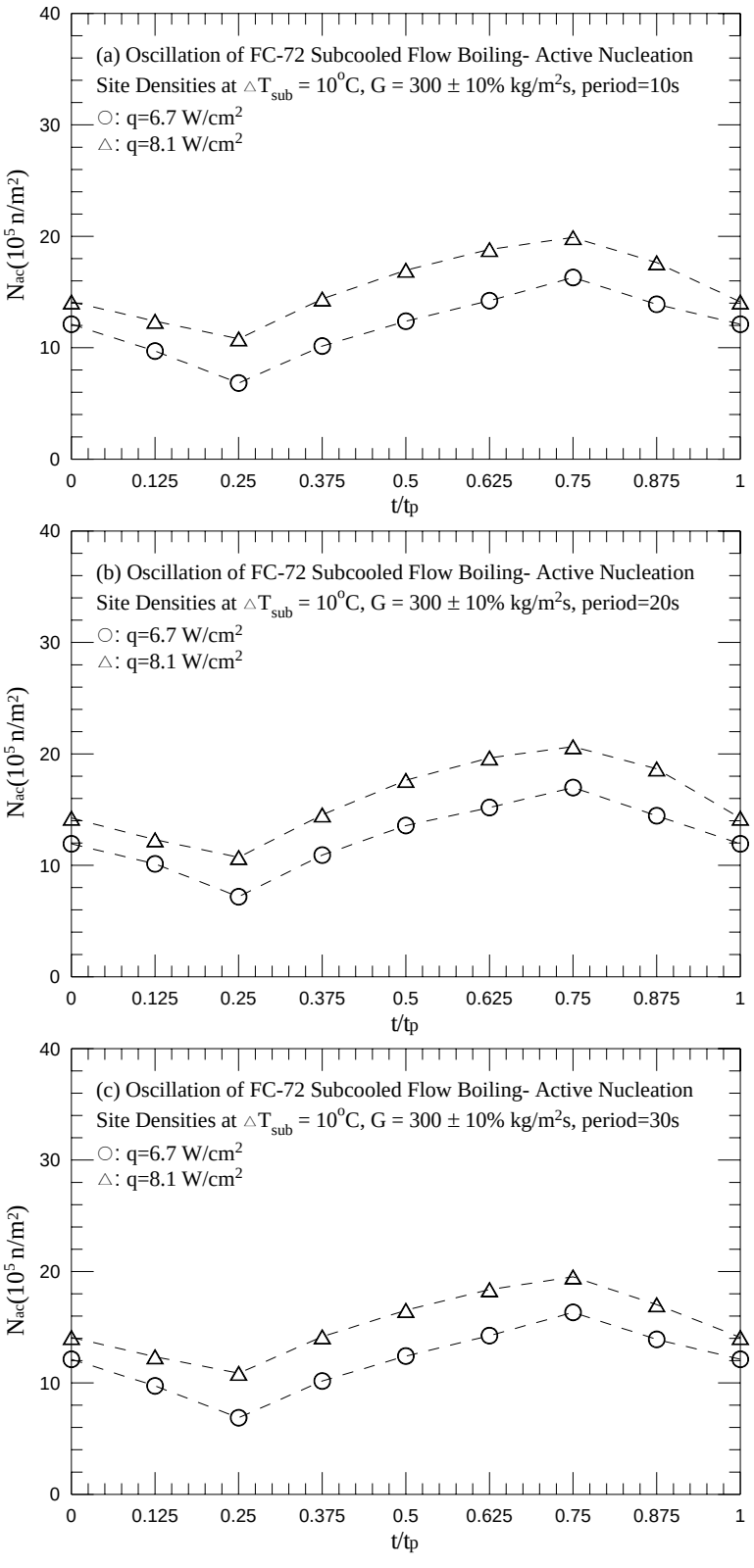

Fig. 5.193 Mean active nucleation site densities for various imposed heat fluxes for transient subcooled flow boiling for G=300±10% kg/m^{2}s and ΔT_{sub} =10°C with t_p=10 sec (a), 20sec (b) and 30 sec (c).

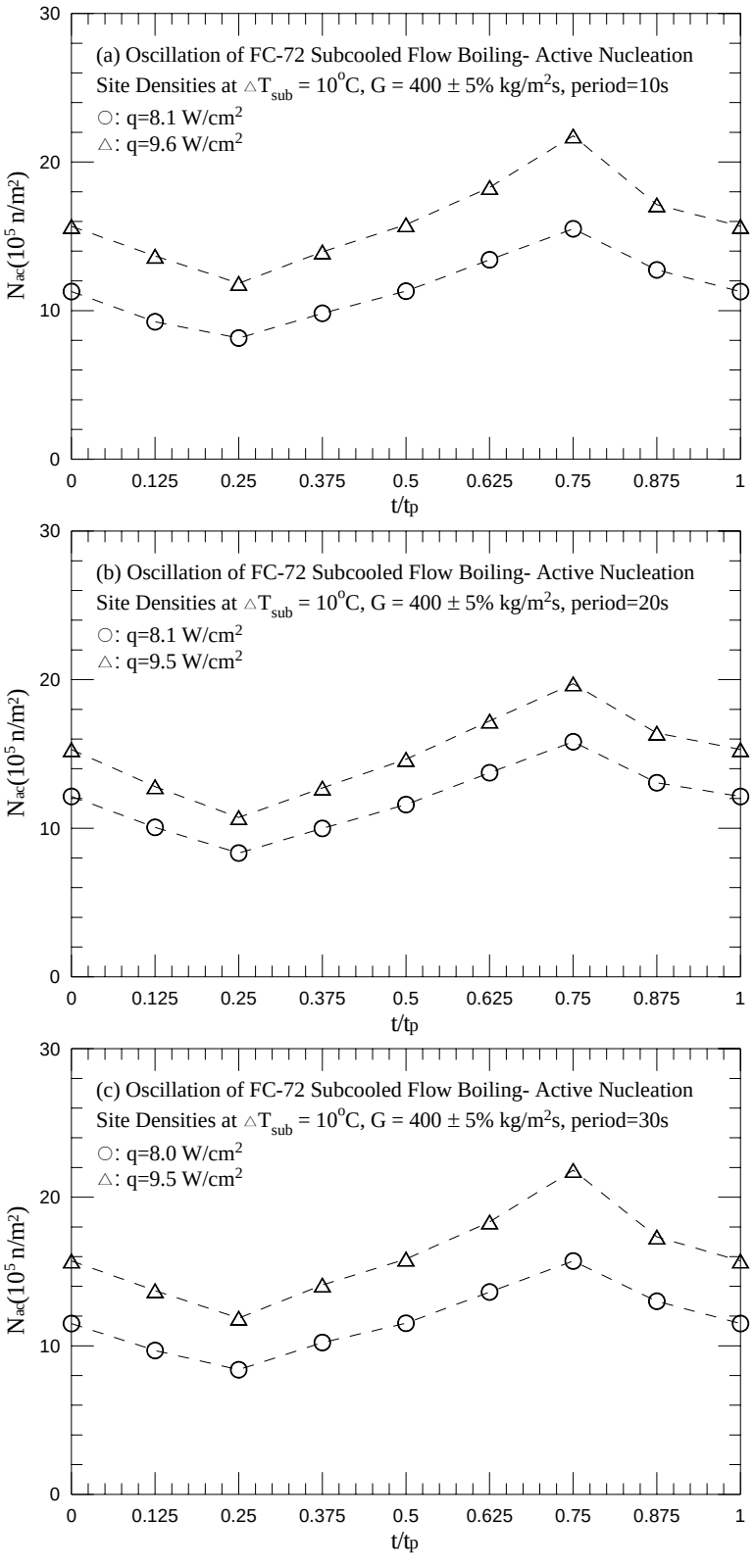

Fig. 5.194 Mean active nucleation site densities for various imposed heat fluxes for transient subcooled flow boiling for G=400±5% kg/m^{2}s and ΔT_{sub} =10^{o}C with t_p=10 sec (a), 20sec (b) and 30 sec (c).

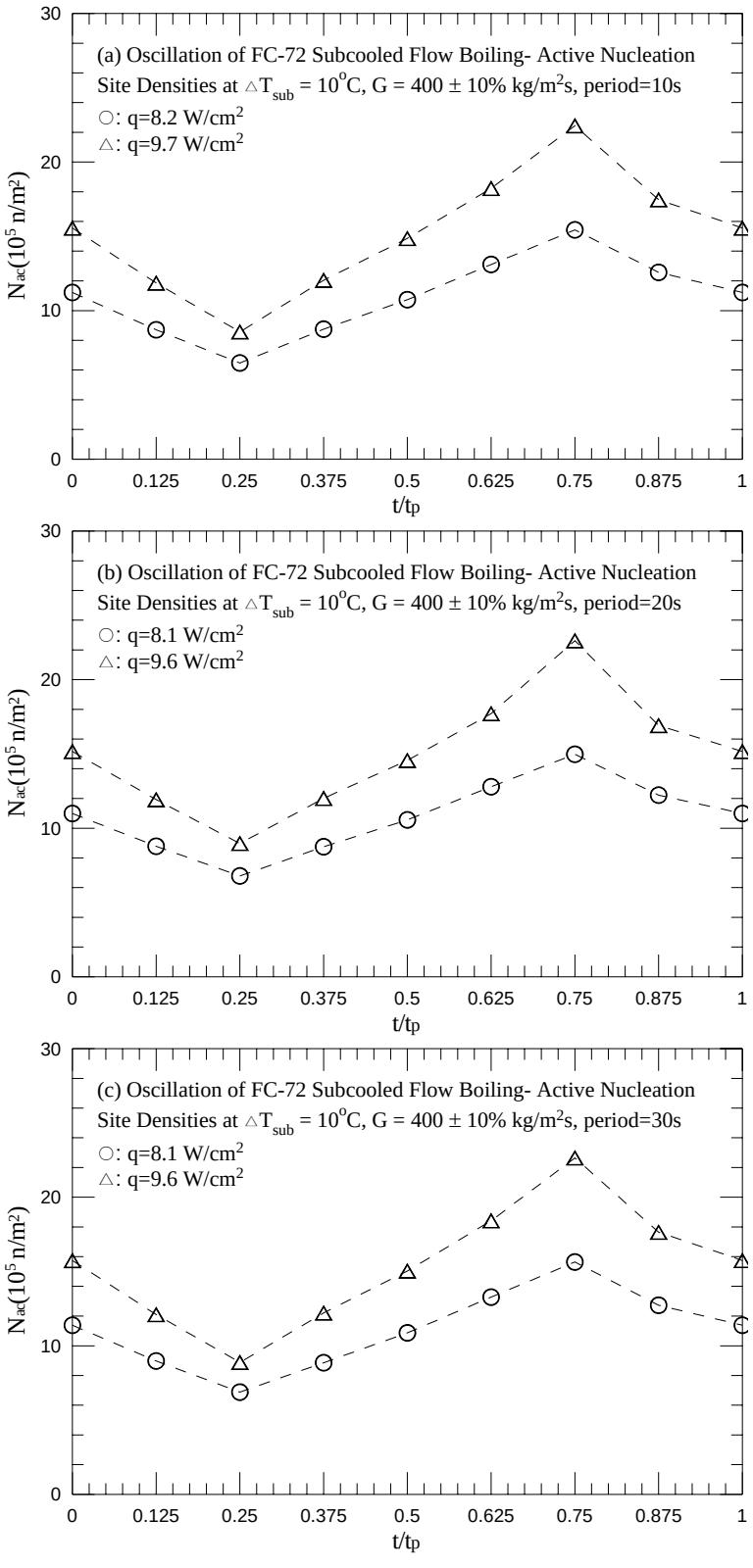

Fig. 5.195 Mean active nucleation site densities for various imposed heat fluxes for transient subcooled flow boiling for G=400±10% kg/m^{2}s and ΔT_{sub} =10°C with t_p=10 sec (a), 20sec (b) and 30 sec (c).

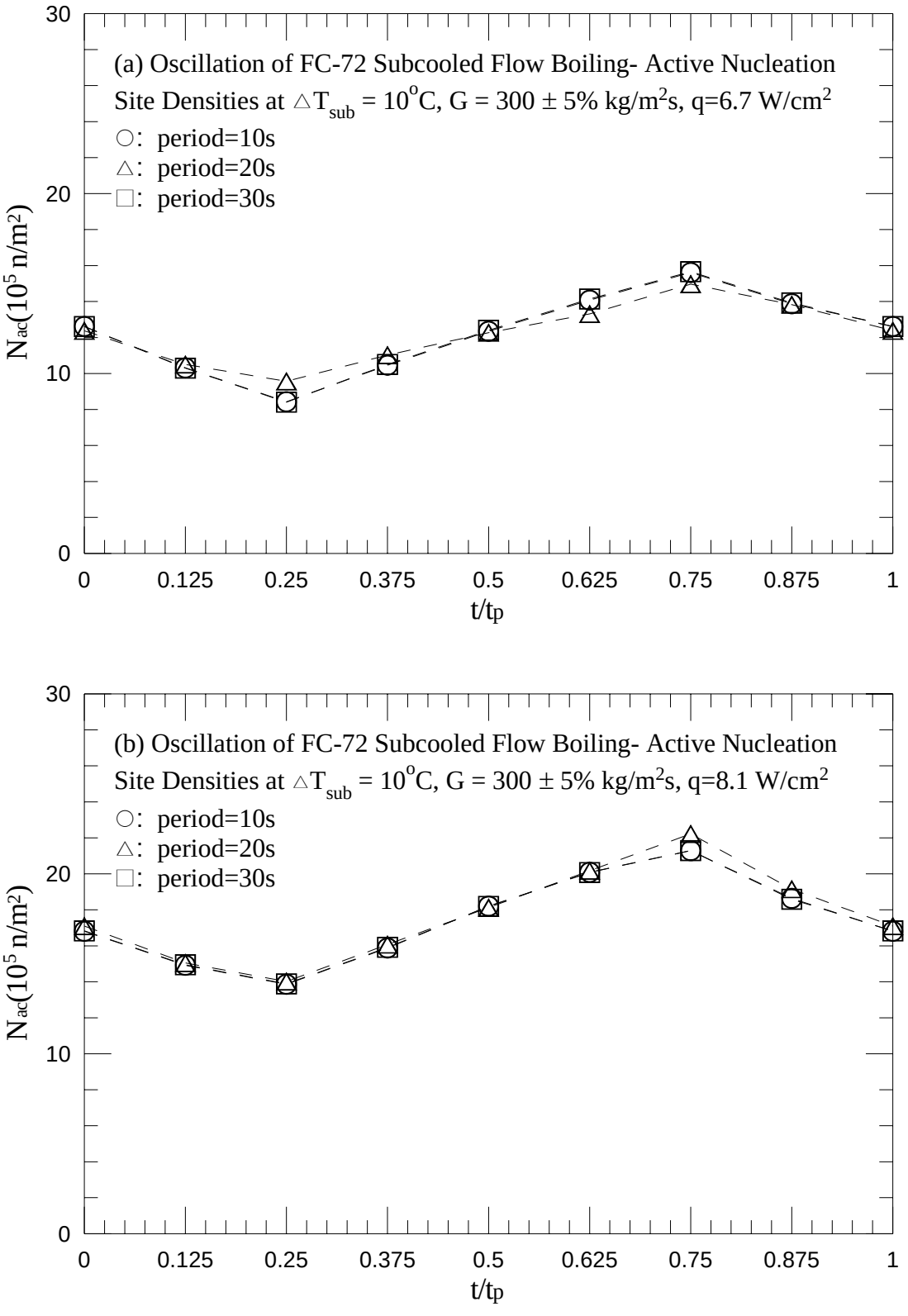

Fig. 5.196 Mean active nucleation site densities for various periods of mass flux oscillation for transient subcooled flow boiling for G=300±5% kg/m^{2}s and ΔT_{sub} =10°C with (a) q=6.7 W/cm^2 and (b) q=8.1 W/cm^2.

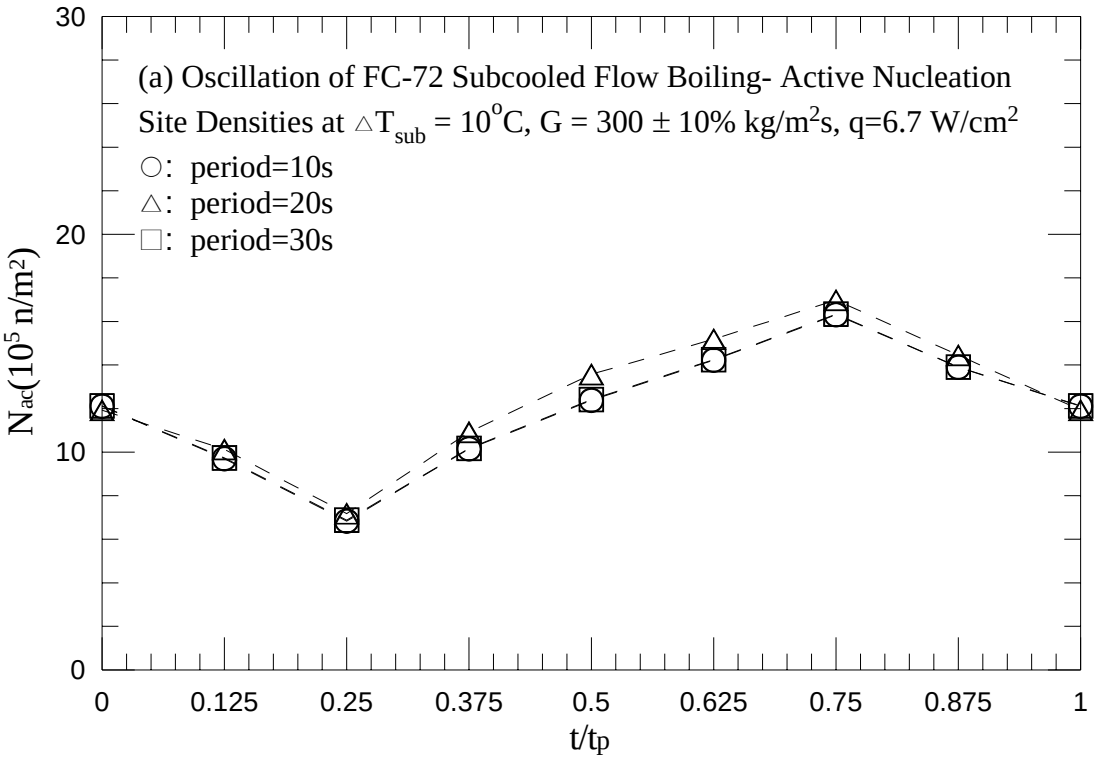

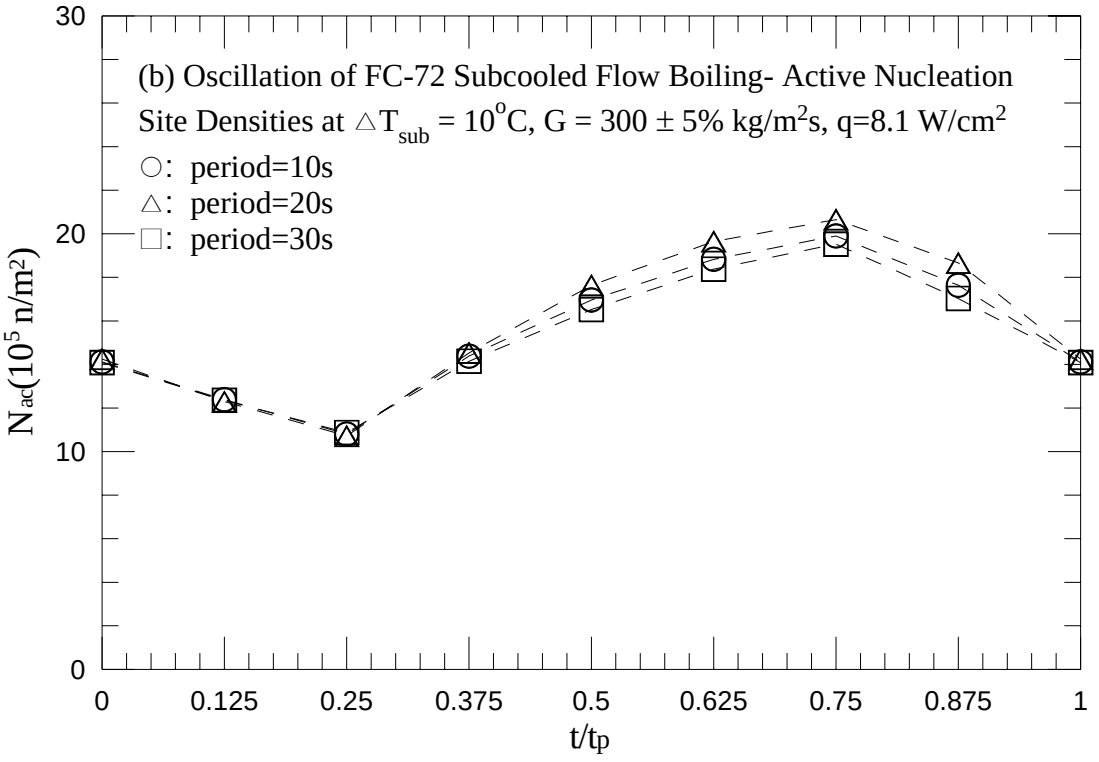

Fig. 5.197 Mean active nucleation site densities for various periods of mass flux oscillation for transient subcooled flow boiling for G=300±10% kg/m^{2}s and ΔT_{sub} =10°C with (a) q=6.7 W/cm^2 and (b) q=8.1 W/cm^2.

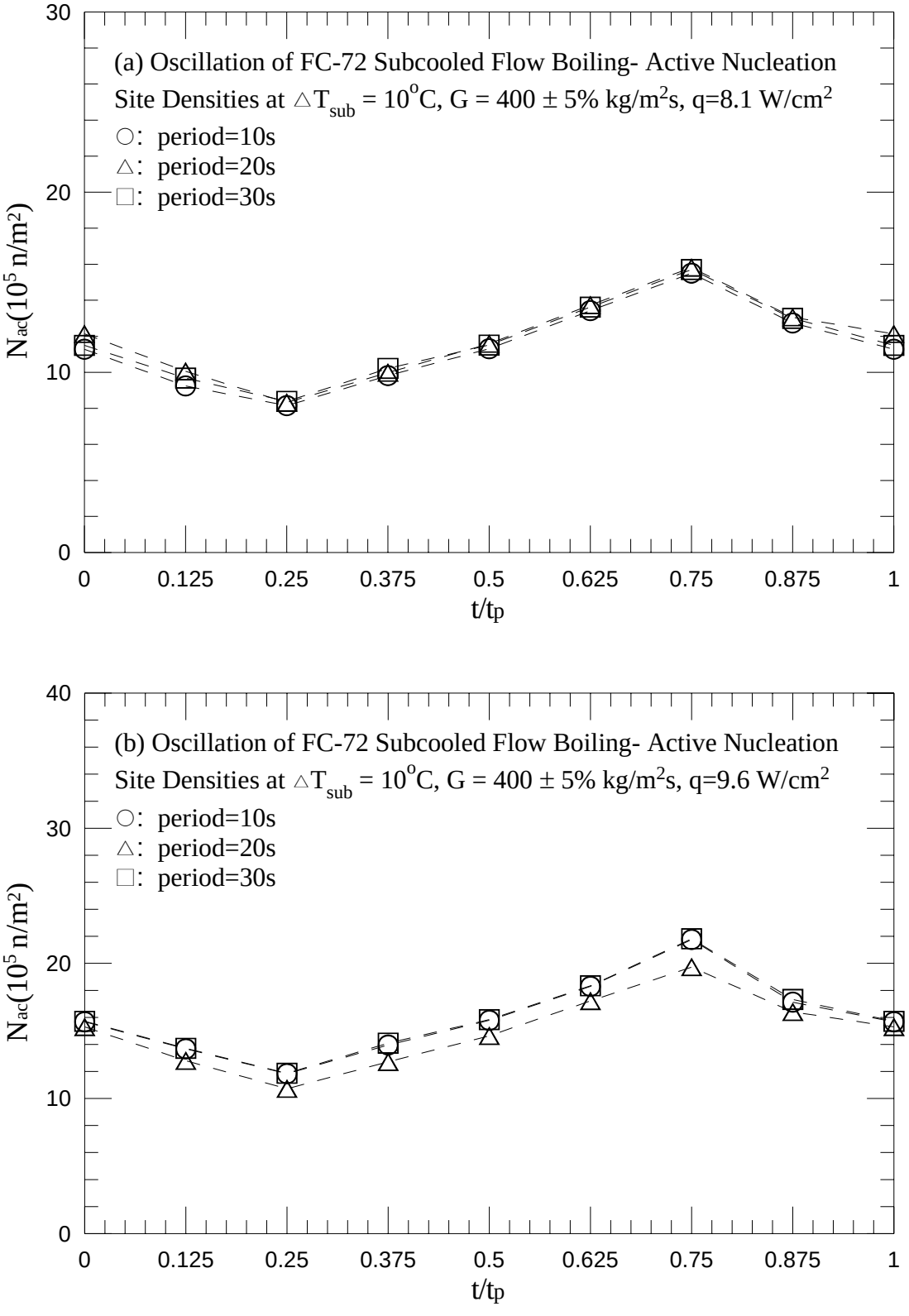

Fig. 5.198 Mean active nucleation site densities for various periods of mass flux oscillation for transient subcooled flow boiling for G=400±5% kg/m^{2}s and ΔT_{sub} =10°C with (a) q=8.1 W/cm^2 and (b) q=9.6 W/cm^2.

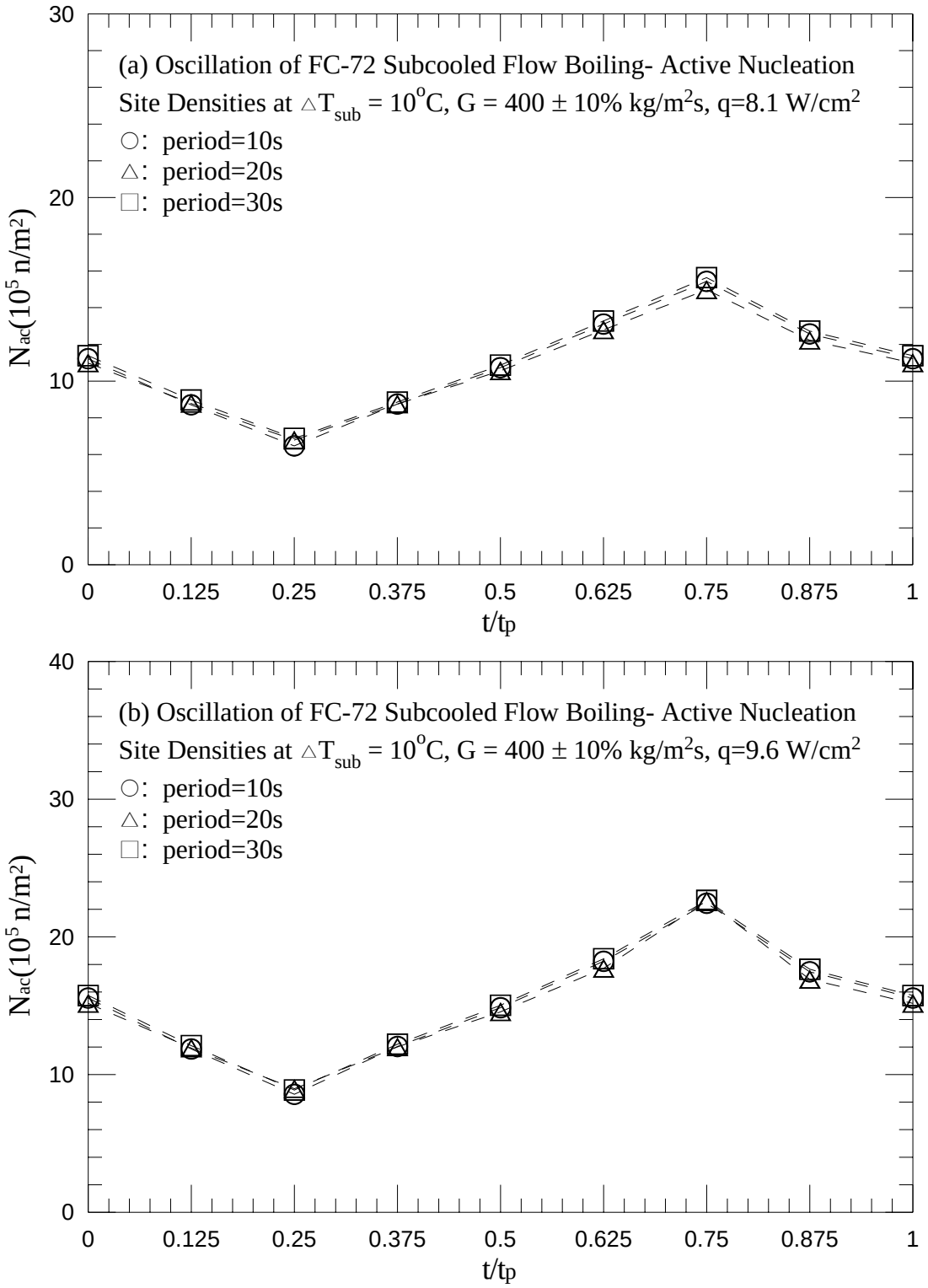

Fig. 5.199 Mean active nucleation site densities for various periods of mass flux oscillation for transient subcooled flow boiling for G=400±10% kg/m^{2}s and ΔT_{sub} =10°C with (a) q=8.1 W/cm^2 and (b) q=9.6 W/cm^2.

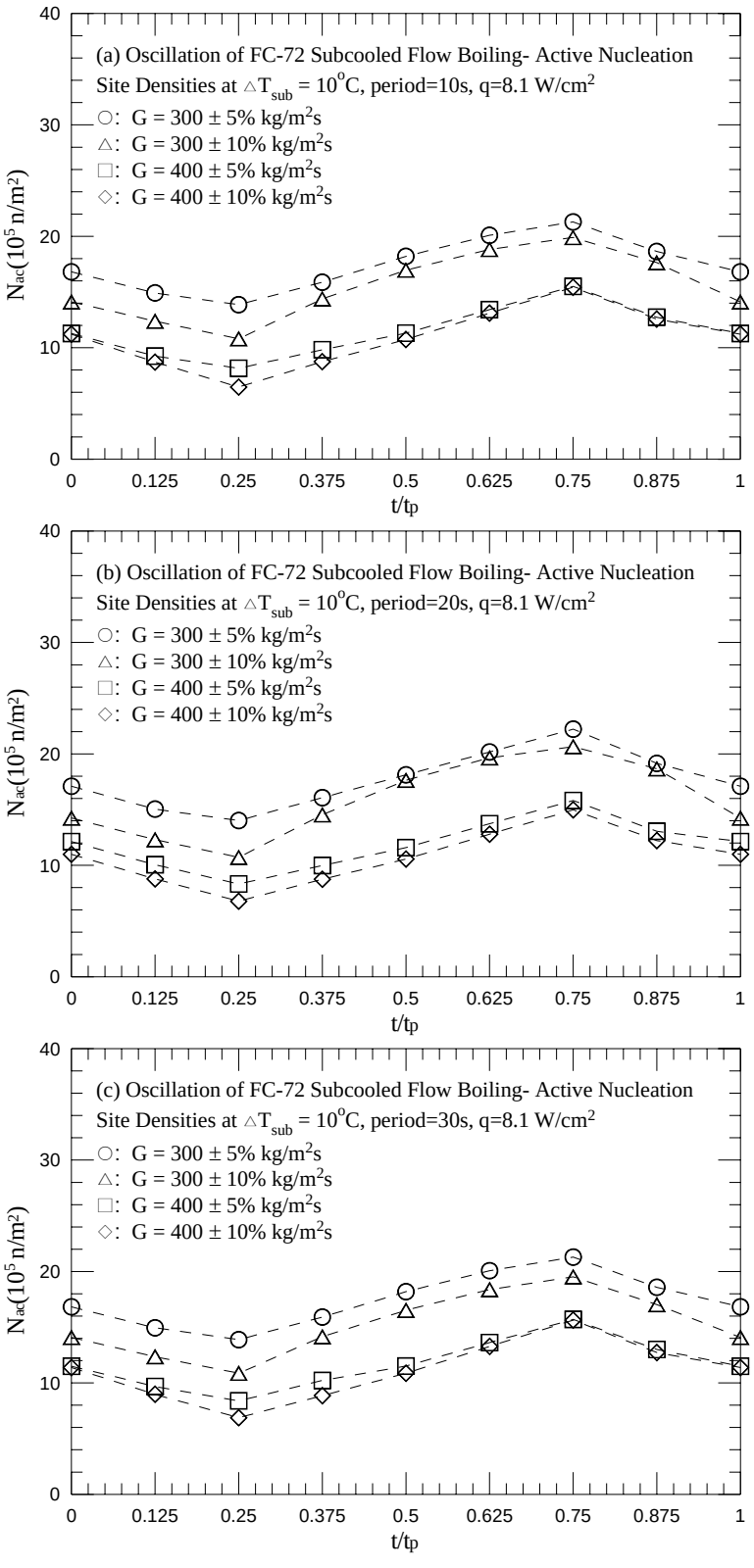

Fig. 5.200 Mean active nucleation site densities for various amplitudes of the mass fluxes oscillation for transient subcooled flow boiling for q=8.1 W/cm^2 and ΔT_{sub} =10^{o}C with period=10 sec (a), 20 sec (b), and 30 sec (c).

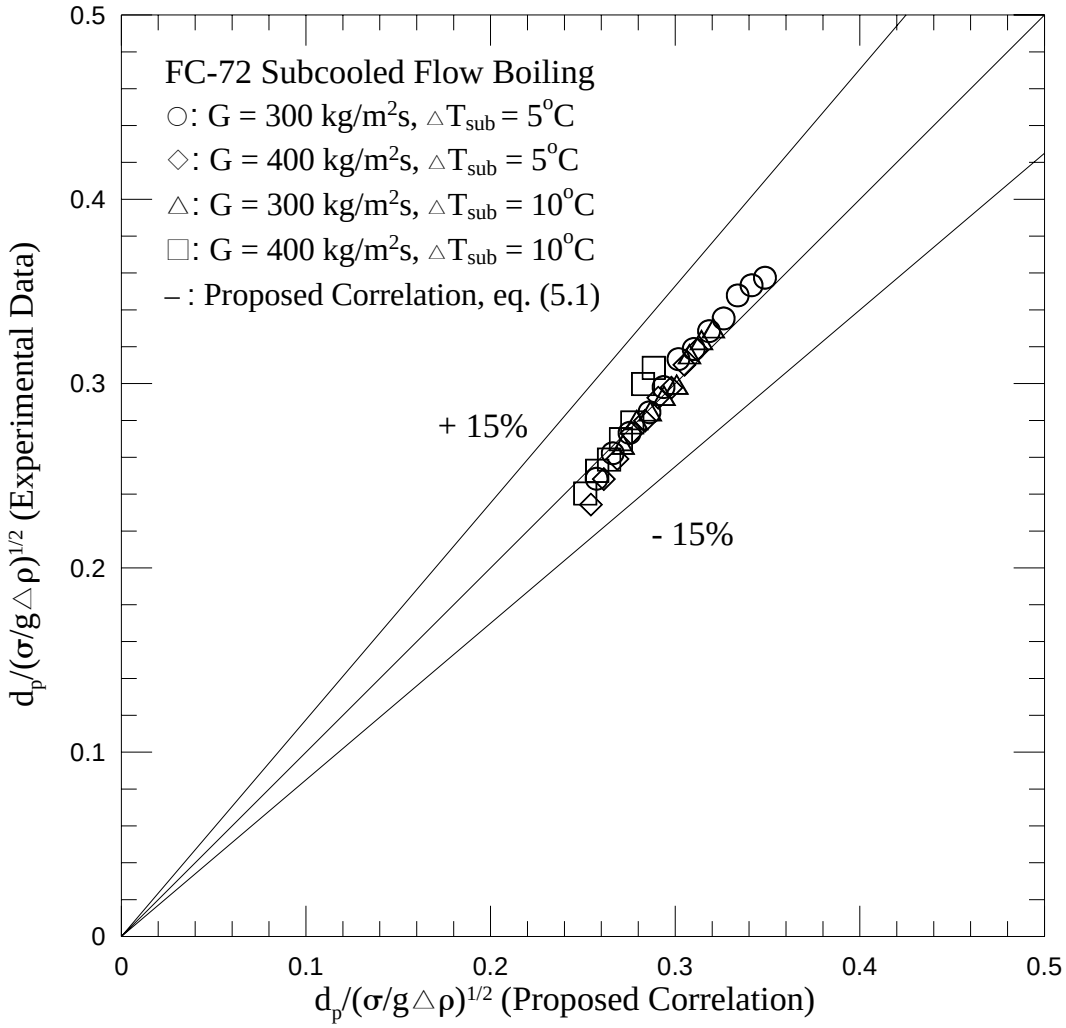

Fig. 5.201 Comparison of the measured data for mean bubble departure diameter for subcooled flow boiling of FC-72 with the proposed correlation.

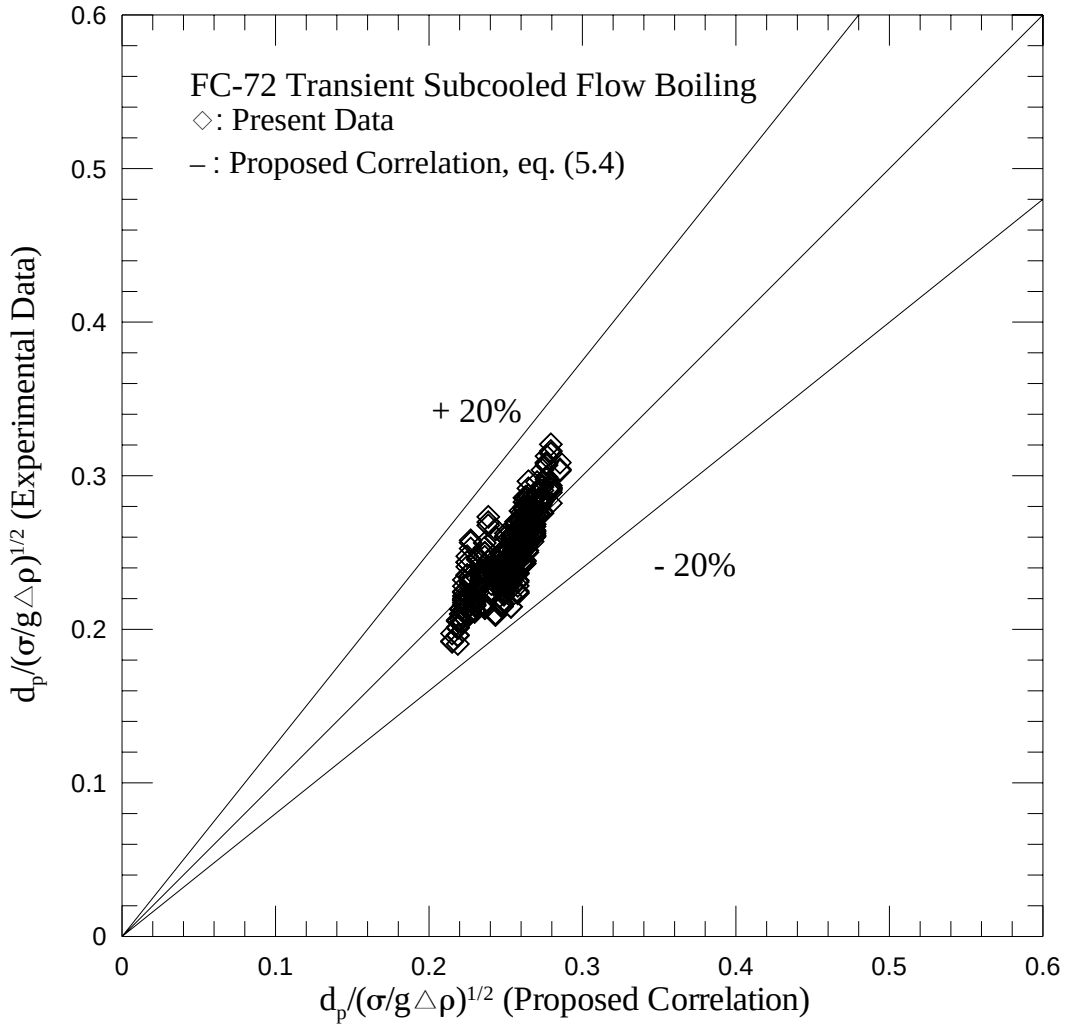

Fig. 5.202 Comparison of the measured data for mean bubble departure diameter for transient subcooled flow boiling of FC-72 with the proposed correlation.

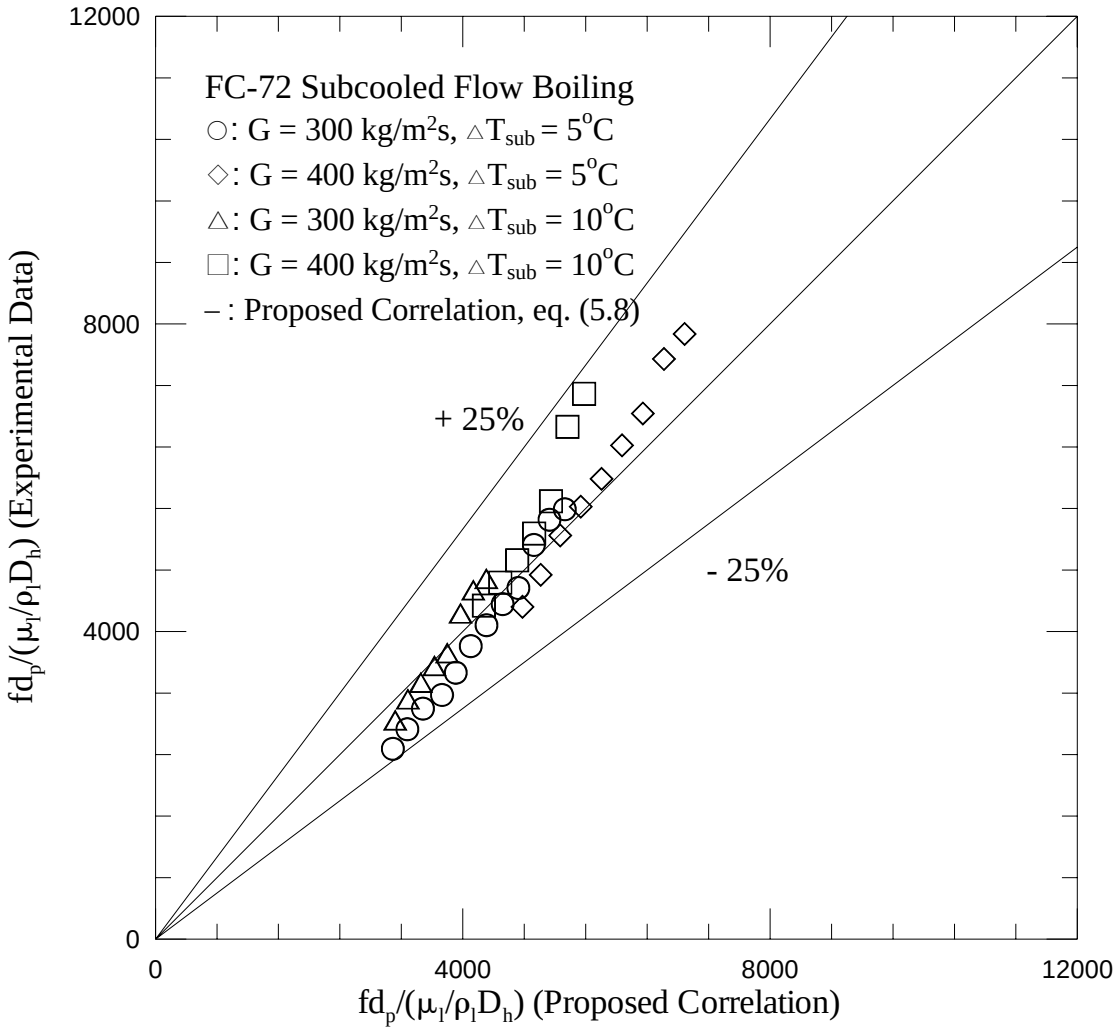

Fig. 5.203 Comparison of the measured data for mean bubble departure frequency for subcooled flow boiling of FC-72 with the proposed correlation.

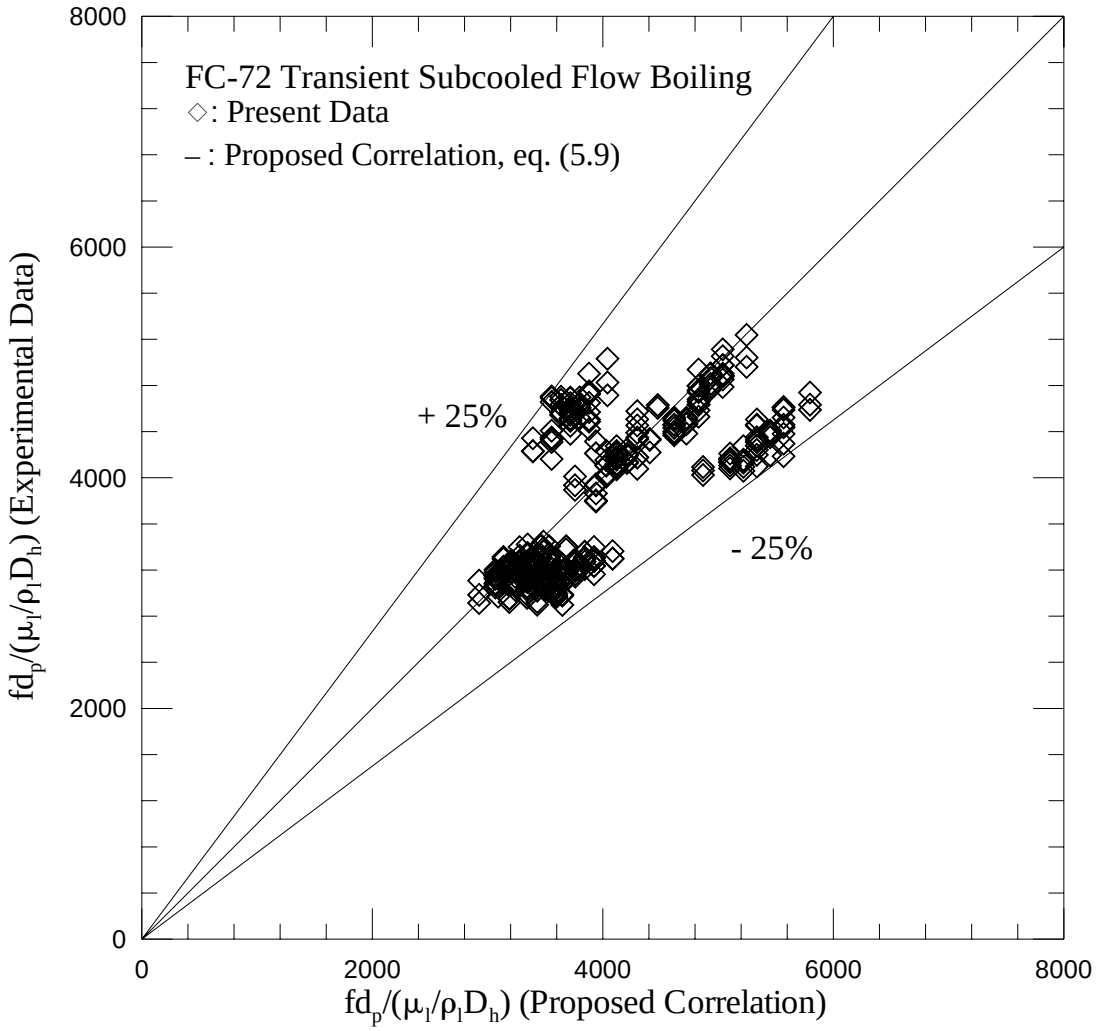

Fig. 5.204 Comparison of the measured data for mean bubble departure frequency for transient subcooled flow boiling of FC-72 with the proposed correlation.

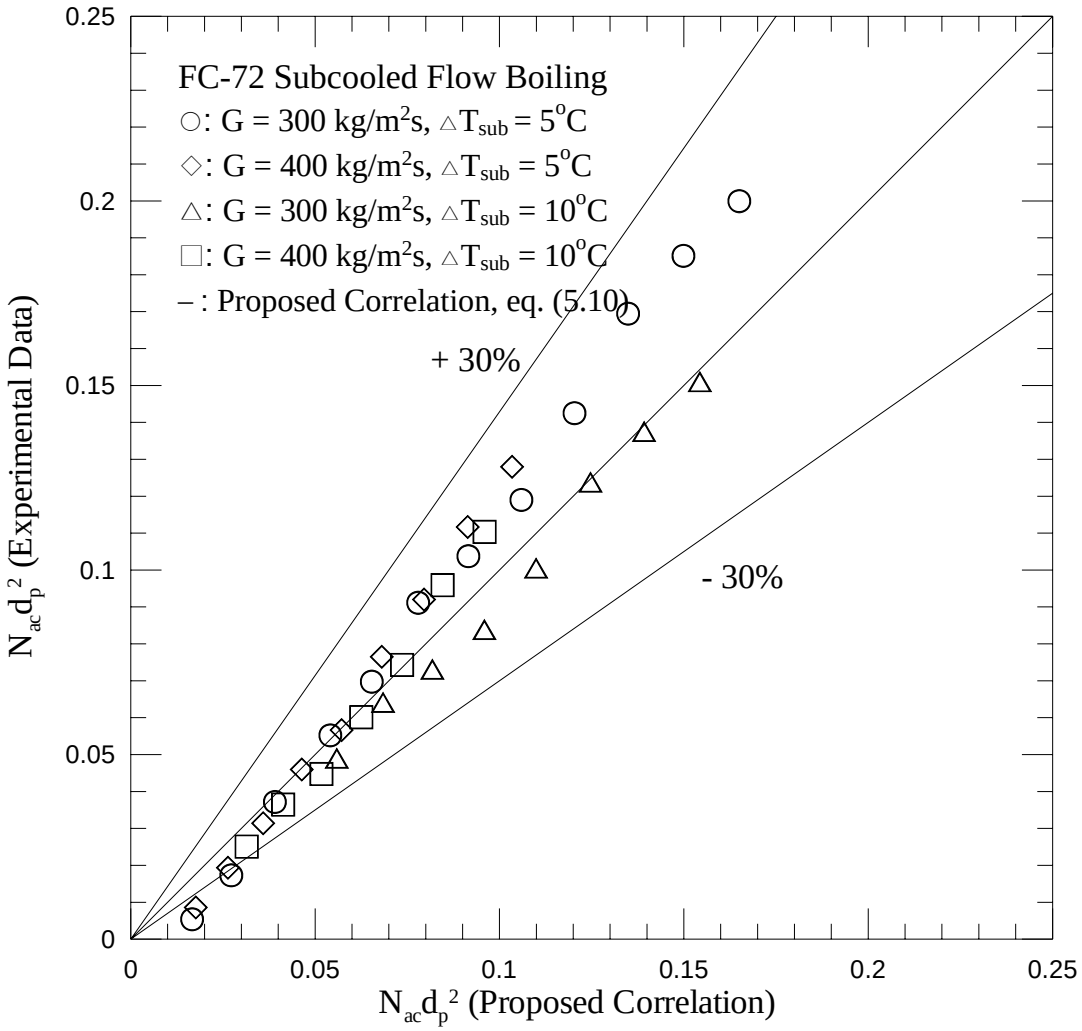

Fig. 5.205 Comparison of the measured data for mean active nucleation site density for subcooled flow boiling of FC-72 with the proposed correlation.

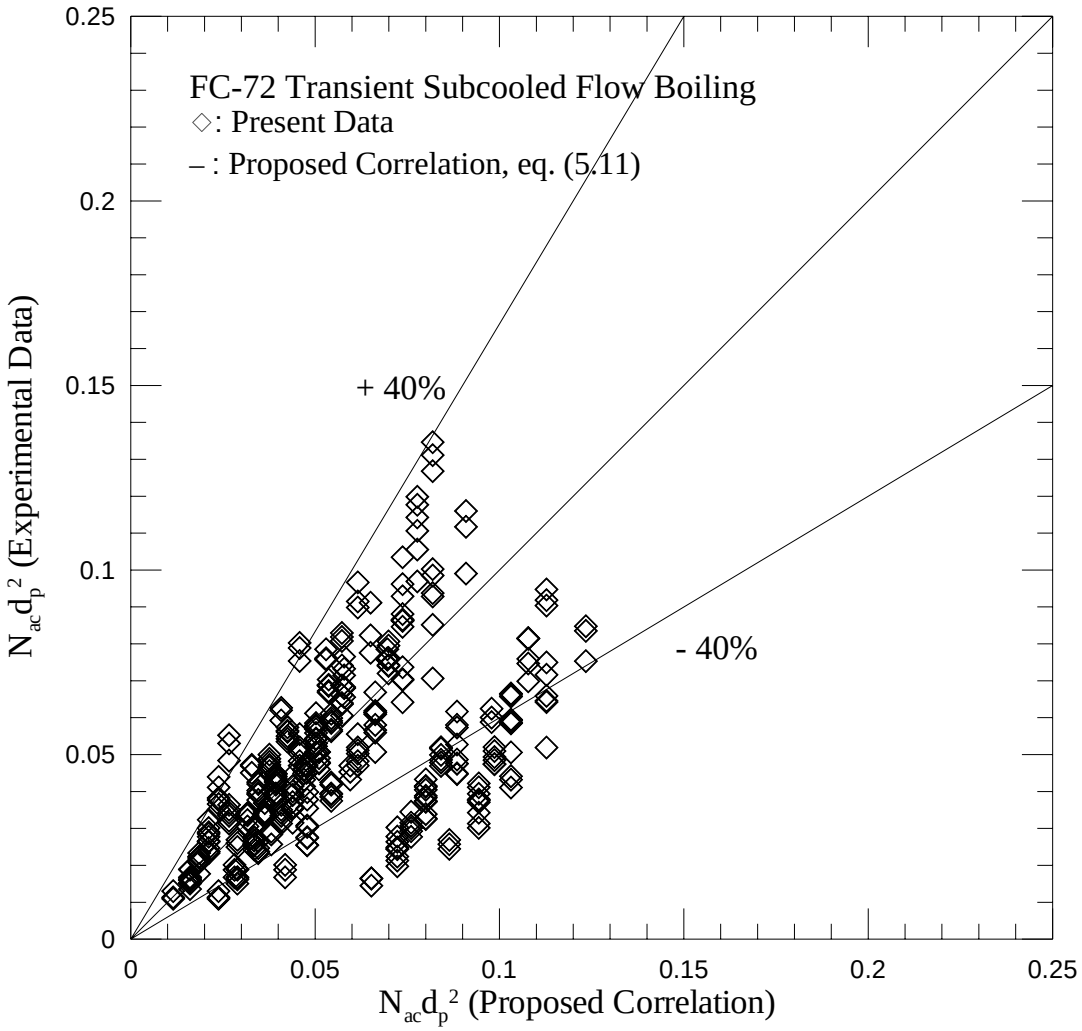

Fig. 5.206 Comparison of the measured data for mean active nucleation site density for transient subcooled flow boiling of FC-72 with the proposed correlation.

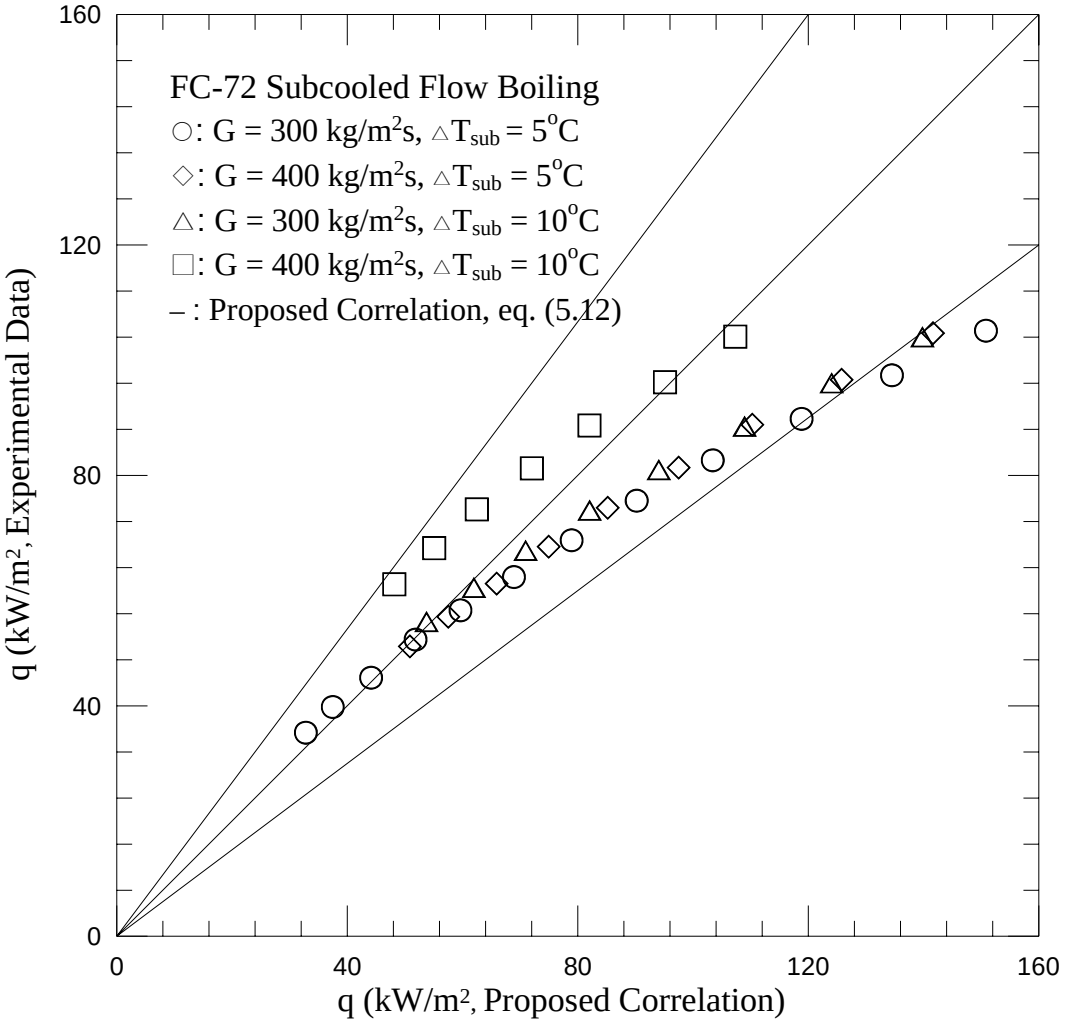

Fig. 5.207 Comparison of the measured data for boiling heat flux for stable subcooled flow boiling of FC-72 with the proposed correlation.

CHAPTER 6

CONCLUDING REMARKS

The FC-72 transient saturated and subcooled flow boiling heat transfer and associated bubble characteristics on a small heated circular copper flat plate flush mounted on the bottom of a rectangular channel have been experimentally investigated. The effects of the mean level and oscillation amplitude and period of the coolant mass flux, inlet liquid subcooling, and the imposed heat flux on the transient FC-72 flow boiling heat transfer coefficients and associated bubble characteristics such as the mean bubble departure diameter, bubble departure frequency, and active nucleation site density have been examined in detail. Major results presented in chapters 4 and 5 can be summarized as follows:

(1) The time-average boiling curves for the transient subcooled and saturated flow boiling of FC-72 are not affected to a noticeable degree by the amplitude and period of the coolant mass flux oscillation. In fact, they resemble that for the stable flow boiling. Similar trend is noted for the time-average boiling heat transfer coefficients.

(2) In the transient saturated flow boiling of FC-72 subject to a time-periodic coolant mass flux oscillation, significant temporal oscillations in the heated surface temperature, boiling heat transfer coefficient, boiling departure diameter and frequency, and active nucleation site density appear for the imposed heat flux slightly higher than that for ONB. These physical quantities oscillate at the same frequency as the mass flux. At a higher imposed heat flux and for a larger amplitude of the mass flux oscillation these oscillations are stronger. The effects of the period of the mass flux oscillation are slight. However, these oscillation are

only slightly affected by the period of the mass flux oscillation. Moreover, the bubbles become smaller and more dispersed when the coolant mass flux increases with time. The opposite processes take place for a decreasing coolant mass flux. Furthermore, reductions in the size of the departing bubbles and active nucleation site density and augmentation in the bubble departure frequency result in the time duration in which the mass flux is rising. When the mass flux is sinking the opposite processes occur.

(3) The temporal variations of the heat transfer and associated bubble characters in the transient FC-72 subcooled flow boiling affected by the coolant mass flux oscillation qualitatively resemble those for the transient saturated flow boiling. Some differences do exist. An increase in the inlet liquid subcooling results in stronger oscillations in the boiling heat transfer coefficient.

REFERENCES

1. R. E. Simons, “Thermal Management of Electronic Packages,” Solid State Technology (1983) 131-137.
2. K. R. Samant and T. W. Simon, “Heat Transfer from a Small Heated Region to R-113 and FC-72,” Transactions of the ASME Journal of Heat Transfer 111 (1989) 1053-1059.
3. S. V. Garimella and P. A. Eibeck, “Heat Transfer Characteristics of an Array of Protruding Elements in Single Phase Forced Convection,” International Journal of Heat and Mass Transfer 33 (12) (1990) 2659-2669.
4. F. P. Incropera, J. S. Kerby, D. F. Moffatt and S. Ramadhyani, “Convection Heat Transfer from Discrete Heat Sources in a Rectangular Channel,” International Journal of Heat and Mass Transfer 29 (7) (1986) 1051-1058.
5. T. J. Heindel, F. P. Incropera, and S. Ramadhyani, “Liquid Immersion Cooling of a Longitudinal Array of Discrete Heat Sources in Protruding Substrates : I – Single-Phase Convection,” Transactions of the ASME Journal of Electronic Package 114 (1992) 55-62.
6. T. J. Heindel, S. Ramadhyani and F. P. Incropera, ”Liquid Immersion Cooling of a Longitudinal Array of Discrete Heat Sources in Protruding Substrates : II – Forced Convection Boiling,” Transactions of the ASME Journal of Electronic Packaging 114 (1992) 63-70.
7. I. Mudawar and D. E. Maddox, “Enhancement of Critical Heat Flux From High Power Microelectronic Heat Sources in a Flow Channel,” Transactions of the ASME Journal of Electronic Package 112 (1990) 241-248.
8. C. O. Gersey and I. Mudawar, “Effects of Orientation on Critical Heat Flux From Chip Arrays During Flow Boiling,” Transactions of the ASME Journal of electronic packaging 114 (1992) 290-299.
9. T. C. Willingham and I. Mudawar, “Forced-Convection Boiling and Critical Heat Flux from a Linear Array of Discrete Heat Sources,” International Journal of Heat and Mass Transfer 35 (11) (1992) 2879-2890.
10. C. P. Tso, K. W. Tou and G. P. Xu, “Flow Boiling Critical Heat Flux of FC-72 from Flush-mounted and Protruded Simulated Chips in a Vertical Rectangular Channel,” International Journal of Multiphase Flow 26 (2000) 351-365.

11. R. Yun, Y. Kim, and M. S. Kim, “Flow boiling heat transfer of carbon dioxide in horizontal mini tubes,” International Journal of Heat and Fluid Flow 26 (2005) 801-809.
12. T. Otsuji and A. Kurosawa, “Critical Heat Flux of Forced Convection Boiling in an Oscillating Acceleration Field : I – General Trends,” Nuclear Engineering and Design 71 (1982) 15-26.
13. T. Otsuji and A. Kurosawa, “Critical Heat Flux of Forced Convection Boiling in an Oscillating Acceleration Field : II – Contribution of Flow Oscillation,” Nuclear Engineering and Design 76 (1983) 13-21.
14. S. Kakac, T. N. Veziroglu, M. M. Padki, L. Q. Fu, and X. J. Chen, “Investigation of Thermal Instabilities in a Forced Convection Upward Boiling System,” Experimental Thermal and Fluid Science 3 (1990) 191-201.
15. M. M. Padki, H. T. Liu, and Kakac, “Two-Phase Flow Pressure-Drop type and Thermal Oscillations,” International Journal of Heat and Fluid Flow 12 (1991) 240-248.
16. Y. Ding, S. Kakac, and X. J. Chen, “Dynamic Instabilities of Boiling Two-Phase Flow in a Single Horizontal Channel,” Experimental Thermal and Fluid Science 11 (1995) 327-342.
17. O. Comakli, S. Karsli, and M. Yilmaz, “Experimental investigation of two phase flow instabilities in a horizontal in-tube boiling system,” Energy Conversion and Management 43 (2002) 249-268
18. P. R. Mawasha and R. J. Gross, “Periodic Oscillations in a Horizontal Single Boiling Channel with Thermal Wall Capacity,” International Journal of Heat and Fluid Flow 22 (2001) 643-649.
19. P. R. Mawasha, R. J. Gross, and D. D. Quinn, “Pressure-Drop Oscillations in a Horizontal Single Boiling Channel,” Heat Transfer Engineering 22 (2001) 26-34.
20. Q. wang, X. J. Chen, S. kakac, and Y. Ding, “Boiling Onset Oscillation : a new type of Dynamic Instability in a Forced-Convection Upflow Boiling System,” International Journal of Heat and Fluid Flow 17(1996) 418-423.
21. D. Brutin, F. Topin, and L. Tadrist, “Experimental Study of Unsteady Convective Boiling in Heated Minichannels,” International Journal of Heat and Mass Transfer 46 (2003) 2957-2965.
22. D. Brutin and L. Tadrist, “Pressure Drop and Heat Transfer Analysis of Flow Boiling in a Minichannel : Influence of the Inlet Condition on Two-phase Flow

Stability," International Journal of Heat and Mass Transfer 47 (2004) 2365-2377.

23. J. Shuai, R. Kulenovic, and M. Groll, "Pressure Drop Oscillations and Flow Patterns for Flow Boiling of Water in Narrow Channel," Proceedings of International Conference on Energy and the Environment, Shanghai, China, May 22-24, 2003.
24. S. H. Chang, I. C. Bang and Won-Pil Baek, "A Photographic Study on the Near-wall Bubble Behavier in Subcooled Flow Boiling," Int. J. Therm. 41 (2002) 609-618.
25. I. C. Bang, S. H. Chang and Won-Pil Baek, "Visualization of the Subcooled Flow Boiling of R-134a in a Vertical Rectangular Channel with an Electrically Heated Wall," International Journal of Heat and Mass Transfer 47 (2004) 4349-4363.
26. S. G. Kandlikar, "Bubble Nucleation and Growth Characteristics in Subcooed Flow Boiling of Water," National Heat Transfer Conference HTD-Vol. 342 4 (1997) 11-18
27. R. Maurus, V. Ilchenko and T. Sattelmayer, "Study of the Bubble Characteristics and the Local Void Fraction in Subcooled Flow Boiling Using Digital Imaging and Analyzing Techniques," Experimental Thermal and Fluid Science 26 (2002) 147-155.
28. R. Maurus, V. Ilchenko and T. Sattelmayer, "Automated high-speed vedio analysis of the bubble dynamics in subcooled flow boiling," International Journal of Heat and Fluid Flow 25 (2004) 149-158.
29. R. Maurus and Sattelmayer, "Bubble and boundary layer behavior in subcooled flow boiling," International Journal of Thermal Sciences 45 (2006) 257-268.
30. G. E. Thorncroft, J. F. Klausner and R. Mei, "An Experimental Investigation of Bubble Growth and Detachment in Vertical Upflow and Downflow Boiling," International Journal of Heat and Mass Transfer 41 (1998) 3857-3871.
31. T. Okawa, T. Ishida, I. Kataoka, and M. Mori, "An experimental study on bubble rise path after the departure from a nucleation site in vertical upflow boiling," Experimental Thermal and Fluid Science 29 (2005) 287-294.
32. T. Okawa, T. Ishida, I. Kataoka, and M. Mori, "Bubble rise characteristics after the departure from a nucleation site in vertical upflow boiling of subcooled water," Nuclear Engineering and Design 235 (2005) 1149-1161.
33. T. Okawa, T. Ishida, I. Kataoka, and M. Mori, "On the rise paths of single vapor bubbles after the departure from nucleation sites in subcooled upflow boiling,"

International Journal of Heat and Mass Transfer 48 (2005) 4446-4459.

34. R. Situ, Y. Mi, M. Ishii, and M. Mori, “Photographic study of bubble behaviors in forced convection subcooled boiling,” International Journal of Heat and Mass Transfer 47 (2004) 3659-3667
35. R. Situ, T. Hibiki, M. Ishii, and M. Mori, “Bubble lift-off size in forced convection subcooled boiling flow,” International Journal of Heat and Mass Transfer 48 (2005) 5536-5548
36. C. P. Yin, Y. Y. Yan, T. F. Lin and B. C. Yang, “Subcooled Flow Boiling Heat Transfer of R-134a and Bubble Characteristics in a Horizontal Annular Duct,” International Journal of Heat and Mass Transfer 43 (2000) 1885-1896.
37. 3M company, Kataoka Japan.
38. S. J. Kline and F. A. McClintock, “Describing Uncertainties in Single-sample Experiments,” Mech. Engng 75 (1953) 3-8.